



MONASH University

Deciphering the modes of action of polymyxins and the synergistic combinations against multidrug-resistant Gram-negative bacteria: A systems pharmacology approach

Mohd Hafidz Mahamad Maifiah

Bachelor of Biomedical Science (Honours)

M. Sc. (Biotechnology Engineering)

A thesis submitted for the degree of
DOCTOR OF PHILOSOPHY

at

Monash University

June 2017

Drug Delivery, Disposition and dynamics
Monash Institute of Pharmaceutical Sciences
Monash University
Melbourne, Victoria, Australia

Copyright notice

© Mohd Hafidz Mahamad Maifiah (2017).

I certify that I have made all reasonable efforts to secure copyright permissions for third-party content included in this thesis and have not knowingly added copyright content to my work without the owner's permission.

This thesis is dedicated to my beloved wife, son and my parents

Table of Contents

ABSTRACT	viii
STATEMENT OF THE ORIGINALITY	x
ACKNOWLEDGEMENTS	xiii
PUBLICATIONS	xv
PRESENTATIONS	xvi
LIST OF TABLES	xvii
LIST OF FIGURES	xx
GLOSSARY OF ABBREVIATIONS	xxiv

Chapter 1: General Introduction	1
1.1 Statement of the problem	2
1.2 Bad bugs, no drugs	3
1.2.1 <i>A. baumannii</i> : an emerging opportunistic pathogen.....	5
1.2.2 <i>P. aeruginosa</i> : an opportunistic ‘superbug’	7
1.3 Polymyxins: an overview	11
1.3.1 Chemical structure.....	12
1.3.2 Mode of action of polymyxins	13
1.3.3 Mechanism of polymyxin resistance	17
1.3.4 Nephrotoxicity and neurotoxicity.....	20
1.3.5 Pharmacokinetics and pharmacodynamics (PK/PD).....	22
1.3.6 Polymyxin combination therapy	26
1.3.6.1 Doripenem	29
1.3.6.2 Rifampicin	31
1.4 Metabolomics	32
1.4.1 Untargeted and targeted metabolomics	34
1.4.2 Sample preparation for bacterial metabolomics	37
1.4.2.1 Sample pre-treatment	38
1.4.2.2 Analytical methods.....	40
1.4.3 Metabolomics data analysis	41
1.4.3.1 IDEOM and MetaboAnalyst 3.0	42
1.4.4 Integrated systems biology.....	44
1.5 Summary	46

1.6 Hypotheses and aims	46
1.7 Significance statement.....	47
1.8 Structure of the thesis	49

Chapter 2: Global metabolic analyses identify key differences in metabolite levels between polymyxin-susceptible and polymyxin-resistant *Acinetobacter baumannii* 50

2.1 Abstract	53
2.2 Introduction	54
2.3 Materials and methods	55
2.3.1 Strains.....	55
2.3.2 Identification of 16S rDNA, genome sequencing and lipid A structural analysis of <i>A. baumannii</i> clinical isolates 03-149.1 and 03-149.2	55
2.3.3 Bacterial culture preparation for metabolomics experiments.....	57
2.3.4 Sample preparation for metabolomic study.....	57
2.3.5 LC-MS analysis.....	58
2.3.6 Data processing, bioinformatics and statistical analyses.....	59
2.4 Results	60
2.4.1 Genomics and lipid A structural analysis of <i>A. baumannii</i> clinical isolates 03-149.1 and 03-149.2	61
2.4.2 Optimal metabolite recovery of MDR <i>A. baumannii</i> by washing with 0.9% NaCl and extraction using chloroform:methanol:water (1:3:1)	66
2.4.3 Multivariate and univariate metabolomics analyses were able to identify key differences between the polymyxin-susceptible and polymyxin-resistant <i>A. baumannii</i> strains	69
2.4.4 Perturbations in sugar and nucleotide metabolism.....	73
2.4.5 Variations of amino acid related metabolites in the polymyxin-resistant 19606R	77
2.4.6 Perturbation of lipids levels in the polymyxin-resistant 19606R.....	80
2.4.7 Untargeted analysis reveals unknown metabolites that are common to both polymyxin-resistant strains	82
2.5 Discussion	82
2.6 Conclusions	90

Chapter 3: Untargeted metabolomics analysis reveals key pathways responsible for the synergistic killing of colistin and doripenem combination against *Acinetobacter baumannii* ..91

3.1 Abstract	94
3.2 Introduction	95
3.3 Materials and methods	97
3.3.1 Strains, antibiotics and reagents	97
3.3.2 Bacterial culture preparation	97
3.3.3 Preparation of cellular metabolite extracts	98
3.3.4 LC-MS analysis of metabolites	99
3.3.5 Data processing, bioinformatics and statistical analyses.....	100
3.4 Results	101
3.4.1 Multivariate and univariate analyses.....	104
3.4.1.1 <i>A. baumannii</i> ATCC 19606.....	104
3.4.1.2 <i>A. baumannii</i> 03-149.1 and 03.149.2 strains.....	106
3.4.2 Colistin alone and in combination with doripenem predominantly induced disruption of bacterial lipids.....	107
3.4.3 Combination of colistin and doripenem induced global metabolic changes via pentose phosphate pathway (PPP) metabolism	112
3.4.4 Colistin and doripenem caused depletion of metabolite levels of energy and nucleotide metabolism.....	115
3.4.5 Colistin and doripenem induced depletion of amino sugar metabolites for cell wall biosynthesis	119
3.4.6 Colistin and doripenem induced alterations in peptide metabolism	120
3.5 Discussion	143
3.6 Conclusions	151

Chapter 4: Untargeted metabolomics study of the synergistic combination of polymyxin B and rifampicin against *Pseudomonas aeruginosa* PAO1 152

4.1 Abstract	153
4.2 Introduction	154
4.3 Materials and methods	155
4.3.1 Strain	155
4.3.2 Antibiotics and reagents	155
4.3.3 Bacterial culture preparation	155

4.3.4 Preparation of cellular metabolite extracts	156
4.3.5 LC-MS analysis of metabolites	157
4.3.6 Data processing, bioinformatics and statistical analyses.....	157
4.4 Results	158
4.4.1 Polymyxin B alone and in combination induced perturbation of membrane lipids	165
4.4.2 Polymyxin B and rifampicin combination up-regulated metabolites of peptidoglycan and LPS biosynthesis	165
4.4.3 Polymyxin B and rifampicin combination causes significant accumulation of nucleotides and perturbation of amino acid metabolites.....	168
4.4.4 Polymyxin B and rifampicin combination induces significant perturbation in the central carbon metabolism	170
4.5 Discussion	179
4.6 Conclusions	183

Chapter 5: The transcriptomic responses of the synergistic combination of polymyxin B and rifampicin against *Pseudomonas aeruginosa* PAO1..... 185

5.1 Abstract	186
5.2 Introduction	187
5.3 Materials and methods	188
5.3.1 Strain	188
5.3.2 Antibiotics and reagents	188
5.3.3 Bacterial culture preparation	188
5.3.4 RNA extraction	189
5.3.5 Analysis of RNA-seq data.....	190
5.4 Results	190
5.4.1 Polymyxin B differentially induced the expression of polymyxin resistance genes at 1 hr.....	196
5.4.2 Rifampicin-induced DEGs at 1 hr	198
5.4.3 Polymyxin B and rifampicin combination differentially induced the repression of virulence factor genes at 1 hr.....	198
5.4.4 The combination of polymyxin B and rifampicin induced significant changes in central carbon metabolism	199

5.4.5 Rifampicin alone and the combination differentially regulated more genes at 24 hr	204
5.5 Discussion	208
5.6 Conclusions	213
Chapter 6: Integrated metabolomics and transcriptomics analyses of the synergistic effect of polymyxin B and rifampicin combination against <i>Pseudomonas aeruginosa</i> PAO1	214
6.1 Abstract	215
6.2 Introduction	216
6.3 Materials and methods	217
6.3.1 Genome-scale metabolic network (GSMN) reconstruction for <i>P. aeruginosa</i> PAO1	217
6.4 Results	218
6.4.1 Metabolomics	218
6.4.2 Transcriptomics	220
6.4.3 Integration of metabolomic and transcriptomic data.....	221
6.4.4 Polymyxin-induced cell envelope changes	223
6.4.5 Polymyxin B induced resistance and the expression of genes related to virulence factor.....	224
6.4.6 The combination of polymyxin B and rifampicin induced significant changes in nucleotide and amino acid metabolism	228
6.4.7 Synergistic polymyxin B and rifampicin combination induced suppression of virulence factors	231
6.4.8 Synergistic polymyxin B and rifampicin combination induced alterations in central carbon metabolism	232
6.4.9 Rifampicin predominantly induced transcriptomic changes in the polymyxin B and rifampicin combination at 24 hr	235
6.5 Discussion	236
6.6 Conclusions	243
Chapter 7: Conclusions and future perspectives.....	245
References	252
Appendices	280

Abstract

Multidrug-resistant (MDR) bacteria are one of the three greatest threats to human health globally and there are few therapeutic options available. Polymyxins (polymyxin B and polymyxin E [i.e. colistin]) have been used as the last-line defence for infections caused by MDR Gram-negative pathogens, such as *Acinetobacter baumannii* and *Pseudomonas aeruginosa*. However, pharmacokinetic/pharmacodynamic (PK/PD) studies indicate that polymyxins often fail to achieve an effective exposure *in vivo* due to the dose-limiting nephrotoxicity, potentially leading to the emergence of resistance. Combination therapy has been strongly recommended to optimise the clinical use of intravenous polymyxins; however, there is a lack of understanding of the exact mechanisms of polymyxin action and their synergistic combinations with other types of antibiotics. Polymyxins enter Gram-negative bacteria via the ‘self-promoted uptake’ pathway, which is initiated by electrostatic interaction with the lipid A of lipopolysaccharide (LPS) in the bacterial outer membrane however the details remain unknown. Metabolomic and transcriptomic analyses are robust, systems-based tools that are increasingly used to investigate the mechanism of drug action. This PhD project is the first to investigate the comparative metabolic profiles of MDR *A. baumannii* strains and revealed that there are significant metabolic differences between polymyxin-susceptible and -resistant strains (Chapter 2). In contrast to its parent strain ATCC 19606, the LPS-deficient, polymyxin-resistant derivative strain 19606R was significantly perturbed in the pentose phosphate pathway (PPP), tricarboxylic acid (TCA) cycle and metabolism of specific amino acids, nucleotides, lipids, LPS and peptidoglycan. Furthermore, *in vitro* and clinical evidence demonstrated that two combination therapies, namely polymyxins with carbapenems, and polymyxins with rifampicin, are synergistic against MDR *A. baumannii* and *P. aeruginosa*. An untargeted metabolomics study of the colistin/doripenem combination against *A. baumannii* showed synergistic killing via a time-dependent inhibition of key metabolic pathways (e.g. lipids, nucleotides, PPP, LPS and peptidoglycan biosynthesis) (Chapter

3). Moreover, the untargeted metabolomics study of polymyxin B/rifampicin combination against *P. aeruginosa* showed that the synergistic action significantly perturbed cell metabolism of lipids, nucleotides, amino acids, central carbon metabolism (i.e. glycolysis, TCA cycle, and PPP), LPS and peptidoglycan biosynthesis. Interestingly, the synergy was predominantly driven by the action of rifampicin but facilitated by polymyxin B (Chapter 4). Transcriptomic data on polymyxin B/rifampicin combination treatment revealed that the synergistic action significantly reduced virulence gene expression in *P. aeruginosa*, suggesting that this combination therapy could affect bacterial pathogenicity (Chapter 5). Furthermore, the results demonstrate the dynamics of cellular respiration of *P. aeruginosa* in adopting anaerobic denitrification process to counteract the effect induced by polymyxin B/rifampicin combination. In turn, treatment with polymyxin B or rifampicin alone induced antibiotic resistance within 1 hr and 24 hr, respectively, signifying the importance of PK/PD optimisation and the significant potential of polymyxin combination therapy. Finally, using genome-scale metabolic network analysis, the complementary metabolomics and transcriptomic data were integrated to examine the synergistic mechanism of polymyxin B and rifampicin in combination (Chapter 6). Overall, this project provides valuable mechanistic insights into the global metabolic differences between polymyxin-susceptible and -resistant isolates. This study also highlights the significance of the dynamic interaction of cellular metabolic and regulatory pathways in response to different classes of antibiotics, and the potential of paradigm-shifting antimicrobial pharmacology.

Declaration

This thesis contains no material which has been accepted for the award of any other degree or diploma at any university or equivalent institution and that, to the best of my knowledge and belief, this thesis contains no material previously published or written by another person, except where due reference is made in the text of the thesis.

A solid black rectangular box used to redact the signature.

Signature:

Print Name: Mohd Hafidz Mahamad Maifiah

Date: 12 June 2017

Statement of originality

Part A Monash University

Declaration for thesis based or partially based on conjointly published or unpublished work

General declaration

In accordance with Monash University Doctorate Regulation 17.2 Doctor of Philosophy and Research Master's regulations the following declarations are made:

I hereby declare that this thesis contains no material which has been accepted for the award of any other degree or diploma at any university or equivalent institution and that, to the best of my knowledge and belief, this thesis contains no material previously published or written by another person, except where due reference is made in the text of the thesis.

This thesis includes two original papers published in peer reviewed journals. The core theme of the thesis is systems pharmacology. The ideas, development and writing up of all the papers in the thesis were the principal responsibility of myself, the student, working within the Faculty of Pharmacy and Pharmaceutical Sciences under the supervision of Professor Jian Li, Dr Darren Creek and Dr Tony Velkov.

The inclusion of co-authors reflects the fact that the work came from active collaboration between researchers and acknowledges input into team-based research.

In the case of Chapters 2 and 3 my contribution to the work involved the following:

Thesis chapter	Publication title	Publication status	Nature and % of student contribution
2	Global metabolic analyses identify key differences in metabolite levels between polymyxin-susceptible and polymyxin-resistant <i>Acinetobacter baumannii</i>	Published	80%
3	Untargeted metabolomics analysis reveals key pathways responsible for the synergistic killing of colistin and doripenem combination against <i>Acinetobacter baumannii</i>	Published	80%

I have renumbered sections of submitted or published papers in order to generate a consistent presentation within the thesis.

Student signature:



Date: 12 June 2017

The undersigned hereby certify that the above declaration correctly reflects the nature and extent of the student's and co-authors' contributions to this work. In instances where I am not the responsible author I have consulted with the responsible author to agree on the respective contributions of the authors.

Main Supervisor signat



Date: 12 June 2017

Acknowledgements

I owe my greatest gratitude to Almighty Allah by his permission, grace and guidance that I am able to finish this PhD study.

First and foremost, I would like to express my deepest thankfulness and appreciation to my supervisors, Professor Jian Li, Dr Darren Creek and Dr Tony Velkov for giving me an opportunity to pursue this wonderful PhD project. Special thanks to Professor Jian Li for his great patience, understanding and excellence guidance throughout this challenging PhD journey. Without his persistent help and inspirational encouragement this PhD thesis would not have been possible. My personal appreciation to Dr Darren Creek for his guidance and help particularly on metabolomic works. To all my supervisors, thanks for your invaluable supports and encouraging advices for making me a better person from time to time.

I also wish to thank members of FADDI in particular Heidi Yu, Jesmin Akter, Dr Veronika Writh, Dr Mohammad Abul Kalam Azad, Dr Soon Ee-Cheah, Dr Matt Johnson, Dr Yan Zhu and others for their full supports. I offer my sincere thanks to my PhD members, Nusaibah Abd Rahim, Mei-ling Han, Bo Yun, Maizbahuddin, Shaz Sivanasen, Thien Tran and others for their advices and kindness thus has made this PhD journey very enjoyable. In addition, I would like to thank members of Darren Creek's group for their direct and indirect supports specifically pertaining to analytical instrumentation for metabolomics work.

Further grateful appreciations and thanks to my sponsors, Malaysian Ministry of Higher Education and International Islamic University Malaysia for giving me this great opportunity to pursue my PhD study in one of the best pharmaceutical schools in the world.

From the bottom of my heart, I wish to express my special thank and gratitude to my beloved wife, Nurul Sakinah Engliman who was the person that instilled me to pursue this PhD. My deepest appreciation for her sacrifice to take care of our son and family. To my son, Muhammad Ukail Umar who always be my motivation to finish this PhD. Last but not least, I also would like to thank to my beloved parents, Mahamad Maifiah Mukari, Siti Aseh Husin, Engliman Roslan and Habibah Dawood, my brothers and sisters for their unconditional supports throughout this PhD study and my life in general.

Publication to support this thesis

1. **Mohd Hafidz Mahamad Maifiah**, Soon-Ee Cheah, Matthew D. Johson, Mei-Ling Han, John D. Boyce, Visanu Thamlikitkul, Alan Forrest, Keith S. Kaye, Paul Hertzog, Anthony W. Purcell, Jiangning Song, Tony Velkov, Darren J. Creek, Jian Li. Global metabolic analyses identify key differences in metabolite levels between polymyxin-susceptible and polymyxin-resistant *Acinetobacter baumannii*. *Sci. Rep.* 6, 22287; doi: 10.1038/srep22287 (2016).
2. **Mohd Hafidz Mahamad Maifiah**, Darren J. Creek, Roger L. Nation, Alan Forrest, Brian T. Tsuji, Tony Velkov, Jian Li. Untargeted metabolomics analysis reveals key pathways responsible for the synergistic killing of colistin and doripenem combination against *Acinetobacter baumannii*. *Sci. Rep.* 7, 45527; doi: 10.1038/srep45527 (2017).

Manuscripts in preparation

3. **Mohd Hafidz Mahamad Maifiah**, Darren J. Creek, Tony Velkov, Jian Li. Metabolic perturbation induced by the synergistic killing of colistin and doripenem combination against *Acinetobacter baumannii*.
4. **Mohd Hafidz Mahamad Maifiah**, Darren J. Creek, Tony Velkov, Jian Li. Integrated metabolomics and transcriptomics analyses of the synergistic effect of polymyxin B and rifampicin combination against *Pseudomonas aeruginosa* PAO1.

Other publication

1. Bhuiyan, M.S., Ellett, F., Murray, G.L., Kostoulas, X., Cerqueira, G.M., Schulze, K.E., **Maifiah, M.H.M.**, Li, J., Creek, D.J., Lieschke, G.J., and Peleg, A.Y. *Acinetobacter baumannii* phenylacetic acid metabolism influences infection outcome through a direct effect on neutrophil chemotaxis. *Proc. Natl. Acad. Sci. USA*, 1-6 (2016).

Presentations

The results of this thesis were presented in the following scientific conferences:

1. **Mohd Hafidz Mahamad Maifiah**, Soon-Ee Cheah, Matthew D. Johson, Mohammad Azad, Tony Velkov, Darren J. Creek, Jian Li. Metabolic profiles of polymyxin-susceptible and –resistant *Acinetobacter baumannii*. 9th Annual Postgraduate Symposium. Monash University, Melbourne, Australia. Poster presentation.
2. **Mohd Hafidz Mahamad Maifiah**, Soon-Ee Cheah, Matthew D. Johson, Jiangning Song, Roger L. Nation, Brian T. Tsuji, Alan Forrest, Keith S. Kaye, Paul Hertzog, Tony Velkov, Darren J. Creek, Jian Li. Untargeted metabolomics of the synergistic combination of colistin and doripenem against *Acinetobacter baumannii*. Interscience Conference on Antimicrobial Agents and Chemotherapy. ICAAC/ICC 2015, San Diego, USA. Poster presentation.
3. **Mohd Hafidz Mahamad Maifiah**, Soon-Ee Cheah, Matthew D. Johson, Jiangning Song, Roger L. Nation, Brian T. Tsuji, Alan Forrest, Keith S. Kaye, Paul Hertzog, Tony Velkov, Darren J. Creek, Jian Li. Untargeted metabolomics of the synergistic combination of colistin and doripenem against *Acinetobacter baumannii*. 2nd International Conference on Polymyxins. 2015, San Diego, USA. Poster presentation.
4. **Mohd Hafidz Mahamad Maifiah**, Soon-Ee Cheah, Matthew D. Johson, Jiangning Song, Roger L. Nation, Brian T. Tsuji, Alan Forrest, Keith S. Kaye, Paul Hertzog, Anthony W. Purcell, Tony Velkov, Darren J. Creek, Jian Li. Untargeted metabolomics of the combination of colistin and doripenem against *Acinetobacter baumannii*. Australian and New Zealand Metabolomics Conference 2016, La Trobe University, Melbourne, Australia. Poster presentation.

List of Tables

Table 1.1 Major mechanisms of polymyxins resistance in MDR Gram-negative bacteria.....	20
Table 2.1 Phylogenetic characterisation by 16S gene sequencing	63
Table 2.2 Mutations identified in the polymyxin-resistant 03-149.2 isolate by high-throughput sequencing and variant calling to <i>A. baumannii</i> ACICU	63
Table 2.3 Validation and reproducibility of metabolite extraction procedure for four different extraction solvents.....	68
Table 2.4 Fold changes (relative intensity) in the abundance of metabolites detected in the LPS-deficient polymyxin-resistant 19606R, relative to the parent strain ATCC 19606.....	78
Table 3.1 Data precision of individual samples represented as the median relative standard deviation (RSD, %) for <i>A. baumannii</i> strains ATCC 19606, 03-149.1 and 03-149.2 (n = 4 biological replicates)	103
Table 3.2 Significant metabolites ($p \leq 0.05$) of ATCC 19606 identified following exposure to colistin (Col) and doripenem (Dor) alone and in combination (Combo) at 15 min.....	124
Table 3.3 Significant metabolites ($p \leq 0.05$) of ATCC 19606 identified following exposure to colistin (Col) and doripenem (Dor) alone and in combination (Combo) at 1 hr.....	125
Table 3.4 Significant metabolites ($p \leq 0.05$) of ATCC 19606 identified following exposure to colistin (Col) and doripenem (Dor) alone and in combination (Combo) at 4 hr.....	126
Table 3.5 Significant metabolites ($p \leq 0.05$) of 03-149.1 identified following exposure to colistin (Col) and doripenem (Dor) alone and in combination (Combo) at 15 min.....	129
Table 3.6 Significant metabolites ($p \leq 0.05$) of 03-149.1 identified following exposure to colistin (Col) and doripenem (Dor) alone and in combination (Combo) at 1 hr	131
Table 3.7 Significant metabolites ($p \leq 0.05$) of 03-149.1 identified following exposure to colistin (Col) and doripenem (Dor) alone and in combination (Combo) at 4 hr	134
Table 3.8 Significant metabolites ($p \leq 0.05$) of 03-149.2 identified following exposure to colistin	

(Col) and doripenem (Dor) alone and in combination (Combo) at 15 min.....	137
Table 3.9 Significant metabolites ($p \leq 0.05$) of 03-149.2 identified following exposure to colistin (Col) and doripenem (Dor) alone and in combination (Combo) at 1 hr	138
Table 3.10 Significant metabolites ($p \leq 0.05$) of 03-149.2 identified following exposure to colistin (Col) and doripenem (Dor) alone and in combination (Combo) at 4 hr.....	140
Table 4.1 Data precision of individual samples for polymyxin B and rifampicin alone and in combination (Combo), untreated control and pooled biological quality control (PBQC) represented as the median relative standard deviation (RSD, %) at 15 min, 1 hr, 4 hr and 24 hr.....	160
Table 4.2 Significant metabolites ($p \leq 0.05$) of PAO1 after treatment with polymyxin B (PB) and rifampicin (RIF) alone and in combination (COMBO) at 15 min.....	172
Table 4.3 Significant metabolites ($p \leq 0.05$) of PAO1 after treatment with polymyxin B (PB) and rifampicin (RIF) alone and in combination (COMBO) at 1 hr	173
Table 4.4 Significant metabolites ($p \leq 0.05$) of PAO1 after treatment with polymyxin B (PB) and rifampicin (RIF) alone and in combination (COMBO) at 4 hr	175
Table 4.5 Significant metabolites ($p \leq 0.05$) of PAO1 after treatment with polymyxin B (PB) and rifampicin (RIF) alone and in combination (COMBO) at 24 hr	178
Table 5.1 DEGs (at least 1.0-log ₂ -fold, $p \leq 0.05$) induced by polymyxin B alone at 1 hr	197
Table 5.2 Common DEGs (at least 1.0-log ₂ -fold, $p \leq 0.05$) induced by polymyxin B alone and the combination at 1 hr and 24 hr.....	197
Table 5.3 DEGs (at least 1.0-log ₂ -fold, $p \leq 0.05$) induced by rifampicin alone at 1 hr	198
Table 5.4 DEGs (at least 1.0-log ₂ -fold, $p \leq 0.05$) induced by the combination at 1 hr	201
Table 5.5 Common DEGs (at least 1.0-log ₂ -fold, $p \leq 0.05$) induced by rifampicin alone and the combination at 24 hr.....	205
Table 5.6 Common DEGs (at least 1.0-log ₂ -fold, $p \leq 0.05$) induced by polymyxin B and	

rifampicin alone and the combination at 24 hr	207
Table 6.1 Significantly changed metabolites and DEGs (at least 1.0-log ₂ -fold, $p \leq 0.05$) associated with amino acid metabolism induced by the polymyxin B and rifampicin combination at 1 hr	230
Table 6.2 DEGs (at least 1.0-log ₂ -fold, $p \leq 0.05$) associated with amino acid metabolism induced by the polymyxin B and rifampicin combination at 24 hr	230
Table 6.3 DEGs (at least 1.0-log ₂ -fold, $p \leq 0.05$) induced by the polymyxin B and rifampicin combination at 1 hr	231

List of Figures

Figure 1.1 The inverse relationship of antibiotic development versus emergence of antibiotic resistance	4
Figure 1.2 A global estimate of death attributable to antimicrobial resistance (AMR) every year by 2050	5
Figure 1.3 Virulence factors of <i>P. aeruginosa</i>	9
Figure 1.4 Chemical structures of polymyxin B and colistin.....	13
Figure 1.5 Structure of Gram-negative bacteria cell envelope and LPS	14
Figure 1.6 Mode of action of polymyxin via the ‘self-promoted uptake’ pathway	16
Figure 1.7 Summary of polymyxin pharmacokinetic pathways.....	24
Figure 1.8 Steady-state plasma concentration versus time profiles of (A) CMS and (B) formed colistin in critically-ill patients.....	24
Figure 1.9 Relationship between bacterial load of log ₁₀ /CFU in the thighs of neutropenic mice at 24 hr and the <i>f</i> AUC/MIC of colistin for <i>P. aeruginosa</i> ATCC 27853	26
Figure 1.10 Chemical structure of doripenem.....	30
Figure 1.11 Chemical structure of rifampicin	31
Figure 1.12 The omics nomenclature	32
Figure 1.13 Untargeted metabolomics workflow	44
Figure 2.1 The mass spectra of lipid A isolated from the <i>A. baumannii</i> clinical isolates	64
Figure 2.2 Structures of lipid A in clinical <i>A. baumannii</i> isolates (A) 03-149.1 and (B) 03-149.2	65
Figure 2.3 Evaluation of washing step and extraction solvents in the sample pre-treatment method.....	67

Figure 2.4 PCA score plot of the untargeted metabolomics dataset of paired polymyxin-resistant 19606R and the wild-type ATCC 19606 and paired of polymyxin-resistant 03-149.2 (blue and labelled with “2”) and polymyxin-susceptible 03-149.1 (red and labelled with “1”) clinical isolates	70
Figure 2.5 (A) PCA score plot of four <i>A. baumannii</i> strains. (B) PCA score plot of paired polymyxin-resistant 19606R and the wild-type ATCC 19606. (C) PCA score plot of paired polymyxin-resistant 03-149.2 and -susceptible 03-149.1 clinical isolates. (D) Pathway-focused representation of the significant metabolites (black bars) and total number of putatively identified metabolites (open bars) for the polymyxin-resistant 19606R relative to the wild-type ATCC 19606 (left) and the polymyxin-resistant clinical isolate 03-149.2 relative to the polymyxin-susceptible isolate 03-149.1 (right).....	71
Figure 2.6 Heat map profiles of metabolite peak intensities in <i>A. baumannii</i>	72
Figure 2.7 Perturbations of identified sugar phosphates in <i>A. baumannii</i>	74
Figure 2.8 Heat map profiles of relative abundance of nucleotides	75
Figure 2.9 Perturbations of TCA cycle intermediates in <i>A. baumannii</i> . TCA cycle of <i>A. baumannii</i>	76
Figure 2.10 Low levels of peptidoglycan biosynthesis metabolites were observed in the polymyxin-resistant <i>A. baumannii</i>	79
Figure 2.11 Relative intensity of glycerophospholipids levels	81
Figure 3.1. Time-kill kinetics of colistin and doripenem alone and in combination against <i>A. baumannii</i> isolates of polymyxin-susceptible (A) ATCC 19606, (B) 03-149.1 and polymyxin-resistant (C) 03-149.2	102
Figure 3.2 PCA score plots of all individual samples of <i>A. baumannii</i> ATCC 19606, 03-149.1 and 03-149.2 strains treated with colistin and doripenem alone and in combination ..	103

Figure 3.3 Multivariate and univariate analyses of global metabolic changes in <i>A. baumannii</i>	
ATCC 19606	105
Figure 3.4 Global metabolic changes in a pair of <i>A. baumannii</i> isolates	107
Figure 3.5 Perturbations of bacterial lipids in <i>A. baumannii</i> ATCC 19606.....	109
Figure 3.6 Perturbations of bacterial lipids in polymyxin-susceptible 03-149.1	110
Figure 3.7 Perturbations of bacterial lipids in polymyxin-resistant 03-149.2.....	111
Figure 3.8 Central metabolic changes in the pentose phosphate pathway (PPP).....	113
Figure 3.9 Central metabolic changes in the pentose phosphate pathway (PPP) in <i>A. baumannii</i>	
clinical isolates	114
Figure 3.10 Depletion of energy and nucleotide metabolite levels in <i>A. baumannii</i>	
ATCC 19606	117
Figure 3.11 Purine and pyrimidine nucleotide changes in <i>A. baumannii</i> clinical isolates.....	118
Figure 3.12 Depletion of amino sugar metabolites for peptidoglycan and LPS biosynthesis in	
<i>A. baumannii</i> ATCC 19606.....	121
Figure 3.13 Peptidoglycan and LPS biosynthesis changes in polymyxin-susceptible 03-149.1	
.....	122
Figure 3.14 Peptidoglycan biosynthesis changes in polymyxin-resistant 03-149.2.....	123
Figure 4.1 Time-kill kinetics of the combination of polymyxin B and rifampicin against	
<i>P. aeruginosa</i> PAO1	159
Figure 4.2 PCA score plot of all individual samples of <i>P. aeruginosa</i> PAO1 treated with	
polymyxin B and rifampicin alone and in combination	160
Figure 4.3 Global metabolic perturbations in <i>P. aeruginosa</i> PAO1	162
Figure 4.4 Heat map profiles of relative abundance of metabolites.....	163
Figure 4.5 The overview of metabolic pathway analysis of the combination of polymyxin B and	
rifampicin	164

Figure 4.6 Heat map profiles of lipid perturbation.....	166
Figure 4.7 Peptidoglycan and LPS biosynthesis changes	167
Figure 4.8 Heat map profiles of (A) nucleotide and (B) amino acid changes.....	169
Figure 4.9 Perturbations of TCA cycle, glycolysis and pentose phosphate pathway (PPP) ...	171
Figure 5.1 Transcriptomics response of <i>P. aeruginosa</i> PAO1	192
Figure 5.2 Gene ontology (GO) enrichment analysis of the combination at 1 hr	193
Figure 5.3 Gene ontology (GO) enrichment analysis of the combination at 24 hr	194
Figure 5.4 The overview of metabolic pathways of the significantly changed enzymatic reactions (edges) of polymyxin B and rifampicin alone and the combination at (A) 1 hr and (B) 24 hr	195
Figure 6.1 Global metabolic changes in <i>P. aeruginosa</i> PAO1 in response to polymyxin B (Poly B) and rifampicin (Rif) alone and in combination (Combo).....	219
Figure 6.2 Gene expression changes in <i>P. aeruginosa</i> PAO1 following exposure to polymyxin B (Poly B) and rifampicin (Rif) alone and in combination (Combo)	221
Figure 6.3 The overview of metabolic pathways of <i>P. aeruginosa</i> PAO1 affected by the combination of polymyxin B and rifampicin at (A) 1 hr and (B) 24 hr	222
Figure 6.4 Perturbation of membrane lipids.....	225
Figure 6.5 GSMN map of peptidoglycan biosynthesis pathway	226
Figure 6.6 GSMN map of LPS modification pathway	227
Figure 6.7 Perturbation of purine and pyrimidine nucleotides.....	229
Figure 6.8 Perturbation of central carbon metabolism by the combination of polymyxin B and rifampicin	234

Glossary of Abbreviations

ATCC	American Type Culture Collection
ANOVA	Analysis of Variance
AMR	Antimicrobial resistance
CF	cystic fibrosis
CM	chlroform:methanol
CMW	chlroform:methanol:water
CDC	The Centers for Disease Control and Prevention
CaMHB	cation-adjusted Mueller-Hinton broth
CMS	Colistin methanesulphonate
DEG	differentially expressed gene
Dab	diaminobutyric acid
EtOH	ethanol
ESI	electro-spray ionisation
ESBL	extended-spectrum β -lactams
FA	fatty acyl
fp	footprint
<i>f</i> AUC	area under free plasma concentration-time curve
FDR	false discovery rate
FT-IR	fourier transform-infrared spectroscopy
GC-MS	gas chromatography-mass spectrometry
GDP	gross domestic product
GalN	galactosamine
GlcN	β -1'-6-linked D-glucosamine
GP	glycerophospholipid

GO	gene ontology
GSH	glutathione
GSSG	glutathione disulfide
GSMN	genome-scale metabolic network
GPR	gene-protein-reaction
HIV	human immunodeficiency virus
HSL	homoserine lactone
HRMS	high-resolution mass spectrometry
HPLC	high-performance liquid chromatography
HILIC	hydrophilic interaction liquid chromatography
HMDB	Human Metabolome Database
IDSA	Infectious Diseases Society of America
IV	intravenous
ICU	intensive care unit
KEGG	Kyoto Encyclopedia of Genes and Genomes
Kdo	3-deoxy-D-manno-octulosonate
LC-MS	liquid chromatography-mass spectrometry
LPS	lipopolysaccharide
L-Ara4N	4-aminoarabinose
MS	mass spectrometry
MDR	multidrug-resistant
MeOH	methanol
MIC	minimal inhibitory concentration
MRSA	methicillin-resistant <i>Staphylococcus aureus</i>
MRM	multiple reaction monitoring

NMR	nuclear magnetic resonance
OM	outer membrane
PBS	phosphate-buffered saline
PCA	principal component analysis
PPP	pentose phosphate pathway
pEtN	phosphoethanolamine
PRPP	5-phospho- α -D-ribose 1-diphosphate
PE	glycerophosphoethanolamine
PS	glycerophosphoserine
PG	glycerophosphoglycerol
PNAG	poly- β -1,6- <i>N</i> -acetylglucosamine
PBQC	pooled biological quality control
PBP	penicillin-binding protein
PK/PD	pharmacokinetics/pharmacodynamics
QC	quality control
QS	Quorum sensing
REVIGO	Reduce and visualise gene ontology
RSD	relative standard deviation
ROS	reactive oxygen species
SDS	sodium dodecyl sulphate
SOD	superoxide dismutase
TCA	tricarboxylic acid
QQQ	triple quadrupole
T6SS	type VI secretion system
UDP-MurNAc	UDP- <i>N</i> -acetylmuramate

UDP-GlcNAc	UDP- <i>N</i> -acetylglucosamine
Vanted	Visualisation and Analysis of Networks containing Experimental Data
VAP	Ventilator-associated pneumonia
WHO	World Health Organization

Chapter One

General Introduction

1.1 Statement of the problem

Among the greatest challenges to human health is the global dissemination of multidrug-resistant (MDR) bacterial pathogens. The paradoxical trend of the constant declining of novel antibiotic discovery as well as the rapid emergence of Gram-negative ‘superbugs’, necessitates a resurgence of polymyxins as the last-line therapy for the treatment of life-threatening infections. The finite *in vivo* pharmacokinetics/pharmacodynamics (PK/PD) of polymyxins show polymyxin monotherapy generate sub-optimal plasma concentrations. This phenomenon can lead to the emergence of polymyxin resistance and significantly compromise their clinical utility. In order to address this crucial problem, polymyxin combination therapy has been suggested as a viable alternative resolution to polymyxin monotherapy. Despite the fact that various efforts have been focused in detailing the action mechanism of polymyxins, the exact mechanism still remains unclear. A comprehensive understanding of the polymyxin action and resistance mechanisms is essential to systematically optimise the clinical use. Systems biology provides powerful tools to obtain a global cross-section of cellular biochemical and regulatory networks under a defined condition. This approach is being increasingly employed in drug development to elucidate the mechanism of drug action. The overall aim of this PhD project was to decipher the mechanisms of antibacterial activity and resistance of polymyxins mono- and combination therapy with carbapenems and rifampicin against MDR pathogens, namely *Acinetobacter baumannii* and *Pseudomonas aeruginosa*. Hypothesis-generating methodologies, metabolomics and transcriptomics were employed. Admittedly, an in-depth understanding of cellular metabolic and regulatory perturbations of MDR Gram-negative bacteria, induced by polymyxins and their combinations provides key information to the discovery of novel potential drug targets. Importantly, the results obtained in this project highlight the significant potential of systems pharmacology in optimisation of antibiotic use in patients and advocate the employment of polymyxin combination therapy.

1.2 Bad bugs, no drugs

Antibiotic resistance is increasing at an exponential rate worldwide. This is exacerbated by the consistently lower rates of novel antibiotic discovery and development pipeline (Figure 1.1) (1). The overwhelming drug resistance evolved predominantly due to the global overuse and misuse of the existing drugs, which has resulted in multidrug-resistant (MDR) pathogens, in particular Gram-negative ‘superbugs’ (2, 3). Worryingly, it has been projected that this critical state of antimicrobial resistance will continue to rise and by 2050 would lead to a mortality rate of 10 million every year, coupled with a reduction of 2% to 3.5% in Gross Domestic Product (GDP) (Figure 1.2) (4). The World Health Organization (WHO) declared the emergence of antibiotic resistance as one of the greatest threats to human health (5).

The Infectious Diseases Society of America (IDSA) ascertains that the major threat of antibiotic resistance is mainly caused by the six ‘superbugs’ ESKAPE (i.e. *Enterococcus faecium*, *Staphylococcus aureus*, *Klebsiella pneumoniae*, *Acinetobacter baumannii*, *Pseudomonas aeruginosa* and *Enterobacter* species), that are characterised by their ability to ‘escape’ antibiotics (6, 7). The Centres for Disease Control and Prevention (CDC) has categorised major MDR pathogens that commonly cause infections in the hospital and the community settings as presenting “Urgent”, “Serious” or “Concerning” Threats (8). Very recently, the WHO ranked a list of antibiotic-resistant “priority pathogens” into three levels, Priority 1 (Critical), Priority 2 (High) and Priority 3 (Medium) based on the urgency and corresponding allocated focus for the research and development of new antibiotics (9).

Proactive counter-measures need to be thoughtfully planned out and implemented by various parties, particularly the pharmaceutical industries, clinicians and researchers. The IDSA previously proposed a goal to develop and approve 10 novel antibiotics by the year 2020 (10).

To achieve this target, strategic clinical research should be focused more intensively to accelerate the process of drug discovery and development. Nevertheless, the current global economic climate and the challenging regulatory requirements necessitate a comprehensive effort to optimise the currently available antibiotics (2). Therefore, the use of an ‘old’ class antibiotic polymyxins as the last-line therapeutic defense is vital (11). This PhD project primarily employed the MDR *A. baumannii* and *P. aeruginosa*, general overviews of both important pathogens are covered in this section.

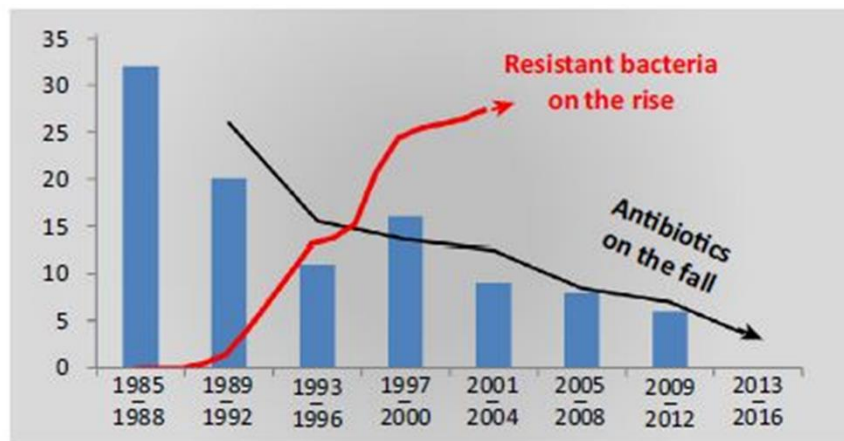


Figure 1.1. The inverse relationship of antibiotic development versus emergence of antibiotic resistance. The rapid increase of antibiotic resistant bacteria coincides with the sharp decrease of new antibiotic discovery. Figure adapted from Schaberle *et al.* (5).

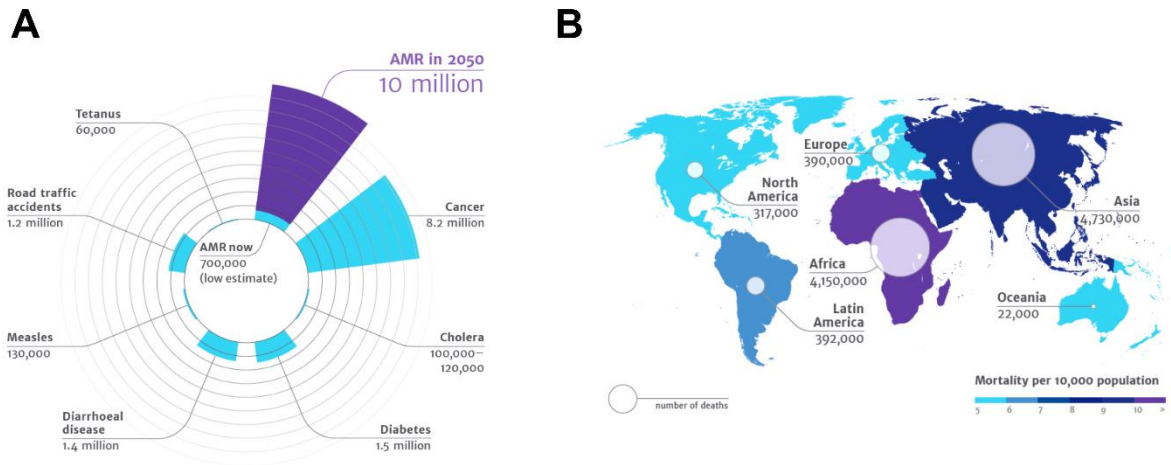


Figure 1.2. A global estimate of death attributable to antimicrobial resistance (AMR) every year by 2050. (A) Comparison between leading causes of death. The problem of antibiotic resistance would lead to 10 million people dying every year. **(B)** Comparison of antibiotic resistance problems between different parts of the world. Figure adapted from O’Neill (4).

1.2.1 *A. baumannii*: an emerging opportunistic pathogen

A. baumannii is an environmental coccobacillus Gram-negative opportunistic pathogen that is rapidly emerging in the clinic (12). The CDC has classified MDR *A. baumannii* as a microorganism with a “Serious Threat” level (8). Due to its resistance to almost all current antibiotics, *A. baumannii* has been rated with the “Critical” level by the WHO in the priority to discover for novel antibiotics (9). This pathogen’s remarkable ability to tolerate and survive in a wide range of environmental conditions, particularly in hospitals for months has predominantly led to serious nosocomial and endemic infections, contributing to high morbidity and mortality rates (13, 14). At least three factors mainly contribute to the persistence of *A. baumannii* in the hospital setting which include their resistance to antibiotics, desiccation and disinfectants (12). *A. baumannii* commonly causes pneumonia, bacteremia, meningitis, urinary tract infection and wound infection (14-16).

Pathogenesis of *A. baumannii* is associated predominantly with several virulence factors, specifically of OmpA, a type of outer membrane protein, their ability to form biofilm and secrete key proteins for example phospholipase C and D (17, 18). Other significant factors that may contribute to the virulence of *A. baumannii* include its presence of lipopolysaccharide (LPS), capsular polysaccharide, penicillin binding proteins (PBPs) and outer membrane vesicles (OMV) (19). Among the treatment preferences for MDR *A. baumannii* infection are carbapenems (e.g. doripenem, imipenem and meropenem), β -lactamase inhibitors (e.g. sulbactam), aminoglycosides (e.g. amikacin and tobramycin) and tigecycline (12). Polymyxins would be administered as the last-line therapy against carbapenem-resistant *A. baumannii* isolates and it is commonly combined with aminoglycosides or rifampicin (20, 21). Analysis of several observational studies indicate that approximately 57-77% of severely ill patients infected with MDR *A. baumannii* were improved following treatment with colistin (13). The combination therapies for treating MDR *A. baumannii* infection that have displayed additive and synergistic killing effects include the rifampicin containing combinations (e.g. imipenem/rifampicin, colistin/rifampicin, tobramycin/rifampicin), imipenem/amikacin and carbapenem/sulbactam (14).

A. baumannii hastily evolves resistance to almost all clinically existing antibiotics by its ability to regulate innate resistance mechanisms, and more alarmingly by the acquisition of external genetic elements (12). Recently, Gao *et al.* reported the longitudinal multicenter surveillance study which revealed a significant increase in a nationwide prevalence of *A. baumannii* resistance from 2004 to 2014 in China (22). The results showed that the rate of antibiotic resistance in *A. baumannii* was approximately $\geq 65\%$ with increased of the prevalence of imipenem resistance from 13% to 70% and that extremely drug-resistant *A. baumannii* from 11% to 60% (22). *A. baumannii* genetically contains several large genomic islands with multiple

resistance genes, and the resistance mechanism can be mediated via mobile genetic elements, particularly plasmids, transposons and integrons (23-32). *A. baumannii* can also potentially develop resistance via enzymatic degradation for example by β -lactamases, metallo- β -lactamases, serine oxacillinases, AmpC cephalosporinases, acetyltransferases, nucleotidyltransferases and phosphotransferases (12). Non-enzymatic mechanisms of resistance in MDR *A. baumannii* include changes in outer membrane proteins and drug-target binding sites, efflux pumps and alterations of PBPs (12, 33-39). It has been shown that MDR *A. baumannii* can develop resistance by the loss of porin channels which are functionally essential to transport drugs into the cell (40). Polymyxin resistance in *A. baumannii* is commonly associated with the modification of the polymyxin binding site, the lipid A domain of LPS structure in the bacterial outer membrane and total LPS loss (41-44). Heteroresistance to polymyxins has been reported in *A. baumannii*, which is characterised by the presence of polymyxin-resistant subpopulations within a susceptible isolate (45-48). The detailed mechanism of polymyxin-induced LPS modification is reviewed in Section 1.3.4.

1.2.2 *P. aeruginosa*: an opportunistic ‘superbug’

P. aeruginosa is an opportunistic aerobic bacillus Gram-negative pathogen commonly exists in both community and hospital setting (49). Predominantly, *P. aeruginosa* is a cause of hospital-acquired acute and chronic infections in patients with immunocompromised, seriously ill in intensive care units (ICU), mechanically ventilated with malignancies or human immunodeficiency virus (HIV) (8, 50-52). In addition, cystic fibrosis (CF) patients are highly susceptible to *P. aeruginosa* which has become a leading cause of chronic lung infection (53, 54). MDR *P. aeruginosa* is majorly responsible for pneumonia, urinary tract infections and bloodstream infections (49). Similar to *A. baumannii*, MDR *P. aeruginosa* has also been assigned a threat level of “Serious” by the CDC and of “Critical” priority by the WHO (8, 9).

The life-threatening infections caused by MDR *P. aeruginosa* has led to significant increases in morbidity and mortality rates worldwide (49, 55). Notably, *P. aeruginosa* displays susceptibility towards α -carboxy- and amino-penicillins, third- and fourth-generation cephalosporins, monobactams, carbapenems, aminoglycosides and fluoroquinolones.

Pathogenesis of *P. aeruginosa* is initiated by bacterial colonisation followed by tissue invasion, as the processes are elicited via numerous cellular virulence factors (Figure 1.3) (50, 51). *P. aeruginosa* colonises the infection site with their structural surface components of flagella and pili which then lead to tissue invasion by a wide range of extracellular products for example elastase, alkaline protease and pyocyanin (51). Notably, isolates of *P. aeruginosa* from acute infections phenotypically display a great extent of virulence determinants compared to isolates from chronic infections (54, 56). Several virulence factors are tightly governed by a complex regulatory and signaling network via a quorum-sensing (QS) system (54, 57). Studies showed that approximately 3-7% of *P. aeruginosa* genome is regulated by the QS system (58).

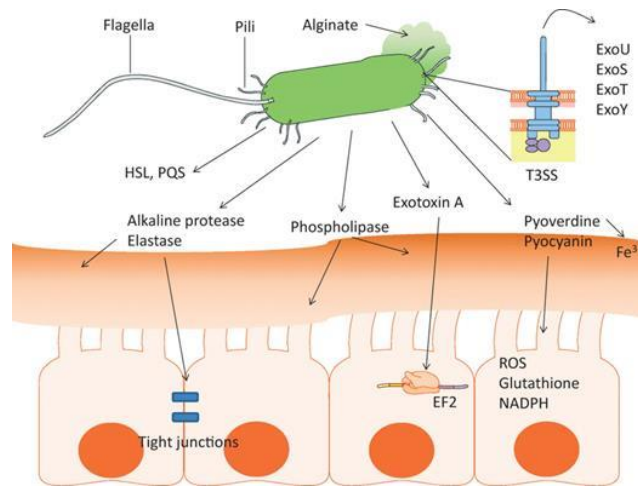


Figure 1.3. Virulence factors of *P. aeruginosa*. Cell-associated virulence factors are flagella, type IV pili and LPS which are essential for bacterial attachment. Secreted virulence factors that exhibit various effects on the host including cytotoxins, proteases, mucins, lipases, phospholipases, pyocyanin and pyoverdine. Figure adapted from Gellatly *et al.* (56).

In general, the QS system is mediated by autoinducers, which are small membrane-diffusible signal molecules, known as acyl homoserine lactones (AHLs) operating in a density-dependent manner by acting upon specific transcriptional regulators (56). The most studied QS systems in *P. aeruginosa* are the *las* and the *rhl* systems (58). The *las* system includes the LasI synthase protein, important for the production of the AHL signal molecule *N*-(3-oxododecanoyl)-L-homoserine lactone (3O-C₁₂-HSL), and the LasR transcriptional regulator. Secondly, the *rhl* system comprises of RhlI, important for the production of the AHL *N*-butyryl-L-homoserine lactone (C₄-HSL), and the RhlR transcriptional regulator. Additionally, a novel QscR has been identified to functionally regulate the production of several other virulence factors via the expression of both *lasI* and *rhlI* (59). It has been demonstrated in several animal models that the deletion of one or more genes associated with the QS system result in decreased virulence in *P. aeruginosa* (60, 61).

As the QS systems and virulence factors are significant for the establishment of infections, these machineries have been examined as potential drug targets (53, 58, 62-64). Studies have been reported on the significant effects of different antibiotic classes on the regulation of many virulence determinants in *P. aeruginosa* (65-71). Azithromycin at sub-inhibitory concentrations significantly inhibited the expression of several virulence factors (e.g. elastase, proteases, lecithinase, DNase and pyocyanin) and caused loss of bacterial motility (65). In addition, it has been reported that the effect of azithromycin, ceftazidime and ciprofloxacin significantly decreased the expression of QS-regulated virulence determinants (e.g. chitinase, protease, elastase, rhamnolipid and type III secretion system), suggesting the reduction of bacterial pathogenicity (67). Cummins *et al.* reported the transcriptome analysis of the effect of sub-inhibitory concentrations of colistin on *P. aeruginosa* which revealed the up-regulation of the *Pseudomonas* quinolone signal (PQS) biosynthesis genes and the phenazine biosynthesis operon (68). Therefore, infections caused by *P. aeruginosa* potentially can be prevented as the QS regulated genes and virulence factors would be an ideal drug target.

Notably, the efficiency of *P. aeruginosa* to develop resistance in response to various classes of antibacterial agents during the treatment has become a significant challenge particularly from patients in ICUs (49). In particular, the resistance rate from CF patients is significantly higher than from non-CF patients (72). An important feature of MDR *P. aeruginosa*, particularly during chronic infection in CF patients is its propensity to form biofilm and over-express the exopolysaccharide alginate to become mucoid (73, 74). MDR *P. aeruginosa* can develop resistance via an intrinsic, acquired and adaptive mechanisms (and sometimes all three at once), which makes their infections extremely tough to treat (56). The intrinsic resistance can be due to the low permeability of this pathogen's outer membrane. It has been reported that its membrane permeability is about 100% lower than outer membrane of *E. coli* (75). Resistance in

P. aeruginosa is also caused by the constitutive expression of membrane efflux-pumps (mex) and the natural occurrence of chromosomal β -lactamase, *ampC*; particularly induced in response to β -lactams, quinolones and aminoglycosides (76). As a consequence of the activation of efflux-pumps and β -lactamases, the entry of small hydrophilic compounds is inhibited while excluding larger molecules altogether. The ability of *P. aeruginosa* to develop resistance to various classes of antibiotics is conferred by its large genome size approximately of 6.26 Mbp which encode 5,567 genes (72, 77). Furthermore, the acquired resistance of *P. aeruginosa* may be the result of plasmid-mediation or mutations (either by single or multiple mutations) which alter the expression and/or function of chromosomally target genes. These pathogens are commonly treated with penicillins, cephalosporins, carbapenems, monobactams, aminoglycosides and fluoroquinolones (49, 56, 78). The effect of external environment and antibiotic treatment can significantly induce adaptive resistance in *P. aeruginosa* (56), and this is reviewed in Section 1.3.4, particularly of polymyxin resistance.

1.3 Polymyxins: an overview

Polymyxins are an ‘old’ class of cationic polypeptide antibiotic firstly isolated in 1947 from the spore-forming Gram-positive soil bacterium, *Paenibacillus polymyxa* (79, 80). Polymyxins were used clinically since the late 1950s, but were never subjected to a systematic drug development procedure (81). Due to reports of toxicity, particularly nephrotoxicity and neurotoxicity, the clinical use of polymyxins was abandoned in the 1970s (82). Nevertheless, since the 1990s polymyxins have been increasingly used as the last-line treatment for MDR Gram-negative bacterial infections.

1.3.1 Chemical structures

Polymyxins are small non-ribosomal cyclic lipopeptide molecules of ~1200 Da in mass. Structurally, it composed of a cyclic heptapeptide ring between the amino group of the side chain of the diaminobutyric acid (Dab) residue at position 4 and the carboxyl group of the C-terminal threonine residue at position 10 (Figure 1.4) (11). The five non-proteogenic Dab residues render their polycationic activity at pH 7.4 with hydrophobic residues at positions 6 and 7 and an *N*-terminal fatty acyl group. The presence of both lipophilic and hydrophilic groups in polymyxin structure are attributed to its amphipathic nature, which is vital for their bactericidal action (11). Two classes of polymyxins are being used clinically, polymyxin B and colistin (also known as polymyxin E) which differ by only an amino acid at position 6 (Figure 1.4) (83). Both polymyxin B and colistin are made up of L-configuration amino acid residues but only differ at their hydrophobic region at position 6 with the presence of D-phenylalanine in polymyxin B while D-leucine in colistin. Two main components that form colistin are colistin A and B, whereas of polymyxin B are polymyxin B1 and B2. There are at least 7 individual polymyxin B and 11 polymyxin E components that have different structures, such as the *N*-terminal fatty acyl groups. The synthesis of polymyxins involves a series of non-ribosomal synthetases with specific domains that govern adenylation, thiolation (peptidyl carrier protein) and condensation (84).

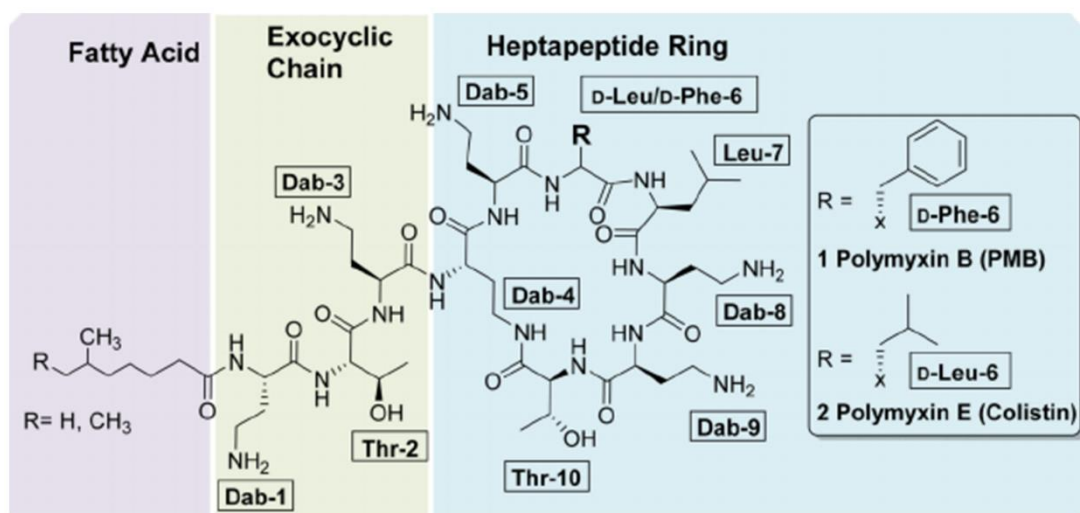


Figure 1.4. Chemical structures of polymyxin B and colistin. Polymyxin structure is characterised by five Dab residues, hydrophobic residues at positions 6 and 7 and an *N*-terminal fatty acyl group. Figure adapted from Godoy *et al.* (85).

1.3.2 Mode of action of polymyxins

The emergence of extremely resistant Gram-negative bacteria towards polymyxins demands detailed understanding on the mechanism of polymyxin action to leverage novel drug discovery strategies. Both colistin and polymyxin B generally display similar modes of bactericidal action with narrow spectra activity against Gram-negative bacteria (86). In order to understand the mechanism of polymyxin action, it is important to firstly appreciate the very fundamental structure of Gram-negative bacterial outer membrane, which serves as a selective permeability barrier (Figure 1.5A) (87). The basic architecture of Gram-negative bacteria cell envelope is made up of an asymmetrical outer membrane and a symmetrical inner membrane (87). The outer membrane characteristically is separated into the outer leaflet which is predominantly constitutes of lipopolysaccharides (LPS) and the inner leaflet which is majorly comprises of phospholipids (87, 88). Three components that make up the structure of LPS are a highly conserved inner core 2-keto-3-deoxyoctonoic acid (Kdo), lipid A and a variable O-antigen of repeating units of polysaccharide (Figure. 1.5) (87). It is widely accepted that the lipid A domain of LPS is the

initial specific binding target for polymyxins (11, 89). The lipid A structure consists of β -1'-6-linked D-glucosamine (GlcN) disaccharide that is phosphorylated at the positions 1- and 4' (Figure. 1.5B). Lipid A commonly contains six acyl chains; four attached directly to the glucosamine sugars are β -hydroxyl chains (usually C12 and C14 in length) and two secondary acyl chains adhered to the β -hydroxyl group. Lipid A functionally acts as a hydrophobic anchor to preserve, maintain and stabilise the structure of outer membrane, conferred by the tight packing of its fatty acyl chains (87).

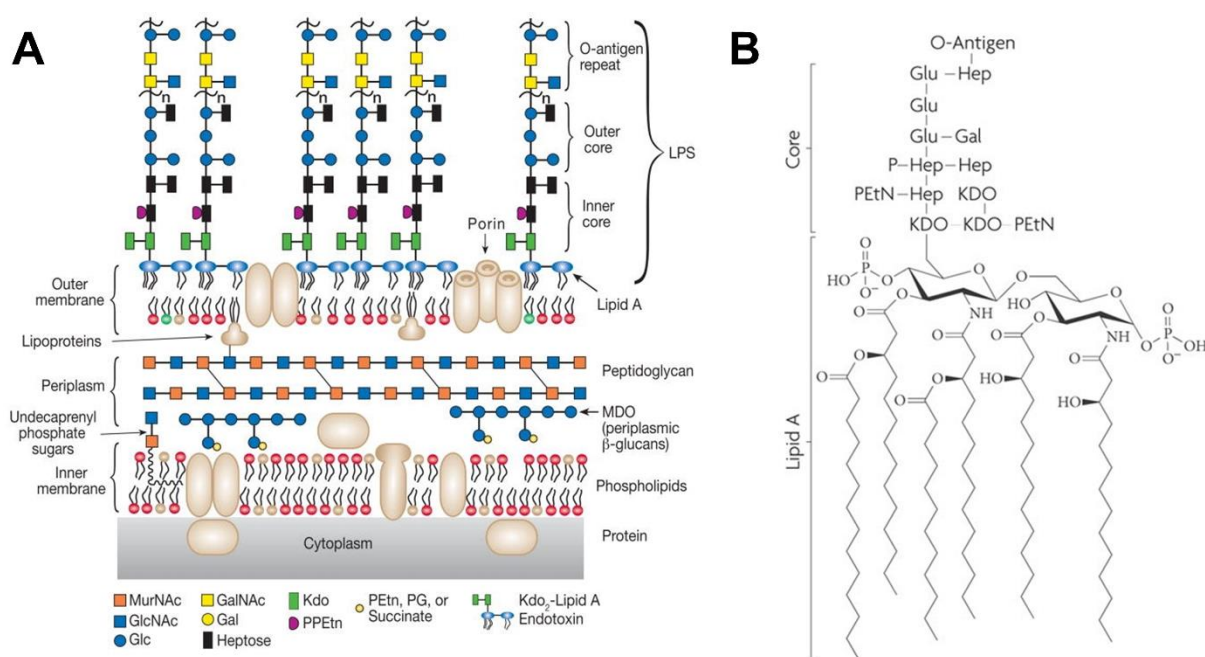


Figure 1.5. Structure of Gram-negative bacteria cell envelope and LPS. (A) Cell envelope is surrounded by outer membrane and inner membrane structures. The outer membrane is composed of asymmetrical outer leaflet, predominantly contains LPS, and symmetrical inner leaflet, mainly composed of phospholipids. (B) The chemical structure of LPS molecule. Lipid A structure of LPS consists of β -1',6-linked disaccharide of glucosamine contains both phosphate and fatty acyl groups. Figure modified from Ruiz *et al.* (90).

A number of models have been described on the mode of action of polymyxins (11, 91-96). Nevertheless, the detailed mechanism of polymyxin-induced bactericidal killing still remains uncertain. The broadly accepted model of polymyxin action is explained by the 'self-promoted uptake' pathway (Figure 1.6). Firstly proposed by Newton, polymyxins execute antibacterial action by its ability to attach to and disorganise the outer membrane structure of Gram-negative bacteria to eventually cause osmotic disturbance (97). Via the electrostatic and hydrophobic interactions, polymyxins specifically attach to their specific target binding sites, lipid A component of LPS structure and also phospholipids in the outer membrane. The results of polymyxin interactions significantly induce membrane disruption, osmotic imbalance and subsequently cell death (93, 94, 98-102). The electrostatic interaction is exerted as a result of the protonation of free amines present on the positively charged Dab residues of polymyxins with the negatively charged phosphate groups of the lipid A domain. The destabilisation of the LPS leaflet of the bacterial outer membrane is predominantly due to the displacement of divalent cations (Mg^{2+} and Ca^{2+}) which are essential for bridging the adjacent LPS molecules. This permits an insertion of the hydrophobic regions of the *N*-terminal fatty acyl tails and amino acid residues at position 6 and 7 of polymyxins into the outer leaflet of outer membrane. Polymyxins may enter the periplasmic space and interact with the phospholipids embedded in the inner leaflet of outer membrane and inner membrane to disrupt bacterial phospholipid membrane structure. The changes cause significant expansion of the outer membrane then lead to a local membrane disturbance and osmotic imbalance. Later, this will increase the permeability of bacterial membrane structure to finally induce cell death (11, 98). Nevertheless, the systematic mechanism of polymyxin permeabilising action presumably does not interconnect with the polymyxin-induced lethal effect (103).

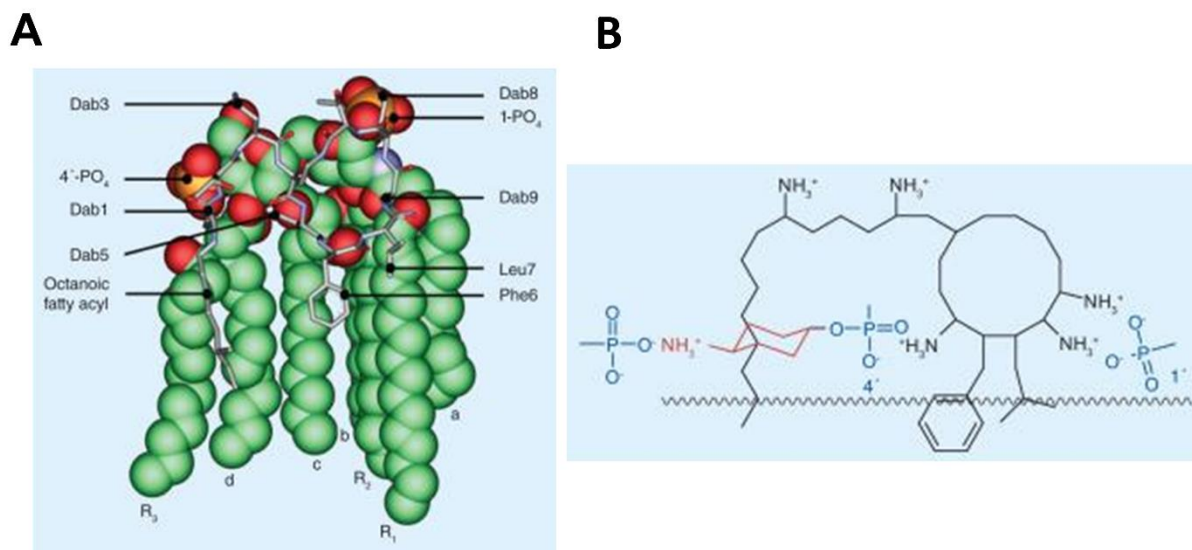


Figure 1.6. Mode of action of polymyxin via the ‘self-promoted uptake’ pathway. (A) The space-filling molecule represents lipid A and the stick molecule represents polymyxin B. **(B)** The electrostatic interaction between the Dab residues on polymyxin and the lipid A phosphoresters of LPS induces the insertion of hydrophobic regions of the *N*-terminal fatty acyl tail and amino acid residues at position 6 and 7. Figure adapted from Velkov *et al.* (11).

Morphological study of *Salmonella typhimurium* and *E. coli* demonstrated that polymyxins predominantly induced blebs, projections of the outer leaflet of the bacterial outer membrane structure (104). The study also showed that polymyxins significantly accumulated in the cells which caused the aggregation of nuclear material and ribosomes (104). Furthermore, polymyxins have been shown to display binding affinity to 16S A-site of *E. coli* ribosomes but with an unclear impact on translation (105). In addition, the effect of polymyxins significantly altered the process of cell division (106, 107). Studies also have shown that the mechanism of polymyxin-induced bacterial killing is partly associated with oxidative stress via the generation of reactive oxygen species (ROS) mainly targeting DNA, RNA, proteins and lipids (108-113). In addition, polymyxins can potentially inhibit the respiratory chain enzymes for example NADH-quinone oxidoreductase, NADH cytochrome c and NADH dehydrogenase (92, 109, 114-

116). Notwithstanding, the link of free radical generation in the mechanism of antibiotic killing is disputable in several literatures (110-112, 117-120). In this PhD project, the key focus of the investigation was to elucidate the mechanism of polymyxin action as a single or in combination with other antibiotics. The novel findings gathered from this PhD project will significantly extend the present understanding on the mechanism of polymyxin action which can be employed for pharmacokinetics/pharmacodynamics (PK/PD) optimisation and developing new generation of polymyxins (Chapters 3 to 6).

1.3.3 Mechanisms of polymyxin resistance

The worldwide increase of polymyxin use has resulted in the emergence of polymyxin resistance. The most common mechanism of polymyxin resistance in Gram-negative bacteria involves the remodelling of LPS structure in the bacterial outer membrane (121). As reviewed in Section 1.3.3, lipid A domain is the specific attachment site for polymyxins to exert its bactericidal effect. Polymyxin treatment can cause modification of the phosphate group of the lipid A structure by the addition of 4-amino-4-deoxy-L-arabinose, phosphoethanolamine or galactosamine (11). This mechanism of polymyxin resistance has been previously demonstrated in *E. coli*, *P. aeruginosa*, *A. baumannii*, *K. pneumoniae* and *Salmonella enterica* serovar Typhimurium (41-43, 122). The modified lipid A domain of the LPS structure caused significant reduction in the net negative charge of the bacterial outer membrane and thus precludes the electrostatic attraction of polymyxins to LPS. Polymyxins also can induce the addition of fatty acyl chains in the lipid A structure of the LPS. The alteration significantly induced the *N*-terminal fatty acyl chain and the hydrophobic amino acid motifs of the polymyxins to be less penetrable towards the outer membrane structure of bacteria (123). Interestingly, lipid A-deficient mutants have been reported in *Neisseria meningitidis* (124) and *A. baumannii* (44, 125) which results in complete LPS loss. These LPS-deficient mutant strains develop a very strong degree of

resistance to polymyxins highly likely due to the inactivation of genes of lipid A biosynthesis (e.g. *lpxA*).

The mechanism of polymyxin adaptive resistance in Gram-negative bacteria is tightly regulated by the two-component systems induced in response to chromosomal mutations (126). Notwithstanding of the extensive study on the mechanism of polymyxin resistance particularly in *P. aeruginosa*, the problem remains unresolved due to the extremely complex bacterial regulatory networks. There are at least five two-component regulatory systems that have been characterised in *P. aeruginosa* namely PmrA/PmrB (127-130), PhoP/PhoQ (131-134), ParR/ParS (135, 136), ColR/ColS and CprR/CprS (137). The PhoPQ and PmrAB systems are the first and most studied two-component systems that linked to polymyxin resistance (127, 131, 138, 139). The two systems, PhoPQ and PmrAB systematically regulate the expression of lipid A modification operon, *arnBCADTEF-pmrE* particularly in response to the limited availability of Mg^{2+} and phosphate independently of the presence of polymyxins. The expression of the *arnBCADTEF-pmrE* operon induced the attachment of 4-aminoarabinose, a sugar with a free amino group to lipid A domain of the LPS structure. The significant reduction in the negative charge of LPS structure as a result of lipid A modification thereby decreasing the binding affinity of polymyxins. On the contrary, a novel ParRS two-component regulatory system is specifically activated by the presence of cationic peptides (i.e. polymyxin B, colistin, indolicidin) independently induced by the limited- Mg^{2+} environmental concentration (135). Interestingly, Muller *et al.*, reported that the ParRS two-component system could be activated in response to no fewer than four different classes of antibiotics including polymyxins, aminoglycosides, fluoroquinolones and β -lactams (140). Therefore, the activation of the ParRS system potentially can induce three different resistance mechanisms via LPS modification, increased efflux pump and reduced porin pathway (140). The ParRS two-component system also has been shown to

control the regulation of multidrug efflux pump (MexEF-OprN) and quorum sensing system in *P. aeruginosa* (141). Furthermore, resistance to polymyxin also can be modulated by the CprRS (cationic peptide resistance) two-component regulatory system upon the exposure to antimicrobial peptides independently regulated by the ParRS system (136).

In addition to LPS modification, polymyxin resistance potentially can be developed due to several other different mechanisms. *K. pneumoniae*, *P. aeruginosa* and *Streptococcus pneumoniae* have been shown to significantly induce the over-expression of anionic capsule polysaccharides (CPS); so as will reduce the number of polymyxins to reach bacterial surface (142). Polymyxins also potentially can induce the up-regulation of outer membrane efflux-pump proteins as demonstrated in *K. pneumoniae*, *P. aeruginosa* and *E. coli* (143-146). Several efflux pumps that have been associated with polymyxin resistance are the AcrAB (143, 146) and KpnEF (144), exhibited by *K. pneumoniae* and *E. coli*, and the MexAB-OprM (145) exhibited by *P. aeruginosa*. Worryingly, for the first time, the emergence of plasmid-mediated colistin resistance, designated as MCR-1 was reported in *E. coli* as being isolated from animals and humans (147). Since then, many studies have been increasingly reported on the occurrence of plasmid-mediated colistin resistance in both animals and humans (148-150). The product of *mcr-1* gene, annotated as a member of the family phosphoethanolamine transferases is attributed to polymyxin resistance via the addition of phosphatidylethanolamine to lipid A structure of the LPS in the bacterial outer membrane (151). More worryingly, the likely co-existence of *mcr-1* gene with other MDR resistance genes of carbapenem and extended-spectrum β -lactams (ESBL) potentially induced the emergence of subpopulation bacterial pathogens with pan-drug resistance properties (152-158). The different mechanisms of polymyxin resistance in Gram-negative bacteria is summarised in Table 1.1.

Table 1.1 Major mechanisms of polymyxins resistance in MDR Gram-negative bacteria. The table is modified from Olaitan *et al.* (159).

Resistance mechanism	Genes involved	Bacterium
Modification of the lipid A or Kdo with aminoarabinose	<i>arnBCADTEF</i> operon and <i>pmrE</i>	<i>Salmonella enterica</i> , <i>K. pneumoniae</i> , <i>E. coli</i> , <i>P. aeruginosa</i> , <i>burkholderia cepacia</i> complex
Modification of the lipid A with phosphoethanolamine	<i>pmrC</i>	<i>S. enterica</i> , <i>K. pneumoniae</i> , <i>A. baumannii</i>
Increased acylation of lipid A enhancing its modification with aminoarabinose	<i>lpxM</i>	<i>S. enterica</i> , <i>K. pneumoniae</i> , <i>E. coli</i>
Loss of LPS	<i>lpxA</i> , <i>lpxC</i> , <i>lpxD</i>	<i>A. baumannii</i>
Efflux pump	<i>acrAB</i> , <i>kpnEF</i> , <i>MexAB-OprM</i>	<i>K. pneumoniae</i> , <i>P. aeruginosa</i>
Over-expression of outer membrane protein OprH	<i>oprH</i>	<i>P. aeruginosa</i>
Activation of LPS-modifying operon by mutations in two-component regulatory system	<i>pmrA/pmrB</i> , <i>phoP/phoQ</i> , <i>colR/colS</i> , <i>cprR/cprS</i> , <i>parR/parS</i>	<i>S. enterica</i> , <i>K. pneumoniae</i> , <i>A. baumannii</i> , <i>P. aeruginosa</i>
Plasmid-mediated	<i>mcr-I</i>	<i>E. coli</i>

1.3.4 Nephrotoxicity and neurotoxicity

The clinical use of intravenous polymyxins has been reported to cause notable nephrotoxicity in up to 60% of patients (82, 160-162). The old studies of polymyxin nephrotoxicity mainly were attributed to intramuscular colistimethate sodium administration, an inactive prodrug form of colistin also known as colistin methanesulphonate (CMS) (163-165). The administration of CMS was markedly associated with the higher daily dosage compared to the current dose recommendation (82). Old literature reported that the incidence of nephrotoxicity of intravenous CMS administration was about 20-36% in studies of patients with pre-existing renal disease (166, 167). It has been shown that patients treated with intravenous CMS had renal impairment

during treatment (26%), prolonged increase of blood urea nitrogen levels (10%), decreased creatinine clearance and an elevated serum creatinine levels (50%) (168-170). Nevertheless, recent data revealed that the incidence of polymyxin-induced nephrotoxicity was lower compared to the previously reported cases in the 1970s. In a comparative study of patients with ventilator-associated pneumonia caused by an *A. baumannii* infection, the results demonstrated that the incidence of CMS-induced nephrotoxicity (24%) was much lower than the effect of intravenous imipenem/cilastatin administration (42%) (171). In addition, Hartzell *et al.* reported that the administration of CMS caused only mild renal dysfunction, without the occurrence of renal replacement therapy and permanent kidney damage (172).

Polymyxins predominantly induce renal insufficiency by the reciprocal rise in serum creatinine levels and decline in creatinine clearance. The administration of polymyxins potentially to cause haematuria, proteinuria, cylindruria, oliguria and acute tubular necrosis (82). Polymyxin-induced nephrotoxicity is known to be dose-dependent effect potentially due to the disruption of cellular membrane integrity, which allows the influx of ions and water to finally cause cell lysis (173, 174). Colistin also significantly increases the transepithelial conductance of the urinary bladder epithelium (175). Nevertheless, the detailed mechanism of polymyxin-induced nephrotoxicity still remains unclear. Furthermore, neurotoxicity occurs less often than nephrotoxicity. The adverse effects associated with neurotoxicity include paraesthesia and the development of respiratory apnoea which also found to be dose-dependent effect (167, 168). Conversely, recent reports demonstrate that the incidence of polymyxin-induced neurotoxicity was not associated with the neuromuscular blockade or apnoea (176-178). The occurrence of neurotoxicity has been linked with the interaction of polymyxin and neurons. Polymyxin induces neuromuscular blockade as it inhibits the release of acetylcholine to the synaptic gap (179, 180). In addition, the neurotoxic effects of polymyxins could cause dizziness, generalised or specific

muscle weakness, facial and peripheral paraesthesia, partial deafness, visual disturbance, vertigo, confusion, hallucinations and seizures.

1.3.5 Pharmacokinetics and pharmacodynamics (PK/PD)

The pharmacokinetics/pharmacodynamics (PK/PD) of polymyxins have been examined in order to optimise their clinical use. Despite the indistinguishable *in vitro* antibacterial activity of polymyxin B and colistin, both show remarkable differences in term of their *in vivo* PK profiles which significantly affecting clinical outcomes of polymyxins in patients (81, 165). Colistin and polymyxin B predominantly differed in term of their parenteral administration. Colistin is generally administered as an inactive prodrug of the sodium salt of colistin methanesulphonate (CMS), also known as colistimethate, whereas the administration of polymyxin B is as its active form (sulphate salt) (163-165). CMS is a chemically-modified form of colistin, masking the primary amines of the Dab residues with methanesulphonate moieties that are negatively charged at a physiological pH (181). The complex chemical feature of CMS renders it as an inactive prodrug, functionally exhibits less potent bactericidal killing and toxic effects as compared to polymyxin B. A greater amount of PK study of polymyxins has been carried out on colistin and CMS compared to polymyxin B as the former has been more broadly used clinically (182-185).

The PK description for CMS, colistin and polymyxin B is simplified in Figure 1.7 (181). After parenteral administration, CMS is converted to colistin with a slow increase in plasma concentration. The route of clearance of CMS is predominantly via the kidneys whereas colistin mainly via other routes as it is extensively reabsorbed in the renal tubules (186, 187). It has been shown that intravenous administration of 3 million units (240 mg) of CMS for every 8 hr takes about 36 hr to achieve colistin steady-state plasma concentration of 2 mg/L in patients with no renal impairment indicating the low plasma exposure to colistin (188). Garonzik *et al.* reported

a largest population PK model (n=105) investigated the disposition of colistin following intravenous CMS administration in critically ill patients (Figure 1.8) (189). In this study, the average steady-state plasma colistin concentration was highly variable between the patients (0.48–9.38 mg/L) given that the plasma concentration of formed colistin is highly influenced by renal function (189). Several clinical studies demonstrated that CMS monotherapy with the currently recommended dosage regimens were unlikely to produce an optimal *in vivo* plasma exposure particularly in patients with moderate-to-good renal function and/or for causative pathogens with MICs of ≥ 1.0 mg/L (190-192). On the contrary, the available clinical studies on PK information of polymyxin B is very limited (193-196). As polymyxin B is administered as active drug, therefore its disposition is relatively simple and rapidly to reach steady-state concentrations (197). Polymyxin B is majorly eliminated via non-renal routes as only less than 1% is excreted through the renal pathway in its unchanged form (98). It has been suggested that plasma concentration of polymyxin B have not been influenced by renal function as shown by minimal interpatient variability in the average steady-state plasma polymyxin B concentration (0.68 mg/L to 4.88 mg/L) (197). Therefore, polymyxin B is better administered in those infections that highly required rapid and reliable optimal concentrations in the systematic circulation (181). Whereas, CMS becomes a treatment preference for urinary tract infections as CMS relatively exists in higher concentrations (181).

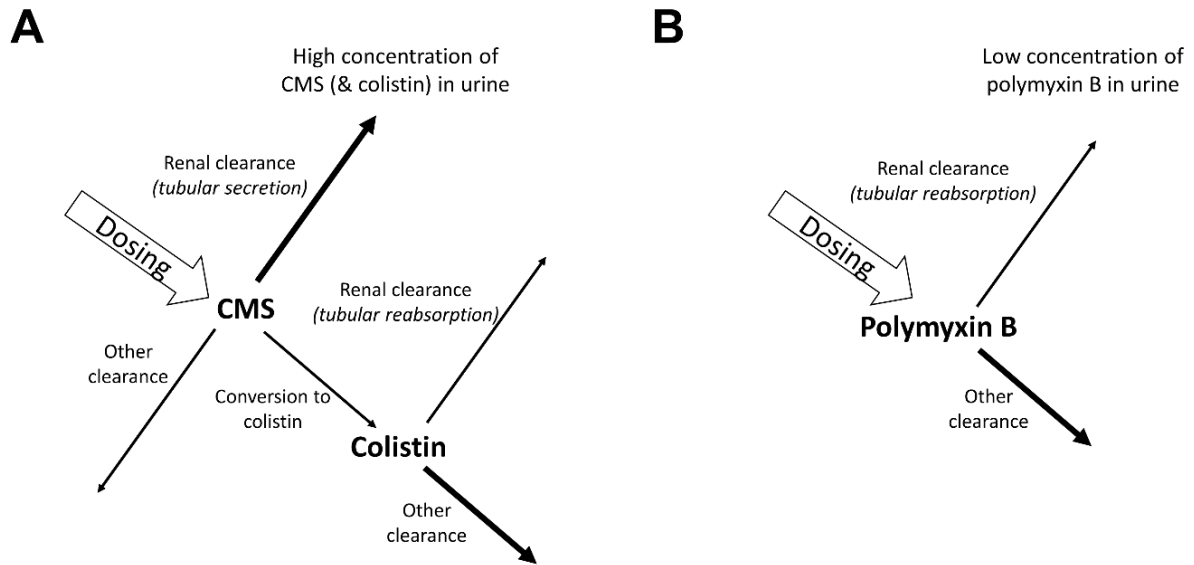


Figure 1.7. Summary of polymyxin pharmacokinetic pathways. (A) CMS and colistin (B) polymyxin B. The relative degree of polymyxin clearance with normal kidney function is represented by the thickness of the arrows. Figure adapted from Nation *et al.* (181).

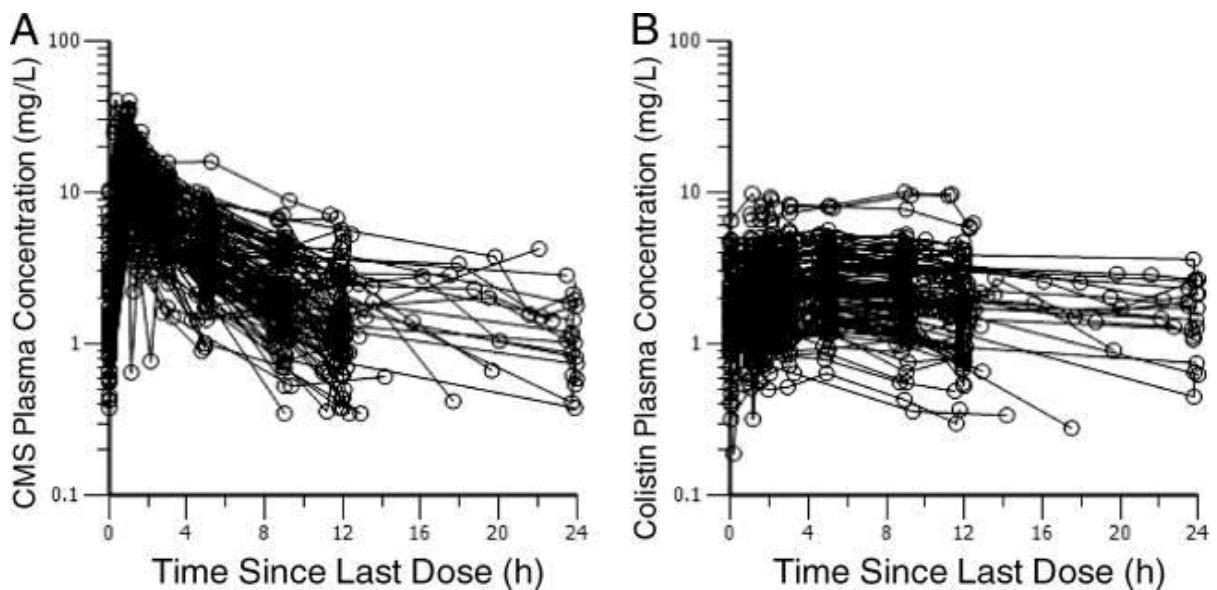


Figure 1.8. Steady-state plasma concentration versus time profiles of (A) CMS and (B) formed colistin in critically-ill patients. The data were gathered from 105 patients in critical conditions with 89 not on renal replacement, 12 on intermittent hemodialysis and four on continuous renal replacement therapy. Figure adapted from Garonzik *et al.* (189).

Compared to polymyxin B, colistin has been extensively reported in many *in vitro* PD study in both static and dynamic time-kill studies. Both colistin and polymyxin B exhibit rapid concentration-dependent killing against Gram-negative bacteria including *A. baumannii*, *K. pneumoniae* and *P. aeruginosa* often following with the rapid re-growth (183-185, 198). In addition, the rate and extent of bacterial killing of polymyxins are influenced by an inoculum effect (198, 199). The rapid emergence of polymyxin resistance is likely due to heteroresistance, a polymyxin-resistant subpopulation in a colony that shows susceptibility based upon minimal inhibitory concentrations (MICs) (46, 81, 184, 199, 200). Polymyxin PK/PD index represents the most predictive correlation of polymyxin activity (i.e. as determined by \log_{10} CFU/mL reductions in the population of bacteria) which is defined by the ratio of the area under free plasma concentration-time curve to MIC value ($fAUC/MIC$) (Figure 1.9) (201, 202). As reviewed in the PK profile of CMS above, polymyxin B is very likely to generate higher $fAUC/MIC$ values than CMS (203). The association of $fAUC/MIC$ with polymyxin bacterial killing effect indicates the significant effect of the time-average exposure to polymyxins than the dosage-average exposure (204). On account of the PK/PD limitations of both colistin and polymyxin B, hence, more data are urgently required from both *in vitro* and *in vivo* studies to provide polymyxins dosage guidelines, especially in critically ill patients.

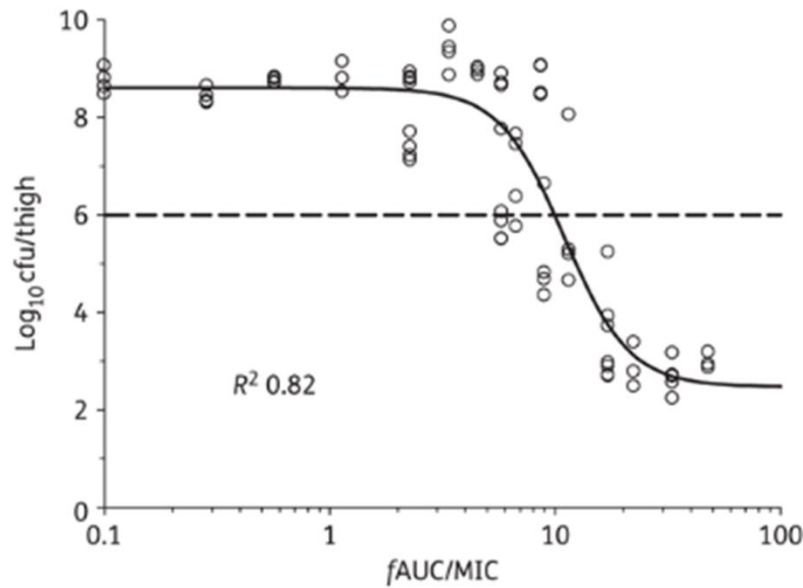


Figure 1.9. Relationship between bacterial load of log₁₀/CFU in the thighs of neutropenic mice at 24 hr and the fAUC/MIC of colistin for *P. aeruginosa* ATCC 27853. Figure adapted from Cheah *et al.* (182).

1.3.6 Polymyxin combination therapy

Evidence from *in vitro* and clinical studies demonstrated that antibiotic combination therapy is a better option for the treatment of MDR Gram-negative pathogens as shown by higher efficacy and lower rate of resistance development (205-208). An observational study recorded that approximately 25-50% of patients with bacteraemia, surgical site infections, pneumonia and septic shock in ICUs have been treated with drug combination therapy (205). A comparative meta-analysis study of carbapenemase-producing *Enterobacteriaceae* infections showed that the mortality rates in combination therapy was 27%, whereas in monotherapy was 38%, suggesting the survival advantage of the antibiotic combination treatment (209). However, evidence on efficacious antibiotic combination therapy in clinical studies is insufficient as more needed to be investigated. Arguably, certain drug combination therapy might potentially lead to even more adverse and harmful toxic effects, further increasing bacterial resistance and finally exorbitant

treatment costs (205). Despite the negative points concerning on drug combination therapy, at least three reasons justify its application: (i) to extend the empiric coverage provided by two different agents aimed at different cellular targets to sufficiently kill the pathogens, by at least one of the two drugs, (ii) to enhance the clinical outcome due to the limited PK/PD profile of drug monotherapy and, (iii) to limit or inhibit the likely emergence of heteroresistant subpopulation bacteria during antibiotic treatment (16, 205, 210-212). In particular circumstances, antibiotic combination therapy is strongly recommended to be used for example for patients with profoundly neutropenic and septic as well as patients in the ICU and ventilator-associated pneumonia (VAP) (205).

As reviewed in Section 1.3.5, polymyxin monotherapy is unlikely to generate *in vivo* optimal plasma concentrations with the potential development of polymyxin heteroresistant subpopulation (81, 189, 197, 213-216). Approximately 47% to 67% mortality rates have been recorded in patients subjected to polymyxin monotherapy (217-221). Polymyxin combination therapy therefore becomes an alternative solution to polymyxin monotherapy and the approach has been increasingly applied in the hospital setting (81, 214). The great advantage of polymyxin combination therapy with other antibiotics allows the use of lower concentrations of each antibiotic, thus reducing its adverse toxic effects (217). Several *in vitro* and clinical studies on polymyxin combination treatment have shown synergy against MDR Gram-negative pathogens, including *A. baumannii*, *P. aeruginosa* and *K. pneumoniae* (98, 217). A number of *in vitro* studies of colistin and carbapenem combination, in particular doripenem synergistically killed MDR *P. aeruginosa*, *K. pneumoniae* and *A. baumannii* (222-227). In addition, the combination of colistin and tigecycline or meropenem have been shown to significantly increase the survival rates of patients (228, 229). It has also been demonstrated that the colistin-carbapenem combination significantly limit the emergence of colistin resistance (16, 227, 230). Furthermore,

evidence from several *in vitro* and clinical studies showed that the combination of polymyxin and rifampicin synergistically kill MDR Gram-negative pathogens (231-236). However, there is still lack of evidence on polymyxin combination therapy in patients and it is usually evaluated only by non-randomised, retrospective analysis, with small and low power prospective trials of undefined patients (206, 214, 228, 237-242). In addition, the dosage regimens and PK data from the clinical studies of polymyxin combination are often missing in the literature.

The synergy between two agents is defined as a greater-than- \log_2 increase in *in vitro* bacterial killing relative to the killing effect of each agent alone (205). Two standard methods to measure the rate of *in vitro* bacterial killing are (1) time-kill curve method, a fixed concentration of a single or multiple agents in combination over time, and (2) checkerboard method, an evaluation of the various concentrations of two different agents (205). Various techniques have been developed to evaluate and determine the type of drug interactions (i.e. synergistic, additive and antagonistic), for example using dose-response based methods namely Loewe additivity (243), isobologram (244) and Chou-Talalay method (245, 246). Using a computational approach, a PPI network-based method termed “NIMS” and neighbour communities have been designed to study drug combinations (247). Despite the efficiency of drug combination therapy and the advanced progress on the method to evaluate drug interactions, the detailed underlying mechanism remains unclear (212). So far, very little work has been undertaken to elucidate the mechanism of action of drug combination therapy. Recently, using systems pharmacology to study antibiotic-induced metabolomic and transcriptomic changes can provide valuable insights into the mechanism of drug interactions with individual biomolecules affecting particular cellular pathways (248). Detailed review of this topic is in Section 1.4.1.

A number of models have been proposed to elucidate the mechanism of action of the synergistic killing of antibiotic combination therapy. Firstly, synergistic killing can be explained by the “simple uptake effects” or the bioavailability model; one drug increases the permeability of bacterial cell envelope to facilitate another drug reaches its specific intracellular target (212, 248-250). Secondly, the parallel pathway inhibition model suggests that the two drugs are synergistic if they inhibit two different targets in parallel pathways that are essential for an observed phenotype (248, 251). It has also been suggested by Pal *et al.* that drug combination potentially could be elucidated by the “collateral sensitivity” model; the organism resistant to drug A may have become more susceptible to drug B (252). Interestingly, the mechanism of polymyxin synergistic killing with other antibiotics has been elucidated by two models namely the subpopulation synergy model and mechanistic synergy model (214). The subpopulation synergy model describes that one drug kills the resistant subpopulation(s) of the other drug, and vice versa, whereas the mechanistic synergy model describes that two drugs acting on different cellular pathways increase the rate or extent of killing of the other drug (214). In this PhD project, two synergistic polymyxin combinations were investigated, including colistin plus doripenem and polymyxin B plus rifampicin (Chapter 3-6). Therefore, doripenem and rifampicin are briefly reviewed in Sections 1.3.6.1 and 1.3.6.2, respectively.

1.3.6.1 Doripenem

Doripenem is a member of antibiotic under a carbapenem class (253). The chemical structure of doripenem is similar to that of other antibiotics in carbapenem class whereas differs from the penicillins with a sulfur atom at position 1 and an unsaturated bond between C2 and C3 (Figure 1.10) (254). Structurally, doripenem is very similar to meropenem with sulfamoylaminoethyl-pyrrolidinylthio group at position 2. Doripenem displays time-dependent broad-spectrum bactericidal activity against Gram-positive, Gram-negative and anaerobic organisms *in vitro*

including ESBL and AmpC-producing Enterobacteriaceae (255, 256). The *in vitro* killing effect of doripenem against Gram-positive bacteria is similar to that of imipenem and better than that of meropenem and ertapenem (257). Whereas, against many Gram-negative bacteria, doripenem displays a relatively similar activity to meropenem and superior to that of imipenem and ertapenem (257). However, doripenem has less activity against methicillin-resistant *Staphylococcus aureus* (MRSA) or vancomycin-resistant enterococci (258). The mechanism of action of doripenem involves the penetration and disruption of bacterial cell wall biosynthesis by inhibiting the action of penicillin-binding proteins (PBPs), enzymes that are essential for the peptidoglycan synthesis of peptide-cross linking process (258, 259). It has been shown that doripenem displays a high affinity for PBP2 and PBP3 in *P. aeruginosa* and PBP2 in *E. coli* (260). As a class of β -lactams, doripenem predominantly requires outer membrane proteins, also known as porins to facilitate its diffusion through the bacterial cell wall (259). Doripenem is generally stable against many β -lactamases but it can be hydrolysed by carbapenemases.

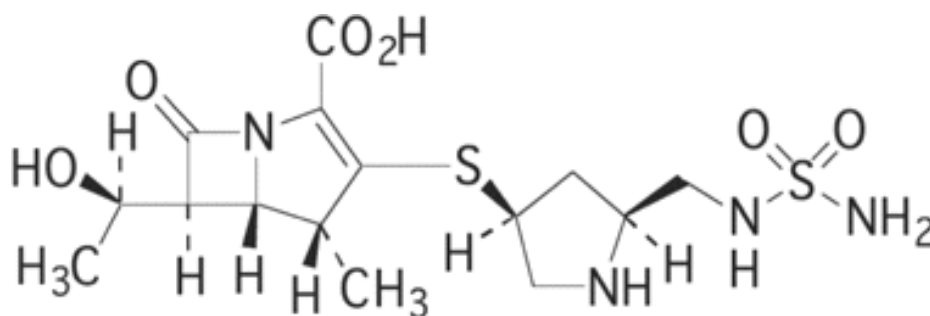


Figure 1.10. Chemical structure of doripenem. Figure adapted from Peterson *et al.* (258).

1.3.6.2 Rifampicin

Rifampicin is an 'old' semisynthetic antibiotic produced from *Streptomyces mediterranei* which was firstly introduced in 1968 (Figure 1.11) (261). Rifampicin displays broad spectrum bactericidal killing against most Gram-positive and Gram-negative bacteria, and remains the main drug for treatment of patients with tuberculosis (261). Rifampicin has been recommended to be used in combination with other drug, mainly isoniazid, pyrazinamide and ethambutol potentially can inhibit the emergence of resistance (261). Rifampicin displays higher MIC values on Gram-negative bacteria compared to Gram-positive bacteria as rifampicin is less permeable to the Gram-negative bacterial outer membrane (262). Rifampicin-induced bacterial killing involves the specific high-affinity binding to, and inhibition of the bacterial DNA-dependent RNA polymerase (i.e. specifically the β subunit) to directly block the RNA transcript elongation step (262-264). Rifampicin resistance occurs as a result of the mutation in the protein sequence of the β subunit of the bacterial RNA polymerase that decreases the sensitivity of the enzyme towards rifampicin (262).

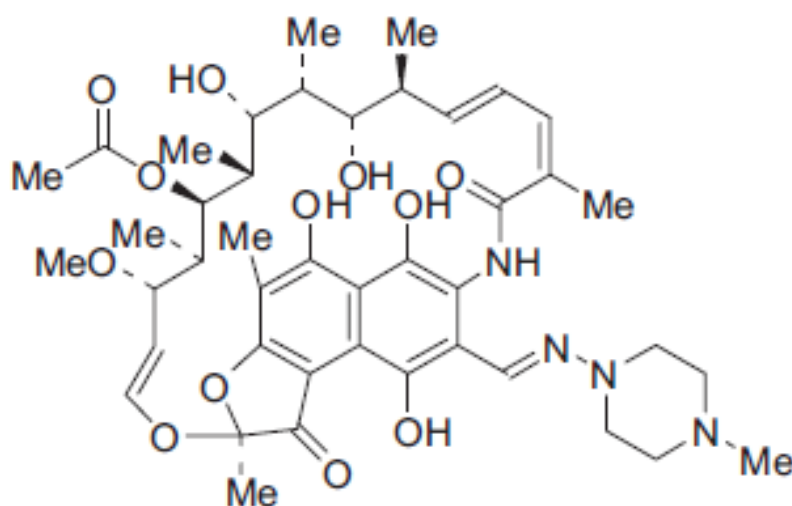


Figure 1.11. Chemical structure of rifampicin. Figure adapted from (265).

1.4 Metabolomics

The central dogma of molecular biology defines that the flow of information is unidirectional from the genomic DNA to messenger RNA (mRNA) and finally translate into proteins (Figure 1.12) (266). Metabolites basically are compounds of protein products of the downstream systems biology components, including enzymes which functionally influence the concentration of their substrates and products in a very specific manner. The balance of cellular metabolite levels is highly vital in controlling many metabolic pathways and flux changes which at the end will determine the phenotype state of an organism (267). Therefore, cellular communication is now understood to be developed on the basis of complex system networks and interactions between DNA, RNA, protein and metabolites significantly interplayed between positive and negative feedback loops (Figure 1.12).

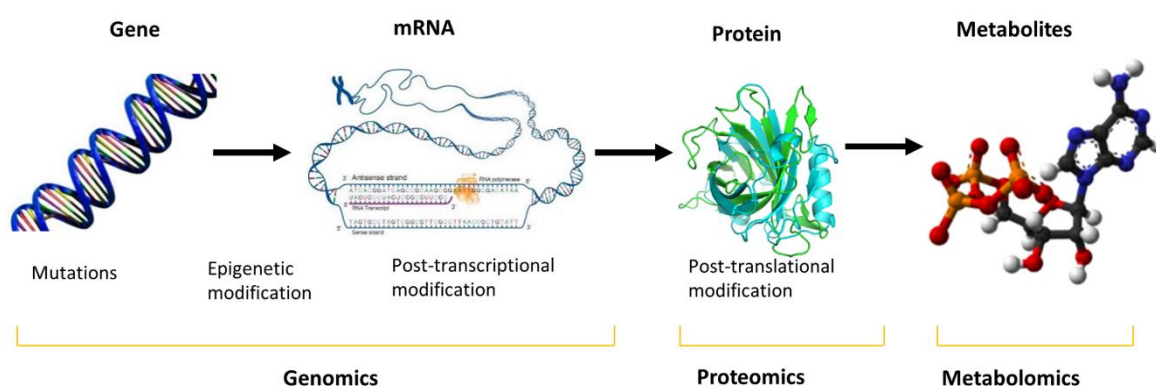


Figure 1.12. The omics nomenclature. Metabolites are the biochemical end products of genomics and proteomics. Metabolites represent the comprehensive signature of the physiological state and unique insight of the specific biochemical processes of an organism. Figure is modified from Patti *et al.* (268).

Revolutions during the period of 1980s and 1990s in the method of biological experiment has developed the new method of omics, an invaluable tool for the study of cell networks and

interactions at systems based levels (269). Although research on metabolic profiling was initiated earlier in the 1970s, the word “metabolome” was firstly used only in 1998 to describe a quantitative phenotypic analysis of *Saccharomyces cerevisiae* (270, 271). Metabolomics is a rapidly evolving systems biology method which has been applied in various research areas including clinical medicine and pharmaceutical (272-278), microbiology (279), agriculture and environmental toxicology, as well as in food analysis (280). At present, metabolomics is significantly adopted in the field of clinical diagnostic and drug discovery and development process (281-285). Metabolomics generally presents a snapshot comparison between healthy and diseased cells or tissues that potentially may lead to a discovery of new disease markers, diagnostic tests or drug targets.

In general, metabolomics is a study aimed to profile all the cellular metabolites and metabolic pathways of the cells in response to a particular set of environmental condition (286, 287). The approach used in metabolomics is comprehensive which encompassed both quantitative and qualitative measurement of metabolites (286, 287). On the contrary, classical biochemical methods are commonly subjected to only a particular single metabolite and metabolic reaction as well as its kinetic property under a defined set of linked reactions and cycles (267, 274). Metabolites are small chemical units typically with a molecular weight of less than 1000 Da generated as a result of complex cellular interactions of genome, transcriptome, proteome and environment. Different classes of metabolites are for example carbohydrates, amino acids, lipids, and nucleotides significantly display a broad range of cellular functions. Collectively, metabolome represents a total pool of metabolites of various chemical compounds from hydrophilic carbohydrates, volatile alcohols, ketones, amino and non-amino organic acids and lipids to a complex mixture of secondary metabolites for example antibiotics, pigments, non-ribosomal peptides and cofactors (267). The levels of metabolites represent a direct functional

reflection of a cellular metabolic state or physiological phenotypes of a cell (268, 288). Therefore, metabolites are always referred to as biomarkers of many biochemical reactions and enzymatic pathways (268, 288).

Understanding the complete nature of cellular metabolic network is extremely challenging due to the complex pathway interactions of metabolites, enzymatic reactions and multi levels of regulatory systems (289). Among the massive challenges in metabolomics research is to deal with the dynamic nature of metabolites as they are influenced by genetic and environmental stimuli (267, 290). The compositions and levels of metabolites are constantly and rapidly transformed likely to generate variations between individual samples (290). A study conducted using a genome-scale model demonstrated that less than 30% of metabolites involved in two metabolic reactions only, whereas about 12% participated in more than 10 reactions (291). Metabolites are highly variables, complex and heterogeneous in their chemical structures and properties particularly in terms of the solubility, polarity and stability (267, 292). Therefore, it is inconceivable to identify and quantify the entire cell metabolome simultaneously by applying only a single analytical method (267, 292). Furthermore, global metabolic profiling is frequently complicated by the annotation of a large set of unknown metabolites that are largely exceeding the number of currently existing compounds in databases (268). Metabolite identification and validation is highly challenging by the tremendous efforts that are required to postulate the biological meaning of the many significantly changed metabolites, as this tends to be the rate limiting step in metabolomic analysis (275).

1.4.1 Untargeted and targeted metabolomics

Methodologies in metabolomics can be categorised into two, untargeted and targeted methods, depending on the experimental question that needs to be answered (268, 269, 293). Untargeted

also known as global metabolomics is basically a hypothesis-generating method which aims to comprehensively measure as many identifiable metabolites as possible at once including those of unknown compounds (275, 294). The steps in untargeted metabolomics include (1) acquiring global mass spectrometry data (2) bioinformatics analysis (3) putative metabolite annotation based on the matched mass/charge ratio and retention time with the respective metabolites available in various databases, and (4) metabolite confirmation via tandem mass spectral data analysis (295). Untargeted metabolomics is often performed to discover potential novel biomarkers and drug targets (269). Key challenges in untargeted metabolomics include metabolite sampling and processing protocols, raw data processing, identifying and characterising unknown molecules and a potential bias towards high-abundance metabolites recovery (269). In addition, the results generated from untargeted metabolomics study are always in the form of sophisticated metadata which highly require an advanced chemometric method analysis in order to produce a feasible dataset.

On the contrary, targeted metabolomics is a hypothesis-driven approach, in which a predetermined set of a compound is measured and analysed qualitatively and quantitatively targeting definite interrelated pathways of interest (268, 275, 296). In targeted metabolomics, the dominant of high abundance metabolites and analytical artefacts likely are avoided and reduced as the sample preparation and processing method can be manipulated and optimised (269). It is important to note that, targeted metabolomics method is commonly employed to justify the hypothesis generated from the result of untargeted metabolomics analysis.

Antibiotic-induced cell death is generally mediated via target specific inhibition (297). However, in detail, the mechanism of action of antibiotic is a very complex process of interactions between regulatory and biochemical networks. To cater the problem of antibiotic resistance, detailed

understanding on the mode of drug action and its resistance is hugely significant for improving current antibiotic therapy and identifying a novel antibiotic target. The traditional program of drug discovery predominantly depends on target-based high-throughput screening of a large library of compounds followed by lead optimisation (298-300). Nevertheless, the progress for searching of potential novel drugs is always hampered by the high tendency rate of failure and erroneous of leads as well as its uncertain *in vivo* activity. At present, systems biology methods such as genomics, transcriptomics, proteomics and metabolomics are increasingly utilised to investigate the mechanism of drug action and resistance (275).

The rapid advancement and development of analytical technologies and bioinformatics analysis methods promote the extent of many advantageous of metabolomics approach in drug-mode-of-action studies (301-303). Vincent *et al.* recently demonstrated the potential of untargeted metabolic profiling method to systematically determine the mechanisms of actions of eight different compounds (304). The changes of cellular metabolites were consistent with the expected modes of actions and targets of the drugs under the study, for example thymidylate kinase for AZ1, isoprenoid biosynthesis for fosmidomycin, acyl transferase for CHIR-090, DNA metabolism for 2-(cyclobutylmethoxy)-5'-deoxyadenosine and changes in cell wall metabolites for ceftazidime (304). In a study of nanoparticles which exhibit antibiotic properties revealed that the nanoparticles significantly induced global metabolic changes predominantly associated with intracellular metabolism of alanine, aspartate and glutamate (305). Halouska *et al.* demonstrated that the results of NMR-based metabolomics systematically clustered the different classes of antibiotics (i.e. 12 known drugs and 3 drugs with unknown mode of action) based on their unique global metabolic changes reflecting to their expected mechanisms of actions (300). Furthermore, treatment of three different antibiotic classes (i.e. ampicillin, kanamycin and norfloxacin) against *E.coli* showed a common pattern of significant metabolic changes at the

early time points (30 min and 60 min) then become more specific at the later time point (90 min) (113). Notably, of the significant metabolic changes observed was the elevation of central carbon metabolism and the reduction of nucleotide and lipid metabolites, suggesting the mechanism of oxidative stress (113). Previously, few studies have been conducted to elucidate the mechanisms of actions of antiprotozoal drugs applying untargeted metabolomics approach (306, 307). To the best of our knowledge, virtually no metabolomics research has been conducted specifically to investigate the modes of actions of polymyxins, either as a single or in combinations with other antibiotics against MDR Gram-negative pathogens.

In this PhD project, untargeted metabolomics was performed to investigate the mechanism of action of polymyxins against MDR Gram-negative pathogens either as a monotherapy or combination therapy (Chapters 3 to 6). To the best of our knowledge, the studies conducted in this research were the first to reveal the different metabolic profiles of MDR *A. baumannii* and *P. aeruginosa* subjected to different polymyxin combination therapies with other antibiotics.

1.4.2 Sample preparation for bacterial metabolomics

A good study design with a robust, sensitive and reproducible method of sample preparation is the cornerstone of metabolomics research as it is essential for producing relevant and statistically significant biological data (308-310). Metabolomics experiment basically includes steps for pre-treatment sample preparation and processing, analytical instrument processing, raw data processing, statistical analysis and finally data interpretation (311). Many studies concerning the development and optimisation of sample preparation methods have been done subjecting to different types of metabolomic samples (309, 310, 312, 313). In microbial metabolomics, it is highly recommended to establish an individual sample preparation protocol on account of the different structural organisations of bacterial cell envelope (314). One general sample

preparation protocol does not fit all. Therefore, a general metabolomics protocol always needs to be optimised to meet the objective of a particular study and to achieve the maximum coverage of the entire metabolome. This is predominantly considering a large number of cellular metabolites with diverse biochemical properties (287). In addition, a preliminary small-scale metabolomic study is highly recommended to be conducted before the ‘real’ experiment to prevent or limit any possible error during the large-scale experimental process (308).

1.4.2.1 Sample pre-treatment

Sample preparation is the most critical step in metabolomics as the product will determine the biological reliability and data quality of a particular experiment. Ideally, sample pre-treatment method for untargeted metabolomics should be simple, unselective and rapid with minimum number of steps (i.e. to avoid metabolite losses) that incorporates a quenching step (287). The protocol should be pragmatic, robust and most importantly reproducible. To certify that the identified metabolites truly reflect its physiological nature, any influence that likely leads to metabolic changes should be avoided or limited. Many cellular metabolites are very labile with high turnover rates, therefore the metabolism of cells firstly must be stopped or quenched (309). Quenching is an essential step in the sample preparation method that is performed to halt or lock cellular metabolism instantaneously by the inactivation of intracellular enzymes (315, 316). In bacterial metabolomics, several sampling methods that are commonly performed include a direct quenching, cold centrifugation and fast vacuum dependent filtration (317). Cold centrifugation and fast filtration methods advantageously reduce the dilution effect and possible contaminants derived from the culture media components. These two methods enable the measurement of both intracellular (fingerprint) and extracellular (footprint) metabolites obtained by the separation of cell pellets and culture supernatants (318). However, sampling using centrifugation is significantly time-consuming and is likely to induce physical stress to cells.

Direct quenching is performed by cold shock or an instant contact with an organic solvent which will likely lyse cells and may lead up to 60% intracellular metabolite leakage (309). Fast vacuum-dependent filtration displays some advantages over the two sampling methods. The step taken in the fast filtration method is technically fast and the metabolite leakage potentially could be avoided as the cells are filtered before treatment with organic solvent (309).

The use of rich culture media to grow microorganisms in metabolomics studies most likely will contaminate and potentially interfere the quantification of cellular-derived metabolites by falsely increasing their levels. To avoid the medium effect, therefore cell washing step is strongly recommended (309). However, under certain conditions, the washing may potentially cause cell leakage of up to 97% of intracellular metabolites (309). The next is cell extraction, a disruption of cell membrane structure to make the cell permeable to release a maximum number of intracellular metabolites while at the same time deactivate intracellular enzymes (316). The method for cell extraction must be non-destructive with the power to release as many metabolites as possible without any bias regardless of the diverse physicochemical properties of metabolites (316). Cell disruption can be either by chemical or mechanical methods. The output recovery of metabolites can be enhanced by combining the two extraction methods but it sometimes can be destructive and likely to decrease the recovery yield of some particular metabolite classes. Extraction using an organic solvent particularly methanol is the most common method used in untargeted metabolomics as the result obtained is always reproducible (309). Some of the frequently applied solvent mixtures used for cell extraction are cold chloroform:methanol:water (1:3:1, v/v), boiled ethanol:water (75:25, v/v), cold methanol:water (80:20, v/v) and acetonitrile:methanol:water (2:2:1, v/v) (319-322). Many studies have been conducted to evaluate and optimise different extraction protocols targeting for various and distinct metabolite classes, but none can comprehensively cover all the cellular metabolites with a single protocol

(319, 323-325). In this PhD project, cell washing and cell extraction steps were evaluated and optimised specifically for bacterial untargeted metabolomic studies (Chapter 2).

1.4.2.2 Analytical methods

The rapid advancement of analytical tools further extends the potential of metabolomics research. In particular, global metabolomics study ideally adopts analytical instrument which can provide broad coverage of different classes of metabolites (292). In addition, the instrument should present high selectivity and sensitivity with high resolution in order to generate biologically sense metabolomics data. The common analytical methods used in metabolomics research include nuclear magnetic resonance (NMR) spectroscopy, fourier transform-infrared spectroscopy (FT-IR) and chromatography separation coupled to mass spectrometry (MS) which are gas chromatography MS (GC-MS) and liquid chromatography MS (LC-MS) (326, 327). NMR spectroscopy is regularly applied for bulk metabolite analysis. Whereas, GC-MS is particularly used for volatile organic compounds which always requires sample pre-treatment processing steps (328). LC-MS allows the separation and detection of compounds of a wide range of polarity and the method is mostly used for untargeted metabolomics (308). Furthermore, high-resolution mass spectrometry (HRMS), in particular, the Orbitrap system, is preferably applied for untargeted metabolomics as it offers better high mass resolution and mass accuracy (100,000 FWHM at m/z 400 and 1 – 2 ppm) (329). For targeted metabolomics study, triple quadrupole (QQQ) mass spectrometry integrated with the multiple reaction monitoring (MRM) technology is commonly used as it is highly sensitive and robust to produce relatively high throughput data (268, 293).

The results of untargeted metabolomics are represented by the relative differences in the integrated mass ion intensities of either chromatogram's peak areas or heights between the

individual groups of samples. Whereas, targeted metabolomics analysis provides an absolute quantitation of a defined set of a metabolite level relative to the isotopically labeled standard (293). As no single analytical method can completely cover the various types of metabolites, therefore, integration of different analytical approaches is strongly recommended to obtain broad metabolite recovery. Previously, Martin *et al.* conducted a large-scale inter-laboratory metabolite recovery analysis of different analytical instruments (i.e. 5 NMR and 11 different mass spectrometers) demonstrated the reliability of untargeted metabolomics results (330). Interestingly, the analysis of same set of samples by the various analytical instruments generated comparable metabolic profiles with high convergence in the spectral information (with an average of 64-91%) irrespective of the type of standardisation, deconvolution methods, LCMS analyser or configuration (330). In addition, several other intra- and inter-laboratory evaluations of different analytical instruments have been reported. The results from the analysis of NMR (331, 332), GC-MS (333) and LC-MS (334) were exceptionally comparable, reliable and reproducible, indicating the high reliability of untargeted metabolomics data.

1.4.3 Metabolomic data analysis

Other major challenges in untargeted metabolomics concern on the complexity of high-throughput data management, analysis and interpretation. The problems always represent the rate-limiting step in metabolomics research. In parallel with the rapid advancement of bioinformatics study field, this greatly facilitates the process of metabolomics data handling and analysis. In metabolomics, data analysis generally encompasses of raw data processing, metabolite identification, statistical analysis, pathway analysis and most importantly biological interpretation. The presence of many omics softwares and programs for example MathDAMP, MetAlign, MZMine, XCMS, IDEOM, MetaboAnalyst 3.0 and iPath provide a better convenient platform for data analysis (268). Depending on its particular functions, these programs are

functionally developed for raw data analysis (e.g. normalisation, peak picking, integration and alignment from the spectral noise), statistical analysis and output visualisation (268).

Metabolites are assigned, either absolutely or putatively based on the signal of mass to charge ratio from the mass spectrum data. For metabolite identification, compounds are searched and matched with the metabolites presence in the various databases such as the Kyoto Encyclopedia of Genes and Genomes (KEGG) (335), METLIN (336), Human Metabolome Database (HMDB) (337) and Lipidmaps (338). A robust statistical analysis of the complex metadata put forth by both univariate and multivariate approaches to determine the group-wise differences between individual samples (288). Univariate statistical analysis is performed basically to reduce a large high-throughput data set to only those that demonstrate significant changes in response to a particular condition. Whereas, multivariate statistical analysis always is the first step to perform to globally visualise and verify the whole data for any unintended issues with the design of experiment. Some of the common approaches include unsupervised methods (e.g. principal component analysis (PCA), clustering algorithms) and supervised methods (e.g. partial least square regression and support vector machine) (288, 339, 340).

1.4.3.1 IDEOM and MetaboAnalyst 3.0

In this PhD project, IDEOM and MetaboAnalyst 3.0 were the primary tools applied for the metabolomics data processing and analysis. IDEOM is a freely available user friendly metabolomic software, accessible in a Microsoft Excel template (341). IDEOM is an automated processing tool, practically applied to analyse high resolution LC-MS data with integrated functions for noise removal, metabolite identification, statistical analysis and result visualisation. IDEOM integrates both the mzMatch (342) and XCMS (343) programs mainly used for raw data processing, peak matching, noise filtering, gap filling and peak annotation. For data analysis,

samples can be assigned based on individual study groups for example as blank, control, treatment and quality control. In addition, consistency of the samples can be automatically monitored based on the average peak high coupled with the normalisation function. Some of the noise filtered in the IDEOM include chromatographic peak shoulders, irreproducible peaks, background or contaminant signals and artefacts (e.g. isotopes, adducts and fragments). Metabolite annotation and identification is based on the accurate mass and retention time matching between the detected peaks with metabolites in reference databases (e.g. KEGG, BioCyc, Lipidmaps and HMDB). In IDEOM, metabolomics data can be analysed by both univariate (e.g. mean, relative intensity, standard deviation, t-test and Fisher ratio) and multivariate (e.g. PCA) approaches. Previously, IDEOM has been validated as an efficient data processing and analysis tool in several untargeted metabolomics studies for example in a study to elucidate the mechanism of action of a combination of eflornithine, a polyamine pathway inhibitor, and nifutimox against *Trypanosoma brucei* (307). Also, IDEOM has been applied to investigate the metabolic response of protozoan parasite *Trypanosoma cruzi* to benznidazole (303). Furthermore, MetaboAnalyst 3.0 was applied to complement the metabolomics data analysis from IDEOM majorly focused on statistical analysis and pathway analysis. MetaboAnalyst 3.0 is a comprehensive web-based omics tool and has been widely applied for data analysis, visualisation and interpretation (344). Three general categories in MetaboAnalyst 3.0 include (i) exploratory statistical analysis (i.e. Statistical Analysis and Time Series Analysis), (ii) functional analysis (i.e. Enrichment Analysis, Pathway Analysis and Integrated Pathway Analysis), and (iii) advanced methods for translational studies (i.e. Biomarker Analysis and Power Analysis). Advantageously, the tool is freely available with a user-friendly interface.

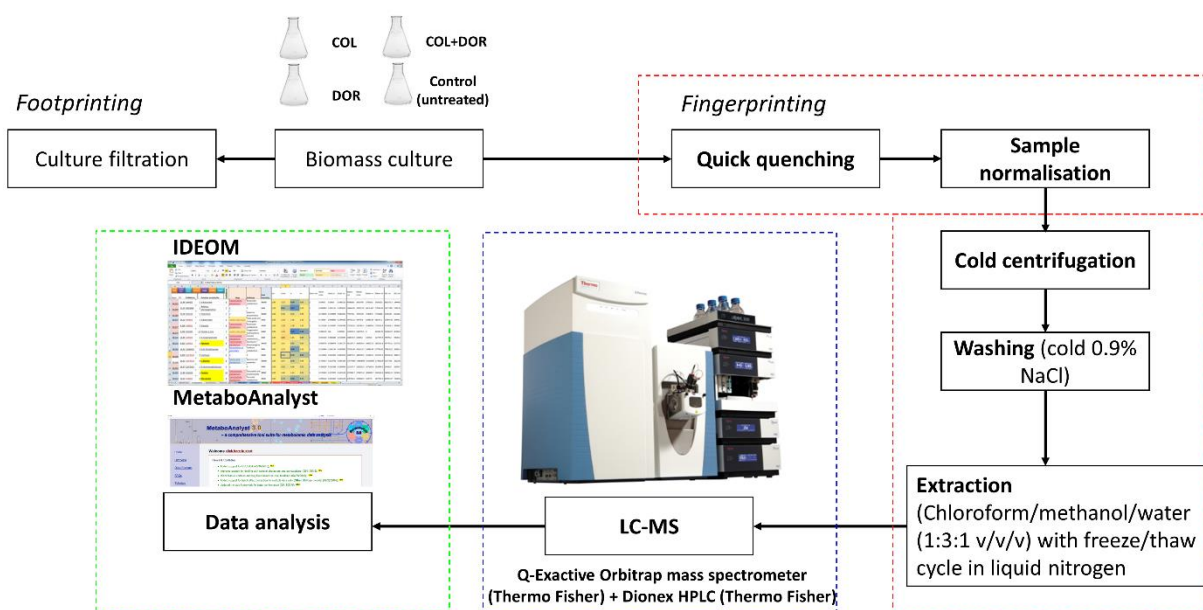


Figure 1.13. Untargeted metabolomics workflow.

1.4.4 Integrated systems biology

Advanced systems biology has enabled the integration of different omics data (e.g. transcriptomics, proteomics and metabolomics) for details elucidation of the underlying mechanism of drug action and resistance (345, 346). The effect of drug treatment generally causes the alteration of cellular metabolic pathways directly affecting the cellular functions of genes, proteins and metabolites (339, 347). However, in certain cases of no direct association between genes and metabolites, the elucidation of a particular biochemical interaction is more complicated (267).

Genome-scale metabolic model (GSMM) is a reconstruction of the metabolic network of a cell annotated based on the interaction between gene-protein-reactions (GPR) and mass-energy balance (348). GSMM has been used widely in the study of systems biology for example in industrial biology and systems medicine (348). The basic reconstruction of a predictive metabolic model is based on the available information from various omics and microbial

physiology studies (267). The study of metabolic response and flux simulation at systems based-level is possible as different multi-omics data can be systematically and concurrently analysed. Coupled with the stoichiometric balance technique, therefore, detailed biological understanding of the mechanism of drug action potentially could be attained via a GSMM method. However, due to the complexity of the codes and scripts underlying the model, the application of GSMM is always limited to those computational expert groups only whereas it is not readily available to biologists. In addition, the limitation of a genome scale modelling include the presence of undefined enzyme sequences (potentially as high as 30-40%) and metabolic reactions, particularly those only regulated under specific external influences (349). Furthermore, the relationship between the GPR is generally qualitative which requires certain assumptions to determine their quantitative relationship (348). As the relationship between fluxes, gene expression levels and enzymes is extremely complex, therefore, making a general assumption is always difficult. Hence, interpretation of the result of a GSMM analysis is better qualitatively rather than quantitatively (348). In other words, the application of a GSMM is much more relevant to determine the presence or absence of a particular reaction with the aim to develop higher quality and more specific model.

In particular, the reconstruction of GSMM of *P. aeruginosa* PAO1 was firstly reported by Oberhardt *et al.* and assigned as iMO1056 (350). The model encompassed of the association of GPR coupled with the stoichiometric and thermodynamic balances, accounts for a total of 1,056 genes encoding for 1,030 proteins and 883 metabolic reactions (350). The pathways generated comprised of those elements important for growth and production of common cellular virulence factors (e.g. alginate, rhamnolipids and QS molecules). The model then was validated that included data of the experimental growth rate, various carbon sources and genome-scale gene from many of *P. aeruginosa* studies. The model of PAO1 has become a major tool to understand

the metabolic and regulatory mechanism of drug action and its resistance, in addition to its potential use for rational drug design and phenotypic prediction. In Chapter 6 of this thesis, a GSMM of *P. aeruginosa* was constructed and analysed to elucidate the relationship between the metabolite-gene-pathways that were significantly altered in response to drug treatment.

1.5 Summary

The overuse and sub-optimal use of antibiotics have led to multidrug-resistance, one of the three greatest threats of human health in modern medicine. With the recent state of the dry discovery and development pipeline for new drugs and the rapid emergence of resistance, this desperately requires optimisation of the clinical use of currently available antibiotics. Due to this crucial situation, polymyxins, an ‘old’ antibiotic class, have been revived as the last-line therapeutic preference for infections caused particularly by MDR Gram-negative bacteria. Notwithstanding, the PK/PD profile of polymyxins demonstrates that polymyxin monotherapy is not likely to generate optimal plasma exposure with the emergence of a resistant sub-population. To cater these problems, polymyxin combination therapy is strongly recommended. There are models that consider the mechanism of polymyxin action, yet the details remain uncertain. The complete understanding of the mode of polymyxin action and resistance is significant to optimise the clinical use. In this PhD project, hypothesis-generating omics strategies were employed to elucidate the mechanisms of activity and resistance of polymyxins against MDR *A. baumannii* and *P. aeruginosa*.

1.6 Hypotheses and aims

The central **hypotheses** of this PhD project were that:

1. Global metabolic profiles are different between polymyxin-susceptible and polymyxin-resistant MDR *A. baumannii* strains in the absence of antibiotic treatment.

2. Synergistic killing by polymyxin combinations is due to mutual perturbations of bacterial global metabolism and gene expression.

The **aims** of this thesis were:

1. To develop an efficient sample pre-treatment method for bacterial metabolomics;
2. To examine the global metabolic profiles of paired polymyxin-susceptible and polymyxin-resistant of *A. baumannii* without antibiotic treatment;
3. To investigate the metabolic profiles of *A. baumannii* with mono- and rational polymyxin combination therapy; and
4. To elucidate the mechanisms of polymyxin synergistic killing against *P. aeruginosa* using metabolomics and transcriptomics.

1.7 Significance statement

1. The comparative global metabolomics study is the first to demonstrate significant metabolic profile changes between pairs of polymyxin-susceptible and polymyxin-resistant *A. baumannii* strains of different mechanisms of polymyxin resistance due to LPS loss and lipid A modifications.
2. Both colistin and polymyxin B significantly perturbed the bacterial lipid metabolism in both *A. baumannii* and *P. aeruginosa* reflecting its general rapid action to cause membrane disruptions.
3. Two conceptual models of antibiotic synergism, the bioavailability model and parallel pathway inhibition model were described via a metabolomics approach; well explained the synergistic killing of colistin and doripenem combination and also polymyxin B and rifampicin combination, respectively.

4. The combination of colistin and doripenem synergistically kills *A. baumannii* by the time-dependent inhibition of key metabolic pathways of lipids, nucleotides, pentose phosphate pathway, peptidoglycan and LPS biosynthesis.
5. The synergistic combination of polymyxin B and rifampicin is predominantly driven by the action of rifampicin and facilitated by the effect of polymyxin B demonstrated by the abundant increases of nucleotides, amino acids, peptidoglycan and LPS biosynthesis metabolites.
6. The synergistic killing of the polymyxin B and rifampicin combination induced significant suppression of many *P. aeruginosa* QS-regulated virulence factors, signifying the inhibition of bacterial pathogenicity.
7. The transient emergence of polymyxin resistance at 1 hr and rifampicin resistance at 24 hr in *P. aeruginosa* highlights the importance of antibiotics optimal dosages and the great potential of polymyxin combinations therapy to reduce or inhibit the development of resistance.
8. The results of metabolomics and transcriptomics study of the polymyxin B and rifampicin combination are complementary, as demonstrated by the significant changes in key metabolic and regulatory pathways of lipids, nucleotides, amino acids, peptidoglycan and LPS biosynthesis, highlighting the potential of a systems pharmacology to elucidate the mechanism of antibiotic action.

Overall, this PhD project provides valuable insights on the mechanisms of polymyxins actions and resistance that may greatly facilitate the discovery of novel antibiotics.

1.8 Structure of the thesis

There are seven chapters in this thesis. Chapter 1 is the background and Chapter 2 and 3 focus on the untargeted metabolomics of *A. baumannii* strains. Chapters 4, 5 and 6 are on the global metabolomics and transcriptomics of *P. aeruginosa*. Chapter 2 and 3 comprise two manuscripts that have already been published and Chapter 6, a manuscript yet to be submitted for publication. The texts and figures in these chapters have been reproduced as published or submitted for publication with modifications for this thesis as per the requirements for this research degree. The final chapter provides a conclusion and discussion of future perspectives.

Chapter Two

Part B**Monash University****Declaration for Thesis Chapter 2****Declaration by candidate**

In the case of Chapter 2, the nature and extent of my contribution to the work was the following:

Nature of contribution	Extent of contribution (%)
Design of the study, laboratory experiments, data analysis and interpretation, preparation of the initial draft of the manuscript and subsequent revisions, and formulation of the conclusions and hypothesis generation from the results of the study	80%

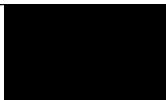
The following co-authors contributed to the work:

Name	Nature of contribution
Soon-Ee Cheah	Advice regarding the thought and design of studies, data analysis and interpretation, review of manuscript drafts and revisions and formulation of conclusions and hypotheses generation from the results of the study
Matthew D. Johnson	Advice regarding the thought and design of studies, laboratory experiments, data analysis and interpretation, review of manuscript drafts and revisions, and formulation of conclusions and hypotheses generation from the results of the study
Mei-Ling Han	Advice regarding the thought and design of studies, laboratory experiments, data analysis and interpretation, review of manuscript drafts and revisions, and formulation of conclusions and hypotheses generation from the results of the study
John D. Boyce	Advice regarding the thought and design of studies, laboratory experiments, data analysis and interpretation, review of manuscript drafts and revisions, and formulation of conclusions and hypotheses generation from the results of the study
Visanu Thamlikitkul	Advice regarding the thought and design of studies, review of manuscript drafts and revisions, and formulation of conclusions and hypotheses generation from the results of the study
Alan Forrest	Advice regarding the thought and design of studies, review of manuscript drafts and revisions, and formulation of conclusions and hypotheses generation from the results of the study
Keith S. Kaye	Advice regarding the thought and design of studies, review of manuscript drafts and revisions, and formulation of conclusions and hypotheses generation from the results of the study

Paul Hertzog	Advice regarding the thought and design of studies, review of manuscript drafts and revisions, and formulation of conclusions and hypotheses generation from the results of the study
Anthony W. Purcell	Advice regarding the thought and design of studies, review of manuscript drafts and revisions, and formulation of conclusions and hypotheses generation from the results of the study
Jiangning Song	Advice regarding the thought and design of studies, review of manuscript drafts and revisions, and formulation of conclusions and hypotheses generation from the results of the study
Tony Velkov	Supervision, advice regarding the thought and design of studies, data analysis and interpretation, review of manuscript drafts and revisions, and formulation of conclusions and hypotheses generation from the results of the study
Darren J. Creek	Supervision, advice regarding the thought and design of studies, data analysis and interpretation, review of manuscript drafts and revisions, and formulation of conclusions and hypotheses generation from the results of the study
Jian Li	Design of the study, supervision, advice regarding the thought and design of studies, data analysis and interpretation, review of manuscript drafts and revisions, and formulation of conclusions and hypotheses generation from the results of the study

The undersigned hereby certify that the above declaration correctly reflects the nature and extent of the candidate's and co-authors' contributions to this work*.

**Candidate's
Signature**

	Date 12 June 2017
---	------------------------------------

**Main
Supervisor's
Signature**

	Date 12 June 2017
--	------------------------------------

*Note: Where the responsible author is not the candidate's main supervisor, the main supervisor should consult with the responsible author to agree on the respective contributions of the authors.

Chapter 2: Global metabolic analyses identify key differences in metabolite levels between polymyxin-susceptible and polymyxin-resistant *Acinetobacter baumannii*

2.1 Abstract

Multidrug-resistant *Acinetobacter baumannii* presents a global medical crisis and polymyxins are used as the last-line therapy. This study aimed to identify metabolic differences between polymyxin-susceptible and polymyxin-resistant *A. baumannii* using untargeted metabolomics. The metabolome of each *A. baumannii* strain was measured using liquid chromatography-mass spectrometry. Multivariate and univariate statistics and pathway analyses were employed to elucidate metabolic differences between the polymyxin-susceptible and -resistant *A. baumannii* strains. Significant differences were identified between the metabolic profiles of the polymyxin-susceptible and -resistant *A. baumannii* strains. The lipopolysaccharide (LPS) deficient, polymyxin-resistant 19606R showed perturbation in specific amino acid and carbohydrate metabolites, particularly pentose phosphate pathway (PPP) and tricarboxylic acid (TCA) cycle intermediates. Levels of nucleotides were lower in the LPS-deficient 19606R. Furthermore, 19606R exhibited a shift in its glycerophospholipid profile towards increased abundance of short-chain lipids compared to the parent polymyxin-susceptible ATCC 19606. In contrast, in a pair of clinical isolates 03-149.1 (polymyxin-susceptible) and 03-149.2 (polymyxin-resistant, due to modification of lipid A), minor metabolic differences were identified. Notably, peptidoglycan biosynthesis metabolites were significantly depleted in both of the aforementioned polymyxin-resistant strains. This is the first comparative untargeted metabolomics study to show substantial differences in the metabolic profiles of the polymyxin-susceptible and -resistant *A. baumannii*.

2.2 Introduction

A. baumannii is a Gram-negative, aerobic bacterium and a major cause of nosocomial infections worldwide, particularly in critically-ill patients (12). *A. baumannii* infections include hospital-acquired pneumonia, bloodstream infection, urinary tract infection, skin and soft tissue infections (13, 351). *A. baumannii* has become a significant global threat and is one of the six ‘superbugs’ identified by the IDSA which required urgent attention for discovery of novel antibiotics (6). Recently, the CDC classified MDR *A. baumannii* as a microorganism with a threat level of “Serious” (8). *A. baumannii* has been characterised as ‘naturally transformable’, since it can rapidly acquire diverse resistance mechanisms and undergo genetic modifications that confer resistance to all current clinically used antibiotics (12, 351, 352).

The clinical use of polymyxins waned in the 1970s due to potential nephrotoxicity and neurotoxicity (Section 1.3.2) (11, 186). However, over the last decade colistin (polymyxin E) and polymyxin B have been widely used as the only effective therapeutic option for patients infected with MDR *A. baumannii* (80, 353, 354). Polymyxins are amphipathic, cationic lipopeptides that contain five L- α , γ -diaminobutyric acid (Dab) residues (Section 1.3.1) (11, 186). The bactericidal activity of polymyxins is exerted via the ‘self-promoted uptake’ pathway, initiated by electrostatic interaction with the lipid A of lipopolysaccharide (LPS) on the outer leaflet of the bacterial outer membrane (Section 1.3.3) (11, 355). In addition, a recent study suggested that polymyxins exert bacterial killing through a specific mechanism via the formation of hydroxyl radicals (109). As reviewed in Section 1.3.4, polymyxin resistance in *A. baumannii* can be acquired via the addition of phosphoethanolamine (41, 42) or galactosamine (43) to lipid A structure. Our group firstly reported that *A. baumannii* ATCC 19606 spontaneously acquired colistin resistance following exposure to high levels of colistin, via the loss of its initial target, LPS (44). Further analyses revealed LPS loss was due to single random mutations in the lipid A

biosynthesis genes, *lpxA*, *lpxC* and *lpxD* (44). Moreover, transcriptomic analyses of the *A. baumannii* LPS-deficient strain 19606R revealed significant up-regulation of genes involved in the cell envelope and membrane biogenesis, in particular of the Lol lipoprotein transport system and the Mla-retrograde phospholipid transport system (356). We therefore hypothesised that the LPS-deficient strain 19606R exhibits significant changes in its metabolic profile in response to LPS loss. For bacteria, metabolomics is a powerful systems biology tool for understanding cell physiology and can complement and validate data from genomics, transcriptomics and proteomics (280, 357, 358). In this study, we report the first comparative untargeted metabolomics analyses of paired polymyxin-susceptible and polymyxin-resistant (via LPS loss or lipid A modifications) *A. baumannii* strains.

2.3 Materials and methods

2.3.1 Strains

The *A. baumannii* wild-type strain ATCC 19606 was obtained from the American Type Culture Collection. The *lpxA* mutant strain 19606R (MIC > 128 mg/L) is an LPS-deficient, polymyxin-resistant derivative of ATCC 19606 (44). The two clinical isolates used in this study were polymyxin-susceptible 03-149.1 (MIC 1 mg/L) and polymyxin-resistant 03-149.2 (MIC > 32 mg/L); both were isolated from the same patient (189). Bacterial strains were grown in cation-adjusted Mueller-Hinton broth (CaMHB; Oxoid, England; 20 - 25 mg/L Ca²⁺ and 10 - 12.5 mg/L Mg²⁺).

2.3.2 Identification of 16S rDNA, genome sequencing and lipid A structural analysis of *A. baumannii* clinical isolates 03-149.1 and 03-149.2

The identification of 16S rDNA and genome sequencing of the clinical isolates of *A. baumannii* were performed by Dr Matthew D. Johnson. The *A. baumannii* clinical isolates 03-149.1 and 03-

149.2 16S were identified using rDNA gene sequencing. Degenerate oligonucleotide primers 16s_Fw CCTACGGGNGGCWGCAG and 16s_Rv GACTACHVGGGTATCTAATCC were used to amplify the 16S gene from each strain by PCR. The 16S fragment was purified by gel extraction (Qiagen) and sequenced using Sanger chemistry (Micromon, Monash University, Australia). Sequences were analysed using Eztaxon (359) and identification of phylogenetic neighbours was conducted using BLASTN (360) program against the database containing published prokaryotic representatives (359). Their genome sequences were determined using 36-bp paired-end sequencing chemistry on an Illumina Genome Analyzer II apparatus (Illumina) at the Micromon Sequencing Facility (Monash University) as previously described (44).

Structural analysis of lipid A of *A. baumannii* clinical isolates was conducted by Mei-Ling Han in our laboratory. Lipid A of the clinical isolates 03-149.1 and 03-149.2 was prepared by mild acid hydrolysis as previously described (361). In detail, 100 mL of broth cultures were harvested at $OD_{600nm} = 0.8$ via centrifugation at $3,220 \times g$ for 20 min and washed twice with phosphate-buffered saline (PBS). Initially, the cells were re-suspended in 4 mL PBS, methanol (10 mL) and chloroform (5 mL) were then added to the suspension, making a single-phase Bligh-Dyer (chloroform/methanol/water, 1:2:0.8, v/v) (362). The mixture was centrifuged at $3,220 \times g$ for 15 min and supernatant was removed. The pellet was washed once with chloroform/methanol/water (1:2:0.8, v/v), re-suspended in the hydrolysis buffer (50 mM sodium acetate pH 4.5, 1% sodium dodecyl sulphate (SDS)), and incubated in a boiling water bath for 45 min. To extract lipid A, the SDS solution was converted into a double-phase Bligh-Dyer mixture by adding 6 mL of chloroform and 6 mL of methanol for a final mixture of chloroform/methanol/water (1:1:0.9, v/v) (362). The lower phase containing lipid A was finally extracted and samples were dried and stored at $-20^{\circ}C$. Structural analysis of lipid A was performed in negative mode on a Q-Exactive Hybrid Quadrupole-Orbitrap Mass Spectrometer (Thermo Fisher).

2.3.3 Bacterial culture preparation for metabolomics experiments

Bacterial strains, subcultured from -80°C frozen stocks, were inoculated onto nutrient agars and incubated for 16 - 18 hr at 37°C. For the polymyxin-resistant strains, *lpxA* mutant 19606R and clinical isolate 03-149.2, the Mueller-Hinton plates were supplemented with polymyxin B (10 mg/L) to maintain the selection pressure. For each culture, a single colony was used to inoculate 10 mL CaMHB for incubation overnight (16 - 18 hr) at 37°C with constant shaking (180 rpm). Three biological replicate reservoirs for different *A. baumannii* colonies, each consisting of 50 mL CaMHB, were prepared for each *A. baumannii* strain. Each reservoir was inoculated with 500 µL of overnight culture and grown at 37°C with shaking (180 rpm) to an OD_{600nm} ~0.5 (mid-exponential growth phase). The polymyxin-resistant strains 19606R and 03-149.2 were grown in CaMHB without colistin. For the blank controls, two CaMHB reservoirs without bacterial inoculation were included in the experiment.

2.3.4 Sample preparation for metabolomic study

Metabolomic sample was prepared as previously described with slight modifications (309). The sample pre-treatment method, washing step and extraction solvents were optimised for improved recovery of cellular metabolites. The final method for cell pellet analyses employed four technical replicates, each consisting of 10 mL mid-exponential culture (OD_{600nm} ~0.5) collected in 50 mL Falcon tubes (Thermo Fisher). The tubes were centrifuged at $3,220 \times g$ at 4°C for 5 min and the supernatant discarded. For each sample, extracellular metabolites and medium components were removed by washing cell pellets twice with 0.5 mL of 0.9% NaCl (4°C). Following each wash, cells were pelleted by centrifugation at $3,220 \times g$ at 4°C for 3 min. To evaluate the washing effect on the metabolite leakage, washing waste supernatant samples were collected and analysed (below). Furthermore, the efficiency of four different extraction solvents were evaluated: (i) absolute methanol (MeOH), (ii) 60% ethanol (60EtOH), (iii)

chloroform:methanol:water (CMW; 1:3:1, v/v), and (iv) chloroform:methanol (CM; 1:2, v/v). In our comparison study of different *A. baumannii* strains, washed cell pellets were resuspended in 0.5 mL metabolite extraction solvent consisting of CMW (1:3:1, v/v; -80°C); the solvent mixture contained the internal standards (CHAPS, CAPS, PIPES and TRIS; 1 μ M of each). These compounds were selected as the internal standards as they are physicochemically diverse small molecules that are not naturally occurring in any microorganism and can be spiked at known concentrations to determine the analytical performance of the method used. Samples were frozen in liquid nitrogen and thawed on ice, and freeze-thaw was repeated three times in order to permeabilise the cells and release intracellular metabolites. The mixtures were centrifuged for 10 min at $3,220 \times g$ at 4°C and 300 μ L of the supernatants containing the extracted metabolites were collected in 1.5-mL centrifuge tubes and stored at -80°C immediately. For analysis, the samples were thawed and further centrifuged at $14,000 \times g$ for 10 min at 4°C and 200 μ L of particle-free supernatant was transferred into the injection vial for LC-MS analysis. For footprint samples, an aliquot of approximately 1.5 mL of the culture was rapidly filtered through a 0.22- μ m filter and stored at -80°C. Prior to analysis, these samples were thawed and 10 μ L combined with 250 μ L extraction solvent (CMW, 1:3:1, v/v) and then centrifuged at $14,000 \times g$ for 10 min at 4°C to collect 200 μ L supernatant for LC-MS analysis (below). Equal volumes from each of the *A. baumannii* strains samples were mixed for a quality control sample (QC). This pooled quality control sample was used to estimate a composite sample profile representing all the analytes that will be encountered during the LC-MS analysis (363).

2.3.5 LC-MS analysis

Hydrophilic interaction liquid chromatography (HILIC) - high-resolution mass spectrometry (HRMS) was employed in this study. Samples were analysed on a Dionex high-performance liquid chromatography (HPLC) system (RSLCU3000, Thermo Fisher) using a ZIC-pHILIC

column (5 μ m, polymeric, 150 \times 4.6 mm; SeQuant, Merck) coupled to a Q-Exactive Orbitrap mass spectrometer (Thermo Fisher) operated at 35,000 resolution in both positive and negative electro-spray ionisation (ESI) mode and a detection range of 85 to 1,275 m/z . The LC solvent consisted of 20 mM ammonium carbonate (A) and acetonitrile (B) with a multi-step gradient system from 80% B to 50% B over 15 min, then to 5% B at 18 min, followed by wash with 5% B for 3 min, and 8 min re-equilibration with 80% B at a flow rate of 0.3 mL/min (364). The run time was 32 min and the injection sample volume was 10 μ L. All samples (3 biological replicates, each with 4 technical replicates) were randomised and analysed in a single LC-MS batch to reduce batch-to-batch variation. The chromatographic peaks, signal reproducibility and analyte stability were monitored by the assessment of pooled quality control sample analysed periodically throughout the run, internal standards and total ion chromatograms for each sample. Mixtures of pure standards containing over 250 metabolites of different classes were analysed within the batch to aid in the identification of metabolites.

2.3.6 Data processing, bioinformatics and statistical analyses

Global metabolomic analyses were performed using mzMatch (342) and IDEOM (<http://mzmatch.sourceforge.net/ideom.php>) free software (341). Raw LC-MS data were converted to mzXML format and chromatogram peaks were detected using XCMS (343) and saved in the peakML format. The program Mzmatch.R was used to align samples and filter peaks based on minimum detectable intensity (100,000), reproducibility (relative standard deviation (RSD) for all replicates < 0.5) and peak shape (codadw > 0.8). Mzmatch.R was also used to retrieve LC-MS peak intensities for missing peaks and for the annotation of related peaks. Unwanted noise and artefact peaks were eliminated using IDEOM with default parameters. Metabolites were putatively identified by the exact mass within 2 ppm, after correction for loss or gain of a proton in negative and positive ESI mode, respectively. Retention time was employed to confirm the

identification of each metabolite based on the available authentic standards. Putative identification of other metabolites was determined using exact mass and predicted retention time based on the Kyoto Encyclopedia of Genes and Genomes (KEGG), MetaCyc and Lipidmaps databases, with preference given to bacterial metabolites annotated in EcoCyc. Quantification of each metabolite was calculated using the raw peak height and is expressed relative to the average peak height for their paired susceptible strain. Univariate statistical analyses utilised a Welch's T-test ($\alpha = 0.01$) and multivariate analyses utilised the metabolomics R package. Metabolic pathway analyses were performed using the free web-based metabolomics tool Pathos (<http://motif.gla.ac.uk/Pathos/>) (365), BioCyc (<http://biocyc.org/>) (366), and Visualisation and Analysis of Networks containing Experimental Data (Vanted) software (367).

2.4 Results

Comparative untargeted metabolomics was employed to identify differences in the metabolic profile between polymyxin-susceptible and polymyxin-resistant *A. baumannii* strains. Two pairs of *A. baumannii* strains were examined: a laboratory-derived polymyxin-resistant, LPS-deficient *lpxA*-mutant strain, 19606R and its polymyxin-susceptible parent strain, ATCC 19606; and two clinical isolates, polymyxin-susceptible 03-149.1 and polymyxin-resistant 03-149.2 obtained from a patient before and after colistin treatment, respectively. The polymyxin-resistant strain 19606R displayed a slower growth rate compared to the parent strain ATCC 19606, as previously reported (44). Whereas, there was no significant difference in the growth rate between the paired polymyxin-susceptible 03-149.1 and polymyxin-resistant 03-149.2 clinical isolates.

2.4.1 Genomics and lipid A structural analysis of *A. baumannii* clinical isolates 03-149.1 and 03-149.2

The paired *A. baumannii* clinical isolates of polymyxin-susceptible 03-149.1 and polymyxin-resistant 03-149.2 strains were initially identified using 16S rDNA gene sequencing; and showed 96.17% and 97.15% sequence similarity to the *A. baumannii* ATCC 19606, respectively (Table 2.1). Furthermore, a comparison of the polymyxin-susceptible 03-149.1 and the polymyxin-resistant 03-149.2 by high-throughput sequencing and variant calling revealed 3 variations unique to the 03-149.2 isolate (Table 2.2). One variation found in 03-149.2 was a deletion of 3 bases in the *pmrB* gene, which conferred an in-frame deletion of alanine 28.

We also investigated the mechanism(s) of polymyxin resistance in the clinical isolate 03-149.2 with lipid A structural analysis. Lipid A samples isolated from both polymyxin-susceptible 03-149.1 and polymyxin-resistant 03-149.2 were characterised with electrospray ionisation (ESI) high-resolution mass spectrometry (HRMS) in the negative-ion mode (Figure 2.1). The mass spectrum of lipid A from the polymyxin-susceptible 03-149.1 shows a predominant peak at m/z 1911.28, which represents a hepta-acylated lipid A with four primary fatty acyls (i.e. two 3-hydroxylaurate [C_{12} (3-OH)] acyl chains and two 3-hydroxymyristate [C_{14} (3-OH)] acyl chains), and three secondary fatty acyls (i.e. one C_{12} (3-OH) acyl chain and two laurate (C_{12}) acyl chains); while the peak at m/z 1933.26 represents the sodium adduct of the hepta-acylated lipid A mentioned above (Figure 2.1A). The peak at m/z 1883.25 is for a hepta-acylated lipid A with four primary C_{14} (3-OH) acyl chains and three secondary fatty acyls (i.e. one C_{12} acyl chain, one C_{12} (3-OH) acyl chain, and one myristate (C_{14}) acyl chain). The peak at m/z 1729.12 corresponds to a hexa-acylated lipid A, indicating the loss of a laurate acyl chain from the hepta-acylated lipid A at m/z 1911.28 ($\Delta m/z = -182$). Additional peaks at m/z 1649.15, 1803.29, 1831.32 differ from the peaks listed above by dephosphorylation at the 1 or 4' position of lipid A ($\Delta m/z = -80$),

while the peaks at m/z 1712.12, 1867.26, and 1895.29 were only different from the corresponding peaks at m/z 1729.12, 1883.25, and 1911.28 by the mass of one oxygen atom ($\Delta m/z = -16$), indicating the absence of 3-hydroxylation at the secondary laurate acyl chain.

Mass spectrometry analyses of lipid A from the polymyxin-resistant 03-149.2 isolate revealed several different types of modifications in the lipid A structure (Figure 2.1B). The predominant peak at m/z 2034.29 represents the hepta-acylated lipid A at m/z 1911.28 modified with a phosphoethanolamine (pEtN) residue ($\Delta m/z = +123$), while the peak at m/z 1954.32 indicates its dephosphorylated form ($\Delta m/z = -80$). Minor peaks at m/z 1990.26, 2006.26, and 2018.29 correspond to lipid A at m/z 1867.26, 1883.25, and 1895.29 which were modified with a pEtN group, respectively. The peak at m/z 2157.30 represents a modified lipid A with the addition of two pEtN moieties to the parent structure at m/z 1911.28. Interestingly, lipid A modified with galactosamine (GalN) was also detected in polymyxin-resistant 03-149.2. In detail, the peaks at m/z 2078.25 and 2094.33 represent lipid A at m/z 1895.29 and 1911.28 modified with a GalN residue ($\Delta m/z = +161$) along with a sodium adduct, respectively, and the peak at m/z 2195.36 corresponds to a lipid A (m/z 1911.28) with both pEtN and GalN additions ($\Delta m/z = +284$) (Figure 2.1B).

Table 2.1 Phylogenetic characterisation by 16S gene sequencing.

Strain name	Length (base pairs) ^a	Closest match ^b	Similarity % ^c	Completeness % ^d
03-149.1	446	ATCC 19606	96.17	30.6
03-149.2	442	ATCC 19606	97.15	30.4

^a Length of input sequence generated by sanger-based sequencing methodologies.

^b Closest match determined by BLASTn against a database of published prokaryotic representatives.

^c Similarity based on BLASTn search against the closest match.

^d Completeness accounts for the entire 16S gene of the closest match.

Table 2.2 Mutations identified in the polymyxin-resistant 03-149.2 isolate by high-throughput sequencing and variant calling to *A. baumannii* ACICU.

Annotation by similarity to <i>A. baumannii</i> ACICU	Sequence		Effect
	03-149.1	03-149.2	
Hypothetical Protein	CTTGAG	GCTTGAG	Frame shift
PmrB Sensor Kinase	AAGC	A	Amino acid deletion (A28-)
Phage-related protein	G	T	Amino acid substitution (I241L)

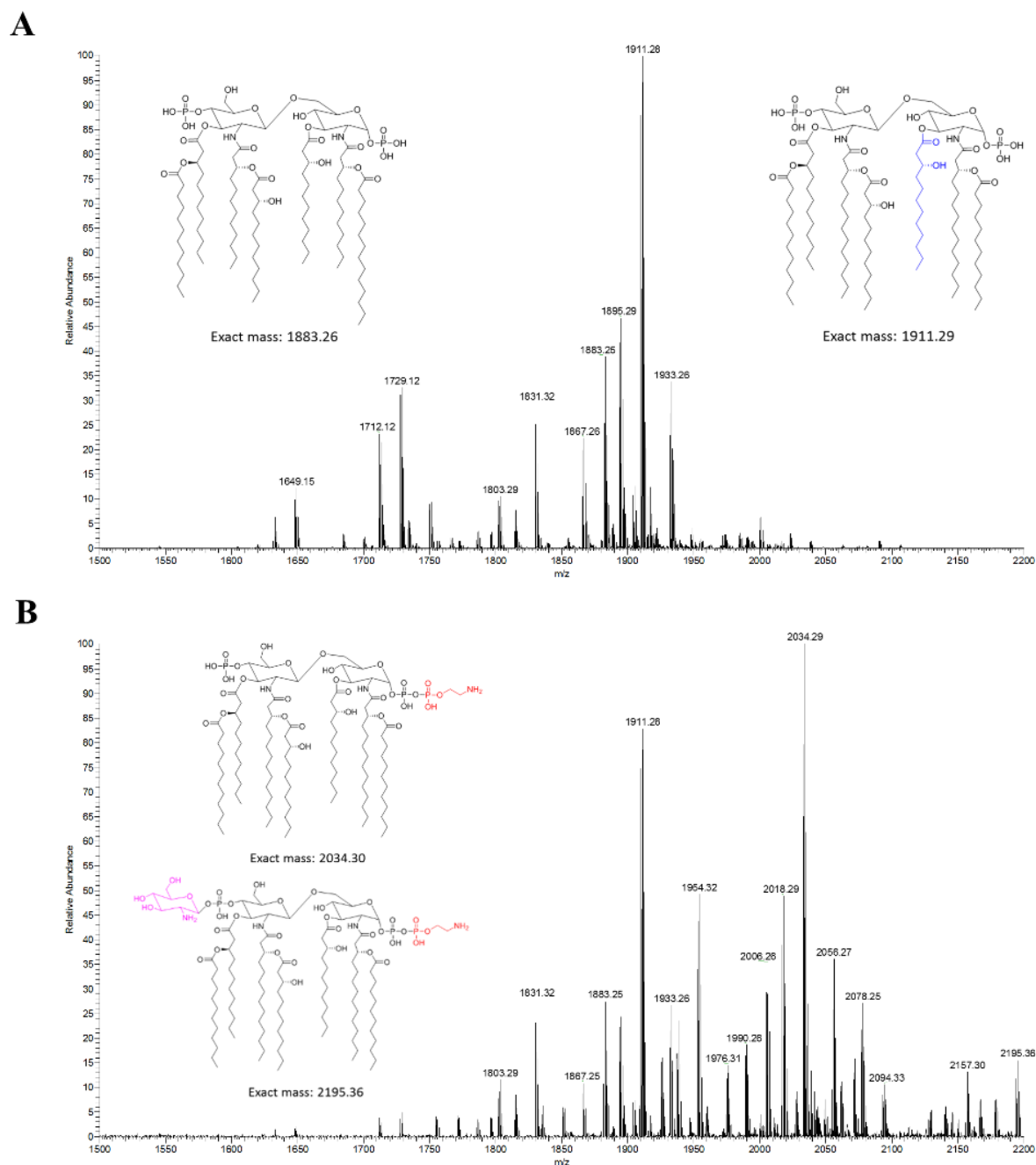
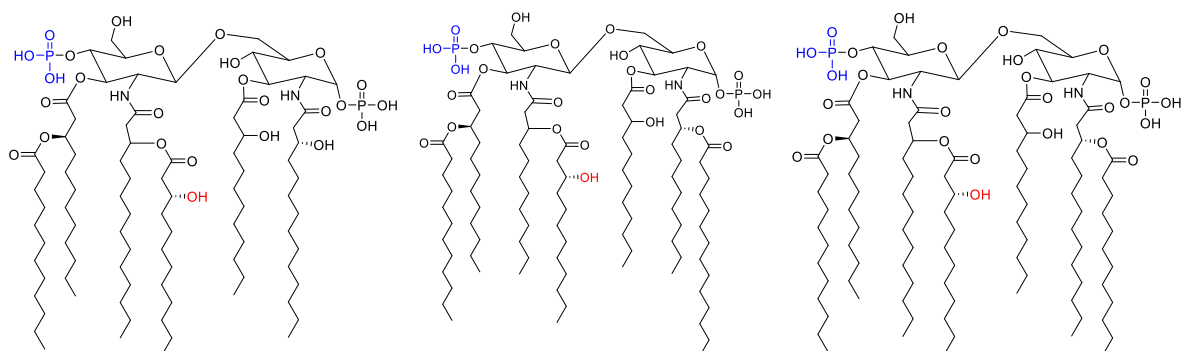


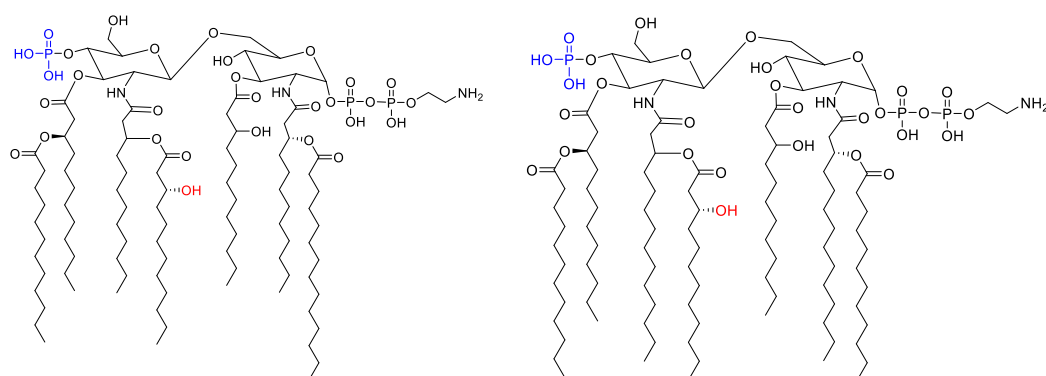
Figure 2.1. The mass spectra of lipid A isolated from the *A. baumannii* clinical isolates. **(A)** Polymyxin-susceptible 03-149.1 without lipid A modifications. **(B)** Polymyxin-resistant 03-149.2 with lipid A modification with phosphoethanolamine (pEtN) and galactosamine (GalN)

A

Exact Mass: 1729.12
 -OH group: 1713.13
 -H₂PO₃ group: 1649.15

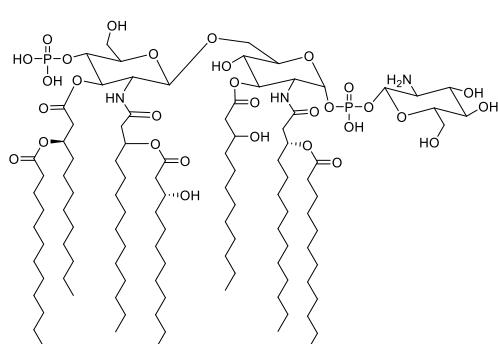
Exact Mass: 1883.26
 -OH group: 1867.26
 -H₂PO₃ group: 1803.29

Exact Mass: 1911.29
 -OH group: 1895.29
 -H₂PO₃ group: 1831.32
 + Na: 1934.28

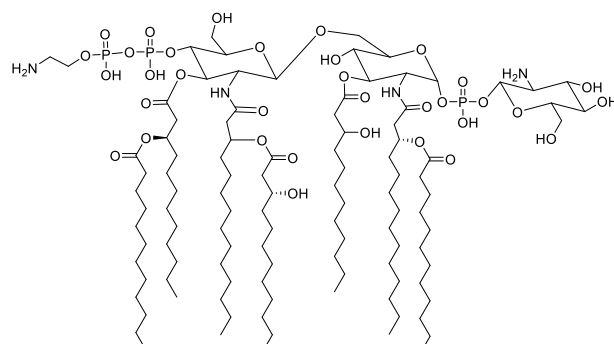
B

Exact Mass: 2006.26
 -OH group: 1990.27

Exact Mass: 2034.30
 -OH group: 2018.30
 -H₂PO₃ group: 1954.33
 + Na: 2057.29



Exact Mass: 2072.36
 + Na: 2095.35



Exact Mass: 2195.36

Figure 2.2. Structures of lipid A in clinical *A. baumannii* isolates (A) 03-149.1 and (B) 03-149.2.

2.4.2 *Optimal metabolite recovery of MDR A. baumannii by washing with 0.9% NaCl and extraction using chloroform:methanol:water (1:3:1)*

Optimisation of the metabolite sampling method was performed prior to the metabolomics analysis of paired polymyxin-susceptible and polymyxin-resistant strains. The potential for metabolite leakage during the washing step was examined by comparing washed and unwashed cell extracts, and analysing the washing waste supernatant. The hierarchical clustered heat map demonstrated that the washing step with 0.9% NaCl successfully removed the majority of culture media components (Figure 2.3A). Recovery of intracellular metabolites (those not present in the broth) was not substantially impacted by washing. Analysis of the supernatant from the washing waste detected leakage of certain cell-derived metabolites, but at very low levels relative to the levels within the cell pellets. Furthermore, evaluation of four extraction solvents showed a total of 1099, 1104, 1070 and 1089 metabolites detected from the LC-MS analyses of metabolite samples extracted by the chloroform:methanol (CM; 1:2, v/v), chloroform:methanol:water (CMW; 1:3:1, v/v), 60% ethanol (60EtOH) and absolute methanol (MeOH) solvents, respectively. CMW was the most promising solvent, demonstrating efficient extraction of a wide range of metabolite classes (Figure 2.3B). In addition, the median relative standard deviation (RSD) for all metabolites in the CMW samples was 22%, which is within an acceptable range and is comparable to the standard MeOH extraction solvent (Table 2.3). In comparison, CM and 60EtOH extraction solvents showed median RSD values of 25% and 24%, respectively. Peak intensities and RSD values for a number of common metabolites are provided in Table 2.3, showing that CMW was the most reproducible compared to the other three extraction solvents.

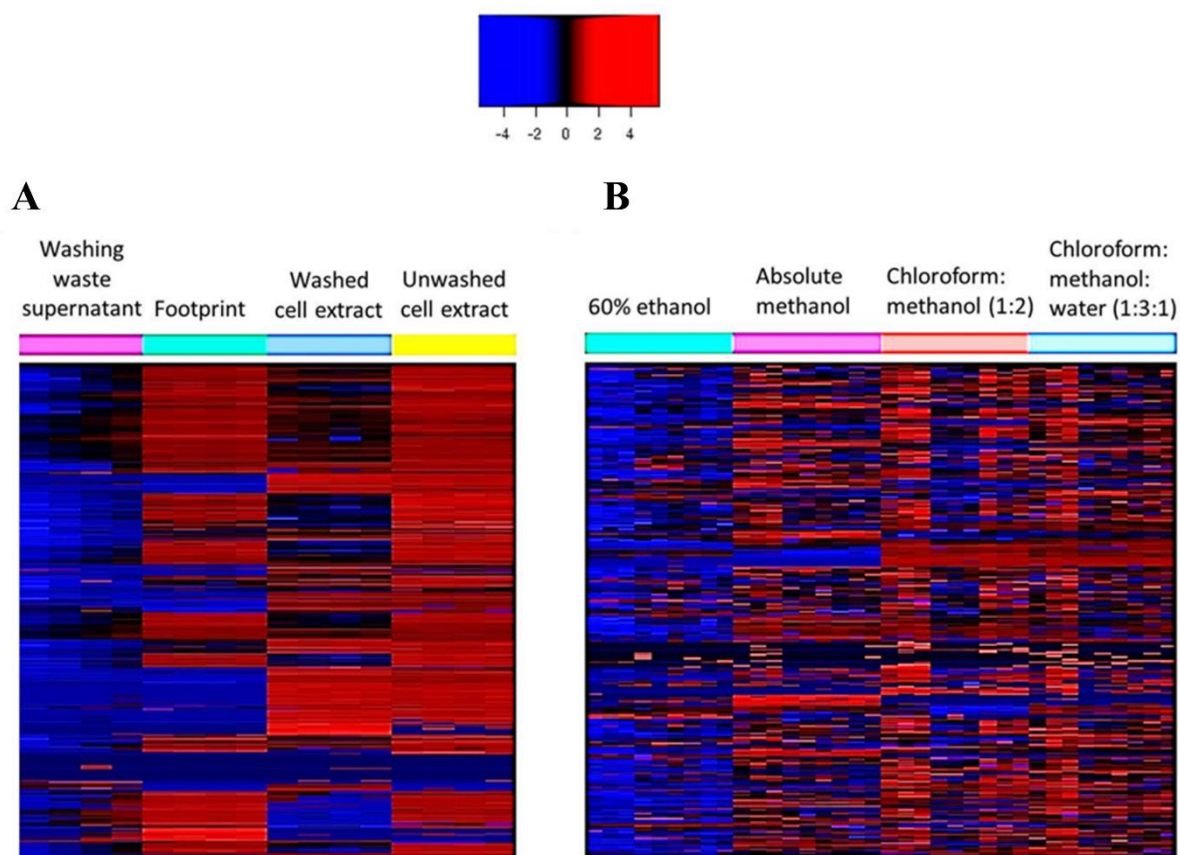


Figure 2.3. Evaluation of washing step and extraction solvents in the sample pre-treatment method. (A) Clustered heat map distinguished the total metabolite recovery between cells subjected to washing with 0.9% NaCl and without washing. (B) Comparison of four different extraction solvents on the global metabolite recovery in *A. baumannii*: 60% ethanol, absolute methanol, chloroform:methanol (1:2, v/v), and chloroform:methanol:water (1:3:1, v/v).

Table 2.3 Validation and reproducibility of metabolite extraction procedure for four different extraction solvents. CM, chloroform:methanol (1:2, v/v); CMW, chloroform:methanol:water (1:3:1, v/v); 60EtOH, 60% ethanol; MeOH, absolute methanol (3 biological samples with 3 technical replicates per condition). *NA, not available as the metabolite was not detected. Data are expressed as mean relative intensity (relative standard deviation, RSD, %).

	CM	CMW	60EtOH	MeOH
Median RSD value (%)	25	22	24	20
Identified compound				
Amino acids				
L-Lysine	4.1 x 10 ⁷ (20.7)	5.7 x 10 ⁷ (16.1)	4.1 x 10 ⁷ (20.4)	4.2 x 10 ⁷ (27.6)
L-Serine	1.7 x 10 ⁷ (22.2)	1.7 x 10 ⁷ (13.7)	1.3 x 10 ⁷ (15.7)	1.8 x 10 ⁷ (7.3)
L-Tyrosine	9.7 x 10 ⁷ (14.0)	9.5 x 10 ⁷ (12.8)	5.6 x 10 ⁷ (17.6)	1.1 x 10 ⁸ (11.2)
L-Methionine	1.8 x 10 ⁸ (11.9)	1.7 x 10 ⁸ (13.9)	1.2 x 10 ⁸ (14.5)	1.9 x 10 ⁸ (10.4)
L-Phenylalanine	3.0 x 10 ⁸ (13.4)	2.7 x 10 ⁸ (13.0)	1.8 x 10 ⁸ (10.8)	2.7 x 10 ⁸ (9.5)
L-Valine	1.0 x 10 ⁷ (14.1)	9.6 x 10 ⁶ (10.2)	7.4 x 10 ⁶ (13.7)	1.0 x 10 ⁷ (5.6)
L-Aspartate	2.8 x 10 ⁷ (11.8)	2.5 x 10 ⁷ (9.4)	2.2 x 10 ⁷ (10.5)	2.6 x 10 ⁷ (6.3)
Energy				
NADPH	5.4 x 10 ⁵ (45.0)	1.6 x 10 ⁶ (11.5)	3.8 x 10 ⁵ (48.3)	6.9 x 10 ⁵ (35.1)
NAD ⁺	4.6 x 10 ⁷ (33.0)	7.6 x 10 ⁷ (9.8)	3.4 x 10 ⁷ (16.1)	5.5 x 10 ⁷ (23.4)
FMN	4.7 x 10 ⁵ (31.3)	6.2 x 10 ⁵ (7.6)	NA*	4.0 x 10 ⁵ (61.7)
Nucleotides				
Adenine	6.7 x 10 ⁶ (46.7)	5.1 x 10 ⁶ (15.6)	2.3 x 10 ⁶ (41.8)	8.8 x 10 ⁶ (26.6)
Cytidine	9.1 x 10 ⁶ (24.1)	8.7 x 10 ⁶ (11.9)	4.0 x 10 ⁶ (10.9)	8.1 x 10 ⁶ (10.1)
Guanine	2.1 x 10 ⁵ (38.6)	2.1 x 10 ⁵ (12.6)	1.5 x 10 ⁵ (28.2)	2.5 x 10 ⁵ (12.9)
Uridine	8.7 x 10 ⁶ (19.2)	8.2 x 10 ⁶ (14.0)	5.0 x 10 ⁶ (15.2)	1.0 x 10 ⁷ (17.3)
Carbohydrate				
Pyruvate	3.0 x 10 ⁵ (19.8)	3.0 x 10 ⁵ (17.0)	2.4 x 10 ⁵ (25.2)	2.8 x 10 ⁵ (10.7)
Sucrose	2.0 x 10 ⁶ (39.2)	1.9 x 10 ⁶ (13.5)	1.1 x 10 ⁶ (13.7)	1.8 x 10 ⁶ (14.7)
Citrate	1.7 x 10 ⁷ (38.7)	2.8 x 10 ⁷ (14.9)	2.7 x 10 ⁷ (20.4)	2.2 x 10 ⁷ (18.6)
cis-aconitate	2.3 x 10 ⁵ (29.3)	4.5 x 10 ⁵ (14.9)	2.6 x 10 ⁵ (17.8)	3.3 x 10 ⁵ (19.5)
Oxalate	2.5 x 10 ⁵ (22.7)	2.7 x 10 ⁵ (19.3)	2.8 x 10 ⁵ (29.2)	2.3 x 10 ⁵ (22.9)
(R,R)-Tartaric acid	3.2 x 10 ⁴ (19.4)	4.0 x 10 ⁴ (17.3)	3.4 x 10 ⁴ (23.3)	3.3 x 10 ⁴ (22.3)

2.4.3 *Multivariate and univariate metabolomics analyses were able to identify key differences between the polymyxin-susceptible and polymyxin-resistant A. baumannii strains*

The metabolomics data from the present LC-MS-based comparative untargeted metabolomics study were highly reproducible. The pooled quality control samples clustered tightly in the principal component analysis (PCA) plot, indicating small analytical variations among the samples (Figure 2.4). Furthermore, the median relative standard deviation (RSD) value for all metabolites in this study was less than 10% (i.e. within 5% retention time for identification of authentic standard). Global metabolome differences between four *A. baumannii* strains were visualised using PCA score plots (Figure 2.5A) and heat map profiles (Figure 2.6), and demonstrate that the polymyxin-resistant and polymyxin-susceptible strains differed significantly in their levels of a number of key cellular metabolites. PCA score plots also clearly show that there were global metabolic differences between the paired *A. baumannii* strains (Figures 2.5B and C). Interestingly, nearly 25% of metabolites in the LPS-deficient polymyxin-resistant strain 19606R, were significantly more abundant than the corresponding polymyxin-susceptible parent strain ATCC 19606 (Figure 2.5D). Peptides were highly enriched in 19606R, and it appears that many of the more abundant metabolites in this polymyxin-resistant strain 19606R were derived from the growth medium (Figure 2.6). The accumulation of medium components within cells was unique to the LPS-deficient 19606R, and was not apparent in the polymyxin-resistant clinical isolate 03-149.2. For univariate analyses, all the putatively identified cellular metabolites (i.e. those more abundant in cell pellets than in footprint samples) were further analysed to reveal those that showed at least 2-fold differences ($*p < 0.05$ and $**p < 0.01$) in relative abundance between the polymyxin-resistant and polymyxin-susceptible *A. baumannii* strains. Several cellular metabolites were differentially abundant in the polymyxin-susceptible ATCC 19606 and polymyxin-resistant 19606R strains including carbohydrate, amino acid, nucleotide and lipid metabolites. In comparison, there were very few metabolic

differences observed in the polymyxin-resistant clinical isolate 03-149.2 and polymyxin-susceptible clinical isolate 03-149.1 (Figure 2.5D).

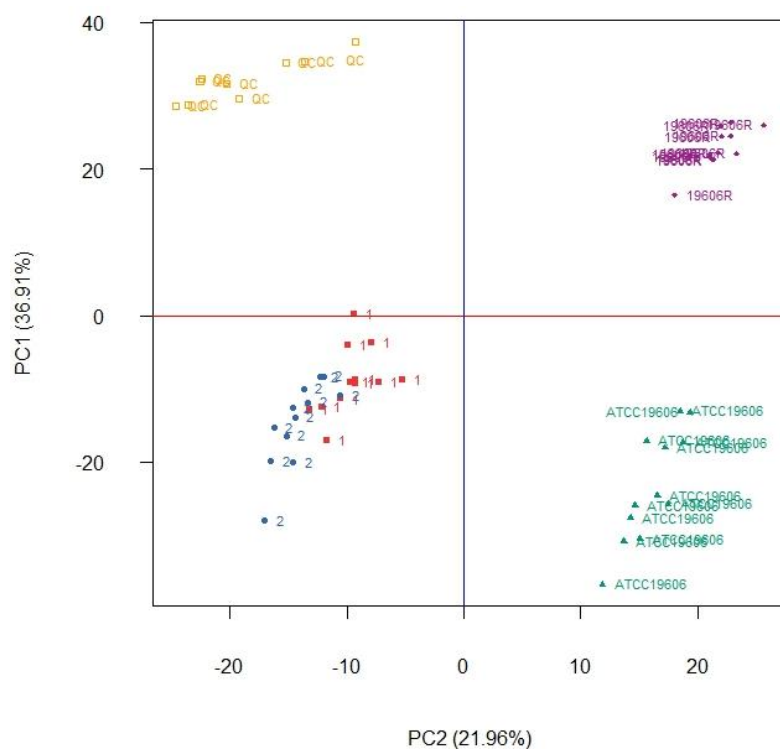


Figure 2.4. PCA score plot of the untargeted metabolomics dataset of paired polymyxin-resistant 19606R and the wild-type ATCC 19606 and paired of polymyxin-resistant 03-149.2 (blue and labelled with “2”) and polymyxin-susceptible 03-149.1 (red and labelled with “1”) clinical isolates. Each data set for individual strains represents a total of 12 sample replicates (3 biological replicates and each with 4 technical replicates). Yellow, pool quality control samples; purple, polymyxin-resistant 19606R; green, ATCC 19606; blue, polymyxin-resistant 03-149.2; and red, polymyxin-susceptible 03-149.1.

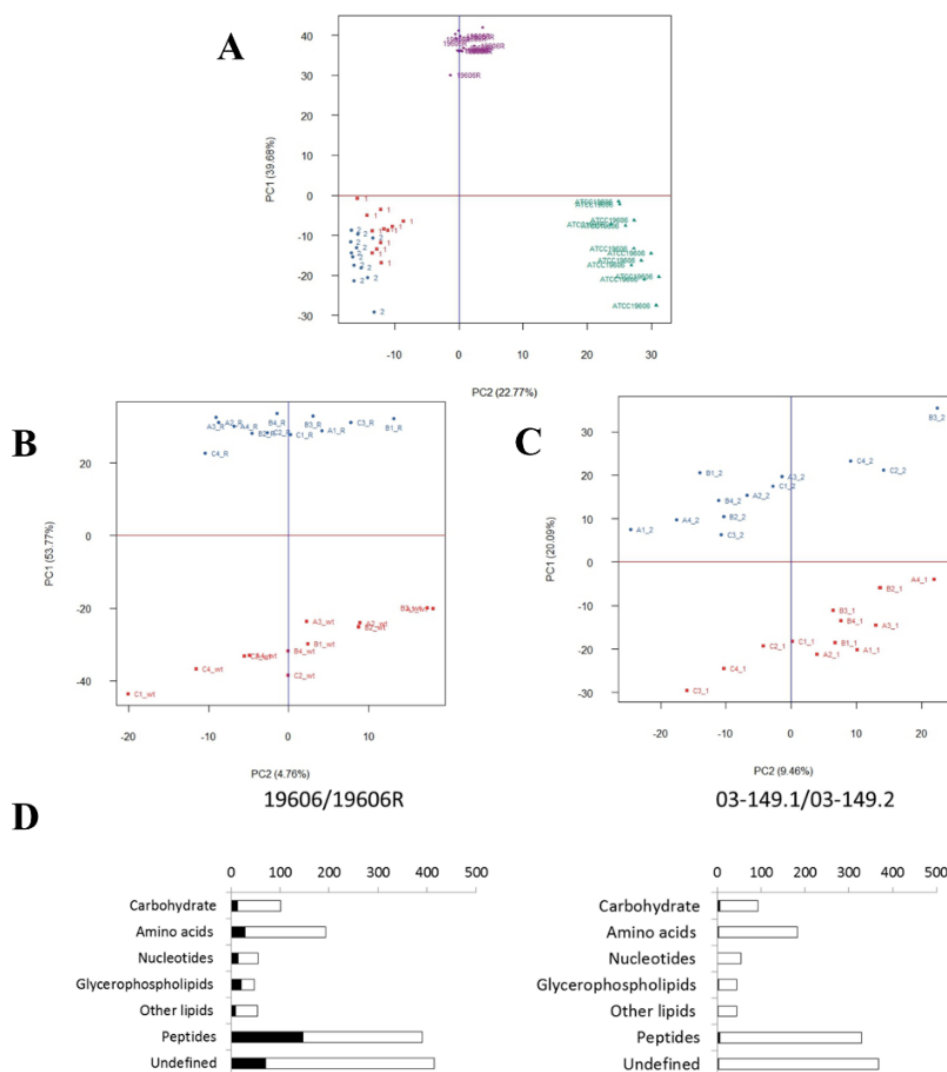


Figure 2.5. (A) PCA score plot of four *A. baumannii* strains. (B) PCA score plot of paired polymyxin-resistant 19606R and the wild-type ATCC 19606. (C) PCA score plot of paired polymyxin-resistant 03-149.2 and -susceptible 03-149.1 clinical isolates. Each data set for individual strains represents a total of 12 sample replicates (3 biological replicates and each with 4 technical replicates). (D) Pathway-focused representation of the significant metabolites (black bars) and total number of putatively identified metabolites (open bars) for the polymyxin-resistant 19606R relative to the wild-type ATCC 19606 (left) and the polymyxin-resistant clinical isolate 03-149.2 relative to the polymyxin-susceptible isolate 03-149.1 (right). Significant metabolites were selected by at least 2-fold difference ($p < 0.05$) in the metabolites levels of polymyxin-resistant strain relative to the polymyxin-susceptible strain.

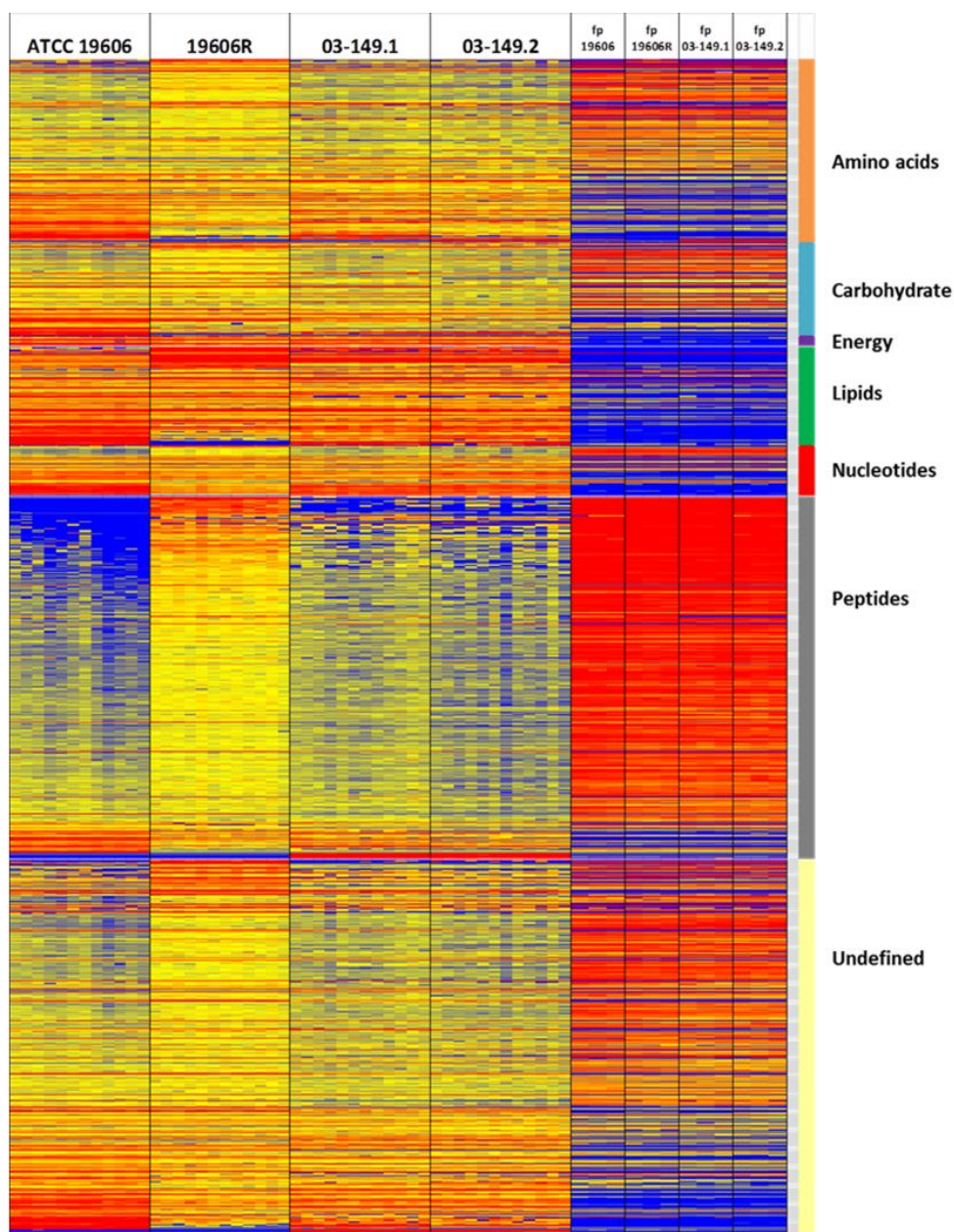


Figure 2.6. Heat map profiles of metabolite peak intensities in *A. baumannii*. Left: paired strains of ATCC 19606 and polymyxin-resistant 19606R, Right: paired clinical isolates polymyxin-susceptible 03-149.1 and polymyxin-resistant 03-149.2. Metabolites are grouped into different classes: amino acids, carbohydrates, energy, lipids, nucleotides, peptides and undefined. Metabolites derived from the footprint (fp) also represented in the heat map. The colors indicate the relative abundance of metabolites based on the relative peak intensity (red = high, yellow = no change, blue = undetectable).

2.4.4 *Perturbations in sugar and nucleotide metabolism*

The polymyxin-resistant strain 19606R showed significant perturbations of several putative sugar phosphate metabolites, including metabolites associated with the pentose phosphate pathway (PPP). In particular, over 2-fold ($p < 0.01$) higher levels were observed for two PPP metabolites, D-erythrose 4-phosphate and D-sedoheptulose 7-phosphate, whereas the PPP-derived nucleotide precursor, 5-phospho- α -D-ribose 1-diphosphate (PRPP) was more than 3-fold ($p < 0.01$) lower than the polymyxin-susceptible parent strain ATCC 19606 (Figure 2.7). On the contrary, the polymyxin-resistant clinical isolate 03-149.2 showed significantly lower abundance of the detected PPP metabolites, D-erythrose 4-phosphate, D-sedoheptulose 7-phosphate, D-glyceraldehyde 3-phosphate, and D-ribose 5-phosphate ($p < 0.05$) than the paired susceptible isolate 03-149.1.

Besides, the levels of most nucleotides were significantly lower in the polymyxin-resistant 19606R than the parent polymyxin-susceptible ATCC 19606 strain (Figure 2.8). However, there were no clear differences in nucleotide levels between the paired clinical isolates. Furthermore, two essential tricarboxylic acid (TCA) cycle intermediates, 2-oxoglutarate and *cis*-aconitate were identified at least 2-fold ($p < 0.05$) lower in relative abundance in the polymyxin-resistant 19606R cells (Figure 2.9). Other TCA cycle metabolites, acetyl-CoA, citrate, and succinate, showed a consistent pattern of lower relative abundance in the polymyxin-resistant strain 19606R, albeit with less than two-fold difference. Interestingly, a similar pattern of metabolic changes were observed in the polymyxin-resistant clinical isolate 03-149.2; which showed lower abundance of citrate, *cis*-aconitate, 2-oxoglutarate and succinate than the polymyxin-susceptible clinical isolate 03-149.1.

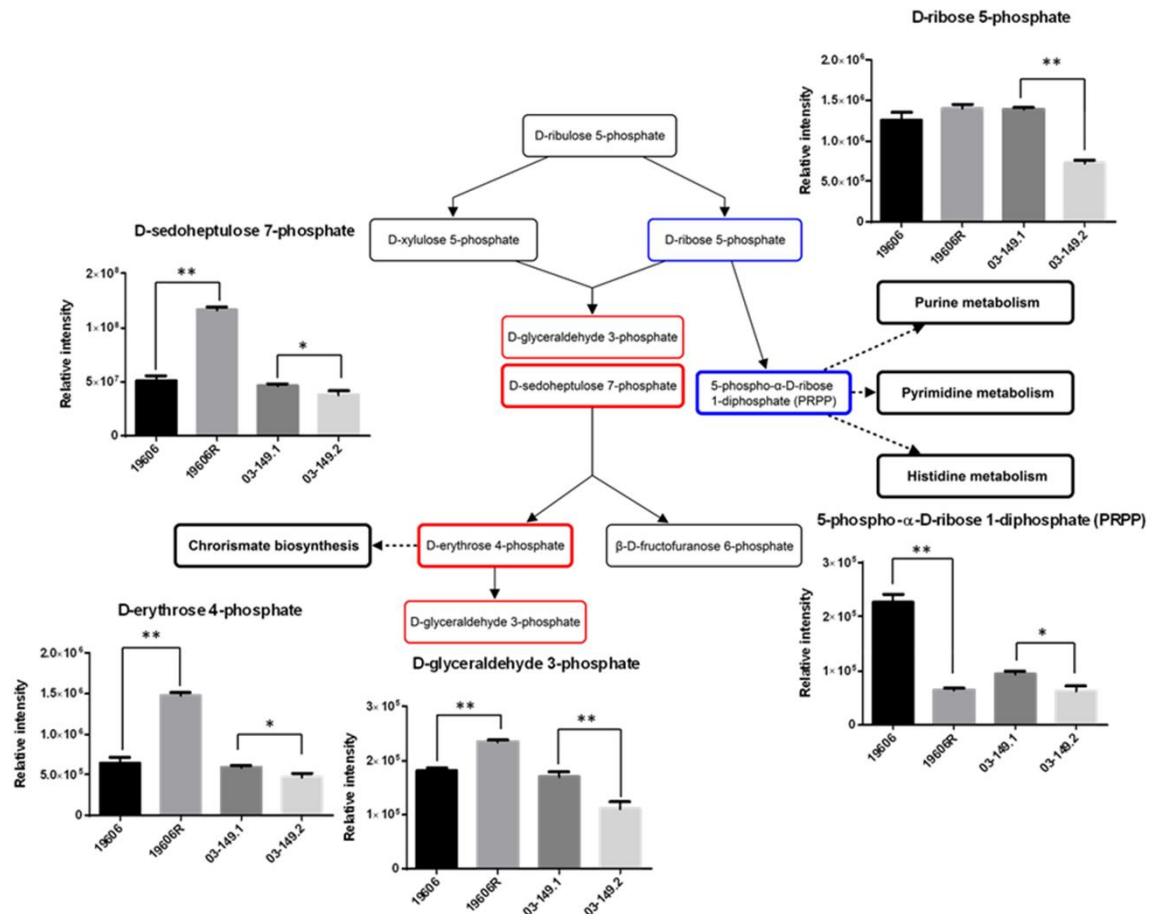


Figure 2.7. Perturbations of identified sugar phosphates in *A. baumannii*. Pentose phosphate pathway (PPP) of *A. baumannii*. PPP intermediates showed significant differences between polymyxin-resistant and polymyxin-susceptible *A. baumannii* strains. Metabolites in the red and bold box indicate metabolites that were at least 2-fold more abundant in polymyxin-resistant 16906R strain than polymyxin-susceptible ATCC 19606 strain. Metabolites in the red box indicate metabolites that were less than 2-fold higher in the 19606R strain. The blue and bold box indicates the metabolite that was at least 2-fold lower in 16906R than ATCC 19606. The blue box indicates the metabolite that was less than 2-fold lower in the 03-149.2 polymyxin-resistant strain than polymyxin-susceptible 03-149.1 strain. The black boxes indicate metabolites that were not detected. * $p < 0.05$; ** $p < 0.01$.

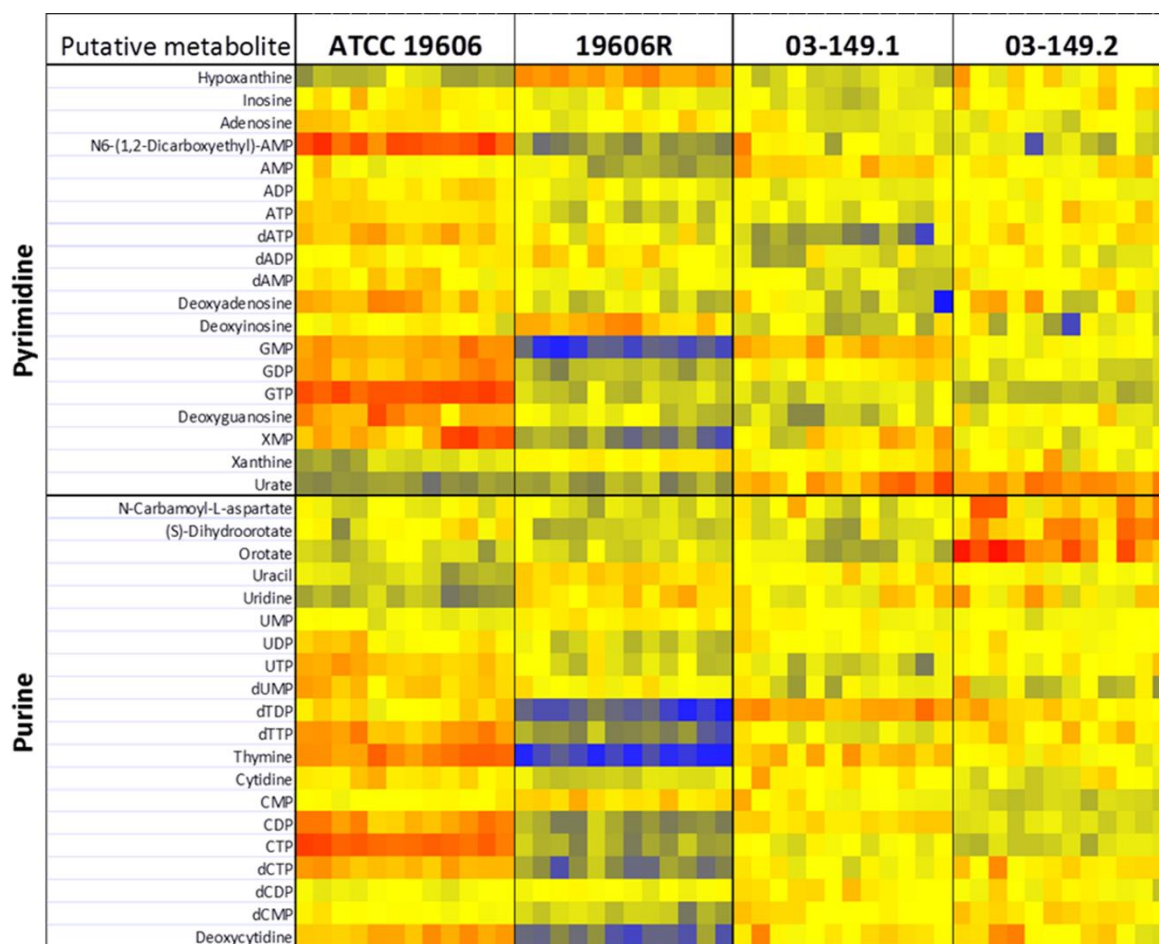


Figure 2.8. Heat map profiles of relative abundance of nucleotides. The polymyxin-resistant 19606R and its parent ATCC 19606 (left) and the clinical isolates polymyxin-resistant 03-149.2 and polymyxin-susceptible 03-149.1 (right). The colors indicate the relative abundance of metabolites based on the relative peak intensity (red = high, yellow = no change, blue = undetectable).

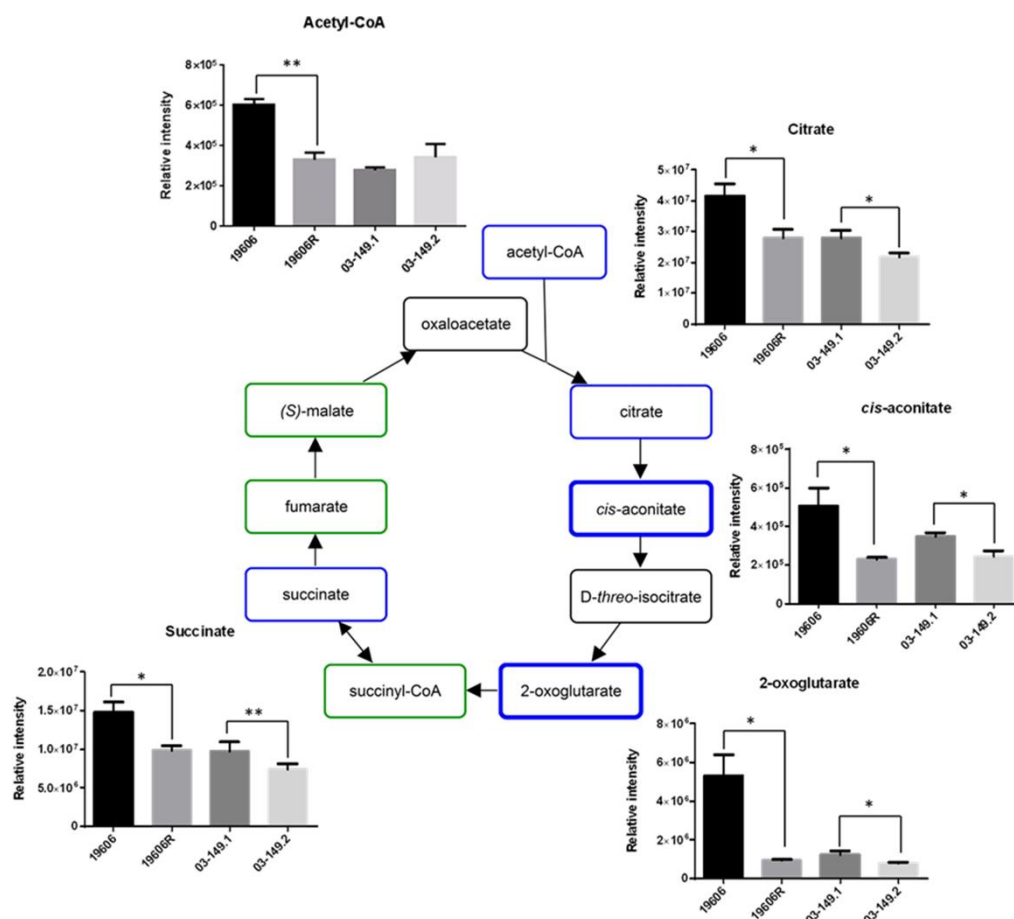


Figure 2.9. Perturbations of TCA cycle intermediates in *A. baumannii*. TCA cycle of *A. baumannii*. The blue and bold box indicates metabolites that were at least 2-fold less abundant in the polymyxin-resistant 19606R strain than polymyxin-susceptible ATCC 19606. Metabolites in the blue box indicate metabolites that were less than 2-fold lower in 19606R than ATCC 19606. The green boxes indicate metabolites that were detected but not significant. The black boxes indicate metabolites that were not detected. * $p < 0.05$; ** $p < 0.01$.

2.4.5 Variations of amino acid related metabolites in the polymyxin-resistant 19606R

The abundance of several metabolites involved in phenylalanine, tyrosine, tryptophan and histidine metabolic pathways were significantly ($p < 0.01$) perturbed in the polymyxin-resistant 19606R strain (Table 2.4). Most notably, two putative metabolites associated with the shikimate pathway, shikimate-3-phosphate and 5-O-(1-Carboxyvinyl)-3-phosphoshikimate were significantly higher in abundance (between 11- to 14-fold) in the polymyxin-resistant 19606R compared to the polymyxin-susceptible parent strain ATCC 19606. Significant depletion was observed in three important peptidoglycan biosynthesis intermediates, *N*-succinyl-L,L-2,6-diaminopimelate, *meso*-diaminopimelate and UDP-*N*-acetylmuramoyl-L-alanyl- γ -D-glutamyl-*meso*-2,6-diaminopimelate which were 2- to 5-fold lower in the polymyxin-resistant 19606R (Figure 2.10A). In addition, levels of these metabolites also decreased in the clinical polymyxin-resistant strain, 03-149.2. Interestingly, choline was undetectable in the polymyxin-resistant 19606R strain (Figure 2.10B), suggesting differential uptake or utilisation of this metabolite from the growth medium. Footprint analysis revealed complete depletion of choline from the growth medium for the polymyxin-resistant 19606R, but not for the polymyxin-susceptible ATCC 19606 or both of the clinical isolates.

Table 2.4 Fold changes (relative intensity) in the abundance of metabolites detected in the LPS-deficient polymyxin-resistant 19606R, relative to the parent strain ATCC 19606.

Formula	Putative metabolite ^a	Pathway/ metabolism	Fold change	<i>p</i> -value
Carbohydrate				
C ₅ H ₁₂ O ₅	Xylitol	Pentose and glucuronate interconversions	3.47	0.00017
C ₁₂ H ₂₃ O ₁₄ P	Lactose 6-phosphate	Galactose metabolism	2.14	0.0018
C ₃ H ₆ O ₉ P ₂	Cyclic 2,3-bisphospho-D-glycerate	Carbohydrate metabolism	-3.01	0.0035
Amino acids				
C ₇ H ₁₁ O ₈ P	Shikimate 3-phosphate	Phenylalanine, tyrosine, tryptophan biosynthesis	14.41	0.0012
C ₁₀ H ₁₃ O ₁₀ P	5-O-(1-Carboxyvinyl)-3-phosphoshikimate	Phenylalanine, tyrosine, tryptophan biosynthesis	11.30	0.0079
C ₈ H ₈ O ₅	3,4-Dihydroxymandelate	Tyrosine	3.03	0.00074
C ₄ H ₆ O ₃	2-Methyl-3-oxopropanoate	Valine, leucine and isoleucine degradation	2.19	0.00060
C ₂ H ₅ O ₅ P	Acetyl phosphate	Taurine and hypotaurine	2.15	9.2E-05
C ₉ H ₈ O ₃	Phenylpyruvate	Phenylalanine	-2.00	5.9E-05
C ₉ H ₁₀ O ₄	3-(2,3-Dihydroxyphenyl)propanoate	Phenylalanine	-2.03	0.0011
C ₁₃ H ₁₅ NO ₆	4-Hydroxyphenylacetylglutamic acid	Tyrosine	-2.08	0.0077
C ₇ H ₁₅ NO ₃	L-Carnitine	Lysine degradation	-2.57	0.00049
C ₆ H ₆ N ₂ O ₂	Urocanate	Histidine	-3.75	0.0031
C ₆ H ₁₀ N ₂ O ₄	<i>N</i> -Formimino-L-glutamate	Histidine	-24.86	0.00095

^a Putative metabolites, identified by exact mass, with at least 2-fold differences at $p < 0.01$ between the polymyxin-resistant 19606R and the polymyxin-susceptible ATCC 19606.

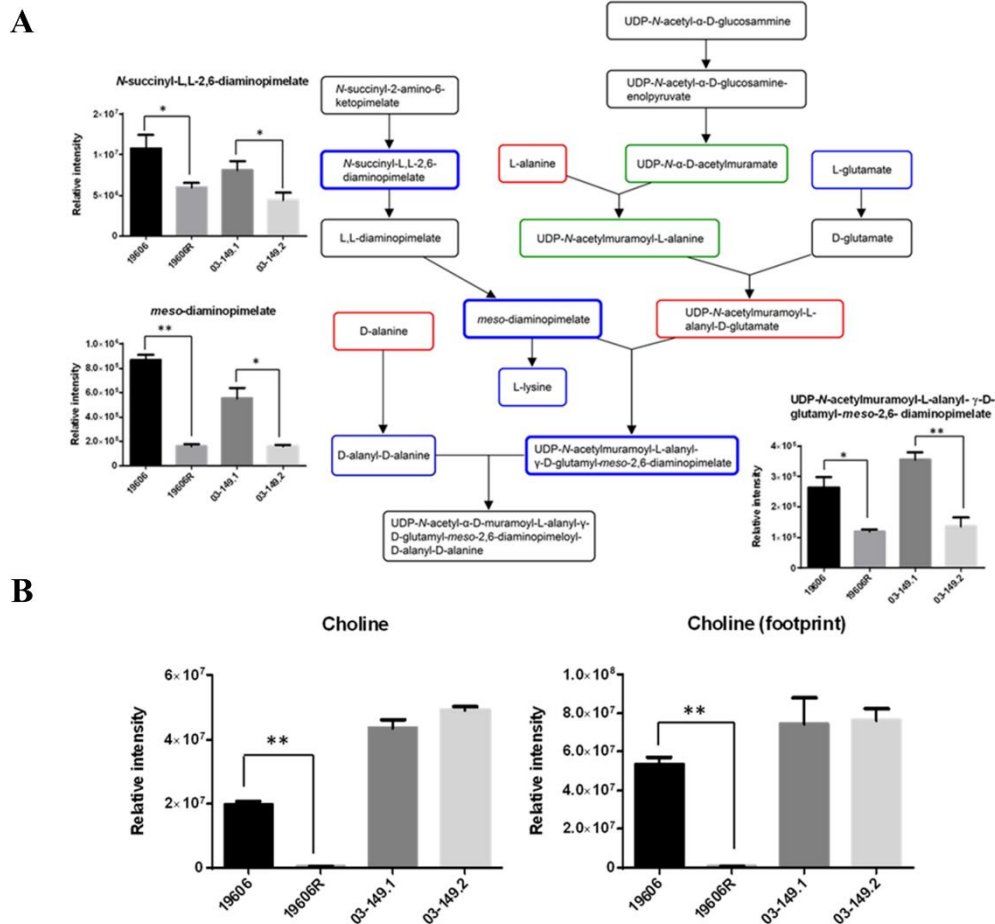


Figure 2.10. Low levels of peptidoglycan biosynthesis metabolites were observed in the polyxmyxin-resistant *A. baumannii*. (A) Peptidoglycan synthesis pathway of *A. baumannii*. Metabolites in the red box indicate metabolites that were less than 2-fold higher in polyxmyxin-resistant strains than polyxmyxin-susceptible strains. The blue and bold boxes indicate metabolites that were at least 2-fold lower in polyxmyxin-resistant strains than polyxmyxin-susceptible strains. Metabolites in the blue box indicate less than 2-fold lower abundance in polyxmyxin-resistant strains than polyxmyxin-susceptible strains. The green box indicates metabolites that were detected but not significant. Metabolites in the black box were not detected. (B) Intracellular and footprint (extracellular) choline shows significantly lower abundance in the polyxmyxin-resistant 19606R than the parent wild-type ATCC 19606. * $p < 0.05$; ** $p < 0.01$.

2.4.6 Perturbation of lipids levels in the polymyxin-resistant 19606R

Analyses of cellular lipid metabolites in the polymyxin-resistant 19606R and polymyxin-susceptible ATCC 19606 revealed profound alteration ($p < 0.05$) of several putatively identified lipid metabolites. The observed accurate masses and retention times indicated that many of these lipids were unsaturated and oxidised fatty acids; precise identification of these fatty acids is beyond the scope of this study. High level identification of glycerophospholipids (GPs) based on molecular formula revealed significant perturbations in the major phospholipid species, glycerophosphoethanolamine (PE), glycerophosphoserine (PS), and glycerophosphoglycerol (PG). In general, GPs with shorter-chain fatty acids (total ≤ 32 carbons) were enriched in the polymyxin-resistant LPS-deficient 19606R, in addition to the shorter-chain lysophospholipids (≤ 18 carbons) (Figure 2.11A). Notably, lipids with longer-chain fatty acids (> 32 carbons) were generally depleted in the LPS-deficient 19606R. However, these trends were not observed in *A. baumannii* of both clinical isolates, polymyxin-susceptible 03-149.1 and polymyxin-resistant 03-149.2 (Figure 2.11B). Furthermore, two key metabolites linked with glycerophospholipid metabolism, ethanolamine phosphate and glycerophosphoethanolamine phosphate were significantly ($p < 0.05$) lower in abundance in the polymyxin-resistant 19606R than the polymyxin-susceptible parent strain ATCC 19606, but not significantly changed in both *A. baumannii* clinical isolates (Figure 2.11C).

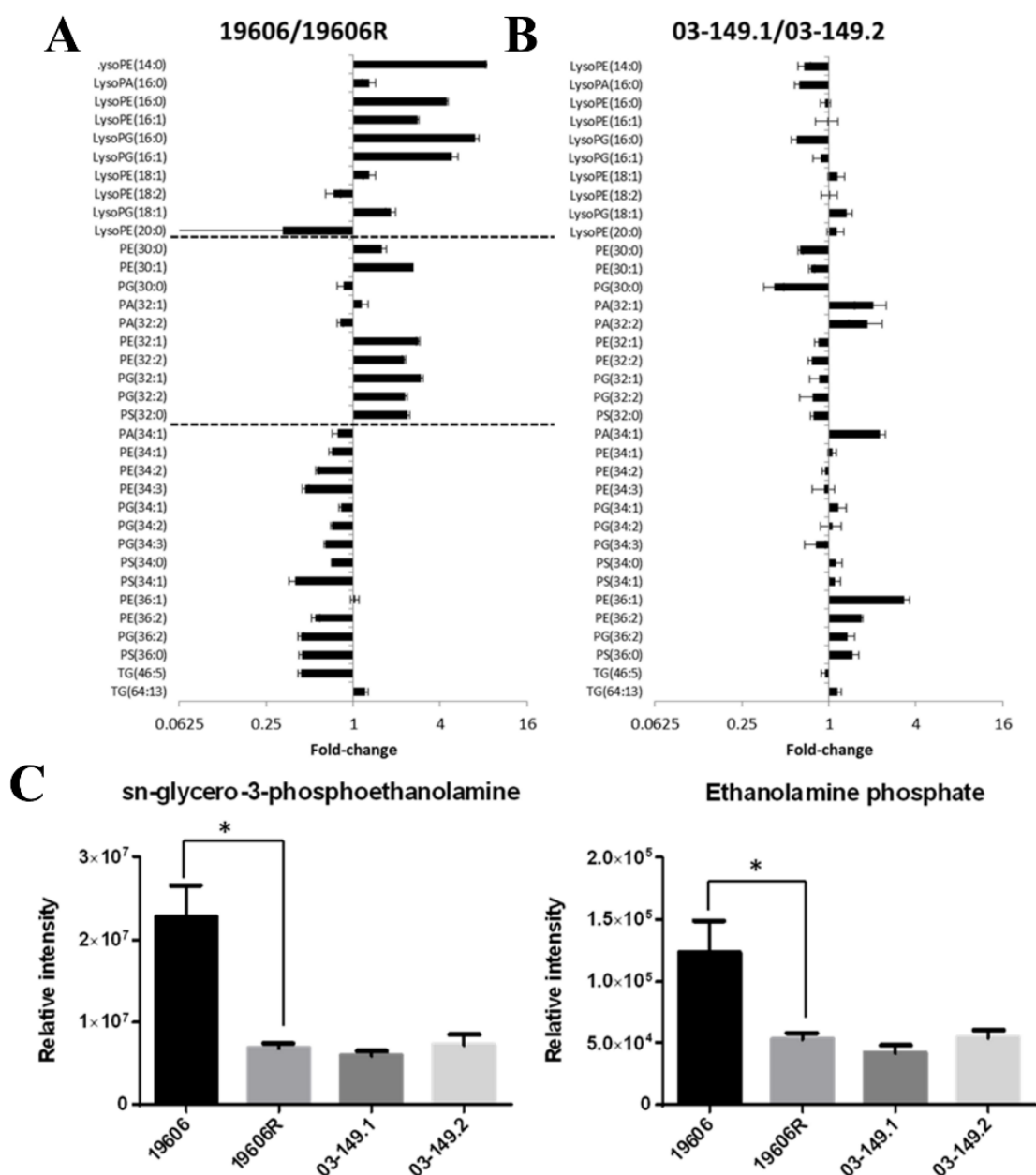


Figure 2.11. Relative intensity of glycerophospholipids levels. (A) LPS-deficient polymyxin-resistant 19606R and its parent strain ATCC 19606; and (B) polymyxin-resistant 03-149.2 and polymyxin-susceptible 03-149. (C) Glyceroethanolamine phosphate and ethanolamine phosphate showed significantly lower levels in the polymyxin-resistant 19606R than its parent ATCC 19606. PE, glycerophosphoethanolamine; PS, glycerophosphoserine; PG, glycerophosphoglycerols; PA, glycerophosphates. Fatty acyl carbon atom number and double bond number are shown in brackets. $*p < 0.05$.

2.4.7 *Untargeted analysis reveals unknown metabolites that are common to both polymyxin-resistant strains*

Four unidentified features were uniquely detected in both polymyxin-resistant strains and not in either of the polymyxin-susceptible strains. Whilst these features could not be identified based on existing bacterial metabolite databases, formula determination based on accurate mass, isotope abundance and retention time suggests that these unique metabolites may be complex amino-sugars: $C_{12}H_{24}N_2O_8$ (mass 324.153; t_R 14.7 min), $C_{30}H_{57}N_2O_{12}P_3$ (mass 730.312; t_R 17.2 min), $C_{13}H_{26}N_2O_6$ (mass 306.179; t_R 19.8 min), and $C_{16}H_{28}N_2O_{11}[Cl^-]$ (mass 460.146; t_R 13.7 min). Notably, three unidentified metabolites were detected in both polymyxin-susceptible strains, but were absent in both of the polymyxin-resistant strains. Accurate mass indicates that these features likely represent metabolites with the formulas $C_9H_{14}N_2O_5S$ (mass 262.063; t_R 13.4 min), $C_7H_{11}NO_3S$ (mass 189.046; t_R 7.5 min) and $C_{11}H_{19}N_3O_7S_2$ (mass 369.066, t_R 16.8 min). The latter formula corresponds to γ -glutamyl cystine, and the presence of sulfur in the other formulas suggest that they may also be cysteine conjugates.

2.5 Discussion

In recent times, untargeted metabolomics has been successfully applied towards the investigation of global metabolic profiles, particularly in microbiology and pharmacology (267, 281, 368). Advantageously, the untargeted metabolomics platform enables the detection of both known and unknown metabolites and has allowed the elucidation of complex interactions between cellular metabolites (280). Significantly, this global metabolomics approach has been beneficial in enhancing our understanding of the biological nature of antimicrobial resistance mechanisms. Global metabolic profiling distinguished differential metabolic patterns between antibiotic-susceptible and antibiotic-resistant strains of *A. baumannii*, *P. aeruginosa*, *Nocardiosis* spp., as well as the protozoan parasites *Trypanosoma brucei* and *Leishmania donovani* (369-373). In a

previous study, both planktonic and biofilm forms of *A. baumannii* were compared to identify metabolic profiles associated with biofilm synthesis (369). In the present study, we employed a global metabolic profiling strategy to identify key metabolic differences between two pairs of polymyxin-susceptible and polymyxin-resistant *A. baumannii* strains, specifically conferred by two different mechanisms of polymyxin resistance, LPS loss and lipid A modifications.

Gram-negative bacteria can develop resistance to most current antimicrobial agents because of their extraordinary metabolic versatility and adaptability to a wide range of environmental conditions (351). The main mechanisms used for conferring polymyxin resistance in Gram-negative bacteria involved modifications of lipid A, the membrane embedded component of LPS (11). In a previous study, we discovered that *A. baumannii* can develop resistance to very high colistin concentrations through a complete loss of LPS, due to spontaneous mutations in any of the three key lipid A biosynthetic genes (44). Polymyxin resistance in 19606R was shown to be conferred by a spontaneous single mutation in *lpxA* gene, resulting in LPS loss (44). RNA expression profiling of polymyxin-resistant 19606R by our group indicated that significant outer-membrane remodelling occurs due to LPS loss (356). This included increased expression of genes involved in cell envelope and membrane biogenesis, in particular the Lol lipoprotein transport system, the Mla-retrograde phospholipid transport system and poly- β -1,6-*N*-acetylglucosamine (PNAG) biosynthesis (356). In addition, polymyxin-resistant 19606R displays a decreased expression of genes predicted to encode the fimbrial subunit FimA and components involved in the type VI secretion system (T6SS) (356).

Our genome sequencing data for the polymyxin-resistant isolate 03-149.2 show that the deletion of 3 bases in the *pmrB* gene conferred an in-frame deletion of alanine 28. This particular mutation has not been characterised previously. However, mutations in *pmrB* have repeatedly been shown

to cause polymyxin resistance in *A. baumannii* by the up-regulation of the phosphoethanolamine transferase, *pmrC*, and subsequent lipid A modification (25). Furthermore, structural analyses of lipid A from both polymyxin-susceptible 03-149.1 and polymyxin-resistant 03-149.2 clinical isolates revealed lipid A modifications with pEtN and GalN in the polymyxin-resistant 03-149.2 strain (Figure 2.2). These lipid A modifications play a role in polymyxin resistance similar to that of aminoarabinose modification in other Gram-negative bacteria (121, 374) which reduce the initial electrostatic interaction with polymyxins by reducing the negative charge on the bacterial outer membrane (11, 91, 375). The results clearly indicate that the mechanism of polymyxin resistance in the polymyxin-resistant 03-149.2 isolate differs from the *A. baumannii* 19606R resistant strain, which was due to the complete loss of LPS (44).

Careful assessment of sample preparation methods is an important pre-requisite step to generate physiological metabolome data based on the differences in cell composition and culture condition (310). In our study, the effect of the washing step and the efficiency of four different extraction solvents were firstly examined. Since a very rich culture medium, CaMHB was used in this study, a washing process was essential to avoid medium effects and to ensure that detected metabolites solely derive from cells (309). Desirably, the leakage of intracellular metabolites into its extracellular environment should be avoided during the washing step (312). As washing with organic solvents at sub-zero temperature leads to the leakage of cellular metabolites (376), we implemented a quenching step at 0°C and washing in aqueous buffer 0.9% NaCl (4°C). The washing process was effective in eliminating most of the extracellular contaminants from the rich growth media whilst avoiding significant leakage of intracellular metabolites. Furthermore, the ideal extraction solvent should be able to extract a broad range of metabolites with different physicochemical properties in high and reproducible yield (377). Several extraction solvents have been reported in the literature for bacterial metabolomics, and four promising solvent

compositions were selected to determine the optimal extraction method specifically for *A. baumannii* in the present study. Unsurprisingly, our analyses showed that different extraction solvents preferentially extract certain metabolites depending on the polarity of the solvent. Overall, CMW (1:3:1, v/v) provided the greatest recovery and reproducibility for the largest number of different classes of metabolites, and is suitable to be used as a one-step method for untargeted metabolomics studies of *A. baumannii*.

Metabolic fingerprinting of two pairs of polymyxin-susceptible and polymyxin-resistant *A. baumannii* strains demonstrated accumulation or depletion of specific metabolite pools, indicating differential regulation of particular metabolic pathways. Interestingly, PCA plots clearly distinguished the metabolic profile differences between the polymyxin-resistant strain 19606R and the three other *A. baumannii* strains, signifying that the metabolic differences were substantially driven by the complete loss of outer membrane LPS. Notably, there were clear metabolic differences between the polymyxin-susceptible ATCC 19606 and polymyxin-resistant 19606R. In contrast, relatively very few metabolite differences were identified between the *A. baumannii* clinical isolates, polymyxin-susceptible 03-149.1 and polymyxin-resistant 03-149.2, demonstrating that lipid A modifications had minimal impact on the global metabolic profile. In general, the results show that different mechanisms of polymyxin resistance lead to unique changes in global metabolic profiles.

Our results demonstrate that peptides derived from the medium component were substantially accumulated in the polymyxin-resistant strain 19606R compared to other *A. baumannii* strains, and suggested that the uptake was facilitated significantly as a result of loss membrane integrity from the total LPS loss. The analyses of carbohydrate associated metabolites displayed higher levels of PPP intermediates in the polymyxin-resistant 19606R than in its susceptible parent

strain ATCC 19606. In contrast, the polymyxin-resistant 03-149.2 showed significantly lower levels of detected PPP-associated metabolites than the polymyxin-susceptible 03-149.1. However, a major end-product of the PPP, PRPP, was 3.5-fold lower in abundance in the polymyxin-resistant 19606R, suggesting diversion of flux through the non-oxidative branch of the PPP. PRPP is an essential precursor for both purine and pyrimidine nucleotide biosynthesis as well as for the biosynthesis of amino acids histidine and tryptophan (378). Coincidentally, decreased levels of nucleotides was observed in 19606R, as well as depletion of two histidine metabolites, *N*-formimino-L-glutamate (24-fold) and urocanate (3-fold), which may be secondary to the decreased concentration of PRPP. However, the significant depletion of nucleotide levels was not observed in the polymyxin-resistant 03-149.2 clinical isolate. The increased level of D-erythrose 4-phosphate (2-fold) generated in the PPP of the polymyxin-resistant 19606R strain appears to facilitate biosynthesis of the aromatic amino acids: phenylalanine, tyrosine and tryptophan through the shikimate pathway, as shown by the significant accumulation of two intermediates, shikimate-3-phosphate (14-fold) and 5-*O*-(1-Carboxyvinyl)-3-phosphoshikimate (11-fold) (379). Apart from the importance of PPP to conserve stable carbon equilibrium, to generate nucleotide and amino acid biosynthesis precursors and to supply reducing molecules for anabolism, PPP also has been found to be essential in the biosynthesis of LPS in Gram-negative bacteria (380). SHI, an enzyme that has been characterised in *Escherichia coli*, *P. aeruginosa* (381) and *Helicobacter pylori* (382) converts sedoheptulose 7-phosphate into the LPS precursor, glycerol-manno-heptose 7-phosphate (381, 383, 384). Interestingly, we identified that the level of this particular metabolite, D-sedoheptulose 7-phosphate was about 2-fold higher (** $p < 0.01$) than the other three *A. baumannii* strains. We hypothesised that, as the polymyxin-resistant 19606R is characterised by the total LPS loss (44), the metabolite, sedoheptulose 7-phosphate was significantly accumulated in the cells since it was not converted into the LPS precursor. The TCA cycle is another essential

central metabolic pathway in bacterial cells, providing substrates for energy and biosynthetic reactions, including precursors for lipids and amino acids (385). Notably, both polymyxin-resistant strains, 19606R and clinical isolate 03-149.2 showed lower abundance of TCA cycle metabolites than their respective polymyxin-susceptible strains. This suggested that, in general, the polymyxin-resistant strains produced less energy through TCA cycle indicating lower cellular metabolism than the polymyxin-susceptible strains and this was significantly observed particularly in the polymyxin-resistant strains, 19606R.

Three intracellular metabolites engaged in the peptidoglycan biosynthesis pathway, *meso*-diaminopimelate, UDP-*N*-acetylmuramoyl-L-alanyl- γ -D-glutamyl-*meso*-2-6-diaminopimelate, and *N*-succinyl-L,L-2,6-diaminopimelate were detected 2- to 5-fold less abundant in the polymyxin-resistant 19606R strain, compared to the parent strain ATCC 19606. Interestingly, these metabolites were also significantly decreased (2- to 3-fold) in the polymyxin-resistant clinical isolate 03-149.2. *Meso*-diaminopimelate is derived from lysine degradation and is conjugated with UDP-*N*-acetylmuramoyl-L-alanyl-D-glutamate (catalysed by MurE ligase) in the cytoplasm to form UDP-*N*-acetylmuramoyl-L-alanyl- γ -D-glutamyl-*meso*-2-6-diaminopimelate (386). This is followed by the addition of dipeptide D-alanyl-D-alanine to form UDP-*N*-acetylmuramoyl-L-alanyl-D-glutamyl-6-carboxy-L-lysyl-D-alanyl-D-alanine (catalysed by MurF ligase). In *E. coli*, the MurE and MurF ligases are encoded by the *murE* and *murF* genes, respectively, co-localised in the genome; these ligases are essential for bacterial viability and are targets for antibacterial chemotherapy (387). The lower levels of the peptidoglycan biosynthesis metabolites indicate that the polymyxin-resistant 19606R and clinical isolate 03-149.2 synthesised less peptidoglycan compared to their polymyxin-susceptible parent strains. Interestingly, choline levels were significantly depleted in the 19606R strain and its culture medium. In our recent transcriptomics study, the expression of choline dehydrogenase, choline-

glycine betaine transporter and choline transport protein BetT was significantly increased (3.0, 3.0 and 4.6 folds, respectively) in the polymyxin-resistant *A. baumannii* 19606R (356). As choline uptake and metabolism have been associated with maintenance of osmotic balance in Gram-negative bacteria (383, 388), our transcriptomics and metabolomics data collectively indicate that choline was required by 19606R in response to the osmolarity pressure due to the less peptidoglycan caused by polymyxin resistance. However, there was no profound change in choline level in the polymyxin-resistant clinical isolate 03-149.2 proposing that choline was not utilised and the level was in equilibrium state between intracellular and extracellular.

The outer membrane (OM) of Gram-negative bacterial cells is composed of an asymmetrical bilayer consisting of an outer leaflet with LPS as a major component, and the inner leaflet mainly containing glycerophospholipids (GPs) (389). The OM serves as an efficient permeability barrier and a first-line defence mechanism, and GPs are the most prevalent component of lipids in the bacteria OM (390). Compared to GPs species in the samples obtained from ATCC 19606, the LPS-deficient, polymyxin-resistant 19606R produced relatively high levels of GP species PE, PS and PG with shorter fatty acyl chains (less than 32 carbons in both chains) and concomitantly less GP species with more than 34 carbons in their fatty acyl chains. This finding agrees with a previous report that showed a LPS-deficient *Neisseria meningitides* mutant preferentially incorporated saturated PE and PG species with shorter fatty acyl chains into its OM (124). Furthermore, the higher abundance of lyso-GPs (those with a single fatty acid chain less than 18 carbons) in the polymyxin-resistant 19606R, compared to the parent strain ATCC 19606, indicate significant GPs turnover; hence, our result supports the hypothesis that the OM structure of polymyxin-resistant bacterial cells is dramatically altered due to LPS loss. The observed increase in the production of GPs, which we hypothesise are mainly exported to the outer leaflet of the OM of the LPS-deficient strain 19606R, further supports the previously described the

compensatory mechanism for the LPS loss which associated with increase in cell envelope and membrane biosynthesis (356). Transcriptomics analyses of the LPS-deficient strain 19606R revealed that there was a significant increase in the expression of genes involved in phospholipid transport (*mlaBCD*) in response to the LPS loss (356). Remarkably, glycerophosphatidylethanolamine phosphate and ethanolamine phosphate showed significantly lower levels in the polymyxin-resistant 19606R than its parent ATCC 19606. Ethanolamine utilisation was suggested to associate with bacterial pathogenesis and virulence (391, 392). Our results support the claim and suggest that ethanolamine is crucial for bacterial metabolism, in particular in the polymyxin-resistant 19606R. The present study utilising HILIC chromatography does not represent the total phospholipid composition and does not reveal the relative distribution of each GP species in the inner and outer membranes of *A. baumannii*. Future membrane lipidomics analysis of LPS-deficient, polymyxin-resistant *A. baumannii* is underway and will further define the total lipid abundance and distribution.

In addition to the perturbations to known metabolic pathways, our untargeted metabolomics analysis revealed four unidentified metabolite features which are consistent with amino-sugars that were unique to the polymyxin-resistant strains, and not in either of the polymyxin-susceptible strains. Metabolite identification is a major bottleneck in untargeted metabolomics, and accurate identification of metabolites that are not present in existing databases requires large-scale fractionation and extensive structural analysis (393-395). Precise structural identification of the unknown metabolites that are unique to polymyxin-resistant strains is beyond the scope of the present study. Nevertheless, with the high-resolution mass spectrometry applied here, features can be annotated with the most likely molecular formulas. Whilst not conclusive, these unique unidentified metabolites suggest the involvement of glycan metabolism in the molecular mechanisms of polymyxin resistance in *A. baumannii*. Further studies are warranted to

characterise these unknown metabolites and their biological functions. Together with our metabolomics and transcriptomics results (356), it will provide additional information about the metabolic differences between polymyxin-susceptible and polymyxin-resistant *A. baumannii* (Figures 2.5 and 2.6).

2.6 Conclusions

To the best of our knowledge, this comparative untargeted metabolomics study is the first to demonstrate significant global metabolic changes in polymyxin-resistant *A. baumannii* strains. In particular, global metabolic differences are associated with different mechanisms of polymyxin resistance due to LPS loss and lipid A modifications. Our study provides a valuable insight into the global metabolism of polymyxin-resistant *A. baumannii* and potentially offers new therapeutic targets

Chapter Three

Part B**Monash University****Declaration for Thesis Chapter 3****Declaration by candidate**

In the case of Chapter 3, the nature and extent of my contribution to the work was the following:

Nature of contribution	Extent of contribution (%)
Design of the study, laboratory experiments, data analysis and interpretation, preparation of the initial draft of the manuscript and subsequent revisions, and formulation of the conclusions and hypothesis generation from the results of the study	80%

The following co-authors contributed to the work:

Name	Nature of contribution
Darren J. Creek	Supervision, advice regarding the thought and design of studies, data analysis and interpretation, review of manuscript drafts and revisions, and formulation of conclusions and hypotheses generation from the results of the study
Roger L. Nation	Advice regarding the thought and design of studies, review of manuscript drafts and revisions, and formulation of conclusions and hypotheses generation from the results of the study
Alan Forrest	Advice regarding the thought and design of studies, review of manuscript drafts and revisions, and formulation of conclusions and hypotheses generation from the results of the study
Brian T. Tsuji	Advice regarding the thought and design of studies, review of manuscript drafts and revisions, and formulation of conclusions and hypotheses generation from the results of the study
Tony Velkov	Supervision, advice regarding the thought and design of studies, data analysis and interpretation, review of manuscript drafts and revisions, and formulation of conclusions and hypotheses generation from the results of the study
Jian Li	Design of the study, supervision, advice regarding the thought and design of studies, data analysis and interpretation, review of manuscript drafts and revisions, and formulation of conclusions and hypotheses generation from the results of the study

The undersigned hereby certify that the above declaration correctly reflects the nature and extent of the candidate's and co-authors' contributions to this work*.

Candidate's Signature		Date 12 June 2017
----------------------------------	---	------------------------------

Main Supervisor's Signature		Date 12 June 2017
--	--	------------------------------

*Note: Where the responsible author is not the candidate's main supervisor, the main supervisor should consult with the responsible author to agree on the respective contributions of the authors.

Chapter 3: Untargeted metabolomics analysis reveals key pathways responsible for the synergistic killing of colistin and doripenem combination against *Acinetobacter baumannii*

3.1 Abstract

Combination therapy is deployed for the treatment of MDR *Acinetobacter baumannii*, as it can rapidly develop resistance to current antibiotics. This is the first study to investigate the synergistic effect of colistin and doripenem combination on the metabolome of *A. baumannii*. The metabolite levels of *A. baumannii* ATCC 19606 and a paired of clinical strains polymyxin-susceptible 03-149 and -resistant 03-149.2 were measured using LC-MS following treatment with colistin (2 mg/L) or doripenem (25 mg/L) alone, and their combination at 15 min, 1 hr and 4 hr (n=4). Colistin predominantly caused disruption of the bacterial outer membrane and cell wall, as shown by perturbation of glycerophospholipids and fatty acids in all the three *A. baumannii* isolates tested. Concentrations of peptidoglycan biosynthesis metabolites decreased in response to doripenem, reflecting its mode of action. The combination induced significant changes to more key metabolic pathways relative to either monotherapy. Down-regulation of cell wall biosynthesis (via D-sedoheptulose 7-phosphate, D-ribulose 5-phosphate) and nucleotide metabolism (via D-ribose 5-phosphate, PRPP) particularly in the *A. baumannii* ATCC 19606 and 03-149.1 strains were associated with perturbations in the pentose phosphate pathway. Notably, the synergistic killing of the combination against the polymyxin-susceptible ATCC 19606 and 03-149.1 displayed common metabolic changes via the time-dependent inhibition of key metabolic pathways. In contrast, the elevated abundances of metabolites (e.g. nucleotides, amino acids) in the *A. baumannii* 03-149.2 strain presumably was the general antibiotic stress response induced by colistin alone and the combination. Overall, our study highlights the significant potential of systems pharmacology in elucidating the mechanism of synergy and optimising antibiotic pharmacokinetics and pharmacodynamics.

3.2 Introduction

MDR *A. baumannii* has been classified by CDC as a “Serious Threat” which is responsible for a plethora of nosocomial infections including pneumonia, bacteraemia, wound infections, urinary tract infections and meningitis (8, 351, 396). As one of the six significant ESKAPE ‘superbugs’ identified by the IDSA, *A. baumannii* represents a challenge as it can rapidly develop resistance to all clinically available antibiotics (6, 397, 398). *A. baumannii* exhibits a wide array of antibiotic resistance strategies, including degradation and modification of enzymes, alteration of target binding sites and activation of efflux pumps (399).

Due to the dry antibiotic discovery pipeline, the re-utilisation of the ‘old’ polymyxin class of antibiotics has become essential for the treatment of life-threatening infections caused by MDR *A. baumannii* (354). Polymyxin B and colistin (i.e. polymyxin E) are non-ribosomal cyclic lipopeptides that contain six basic L- α - γ -diaminobutyric acid (Dab) residues, two hydrophobic amino acids, and an *N*-terminal fatty acyl group (Section 1.3.1) (11). Polymyxins interact electrostatically with the phosphate groups of the lipid A component of lipopolysaccharide (LPS) followed by non-polar interactions of hydrophobic domains on both molecules to initiate the rapid bactericidal effect (Section 1.3.3) (11, 400). Destabilisation of the LPS leaflet of the outer membrane has generally been thought to cause local disturbance, osmotic imbalance and finally cell death, although the ultimate mechanism of cell death is not completely understood (96).

Polymyxin monotherapy may lead to treatment failure as it is not always possible to generate reliably efficacious plasma exposure and bacterial resistance may emerge (Section 1.3.5) (45, 48, 212, 401-403). *A. baumannii* can become resistant to polymyxins by the addition of phosphoethanolamine (pEtN), galactosamine (GalN) or both (41-43, 404-406) to its lipid A structure, or by the loss of LPS (Section 1.3.4) (44). These modifications significantly reduce

the negative charge on the bacterial outer membrane, thus diminishing the binding of polymyxins (11). A number of *in vitro* studies have shown that colistin and doripenem combination therapy is synergistic against MDR *Pseudomonas aeruginosa*, *Klebsiella pneumoniae* and *A. baumannii* (222-226, 407). In addition, the colistin-carbapenem combination has been shown to significantly limit the emergence of colistin resistance in *A. baumannii* (16). Therefore, polymyxin-carbapenem combinations are often employed to enhance therapeutic response and minimise potential polymyxin resistance.

The mechanisms that underlie the synergistic action of polymyxins and carbapenems have not been fully elucidated. Metabolomics provides the opportunity to gain a system-wide snapshot of cellular biochemical networks under defined conditions, and has been increasingly employed in bacterial physiology and drug discovery to elucidate the mechanism of drug action (304, 408-410). Furthermore, a detailed understanding of cellular metabolic perturbations in response to antibiotic treatment can potentially facilitate the discovery of novel alternative drug targets (248). To elucidate the mechanism of synergistic killing of the colistin and doripenem combination against *A. baumannii*, we conducted an untargeted metabolomics study. Our study is the first to reveal the metabolic perturbations induced by the combination were predominantly associated with the effect of colistin at the early time points (15 min and 1 hr), followed by the effect of doripenem at the later time points (4 hr). Notably, significant metabolic changes via disorganisation of membrane lipids and depletion of nucleotides, energy and amino sugar metabolites were evident following treatment with colistin alone, and were enhanced by its combination with doripenem. Our data provide a novel insight into the mechanism of synergistic killing against *A. baumannii* by the colistin-doripenem combination.

3.3 Materials and methods

3.3.1 Strains, antibiotics and reagents

A. baumannii ATCC 19606 (American Type Culture Collection [ATCC], Manassas, USA) was susceptible to both colistin and doripenem with MICs of 1 mg/L for both antibiotics. The pair of *A. baumannii* strains, 03-149.1 and 03-149.2 were clinically isolated from the similar patient (189). The 03-149.1 and 03-149.2 strains were polymyxin-susceptible (MIC 1 mg/L) and polymyxin-resistant (MIC > 32 mg/L), respectively and both were resistant to doripenem (MIC > 32 mg/L). The strains were grown in cation-adjusted Mueller-Hinton broth (CaMHB; Oxoid, Australia; 20 - 25 mg/L Ca²⁺ and 10 - 12.5 mg/L Mg²⁺). Colistin (Sigma-Aldrich, Saint Louis, USA) and doripenem (Doribax, Shinogi Inc, Osaka, Japan) were prepared using Milli-Q water (Millipore Australia, North Ryde, New South Wales, Australia) prior to each experiment and sterilised by filtration with a 0.22-µm pore size Millex GP filter (Millipore, Bedford, MA).

3.3.2 Bacterial culture preparation

The bacterial culture preparation for *A. baumannii* ATCC 19606 was conducted independently of the two *A. baumannii* clinical strains. Whereas the study for both *A. baumannii* clinical 03-149.1 and 03-149.2 strains was conducted in parallel. Culture of polymyxin-susceptible *A. baumannii* ATCC 19606 and 03-149.1 strains were prepared on nutrient agar plates while polymyxin-resistant 03-149.2 strain was plated on Mueller-Hinton agar supplemented with polymyxin B (10 mg/L) to maintain selection pressure. The plates were incubated for 16 - 18 hr at 37°C. For the overnight culture, colonies of *A. baumannii* strains were separately inoculated into 15 mL CaMHB and incubated for 16 - 18 hr at 37°C with shaking at 150 rpm. As different types of growth media have significant impacts on bacterial growth and antibiotic susceptibility, CaMHB was selected as the culture medium for PAO1 in this study. For the main culture, 1:100 dilution of the overnight culture was sub-cultured into four different reservoirs containing 200

mL fresh MHB and grown to an optical density at 600 nm (OD_{600}) of ~0.5 to achieve the starting inoculum $\sim 10^8$ colony-forming units (CFU)/mL (in order to obtain enough cells) of an early exponential growth phase. Bacterial culture was treated with colistin (2 mg/L), doripenem (25 mg/L) and combination of colistin and doripenem (2 mg/L + 25 mg/L, respectively); concentrations of colistin and doripenem were chosen based on their pharmacokinetics in patients (222). Bacterial culture without any antibiotic treatment served as a control. Four biological replicates were prepared independently from different colonies of *A. baumannii* ATCC 19606, 03-149.1 and 03-149.2 strains on different days.

3.3.3 Preparation of cellular metabolite extracts

The untargeted metabolomics study was performed to investigate global metabolic alterations in *A. baumannii* ATCC 19606 and paired clinical isolates polymyxin-susceptible 03-149.1 and -resistant 03-149.2 due to colistin, doripenem and the combination treatments in an *in vitro* static time-kill study. Cellular metabolites of *A. baumannii* were extracted by the previously optimised method with slight modifications (Section 2.3.4). Samples were collected before treatment with colistin, doripenem and the combination (i.e. time = 0), and at 15 min, 1 hr and 4 hr for metabolite extraction and viable counting. For the fingerprint samples (i.e. intracellular metabolites), 15 mL of the bacterial culture was collected and immediately transferred on ice. All the samples were rapidly quenched in a dry ice/ethanol bath and preserved on ice for all following steps. Samples were normalised by optical density ($OD_{600\text{ nm}}$) and centrifuged for 10 min at $3,220 \times g$ at 4°C. The supernatant was collected for extracellular metabolites (i.e. footprint). The cell pellets were washed three times with sterile saline (4°C) and centrifuged for 3 min at $3,220 \times g$ at 4°C. Cellular metabolites were extracted with chloroform:methanol:water (CMW, 1:3:1, v/v; -80°C) (total volume of 300 μ L) containing generic internal standards (CHAPS, CAPS, PIPES and TRIS) at 1 μ M. Samples were immediately frozen in liquid nitrogen

and allowed to thaw on ice, and the freeze-thaw process was repeated three times to lyse the cells and release cellular metabolites. The extracted samples were centrifuged for 10 min at $3,220 \times g$ at 4°C and the supernatant was collected and further centrifuged at $14,000 \times g$ for 10 min at 4°C . The final supernatant samples (200 μL) were collected into injector vials for LC-MS analysis. For footprint samples, aliquots of the culture supernatant were rapidly filtered through a 0.22- μm membrane filter, and 10 μL of the supernatant was mixed with 250 μL of CMW (1:3:1, v/v) and centrifuged at $14,000 \times g$ for 10 min at 4°C to collect particle-free supernatant for LC-MS analysis.

3.3.4 LC-MS analysis of metabolites

Samples were analysed on a Q-Exactive Orbitrap mass spectrometer (Thermo Fisher), coupled to a Dionex high-performance liquid chromatograph (U3000 RSLC HPLC, Thermo Fisher) with a ZIC-pHILIC column (5 μm , polymeric, 150×4.6 mm; SeQuant, Merck). The MS system was operated at 35,000 resolution in both positive and negative electro-spray ionisation (ESI) mode (rapid switching) and a detection range of 85 to 1,275 m/z . The LC mobile phase consisted of 20 mM ammonium carbonate (A) and acetonitrile (B) with a multi-step gradient system from 80% B to 50% B over 15 min, then to 5% B at 18 min, followed by a wash with 5% B for 3 min, and re-equilibration for 8 min with 80% B at a flow rate of 0.3 mL/min (122). The injection sample volume was 10 μL and the run time was 32 min. All samples were analysed in the same run and the chromatographic peaks, signal reproducibility and analyte stability were monitored by assessment of pooled biological quality control (PBQC) samples (aliquot of 10 μL of each sample, including both footprints and fingerprints) analysed periodically throughout the batch, internal standards and total ion chromatograms for each sample. Mixtures of pure standards containing over 200 metabolites were analysed within the batch to aid in the identification of metabolites.

3.3.5 Data processing, bioinformatics and statistical analyses

Metabolomics data analyses were performed as previously described in Section 2.3.6 using mzMatch (342) and IDEOM (<http://mzmatch.sourceforge.net/ideom.php>) (341). Quantification of each metabolite was conducted using the raw peak height. Univariate and multivariate analyses utilised MetaboAnalyst 3.0 (344). For the *A. baumannii* ATCC 19606, prior to analysis, relative peak intensity data were normalised by the median, log transformed and scaled (by auto scale function) to reduce variance between the samples. In turn, for the *A. baumannii* 03-14.9.1 and 03-149.2 isolates, the data were log transformed and scaled (by auto scale function) without median normalisation. The global metabolic profiles of samples with antibiotic treatments at each time point were analysed using multivariate statistical analysis by unsupervised principal component analysis (PCA). One-way Analysis of Variance (ANOVA) ($p < 0.05$, $\text{FDR} \leq 0.1$) for multiple comparison and post hoc analysis using Tukey's Honestly Significant Difference were applied to identify significant metabolite changes between treated and untreated control samples at each time point. Metabolites that were detected as isomeric peaks with opposite abundance changes (increased and decreased levels) were excluded. To further increase the reliability of the data, significant metabolites were filtered by selection of only those that showed a ≥ 1.5 -log₂-fold change relative to the untreated control samples and an identification confidence score of 6 or more in IDEOM (i.e. removing likely LC-MS artefacts). Metabolic pathway analysis was performed based on the statistically significant identified metabolites (≥ 1.5 -log₂-fold; $p \leq 0.05$, $\text{FDR} \leq 0.1$, one-way ANOVA for multiple comparison). Visualisation and Analysis of Networks containing Experimental Data (Vanted) software was utilised to visualise the associated metabolic pathways (367).

3.4 Results

Untargeted metabolomics was applied to profile the metabolic changes in *A. baumannii* ATCC 19606 and a pair of clinical isolates of polymyxin-susceptible 03-149.1 and -resistant 03-149.2 treated with colistin and doripenem mono- and combination therapy at 15 min, 1 hr and 4 hr. Four biological replicates were independently prepared from different cultures on separate days. The *A. baumannii* ATCC 19606 samples were analysed in a single LC-MS batch independently of the *A. baumannii* 03-149.1 and 03.149.2 samples. The time-kill kinetics curve demonstrates that there was no significant killing by colistin alone against ATCC 19606 strain at each time point whereas doripenem alone and the combination showed quite significant killing effect particularly at 1 hr (~ 0.5 -log) and 4 hr (~ 2 -log) (Figure 3.1A). To reduce the variance between the sample groups due to the killing effects of doripenem alone and the combination in the ATCC 19606 study, median normalisation was applied in the data analysis (detail is described in Section 3.3.5). Furthermore, colistin alone and the combination against 03-149.1 strain caused minimal killing at each time point whereas no effect induced by doripenem alone (Figure 3.1B). In turn, colistin alone caused no significant bacterial killing whereas there were slight killing by doripenem alone and in combination in the 03-149.2 strain at each time point (Figure 3.1C). Significant changes in the metabolite relative intensity levels between antibiotic treated samples and untreated control samples were defined as at least 1.5 log₂-fold difference (ANOVA for multiple comparison, $p \leq 0.05$, FDR ≤ 0.1). Global metabolome changes and the number of significantly perturbed metabolites following treatments with antibiotic at each time point were visualised by PCA plots and summarised in Venn diagrams, respectively (Figures 3.3 and 3.4). Metabolic pathway analysis then was performed based on the list of significantly altered metabolites to elucidate the modes of action of colistin and doripenem alone and in combination.

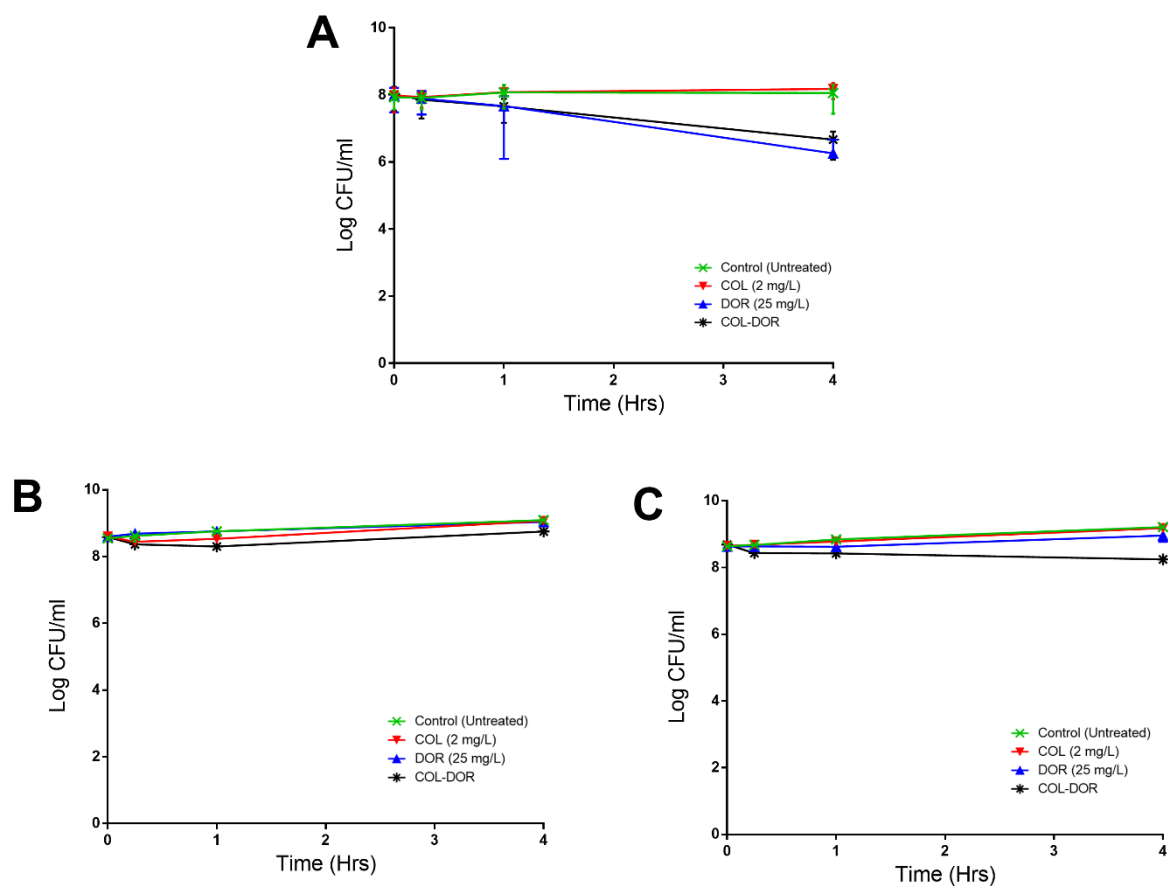


Figure 3.1. Time-kill kinetics of colistin and doripenem alone and in combination against *A. baumannii* isolates of polymyxin-susceptible (A) ATCC 19606, (B) 03-149.1 and polymyxin-resistant (C) 03-149.2.

Table 3.1 Data precision of individual samples represented as the median relative standard deviation (RSD, %) for *A. baumannii* strains ATCC 19606, 03-149.1 and 03-149.2 (n=4 biological replicates). Pooled biological quality controls = PBQCs.

	ATCC 19606	03-149.1	03-149.2
15 min			
Control	18	18	19
Colistin	28	18	24
Doripenem	19	21	19
Combo	30	17	16
1 hr			
Control	18	18	12
Colistin	23	22	17
Doripenem	22	16	18
Combo	19	26	23
4 hr			
Control	26	19	17
Colistin	24	17	14
Doripenem	29	19	18
Combo	21	21	15
PBQCs	14	11	11

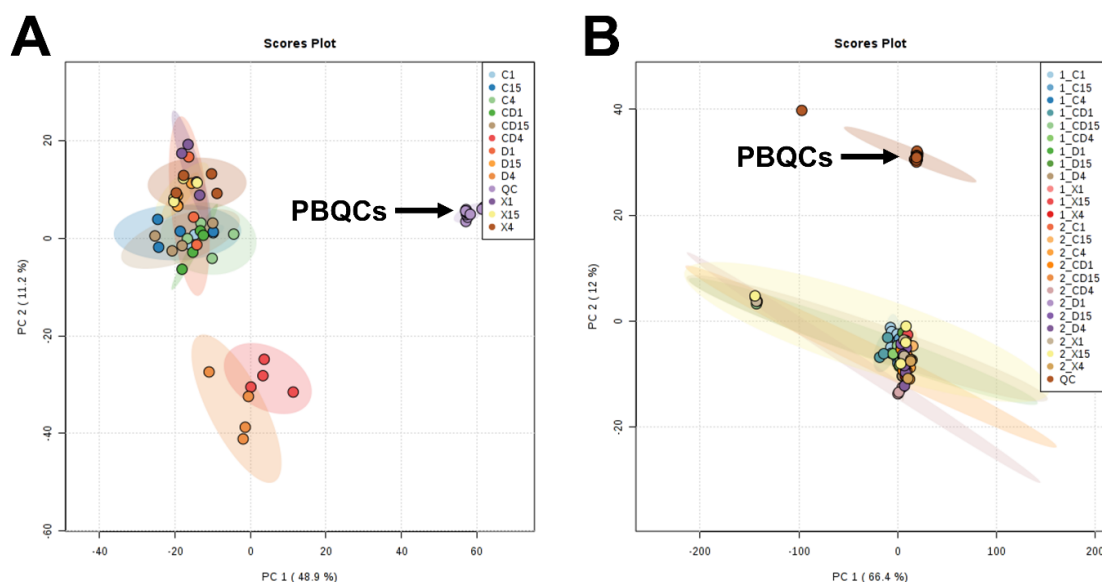


Figure 3.2. PCA score plots of all individual samples of *A. baumannii* (A) ATCC 19606 and (B) 03-149.1 and 03-149.2 strains treated with colistin and doripenem alone and in combination. Pooled biological quality controls (PBQCs) were analysed throughout each of the LC-MS batch for *A. baumannii* isolates ATCC 19606 and, 03-149.1 and 03-149.2.

3.4.1 *Multivariate and univariate analyses*

3.4.1.1 *A. baumannii ATCC 19606*

The within-experiment technical (analytical) variations were monitored based on periodic analysis of pooled biological quality control (PBQC) samples in the batch. We showed that the median relative standard deviation (RSD) of the PBQC, an indicator for analytical reproducibility, of ATCC 19606 study was 14% which is well within the acceptable limits for metabolomics ($\leq 20\%$) (Table 3.1) (411). In addition, the PCA plot showed the PBQC samples tightly clustered together, indicating minimal technical variation (Figure 3.2A). The median RSD value for each sample group was between 19-30%, showing the dynamics of bacterial metabolism due to antibiotic treatments (Table 3.1). A total of 1,577, 1,583, and 1,637 unique metabolites (carbohydrates, energy, amino acids, nucleotides, lipids, peptides, and others) were putatively identified at 15 min, 1 hr and 4 hr, respectively. Univariate analysis of these features revealed that 5-11% of metabolites were significantly altered following treatment with monotherapy and the combination at each time point (Figure 3.3B). Colistin induced significant global metabolic changes as early as at 15 min. In contrast, the most substantial metabolic changes associated with doripenem monotherapy were observed at 4 hr, signifying the time-dependent effect of doripenem. Treatment with the colistin and doripenem combination affected 31 additional metabolites that were not altered by either colistin or doripenem treatment alone at 15 min and 1 hr, indicating a synergistic effect of this combination. Interestingly, the PCA plot shows relatively similar metabolic profiles between the treatment with colistin monotherapy and the combination of colistin and doripenem at 15 min (Figure 3.3A (i)). There was also considerable overlap at 1 hr as almost half of the perturbed metabolites from the combination treatment were also perturbed by colistin alone (Figures 3.3A (ii) and B (ii)). However, at 4 hr the impact of colistin alone was minimal and the combination treatment shared many metabolic features with the doripenem monotherapy (Figure 3.3A (iii) and B (iii)).

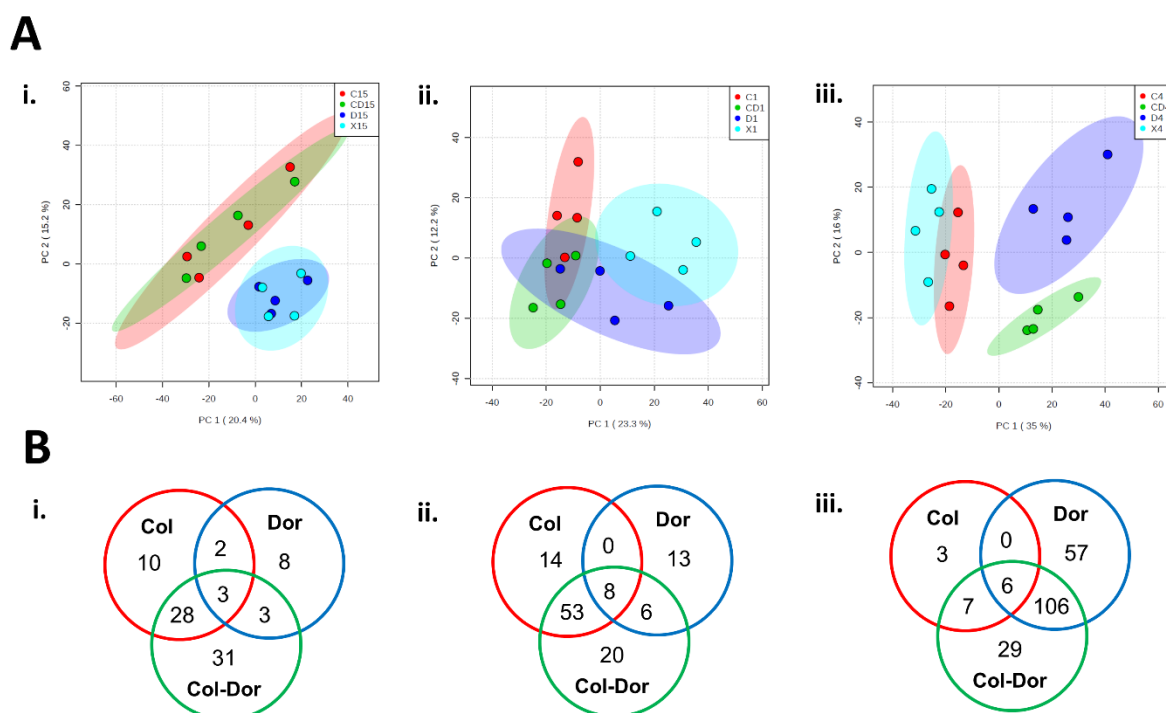


Figure 3.3. Multivariate and univariate analyses of global metabolic changes in *A. baumannii* ATCC 19606. (A) PCA score plots of the first two principal components for metabolite levels from samples treated with colistin, doripenem and the combination at (i) 15 min, (ii) 1 hr and (iii) 4 hr. Each data set represents a total of 16 samples of 4 biological replicates of each condition. Red = colistin alone (C); Dark blue = doripenem alone (D); Green = colistin and doripenem combination (CD); Light blue = untreated control (X). (B) Venn diagrams represent the number of metabolites significantly affected by each treatment at (i) 15 min, (ii) 1 hr and (iii) 4 hr. Significant metabolites were selected with ≥ 1.5 -log₂-fold, $p \leq 0.05$, FDR ≤ 0.1 (one-way ANOVA for multiple comparison).

3.4.1.2 *A. baumannii* 03-149.1 and 03.149.2 strains

Preliminary analyses via PCA plots and median RSD values indicated that there were several outliers generated from few replicates in some sample groups of *A. baumannii* 03-149.1 and 03.149.2 strains (data not shown). To reduce the variance between the samples and further enhance the reliability of the data, those replicates have been removed from the analysis. The median RSD value of the PBQC was 11% which is well within the acceptable limits for metabolomics ($\leq 20\%$) (i.e. within 5% retention time for the identification of authentic standards) (Table 3.1) (411). For each individual sample group, the median RSD value was between 16-26% for 03-149.1 strain and 12-24% for 03-149.2 strain, signifying the metabolic perturbations induced by antibiotics (Table 3.1). A total of 2,700 metabolites of different classes (e.g. carbohydrates, amino acids, nucleotides, lipids, energy and others) were putatively annotated and identified in *A. baumannii* 03-149.1 and 03.149.2 strains. PCA plots of both isolates at 15 min and 1 hr demonstrated that colistin alone and the combination closely clustered together which were distinguished from doripenem alone and control untreated groups, suggesting general metabolic responses induced by colistin (Figure 3.4A and B). There is no clear separation between the antibiotic-treated groups of 03-149.1 strain at 4 hr (Figure 3.4A (i)). Interestingly, at 4 hr, the PCA plot of 03-149.2 strain showed that the combination was slightly separated from the colistin and doripenem monotherapy and control-untreated group (Figure 3.4B(i)).

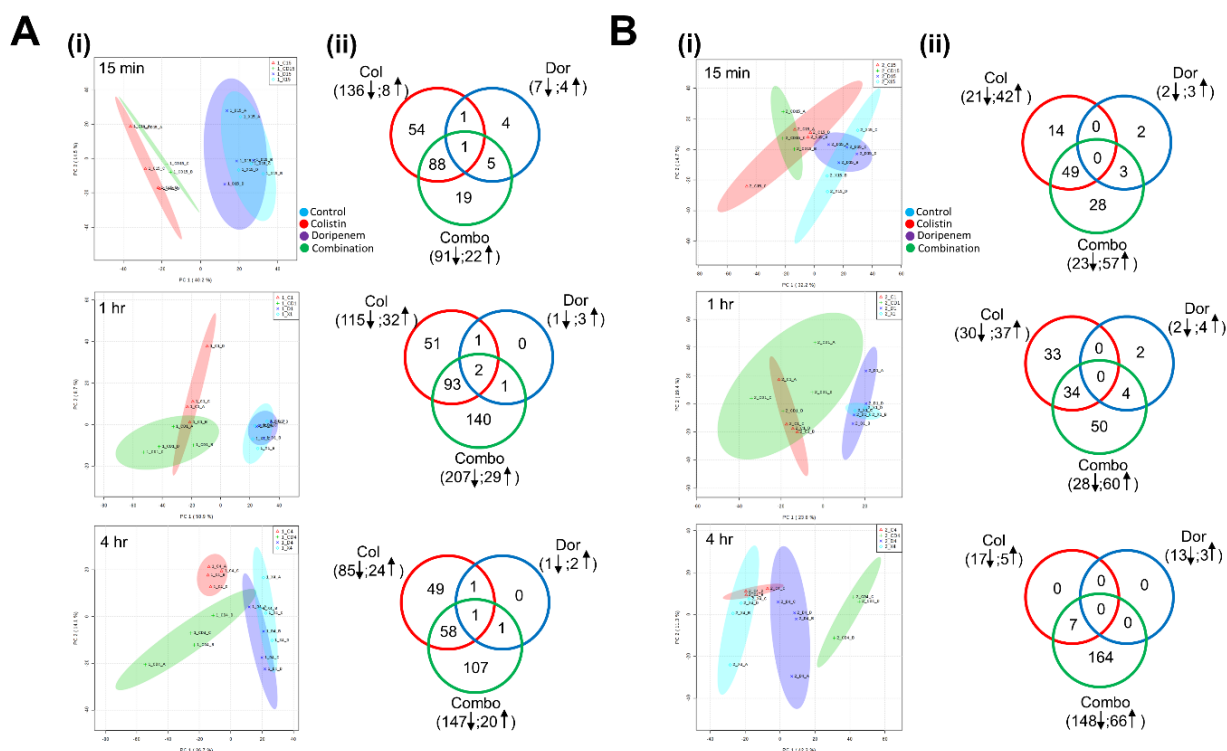


Figure 3.4. Global metabolic changes in a pair of *A. baumannii* isolates. PCA plots (left) and Venn diagrams (right) of *A. baumannii* (A) polymyxin-susceptible 03-149.1 and (B) polymyxin-resistant 03-149.2 strains treated with colistin and doripenem alone and in combination at 15 min, 1 hr and 4 hr. The numbers in brackets represent number of metabolites that were significantly changed. Colistin = Col; doripenem = Dor; colistin and doripenem combination = Combo. Significant metabolites were selected with ≥ 1.5 -log₂-fold, $p \leq 0.05$.

3.4.2 Colistin alone and in combination with doripenem predominantly induced disruption of bacterial lipids

Unique patterns of changes in the levels of lipids were observed in ATCC 19606 treated with either colistin monotherapy or combination with doripenem at 15 min, 1 hr and 4 hr (Figure 3.5). Treatment with colistin alone induced significant perturbation in the levels of membrane lipids at 15 min and 1 hr, predominantly the glycerophospholipids (GPs) and fatty acids (FAs) (≥ 1.5 -

log₂-fold, $p \leq 0.05$) (Figure 3.5A(i) and (ii)). Significant changes in the levels of GPs were observed after treatment with colistin and doripenem combination at all three time points, including the depletion of several lysophosphatidylethanolamines (lysoPE) while only very few FAs were affected (Figure 3.5A). Doripenem alone showed no significant changes to lipid levels at 15 min and 1 hr. However, doripenem alone caused substantial perturbation in the levels of cellular lipids, predominantly accumulation of FAs at 4 hr (Figure 3.5A (iii)). Colistin alone and in combination also significantly induced similar trends of lipid changes predominantly of FAs and GPs in both 03-149.1 and 03-149.2 strains across 4 hr (Figures 3.6 and 3.7). However, perturbation of lipids was not clearly observed following exposure to doripenem alone in 03-149.1 strain at each time point (Figure 3.6). Slight changes in FAs and GPs levels were noticed in the 03-149.2 strain following treatment with doripenem alone at 4 hr but no changes at the early time points (Figure 3.7). Interestingly, the metabolite arising from PE metabolism, *sn*-glycero-3-phosphoethanolamine, significantly decreased (≥ 1.5 -log₂-fold, $p \leq 0.0001$) after treatment with colistin monotherapy and the combination across all time points in ATCC 19606 (Figure 3.5B). In addition, the combination therapy significantly decreased the level of *sn*-glycero-3-phosphate (≥ 1.5 -log₂-fold, $p \leq 0.001$), another metabolite associated with GP metabolism (Figure 3.5B). Notably, *sn*-glycero-3-phosphate, *sn*-glycero-3-phosphoethanolamine and *sn*-glycero-3-phosphocholine also were significantly depleted (≤ 1.5 -log₂-fold, $p \leq 0.001$) by colistin alone and the combination in the 03-149.1 strain (Figure 3.6B). Treatment with colistin alone and the combination against 03-149.2 strain similarly decreased the level of *sn*-glycero-3-phosphoethanolamine at each time point whereas *sn*-glycero-3-phosphocholine was significantly depleted only at 4 hr by the combination (Figure 3.7B).

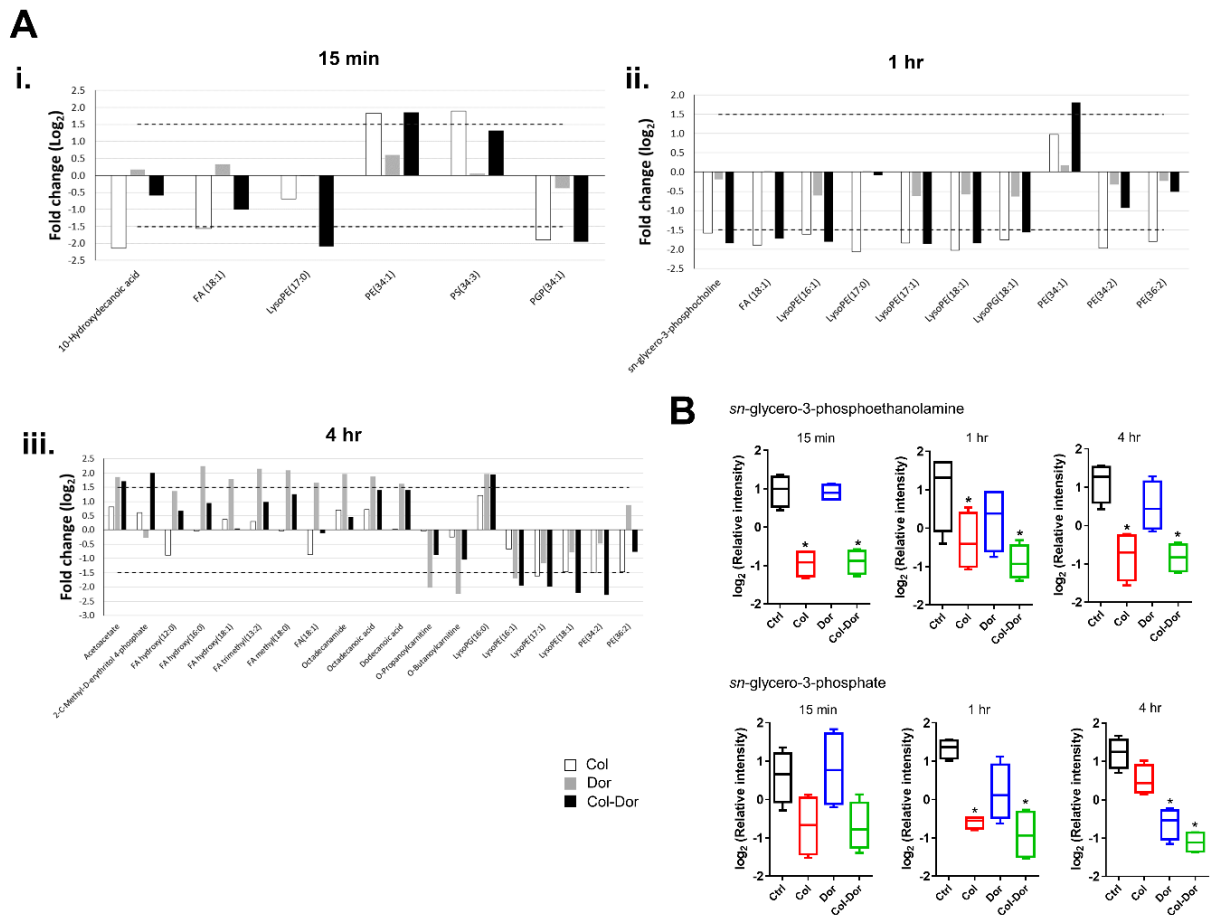


Figure 3.5. Perturbations of bacterial lipids in *A. baumannii* ATCC 19606. (A) Significantly perturbed lipids following treatment with colistin (Col), doripenem (Dor) and the combination (Col-Dor) at (i) 15 min, (ii) 1 hr and (iii) 4 hr. Lipid names are putatively assigned based on accurate mass. **(B)** Depletion of *sn*-glycero-3-phosphoethanolamine and *sn*-glycero-3-phosphate after treatment with colistin, doripenem and the combination across all three time points. Box plots indicate upper and lower quartiles (top and bottom of box); median (line within box); and the spread of data that are not outliers (whiskers). * ≥ 1.5 -log₂-fold, $p \leq 0.05$.

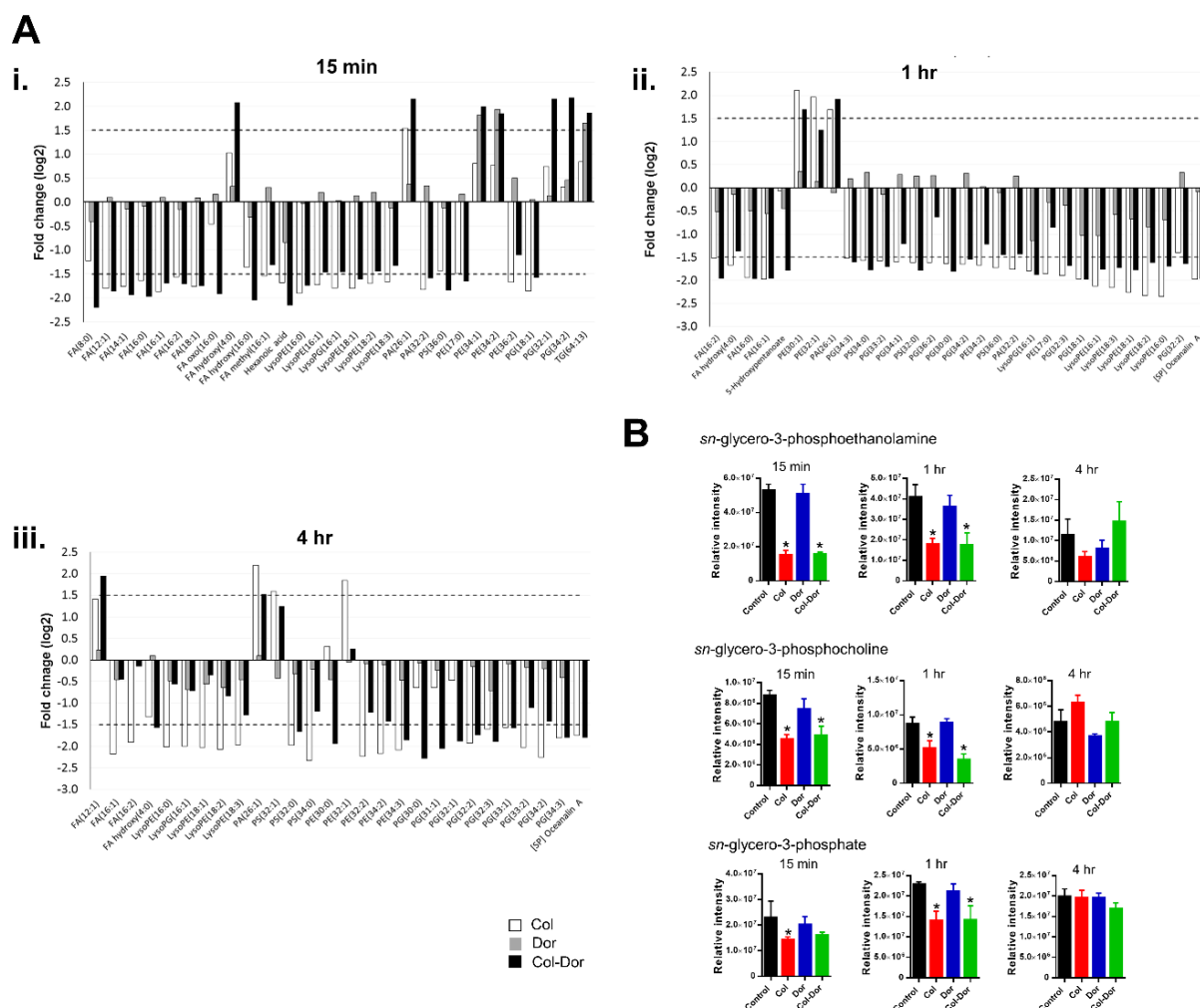


Figure 3.6. Perturbations of bacterial lipids in polymyxin-susceptible 03-149.1. (A) Colistin alone and the combination significantly perturbed the levels of glycerophospholipids and fatty acyls at (i) 15 min, (ii) 1 hr and (iii) 4 hr. Lipids were putatively annotated based on the accurate masses. (B) Perturbations of metabolites associated with lipid metabolism, *sn*-glycero-3-phosphoethanolamine, *sn*-glycero-3-phosphocholine and *sn*-glycero-3-phosphate. * $\geq 1.5\text{-log}_2\text{-fold}$.

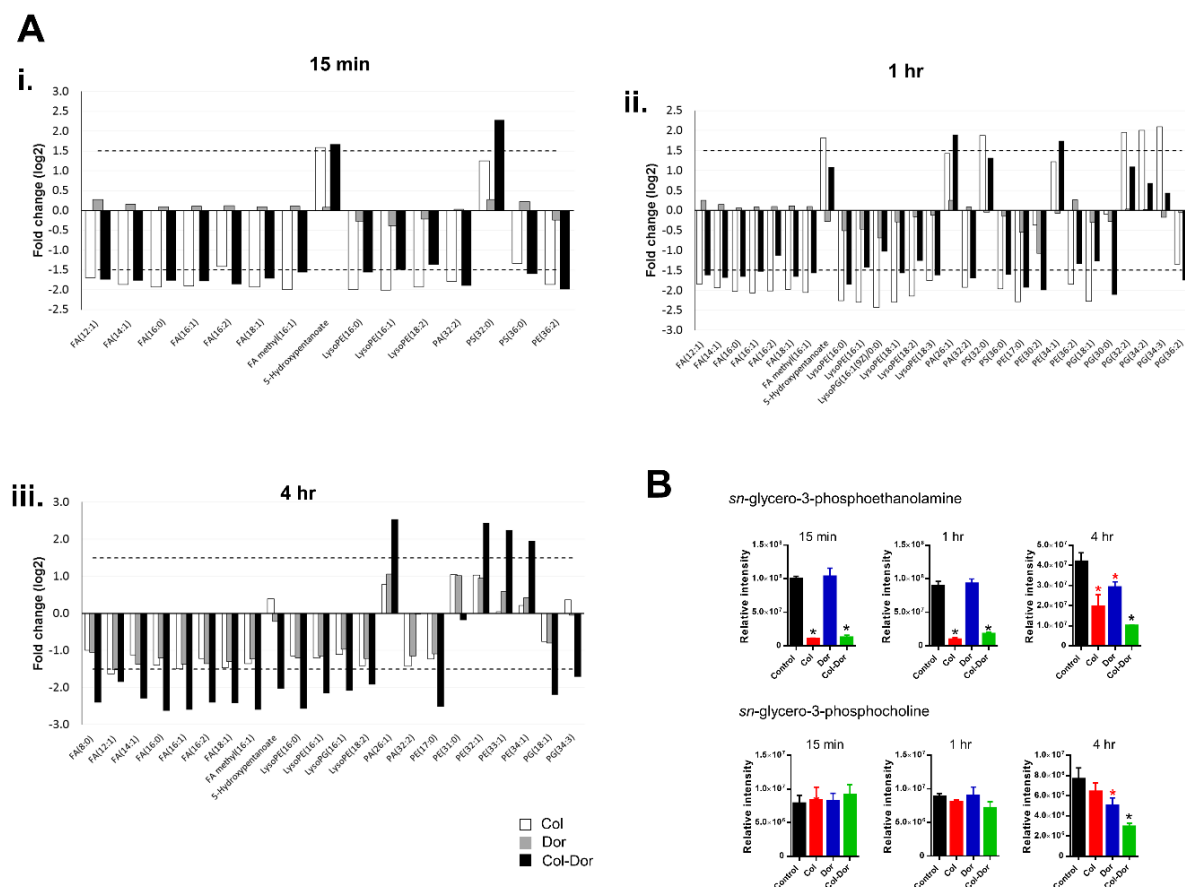


Figure 3.7. Perturbations of bacterial lipids in polymyxin-resistant 03-149.2. (A) Colistin alone predominantly perturbed the levels of glycerophospholipids and fatty acyls at (i) 15 min and (ii) 1 hr, whereas the combination significantly perturbed the lipids across all time points including at (iii) 4 hr. Lipids were putatively annotated based on the accurate masses. **(B)** Perturbations of metabolites associated with lipid metabolism, *sn*-glycero-3-phosphoethanolamine and *sn*-glycero-3-phosphocholine. * $\geq 1.5\text{-log}_2\text{-fold}$, * $\leq 1.5\text{-log}_2\text{-fold}$, $p \leq 0.05$.

3.4.3 *Combination of colistin and doripenem induced global metabolic changes via pentose phosphate pathway (PPP) metabolism*

The combination of colistin and doripenem caused significant changes in the levels of metabolites of central carbon metabolism, primarily associated with bacterial anabolic metabolism of the PPP in *A. baumannii* at 15 min, 1 hr and 4 hr ($\geq 1.5\text{-log}_2\text{-fold}$, $p \leq 0.05$) (Figures 3.8 and 3.9). In particular, the combination of colistin and doripenem induced significant decreases in the levels of three essential metabolites of PPP in ATCC 19606 at all time points, D-ribose 5-phosphate, D-sedoheptulose 7-phosphate and D-erythrose 4-phosphate, key precursors for biosynthesis of nucleotides, LPS and aromatic amino acids, respectively (Figure 3.8). In the ATCC 19606, these metabolites were depleted by colistin monotherapy at the early time points (significant at 1 hr), but not by doripenem; whereas significant depletion at 4 hr was observed for doripenem monotherapy, but not colistin. In addition to these PPP metabolites, a related metabolite, 2-deoxy-D-ribose-5-phosphate was consistently decreased as a result of the combination of colistin and doripenem at 1 hr and 4 hr. Similarly, the levels of D-sedoheptulose 7-phosphate, D-glucono-1,5-lactone 6-phosphate, 2-deoxy-D-ribose-5-phosphate, deoxyribose and D-ribose were significantly depleted ($\leq 1.5\text{-log}_2\text{-fold}$, $p \leq 0.05$) following exposure to colistin alone and the combination in the 03-149.1 strain particularly at 1 hr and 4 hr (Figure 3.9; Tables 3.6 and 3.7). However, doripenem alone induced no significant effects on these PPP metabolites in the 03-149.1 strain at all time points. In turn, for the 03-149.2 strain, significant depletions ($\leq 1.5\text{-log}_2\text{-fold}$, $p \leq 0.05$) in the levels of D-glucono-1,5-lactone 6-phosphate, D-gluconic acid and 6-phospho-D-gluconate metabolites were observed following treatment with the colistin and doripenem combination at 4 hr but no changes by single colistin and doripenem treatment (Figure 3.9 and Table 3.10). In contrast, at 4 hr, the levels of metabolites D-erythrose 4-phosphate and D-sedoheptulose 7-phosphate were notably increased

($\geq 1.5\text{-log}_2\text{-fold}$, $p \leq 0.05$) by the colistin and doripenem combination treatment in the 03-149.2 strain (Figure 3.9).

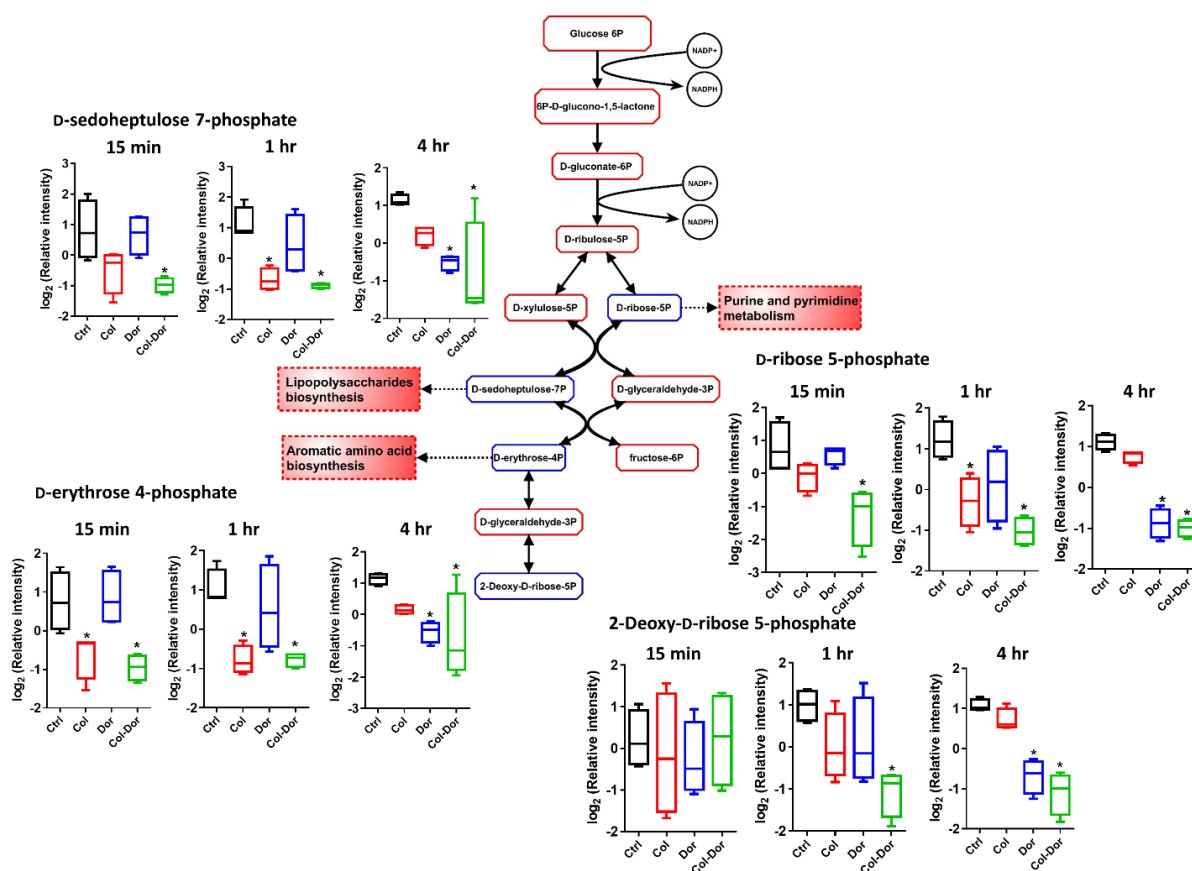


Figure 3.8. Central metabolic changes in the pentose phosphate pathway (PPP). Antibiotic treatment of *A. baumannii* ATCC 19606 significantly decreased the levels of three PPP metabolites (i.e. D-sedoheptulose 7-phosphate, D-erythrose 4-phosphate and D-ribose 5-phosphate) that are essential anabolic precursors of related pathways. The combined colistin and doripenem significantly decreased the levels of the three precursor metabolites at all time points. Additionally, 2-deoxy-D-ribose 5-phosphate significantly decreased followed by the combination at 1 hr and 4 hr. In the pathway flow chart (adapted from biocyc.org with reference to *E. coli* K-12), blue boxes indicate the metabolites that were significantly decreased and red boxes indicate the metabolites that were not significantly changed. Box plots indicate upper and lower quartiles (top and bottom of box); median (line within box); and the spread of data that are not outliers (whiskers). * $\geq 1.5\text{-log}_2\text{-fold}$, $p \leq 0.05$.

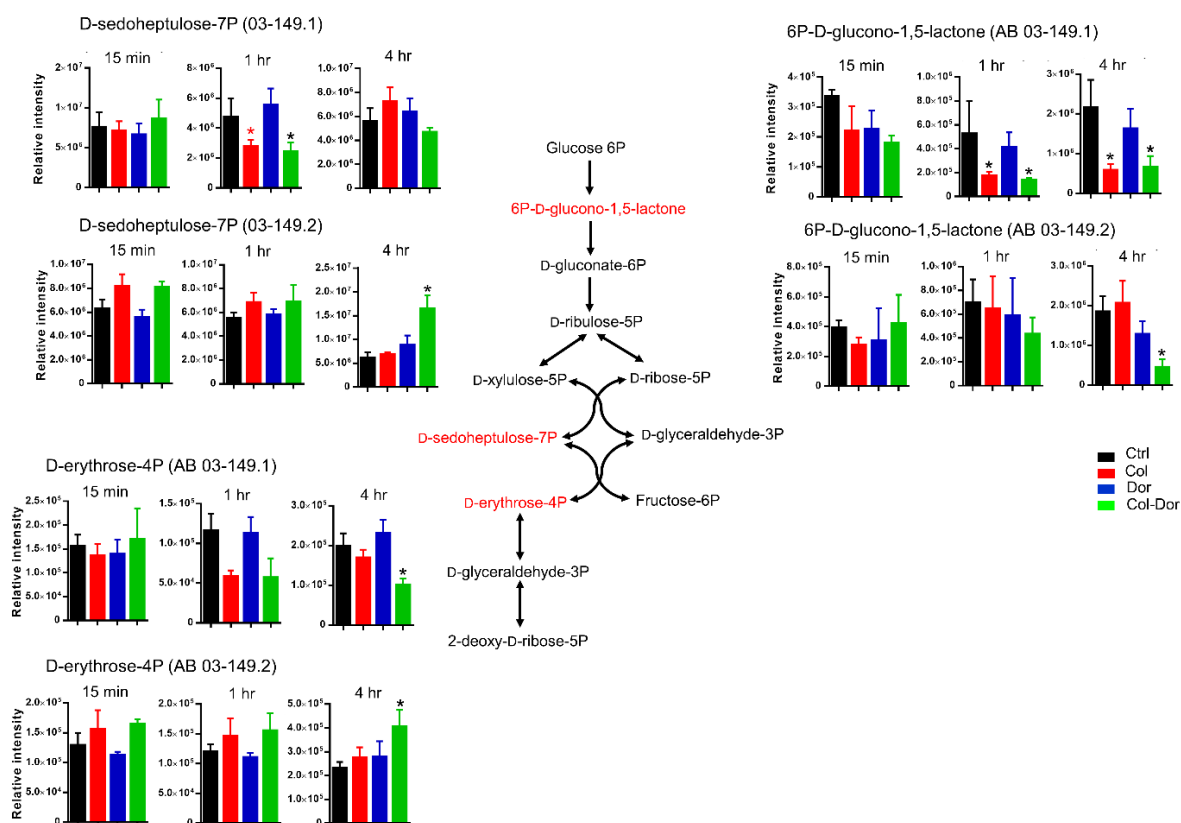


Figure 3.9. Central metabolic changes in the pentose phosphate pathway (PPP) in *A. baumannii* clinical isolates. The combination of colistin and doripenem significantly depleted the PPP metabolite levels in the polymyxin-susceptible 03-149.1 strain predominantly at 1 hr and 4 hr. Colistin and doripenem combination significantly perturbed (i.e. increased and decreased) the metabolite levels in the polymyxin-resistant 03-149.2 strain particularly at 4 hr. Metabolites with red and black colours indicate metabolites that were significantly changed and not significantly changed, respectively. * $\geq 1.5\text{-log}_2\text{-fold}$, * $\leq 1.5\text{-log}_2\text{-fold}$, $p \leq 0.05$.

3.4.4 *Colistin and doripenem caused depletion of metabolite levels of energy and nucleotide metabolism*

Significant depletion in the levels of intracellular metabolites of energy metabolism, namely ATP, NAD⁺ and NADP⁺ was observed in the ATCC 19606 strain following treatment with the colistin and doripenem combination across all three time points ($\geq 1.5\text{-log}_2\text{-fold}$, $p \leq 0.01$) (Figure 3.10A). Treatment with colistin alone decreased the levels of these energy metabolites at 15 min and 1 hr, while doripenem-associated depletion was only significant at 4 hr in the ATCC 19606 strain. Significant decreases of energy metabolites (i.e. ATP, ADP, NAD⁺ and NADP⁺) were also observed in the 03-149.1 strain following treatment with colistin alone at 15 min and 1 hr, colistin and doripenem combination at each time point, but no significant changes by doripenem alone (Tables 3.5-3.7). In contrast, for the 03-149.2 strain, energy metabolites (i.e. ATP, NAD⁺) were significantly increased by colistin alone at 15 min and 1 hr, the combination at all time points but no changes by doripenem alone (Tables 3.8-3.10). Notably, significant perturbations of TCA cycle intermediates, fumarate and *cis*-aconitate were identified in samples treated with colistin and doripenem alone and in combination in the *A. baumannii* ATCC 19606 particularly at 15 min and 4 hr (Tables 3.2 and 3.4). Our results also showed that, the levels of several TCA cycle intermediates (e.g. 2-oxoglutarate, (*S*)-malate, succinate, citrate) were significantly changed in both *A. baumannii* 03-149.1 and 03-149.2 strains (Tables 3.5-3.10). In particular, notable increase of succinate was observed following treatment with the combination against 03-149.2 strain at 1 hr and 4 hr (Tables 3.9 and 3.10).

Furthermore, significant depletion in the levels of nucleotides, both purines and pyrimidines, were observed in the ATCC 19606 after colistin alone at 1 hr, doripenem alone at 4 hr and the combination treatment at each time point ($\geq 1.5\text{-log}_2\text{-fold}$, $p \leq 0.01$) (Figure 3.10B). In the 03-149.1 strain, the levels of many nucleotides were significantly lowered ($\leq 1.5\text{-log}_2\text{-fold}$, $p \leq 0.05$)

by colistin alone and the combination at all time points, whereas doripenem alone showed no significant effect (Figure 3.11A). In contrast, significant increases (≥ 1.5 -log₂-fold, $p \leq 0.05$) in the levels of nucleotides were notified following exposure to colistin alone and in combination in the 03-149.2 strain at the early time points, 15 min and 1 hr (Figure 3.11B). Interestingly, at 4 hr, colistin and doripenem combination caused significant depletion in the levels of nucleotides in the 03-149.2 strain whereas no changes induced by colistin and doripenem monotherapy (Figure 3.11B). The results also showed that the level of 5-phospho- α -D-ribose-1-diphosphate (PRPP), a key precursor for nucleotide biosynthesis significantly depleted (≥ 1.5 -log₂-fold, $p \leq 0.01$) in the 03-149.1 strain after exposure to colistin alone and the combination at each time point. Whereas in the 03-149.2 strain, the PRPP was significantly depleted at 4 hr by the combination (Figure 3.11C). However, there was no significant change in the level of PRPP in the 03-149.2 strain by the colistin and doripenem combination at 15 min and 1 hr whereas only colistin alone caused significant increase at 15 min (Figure 3.11C). Furthermore, many of amino acid metabolites were significantly decreased (≤ 1.5 -log₂-fold, $p \leq 0.05$) by colistin alone and the combination in the ATCC 19606 and 03-149.1 strains (Tables 3.2-3.7), whereas these were significantly increased (≥ 1.5 -log₂-fold, $p \leq 0.05$) in the 03-149.2 strain (Tables 3.8-3.10).

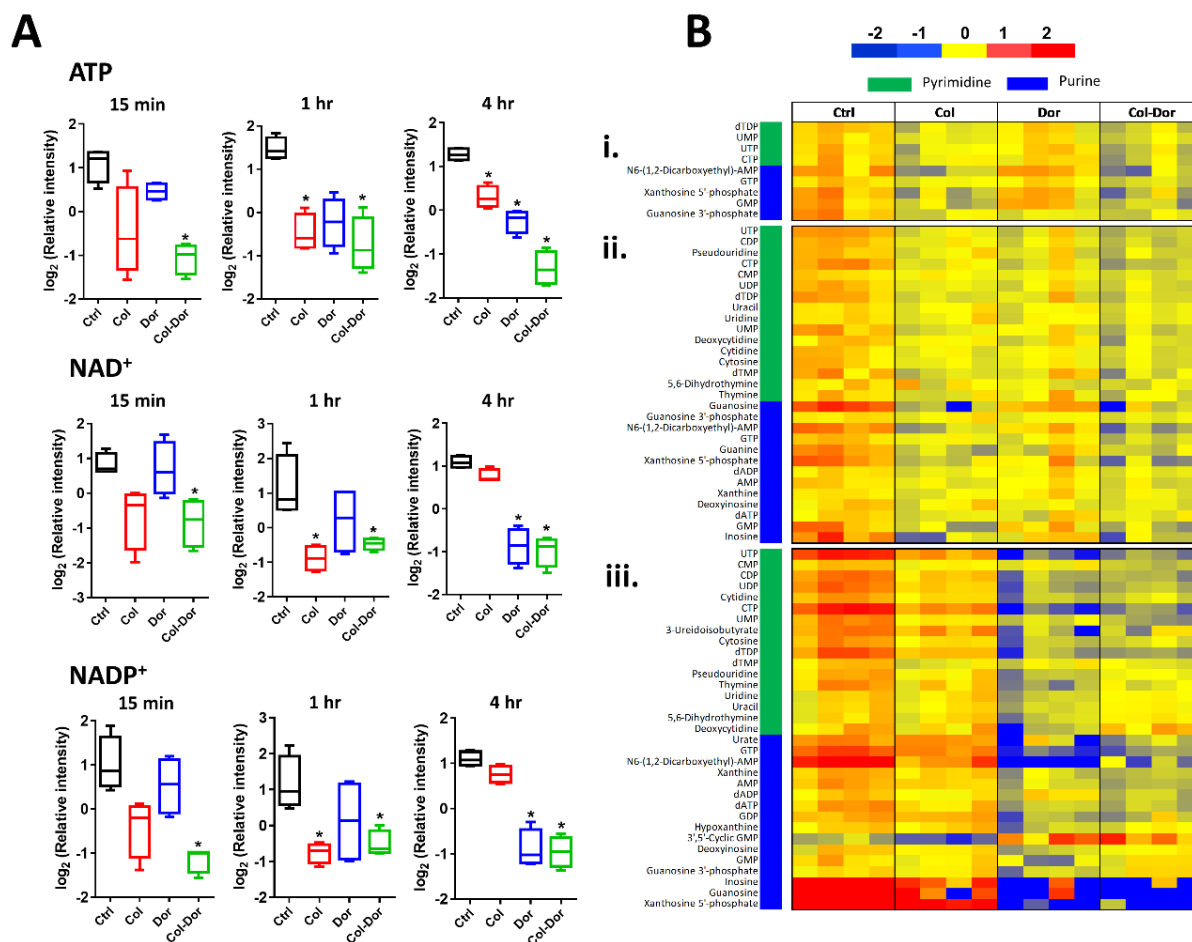


Figure 3.10. Depletion of energy and nucleotide metabolite levels in *A. baumannii* ATCC 19606. (A) Decreased levels of key energy-associated metabolites, ATP, NAD⁺ and NADP⁺ induced by colistin, doripenem and the combination. Box plots indicate upper and lower quartiles (top and bottom of box); median (line within box); and the spread of data that are not outliers (whiskers). * ≥ 1.5 -log₂-fold, $p \leq 0.05$. (B) Heatmap profile of relative abundance of significantly perturbed nucleotides at (i) 15 min, (ii) 1 hr and (iii) 4 hr after treatment with colistin (Col), doripenem (Dor) and the combination (Col-Dor) (n = 4). Antibiotics decreased the levels of nucleotides, both purines and pyrimidines.

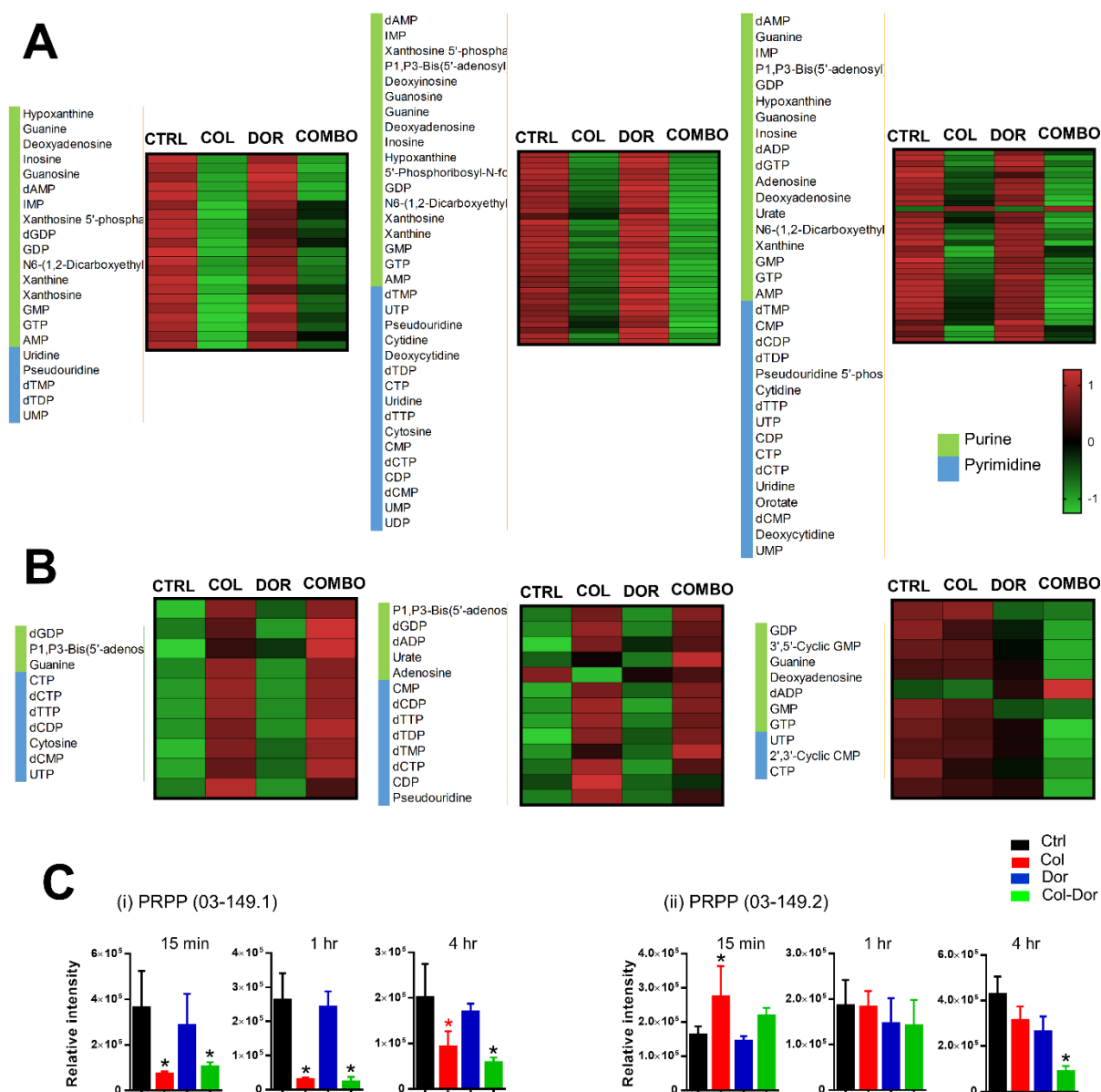


Figure 3.11. Purine and pyrimidine nucleotide changes in *A. baumannii* clinical isolates.

Heatmap profiles of the significantly changed nucleotides in the *A. baumannii* (A) polymyxin-susceptible 03-149.1 and (B) polymyxin-resistant 03-149.2 strains exposed to colistin and doripenem alone and the combination at 15 min (left), 1 hr (centre) and 4 hr (right). (C) Perturbation of PRPP metabolite, a key precursor for nucleotide biosynthesis in *A. baumannii* (i) 03-149.1 and (ii) 03-149.2 strains. Colistin = Col; Doripenem = Dor; Colistin and doripenem combination = Combo; Control = Ctrl. * $\geq 1.5\text{-log}_2\text{-fold}$, * $\leq 1.5\text{-log}_2\text{-fold}$, $p \leq 0.05$.

3.4.5 Colistin and doripenem induced depletion of amino sugar metabolites for cell wall biosynthesis

Colistin alone significantly decreased the intracellular levels of several important metabolites associated with amino sugar and nucleotide sugar metabolism in the ATCC 19606, in particular at 1 hr ($\geq 1.5\text{-log}_2\text{-fold}$, $p \leq 0.05$) (Figure 3.12A). The levels of two major precursor metabolites of cell wall biosynthesis significantly decreased after treatment with colistin alone at 1 hr, namely UDP-*N*-acetylmuramate (UDP-MurNAc) and UDP-*N*-acetylglucosamine (UDP-GlcNAc) ($\geq 1.5\text{-log}_2\text{-fold}$, $p \leq 0.01$). Significant decreases in the levels of both metabolites were also observed following treatment with the combination of colistin and doripenem at 1 hr and 4 hr. Doripenem alone significantly decreased the amino sugar associated metabolites only at 4 hr. Two metabolites of peptidoglycan biosynthesis were identified to significantly decrease at 4 hr after doripenem treatment in the ATCC 19606, meso-2,6-Diaminoheptanedioate and UDP-*N*-acetylmuramoyl-L-alanyl-D-glutamyl-6-carboxy-L-lysyl-D-alanyl-D-alanine ($\geq 1.5\text{-log}_2\text{-fold}$, $p \leq 0.01$) (Figure 3.12B). Only UDP-*N*-acetylmuramoyl-L-alanyl-D-glutamyl-6-carboxy-L-lysyl-D-alanyl-D-alanine was found to significantly decrease after treatment with combined colistin and doripenem at 4 hr. The changes in cell wall metabolism were also observed in both 03-149.1 and 03-149.2 isolates predominantly induced by the combination of colistin and doripenem (Figures 3.13 and 3.14). Colistin alone and in combination generally induced significant depletion ($\leq 1.5\text{-log}_2\text{-fold}$, $p \leq 0.05$) in the levels of many peptidoglycan biosynthesis associated metabolites in the 03-149.1 strain particularly at 15 min and 1 hr (Figure 3.13). On the contrary, the metabolite levels of peptidoglycan biosynthesis were significantly increased by the colistin and doripenem combination in the 03-149.2 isolate (Figure 3.14). Notably, the levels of UDP-MurNAc-L-Ala-gamma-D-Glu-meso-2,6-diaminopimelate and UDP-MurNAc-L-Ala-gamma-D-Glu-meso-2,6-diaminopimeloyl D-Ala-D-Ala were significantly altered ($\leq 1.5\text{-log}_2\text{-fold}$, $p \leq 0.001$) by doripenem alone in both *A. baumannii* clinical isolates (Figures 3.13 and 3.14). In

addition, marked decreases ($\leq 1.5\text{-log}_2\text{-fold}$, $p \leq 0.01$) of LPS biosynthesis metabolites, D-ribulose-5-phosphate and 3-deoxy-D-manno-octulosonate (KDO) were noticed following colistin alone and the combination in the 03-149.1 strain particularly at 1 hr and 4 hr, but not in the 03-149.2 strain (Figure 3.13B).

3.4.6 *Colistin and doripenem induced alterations in peptide metabolism*

Treatment with doripenem alone and the combination of colistin and doripenem showed unique changes in the levels of short peptides in the ATCC 19606 (Tables 3.2-3.4). The number of significantly perturbed peptides increased across the time points after treatment with doripenem alone and the combination of colistin and doripenem ($\geq 1.5\text{-log}_2\text{-fold}$, $p \leq 0.05$). However, colistin alone showed significant changes in the levels of only a few cellular peptides. Interestingly, a unique putative metabolite, tyramine ($m/z = 137.08$, $t_R = 9.03$ min; MSI level 2), which is associated with tyrosine metabolism was found to significantly increase only after treatment with doripenem alone and the combination of colistin and doripenem across all time points in all the *A. baumannii* strains ($\geq 1.5\text{-log}_2\text{-fold}$, $p \leq 0.0001$) (Tables 3.2-3.10).

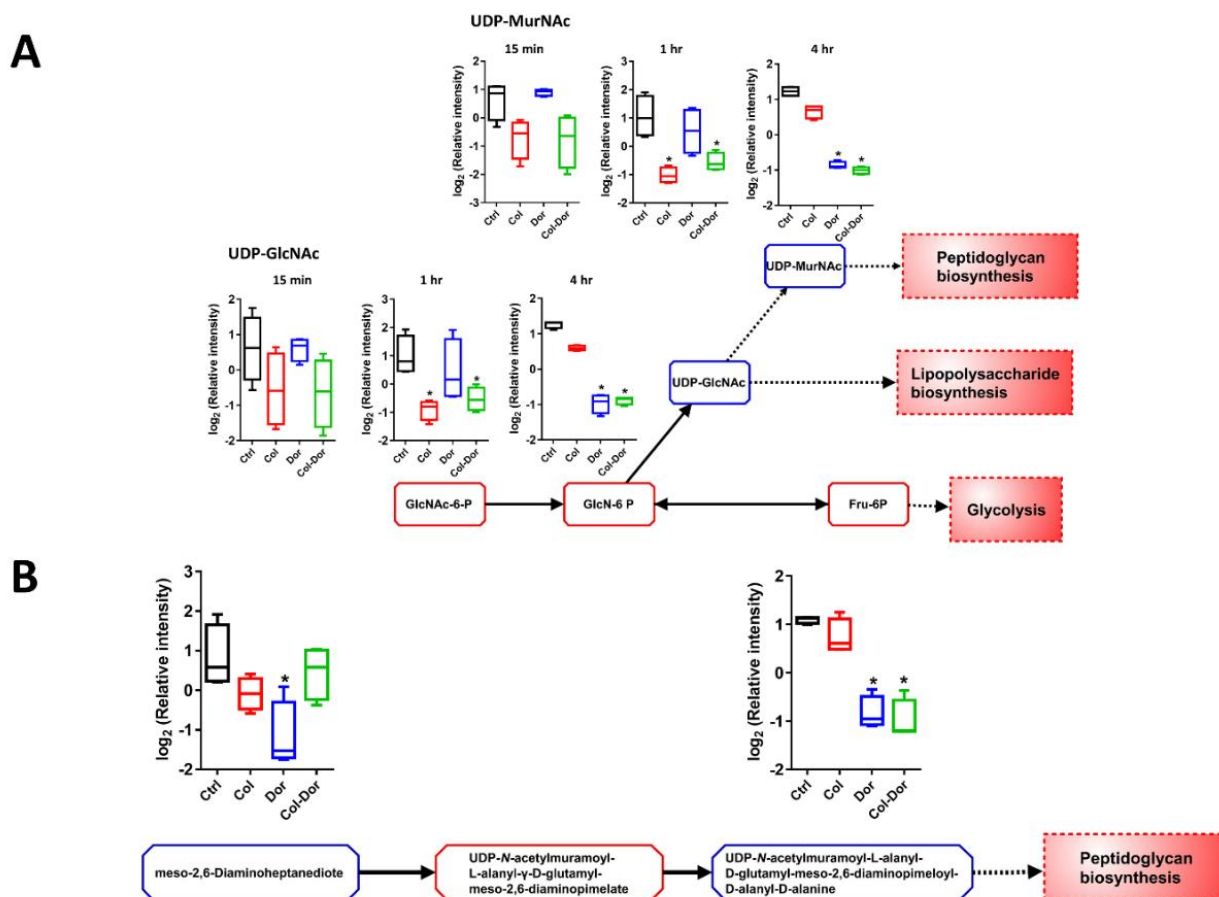


Figure 3.12. Depletion of amino sugar metabolites for peptidoglycan and LPS biosynthesis in *A. baumannii* ATCC 19606. (A) Significant decreases in the levels of two amino sugar metabolites at 1 hr and 4 hr by colistin, doripenem and the combination. UDP-GlcNAc is a key precursor metabolite for LPS and peptidoglycan biosynthesis. (B) Levels of two key metabolites of peptidoglycan biosynthesis significantly decreased after treatment with doripenem alone at 4 hr. The combination of colistin and doripenem also significantly decreased UDP-*N*-acetylmuramoyl-L-alanyl-D-glutamyl-meso-2,6-diaminopimeloyl-D-alanyl-D-alanine (≥ 2.0 -log₂-fold) at 4 hr. The blue boxes in the flow charts indicate the metabolites that were significantly decreased. The red boxes indicate the metabolites that were not significantly changed. Box plots indicate upper and lower quartiles (top and bottom of box); median (line within box); and the spread of data that are not outliers (whiskers). * ≥ 1.5 -log₂-fold, $p \leq 0.05$.

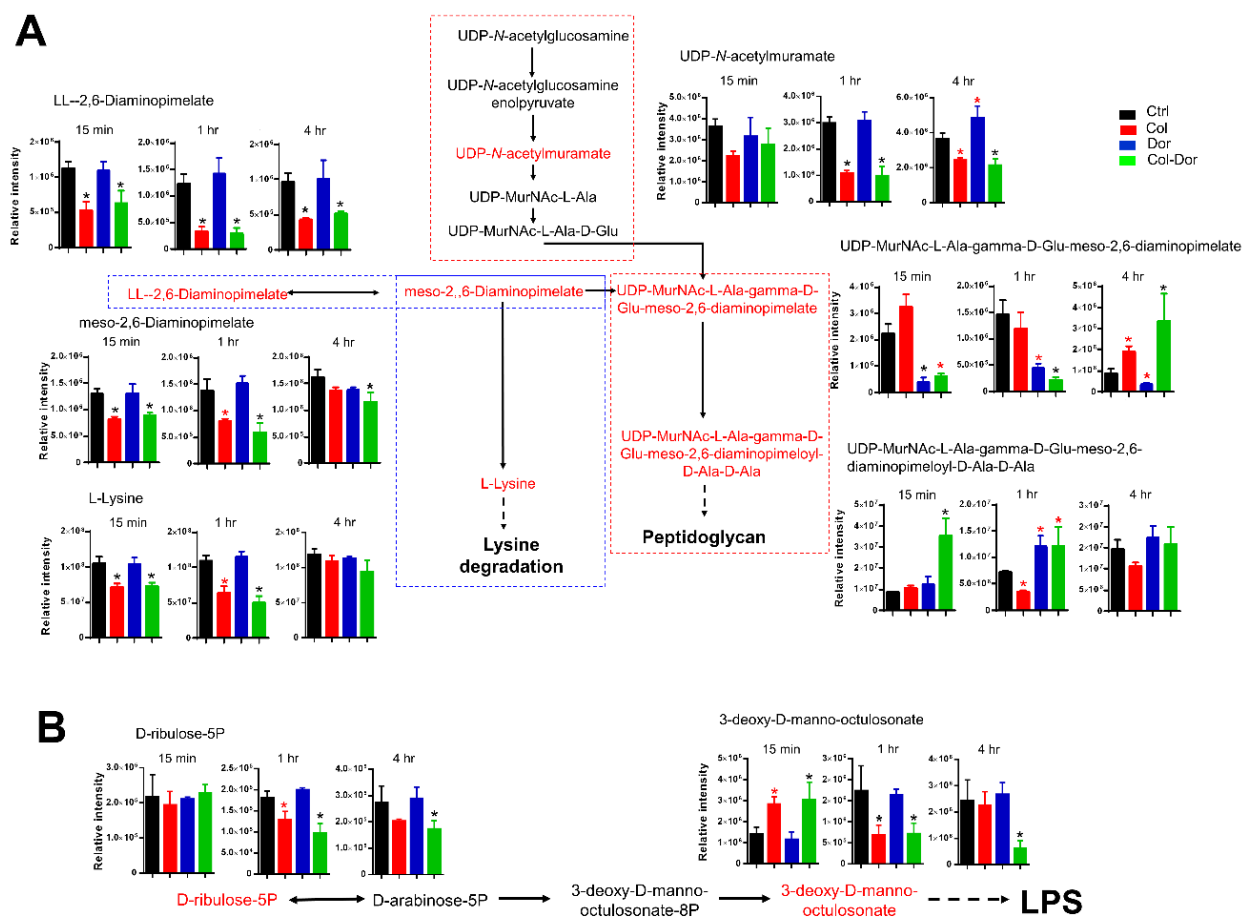


Figure 3.13. Peptidoglycan and LPS biosynthesis changes in polymyxin-susceptible 03-149.1. (A) Peptidoglycan biosynthesis. Colistin alone and the combination significantly decreased the levels of many metabolites whereas doripenem alone particularly affected UDP-MurNAc-L-Ala-gamma-D-Glu-meso-2,6-diaminopimelate and UDP-MurNAc-L-Ala-gamma-D-Glu-meso-2,6-diaminopimeloyl D-Ala-D-Ala. (B) LPS biosynthesis. Colistin alone and the combination significantly altered the levels of D-ribulose-5-phosphate and 3-deoxy-D-manno-octulosonate. Red and black colours indicate metabolites that were significantly changed and not significantly changed, respectively. * $\geq 1.5\text{-log}_2\text{-fold}$, * $\leq 1.5\text{-log}_2\text{-fold}$, $p \leq 0.05$.

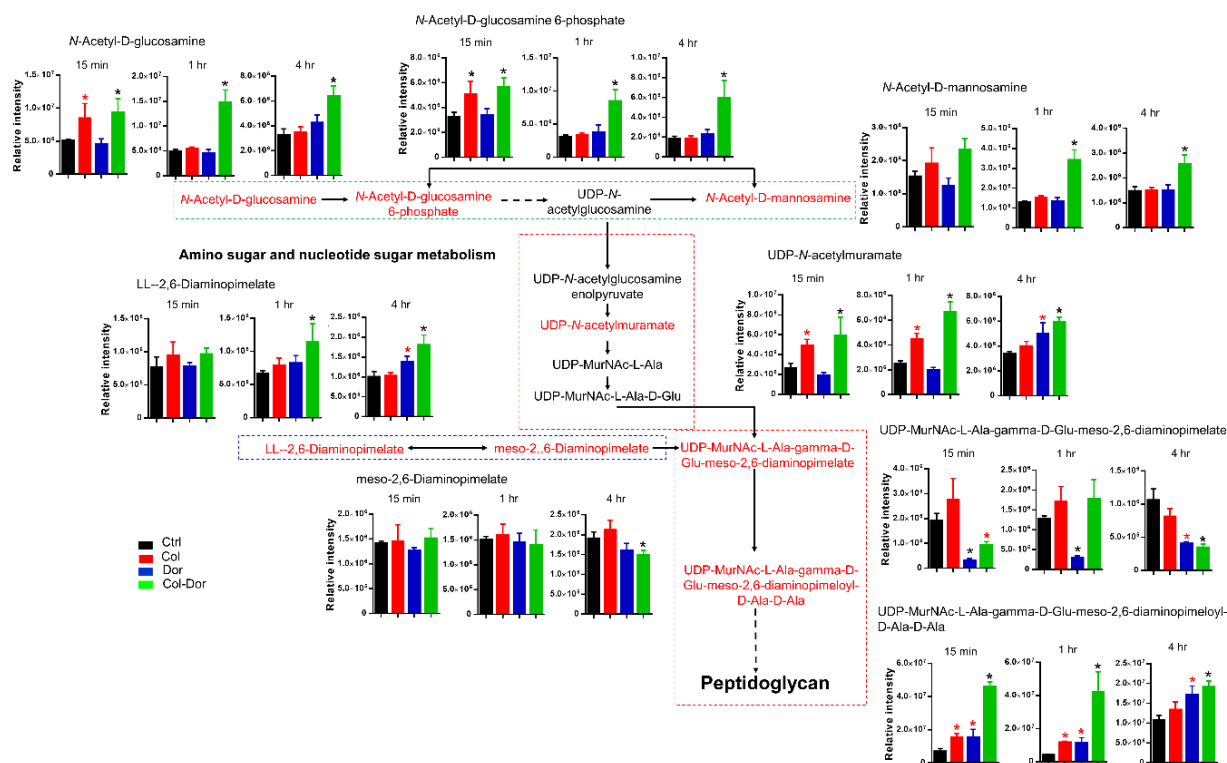


Figure 3.14. Peptidoglycan biosynthesis changes in polymyxin-resistant 03-149.2. The combination of colistin and doripenem significantly increased the levels of many metabolites whereas doripenem alone particularly affected UDP-MurNac-L-Ala-gamma-D-Glu-meso-2,6-diaminopimelate and UDP-MurNac-L-Ala-gamma-D-Glu-meso-2,6-diaminopimeloyl D-Ala-D-Ala. Red and black colours indicate metabolites that were significantly changed and not significantly changed, respectively. * $\geq 1.5\text{-log}_2\text{-fold}$, * $\leq 1.5\text{-log}_2\text{-fold}$, $p \leq 0.05$.

Table 3.2 Significant metabolites ($p \leq 0.05$) of ATCC 19606 identified following exposure to colistin (Col) and doripenem (Dor) alone and in combination (Combo) at 15 min. Significant fold-changes are highlighted in yellow.

Formula	Map	Pathway	Metabolite	Col	Dor	Combo	p-value
C ₄ H ₇ NO ₄	Amino Acid	Alanine and aspartate	L-Aspartate	1.68	-0.15	1.43	0.001199
C ₁₅ H ₂₂ N ₆ O ₅ S			S-Adenosyl-L-methionine	-1.22	-1.30	-2.33	0.001057
C ₅ H ₉ NO ₄			L-Glutamate	-1.58	-0.57	-2.02	0.002507
C ₇ H ₁₁ NO ₅			N-Acetyl-L-glutamate	-1.54	-0.29	-1.88	0.002564
C ₈ H ₁₅ NO ₆		Glutamate	N-Acetyl-D-glucosamine	1.60	-0.61	-0.31	0.000346
C ₂₀ H ₃₂ N ₆ O ₁₂ S ₂			Glutathione disulfide	-1.64	-0.06	-1.83	0.000270
C ₃ H ₄ O ₄		Glycine, serine and threonine	Hydroxypyruvate	1.89	0.25	2.03	1.74E-06
C ₄₁ H ₆₅ N ₉ O ₂₈ P ₂		Lysine biosynthesis	UDP-N-acetylmuramoyl-L-alanyl-D-glutamyl-6-carboxy-L-lysyl-D-alanyl-D-alanine	-0.70	1.68	1.15	3.10E-07
C ₅ H ₈ O ₃		Lysine degradation	5-Oxopentanoate	1.35	0.00	1.76	0.003292
C ₉ H ₁₀ O ₄		Phenylalanine	3-(2,3-Dihydroxyphenyl)propanoate	-1.42	-0.53	-2.15	0.001055
C ₉ H ₁₁ NO ₂			L-Phenylalanine	2.12	0.33	0.77	0.002122
C ₂ H ₅ O ₅ P		Taurine and hypotaurine	Acetyl phosphate	-1.34	-0.22	-1.67	0.020874
C ₈ H ₁₁ NO		Tyrosine	Tyramine	0.05	2.00	1.91	2.14E-14
C ₆ H ₁₀ O ₃		Valine, leucine and isoleucine degradation	(S)-3-Methyl-2-oxopentanoic acid	1.93	0.21	1.34	0.002784
C ₅ H ₈ O ₃			3-Methyl-2-oxobutanoic acid	1.52	-0.07	1.95	2.18E-05
C ₆ H ₁₀ O ₃			4-Methyl-2-oxopentanoate	1.42	-0.05	2.06	5.65E-06
C ₁₅ H ₁₀ O ₅	Biosynthesis of Secondary Metabolites	Isoflavonoid biosynthesis	2'-Hydroxydaidzein	1.67	0.38	1.70	0.007274
C ₆ H ₁₃ NO ₅	Carbohydrate	Aminosugars	D-Glucosamine	-0.28	-0.11	-1.90	0.005587
C ₆ H ₁₁ NO ₄		C5-Branched dibasic acid	4-Methyl-L-glutamate	-1.56	-0.69	-2.31	0.000113
C ₆ H ₁₀ O ₅		Fructose and mannose	2-Dehydro-3-deoxy-L-rhamnonate	-0.02	-0.70	-1.77	0.018008
C ₃ H ₅ O ₆ P		Glycolysis / Gluconeogenesis	Phosphoenolpyruvate	1.64	-0.21	1.58	0.000217
C ₃ H ₇ O ₇ P			3-Phospho-D-glycerate	1.40	0.36	1.85	0.009620
C ₆ H ₁₂ O ₇		Pentose and glucuronate interconversions	D-Mannate	1.74	0.29	1.73	0.002352
C ₄ H ₉ O ₇ P		Pentose phosphate pathway	D-Erythrose 4-P	-1.38	0.09	-1.71	0.002240
C ₅ H ₁₁ O ₈ P			D-Ribose 5-P	-0.88	-0.22	-2.05	0.002698
C ₇ H ₁₅ O ₁₀ P			D-Sedoheptulose 7-P	-1.32	-0.15	-1.80	0.006959
C ₆ H ₁₃ NO ₆			2-Amino-2-deoxy-D-gluconate	1.47	0.32	1.73	0.01307
C ₃ H ₇ O ₅ P		Propanoate	Propanoyl phosphate	-1.67	-0.08	-1.68	0.001283
C ₆ H ₁₃ O ₉ P		Starch and sucrose	D-Glucose 6-P	1.60	-0.36	0.83	0.008075
C ₄ H ₄ O ₄		TCA cycle	Fumarate	1.73	2.14	1.48	0.002026
C ₈ H ₁₈ NO ₁₀ P		undefined	N-Gluconyl ethanolamine phosphate	-1.75	-0.28	-1.84	0.000740
C ₇ H ₇ NO ₂	Cofactors & Vitamins	Nicotinate & nicotinamide	N-Methylnicotinate	1.79	0.14	1.77	0.000285
C ₅ H ₉ NO ₃		Porphyrin & chlorophyll	(S)-4-Amino-5-oxopentanoate	-1.55	-1.36	-2.13	0.004471
C ₁₃ H ₂₂ N ₄ O ₈ S ₂	Peptide	Acidic peptide	Asp-Cys-Cys-Ser	-1.64	-0.51	-2.04	0.001071
C ₁₃ H ₂₁ N ₅ O ₈			Ala-Asn-Asp-Gly	1.58	0.33	1.74	0.008051
C ₁₃ H ₂₃ N ₅ O ₆			Glu-Pro-Pro	1.37	1.73	0.01	0.004429
C ₂₁ H ₃₆ N ₆ O ₁₀		Basic peptide	Glu-Glu-Gln-Lys	-0.08	2.07	1.66	4.53E-12
C ₂₂ H ₃₄ N ₄ O ₇ S		Hydrophobic peptide	Cys-Leu-Thr-Tyr	-0.78	-1.86	-1.08	0.046288
C ₁₄ H ₂₅ N ₃ O ₆			Glu-Ala-Ile	0.46	-1.69	-0.76	0.001490
C ₁₄ H ₂₄ N ₄ O ₅		Nonpolar peptide	Ala-Ala-Ala-Pro	-0.07	-1.85	0.01	0.003101

Table 3.3 Significant metabolites ($p \leq 0.05$) of ATCC 19606 identified following exposure to colistin (Col) and doripenem (Dor) alone and in combination (Combo) at 1 hr. Significant fold-changes are highlighted in yellow.

Formula	Map	Pathway	Metabolite	Col	Dor	Combo	p value
C ₄ H ₇ NO ₄	Amino Acid	Alanine and aspartate	L-Aspartate	1.76	1.00	2.01	0.004135
C ₉ H ₁₈ N ₄ O ₄		Arginine and proline	N2-(D-1-Carboxyethyl)-L-arginine	-1.56	-1.75	-2.27	0.000452
C ₇ H ₁₁ NO ₅			N-Acetyl-L-glutamate	-1.80	-0.87	-2.12	0.000932
C ₅ H ₉ NO ₄			L-Glutamate	-1.93	-0.61	-1.63	0.005325
C ₁₅ H ₂₂ N ₆ O ₅ S			S-Adenosyl-L-methionine	-1.98	-1.36	-1.54	0.012693
C ₁₀ H ₁₈ N ₄ O ₆			N-(L-Arginino)succinate	-1.76	-0.90	-2.22	0.000369
C ₃ H ₇ NO ₅ S		Cysteine	L-Cysteate	-1.25	-0.90	-2.11	0.008426
C ₂₀ H ₃₁ N ₃ O ₁₉ P ₂		D-Glutamine and D-glutamate	UDP-N-acetylmuramate	-2.07	-0.52	-1.61	0.000964
C ₈ H ₁₆ NO ₉ P		Glutamate	N-Acetyl-D-glucosamine 6-phosphate	-1.70	0.11	-1.21	0.005099
C ₂₀ H ₃₂ N ₆ O ₁₂ S ₂		Glutamate	Glutathione disulfide	-1.86	-0.42	-1.87	0.000538
C ₄₁ H ₆₅ N ₉ O ₂₈ P ₂		Lysine biosynthesis	UDP-N-acetylmuramoyl-L-alanyl-D-glutamyl-6-carboxy-L-lysyl-D-alanyl-D-alanine	-0.82	1.46	1.17	0.000003
C ₈ H ₁₆ N ₂ O ₃			N2-Acetyl-L-lysine	-1.96	-1.38	-2.06	0.001197
C ₄ H ₇ NO ₂		Methionine	1-Aminocyclopropane-1-carboxylate	1.21	1.68	-0.01	0.011663
C ₉ H ₁₀ O ₄		Phenylalanine	3-(2,3-Dihydroxyphenyl)propanoate	-1.70	-1.18	-1.70	0.029722
C ₈ H ₁₁ N			Phenethylamine	1.14	1.30	1.88	0.036894
C ₂ H ₅ O ₅ P		Taurine and hypotaurine	Acetyl phosphate	-1.86	-0.71	-1.93	0.001824
C ₈ H ₁₁ NO		Tyrosine	Tyramine	0.04	2.01	1.90	1.62E-14
C ₇ H ₁₂ O ₅		Valine, leucine & isoleucine biosynthesis	(2S)-2-Isopropylmalate	-1.89	-1.23	-1.57	0.020365
C ₆ H ₁₀ O ₃			4-Methyl-2-oxopentanoate	1.85	0.20	1.02	0.014174
C ₁₅ H ₁₀ O ₅	Biosynthesis of secondary metabolites	Isoflavonoid biosynthesis	2'-Hydroxydaidzein	2.22	0.75	2.01	4.74E-06
C ₈ H ₁₈ NO ₁₀ P	Carbohydrate	0	N-Gluconyl ethanolamine phosphate	-1.99	-0.80	-2.05	0.000269
C ₁₇ H ₂₅ N ₃ O ₁₈ P ₂		Aminosugars	UDP-N-acetyl-D-mannosaminuronate	-1.98	-1.18	-1.75	0.006717
C ₁₇ H ₂₇ N ₃ O ₁₇ P ₂			UDP-N-acetyl-D-glucosamine	-1.89	-0.55	-1.52	0.008819
C ₆ H ₁₃ NO ₅			D-Glucosamine	-1.47	-1.78	-1.14	0.041123
C ₅ H ₆ O ₄		Ascorbate and aldarate	2,5-Dioxopentanoate	0.92	1.44	1.97	0.015363
C ₆ H ₁₁ NO ₄		C5-Branched dibasic acid	4-Methyl-L-glutamate	-2.13	-0.97	-1.55	0.003676
C ₆ H ₆ O ₆		TCA cycle	cis-Aconitate	-0.88	-1.74	-1.52	0.040753
C ₄ H ₄ O ₄			Fumarate	-0.95	-1.87	-0.79	0.047604
C ₆ H ₁₀ O ₅		Fructose and mannose	2-Dehydro-3-deoxy-L-rhamnonate	-1.07	-1.70	-2.00	0.006820
C ₃ H ₈ O ₃		Galactose	Glycerol	-0.83	0.49	-1.58	0.003247
C ₇ H ₁₅ O ₁₀ P		PPP	D-Sedoheptulose 7-P	-1.83	-0.70	-2.03	0.000868
C ₄ H ₉ O ₇ P			D-Erythrose 4-P	-1.83	-0.51	-1.82	0.002133
C ₅ H ₁₁ O ₈ P			D-Ribose 5-P	-1.52	-1.10	-2.25	0.001589
C ₆ H ₁₂ O ₇			D-Gluconic acid	1.21	1.43	2.05	0.011645
C ₅ H ₁₁ O ₇ P			2-Deoxy-D-ribose 5-P	-1.00	-0.90	-2.06	0.014475
C ₃ H ₇ O ₅ P			Propanoate	-1.78	-0.24	-2.00	0.000034
C ₈ H ₁₄ O ₈	Glycan biosynthesis & metabolism	LPS biosynthesis	3-Deoxy-D-manno-octulosonate	-1.74	-1.32	-1.96	0.007821
C ₁₀ H ₁₈ N ₂ O ₃ S		biotin biosynthesis II	9-mercaptodethiobiotin	-0.55	1.57	-0.30	0.001057

C ₉ H ₂₀ N ₂ O ₂	Cofactors & vitamins	Biotin	7,8-Diaminononanoate	-1.97	-1.30	-1.37	0.019147
C ₇ H ₇ NO ₂		Nicotinate & nicotinamide	N-Methylnicotinate	1.77	1.67	2.28	0.000284
C ₁₁ H ₁₅ N ₂ O ₈ P			Nicotinamide D-ribonucleotide	-2.01	-1.28	-2.16	0.000342
C ₇ H ₆ O ₃		Ubiquinone biosynthesis	4-Hydroxybenzoate	-1.84	-0.73	-2.04	0.000841
C ₁₂ H ₂₀ N ₄ O ₈	Peptide	Acidic peptide	Ala-Asp-Gly-Ser	1.30	-0.15	1.90	0.000208
C ₁₃ H ₂₂ N ₄ O ₈ S ₂			Asp-Cys-Cys-Ser	-1.91	-0.60	-1.83	0.00158
C ₁₄ H ₂₀ N ₄ O ₁₁			Asp-Asp-Asp-Gly	0.06	1.50	1.52	0.01172
C ₁₃ H ₂₁ N ₃ O ₉			Glu-Asp-Thr	0.33	-1.71	-1.24	0.000442
C ₁₁ H ₁₉ N ₃ O ₇			Glu-Ala-Ser	-1.79	-0.07	-1.48	0.001976
C ₁₂ H ₁₉ N ₃ O ₉			Glu-Asp-Ser	-1.12	-1.09	-1.98	0.025683
C ₁₄ H ₂₁ N ₃ O ₈			Glu-Asp-Pro	-0.84	-2.07	-0.73	0.010812
C ₂₁ H ₃₆ N ₆ O ₁₀		Basic peptide	Glu-Glu-Gln-Lys	0.02	2.11	1.75	8.21E-16
C ₁₄ H ₂₆ N ₆ O ₆			Glu-Ala-Arg	1.82	1.19	1.74	0.015739
C ₁₉ H ₃₄ N ₄ O ₅ S ₂		Hydrophobic peptide	Cys-Leu-Met-Pro	1.87	1.29	2.29	0.000195
C ₂₁ H ₂₉ N ₅ O ₅ S			Ala-Met-Trp-Gly	-0.42	-1.90	-0.45	0.019406
C ₂₀ H ₃₂ N ₄ O ₇			Asp-Leu-Pro-Pro	0.54	-1.55	-0.41	0.006251
C ₁₅ H ₂₅ N ₃ O ₆			Glu-Pro-Val	-1.48	-1.90	-1.77	0.007997
C ₁₆ H ₃₁ N ₃ O ₄			Ile-Val-Val	1.04	1.53	1.91	0.020099
C ₁₇ H ₃₃ N ₃ O ₄			Ile-Ile-Val	0.51	1.50	1.84	0.012618
C ₁₁ H ₂₁ N ₃ O ₄			Ile-Ala-Gly	1.19	1.18	2.14	0.007660
C ₉ H ₁₅ N ₃ O ₄			Asparaginy-Proline	-0.62	-1.86	-1.82	0.003038
		0					

Table 3.4 Significant metabolites ($p \leq 0.05$) of ATCC 19606 identified following exposure to colistin (Col) and doripenem (Dor) alone and in combination (Combo) at 4 hr. Significant fold-changes are highlighted in yellow.

Formula	Map	Pathway	Metabolite	Col	Dor	Combo	P value
C ₄ H ₇ NO ₄	Amino Acid	Alanine and aspartate	L-Aspartate	1.67	1.82	2.43	0.000015
C ₅ H ₉ NO ₄			Arginine and proline	-1.09	-2.26	-2.20	7.58E-07
C ₇ H ₁₁ NO ₅		Arginine and proline	N-Acetyl-L-glutamate	-1.02	-2.31	-2.26	1.95E-10
C ₁₀ H ₁₈ N ₄ O ₆			N-(L-Arginino)succinate	-0.95	-2.15	-2.18	8.59E-06
C ₆ H ₁₃ N ₃ O ₃			L-Citrulline	-0.84	-2.45	-1.23	0.000062
C ₆ H ₁₃ NO ₇			N-Succinyl-L-glutamate	-0.76	-2.08	-1.95	0.000198
C ₁₅ H ₂₂ N ₆ O ₅ S			S-Adenosyl-L-methionine	-0.61	-2.24	-2.11	1.79E-11
C ₉ H ₁₈ N ₄ O ₄			N2-(D-1-Carboxyethyl)-L-arginine	-0.53	-2.35	-1.20	0.000074
C ₉ H ₁₆ N ₂ O ₅			N2-Succinyl-L-ornithine	-0.24	-2.09	-1.90	4.35E-08
C ₉ H ₁₃ NO ₆			N-Succinyl-L-glutamate 5-semialdehyde	-0.20	1.62	1.85	1.46E-06
C ₁₀ H ₁₈ N ₄ O ₅			N2-Succinyl-L-arginine	-0.16	-2.12	-1.81	8.03E-09
C ₅ H ₉ NO ₂			L-Proline	0.20	-1.77	-0.23	0.005147
C ₉ H ₁₉ N ₃ O ₃			gamma-L-Glutamylputrescine	0.38	1.47	1.90	0.005666
C ₉ H ₁₆ N ₂ O ₅			gamma-Glutamyl-gamma-aminobutyrate	0.61	1.91	1.95	0.000544
C ₆ H ₁₂ N ₂ O ₄ S ₂		Cysteine	L-Cystine	-0.19	-2.24	-1.54	4.76E-07
C ₆ H ₁₂ N ₂ O ₃		D-Alanine	D-Alanyl-D-alanine	-0.27	-1.96	-2.09	3.47E-09
C ₂₀ H ₃₁ N ₃ O ₁₉ P ₂		D-Glutamine & D-glutamate	UDP-N-acetylmuramate	-0.57	-2.09	-2.23	2.19E-11
C ₈ H ₁₆ NO ₉ P		Glutamate	N-Acetyl-D-glucosamine 6-P	-0.91	-2.33	-2.06	4.11E-07
C ₄ H ₆ O ₃			Succinate semialdehyde	0.97	2.12	2.23	5.80E-06
C ₂₀ H ₃₂ N ₆ O ₁₂ S ₂			Glutathione disulfide	-0.72	-2.19	-2.25	1.74E-14
C ₅ H ₁₃ NO		Glycine, serine and threonine	Choline	-0.42	-2.23	-1.35	0.000225
C ₃ H ₇ NO ₂ S			L-Cysteine	-0.13	-2.17	-1.27	0.000043
C ₃ H ₄ O ₄			Hydroxypyruvate	0.96	2.24	1.78	0.000327

C ₆ H ₆ N ₂ O ₂		Histidine	Urocanate	0.00	2.19	1.37	2.45E-07
C ₇ H ₁₄ N ₂ O ₄		Lysine biosynthesis	meso-2,6-Diaminoheptanedioate	-0.91	-2.00	-0.37	0.008712
C ₈ H ₁₆ N ₂ O ₃			N2-Acetyl-L-lysine	-0.47	-2.20	-2.01	3.80E-09
C ₄₁ H ₆₅ N ₉ O ₂₈ P ₂			UDP-N-acetylmuramoyl-L-alanyl-D-glutamyl-6-carboxy-L-lysyl-D-alanyl-D-alanine	-0.36	-1.94	-2.09	1.02E-06
C ₅ H ₈ O ₃		Lysine degradation	5-Oxopentanoate	0.13	2.24	1.49	9.32E-08
C ₈ H ₁₆ N ₂ O ₄			N6-Acetyl-N6-hydroxy-L-lysine	0.38	1.42	1.98	0.003456
C ₆ H ₁₁ NO ₄		Methionine	O-Acetyl-L-homoserine	-0.16	-1.76	-1.57	0.002840
C ₁₄ H ₂₀ N ₆ O ₅ S			S-Adenosyl-L-homocysteine	0.06	-0.69	-1.78	0.012369
C ₉ H ₁₀ O ₄		Phenylalanine	3-(2,3-Dihydroxyphenyl)propanoate	-0.32	-2.13	-1.96	6.16E-09
C ₈ H ₁₁ N			Phenethylamine	0.50	1.88	0.54	0.027898
C ₉ H ₈ O ₃			Phenylpyruvate	0.79	2.01	2.32	3.19E-07
C ₁₀ H ₁₃ O ₁₀ P		Phenylalanine, tyrosine and tryptophan biosynthesis	5-O-(1-Carboxyvinyl)-3-phosphoshikimate	-0.08	-2.10	-1.46	0.000018
C ₂ H ₅ O ₅ P		Taurine and hypotaurine	Acetyl phosphate	-1.07	-1.62	-2.00	0.009353
C ₁₁ H ₁₂ N ₂ O ₂		Tryptophan	L-Tryptophan	0.07	-1.55	-1.33	0.011505
C ₁₀ H ₉ NO ₂			N-Acetylindoxyl	0.53	1.85	2.19	0.000010
C ₈ H ₁₁ NO		Tyrosine	Tyramine	0.06	1.94	1.97	3.43E-12
C ₉ H ₈ O ₅			3-(3,4-Dihydroxyphenyl)pyruvate	0.07	1.99	1.92	9.94E-11
C ₈ H ₈ O ₄			3,4-Dihydroxyphenylacetate	0.35	-1.71	-1.10	0.000973
C ₉ H ₈ O ₄			3-(4-Hydroxyphenyl)pyruvate	0.78	1.74	2.12	0.000969
C ₉ H ₈ O ₃			4-Coumarate	1.69	1.51	1.80	0.01506
C ₅ H ₁₀ O ₄		Valine, leucine and isoleucine biosynthesis	(R)-2,3-Dihydroxy-3-methylbutanoate	-1.43	-2.05	-2.12	0.000345
C ₇ H ₁₂ O ₅			(2S)-2-Isopropylmalate	-0.88	-2.10	-2.18	0.000012
C ₆ H ₁₀ O ₄			(S)-2-Aceto-2-hydroxybutanoate	-0.29	1.80	0.63	0.002162
C ₆ H ₁₀ O ₃		Valine, leucine and isoleucine degradation	(S)-3-Methyl-2-oxopentanoic acid	0.25	2.21	1.56	0.000004
C ₄ H ₆ O ₃			2-Methyl-3-oxopropanoate	0.26	1.90	0.35	0.010738
C ₅ H ₈ O ₃			3-Methyl-2-oxobutanoic acid	0.42	2.28	1.70	1.49E-06
C ₆ H ₁₀ O ₃			4-Methyl-2-oxopentanoate	0.61	2.22	2.07	2.31E-08
C ₁₅ H ₁₀ O ₅	Biosynthesis of Secondary Metabolites	Flavonoid biosynthesis	Apigenin	0.55	2.41	0.80	0.000022
C ₁₅ H ₁₀ O ₅		Isoflavonoid biosynthesis	2'-Hydroxydaidzein	1.33	2.55	1.78	1.01E-06
C ₆ H ₁₃ NO ₅	Carbohydrate	Aminosugars	D-Glucosamine	-0.82	-2.35	-1.38	0.000320
C ₁₇ H ₂₇ N ₃ O ₁₇ P ₂			UDP-N-acetyl-D-glucosamine	-0.67	-2.24	-2.15	1.84E-10
C ₅ H ₆ O ₄		Ascorbate and aldarate	2,5-Dioxopentanoate	-0.04	1.56	1.96	0.000016
C ₆ H ₁₁ NO ₄		C5-Branched dibasic acid	4-Methyl-L-glutamate	-1.19	-2.07	-1.84	0.002295
C ₆ H ₆ O ₆		TCA cycle	cis-Aconitate	0.40	1.16	2.20	0.000681
C ₄ H ₄ O ₄			Fumarate	1.57	1.88	2.36	0.000060
C ₆ H ₁₀ O ₅		Fructose and mannose	2-Dehydro-3-deoxy-L-rhamnonate	-1.44	-2.39	-2.10	1.78E-06
C ₁₂ H ₂₂ O ₁₁		Galactose	Lactose	-0.73	-1.44	-2.60	3.38E-10
C ₃ H ₇ O ₇ P		Glycolysis / Gluconeogenesis	3-Phospho-D-glycerate	-0.01	-2.05	-1.53	7.76E-06
C ₃ H ₇ O ₆ P			Glycerone phosphate	0.10	-1.83	-1.75	1.54E-06
C ₃ H ₅ O ₆ P			Phosphoenolpyruvate	0.15	-1.91	-1.49	0.000015
C ₁₅ H ₂₄ N ₂ O ₁₇ P ₂		Pentose & glucuronate interconversions	UDP-glucose	-0.92	-2.27	-2.26	7.87E-11
C ₆ H ₁₂ O ₇			D-Mannosate	0.81	2.35	0.85	0.000404
C ₄ H ₉ O ₇ P		PPP	D-Erythrose 4-P	-0.99	-1.69	-1.88	0.012929
C ₇ H ₁₅ O ₁₀ P			D-Sedoheptulose 7-P	-0.93	-1.65	-1.97	0.008206
C ₅ H ₁₁ O ₇ P			2-Deoxy-D-ribose 5-P	-0.36	-1.75	-2.17	0.000004
C ₅ H ₁₁ O ₈ P			D-Ribose 5-P	-0.34	-1.99	-2.11	2.56E-08
C ₆ H ₁₃ O ₁₀ P			6-Phospho-D-gluconate	-0.32	-2.24	-1.74	2.21E-07
C ₆ H ₁₂ O ₇			D-Gluconic acid	0.23	1.82	2.03	5.42E-06
C ₆ H ₁₃ NO ₆			2-Amino-2-deoxy-D-gluconate	0.59	0.74	1.86	0.04274
C ₇ H ₁₀ O ₇		Propanoate	2-Methylcitrate	-0.54	-1.73	-2.29	6.43E-06
C ₃ H ₇ O ₅ P			Propanoyl phosphate	-0.38	1.64	0.09	0.005821
C ₁₂ H ₂₃ O ₁₄ P		Starch & sucrose	Sucrose 6-P	-2.27	-1.87	-2.24	2.38E-07

C ₈ H ₁₈ NO ₁₀ P		undefined	N-Gluconyl ethanolamine phosphate	-0.73	-2.30	-1.80	0.000016
C ₂₂ H ₃₂ O ₁₃			(S)-Multifidol 2-[apiosyl-(1->6)-glucoside]	-0.38	-2.17	-1.81	0.000002
C ₁₈ H ₃₃ NO ₁₅			beta-D-Galactopyranosyl-(1->4)-2-amino-2-deoxy-beta-D-glucopyranosyl-(1->6)-D-mannose	-0.29	-2.07	-1.71	0.000044
C ₆ H ₁₄ O ₁₂ P ₂	Energy	Carbon fixation	D-Fructose 1,6-bisphosphate	-0.05	-1.98	-1.84	5.43E-08
C ₈ H ₁₄ O ₈	Glycan Biosynthesis & Metabolism	LPS biosynthesis	3-Deoxy-D-manno-octulosonate	-0.67	-2.10	-2.25	1.84E-09
C ₇ H ₁₆ O ₁₃ P ₂			D-glycero-D-manno-Heptose 1,7-bisphosphate	0.04	-2.02	-1.52	5.85E-06
C ₁₀ H ₁₈ N ₂ O ₅ S	Cofactors & Vitamins	biotin biosynthesis II	9-mercaptopdethiobiotin	1.59	2.18	1.99	0.000276
C ₉ H ₂₀ N ₂ O ₂		Biotin	7,8-Diaminononanoate	-0.32	-1.81	-2.00	0.000054
C ₁₁ H ₁₅ N ₂ O ₈ P		Nicotinate and nicotinamide	Nicotinamide D-ribonucleotide	-0.22	-2.17	-1.62	0.000003
C ₆ H ₈ O ₃		pantothenate and coenzyme A biosynthesis III	Dihydro-4,4-dimethyl-2,3-Furandione	0.94	2.05	1.45	0.009185
C ₇ H ₆ O ₃		Ubiquinone biosynthesis	4-Hydroxybenzoate	-1.24	-1.89	-2.10	0.001408
C ₈ H ₁₃ N ₂ O ₅ P		Vitamin B6	Pyridoxamine phosphate	-0.23	-1.75	-1.86	0.000421
C ₁₃ H ₂₂ N ₄ O ₈ S ₂	Peptide	Acidic peptide	Asp-Cys-Cys-Ser	-0.58	-2.22	-2.12	1.28E-11
C ₁₅ H ₂₄ N ₄ O ₉			Asp-Pro-Ser-Ser	-0.16	-1.30	-1.84	0.005634
C ₁₄ H ₂₀ N ₄ O ₁₁			Asp-Asp-Asp-Gly	0.05	1.86	2.00	3.60E-09
C ₁₃ H ₂₁ N ₅ O ₈			Ala-Asn-Asp-Gly	1.32	2.41	1.77	0.000059
C ₁₁ H ₁₉ N ₃ O ₇			Glu-Ala-Ser	-0.96	-2.19	-2.27	1.36E-07
C ₁₃ H ₂₁ N ₃ O ₈			Glu-Ala-Glu	-0.48	-2.04	-1.60	0.001209
C ₁₂ H ₁₉ N ₃ O ₉			Glu-Asp-Ser	0.03	-1.69	-1.48	0.00215
C ₁₃ H ₂₁ N ₃ O ₇			Glu-Pro-Ser	0.06	-0.53	-1.66	0.032719
C ₁₃ H ₂₃ N ₃ O ₈			Glu-Thr-Thr	0.62	0.42	-1.58	0.000192
C ₂₁ H ₃₆ N ₆ O ₁₀		Basic peptide	Glu-Glu-Gln-Lys	-0.18	1.83	1.83	1.90E-11
C ₂₄ H ₃₂ N ₆ O ₈ S		Hydrophobic peptide	Asn-Met-Trp-Asp	-0.32	0.95	1.65	0.004643
C ₂₀ H ₃₃ N ₅ O ₈			Asn-Glu-Ile-Pro	-0.11	0.21	1.74	0.009794
C ₂₅ H ₃₇ N ₅ O ₅			Ala-Leu-Trp-Val	-0.01	1.57	2.12	3.36E-08
C ₁₈ H ₃₁ N ₅ O ₇			Asn-Thr-Val-Pro	0.15	1.62	2.00	0.000065
C ₁₆ H ₂₈ N ₄ O ₆			Ala-Val-Pro-Ser	0.32	-1.64	-1.67	3.73E-06
C ₁₉ H ₃₄ N ₄ O ₅ S ₂			Cys-Leu-Met-Pro	0.41	-1.51	-1.41	0.000480
C ₁₆ H ₂₈ N ₄ O ₅			Ala-Leu-Gly-Pro	0.57	-1.67	-0.20	0.000994
C ₁₈ H ₃₁ N ₅ O ₉			Asn-Glu-Ile-Ser	0.61	1.11	2.31	0.000396
C ₂₀ H ₃₂ N ₄ O ₇			Asp-Leu-Pro-Pro	0.79	-0.32	1.57	0.014219
C ₁₄ H ₂₆ N ₄ O ₆			Ala-Thr-Val-Gly	0.84	1.60	1.88	0.014772
C ₁₃ H ₂₃ N ₃ O ₆ S			Ile-Asp-Cys	0.18	2.30	1.28	1.39E-06
C ₁₇ H ₃₃ N ₃ O ₄			Ile-Ile-Val	0.33	1.75	1.47	0.012734
C ₁₄ H ₂₅ N ₃ O ₅			Ile-Pro-Ser	0.94	1.20	2.31	0.001212
C ₁₁ H ₂₁ N ₃ O ₄			Ile-Ala-Gly	1.11	1.97	1.54	0.014116
C ₁₉ H ₂₅ N ₃ O ₄			Phe-Pro-Pro	1.23	0.40	1.99	0.006365
C ₁₂ H ₂₂ N ₄ O ₆		Polar peptide	Ala-Thr-Ala-Gly	-0.39	-2.23	-0.65	0.000425
C ₁₃ H ₂₄ N ₄ O ₅			Ala-Gly-Pro-Pro	0.69	-1.52	0.44	0.000285
C ₁₇ H ₂₇ N ₅ O ₆			Ala-Asn-Pro-Pro	0.86	1.30	2.39	0.000206
C ₁₀ H ₁₉ N ₅ O ₅		undefined	Aspartyl-Arginine	-0.01	-1.81	-0.73	0.013069
C ₁₁ H ₂₀ N ₂ O ₅			L-γ-glutamyl-L-leucine	0.10	0.95	2.18	0.000108
C ₁₀ H ₁₈ N ₂ O ₅			L-β-aspartyl-L-leucine	0.85	1.32	2.00	0.016341
C ₁₁ H ₂₀ N ₂ O ₅			L-γ-glutamyl-L-isoleucine	1.14	1.64	2.56	1.25E-06

Table 3.5 Significant metabolites ($p \leq 0.05$) of 03-149.1 identified following exposure to colistin (Col) and doripenem (Dor) alone and in combination (Combo) at 15 min. Significant fold-changes are highlighted in yellow.

Formula	Map	Pathway	Metabolite	Col	Dor	Combo	P value
C ₉ H ₁₈ N ₂ O ₄	Amino Acid	0	Meprobamate	-1.1	-0.9	-2.2	0.019377
C ₉ H ₁₉ N ₃ O ₄			Lysinoalanine	-0.8	-0.5	-2.1	0.015845
C ₁₁ H ₁₃ NO ₄			N-Acetyl-L-tyrosine	-2.1	-0.6	-1.7	0.001328
C ₉ H ₁₄ N ₄ O ₃		Alanine and aspartate	Carnosine	-1.5	-0.1	-1.6	0.011253
C ₆ H ₉ NO ₅			N-Acetyl-L-aspartate	-2.1	-0.4	-1.2	0.002834
C ₆ H ₁₄ N ₄ O ₂		Arginine and proline	L-Arginine	-2.1	-0.4	-2.0	4.55E-06
C ₅ H ₉ NO ₄			L-Glutamate	-1.8	-0.3	-1.9	0.000886
C ₉ H ₁₃ NO ₇			N-Succinyl-L-glutamate	-2.0	-0.4	-1.8	0.000363
C ₁₅ H ₂₂ N ₆ O ₅ S			S-Adenosyl-L-methionine	-1.8	0.0	-1.7	0.000223
C ₅ H ₁₂ N ₂ O ₂			L-Ornithine	-1.8	0.1	-1.4	0.001101
C ₆ H ₉ NO ₂			L-Proline	-1.8	-0.2	-1.4	0.008895
C ₉ H ₁₆ N ₂ O ₅			gamma-Glutamyl-gamma-aminobutyrate	-1.6	0.0	-1.3	0.017451
C ₇ H ₁₁ NO ₅			N-Acetyl-L-glutamate	-1.9	-0.2	-1.2	0.003129
C ₆ H ₁₃ N ₃ O ₃			L-Citrulline	-1.7	0.1	-0.9	0.006036
C ₈ H ₁₅ N ₃ O ₄			N-Acetyl-L-citrulline	-1.4	-0.6	-2.2	0.004982
C ₃ H ₅ NO ₂		arginine biosynthesis III					
C ₆ H ₁₂ N ₂ O ₃		Cysteine metabolism	2-Aminoacrylate	0.5	2.0	-0.2	0.000718
C ₆ H ₁₁ N ₃ O ₃		D-Alanine metabolism	D-Alanyl-D-alanine	-2.0	0.4	-0.9	2.48E-07
C ₃ H ₁₀ N ₂ O ₃		D-Arginine and D-ornithine	5-Guanidino-2-oxopentanoate	-2.0	-0.4	-1.4	0.002740
C ₈ H ₁₄ N ₂ O ₅ S		Glutamate	L-Glutamine	-1.9	-0.2	-2.0	7.47E-06
C ₈ H ₁₅ NO ₆			gamma-L-Glutamyl-L-cysteine	-1.9	0.0	-1.8	1.43E-07
C ₆ H ₁₄ NO ₈ P			N-Acetyl-D-glucosamine	0.2	-1.7	0.6	0.000151
C ₈ H ₁₆ NO ₉ P			D-Glucosamine 6-phosphate	0.9	-0.1	2.2	0.000062
C ₄ H ₉ N ₃ O ₂			N-Acetyl-D-glucosamine 6-phosphate	1.4	0.1	2.3	0.000019
C ₆ H ₁₀ N ₂ O ₂		Glycine, serine and threonine	Creatine	-2.1	-0.7	-2.0	0.000311
C ₅ H ₉ NO ₃			Ectoine	-2.2	-0.9	-1.9	0.000080
C ₁₀ H ₁₄ N ₂ O ₆			5-Aminolevulinate	-2.2	-0.2	-1.7	1.88E-10
C ₁₀ H ₁₅ N ₂ O ₉ P		Histidine	(1-Ribosylimidazole)-4-acetate	-2.0	-1.0	-1.9	0.002090
C ₉ H ₁₅ N ₃ O ₂			1-(5-Phosphoribosyl)imidazole-4-acetate	-1.9	-0.1	-1.5	0.001418
C ₆ H ₁₀ N ₂ O ₄			Hercynine	-1.5	0.1	-1.5	0.009637
C ₆ H ₁₄ N ₂ O ₂			N-Formimino-L-glutamate	-2.0	-0.4	-1.3	0.003868
C ₇ H ₁₄ N ₂ O ₄		Lysine biosynthesis	L-Lysine	-1.9	-0.1	-1.8	0.000025
C ₇ H ₁₄ N ₂ O ₄			meso-2,6-Diaminoheptanedioate	-2.0	0.0	-1.6	0.000014
C ₃₅ H ₅₅ N ₇ O ₂₆ P ₂			LL-2,6-Diaminoheptanedioate	-1.9	-0.1	-1.5	0.000166
C ₈ H ₁₆ N ₂ O ₃			UDP-N-acetylmuramoyl-L-alanyl-D-gamma-glutamyl-meso-2,6-diaminopimelate	0.4	-1.8	-1.3	1.23E-06
C ₆ H ₁₁ NO ₄			N2-Acetyl-L-lysine	-1.8	0.3	-1.3	6.30E-06
C ₇ H ₉ NO ₄		Lysine degradation	L-2-Aminoadipate	-2.0	0.1	-1.3	0.000028
C ₄₁ H ₆₅ N ₉ O ₂₈ P ₂			2,3,4,5-Tetrahydrodipicolinate	-1.9	-0.3	-1.2	0.004910
C ₉ H ₂₀ N ₂ O ₂			UDP-N-acetylmuramoyl-L-alanyl-D-glutamyl-6-carboxy-L-lysyl-D-alanyl-D-alanine	0.3	0.6	2.5	0.000023
C ₉ H ₁₈ N ₂ O ₄			N6,N6,N6-Trimethyl-L-lysine	-1.9	-0.1	-1.7	0.000060
C ₇ H ₁₅ NO ₃			N2-(D-1-Carboxyethyl)-L-lysine	-2.0	0.0	-1.7	1.10E-07
C ₈ H ₁₆ N ₂ O ₃			L-Carnitine	-1.9	-0.2	-1.3	0.006004
			N6-Acetyl-L-lysine	-1.9	-1.6	-0.6	0.007393

C ₆ H ₉ NO ₂		Methionine	2,3,4,5-Tetrahydropyridine-2-carboxylate	0.6	-0.5	1.8	0.003195
C ₃ H ₁₁ NO ₂ S			L-Methionine	-1.7	-0.1	-1.6	0.001898
C ₆ H ₁₁ NO ₄			O-Acetyl-L-homoserine	-1.8	0.2	-1.6	0.000038
C ₅ H ₁₁ NO ₃ S			L-Methionine S-oxide	-2.2	-0.3	-1.5	0.000028
C ₈ H ₁₃ NO ₆			O-Succinyl-L-homoserine	-2.0	-0.2	-1.1	0.002475
C ₉ H ₁₁ NO ₂		Phenylalanine	L-Phenylalanine	-1.7	0.3	-1.6	0.000010
C ₉ H ₈ O ₃			Phenylpyruvate	1.8	-0.2	1.8	9.78E-07
C ₆ H ₇ NO		Tryptophan	2-Aminophenol	-1.6	0.1	-1.7	0.000381
C ₁₁ H ₁₂ N ₂ O ₂			L-Tryptophan	-1.8	0.1	-1.5	0.000369
C ₁₀ H ₉ NO ₄			4-(2-Aminophenyl)-2,4-dioxobutanoate	-1.7	0.0	-1.2	0.01511
C ₈ H ₇ N			Indole	-1.6	0.3	-1.2	0.004602
C ₁₀ H ₉ NO ₂			Indole-3-acetate	1.4	-0.2	1.6	0.005537
C ₉ H ₁₁ NO ₃		Tyrosine	L-Tyrosine	-1.8	-0.6	-2.0	0.003006
C ₉ H ₉ NO ₄			Dopaquinone	-1.9	-0.7	-0.4	0.017413
C ₉ H ₈ O ₄			2-Hydroxy-3-(4-hydroxyphenyl)propenoate	1.6	-0.5	1.3	0.000037
C ₈ H ₁₁ NO ₃			L-Noradrenaline	1.0	-0.2	1.9	0.002437
C ₈ H ₁₁ NO			Tyramine	0.1	1.9	2.0	1.24E-08
C ₆ H ₁₀ O ₄		Valine, leucine and isoleucine biosynthesis	(S)-2-Aceto-2-hydroxybutanoate	1.8	0.1	1.7	0.000158
C ₆ H ₁₃ NO ₂			L-Leucine	-2.0	-0.2	-1.7	0.000244
C ₆ H ₁₃ NO ₂			L-Isoleucine	-1.9	-0.1	-1.7	0.000210
C ₄ H ₈ O ₃			(S)-3-Hydroxyisobutyrate	-1.7	0.2	-1.7	0.000043
C ₅ H ₁₁ NO ₂			L-Valine	-2.0	-0.2	-1.6	0.000118
C ₁₅ H ₂₄ O	Biosynthesis of Secondary Metabolites	0	2-trans,6-trans-Farnesal	2.0	0.4	1.8	0.000318
C ₇ H ₉ NO ₃		(5R)-carbapenem biosynthesis	(3S,5S)-carbapenam	-0.4	1.6	1.7	8.23E-08
C ₉ H ₁₈ N ₄ O ₄		Clavulanic acid biosynthesis	L-N ₂ -(2-Carboxyethyl)arginine	-2.1	-0.2	-1.6	5.58E-06
C ₁₆ H ₂₅ N ₅ O ₆		Zeatin biosynthesis	Dihydrozeatin-O-glucoside	-1.8	-0.3	-1.1	0.020626
C ₈ H ₁₈ NO ₁₀ P	Carbohydrate	0	N-Gluconyl ethanolamine phosphate	-1.8	0.0	-1.8	0.000010
C ₁₂ H ₂₀ N ₂ O ₇			Deoxyfructosazine	-2.1	-0.6	-1.0	0.003836
C ₈ H ₁₅ NO ₆		Aminosugars	N-Acetyl-D-mannosamine	1.7	-0.3	1.7	9.67E-07
C ₂₀ H ₂₉ N ₅ O ₁₉ P ₂			UDP-N-acetyl-3-(1-carboxyvinyl)-D-glucosamine	1.8	0.0	2.0	2.53E-09
C ₆ H ₁₀ O ₈		Ascorbate and aldarate	D-Glucarate	-1.7	-0.3	-1.7	0.004616
C ₄ H ₈ O ₅			[FA trihydroxy(4:0)] 2,3,4-trihydroxy-butanoic acid	-1.8	0.0	-1.3	0.003263
C ₅ H ₆ O ₄			2,5-Dioxopentanoate	-1.7	0.2	-0.7	0.005769
C ₅ H ₈ O ₄		Butanoate	2-Acetolactate	-1.9	-0.3	-1.3	0.010647
C ₄ H ₆ O ₅		TCA cycle	(S)-Malate	-2.1	-0.6	-2.0	0.000031
C ₅ H ₆ O ₅			2-Oxoglutarate	-1.8	-1.5	-1.9	0.009938
C ₂₁ H ₃₆ N ₇ O ₁₆ P ₃ S			CoA	-1.9	0.0	-1.7	6.08E-06
C ₂₄ H ₄₂ O ₂₁		Galactose	Stachyose	-1.7	0.1	-1.6	0.000525
C ₆ H ₁₀ O ₆			2-Dehydro-3-deoxy-D-galactonate	-1.9	-0.3	-1.4	0.006064
C ₁₂ H ₂₄ O ₁₁			Melibiose	-1.7	-0.1	-1.4	0.015204
C ₁₂ H ₂₂ O ₁₁		glycogen degradation I	beta-Maltose	-1.8	0.1	-1.3	0.000663
C ₂₃ H ₃₈ N ₇ O ₁₇ P ₃ S		Glycolysis /	Acetyl-CoA	-1.7	-0.2	-1.8	0.001909
C ₁₂ H ₁₈ N ₄ O ₇ P ₂ S		Gluconeogenesis	Thiamin diphosphate	-1.9	-0.2	-1.2	0.006093
C ₆ H ₁₀ O ₅		Glyoxylate and dicarboxylate	3-Ethylmalate	-0.9	-0.1	-2.1	0.005695
C ₆ H ₁₀ O ₆		Inositol metabolism	2,4,6/3,5-Pentahydroxycyclohexanone	-1.7	0.1	-1.1	0.010751
C ₇ H ₁₄ O ₆			1-O-Methyl-myo-inositol	-1.7	0.2	-1.3	0.001638
C ₅ H ₁₀ O ₆		Pentose & glucuronate interconversions	L-Lyxonate	-1.6	0.2	-1.4	0.001413
C ₅ H ₁₀ O ₆			D-Xylonate	-0.4	-1.9	-0.3	0.009746
C ₅ H ₁₃ O ₁₄ P ₃		PPP	5-Phospho-alpha-D-ribose 1-diphosphate	-2.1	-0.4	-1.6	0.000290
C ₅ H ₁₀ O ₄			Deoxyribose	-1.7	0.1	-1.3	0.002155
C ₅ H ₁₀ O ₅			D-Ribose	-1.8	0.2	-1.2	0.000445
C ₆ H ₁₀ O ₆			2-Dehydro-3-deoxy-D-gluconate	-1.7	0.0	-1.1	0.01354
C ₃ H ₇ O ₅ P		Propanoate metabolism	Propanoyl phosphate	-2.1	-0.5	-1.9	0.000013
C ₆ H ₁₃ O ₉ P		Starch and sucrose	D-Glucose 6-phosphate	-1.6	-0.3	-1.7	0.010495
C ₁₀ H ₁₅ N ₅ O ₁₀ P ₂	Energy	Oxidative phosphorylation	ADP	-1.9	-0.3	-1.5	0.001803
C ₁₀ H ₁₆ N ₅ O ₁₃ P ₃			ATP	-2.0	-0.4	-1.3	0.002432
C ₂₁ H ₂₈ N ₇ O ₁₇ P ₃		Photosynthesis	NADP+	-1.8	-0.6	-1.8	0.005682

C ₈ H ₁₄ O ₈	Glycan Biosynthesis & Metabolism	LPS biosynthesis	3-Deoxy-D-manno-octulosonate	1.4	-0.5	1.5	0.000538
C ₆ H ₅ NO ₂	Cofactors & Vitamins	Nicotinate & nicotinamide	Nicotinate	1.8	-0.1	1.4	0.000340
C ₁₄ H ₁₈ N ₂ O ₄		Riboflavin	α -Ribazole	-1.5	0.2	-1.6	0.001781
C ₈ H ₁₃ N ₂ O ₅ P		Vitamin B6	Pyridoxamine phosphate	-1.8	-0.2	-1.6	0.002969

Table 3.6 Significant metabolites ($p \leq 0.05$) of 03-149.1 identified following exposure to colistin (Col) and doripenem (Dor) alone and in combination (Combo) at 1 hr. Significant fold-changes are highlighted in yellow.

Formula	Map	Pathway	Metabolite	Col	Dor	Combo	P value
C ₉ H ₁₉ N ₃ O ₄	Amino Acid	0	Lysinoalanine	-0.1	-0.4	-2.2	6.68E-05
C ₁₃ H ₁₄ N ₂ O ₂			(1xi,3xi)-1,2,3,4-Tetrahydro-1-methyl- β -carboline-3-carboxylic acid	-1.3	0.2	-2.0	4.79E-06
C ₁₂ H ₂₄ N ₂ O ₇			1-[(5-Amino-5-carboxypentyl)amino]-1-deoxyfructose	-1.3	0.0	-2.0	0.000126
C ₁₀ H ₁₈ N ₂ O ₆ S			γ -L-Glutamyl-L-methionine sulfoxide	-0.6	0.1	-2.0	0.001011
C ₆ H ₁₂ N ₂ O			L-Lysine 1,6-lactam	-1.2	0.2	-1.9	0.000122
C ₉ H ₁₄ N ₂ O ₅			(2S,3'S)- α -Amino-2-carboxy-5-oxo-1-pyrrolidinebutanoic acid	-1.6	0.0	-1.9	8.66E-05
C ₁₁ H ₁₃ NO ₄			N-Acetyl-L-tyrosine	-1.4	0.4	-1.8	3.65E-06
C ₁₂ H ₂₄ N ₄ O ₇			N2-Fructopyranosylarginine	-1.3	0.2	-1.8	0.000686
C ₁₂ H ₁₂ N ₂ O ₂			L-1,2,3,4-Tetrahydro-beta-carboline-3-carboxylic acid	-1.2	0.2	-1.7	0.001738
C ₆ H ₁₃ N ₃ O ₄			4-Hydroxycitrulline	-1.8	0.0	-1.7	0.000205
C ₇ H ₁₁ N ₃ O ₃			(S)-N-(4,5-Dihydro-1-methyl-4-oxo-1H-imidazol-2-yl)alanine	-1.2	0.3	-1.6	0.005470
C ₆ H ₁₈ N ₂ O ₄			Meprobamate	0.4	0.1	-1.6	0.007501
C ₉ H ₁₄ N ₄ O ₃		Alanine and aspartate	Carnosine	-1.6	0.2	-2.0	3.90E-07
C ₆ H ₉ NO ₅			N-Acetyl-L-aspartate	-1.8	0.1	-1.9	1.31E-08
CH ₃ O ₄ P		Aminophosphonate	Hydroxymethylphosphonate	-1.0	-1.6	0.3	0.005838
C ₉ H ₁₆ N ₂ O ₅		Arginine and proline	gamma-Glutamyl-gamma-aminobutyrate	-0.9	0.1	-2.1	4.75E-05
C ₆ H ₁₄ N ₄ O ₂			L-Arginine	-1.4	-0.1	-2.1	8.69E-05
C ₁₅ H ₂₂ N ₆ O ₅ S			S-Adenosyl-L-methionine	-1.6	0.1	-2.1	4.49E-08
C ₉ H ₁₈ N ₄ O ₄			N2-(D-1-Carboxyethyl)-L-arginine	-1.5	0.0	-2.0	2.21E-06
C ₁₀ H ₁₈ N ₄ O ₅			N2-Succinyl-L-arginine	-1.6	0.0	-2.0	4.45E-05
C ₆ H ₁₃ N ₃ O ₃			L-Citrulline	-1.6	0.2	-2.0	2.61E-10
C ₉ H ₁₆ N ₂ O ₄			gamma-Glutamyl-gamma-aminobutyraldehyde	-1.5	0.2	-1.9	2.58E-06
C ₇ H ₁₁ NO ₅			N-Acetyl-L-glutamate	-1.7	0.2	-1.9	5.01E-08
C ₈ H ₁₁ N ₃ O ₂			4-Guanidinobutanoate	-1.2	0.1	-1.9	0.000938
C ₅ H ₁₂ N ₂ O ₂			L-Ornithine	-1.8	-0.1	-1.8	9.44E-05
C ₅ H ₉ NO ₂			L-Proline	-1.6	0.0	-1.8	0.000255
C ₉ H ₁₆ N ₂ O ₅			N2-Succinyl-L-ornithine	-1.5	0.3	-1.8	3.55E-06
C ₇ H ₁₄ N ₂ O ₃			N-Acetylornithine	-1.8	0.1	-1.8	6.94E-06
C ₉ H ₁₃ NO ₇			N-Succinyl-L-glutamate	-2.0	0.0	-1.6	6.63E-06
C ₅ H ₉ NO ₄			L-Glutamate	-1.2	0.3	-2.0	8.85E-06
C ₈ H ₁₅ N ₃ O ₄		arginine biosynthesis III	N-Acetyl-L-citrulline	-0.2	0.0	-1.8	0.012019
C ₉ H ₁₇ NO ₅		beta-Alanine	Pantothenate	-1.3	0.1	-1.9	0.000242

C ₉ H ₁₉ N ₅ O ₃			beta-Alanyl-L-arginine	0.5	0.0	-1.5	0.008931
C ₅ H ₉ NO ₃			N-Acetyl-beta-alanine	-0.7	0.9	-1.5	3.73E-05
C ₉ H ₁₉ N ₃ O ₃			beta-Alanyl-L-lysine	0.8	-0.1	-1.4	0.004656
C ₆ H ₁₂ N ₂ O ₄ S ₂		Cysteine	L-Cystine	-1.1	0.3	-1.6	0.006243
C ₃ H ₅ NO ₂			2-Aminoacrylate	-2.4	-0.2	-0.8	2.15E-07
C ₆ H ₁₂ N ₂ O ₃		D-Alanine	D-Alanyl-D-alanine	-1.7	0.4	-1.5	4.45E-07
C ₆ H ₁₁ N ₃ O ₃		D-Arginine and D-ornithine	5-Guanidino-2-oxopentanoate	-1.6	0.0	-2.0	3.66E-06
C ₃ H ₁₂ N ₂ O ₂			(2R,4S)-2,4-Diaminopentanoate	-1.5	0.3	-1.8	1.72E-07
C ₂₀ H ₃₁ N ₃ O ₁₉ P ₂			UDP-N-acetylmuramate	-1.7	0.1	-1.9	1.08E-06
C ₅ H ₁₀ N ₂ O ₃		Glutamate	L-Glutamine	-1.7	0.0	-2.1	3.13E-10
C ₆ H ₁₄ NO ₈ P			D-Glucosamine 6-phosphate	-1.5	0.1	-2.0	1.21E-06
C ₈ H ₁₄ N ₂ O ₅ S			gamma-L-Glutamyl-L-cysteine	-1.9	0.0	-1.9	1.09E-07
C ₅ H ₁₀ N ₂ O ₃ S		Glutathione	Cys-Gly	-1.9	-0.1	-1.8	2.29E-05
C ₅ H ₇ NO ₃			5-Oxoproline	-0.7	0.0	-1.8	0.016431
C ₄ H ₉ N ₃ O ₂		Glycine, serine and threonine	Creatine	-1.4	0.1	-2.0	4.41E-06
C ₅ H ₉ NO ₃			5-Aminolevulinate	-1.7	-0.5	-2.0	0.001249
C ₆ H ₁₀ N ₂ O ₂			Ectoine	-1.3	0.1	-1.9	0.000473
C ₄ H ₉ NO ₂			N,N-Dimethylglycine	-2.0	-0.1	-1.4	6.91E-05
C ₃ H ₇ NO ₃			L-Serine	-1.7	-0.2	-2.0	2.18E-05
C ₁₀ H ₁₄ N ₂ O ₆		Histidine	(1-Ribosylimidazole)-4-acetate	-1.3	0.0	-2.1	2.47E-06
C ₉ H ₁₅ N ₃ O ₂			Hercynine	-1.4	0.1	-2.1	1.76E-06
C ₁₀ H ₁₅ N ₂ O ₉ P			1-(5-Phosphoribosyl)imidazole-4-acetate	-1.6	0.1	-2.0	4.45E-09
C ₆ H ₁₀ N ₂ O ₄			N-Formimino-L-glutamate	-1.3	0.1	-2.0	1.24E-05
C ₆ H ₁₀ N ₂ O ₅			N-Carbamyl-L-glutamate	-1.2	0.0	-1.9	0.002804
C ₆ H ₉ N ₃ O ₂			L-Histidine	-1.2	0.3	-1.6	0.002982
C ₃₀ H ₃₉ N ₉ O ₁₂		homoserine and methionine biosynthesis	5-Methyltetrahydropteroyltri-L-glutamate	-1.7	0.4	-1.7	2.34E-09
C ₃₅ H ₅₅ N ₇ O ₂₆ P ₂		Lysine biosynthesis	UDP-N-acetylmuramoyl-L-alanyl-D-gamma-glutamyl-meso-2,6-diaminopimelate	-0.3	-1.4	-2.3	3.67E-07
C ₉ H ₁₆ N ₂ O ₅			N6-Acetyl-LL-2,6-diaminoheptanedioate	-0.8	0.1	-2.1	6.87E-05
C ₆ H ₁₄ N ₂ O ₂			L-Lysine	-1.4	0.1	-2.0	3.56E-06
C ₇ H ₁₄ N ₂ O ₄			meso-2,6-Diaminoheptanedioate	-1.3	0.2	-2.0	1.43E-05
C ₇ H ₁₄ N ₂ O ₄			LL-2,6-Diaminoheptanedioate	-1.6	0.2	-1.9	7.86E-07
C ₇ H ₉ NO ₄			2,3,4,5-Tetrahydrodipicolinate	-1.7	0.2	-1.9	5.86E-08
C ₈ H ₁₆ N ₂ O ₃			N2-Acetyl-L-lysine	-1.6	0.3	-1.8	2.52E-07
C ₆ H ₁₁ NO ₄			L-2-Aminoadipate	-1.8	0.1	-1.7	4.53E-06
C ₄₁ H ₆₅ N ₉ O ₂₈ P ₂			UDP-N-acetylmuramoyl-L-alanyl-D-glutamyl-6-carboxy-L-lysyl-D-alanyl-D-alanine	-1.4	0.9	0.9	1.59E-06
C ₈ H ₁₆ N ₂ O ₃		Lysine degradation	N6-Acetyl-L-lysine	-0.9	0.1	-2.2	3.24E-06
C ₉ H ₁₈ N ₂ O ₄			N2-(D-1-Carboxyethyl)-L-lysine	-1.7	0.0	-2.0	4.01E-08
C ₉ H ₂₀ N ₂ O ₂			N6,N6,N6-Trimethyl-L-lysine	-1.5	0.2	-2.0	4.62E-07
C ₇ H ₁₅ NO ₃			L-Carnitine	-1.6	-0.1	-1.9	0.000126
C ₅ H ₁₁ NO ₂			5-Aminopentanoate	-1.8	0.2	-1.8	3.51E-07
C ₈ H ₁₆ N ₂ O ₄			N6-Acetyl-N6-hydroxy-L-lysine	0.2	0.1	-1.7	0.002574
C ₆ H ₉ NO ₂			2,3,4,5-Tetrahydropyridine-2-carboxylate	-1.5	0.1	-1.5	0.003951
C ₃ H ₁₁ NO ₂ S		Methionine	L-Methionine	-1.5	0.0	-2.0	2.64E-05
C ₅ H ₁₁ NO ₃ S			L-Methionine S-oxide	-1.3	0.0	-2.0	9.93E-05
C ₈ H ₁₃ NO ₆			O-Succinyl-L-homoserine	-1.6	0.1	-2.0	1.07E-07
C ₆ H ₁₁ NO ₄			O-Acetyl-L-homoserine	-1.9	-0.1	-2.0	3.06E-08
C ₉ H ₁₁ NO ₂		Phenylalanine	D-Phenylalanine	-1.7	0.1	-2.0	5.11E-09
C ₁₃ H ₁₆ N ₂ O ₄			α-N-Phenylacetyl-L-glutamine	-1.4	0.0	-1.9	0.000320
C ₆ H ₁₁ NO ₂			L-Phenylalanine	-1.7	0.1	-1.9	3.61E-06
C ₉ H ₈ O ₃			trans-2-Hydroxycinnamate	-1.4	0.1	-1.9	0.000264
C ₁₁ H ₁₃ NO ₃			N-Acetyl-L-phenylalanine	-1.5	0.4	-1.6	6.35E-06
C ₉ H ₈ O ₃			Phenylpyruvate	1.8	-0.3	1.1	0.000774
C ₇ H ₁₀ O ₅		Phenylalanine, tyrosine and tryptophan biosynthesis	Shikimate	-1.5	0.2	-1.9	3.91E-06
C ₁₀ H ₁₃ O ₁₀ P			5-O-(1-Carboxyvinyl)-3-phosphoshikimate	1.7	-0.1	1.0	0.009833
C ₈ H ₇ N		Tryptophan	Indole	-1.6	-0.3	-2.2	4.32E-06
C ₁₁ H ₁₂ N ₂ O ₄			L-Formylkynurenine	-1.5	0.1	-1.9	8.19E-05
C ₁₁ H ₁₂ N ₂ O ₂			L-Tryptophan	-1.6	0.2	-1.9	1.03E-06
C ₆ H ₇ NO			2-Aminophenol	-1.6	0.2	-1.9	8.35E-07

C ₁₀ H ₉ NO ₄		Tyrosine	4-(2-Aminophenyl)-2,4-dioxobutanoate	-1.1	0.4	-1.7	0.000770
C ₁₁ H ₁₁ NO ₃			Indolelactate	-1.5	0.2	-1.6	0.001018
C ₉ H ₁₁ NO ₃			L-Tyrosine	-1.3	0.1	-2.0	0.000199
C ₉ H ₁₀ O ₄			3-(4-Hydroxyphenyl)lactate	-1.4	0.1	-1.8	0.000373
C ₈ H ₁₁ NO			Tyramine	0.3	2.1	2.0	2.97E-09
C ₆ H ₁₃ NO ₂		Valine, leucine and isoleucine degradation	L-Isoleucine	-1.7	0.1	-1.9	1.67E-06
C ₆ H ₁₃ NO ₂			L-Leucine	-1.6	0.1	-1.9	7.25E-06
C ₅ H ₁₁ NO ₂			L-Valine	-1.7	0.1	-1.8	1.02E-05
C ₂₆ H ₄₄ N ₇ O ₁₈ P ₃ S			(2S,3S)-3-Hydroxy-2-methylbutanoyl-CoA	-0.3	-0.3	-1.7	0.041719
C ₄ H ₈ O ₃	Biosynthesis of Secondary Metabolites	0	(S)-3-Hydroxyisobutyrate	-1.3	0.2	-1.6	0.006279
C ₁₅ H ₂₄ O			2-trans,6-trans-Farnesal	1.6	-0.3	1.4	0.000517
C ₇ H ₉ NO ₃			(3S,5S)-carbapenam	-0.5	1.7	1.5	6.78E-08
C ₈ H ₁₄ N ₂ O ₄			Clavulanic acid biosynthesis	-1.1	0.2	-2.0	2.72E-05
C ₉ H ₁₈ N ₄ O ₄			L-N2-(2-Carboxyethyl)arginine	-1.7	0.1	-2.0	8.92E-08
C ₁₆ H ₂₅ N ₅ O ₆	Carbohydrate	0	Zeatin biosynthesis	-1.4	0.2	-1.9	2.06E-05
C ₈ H ₁₈ NO ₁₀ P			N-Gluconyl ethanolamine phosphate	-1.4	0.0	-2.2	1.29E-06
C ₁₅ H ₁₆ O ₁₀			Caffeic acid 3-O-glucuronide	-1.4	0.0	-2.0	8.64E-05
C ₁₅ H ₁₆ O ₁₀			Caffeic acid 4-O-glucuronide	-1.2	0.2	-2.0	1.34E-05
C ₁₂ H ₂₀ N ₂ O ₇			Deoxyfructosazine	-1.5	0.2	-2.0	1.57E-06
C ₁₈ H ₃₃ NO ₁₅			beta-D-Galactopyranosyl-(1->4)-2-amino-2-deoxy-beta-D-glucopyranosyl-(1->6)-D-mannose	-1.7	0.0	-1.8	0.000130
C ₄ H ₈ O ₄			L-Erythrose	-1.4	0.5	-1.8	2.17E-07
C ₁₁ H ₁₉ NO ₇			N-(1-Deoxy-1-fructosyl)proline	-1.5	0.3	-1.7	7.11E-05
C ₆ H ₁₃ O ₉ P			Hexose phosphate	-1.2	0.2	-1.7	0.003243
C ₁₂ H ₂₃ NO ₇			N-(1-Deoxy-1-fructosyl)isoleucine	-1.1	0.2	-1.6	0.009169
C ₁₂ H ₁₉ N ₃ O ₇			N-(1-Deoxy-1-fructosyl)histidine	-1.2	0.1	-1.6	0.009751
C ₁₇ H ₂₅ N ₃ O ₁₈ P ₂		Aminosugars	UDP-N-acetyl-2-amino-2-deoxy-D-glucuronate	-1.8	-0.1	-1.9	1.58E-05
C ₁₇ H ₂₇ N ₃ O ₁₇ P ₂			UDP-N-acetyl-D-galactosamine	-1.4	0.3	-1.8	9.03E-06
C ₂₀ H ₃₁ N ₄ O ₁₆ P			CMP-N-acetylneuraminate	-1.8	0.0	-1.7	4.74E-05
C ₆ H ₁₃ NO ₅			D-Glucosamine	-1.9	0.2	-1.7	4.42E-08
C ₁₁ H ₁₉ NO ₉			N-Acetylneuraminate	-1.3	0.1	-1.7	0.003332
C ₈ H ₁₅ NO ₆			N-Acetyl-D-mannosamine	1.9	-0.1	0.0	0.001226
C ₆ H ₁₀ O ₈		Ascorbate and aldarate	D-Glucarate	-1.3	-0.2	-2.1	0.000175
C ₆ H ₆ O ₆			L-Dehydroascorbate	-1.5	-0.1	-2.1	1.38E-05
C ₄ H ₈ O ₅			[FA trihydroxy(4:0)] 2,3,4-trihydroxy-butanoic acid	-1.6	0.0	-2.0	3.51E-06
C ₅ H ₆ O ₄			2,5-Dioxopentanoate	-1.6	-0.1	-1.6	0.004669
C ₅ H ₈ O ₄		Butanoate	2-Acetolactate	-1.6	-0.1	-2.0	7.93E-05
C ₄ H ₄ O ₂			3-Butynoate	-1.4	0.4	-1.9	5.35E-07
C ₆ H ₁₀ N ₂ O ₃		C5-Branched dibasic acid	4-Methylene-L-glutamine	-1.7	0.0	-1.8	0.000250
C ₅ H ₆ O ₄			Mesaconate	-1.5	0.2	-1.7	0.000310
C ₆ H ₁₁ NO ₄			4-Methyl-L-glutamate	-1.1	0.3	-1.6	0.006065
C ₄ H ₆ O ₅		TCA cycle	(S)-Malate	-1.3	-0.3	-2.2	0.000215
C ₄ H ₆ O ₄			Succinate	-1.9	-0.4	-2.0	7.64E-05
C ₆ H ₈ O ₇			Citrate	-1.2	0.0	-2.0	0.000813
C ₂₁ H ₃₆ N ₇ O ₁₆ P ₃ S			CoA	-1.7	0.5	-1.5	1.10E-07
C ₆ H ₁₃ O ₈ P		Fructose and mannose	L-Fuculose 1-phosphate	-1.6	-0.2	-2.2	1.04E-07
C ₆ H ₁₂ O ₆			D-Fructose	-1.5	0.1	-2.1	4.90E-08
C ₆ H ₁₂ O ₆			D-Mannose	-1.7	0.2	-1.7	2.14E-05
C ₂₄ H ₄₂ O ₂₁		Galactose	Stachyose	-1.3	0.2	-2.1	4.27E-06
C ₆ H ₁₀ O ₆			2-Dehydro-3-deoxy-D-galactonate	-1.2	0.3	-1.9	1.10E-05
C ₁₈ H ₃₂ O ₁₆			Raffinose	-1.1	0.0	-1.8	0.006123
C ₁₂ H ₂₄ O ₁₁			Melibiose	-1.1	0.1	-1.8	0.005658
C ₁₂ H ₂₂ O ₁₁		glycogen degradation I	β-Maltose	-1.7	0.1	-1.9	4.74E-06
C ₃ H ₇ O ₆ P		Glycolysis / Gluconeogenesis	Glycerone phosphate	-1.0	-0.5	-1.9	0.030454
C ₃ H ₇ O ₇ P			3-Phospho-D-glycerate	-1.2	-0.2	-1.7	0.015781
C ₁₂ H ₁₈ N ₄ O ₇ P ₃ S			Thiamin diphosphate	-1.2	0.1	-1.7	0.005908
C ₂₃ H ₃₈ N ₇ O ₁₇ P ₃ S			Acetyl-CoA	-0.6	0.8	-1.4	0.001260
C ₆ H ₁₀ O ₅			3-Ethylmalate	-1.9	-0.8	-1.9	0.002355
C ₇ H ₁₂ O ₅		Glyoxylate and dicarboxylate	3-Propylmalate	-1.4	0.2	-1.7	0.000773
C ₆ H ₁₂ O ₆		Inositol	myo-Inositol	-1.4	0.1	-2.0	1.34E-06

C ₆ H ₁₀ O ₆			2,4,6/3,5-Pentahydroxycyclohexanone	-1.3	0.3	-1.9	4.68E-05
C ₇ H ₁₄ O ₆		Inositol phosphate	1-O-Methyl-myo-inositol	-1.6	0.1	-2.0	9.84E-08
C ₁₅ H ₂₄ N ₂ O ₁₇ P ₂		Pentose and glucuronate interconversions	UDP-glucose	-1.3	0.2	-2.0	1.77E-05
C ₅ H ₁₀ O ₆			L-Lyxonate	-1.6	0.2	-1.9	5.94E-07
C ₅ H ₁₀ O ₆			D-Xylonate	-2.2	0.2	-0.9	1.62E-09
C ₆ H ₁₁ O ₉ P		Pentose phosphate pathway	D-Glucono-1,5-lactone 6-P	-1.6	-0.3	-2.0	0.000278
C ₅ H ₁₃ O ₁₄ P ₃			5-Phospho-α-D-ribose 1-diphosphate	-1.6	0.0	-2.0	3.99E-06
C ₅ H ₁₁ O ₈ P			D-Ribulose 5-P	-1.0	0.3	-1.9	4.45E-05
C ₅ H ₁₀ O ₄			Deoxyribose	-1.8	-0.1	-1.9	8.23E-06
C ₅ H ₁₀ O ₅			D-Ribose	-1.6	0.2	-1.9	5.76E-07
C ₆ H ₁₀ O ₆			2-Dehydro-3-deoxy-D-gluconate	-1.4	0.3	-1.9	3.56E-05
C ₅ H ₁₁ O ₇ P			2-Deoxy-D-ribose 5-P	-1.7	0.1	-1.8	1.02E-05
C ₅ H ₁₁ O ₈ P			D-Ribose 5-P	-0.7	0.1	-1.7	0.02267
C ₇ H ₁₅ O ₁₀ P			D-Sedoheptulose 7-P	-1.2	0.4	-1.6	0.000466
C ₇ H ₁₀ O ₇		Propanoate	2-Methylcitrate	-1.7	-0.1	-1.7	0.000926
C ₆ H ₁₀ O ₅		Pyruvate	(R)-2-Ethylmalate	-1.2	0.3	-1.8	0.000435
C ₁₂ H ₂₃ O ₁₄ P		Starch and sucrose	α,α'-Trehalose 6-P	-1.8	0.2	-1.8	1.18E-09
C ₆ H ₁₃ O ₉ P			D-Glucose 6-P	-1.7	0.1	-1.5	0.000678
C ₆ H ₁₄ O ₁₂ P ₂	Energy	Carbon fixation	D-Fructose 1,6-bisphosphate	-1.1	-0.2	-2.0	0.003926
C ₁₀ H ₁₆ N ₅ O ₁₃ P ₃		Oxidative phosphorylation	ATP	-1.4	0.1	-2.0	1.16E-05
C ₁₀ H ₁₅ N ₅ O ₁₀ P ₂			ADP	-1.4	0.3	-1.9	1.91E-06
C ₂₁ H ₂₇ N ₇ O ₁₄ P ₂			NAD+	-1.6	0.2	-1.9	1.66E-07
C ₂₁ H ₂₈ N ₇ O ₁₇ P ₃		Photosynthesis	NADP+	-1.5	0.0	-2.0	2.20E-05
C ₈ H ₁₄ O ₈	Glycan Biosynthesis & Metabolism	LPS biosynthesis	3-Deoxy-D-manno-octulosonate	-1.7	0.0	-1.6	0.001085
C ₆ H ₈ O ₄	Cofactors and Vitamins	Nicotinate and nicotinamide	2,3-Dimethylmaleate	-1.5	0.3	-1.9	5.69E-07
C ₆ H ₅ NO ₂			Nicotinate	2.0	0.3	2.0	2.77E-07
C ₉ H ₁₈ NO ₈ P		Pantothenate and CoA biosynthesis	D-4'-Phosphopantothenate	-1.7	0.2	-1.7	3.21E-05
C ₆ H ₈ O ₃		pantothenate and coenzyme A biosynthesis III	Dihydro-4,4-dimethyl-2,3-Furandione	-0.2	0.1	-1.7	0.012973
C ₁₄ H ₁₈ N ₂ O ₄		Riboflavin	α-Ribazole	-0.3	0.3	-1.9	0.000234
C ₇ H ₉ NO ₅		Vitamin B6	2-(Acetamidomethylene)succinate	-1.4	0.1	-1.9	0.000165
C ₈ H ₁₃ N ₂ O ₅ P			Pyridoxamine phosphate	-1.7	0.1	-1.9	5.61E-07

Table 3.7 Significant metabolites ($p \leq 0.05$) of 03-149.1 identified following exposure to colistin (Col) and doripenem (Dor) alone and in combination (Combo) at 4 hr. Significant fold-changes are highlighted in yellow.

Formula	Map	Pathway	Metabolite	Col	Dor	Combo	p-value
C ₉ H ₁₉ N ₃ O ₄	Amino Acid	0	Lysinoalanine	-0.8	-1.0	-2.1	0.009080
C ₆ H ₁₃ N ₃ O ₄			4-Hydroxycitrulline	-1.4	0.1	-2.1	4.06E-06
C ₁₃ H ₁₄ N ₂ O ₂			(1 <i>xi</i> ,3 <i>xi</i>)-1,2,3,4-Tetrahydro-1-methyl-β-carboline-3-carboxylic acid	-1.1	-0.2	-2.0	0.006071
C ₁₀ H ₁₈ N ₂ O ₆ S			γ-L-Glutamyl-L-methionine sulfoxide	-0.5	-0.1	-1.9	0.005148
C ₆ H ₁₂ N ₂ O			L-Lysine 1,6-lactam	-0.3	-0.1	-1.8	0.015564
C ₆ H ₉ NO ₅		Alanine and aspartate	N-Acetyl-L-aspartate	-2.1	-0.1	-1.3	3.55E-05
CH ₅ O ₄ P		Aminophosphonate	Hydroxymethylphosphonate	-2.0	-0.5	-0.2	0.004324

C ₇ H ₁₁ NO ₅	Arginine and proline	N-Acetyl-L-glutamate	-1.2	-0.1	-2.2	7.09E-05
C ₁₅ H ₂₂ N ₆ O ₅ S		S-Adenosyl-L-methionine	-1.2	0.0	-2.1	1.01E-05
C ₅ H ₁₁ N ₃ O ₂	4-Guanidinobutanoate	4-Guanidinobutanoate	-0.8	-0.3	-2.1	0.002874
C ₁₀ H ₁₈ N ₄ O ₅		N2-Succinyl-L-arginine	-1.5	-0.2	-2.0	0.000124
C ₄ H ₇ N ₃ O	Creatinine	Creatinine	-0.8	-0.1	-1.9	0.005081
C ₅ H ₉ NO ₄		L-Glutamate	-1.2	0.1	-1.9	0.000930
C ₉ H ₁₃ NO ₇	N-Succinyl-L-glutamate	N-Succinyl-L-glutamate	-0.8	0.1	-1.9	0.002495
C ₉ H ₁₆ N ₂ O ₅		gamma-Glutamyl-gamma-aminobutyrate	-0.6	-0.5	-1.9	0.027147
C ₆ H ₁₃ N ₃ O ₃	L-Citrulline	L-Citrulline	-0.5	0.5	-1.9	0.000139
C ₇ H ₁₄ N ₂ O ₃		N-Acetylornithine	-1.7	-0.4	-1.7	0.008371
C ₅ H ₇ NO ₂	1-Pyrroline-2-carboxylate	1-Pyrroline-2-carboxylate	0.2	0.1	2.0	0.000583
C ₈ H ₁₅ N ₃ O ₄		N-Acetyl-L-citrulline	-1.2	-0.3	-2.0	0.002877
C ₃ H ₅ NO ₂	Cysteine	2-Aminoacrylate	-1.3	0.0	-1.7	0.004637
C ₆ H ₁₂ N ₂ O ₄ S ₂		L-Cystine	1.7	0.0	1.5	0.000904
C ₆ H ₁₂ N ₂ O ₃	D-Alanine	D-Alanyl-D-alanine	-1.7	0.2	-1.7	1.60E-06
C ₆ H ₁₁ N ₃ O ₃		5-Guanidino-2-oxopentanoate	-0.7	0.1	-2.0	0.000525
C ₂₀ H ₃₁ N ₃ O ₁₉ P ₂	D-Glutamine and D-glutamate	UDP-N-acetylmuramate	-1.1	0.8	-1.5	1.99E-06
C ₂₈ H ₄₃ N ₅ O ₂₃ P ₂		UDP-N-acetylmuramoyl-L-alanyl-D-glutamate	2.2	0.0	0.4	1.35E-05
C ₅ H ₁₀ N ₂ O ₃	Glutamate	L-Glutamine	-1.3	-0.1	-2.1	4.03E-05
C ₆ H ₁₄ NO ₈ P		D-Glucosamine 6-P	-0.3	0.1	-2.1	3.88E-05
C ₈ H ₁₄ N ₂ O ₅ S	gamma-L-Glutamyl-L-cysteine	gamma-L-Glutamyl-L-cysteine	-1.4	0.1	-1.9	0.000145
C ₈ H ₁₆ NO ₉ P		N-Acetyl-D-glucosamine 6-P	2.1	0.4	1.6	0.000260
C ₈ H ₁₅ NO ₆	N-Acetyl-D-glucosamine	N-Acetyl-D-glucosamine	1.5	0.8	2.5	4.52E-06
C ₃ H ₁₀ N ₂ O ₃ S		Cys-Gly	-2.0	-0.2	-1.8	2.14E-05
C ₄ H ₉ N ₃ O ₂	Glutathione	Glutathione	-1.0	-0.1	-1.8	0.013316
C ₃ H ₈ NO ₆ P		Glycine, serine and threonine				
C ₆ H ₁₀ N ₂ O ₄	Glycine, serine and threonine	O-Phospho-L-serine	1.8	-0.1	1.5	0.000187
C ₆ H ₉ N ₃ O ₂		Histidine				
C ₉ H ₁₅ N ₃ O ₂	N-Formimino-L-glutamate	N-Formimino-L-glutamate	-0.6	-0.4	-2.3	0.000244
C ₇ H ₁₀ O ₇		L-Histidine	-0.8	-0.2	-2.0	0.004350
C ₈ H ₁₆ N ₂ O ₃	Hercynine	Hercynine	-1.2	-0.1	-1.9	0.004723
C ₇ H ₉ NO ₄		Lysine biosynthesis				
C ₇ H ₁₄ N ₂ O ₄	Homocitrate	Homocitrate	-0.8	-0.2	-2.4	1.14E-06
C ₃₅ H ₅₅ N ₇ O ₂₆ P ₂		N2-Acetyl-L-lysine	-1.1	-0.2	-2.3	4.12E-05
C ₈ H ₁₃ NO ₅	2,3,4,5-Tetrahydronicotinamide	2,3,4,5-Tetrahydronicotinamide	-1.2	-0.1	-2.2	4.90E-05
C ₆ H ₁₁ NO ₄		meso-2,6-Diaminoheptanedioate	-1.0	-1.0	-2.2	0.005969
C ₉ H ₁₆ N ₂ O ₅	L-2-Aminoadipate	L-2-Aminoadipate	-0.9	-0.1	-2.2	0.000179
C ₇ H ₁₄ N ₂ O ₄		N6-Acetyl-L-lysine	-0.6	-0.5	-1.9	0.02643
C ₃₅ H ₅₅ N ₇ O ₂₆ P ₂	LL-2,6-Diaminoheptanedioate	LL-2,6-Diaminoheptanedioate	-2.0	0.0	-1.6	1.31E-05
C ₈ H ₁₃ NO ₅		UDP-N-acetylmuramoyl-L-alanyl-D-γ-glutamyl-meso-2,6-diaminopimelate	0.9	-1.0	1.5	9.36E-07
C ₆ H ₁₁ NO ₃	N2-Acetyl-L-aminoadipate	N2-Acetyl-L-aminoadipate	1.5	0.8	2.5	2.13E-06
C ₈ H ₁₆ N ₂ O ₃		6-Amino-2-oxohexanoate	-1.2	-0.3	-2.3	3.35E-06
C ₉ H ₂₀ N ₂ O ₂	N6-Acetyl-L-lysine	N6-Acetyl-L-lysine	-0.8	-0.7	-2.1	0.004809
C ₆ H ₉ NO ₂		N6,N6,N6-Trimethyl-L-lysine	-0.9	0.1	-2.0	0.000109
C ₇ H ₁₅ NO ₃	2,3,4,5-Tetrahydropyridine-2-carboxylate	2,3,4,5-Tetrahydropyridine-2-carboxylate	-1.2	0.2	-1.9	0.000368
C ₇ H ₁₅ NO ₂		L-Carnitine	-1.8	0.0	-1.7	9.48E-05
C ₅ H ₁₁ NO ₂	4-Trimethylammonibutanoate	4-Trimethylammonibutanoate	-1.5	0.2	-1.6	0.001508
C ₆ H ₁₁ NO ₄		5-Aminopentanoate	-2.0	0.4	-0.8	1.07E-05
C ₃ H ₁₁ NO ₂ S	O-Acetyl-L-homoserine	O-Acetyl-L-homoserine	-1.3	0.0	-2.0	0.000397
C ₅ H ₁₁ NO ₃ S		L-Methionine	-1.1	0.0	-1.9	0.003462
C ₁₁ H ₁₃ NO ₃	L-Methionine S-oxide	L-Methionine S-oxide	-1.1	0.0	-1.8	0.006439
C ₉ H ₁₁ NO ₂		Phenylalanine				
C ₈ H ₈ O ₂	N-Acetyl-L-phenylalanine	N-Acetyl-L-phenylalanine	-1.9	0.1	-1.3	0.000371
C ₉ H ₈ O ₃		L-Phenylalanine	-1.7	0.1	-0.7	0.020459
C ₁₀ H ₁₃ O ₁₀ P	Phenylacetic acid	Phenylacetic acid	1.7	-0.3	0.0	0.004279
C ₉ H ₁₆ N ₂ O ₅ Se		Phenylpyruvate	-0.9	-0.2	1.5	8.97E-05
C ₁₁ H ₁₂ N ₂ O ₂	5-O-(1-Carboxyvinyl)-3-phosphoshikimate	5-O-(1-Carboxyvinyl)-3-phosphoshikimate	1.8	-0.6	0.9	7.79E-06
C ₆ H ₇ NO		Selenoamino acid				
C ₈ H ₇ N		γ-Glutamyl-Se-methylselenocysteine	2.1	0.3	1.9	7.18E-08
	Tryptophan	L-Tryptophan	-1.5	-0.1	-1.6	0.007505
		2-Aminophenol	-1.8	-0.2	-1.3	0.008169
		Indole	-1.9	-0.1	-0.7	0.009161

C ₁₀ H ₉ NO ₂			Indole-3-acetate	1.6	-0.3	-0.2	0.005570
C ₇ H ₅ NO ₄			Pyridine-2,3-dicarboxylate	1.6	0.0	1.3	0.013755
C ₁₁ H ₁₁ NO ₃			Indolelactate	-0.8	0.0	1.5	0.000751
C ₈ H ₁₁ NO ₃		Tyrosine	L-Noradrenaline	-1.1	0.2	-1.9	0.000114
C ₉ H ₁₁ NO ₃			L-Tyrosine	-1.8	-0.3	-1.7	0.001670
C ₈ H ₈ O ₄			Homogentisate	-1.8	-0.9	-0.2	0.016084
C ₈ H ₁₁ NO			Tyramine	0.0	1.5	2.2	3.32E-08
C ₆ H ₁₀ O ₄		Valine, leucine and isoleucine biosynthesis	(S)-2-Aceto-2-hydroxybutanoate	1.9	0.4	0.8	0.017458
C ₂₆ H ₄₂ N ₇ O ₁₇ P ₃ S			3-Methylcrotonyl-CoA	-1.0	-0.5	-2.4	8.36E-06
C ₂₆ H ₄₄ N ₇ O ₁₈ P ₃ S			(2S,3S)-3-Hydroxy-2-methylbutanoyl-CoA	-0.9	-0.4	-2.4	2.95E-05
C ₆ H ₁₃ NO ₂			L-Isoleucine	-1.1	0.0	-1.6	0.021256
C ₅ H ₈ O ₃			3-Methyl-2-oxobutanoic acid	1.6	-0.3	-0.4	0.002311
C ₁₅ H ₂₄ O	Biosynthesis of secondary metabolites	0	2-trans,6-trans-Farnesal	1.8	0.0	0.9	0.010408
C ₇ H ₉ NO ₃		(5R)-carbapenem biosynthesis	(3S,5S)-carbapenam	-0.4	0.9	1.8	0.000378
C ₉ H ₁₈ N ₄ O ₄		Clavulanic acid biosynthesis	L-N2-(2-Carboxyethyl)arginine	-1.3	-0.7	-2.4	0.000147
C ₈ H ₁₄ N ₂ O ₄			Proclavaminc acid	-0.6	-0.5	-2.0	0.010676
C ₄ H ₈ O ₄	Carbohydrate	0	D-Threose	-1.6	0.0	-2.1	7.45E-09
C ₁₈ H ₃₃ NO ₁₅			β-D-Galactopyranosyl-(1->4)-2-amino-2-deoxy-β-D-glucopyranosyl-(1->6)-D-mannose	-1.0	0.0	-2.1	6.14E-05
C ₈ H ₁₈ NO ₁₀ P			N-Gluconyl ethanolamine phosphate	-1.3	0.1	-1.7	0.002154
C ₆ H ₁₃ O ₉ P			Hexose phosphate	0.3	0.2	-1.7	0.000918
C ₂₀ H ₃₁ N ₄ O ₁₆ P			CMP-N-acetylneuraminate	-0.1	0.5	-1.9	6.59E-06
C ₁₇ H ₂₇ N ₃ O ₁₇ P ₂			UDP-N-acetyl-D-galactosamine	-0.8	0.2	-1.7	0.006375
C ₆ H ₁₃ NO ₅		Aminosugars	D-Glucosamine	-2.1	0.4	-0.7	3.16E-07
C ₈ H ₁₅ NO ₆			N-Acetyl-D-mannosamine	2.2	0.2	1.5	1.69E-05
C ₆ H ₁₀ O ₈		Ascorbate and aldarate	D-Glucarate	-1.2	-0.6	-2.4	0.000106
C ₄ H ₈ O ₅			[FA trihydroxy(4:0)] 2,3,4-trihydroxy-butanoic acid	-1.6	-0.2	-2.0	0.000136
C ₅ H ₆ O ₄		Butanoate	2,5-Dioxopentanoate	1.9	0.6	0.8	0.024633
C ₈ H ₁₄ O ₅			(R)-3-((R)-3-Hydroxybutanoyloxy)butanoate	-1.3	-0.2	-2.3	3.34E-06
C ₄ H ₆ O ₂			Diacetyl	-1.7	-0.1	-2.2	1.49E-08
C ₄ H ₄ O ₂			3-Butyrate	-0.2	-0.3	-2.0	0.002559
C ₆ H ₁₁ NO ₄		C5-Branched dibasic acid	4-Methyl-L-glutamate	-1.1	0.0	-2.1	0.000117
C ₅ H ₆ O ₄			Itaconate	-1.1	0.1	-2.1	1.74E-05
C ₆ H ₁₀ N ₂ O ₃		4-Methylene-L-glutamine	4-Methylene-L-glutamine	-1.4	0.1	-2.0	7.18E-06
C ₆ H ₈ O ₇			Citrate	-1.2	-0.1	-2.3	3.85E-06
C ₆ H ₁₂ O ₆		Fructose & mannose	D-Fructose	-1.8	-1.1	-2.1	0.002184
C ₆ H ₁₀ O ₅			2-Dehydro-3-deoxy-D-fuconate	-1.3	-0.5	-2.0	0.004792
C ₁₂ H ₂₂ O ₁₁		Galactose	Lactose	-1.6	-0.1	-2.2	1.56E-09
C ₁₂ H ₂₂ O ₁₁		glycogen degradation I	β-Maltose	-1.7	0.0	-2.1	1.33E-10
C ₂₃ H ₃₈ N ₇ O ₁₇ P ₃ S		Glycolysis / Gluconeogenesis	Acetyl-CoA	-1.0	0.0	-2.0	0.000970
C ₇ H ₁₂ O ₅		Glyoxylate & dicarboxylate	3-Propylmalate	-0.9	-0.3	-2.3	9.07E-05
C ₆ H ₁₀ O ₅			3-Ethylmalate	-1.7	-0.1	-2.1	9.23E-09
C ₂₆ H ₄₄ N ₇ O ₁₇ P ₃ S			Pentanoyl-CoA	-1.8	-0.2	-2.0	7.88E-06
C ₇ H ₁₄ O ₆		Inositol phosphate	1-O-Methyl-myo-inositol	-1.0	-0.5	-2.1	0.002990
C ₁₅ H ₂₄ N ₂ O ₁₇ P ₂		Pentose & glucuronate interconversions	UDP-glucose	-1.0	-0.3	-2.0	0.005981
C ₅ H ₁₀ O ₆			L-Lyxonate	-1.4	0.0	-1.9	0.000591
C ₅ H ₁₃ O ₁₄ P ₃		PPP	5-Phospho-alpha-D-ribose 1-diphosphate	-1.3	-0.2	-2.0	0.000747
C ₅ H ₁₁ O ₇ P			2-Deoxy-D-ribose 5-P	-1.4	0.1	-2.0	2.99E-05
C ₅ H ₁₀ O ₅			D-Ribose	-1.7	-0.1	-2.0	7.02E-05
C ₄ H ₉ O ₇ P			D-Erythrose 4-P	-0.4	0.5	-1.9	3.98E-05
C ₆ H ₁₁ O ₈ P			D-Glucono-1,5-lactone 6-P	-1.9	-0.4	-1.8	0.000753
C ₅ H ₁₁ O ₈ P			D-Ribulose 5-P	-1.0	0.2	-1.7	0.005209
C ₃ H ₁₀ O ₄			Deoxyribose	-2.2	-0.2	-1.4	2.63E-05
C ₅ H ₁₁ O ₈ P			D-Ribose 5-P	1.9	0.2	0.3	0.008862
C ₇ H ₁₀ O ₇		Propanoate	2-Methylcitrate	-1.0	-0.3	-2.4	5.16E-07
C ₆ H ₁₃ O ₉ P		Starch and sucrose	D-Glucose 6-P	1.8	0.2	0.0	0.005044
C ₁₀ H ₁₃ N ₅ O ₁₀ P ₂	Energy	Oxidative phosphorylation	ADP	-1.2	-0.1	-2.2	8.79E-06
C ₁₀ H ₁₆ N ₅ O ₁₃ P ₃			ATP	-0.6	-0.2	-2.1	0.000939
C ₂₁ H ₂₇ N ₇ O ₁₄ P ₂			NAD+	-1.5	-0.2	-1.9	0.000768

C ₂₁ H ₂₈ N ₇ O ₁₇ P ₃		Photosynthesis	NADP+	-1.4	-0.5	-2.1	0.002394
C ₈ H ₁₄ O ₈	Glycan biosynthesis & metabolism	LPS biosynthesis	3-Deoxy-D-manno-octulosonate	-0.1	0.2	-2.0	5.50E-05
C ₆ H ₈ O ₄	Cofactors & vitamins	Nicotinate & nicotinamide	2,3-Dimethylmaleate	0.0	0.0	-1.9	0.001107
C ₉ H ₁₈ NO ₈ P		Pantothenate & CoA biosynthesis	D-4'-Phosphopantothenate	-1.1	-0.4	-2.4	4.93E-06
C ₆ H ₁₀ N ₃ O ₄ P		Thiamine	4-Amino-2-methyl-5-phosphomethylpyrimidine	0.0	-0.7	1.7	2.63E-05

Table 3.8 Significant metabolites ($p \leq 0.05$) of 03-149.2 identified following exposure to colistin (Col) and doripenem (Dor) alone and in combination (Combo) at 15 min. Significant fold-changes are highlighted in yellow.

Formula	Map	Pathway	Metabolite	Col	Dor	Combo	p-value
C ₆ H ₉ NO ₅	Amino Acid	Alanine and aspartate	N-Acetyl-L-aspartate	1.3	0.0	2.0	0.003542
CH ₅ O ₄ P		Aminophosphonate	Hydroxymethylphosphonate	-1.9	-0.1	-1.9	3.00E-06
C ₆ H ₁₁ NO ₂		Arginine and proline	N4-Acetylaminobutanal	0.9	-0.4	1.9	0.001355
C ₁₀ H ₁₈ N ₄ O ₅			N2-Succinyl-L-arginine	1.5	-0.1	2.0	3.22E-05
C ₇ H ₁₁ NO ₅			N-Acetyl-L-glutamate	1.6	0.3	2.1	0.002358
C ₇ H ₁₄ N ₂ O ₃			N-Acetylornithine	1.4	0.2	2.3	0.000193
C ₃ H ₅ NO ₂		Cysteine	2-Aminoacrylate	-2.0	-0.3	0.4	1.76E-05
C ₂₀ H ₃₁ N ₃ O ₁₉ P ₂		D-Glutamine and D-glutamate	UDP-N-acetylmuramate	1.2	-0.7	1.5	4.60E-05
C ₈ H ₁₅ NO ₆		Glutamate	N-Acetyl-D-glucosamine	1.3	-0.4	1.6	0.001424
C ₈ H ₁₆ NO ₉ P			N-Acetyl-D-glucosamine 6-P	1.6	0.1	2.0	0.001752
C ₆ H ₁₄ NO ₈ P			D-Glucosamine 6-P	0.7	0.4	2.5	9.41E-05
C ₅ H ₁₀ N ₂ O ₃			L-Glutamine	1.6	-0.5	1.4	6.43E-05
C ₄ H ₆ O ₃			Succinate semialdehyde	-1.4	-0.8	-2.4	0.005640
C ₃ H ₈ NO ₆ P		Glycine, serine and threonine	O-Phospho-L-serine	1.7	-0.4	1.2	0.000305
C ₈ H ₁₃ NO ₅							
C ₇ H ₁₀ O ₇		Lysine biosynthesis	N2-Acetyl-L-aminoadipate	1.2	-0.5	1.7	0.000362
C ₇ H ₉ NO ₄			Homoisocitrate	1.5	-0.2	1.8	0.000388
C ₃₅ H ₅₅ N ₇ O ₂₆ P ₂			2,3,4,5-Tetrahydrodipicolinate	1.4	0.0	1.9	0.004400
C ₄₁ H ₆₅ N ₉ O ₂₈ P ₂			UDP-N-acetylmuramoyl-L-alanyl-D-γ-glutamyl-meso-2,6-diaminopimelate	0.4	-2.0	-0.7	2.29E-06
C ₆ H ₉ NO ₂		Lysine degradation	UDP-N-acetylmuramoyl-L-alanyl-D-glutamyl-6-carboxy-L-lysyl-D-alanyl-D-alanine	1.2	1.2	2.8	7.31E-06
C ₆ H ₁₁ NO ₃			2,3,4,5-Tetrahydropyridine-2-carboxylate	1.1	-0.1	2.2	5.82E-05
C ₃ H ₁₁ NO ₂			6-Amino-2-oxohexanoate	1.8	0.7	2.3	0.000581
C ₅ H ₁₁ NO ₂			5-Aminopentanoate	1.5	-0.1	1.9	0.001853
C ₁₁ H ₁₁ NO ₃		Phenylalanine	D-Phenylalanine	1.6	-0.4	1.4	8.58E-05
C ₉ H ₁₀ O ₄		Tryptophan	Indolelactate	-1.2	0.5	-1.5	0.002021
C ₈ H ₁₁ NO ₃		Tyrosine	3-(4-Hydroxyphenyl)lactate	-1.1	0.3	-1.7	0.008127
C ₈ H ₁₁ NO			L-Noradrenaline	1.2	-0.2	2.1	0.000120
C ₆ H ₁₀ O ₄			Tyramine	0.1	2.0	2.0	1.09E-08
C ₃ H ₈ O ₄		Valine, leucine and isoleucine biosynthesis	(S)-2-Aceto-2-hydroxybutanoate	1.8	0.3	1.9	0.001318
C ₂₆ H ₄₄ N ₇ O ₁₈ P ₃ S			(S)-2-Acetolactate	1.6	0.1	2.0	0.000821
C ₂₆ H ₄₂ N ₇ O ₁₇ P ₃ S		Valine, leucine and isoleucine degradation	(2S,3S)-3-Hydroxy-2-methylbutanoyl-CoA	1.6	-0.3	1.7	7.09E-06
			3-Methylcrotonyl-CoA	1.5	-0.5	1.5	4.63E-05

C ₇ H ₉ NO ₃	Biosynthesis of secondary metabolites	(5R)-carbapenem biosynthesis	(3S,5S)-carbapenam	0.4	2.1	2.1	8.85E-08
C ₆ H ₁₃ O ₉ P	Carbohydrate	0	Hexose phosphate	1.5	-0.5	1.5	0.000112
C ₆ H ₁₃ NO ₅		Aminosugars	D-Glucosamine	1.2	-0.3	1.8	0.001683
C ₂₀ H ₃₁ N ₄ O ₁₆ P			CMP-N-acetylneuraminate	1.1	-0.2	1.9	0.003298
C ₁₇ H ₂₅ N ₃ O ₁₈ P ₂			UDP-N-acetyl-2-amino-2-deoxy-D-glucuronate	1.6	-0.1	1.9	6.67E-05
C ₁₇ H ₂₇ N ₃ O ₁₇ P ₂			UDP-N-acetyl-D-galactosamine	1.5	-0.3	2.0	1.03E-06
C ₂₁ H ₃₆ N ₇ O ₁₆ P ₃ S		TCA cycle	CoA	-2.0	0.2	-1.5	7.44E-09
C ₃ H ₆ O ₄		Glycine, serine and threonine	D-Glycerate	2.1	0.2	1.3	0.000906
C ₃ H ₅ O ₆ P		Glycolysis / Gluconeogenesis	Phosphoenolpyruvate	1.8	-0.3	1.4	5.33E-05
C ₃ H ₇ O ₇ P			3-Phospho-D-glycerate	1.8	-0.2	1.3	0.000460
C ₂₆ H ₄₄ N ₇ O ₁₇ P ₃ S		Glyoxylate & dicarboxylate	Pentanoyl-CoA	1.5	-0.5	1.4	9.51E-05
C ₅ H ₁₀ O ₆		Pentose & glucuronate interconversions	D-Xylonate	0.3	-1.6	0.1	0.005754
C ₁₅ H ₂₄ N ₂ O ₁₇ P ₂			UDP-glucose	1.6	0.0	1.8	0.002529
C ₆ H ₁₂ O ₇		PPP	D-Gluconic acid	2.4	1.1	1.3	0.001664
C ₅ H ₁₃ O ₁₄ P ₃			5-Phospho-α-D-ribose 1-diphosphate	1.6	-0.4	1.0	0.005792
C ₇ H ₁₀ O ₇		Propanoate	2-Methylcitrate	1.6	-0.2	1.7	0.000167
C ₃ H ₇ O ₅ P			Propanoyl phosphate	-2.0	0.0	-1.8	1.03E-08
C ₆ H ₁₃ O ₉ P		Starch & sucrose	D-Glucose 6-P	-1.7	0.1	-1.6	0.000661
C ₂₁ H ₂₇ N ₇ O ₁₄ P ₂	Energy	Oxidative phosphorylation	NAD+	1.7	0.3	1.9	0.007467
C ₁₀ H ₁₆ N ₅ O ₁₃ P ₃			ATP	1.8	0.2	1.6	0.004439
C ₁₁ H ₁₅ N ₂ O ₈ P	Cofactors & vitamins	Nicotinate & nicotinamide	Nicotinamide D-ribonucleotide	-1.5	0.1	-2.0	2.82E-05
C ₆ H ₈ O ₄			2,3-Dimethylmaleate	1.1	-0.2	1.7	0.010022
C ₆ H ₅ NO ₂			Nicotinate	-1.6	0.2	-1.8	4.08E-05
C ₇ H ₆ O ₄	Xenobiotics Biodegradation & Metabolism	Benzoate degradation via hydroxylation	3,4-Dihydroxybenzoate	1.8	0.2	1.6	0.008062

Table 3.9 Significant metabolites ($p \leq 0.05$) of 03-149.2 identified following exposure to colistin (Col) and doripenem (Dor) alone and in combination (Combo) at 1 hr. Significant fold-changes are highlighted in yellow.

Formula	Map	Pathway	Metabolite	Col	Dor	Combo	p-value
C ₆ H ₁₉ N ₃ O ₄	Amino Acid	0	Lysinoalanine	-0.3	-0.3	-2.1	0.002179
C ₆ H ₁₃ N ₃ O ₄		Alanine and aspartate	4-Hydroxycitrulline	0.0	-0.1	1.8	0.004257
C ₄ H ₇ NO ₄			L-Aspartate	1.3	-0.1	1.7	0.005514
CH ₂ O ₄ P		Aminophosphonate	Hydroxymethylphosphonate	-1.8	-0.9	0.1	0.008930
C ₉ H ₁₈ N ₄ O ₄		Arginine and proline	N ₂ -(D-1-Carboxyethyl)-L-arginine	2.1	1.0	1.6	0.011513
C ₇ H ₁₄ N ₂ O ₃			N-Acetylornithine	2.1	0.3	1.8	0.000015
C ₈ H ₁₅ N ₃ O ₄		arginine biosynthesis III	N-Acetyl-L-citrulline	-1.2	-0.1	-1.9	0.007131
C ₆ H ₁₂ N ₂ O ₄ S ₂		Cysteine	L-Cystine	0.1	0.6	2.0	0.005740
C ₂₀ H ₃₁ N ₃ O ₁₉ P ₂		D-Glutamine and D-glutamate	UDP-N-acetylmuramate	1.1	-0.4	1.9	2.85E-08
C ₂₈ H ₄₃ N ₅ O ₂₃ P ₂			UDP-N-acetylmuramoyl-L-alanyl-D-glutamate	0.4	-0.3	2.1	1.05E-07
C ₈ H ₁₅ NO ₆		Glutamate	N-Acetyl-D-glucosamine	0.2	-0.2	2.1	4.92E-07
C ₈ H ₁₆ NO ₉ P			N-Acetyl-D-glucosamine 6-P	0.2	0.4	2.2	0.000129
C ₁₀ H ₁₄ N ₂ O ₆		Histidine	(1-Ribosylimidazole)-4-acetate	1.7	-0.1	-0.5	0.000474
C ₃₀ H ₃₉ N ₉ O ₁₂		homoserine and methionine biosynthesis	5-Methyltetrahydropteroyltri-L-glutamate	2.2	0.5	2.1	1.57E-06
C ₇ H ₁₄ N ₂ O ₄		Lysine biosynthesis	LL-2,6-Diaminoheptanedioate	0.7	0.9	2.1	0.012385

C ₈ H ₁₃ NO ₅			N2-Acetyl-L-aminoadipate	0.3	-0.1	2.2	1.41E-06
C ₆ H ₁₁ NO ₄			L-2-Aminoadipate	1.7	0.0	1.4	0.005904
C ₃₅ H ₅₅ N ₇ O ₂₆ P ₂			UDP-N-acetylmuramoyl-L-alanyl-D-γ-glutamyl-meso-2,6- diaminopimelate	0.3	-1.8	0.4	4.34E-07
C ₄₁ H ₆₅ N ₉ O ₂₈ P ₂			UDP-N-acetylmuramoyl-L-alanyl-D-glutamyl-6-carboxy-L-lysyl-D-alanyl-D-alanine	1.3	1.2	2.8	9.46E-08
C ₉ H ₁₈ N ₂ O ₄		Lysine degradation	N2-(D-1-Carboxyethyl)-L-lysine	2.0	0.4	0.3	0.011946
C ₆ H ₉ NO ₂			2,3,4,5-Tetrahydropyridine-2-carboxylate	1.3	0.1	2.0	0.001367
C ₅ H ₁₁ NO ₂			5-Aminopentanoate	0.7	0.0	2.0	0.001945
C ₈ H ₁₃ NO ₆		Methionine	O-Succinyl-L-homoserine	1.7	-0.2	-0.5	0.000132
C ₁₃ H ₁₆ N ₂ O ₄		Phenylalanine	α-N-Phenylacetyl-L-glutamine	1.9	-0.1	1.0	0.005014
C ₁₁ H ₁₃ NO ₃			N-Acetyl-L-phenylalanine	1.6	0.2	1.8	0.009534
C ₇ H ₁₀ O ₅		Phenylalanine, tyrosine and tryptophan biosynthesis	Shikimate	1.6	0.3	1.9	0.004118
C ₉ H ₁₀ O ₄		Tyrosine	3-(4-Hydroxyphenyl)lactate	-1.6	-0.1	-1.5	0.013233
C ₈ H ₁₁ NO ₃			L-Noradrenaline	1.4	0.3	2.1	0.001578
C ₈ H ₁₁ NO			Tyramine	0.1	2.0	2.0	1.26E-11
C ₈ H ₈ O ₄			Homogentisate	0.4	-0.6	1.6	0.002873
C ₆ H ₁₀ O ₄		Valine, leucine and isoleucine biosynthesis	(S)-2-Aceto-2-hydroxybutanoate	-0.2	-0.2	-2.2	0.000041
C ₃ H ₈ O ₄			(S)-2-Acetolactate	1.8	-0.3	1.2	0.000553
C ₂₆ H ₄₄ N ₇ O ₁₈ P ₃ S		Valine, leucine and isoleucine degradation	(2S,3S)-3-Hydroxy-2-methylbutanoyl-CoA	1.8	-0.3	1.4	0.000018
C ₄ H ₈ O ₃			(S)-3-Hydroxyisobutyrate	0.4	0.8	2.1	0.008133
C ₇ H ₉ NO ₃	Biosynthesis of Secondary Metabolites	(5R)-carbapenem biosynthesis	(3S,5S)-carbapenam	0.3	2.1	1.9	4.98E-06
C ₄ H ₈ O ₄	Carbohydrate	0	L-Erythrulose	1.0	0.2	2.0	0.004918
C ₁₈ H ₃₃ NO ₁₅			beta-D-Galactopyranosyl-(1->4)-2-amino-2-deoxy-β-D-glucopyranosyl-(1->6)-D-mannose	0.9	0.1	2.1	0.000492
C ₁₇ H ₂₅ N ₃ O ₁₈ P ₂		Aminosugars	UDP-N-acetyl-2-amino-2-deoxy-D-glucuronate	1.6	-0.1	1.5	0.005146
C ₂₀ H ₃₁ N ₄ O ₁₆ P			CMP-N-acetylneuraminate	0.8	-0.2	1.9	0.000552
C ₁₇ H ₂₇ N ₃ O ₁₇ P ₂			UDP-N-acetyl-D-galactosamine	1.9	0.2	2.0	0.000018
C ₆ H ₁₃ NO ₅			D-Glucosamine	0.6	0.1	2.1	0.001238
C ₈ H ₁₅ NO ₆			N-Acetyl-D-mannosamine	0.4	0.0	2.2	5.08E-07
C ₆ H ₁₀ N ₂ O ₃			4-Methylene-L-glutamine	-0.4	0.1	1.7	0.005430
C ₂₁ H ₃₆ N ₇ O ₁₆ P ₃ S		C5-Branched dibasic acid	4-Methylene-L-glutamine	-0.4	0.1	1.7	0.005430
C ₄ H ₆ O ₄		TCA cycle	CoA	-1.7	0.4	-1.3	0.000022
C ₁₂ H ₂₂ O ₁₁			Succinate	0.0	-0.4	1.6	0.002918
C ₃ H ₆ O ₄		Galactose	Lactose	0.7	-0.1	1.9	0.002751
C ₃ H ₆ O ₄		Glycine, serine and threonine	D-Glycerate	1.9	0.0	1.4	0.001496
C ₃ H ₇ O ₇ P			3-Phospho-D-glycerate	1.7	-0.4	1.1	0.000632
C ₅ H ₁₀ O ₆		Glycolysis / Gluconeogenesis	3-Phospho-D-glycerate	1.7	-0.4	1.1	0.000632
C ₅ H ₁₀ O ₆		Pentose and glucuronate interconversions	D-Xylonate	0.6	0.1	2.1	0.000229
C ₃ H ₇ O ₅ P		Propanoate	Propanoyl phosphate	-2.2	0.1	-1.3	1.45E-07
C ₁₂ H ₂₃ O ₁₄ P		Starch and sucrose	alpha, alpha'-Trehalose 6-P	0.6	-0.4	-1.8	0.000028
C ₆ H ₁₃ O ₉ P			D-Glucose 6-P	-0.2	-0.2	1.8	0.000308
C ₂₁ H ₂₇ N ₇ O ₁₄ P ₂	Energy	Oxidative phosphorylation	NAD+	1.6	-0.3	1.0	0.008434
C ₁₀ H ₁₅ N ₅ O ₁₀ P ₂			ADP	1.3	0.5	2.0	0.01291
C ₂₁ H ₂₈ N ₇ O ₁₇ P ₃		Photosynthesis	NADP+	1.7	0.1	-0.4	0.003460
C ₈ H ₁₂ O ₇	Cofactors & vitamins	coenzyme B biosynthesis	(-)-threo-iso(homo)2citrate	-1.7	-0.1	-2.0	0.000134
C ₁₁ H ₁₅ N ₂ O ₈ P		Nicotinate and nicotinamide	Nicotinamide D-ribonucleotide	-1.8	0.0	-1.2	0.004446
C ₆ H ₅ NO ₂			Nicotinate	-1.6	-0.1	-1.8	0.001814
C ₂₇ H ₃₃ N ₉ O ₁₅ P ₂		Riboflavin	FAD	0.6	0.6	2.1	0.012606
C ₇ H ₆ O ₄	Xenobiotics biodegradation & metabolism	Benzoate degradation via hydroxylation	3,4-Dihydroxybenzoate	1.0	0.5	2.3	0.001400

Table 3.10 Significant metabolites ($p \leq 0.05$) of 03-149.2 identified following exposure to colistin (Col) and doripenem (Dor) alone and in combination (Combo) at 4 hr. Significant fold-changes are highlighted in yellow.

Formula	Map	Pathway	Metabolite	Col	Dor	Combo	p-value
C ₉ H ₁₉ N ₃ O ₄	Amino Acid	0	Lysinoalanine	-0.7	-0.8	-2.5	0.000269
C ₉ H ₁₈ N ₂ O ₄			Meprobamate	-0.2	-0.6	-2.2	0.001450
C ₆ H ₁₃ N ₃ O ₄			4-Hydroxycitrulline	-0.2	-0.9	-2.1	0.003498
C ₁₀ H ₁₈ N ₂ O ₆ S			γ-L-Glutamyl-L-methionine sulfoxide	-0.2	-0.4	-2.0	0.011608
C ₁₁ H ₁₃ NO ₄			N-Acetyl-L-tyrosine	-0.3	-0.3	-1.9	0.008451
C ₁₂ H ₂₄ N ₂ O ₇			1-[(5-Amino-5-carboxypentyl)amino]-1-deoxyfructose	0.4	-0.2	-1.8	0.004288
C ₉ H ₁₄ N ₄ O ₃		Alanine and aspartate	Carnosine	0.2	-0.5	-2.2	0.000157
CH ₅ O ₄ P		Aminophosphonate	Hydroxymethylphosphonate	-1.6	-1.2	-2.4	0.000599
C ₉ H ₁₆ N ₂ O ₅		Arginine and proline	γ-Glutamyl-gamma-aminobutyrate	-0.3	-0.7	-2.4	0.000400
C ₉ H ₁₆ N ₂ O ₄			γ-Glutamyl-gamma-aminobutyraldehyde	0.0	-0.6	-2.3	0.000029
C ₅ H ₁₁ N ₃ O ₂			4-Guanidinobutanoate	0.1	-0.3	-1.9	0.003726
C ₁₀ H ₁₈ N ₄ O ₅			N2-Succinyl-L-arginine	0.6	0.0	-1.5	0.007850
C ₆ H ₁₃ N ₃ O ₃			L-Citrulline	0.5	0.3	1.8	0.016178
C ₉ H ₁₆ N ₂ O ₅			N2-Succinyl-L-ornithine	0.1	0.7	2.1	0.007757
C ₇ H ₁₄ N ₂ O ₃			N-Acetylornithine	0.9	1.2	2.5	0.000164
C ₆ H ₁₄ N ₄ O ₂			L-Arginine	0.1	-0.6	-2.3	8.22E-06
C ₅ H ₁₂ N ₂ O ₂			L-Ornithine	1.6	1.4	1.7	0.004537
C ₁₅ H ₂₂ N ₆ O ₅ S			S-Adenosyl-L-methionine	0.8	1.2	2.2	0.002008
C ₈ H ₁₅ N ₃ O ₄		arginine biosynthesis III	N-Acetyl-L-citrulline	-0.3	-0.9	-2.3	0.000979
C ₉ H ₁₉ N ₅ O ₃		beta-Alanine	β-Alanyl-L-arginine	-0.2	-0.6	-2.0	0.015251
C ₉ H ₁₉ N ₃ O ₃			β-Alanyl-L-lysine	0.1	-0.3	-1.9	0.006409
C ₆ H ₁₂ N ₂ O ₄ S ₂		Cysteine	L-Cystine	-0.7	0.5	1.8	0.000224
C ₂₀ H ₃₁ N ₃ O ₁₉ P ₂		D-Glutamine and D-glutamate	UDP-N-acetylmuramate	0.7	0.6	2.3	0.000377
C ₈ H ₁₅ NO ₆		Glutamate metabolism	N-Acetyl-D-glucosamine	0.2	0.7	2.3	0.000789
C ₈ H ₁₆ NO ₉ P			N-Acetyl-D-glucosamine 6-P	0.0	0.8	2.3	0.000128
C ₅ H ₁₀ N ₂ O ₃			L-Glutamine	-0.2	-1.0	-1.8	0.00329
C ₅ H ₉ NO ₃		Glycine, serine and threonine metabolism	5-Aminolevulinate	0.2	0.7	2.3	0.000890
C ₁₀ H ₁₄ N ₂ O ₆		Histidine	(1-Ribosylimidazole)-4-acetate	-0.6	-0.7	-2.4	0.000439
C ₆ H ₁₀ N ₂ O ₄			N-Formimino-L-glutamate	0.3	-0.3	-2.0	0.001137
C ₉ H ₁₅ N ₃ O ₂			Hercynine	0.4	-0.2	-1.9	0.000148
C ₆ H ₉ N ₃ O ₂			L-Histidine	-0.2	-0.5	-2.1	0.003870
C ₉ H ₁₆ N ₂ O ₅		Lysine biosynthesis	N6-Acetyl-LL-2,6-diaminoheptanedioate	-0.3	-0.7	-2.4	0.000400
C ₇ H ₁₀ O ₇			Homoisocitrate	0.5	-0.2	-1.9	0.000270
C ₇ H ₁₄ N ₂ O ₄			meso-2,6-Diaminoheptanedioate	0.6	0.1	-1.5	0.004920
C ₈ H ₁₃ NO ₅			N2-Acetyl-L-aminoadipate	-0.3	0.5	2.1	0.000617
C ₇ H ₁₄ N ₂ O ₄			LL-2,6-Diaminoheptanedioate	0.1	0.5	2.2	0.000289
C ₃₅ H ₅₅ N ₇ O ₂₆ P ₂			UDP-N-acetylmuramoyl-L-alanyl-D-γ-glutamyl-meso-2,6-diaminopimelate	-0.5	-0.4	-2.2	1.36E-06
C ₄₁ H ₆₅ N ₉ O ₂₈ P ₂			UDP-N-acetylmuramoyl-L-alanyl-D-glutamyl-6-carboxy-L-lysyl-D-alanyl-D-alanine	0.8	0.5	2.2	0.000458
C ₈ H ₁₆ N ₂ O ₃		Lysine degradation	N6-Acetyl-L-lysine	0.0	-0.6	-2.3	0.000050
C ₉ H ₁₈ N ₂ O ₄			N2-(D-1-Carboxyethyl)-L-lysine	-0.7	-0.6	-2.0	0.018994
C ₇ H ₁₅ NO ₂			4-Trimethylammoniobutanoate	0.1	0.5	1.9	0.022474
C ₆ H ₉ NO ₂			2,3,4,5-Tetrahydropyridine-2-carboxylate	0.3	0.9	2.4	0.000297
C ₅ H ₁₁ NO ₂			5-Aminopentanoate	1.1	1.0	2.4	0.001679
C ₄ H ₈ O ₂ S		Methionine	3-(Methylthio)propionic acid	0.1	-0.1	-1.8	0.004468

C ₈ H ₁₃ NO ₆		Phenylalanine	O-Succinyl-L-homoserine	-0.6	-0.8	-2.5	0.000300
C ₈ H ₈ O ₂			Phenylacetic acid	0.7	1.3	1.9	0.000560
C ₇ H ₁₀ O ₅			Shikimate	0.7	1.1	2.5	0.000077
C ₉ H ₁₆ N ₂ O ₅ Se		Selenoamino acid	γ-Glutamyl-Se-methylselenocysteine	0.1	0.6	2.3	0.000170
C ₂ H ₄ O ₅ S		Taurine and hypotaurine	Sulfoacetate	0.1	-0.2	-2.0	0.000443
C ₂ H ₅ O ₅ P			Acetyl phosphate	0.5	0.8	2.3	0.003220
C ₁₁ H ₁₂ N ₂ O ₄		Tryptophan	L-Formylkynurenine	-0.5	-0.4	-2.0	0.009990
C ₆ H ₇ NO			2-Aminophenol	0.2	-0.2	-1.9	0.004606
C ₈ H ₁₁ NO ₃		Tyrosine	L-Noradrenaline	0.1	0.8	2.4	0.000026
C ₈ H ₁₁ NO			Tyramine	0.1	0.0	1.9	6.27E-08
C ₂₆ H ₄₄ N ₇ O ₁₈ P ₃ S		Valine, leucine and isoleucine degradation	(2S,3S)-3-Hydroxy-2-methylbutanoyl-CoA	0.8	0.2	-1.5	0.000095
C ₆ H ₁₀ O ₃			4-Methyl-2-oxopentanoate	0.2	0.0	-1.8	0.000099
C ₅ H ₈ O ₃			3-Methyl-2-oxobutanoic acid	-0.2	-0.5	-2.4	0.000013
C ₉ H ₁₈ N ₄ O ₄	Biosynthesis of Secondary Metabolites	Clavulanic acid biosynthesis	L-N2-(2-Carboxyethyl)arginine	0.1	-0.6	-2.4	4.10E-06
C ₁₅ H ₁₆ O ₁₀	Carbohydrate	0	Caffeic acid 4-O-glucuronide	-1.0	-0.7	-2.4	0.000050
C ₄ H ₈ O ₄			D-Threose	0.0	-0.8	-2.4	6.99E-06
C ₁₆ H ₂₃ N ₃ O ₁₀			3'-Amino-3'-deoxythymidine glucuronide	-0.3	-0.6	-2.2	0.003316
C ₁₁ H ₁₉ NO ₇			N-(1-Deoxy-1-fructosyl)proline	-0.6	-0.5	-2.2	0.001037
C ₁₂ H ₂₀ N ₂ O ₇			Deoxyfructosazine	0.0	-0.2	-1.9	0.000778
C ₆ H ₁₃ O ₉ P			Hexose phosphate	0.7	0.8	2.2	0.015188
C ₄ H ₈ O ₄			L-Erythrulose	0.3	0.8	2.4	0.000187
C ₁₈ H ₃₃ NO ₁₅			β-D-Galactopyranosyl-(1->4)-2-amino-2-deoxy-β-D-glucopyranosyl-(1->6)-D-mannose	0.8	0.9	2.4	0.001075
C ₁₇ H ₂₅ N ₃ O ₁₈ P ₂		Aminosugars	UDP-N-acetyl-2-amino-2-deoxy-D-glucuronate	-0.1	0.0	-1.6	0.004551
C ₈ H ₁₅ NO ₆			N-Acetyl-D-mannosamine	0.1	0.9	2.2	0.000664
C ₁₇ H ₂₇ N ₃ O ₁₇ P ₂			UDP-N-acetyl-D-galactosamine	0.5	1.0	2.3	0.001294
C ₆ H ₁₃ NO ₅			D-Glucosamine	0.7	1.0	2.5	0.000090
C ₆ H ₁₀ O ₈		Ascorbate and aldarate	D-Glucarate	0.3	-0.3	-2.2	4.00E-06
C ₅ H ₆ O ₄			2,5-Dioxopentanoate	0.4	1.1	2.1	0.003667
C ₆ H ₆ O ₆			L-Dehydroascorbate	0.1	-0.4	-2.2	0.000196
C ₈ H ₁₄ O ₅		Butanoate	(R)-3-((R)-3-Hydroxybutanoyloxy)butanoate	0.1	-0.5	-2.3	2.55E-06
C ₄ H ₆ O ₂			Diacetyl	0.1	-0.3	-1.9	0.009602
C ₅ H ₈ O ₄			2-Acetolactate	2.2	1.2	2.3	7.84E-09
C ₆ H ₁₀ N ₂ O ₃		C5-Branched dibasic acid	4-Methylene-L-glutamine	-0.2	-0.9	-2.0	0.008660
C ₆ H ₁₁ NO ₄			4-Methyl-L-glutamate	1.7	1.2	1.9	0.015476
C ₂₁ H ₃₆ N ₇ O ₁₆ P ₃ S		TCA cycle	CoA	-1.2	-1.4	-2.5	0.000001
C ₆ H ₈ O ₇			Citrate	0.3	-0.2	-1.8	0.009505
C ₄ H ₆ O ₄			Succinate	0.5	1.3	1.8	0.000220
C ₆ H ₁₂ O ₆		Fructose and mannose	L-Sorbose	0.0	-0.2	-1.9	0.003560
C ₆ H ₁₀ O ₅			2-Dehydro-3-deoxy-D-fuconate	0.3	-0.3	-1.9	0.006055
C ₆ H ₁₂ O ₆			D-Mannose	0.9	0.8	2.3	0.002399
C ₆ H ₁₂ O ₆			D-Fructose	-0.1	-0.6	-2.4	5.35E-06
C ₂₄ H ₄₂ O ₂₁		Galactose	Stachyose	-0.9	-1.0	-2.6	0.000033
C ₁₂ H ₂₂ O ₁₁			Lactose	0.0	-0.8	-2.4	1.96E-06
C ₃ H ₆ O ₄		Glycine, serine and threonine	D-Glycerate	0.0	-0.1	-1.7	0.019384
C ₁₂ H ₂₂ O ₁₁		glycogen degradation I	β-Maltose	-0.1	-0.8	-2.5	6.01E-07
C ₃ H ₇ O ₆ P		Glycolysis / Gluconeogenesis	Glycerone phosphate	0.0	-0.7	-2.1	0.003990
C ₆ H ₁₀ O ₅		Glyoxylate and dicarboxylate	3-Ethylmalate	0.0	-0.8	-2.4	3.24E-06
C ₇ H ₁₂ O ₅			3-Propylmalate	0.0	-0.4	-2.0	0.007022
C ₇ H ₁₄ O ₆		Inositol phosphate	1-O-Methyl-myo-inositol	0.0	-0.4	-2.2	0.000123
C ₆ H ₁₁ O ₉ P		PPP	D-Glucono-1,5-lactone 6-P	0.2	-0.6	-2.2	0.000239
C ₆ H ₁₂ O ₇			D-Gluconic acid	0.4	-0.4	-2.1	0.000034
C ₆ H ₁₃ O ₁₀ P			6-Phospho-D-gluconate	0.4	-0.4	-2.1	0.000381
C ₇ H ₁₅ O ₁₀ P			D-Sedoheptulose 7-P	0.3	0.8	2.4	0.000258
C ₄ H ₉ O ₇ P			D-Erythrose 4-P	0.6	0.9	2.1	0.023033
C ₅ H ₁₃ O ₁₄ P ₃			5-Phospho-α-D-ribose 1-diphosphate	-0.5	-1.0	-2.5	0.000037
C ₇ H ₁₀ O ₇		Propanoate	2-Methylcitrate	0.5	-0.3	-2.0	0.000062
C ₃ H ₇ O ₅ P			Propanoyl phosphate	-1.0	-1.0	-2.4	0.000961
C ₆ H ₁₀ O ₅		Pyruvate	(R)-2-Ethylmalate	0.3	0.1	-1.5	0.007353

$C_{18}H_{32}O_{18}$		Starch and sucrose	1-4- β -D-Glucan	0.2	-0.4	-2.1	0.000670
$C_{10}H_{16}N_5O_{13}P_3$	Energy	Oxidative phosphorylation	ATP	-0.3	0.3	1.8	0.008598
$C_{10}H_{18}N_2O_3$	Cofactors & vitamins	Biotin	Dethiobiotin	0.3	-0.3	-2.1	0.000044
$C_9H_{18}NO_8P$		Pantothenate and CoA biosynthesis	D-4'-Phosphopantothenate	0.0	-0.7	-2.4	0.000061

3.5 Discussion

The global spread of MDR Gram-negative bacteria is alarming and it is crucial to understand the detailed mechanisms of antibiotic action and resistance. Bacterial metabolic responses to antibiotics have not been well examined with cutting-edge metabolomics, and deciphering the metabolome of bacterial cells can potentially lead to innovative strategies for effective antibacterial therapy. Polymyxins and carbapenems display their primary antibacterial activity via initial interactions with LPS and binding to penicillin-binding proteins (PBPs), respectively (11, 258). Notwithstanding, increasing evidence indicates that the rarely explored effects on bacterial metabolism are crucial for the antibacterial activity of antibiotics (113). The combination of polymyxins with carbapenems has been shown to be synergistic against MDR Gram-negative bacteria; albeit, the detailed mechanism of their synergistic action(s) has not been examined (222-226). Previously, our transcriptomics data revealed that the combination of colistin and doripenem altered the gene expression profiles in *A. baumannii* at 1 hr in a similar manner to that of colistin treatment alone. These genes were primarily associated with outer membrane biogenesis, fatty acid metabolism and phospholipid trafficking (412). Interestingly, similar transcriptional changes were also observed in the *A. baumannii* LPS-deficient strain without colistin treatment (356). Our present study is the first to elucidate the synergistic killing mechanism of the combination of colistin and doripenem against *A. baumannii*. The most significant findings on the synergistic combination in this metabolomics study include: (1) differential time-dependent inhibition of key metabolic pathways; (2) perturbation of the PPP and the downstream metabolism of LPS and nucleotides; and (3) inhibition of cell wall synthesis via different targets.

In the present study, global metabolic changes of *A. baumannii* ATCC 19606 and a pair of clinical strains of polymyxin-susceptible 03-149.1 and polymyxin-resistant 03-149.2 were

investigated following exposure to colistin and doripenem individually and in combination over 4 hr. Our results show, for the first time, that colistin, doripenem and the combination induced common global metabolic perturbations in *A. baumannii*, and metabolisms of cellular lipids, nucleotides, amino sugars and energy are the common pathways involved in the synergistic action of colistin and doripenem. The initial cellular metabolic perturbations following treatment with colistin monotherapy at 15 min and 1 hr impacted several essential metabolic pathways, namely lipid metabolism, nucleotide metabolism, amino sugar metabolism and energy metabolism. Similar metabolic alterations were observed following treatment with doripenem alone at 4 hr, indicating the effects of each antibiotic occur in a differential time-dependent manner. With the combination treatment, the perturbations were observed across all time points in *A. baumannii* strains ATCC 19606, 03-149.1 and 03-149.2. This mechanistic finding has important implications for the pharmacokinetics/pharmacodynamics (PK/PD) of the colistin and doripenem combination, supporting its use in the clinic for maintaining persistent antibacterial effect and minimising the potential bacterial regrowth due to colistin monotherapy (185, 413).

Two key models have been proposed to explain mechanisms of drug synergism, the parallel pathway inhibition model and the bioavailability model (reviewed in Section 1.3.6) (249-251, 414). The parallel pathway inhibition model suggests that two drugs are synergistic if they inhibit two different targets in parallel pathways that are essential for an observed phenotype (251). The bioavailability model suggests that two drugs are synergistic if one drug's action enhances another drug's availability in the target cell, either by increasing the second drug's entry into the cell or by decreasing the second drug's degradation or efflux (250). As doripenem itself can access its target in the periplasmic space in *A. baumannii*, the bioavailability model is unlikely to explain the synergistic activity of colistin and doripenem, and is not supported by our metabolomics data. Our metabolomics analysis indicates that the parallel pathway inhibition

model explains well the synergistic killing by colistin and doripenem against *A. baumannii*. Notably, treatment with colistin or doripenem alone or in combination at different time points significantly decreased the cellular levels of PPP intermediates (e.g. D-sedoheptulose 7-phosphate) and key precursor and intermediate metabolites for the biosynthesis of peptidoglycan and LPS (e.g. UDP-GlcNAc, UDP-MurNAc) in all three *A. baumannii* strains (Figures 3.8, 3.9, and, 3.12-3.14). Our metabolomics data also demonstrate that colistin and doripenem generally perturb various key pathways related to cell envelope biosynthesis, namely GPs, FAs, LPS and peptidoglycan biosynthesis (Figures 3.5-3.7 and 3.12-3.14). Importantly, our study is the first to reveal that colistin itself also caused inhibition of cell wall synthesis, particularly peptidoglycan by decreasing the essential precursor metabolites (e.g. UDP-GlcNAc, UDP-MurNAc), a different mechanism from doripenem which acts via binding to PBPs.

The Gram-negative bacterial cell envelope is composed of an asymmetrical outer membrane (OM), a thin cell wall, and a symmetrical inner membrane (reviewed in Section 1.3.3) (87). The outer leaflet of the OM is predominantly constituted of LPS and the inner leaflet is mainly comprised of phospholipids (87, 88). In line with the primary mode of action of colistin, our metabolomics data revealed that colistin treatment at 15 min and 1 hr caused significant perturbations in the levels of OM lipids, specifically GPs and FAs in all three *A. baumannii* strains (Figures 3.5-3.7). Consistent with our findings, it has been demonstrated *in vitro* that, liposomes prepared from phosphatidylethanolamine were extremely sensitive to polymyxin B indicating the binding affinity of polymyxin towards phospholipids (94). In addition, our previous transcriptomics results showed that colistin treatment up-regulated the expression of the Mla system (Maintenance of OM lipid asymmetry) in *A. baumannii* ATCC 19606, which is responsible for transporting excess phospholipids in the outer leaflet back to the inner membrane to maintain the OM asymmetry (412, 415, 416). Significant changes to the OM lipids, as

observed at both the transcriptomics and metabolomics levels, are highly consistent with the proposed bactericidal mechanism of colistin via lipid exchange between the inner and outer membrane (400). Furthermore, our previous transcriptomics data showed that colistin treatment induced the up-regulation of genes involved in fatty acid β -oxidation/degradation and down-regulation of genes involved in fatty acid biosynthesis (412), which well explains the colistin-induced fatty acid perturbations observed in this study. Notably, doripenem treatment at 15 min and 1 hr did not produce any appreciable changes in the levels of GPs and FAs relative to the untreated control in all the three *A. baumannii* strains. The expression of lipid metabolism genes was not affected at 15 min, although significant transcriptomics changes were reported for doripenem treatment at 1 hr (i.e. retrograde phospholipid transport and lipoprotein transport) in the ATCC 19606 (412). However, doripenem treatment at 4 hr produced a similar pattern of lipid changes (i.e. GPs, FAs) as per the aforementioned colistin treatment particularly in the ATCC 19606. There were no significant lipid changes observed in both polymyxin-susceptible 03-149.11 and polymyxin-resistant 03-149.2 by doripenem alone likely due to their resistance to doripenem. Interestingly, the entire time-course of the combination treatment against the ATCC 19606 displayed a distinct pattern of lipid changes, wherein only the GPs were significantly perturbed while the FA levels remained largely unaffected. One metabolite involved in glycerophospholipid metabolism, *sn*-glycero-3-phosphoethanolamine, was specifically associated with colistin treatment, both alone and in combination was steadily decreased in all three *A. baumannii* strains. Interestingly, *sn*-glycero-3-phosphoethanolamine was also significantly depleted in the LPS-deficient polymyxin-resistant strain *A. baumannii* 19606R relative to the wild-type ATCC 19606 strain in the absence of polymyxin treatment, suggesting the importance of the metabolite in response to polymyxin (as reported in Section 2.4.6).

In terms of the impact on energy metabolism, treatment with the colistin and doripenem combination significantly decreased intracellular ATP, NADP⁺ and NAD⁺ levels and the levels of major metabolites of PPP, namely D-sedoheptulose 7-phosphate, D-ribose 5-phosphate and D-erythrose 4-phosphate in the ATCC 19606. ADP-heptose, a key downstream metabolite of the heptose biosynthesis pathway, is an important component of the LPS inner core (381, 417). Mutations in the gene (*GmhA*) associated with ADP-glyceromannoheptose synthesis in *Haemophilus influenza*, which cause deficiencies in heptose biosynthesis, result in an avirulent phenotype, increased membrane permeability and increased susceptibility to antibiotics (381, 418, 419). Excitingly, our data revealed significant depletion in the levels of D-sedoheptulose 7-phosphate in the ATCC 19606 strain under all treatment conditions across 4 hr, in the 03-149.1 particularly at 1 hr and in the 03-149.2 at 4 hr (Figures 3.8 and 3.9). As D-sedoheptulose 7-phosphate is also a key early precursor metabolite in the heptose biosynthesis pathway, our data suggest that colistin, doripenem and their combination perturb the biosynthesis of ADP-heptose in *A. baumannii* via inhibition of the PPP.

Another metabolite in the PPP, D-ribose 5-phosphate, was significantly depleted after treatment with colistin, doripenem and the combination in the ATCC 19606 (Figure 3.8). D-Ribose 5-phosphate is a key initial precursor metabolite in purine and pyrimidine metabolism, and hence all treatment conditions caused significant decreases in the levels of nucleotides, both purine and pyrimidine (Figure 3.10B). In turn, the significant decreased of purine and pyrimidine nucleotides in the 03-149.1 strain was consistent with the low levels of the precursor metabolite, PRPP at 15 min, 1 hr and 4 hr (Figure 3.11C) (420). In contrast to the findings that were observed in both polymyxin-susceptible ATCC 19606 and 03-149.1 strains, our results showed that treatment with colistin alone and the combination against 03-149.2 strain induced significant elevation in nucleotide levels at 15 min and 1 hr (Figure 3.11B). We speculated that the

accumulation of the metabolites in the 03-149.2 strain was due to the general stress response induced by colistin alone and the combination. As a result, the bacteria presumably tried to produce more metabolites to cope with the toxic effects conferred by the antibiotics. In addition, the increased levels of many amino acid (e.g. arginine, proline and lysine metabolism) and carbohydrate (e.g. PPP metabolism) metabolites were likely to support the hypothesis of antibiotic-induced stress response in the 03-149.2 strain. Furthermore, as the synergistic effect of the colistin and doripenem combination significantly decreased the levels of nucleotides in the 03-149.2 strain at 4 hr, the result was in line with the decreased level of nucleotide precursor, PRPP (Figure 3.11B and C) (420).

Previous metabolomics studies have shown total depletion of the nucleotide pool following antibiotic treatment (ampicillin, kanamycin, norfloxacin, vancomycin) in both Gram-negative (*Escherichia coli*) and Gram-positive (*Staphylococcus aureus*) bacteria (113, 421). The significant changes in nucleotide levels in antibiotic-treated samples were suggestive of nucleotide degradation (113). Interestingly, significant depletion in the levels of nucleotides in the polymyxin-resistant LPS-deficient strain *A. baumannii* 19606R was observed even without polymyxin treatment (as discussed in Section 2.4.4). Significant depletion in the levels of energy metabolites (ATP, NADP⁺, NAD⁺) in *A. baumannii* is likely secondary to the nucleotide pool depletion, but may also be indicative of altered oxidative phosphorylation. It has been reported that polymyxins predominantly inhibit the process of respiration which reduced the level of the intracellular ATP pool (79). In addition, significant alteration in the levels of TCA cycle metabolites (e.g. fumarate, *cis*-aconitate) in all *A. baumannii* strains were observed in the present study. It is likely that the depletion of energy related metabolites by colistin, doripenem and the combination also is a secondary effect to their antibacterial activity against MDR Gram-negative bacteria, in particular *A. baumannii*.

The broad-spectrum antibacterial effect of doripenem against Gram-positive and Gram-negative bacteria is by virtue of its ability to inhibit biosynthesis of the key building block of the bacterial cell wall, peptidoglycan (258, 422, 423). Fundamentally, doripenem is a substrate analogue that binds to the C-terminal transpeptidase active site of PBPs in a non-reversible manner, thus inhibiting the peptidoglycan polymerisation process (424). Notably, following treatment with doripenem alone or in combination at 4 hr, we observed significant decreases in the levels of peptidoglycan biosynthesis metabolites, meso-2,6-diaminoheptanedioate and UDP-*N*-acetylmuramoyl-L-alanyl-D-glutamyl-6-carboxy-L-lysyl-D-alanyl-D-alanine in the ATCC 19606 (Figure 3.12). Significant changes in the levels of peptidoglycan biosynthesis metabolites were consistently observed in both *A. baumannii* clinical isolates (Figures 3.13 and 3.14). As mentioned above, colistin monotherapy also significantly decreased the levels of the essential peptidoglycan biosynthesis metabolites (e.g. UDP-GlcNAc, UDP-MurNAc) as observed particularly in the polymyxin-susceptible strains ATCC 19606 and 03-149.1. Interestingly, our previous transcriptomics results showed that peptidoglycan-associated lipoproteins were significantly up-regulated in *A. baumannii* ATCC 19606 in response to treatment with colistin and doripenem alone or in combination (412). The up-regulation of peptidoglycan-associated lipoproteins may be a protective action by *A. baumannii* to cope with the inhibition of peptidoglycan synthesis by doripenem and/or colistin. Taken together, our current metabolomics study reveals that, in addition to disorganising the OM, colistin also interferes cell wall synthesis via inhibition of peptidoglycan metabolism; this mechanism also explains the synergistic killing effect of its combination with a carbapenem.

Studies have shown that the mechanism of polymyxin activity was partly associated with oxidative stress via the formation of hydroxyl radicals, with reactive oxygen species mainly targeting DNA, RNA, proteins and lipids (108), or by inhibition of respiratory chain enzymes

(e.g. NADH-quinone oxidoreductase) (92, 109). However, the association of free radicals in the mechanism of antibiotic bacterial killing is disputable (110-112, 117, 118). In our analysis of *A. baumannii* ATCC 19606, the reduced form of glutathione (GSH), an important indicator of oxidative stress, was not detected, as it was likely oxidised to glutathione disulfide (GSSG) during sample preparation and/or storage (425). Nevertheless, the total glutathione content, measured as GSSG, was significantly depleted following exposure to colistin and doripenem alone and in combination in the ATCC 19606 (Tables 3.3 and 3.4); this result is in line with the utilisation of glutathione pools to compensate for antibiotic-induced oxidative damage, albeit not consistent with the increased levels of reduced glutathione previously reported (113). We identified that GSH was significantly depleted in the *A. baumannii* 03-149.1 strain in response to colistin alone and in combination (data not shown). As GSH is easily oxidised to GSSG during sample preparation and/or storage, thus we carefully considered the changes was predominantly due to the oxidation. However, as GSSG was significantly depleted in the *A. baumannii* 03-149.1 strain following colistin alone and the combination, similarly we hypothesised that the change was due to the utilisation of glutathione pools as observed in the ATCC 19606. Furthermore, there was no appreciable change in the GSSG level in the *A. baumannii* 03-149.2 strain. Even though we were unable to detect specific markers of oxidative stress from the TCA cycle intermediate (i.e. α -ketoglutarate) and product (i.e. NADH), the changes to other TCA metabolites (e.g. fumarate, *cis*-aconitate) in all the *A. baumannii* strains clearly indicate the perturbation of the TCA cycle in response to single and combination treatments of colistin and doripenem. Our group previously demonstrated that *A. baumannii* ATCC 19606 treated with colistin significantly increased the expression of superoxide dismutase (SOD) enzyme, HMPREF0010_02336 (*sodB* encoding a predicted FeSOD) and HMPREF0010_02564 (encoding a predicted Cu-ZnSOD), suggesting the association of hydroxyl radicals in colistin antibacterial activity (412).

3.6 Conclusions

To the best of our knowledge, this is the first metabolomics study to investigate the mechanism of action of colistin either as monotherapy, or in combination with doripenem, against *A. baumannii*. Notwithstanding the complex of cellular biochemical networks and interactions in bacteria, our study significantly highlights the bacterial metabolic responses to antibiotics which potentially could be exploited to develop new, effective means to combat MDR infections. Our study reveals significant perturbations to cell envelope biosynthesis, nucleotide metabolism and energy metabolism induced by colistin and its synergistic combination with doripenem. The convergence of antibiotic-induced metabolic profiles on the depletion of PPP and amino-sugar metabolites indicates that these pathways play key roles in the antibacterial activity of colistin alone and its combination with doripenem. Importantly, we are the first to demonstrate that the combination of colistin with doripenem synergistically kills *A. baumannii* via inhibiting different key metabolic pathways in a time-dependent manner, which highlights the essentiality of mechanism-based optimisation of this combination using PK/PD. Overall, this study highlights the significant potential of systems pharmacology in paradigm-shifting optimisation of antibiotic use in patients.

Chapter Four

Chapter 4: Untargeted metabolomics study of the synergistic combination of polymyxin B and rifampicin against *Pseudomonas aeruginosa* PAO1

4.1 Abstract

The emergence of antimicrobial resistance in parallel with the dry discovery of new antibiotics, desperately needs the full exploitation of the last-line antibiotic class polymyxins. Understanding the detailed underlying mode of action of polymyxins is highly relevant in optimising its clinical use. An untargeted metabolomics study was performed to profile the global metabolic changes of *Pseudomonas aeruginosa* PAO1 following treatment with polymyxin B (1 mg/L) and rifampicin (2 mg/L) alone and in combination at 15 min, 1 hr, 4 hr and 24 hr (n=4). Polymyxin B alone and in combination significantly altered the PAO1 lipid metabolism at 15 min, 1 hr and 4 hr, reflecting the general action of polymyxin B to trigger membrane disruptions. Notable metabolic perturbations of purine and pyrimidine nucleotides, amino acids metabolites, central carbon metabolism (i.e. TCA cycle, glycolysis and pentose phosphate pathway), peptidoglycan and LPS biosynthesis were subjected to the synergistic effect of the combination at 15 min, 1 hr and 4 hr. Nevertheless, rifampicin alone induced no appreciable changes across all time points. The abundance of metabolites (e.g. nucleotides, amino acids) following the combination treatment suggesting that PAO1 was in a state of cellular metabolic arrest which in line with the mode of action of rifampicin as an RNA synthesis inhibitor. The mechanism of synergistic killing of the combination is clearly elucidated by the simple uptake effect as polymyxin B induced the disruption of outer membrane to facilitate the entry of rifampicin for the latter to reach its intracellular target. Overall, this study significantly provides vast information on polymyxin B-rifampicin synergistic interaction which is highly useful for the pharmacokinetics/pharmacodynamics optimisation of polymyxins.

4.2 Introduction

The aerobic Gram-negative *P. aeruginosa* has been labelled as a “Serious-Threat” and “Critical-Priority” opportunistic pathogen due to its remarkable ability to develop resistance towards almost all current antibiotics (8, 9, 388). Treatment of MDR *P. aeruginosa* infection necessitates the revisit of polymyxins, an ‘old’ antibiotic class (11, 398). Polymyxin-induced bacterial killing is well elucidated by the ‘self-promoted uptake’ pathway (Section 1.3.3) (11). Considering its dose-limiting toxicity (82, 160-162), polymyxin monotherapy is unlikely to produce an optimal *in vivo* plasma concentration with the potential emergence of polymyxin heteroresistant sub-population (Section 1.3.5) (81, 189). Evidence showed that polymyxin combination therapy potentially could cater these limitations (98, 214). In particular, the combination of polymyxin with rifampicin has been shown to synergistically killed MDR Gram-negative pathogens including *P. aeruginosa*, *K. pneumoniae* and *A. baumannii* (231-236). Notwithstanding, the detailed mechanistic killing action of polymyxins either as a single or in combination largely remains to be explored to further optimise its application in clinical setting.

The study of metabolomics has become an important component in the drug development pipeline used to elucidate the mechanism of action of a particular new drug (275). The abundance of metabolites, either of its substrates or products generally is a direct reflection of an enzyme’s inhibition of a particular reaction (304). For the first time, global metabolite profiling of a single and combination of polymyxin B and rifampicin treatment against *P. aeruginosa* PAO1 was conducted across four time points at 15 min, 1 hr, 4 hr and 24 hr. The synergistic action of the combination induced significant perturbation in the levels of metabolites associated with lipid, cell envelope biosynthesis, nucleotide, amino acid and central carbon metabolisms. The predominant effect of polymyxin B at the early time point (15 min) caused membrane lipid disorganisation that facilitate the intracellular entry of rifampicin to induce the global metabolic

changes. Overall, this study highlights the global insights of the PAO1 metabolic changes of single and combination of polymyxin B treatment potentially beneficial to be used for polymyxin PK/PD optimisation and discovery of novel polymyxin cellular targets.

4.3 Materials and methods

4.3.1 Strain

P. aeruginosa PAO1 strain was from the American Type Culture Collection (ATCC). The PAO1 was susceptible to polymyxin B and resistant to rifampicin with broth microdilution MICs of 0.5 mg/L and 32 mg/L, respectively. The strain was grown in cation-adjusted Mueller-Hinton broth (CaMHB; Oxoid, Australia; 20-25 mg/L Ca^{2+} and 10-12.5 mg/L Mg^{2+}).

4.3.2 Antibiotics and reagents

Polymyxin B was prepared using Milli-Q water (Millipore Australia, North Ryde, New South Wales, Australia) while rifampicin was solubilised by DMSO prior to each experiment and sterilised by filtration with a 0.22- μm pore size Millex GP filter (Millipore, Bedford, MA).

4.3.3 Bacterial culture preparation

The culture of *P. aeruginosa* PAO1 was prepared on a nutrient agar plate from the frozen stock (-80°C) and incubated for 16 - 18 hr at 37°C . As different types of growth media have significant impacts on bacterial growth and antibiotic susceptibility, CaMHB was selected as the culture medium for PAO1 in this study. For the overnight culture, a colony of *P. aeruginosa* PAO1 was inoculated into 15 mL CaMHB and incubated for 16 - 18 hr at 37°C with shaking at 150 rpm. The overnight culture was diluted with 1:100 into four different reservoirs of 200 mL fresh CaMHB. To obtain enough cells for the metabolomics experiment, the culture was grown to an optical density at 600 nm ($\text{OD}_{600\text{ nm}}$) of ~ 0.5 ($\sim 10^8$ CFU/mL). Bacterial culture of each reservoirs

was treated with polymyxin B (1 mg/L), rifampicin (2 mg/L) and the combination of polymyxin B and rifampicin (1 mg/L + 2 mg/L); concentrations of polymyxin B and rifampicin were clinically relevant. Untreated bacterial culture served as a control sample. The study was conducted with four biological replicates independently from different colonies of PAO1 on different days

4.3.4 Preparation of cellular metabolite extracts

Cellular metabolites of *P. aeruginosa* PAO1 were extracted by the previously optimised method with slight modifications (Section 2.3.4). Samples were collected before treatment with polymyxin B, rifampicin and the combination (i.e. time = 0), and at 15 min, 1 hr, 4 hr and 24 hr for metabolite extraction and viable counting. For the fingerprint samples (i.e. intracellular metabolites), 20 mL of the bacterial culture was collected and immediately transferred onto the ice. Quickly, all the samples were quenched in a dry ice/ethanol bath and preserved on ice for all following steps. Samples were normalised by OD_{600 nm} of ~0.5 (~10⁸ CFU/mL). The samples then were centrifuged for 10 min at 3,220 x g at 4°C. The supernatant was collected for extracellular metabolite preparation (i.e. footprint). The cell pellets were washed three times with 0.9% NaCl (4°C) and centrifuged for 3 min at 3,220 g at 4°C. Cellular metabolites were extracted with chloroform:methanol:water (CMW; 1:3:1, v/v; -80°C) mixture solvent (total volume of 250 µL) containing generic internal standards (CHAPS, CAPS, PIPES and TRIS) at 1 µM. Samples were frozen in liquid nitrogen and allowed to thaw on ice, and the freeze-thaw process was repeated three times to lyse the cells and release cellular metabolites. The extracted samples were centrifuged for 10 min at 3,220 x g at 4°C and the supernatant was collected and further centrifuged at 14,000 x g for 10 min at 4°C. The final supernatant samples (200 µL) were collected into the injector vial for LC-MS analysis. For footprint samples, aliquots of the culture supernatant were rapidly filtered through a 0.22-µm membrane filter, and 10 µL of the

supernatant was mixed with 250 μ L of CMW (1:3:1, v/v) and centrifuged at 14,000 \times g for 10 min at 4°C to collect particle-free supernatant for LC-MS analysis.

4.3.5 LC-MS analysis of metabolites

Analyses were performed on a Q-Exactive Orbitrap mass spectrometer (Thermo Fisher) coupled to a Dionex high-performance liquid chromatograph (U3000 RSLC HPLC, Thermo Fisher) with a ZIC-pHILIC column (5 μ m, polymeric, 150 \times 4.6 mm; SeQuant, Merck). The MS system was operated at 35,000 resolution in both positive and negative electrospray ionisation (ESI) mode (rapid switching) and a detection range of 85 to 1,275 m/z . The LC solvent consisted of 20 mM ammonium carbonate (A) and acetonitrile (B) with a multi-step gradient system from 80% B to 50% B over 15 min, then to 5% B at 18 min, followed by a wash with 5% B for 3 min, and re-equilibration for 8 min with 80% B at a flow rate of 0.3 mL/min (Section 2.3.5). The injection sample volume was 10 μ L and the run time was 32 min. All samples were analysed in the same run. The chromatographic peaks, signal reproducibility and analyte stability were periodically monitored by the assessment of pooled quality control samples (aliquot of 10 μ L of each sample, including both footprints and fingerprints), internal standards and total ion chromatograms throughout the batch. Mixtures of pure standards containing over 200 metabolites were analysed within the batch to aid in the identification of metabolites.

4.3.6 Data processing, bioinformatics and statistical analyses

Metabolomics data analyses were performed as previously described in Section 2.3.6 using mzMatch (342) and IDEOM (<http://mzmatch.sourceforge.net/ideom.php>) (341). The quantification of each metabolite was conducted using the chromatogram raw peak height. Univariate and multivariate analyses utilised MetaboAnalyst 3.0 (344). Prior to analysis, relative peak intensity data were normalised by the median, log transformed and scaled (by auto scale

function) to reduce variance between the samples (Section 3.3.5). Unsupervised principal component analysis (PCA) was applied to analyse the global metabolic profiles at each time point. Significantly changed metabolites of the treated samples at each time point were identified by One-way Analysis of Variance (ANOVA) ($p < 0.05$, $FDR \leq 0.05$) for multiple comparison coupled with post hoc analysis using Tukey's Honestly Significant Difference (Tukey's HSD). Those metabolites that showed a ≥ 1.0 -log₂-fold change were further analysed and subjected to metabolic pathway analysis.

4.4 Results

The present study aimed to profile the global metabolic changes of *P. aeruginosa* PAO1 induced by the synergistic killing of the combination of polymyxin B and rifampicin treatment at 15 min, 1 hr, 4 hr and 24 hr (n=4) (Figure 4.1). The coupling of hydrophilic interaction liquid chromatography (pHILIC) method with the Q-Exactive mass spectrometry advantageously maximised the separation and fragmentation of metabolites. Absolute identification of metabolites was determined based on the matched metabolite retention time and mass with the reference standard compounds that were available. Whereas, those metabolites that do not have reference standards were putatively annotated based on the calculated retention time and mass of the standards compounds. IDEOM (341) analysis annotated about 2,520 metabolite features (including their isomers) with reference to the *P. aeruginosa* and few other central databases (e.g. KEGG, Lipidmaps). The reproducibility of the metabolomics data, both the analytical (instrument) and the between individual sample groups was firstly determined based on the median relative standard deviation (RSD) values. The pooled biological quality control (PBQC) samples was used for determination of the analytical instrument performance which demonstrated the median RSD value of 20% (i.e. within the acceptable limit of metabolomics study of $\leq 20\%$) (Table 4.1). In addition, identification of the authentic standard was set within

5% retention time. Consistently, the principal component analysis (PCA) plot of all the individual sample groups at all time points shows that the PBQC samples are well clustered (Figure 4.2). Interestingly, the median RSD values for the combination of polymyxin B and rifampicin (23-34%) are more reproducible as compared to the single polymyxin B and rifampicin as well as untreated control (Table 4.1). The broad values of the median RSD (23-61%) of the sample groups indicate the highly dynamic nature of *P. aeruginosa* metabolism.

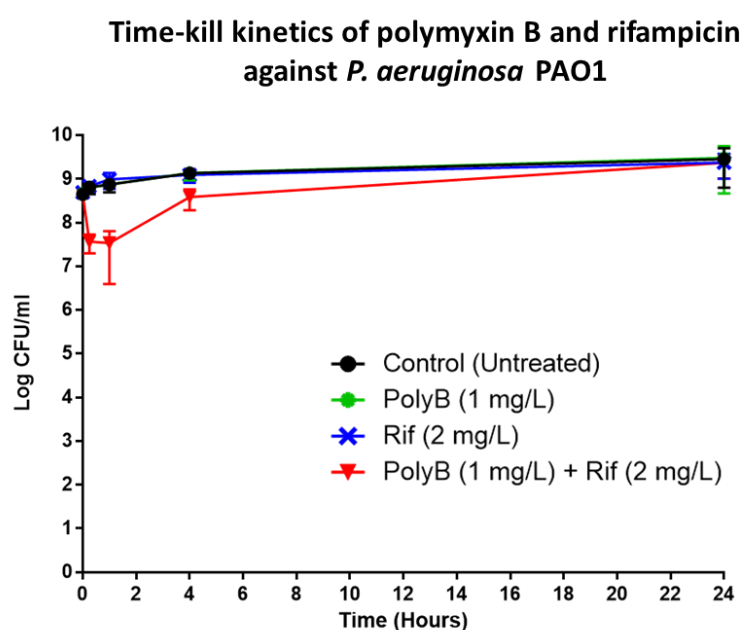


Figure 4.1. Time-kill kinetics of the combination of polymyxin B and rifampicin against *P. aeruginosa* PAO1. PAO1 cells were treated at OD₆₀₀ of ~0.5 with single and the combined polymyxin B and/or rifampicin. Metabolomics samples were collected at 0 hr, 15 min, 1 hr, 4 hr and 24 hr (n=4).

Table 4.1 Data precision of individual samples for polymyxin B and rifampicin alone and in combination (Combo), untreated control and pooled biological quality control (PBQC) represented as the median relative standard deviation (RSD, %) at 15 min, 1 hr, 4 hr and 24 hr.

	15 min	1 hr	4 hr	24 hr
PBQCs (throughout a batch)	20			
Control	25	48	33	32
Polymyxin B	25	34	37	61
Rifampicin	26	30	28	42
Combo	34	23	25	27

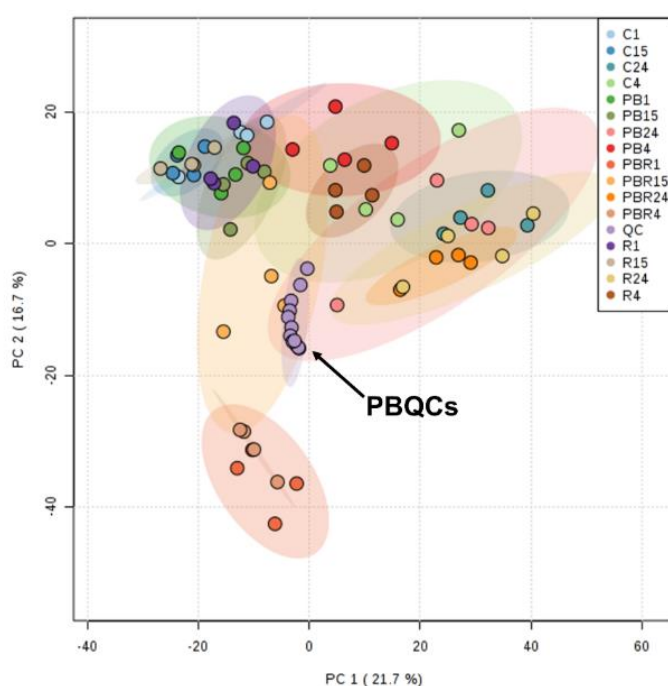


Figure 4.2. PCA score plot of all individual samples of *P. aeruginosa* PAO1 treated with polymyxin B and rifampicin alone and in combination. Twelve pooled biological quality control (PBQC) samples were analysed throughout the LC-MS batch. Each dataset represents four biological replicates of sample groups at all time points.

PCA plot was utilised to demonstrate the global metabolome changes of individual sample groups at each time point (Figure 4.3). The number of metabolites that were significantly changed (one way ANOVA; $\geq 1.0\text{-log}_2\text{-fold}$, $p \leq 0.05$, $\text{FDR} \leq 0.05$) by polymyxin B and rifampicin monotherapy and the combination at each time point were summarised in Venn diagrams (Figure 4.3). PCA plot at 15 min shows that polymyxin B alone well clustered and slightly overlapped with the polymyxin B and rifampicin combination (Figure 4.3A). In addition, the pattern of metabolic changes shown in the heat map profile at 15 min is likely in common between polymyxin B alone and the combination (Figure 4.4A). The combination of polymyxin B and rifampicin is distinctly separated from single polymyxin B and rifampicin monotherapy and control untreated sample at 1 hr and 4 hr (Figures 4.3B, C, and 4.4B, C). Notably, all the groups are indistinguishably separated by the antibiotic treatments at 24 hr (Figures 4.3D and 4.4D). Single polymyxin B induced subtle metabolic changes (0.2-1.8%) at 15 min, 1 hr and 4 hr, while rifampicin alone induced almost no changes (0.03-0.4%) at all time points (Figure 4.3). On the contrary, the synergistic action of the combination of polymyxin B and rifampicin significantly altered approximately 4-8% of the identified metabolites at 15 min, 1 hr and 4 hr, whereas 0.5% metabolites at 24 hr (Figure 4.3). Furthermore, metabolic pathway analysis demonstrated that the combination significantly altered several key metabolic pathways of PAO1 including purine and pyrimidine nucleotide metabolism, peptidoglycan biosynthesis, amino sugar and nucleotide sugar metabolism and pyruvate metabolism across the 4 hr (Figure 4.5).

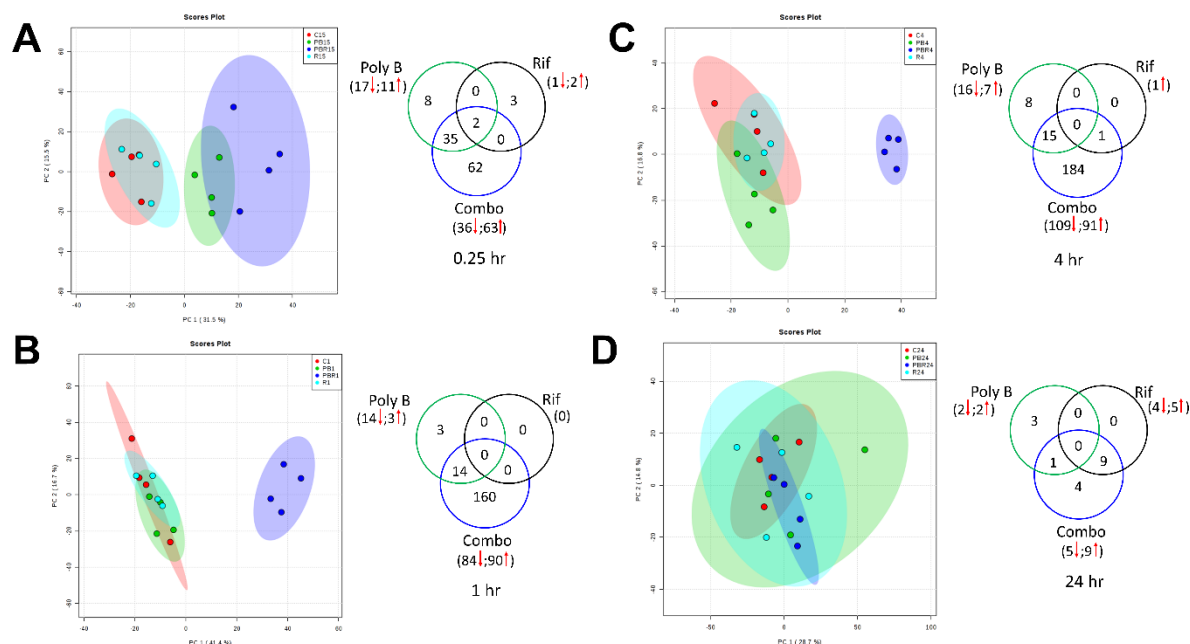


Figure 4.3. Global metabolic perturbations in *P. aeruginosa* PAO1. PCA plots (left) and Venn diagrams (right) of metabolite changes of samples treated with polymyxin B and rifampicin alone and the combination at (A) 15 min, (B) 1 hr, (C) 4 hr and (D) 24 hr. The numbers in brackets represent the metabolites that were significantly changed (up- and down-regulated). Green = polymyxin B (PB); Light blue = rifampicin (R); Dark blue = combination (PBR); Red = control (C). Significant metabolites were selected with ≥ 1.0 -log₂-fold, $p \leq 0.05$, $FDR \leq 0.05$ (one-way ANOVA for multiple comparison).

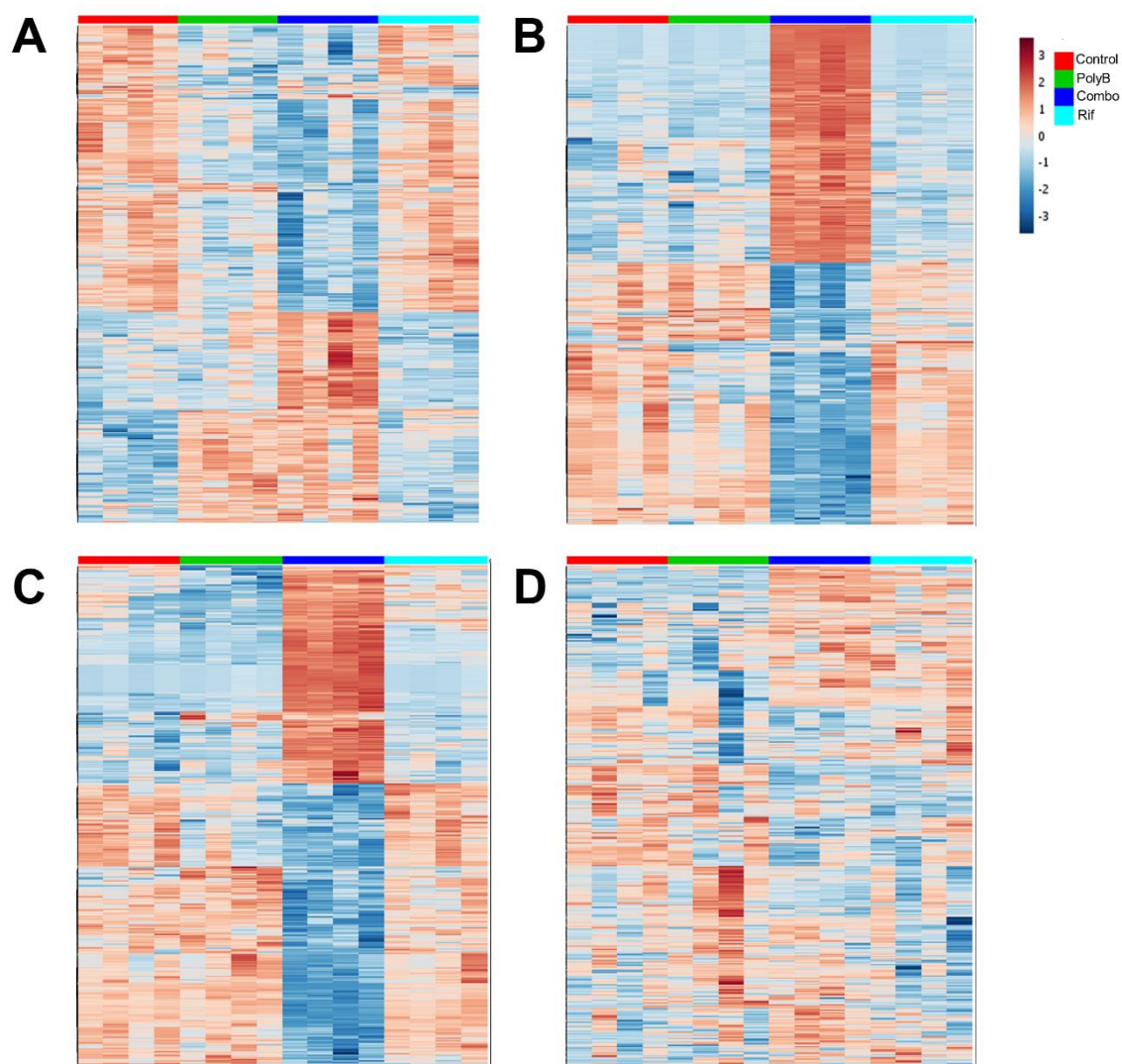


Figure 4.4. Heat map profiles of relative abundance of metabolites. The heat maps were hierarchically clustered based on the top 500 of significantly changed metabolites ($p \leq 0.05$) by polymyxin B and rifampicin alone and the combination at (A) 15 min, (B) 1 hr, (C) 4 hr and (D) 24 hr.

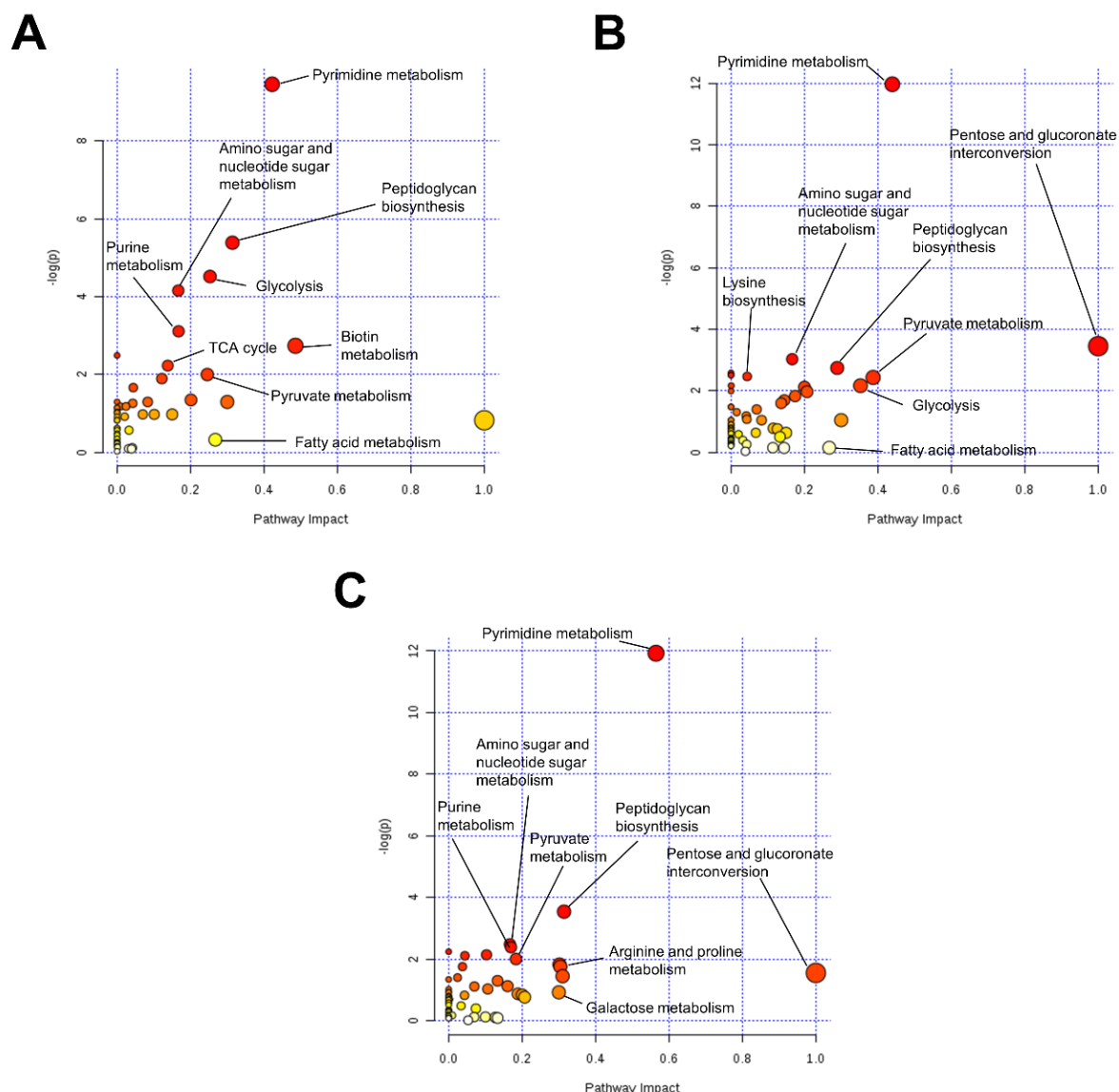


Figure 4.5. The overview of metabolic pathway analysis of the combination of polymyxin B and rifampicin. Metabolic pathways of *P. aeruginosa* PAO1 that were significantly perturbed by the combination of polymyxin B and rifampicin at (A) 15 min, (B) 1 hr and (C) 4 hr. The analysis was according to p -values from pathway enrichment analysis and pathway impact values from pathway topology analysis. The circle size represents the pathway impact score whereas the colour intensity represents the significance of the pathway. Significant metabolites were selected with ≥ 1.0 -log₂-fold, $p \leq 0.05$.

4.4.1 *Polymyxin B alone and in combination induced perturbation of membrane lipids*

Treatment with polymyxin B alone predominantly altered ($\leq 1.0\text{-log}_2\text{-fold}$, $p \leq 0.05$) the levels of several membrane lipids mainly of fatty acyls (FAs) and glycerophospholipids (GPs) at 15 min, 1 hr and 4 hr whereas rifampicin alone caused no significant changes (Figure 4.6). Substantial perturbations ($\geq 1.0\text{-log}_2\text{-fold}$, $p \leq 0.05$) of FAs and GPs were notified by the combination of polymyxin B and rifampicin treatment at 15 min, 1 hr and 4 hr (Figure 4.6). Unique patterns of lipid changes predominantly of GPs with long fatty acyls chains of phosphatidylethanolamine (PE) and phosphatidylglycerol (PG) species were observed following treatment with the combined polymyxin B and rifampicin at 1 hr and 4 hr. Interestingly, a comparable lipid perturbation particularly of FAs was observed at 24 hr between rifampicin alone and the combination. Furthermore, at 15 min and 1 hr, the level of *sn*-glycero-3-phosphocholine, a metabolite of lipid metabolism was significantly depleted by polymyxin B alone and the combination of polymyxin B and rifampicin.

4.4.2 *Polymyxin B and rifampicin combination up-regulated metabolites of peptidoglycan and LPS biosynthesis*

Significant increases ($\geq 1.5\text{-log}_2\text{-fold}$, $p \leq 0.05$) of four peptidoglycan biosynthesis metabolites namely UDP-*N*-acetylglucosamine (UDP-GlcNAc), UDP-*N*-acetylmuramate (UDP-MurNAc), UDP-MurNAc-L-Ala- γ -D-Glu-meso-2,6-diaminopimelate and UDP-MurNAc-L-Ala- γ -D-Glu-meso-2,6-diaminopimeloyl-D-Ala-D-Ala were notified following treatment with the combination of polymyxin B and rifampicin at 15 min, 1 hr and 4 hr (Figure 4.7A). In addition, the combination also significantly up-regulated ($\geq 1.5\text{-log}_2\text{-fold}$, $p \leq 0.05$) the level of 3-deoxy-D-manno-octulosonate (KDO), a metabolite of LPS biosynthesis in PAO1 at 15 min, 1 hr and 4 hr (Figure 4.7B). However, no significant changes of any peptidoglycan biosynthesis

metabolite were detected in response to polymyxin B and rifampicin monotherapy at all time points.

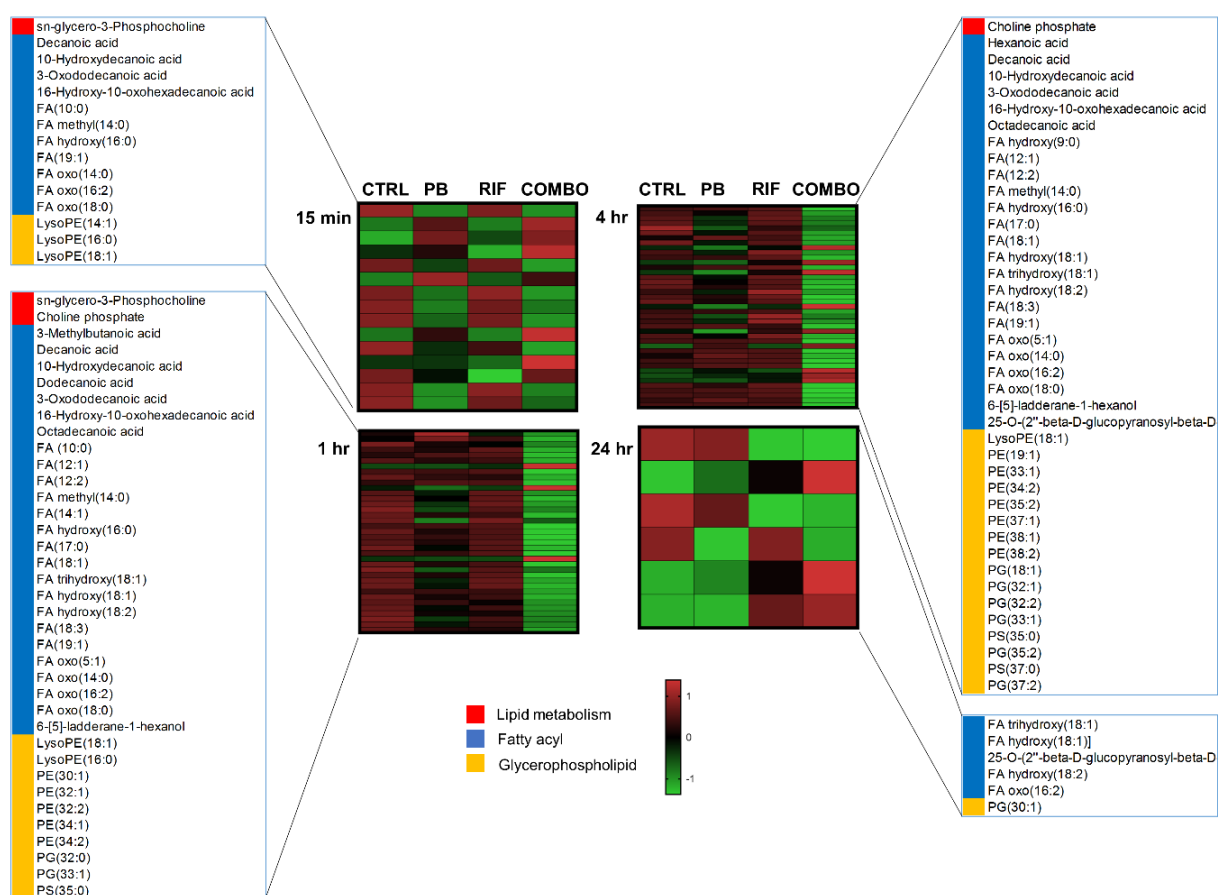


Figure 4.6. Heat map profiles of lipid perturbation. Polymyxin B alone and the combination of polymyxin B and rifampicin induced significant lipid changes majorly of fatty acyls (FAs) and glycerophospholipids (GPs) in *P. aeruginosa* PAO1 at 15 min, 1 hr and 4 hr. Several FAs were significantly perturbed by both rifampicin alone and the combination at 24 hr. Control = CTRL; polymyxin B = PB; rifampicin = RIF; combination = COMBO. Lipids were putatively annotated with reference to accurate mass and significantly selected with $\geq 1.0\text{-log}_2\text{-fold}$, $p \leq 0.05$.

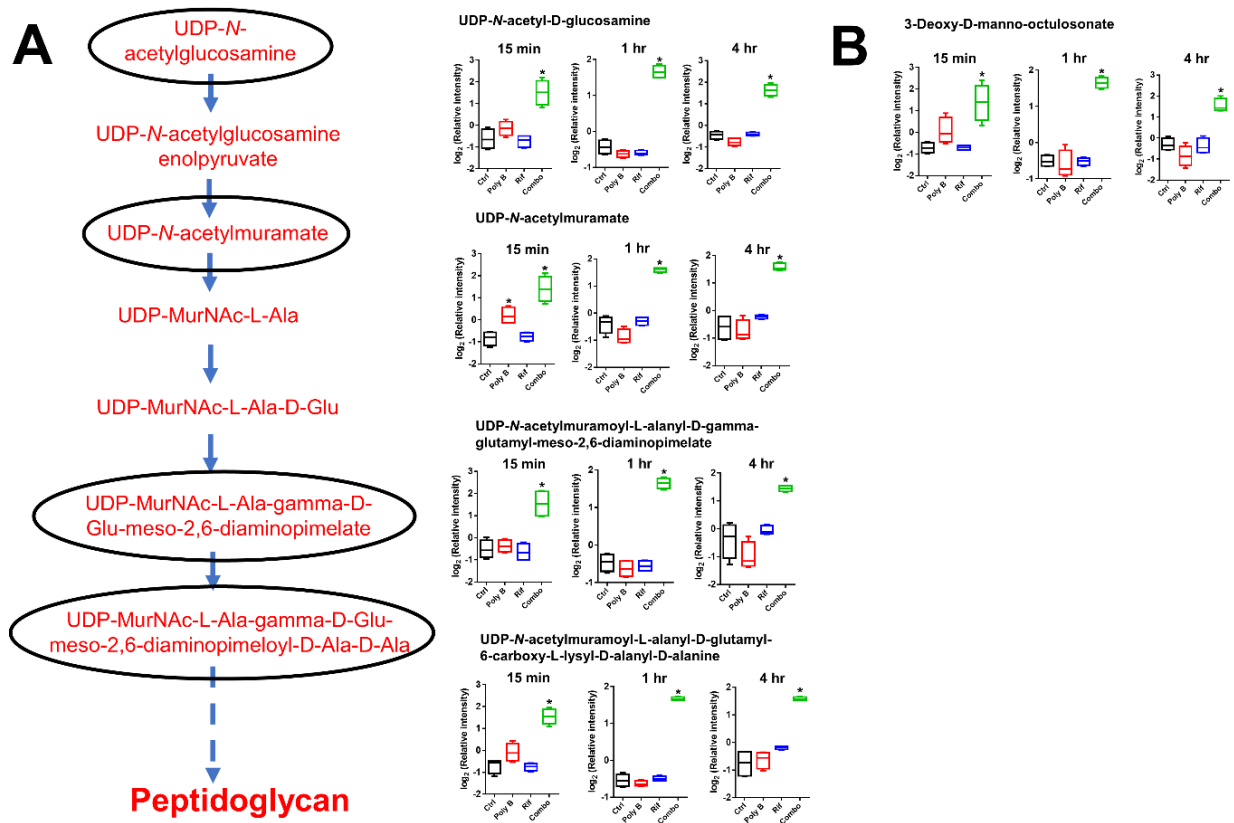


Figure 4.7. Peptidoglycan and LPS biosynthesis changes. The combination of polymyxin B and rifampicin significantly increased the levels of **(A)** four peptidoglycan biosynthesis metabolites and **(B)** a LPS biosynthesis metabolite at 15 min, 1 hr and 4 hr. Polymyxin B and rifampicin monotherapy induced no significant changes on these metabolites at each time point. The black circles indicate the significantly changed metabolite. Box plots indicate upper and lower quartiles (top and bottom of box); median (line within box); and the spread of data that are not outliers (whiskers). * ≥ 1.0 -log₂-fold, $p \leq 0.05$. The figure is modified from the BioCyc.

4.4.3 *Polymyxin B and rifampicin combination caused significant accumulation of nucleotides and perturbation of amino acid metabolites*

The combination of polymyxin B and rifampicin significantly up-regulated ($\geq 1.0\text{-log}_2\text{-fold}$, $p \leq 0.05$) the levels of most identified purine and pyrimidine nucleotides at 15 min, 1 hr and 4 hr (Figure 4.8A). Notable decreases ($\leq 1.0\text{-log}_2\text{-fold}$, $p \leq 0.05$) of a few nucleotides were observed by polymyxin B alone at 15 min, 1 hr and 4 hr whereas no significant changes were detected by rifampicin alone at any time point. At 24 hr, the results showed that there were no significant changes in the relative abundance of nucleotides following exposure to polymyxin B and rifampicin alone and the combination. Furthermore, the combination of polymyxin B and rifampicin also significantly perturbed PAO1 amino acid metabolism predominantly of arginine, proline, glycine, serine, threonine, valine, leucine and isoleucine at 15 min, 1 hr and 4 hr (Figure 4.8B and Tables 4.2-4.4). Notably, few amino acid metabolites were significantly changed by polymyxin B alone particularly at 15 min and 4 hr but no significant changes were induced by rifampicin alone (Figure 4.8B and Tables 4.2 and 4.4).

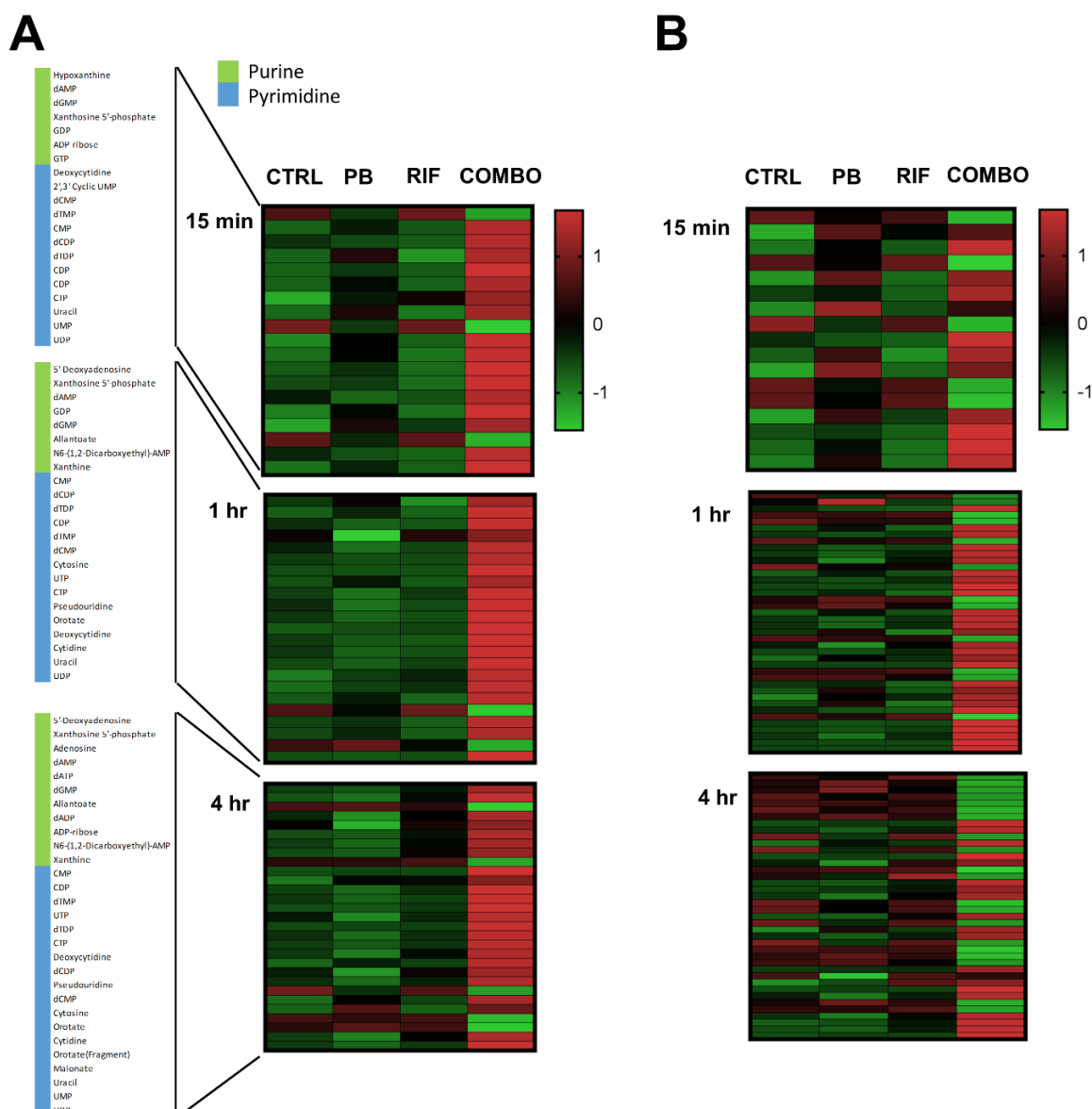


Figure 4.8. Heat map profiles of (A) nucleotide and (B) amino acid changes. The combination of polymyxin B and rifampicin predominantly increased the levels of purine and pyrimidine nucleotides and significantly perturbed the levels of amino acid metabolites at 15 min, 1 hr and 4 hr. Polymyxin B alone significantly induced few nucleotide and amino acid changes whereas rifampicin alone showed no significant effect across 4 hr. Control=CTRL; Polymyxin B=PB; Rifampicin=RIF; Combination=Combo. Metabolites were significantly selected with $\geq 1.0\text{-log}_2\text{-fold}$, $p \leq 0.05$.

4.4.4 *Polymyxin B and rifampicin combination induced significant perturbation in the central carbon metabolism*

The synergistic killing of the combination significantly altered the levels (≥ 1.0 -log₂-fold, $p \leq 0.05$) of several metabolites of central carbon metabolism including glycolysis, tricarboxylic acid (TCA) cycle and pentose phosphate pathway (PPP) at 15 min, 1 hr and 4 hr (Figure 4.9). However, no significant metabolic changes were notified by polymyxin B and rifampicin monotherapy at each time point. The combination of polymyxin B and rifampicin significantly up-regulated and down-regulated the levels of phosphoenolpyruvate and pyruvate, respectively, the metabolites of glycolytic pathway particularly at 1 hr and 4 hr. Several metabolites of TCA cycle pathway that were significantly perturbed by the combination were (*S*)-malate, acetyl-CoA (both were up-regulated) and 2-oxoglutarate (down-regulated). Nevertheless, there were no particular pattern in term of time-dependent changes as (*S*)-malate notably changed at 4 hr, acetyl-CoA at 15 min and 1 hr and 2-oxoglutarate across the 4 hr. Furthermore, three metabolites of PPP, D-sedoheptulose 7-phosphate, D-ribose 5-phosphate and fructose 6-phosphate were steadily increased (≥ 1.0 -log₂-fold, $p \leq 0.05$) by the combination of polymyxin B and rifampicin particularly at 1 hr and 4 hr.

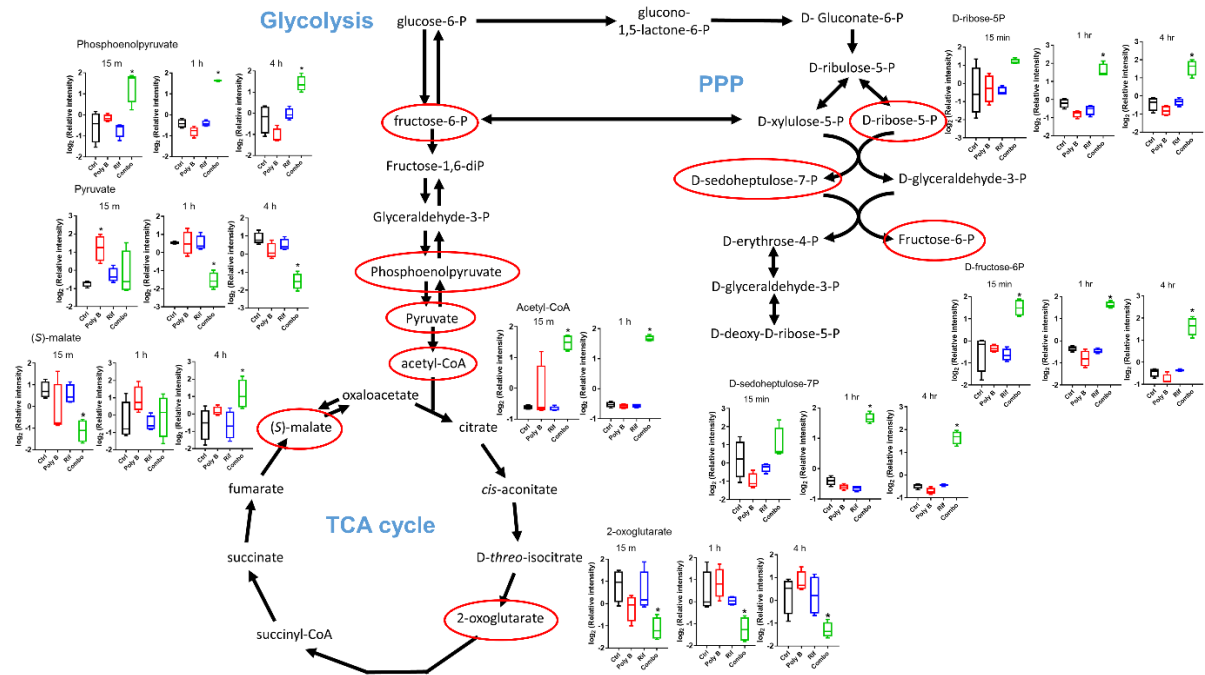


Figure 4.9. Perturbations of TCA cycle, glycolysis and pentose phosphate pathway (PPP).

The combination of polymyxin B and rifampicin significantly perturbed the levels of glycolysis and TCA cycle metabolites of PAO1 at 15 min, 1 hr and 4 hr. The combination also predominantly increased the levels of three PPP metabolites particularly at 1 hr and 4 hr. Polymyxin B and rifampicin alone induced no significant changes at each time point. Red circles indicate the significantly changed metabolites. Box plots indicate upper and lower quartiles (top and bottom of box); median (line within box); and the spread of data that are not outliers (whiskers). * ≥ 1.0 -log₂-fold, $p \leq 0.05$. The figure is modified from the BioCyc.

Table 4.2 Significant metabolites ($p \leq 0.05$) of PAO1 after treatment with polymyxin B (PB) and rifampicin (RIF) alone and in combination (COMBO) at 15 min. Significant fold-changes are highlighted in yellow.

Formula	Map	Pathway	Metabolite	PB	RIF	COMBO	p-value
C ₈ H ₁₄ O ₈	Glycan Biosynthesis & Metabolism	LPS biosynthesis	3-Deoxy-D-manno-octulosonate	0.77	0.01	2.08	0.000407
C ₁₀ H ₁₅ N ₅ O ₁₀ P ₂	Energy	Oxidative phosphorylation	ADP	-0.51	-0.49	1.42	0.003593
C ₆ H ₁₄ O ₁₂ P ₂		Carbon fixation	D-Fructose 1,6-bisphosphate	2.03	0.59	1.88	0.000256
C ₈ H ₁₃ N ₂ O ₅ P	Cofactors & Vitamins	Vitamin B7	Pyridoxamine phosphate	0.29	-0.40	1.82	0.000629
C ₈ H ₁₁ NO ₆		Vitamin B6	2-(Hydroxymethyl)-3-(acetamidomethylene)succinate	-0.93	-0.29	-1.99	0.006781
C ₁₄ H ₁₈ N ₂ O ₄		Riboflavin	α -Ribazole	-1.01	-0.27	-2.10	0.001600
C ₆ H ₈ O ₄		Nicotinate and nicotinamide	2,3-Dimethylmaleate	-0.62	0.69	-1.49	0.002293
C ₁₀ H ₁₈ N ₂ O ₅ S		biotin biosynthesis II	9-mercaptopdethiobiotin	-1.38	-0.26	-1.89	0.004652
C ₁₀ H ₁₆ N ₂ O ₅ S		Biotin	Biotin	-1.22	-0.73	-2.41	9.27E-05
C ₁₀ H ₁₈ N ₂ O ₃			Dethiobiotin	-0.98	-0.29	-2.16	0.000870
C ₂₁ H ₃₆ N ₇ O ₁₆ P ₃ S		TCA cycle	CoA	0.76	-0.10	1.87	0.003567
C ₃ H ₇ O ₅ P		Propanoate	Propanoyl phosphate	-1.46	0.04	-2.14	8.80E-08
C ₃ H ₁₁ O ₇ P		PPP	2-Deoxy-D-ribose 1-P	2.20	0.54	1.59	0.000215
C ₁₅ H ₂₄ N ₂ O ₁₇ P ₂	Carbohydrate	Pentose & glucuronate interconversions	UDP-glucose	-0.24	-0.06	1.90	0.000117
C ₆ H ₁₂ O ₆		Glycolysis / Gluconeogenesis	D-Glucose	-0.91	-0.66	-2.23	0.001888
C ₃ H ₇ O ₆ P			Glycerone phosphate	2.28	0.79	1.70	0.000139
C ₃ H ₇ O ₇ P			3-Phospho-D-glycerate	-0.04	-0.26	1.67	0.005657
C ₆ H ₁₂ O ₅		Fructose & mannose	L-Rhamnofuranose	2.18	1.63	2.00	0.000203
C ₆ H ₁₃ O ₈ P			L-Fucose 1-phosphate	1.91	1.07	2.05	0.001544
C ₈ H ₁₅ NO ₆		Aminosugars	N-Acetyl-D-mannosamine	2.10	0.68	1.76	0.000671
C ₁₅ H ₁₆ O ₁₀		0	Caffeic acid 4-O-glucuronide	-1.10	0.04	-2.26	5.09E-08
C ₁₄ H ₂₆ O ₁₀			Isopropyl apiosylglucoside	1.82	0.52	1.79	0.002914
C ₂₇ H ₃₈ O ₁₈			cis-Ferulic acid [arabinosyl-(1->3)-[glucosyl-(1->6)]-glucosyl] ester	1.74	0.81	2.23	0.000252
C ₁₆ H ₂₆ N ₂ O ₁₅ P ₂	Biosynthesis of Secondary Metabolites	Novobiocin biosynthesis	dTDP-6-deoxy-L-mannose	0.53	-0.03	2.09	0.000194
C ₈ H ₁₄ N ₂ O ₄		Clavulanic acid biosynthesis	Proclavaminic acid	-1.35	-0.62	-2.16	0.001912
C ₁₀ H ₉ NO ₄	Amino Acid	Tryptophan	4-(2-Aminophenyl)-2,4-dioxobutanoate	-0.85	-0.19	-1.91	0.010949
C ₂ H ₅ O ₅ P		Taurine and hypotaurine	Acetyl phosphate	2.04	0.42	1.30	0.003585
C ₈ H ₁₃ NO ₅		Lysine biosynthesis	N2-Acetyl-L-aminoadipate	2.04	0.41	1.95	1.04E-05
C ₆ H ₁₀ N ₂ O ₄		Histidine	N-Formimino-L-glutamate	1.04	-0.33	1.84	0.000260
C ₆ H ₆ N ₂ O ₂			Urocanate	1.67	0.28	2.04	0.000122
C ₄ H ₉ N ₃ O ₂		Glycine, serine and threonine	Creatine	-0.59	0.13	-2.02	0.000350
C ₄ H ₆ O ₃		Glutamate metabolism	Succinate semialdehyde	-0.66	-0.26	-1.96	0.009503
C ₅ H ₈ O ₅		glutamate degradation V	(R)-2-Hydroxyglutarate	-0.27	-0.35	1.77	0.000178
C ₆ H ₁₂ N ₂ O ₄ S ₂		Cysteine	L-Cystine	1.47	0.68	2.21	0.000920
C ₅ H ₉ NO ₄		Arginine and proline	L-Glutamate	-1.35	-0.45	-2.24	0.000237
C ₉ H ₁₆ N ₂ O ₄			gamma-Glutamyl-gamma-aminobutyraldehyde	-0.72	-0.07	-1.99	0.002454
C ₆ H ₁₁ NO ₂			N4-Acetylaminobutanal	0.78	0.20	2.23	0.000114
C ₂ H ₅ O ₅ P		Aminophosphonate	Phosphonoacetate	0.25	-0.22	1.65	0.015136
CH ₃ O ₄ P			Hydroxymethylphosphonate	1.81	1.12	1.78	0.014269

C ₁₈ H ₃₂ O ₃	Undefined	vernolic acid biosynthesis	vernolate	-1.08	-0.15	-1.81	0.013949
C ₁₃ H ₂₄ O ₁₁		galactosylcyclitol biosynthesis	D-galactosylononitol	-1.83	-0.45	-1.49	0.010712
C ₁₂ H ₁₀ N ₂ O		beta-carboline biosynthesis	Harmalol	1.76	-0.10	0.95	0.007413
C ₂₉ H ₄₁ N ₅ O ₉		undefined	Neocasomorphin (1-5)	-1.08	-0.33	-2.20	0.000473
C ₆ H ₁₅ O ₈ P			Glycerophosphoglycerol	-1.39	0.07	-2.15	6.21E-08
C ₃ H ₉ O ₆ P			sn-glycerol-1-P	-1.37	0.07	-2.15	1.59E-07
C ₁₂ H ₁₆ N ₂ O ₃			Carbetamide	-0.84	-0.25	-2.05	0.003297
C ₁₂ H ₁₆ N ₂ O ₄			3-Hydroxyhexobarbital	-1.14	-0.11	-2.00	0.001435
C ₁₈ H ₁₁ NO ₈ S ₂			Quinoline yellow	-1.33	-0.06	-1.76	0.005547
C ₃ H ₇ NO ₂			3,4-Dihydro-2H-Pyrrole-2-carboxylate	1.62	0.26	1.51	0.016637
C ₁₁ H ₁₇ NO ₇			1,6-anhydro-N-acetylmuramate	2.01	0.17	1.58	0.000140
C ₆ H ₁₄ NO ₈ P			glycerophosphoserine	1.78	0.21	1.74	0.000884
C ₁₁ H ₈ N ₂			beta-Carboline	2.01	0.47	1.76	0.000460
C ₁₀ H ₁₅ N ₅ O ₄			formycin A	0.08	-0.27	1.80	0.001451
CH ₃ O ₄ P			methylphosphate	1.92	0.45	1.87	0.000376
C ₅ H ₆ N ₂ O ₂			Imidazol-4-ylacetate	0.32	-0.26	1.89	0.000660
C ₆ H ₁₁ NO ₂			(R)-piperidine-3-carboxylate	0.66	-0.16	1.90	0.001681
C ₁₅ H ₂₄ N ₅ O ₁₇ P ₃			ADPribose 2'-phosphate	0.35	-0.09	1.93	0.001441
C ₈ H ₁₁ N ₃ O ₃			N-Acetyl-L-histidine	1.25	-0.06	2.04	5.90E-05
C ₁₁ H ₁₉ NO ₈			N-Acetylmuramate	2.05	1.21	2.09	0.000433

Table 4.3 Significant metabolites ($p \leq 0.05$) of PAO1 after treatment with polymyxin B (PB) and rifampicin (RIF) alone and in combination (COMBO) at 1 hr. Significant fold-changes are highlighted in yellow.

Formula	Map	Pathway	Metabolite	PB	RIF	COMBO	p-value
C ₈ H ₁₄ O ₈	Glycan Biosynthesis & Metabolism	LPS biosynthesis	3-Deoxy-D-manno-octulosonate	-0.10	-0.01	2.15	1.07E-08
C ₆ H ₁₄ O ₁₂ P ₂	Energy	Carbon fixation	D-Fructose 1,6-bisphosphate	-0.01	0.33	2.23	5.34E-07
C ₁₀ H ₁₆ N ₅ O ₁₃ P ₃		Oxidative phosphorylation	ATP	-0.48	-0.07	1.74	0.000308
C ₁₀ H ₁₅ N ₅ O ₁₀ P ₂			ADP	-0.60	-0.22	1.64	0.000289
C ₈ H ₈ N ₂ O ₃	Cofactors and Vitamins	Nicotinate and nicotinamide	Nicotinurate	0.26	-0.17	-1.92	0.000271
C ₆ H ₅ NO ₃			6-Hydroxynicotinate	-0.15	0.06	2.11	6.74E-07
C ₈ H ₁₃ N ₂ O ₅ P		Vitamin B6	Pyridoxamine phosphate	-1.09	0.09	1.44	2.02E-05
C ₁₅ H ₁₆ O ₁₀	Carbohydrate	0	Caffeic acid 4-O-glucuronide	0.33	-0.10	-2.12	7.67E-12
C ₁₄ H ₂₆ O ₁₀			Isopropyl apiosylglucoside	-0.09	0.24	-1.94	0.000147
C ₂₇ H ₃₈ O ₁₈			cis-Ferulic acid [arabinosyl-(1->3)-[glucosyl-(1->6)]-glucosyl] ester	-0.60	0.62	1.80	4.77E-05
C ₂₁ H ₃₆ N ₇ O ₁₆ P ₃ S		TCA cycle	CoA	0.16	-0.12	2.22	7.06E-11
C ₄ H ₆ O ₄			Succinate	0.07	-0.18	2.06	5.28E-06
C ₃ H ₇ O ₇ P		Glycolysis / Gluconeogenesis	3-Phospho-D-glycerate	0.01	-0.21	2.15	2.83E-13
C ₁₅ H ₂₂ N ₂ O ₁₈ P ₂		Pentose & glucuronate interconversions	UDP-glucuronate	1.39	-0.05	2.23	4.01E-13
C ₁₅ H ₂₄ N ₂ O ₁₇ P ₂			UDP-glucose	-0.10	0.00	2.19	1.80E-12
C ₃ H ₇ O ₅ P		Propanoate	Propanoyl phosphate	0.47	-0.41	-2.04	3.37E-08
C ₆ H ₁₀ O ₅		Pyruvate	(R)-2-Ethylmalate	-0.10	-0.65	-2.10	0.000662
C ₁₂ H ₂₂ O ₁₁	Biosynthesis of Secondary Metabolites	Starch and sucrose	Maltose	0.53	-0.14	1.78	0.007983
C ₁₆ H ₂₆ N ₂ O ₁₅ P ₂		Novobiocin biosynthesis	dTDP-6-deoxy-L-mannose	-0.13	-0.12	2.14	3.17E-12
C ₁₅ H ₂₉ N ₃ O ₅	Amino Acid	0	Marimastat	-0.38	0.03	-2.23	7.71E-07
C ₁₁ H ₁₂ N ₂ O ₂			D-Tryptophan	0.04	-0.45	-1.84	0.007313

C ₁₃ H ₁₄ N ₂ O ₂			(1xi,3xi)-1,2,3,4-Tetrahydro-1-methyl-beta-carboline-3-carboxylic acid	0.11	-0.34	1.92	6.84E-05
C ₆ H ₁₂ N ₂ O			L-Lysine 1,6-lactam	-0.28	0.18	1.92	0.000183
C ₃ H ₇ NO ₂		Alanine and aspartate	L-Alanine	-0.95	0.09	-1.74	0.009925
C ₅ H ₁₁ NO ₂		Amino Fatty Acids	[FA amino(5:0)] 2S-amino-pentanoic acid	-0.58	-0.35	-2.12	0.001927
C ₂ H ₅ O ₅ P		Aminophosphonate	Phosphonoacetate	0.25	-0.25	2.15	1.79E-08
C ₆ H ₁₁ NO ₂		Arginine and proline	N4-Acetylaminobutanal	-0.81	0.08	1.65	3.25E-05
C ₉ H ₁₆ N ₂ O ₅			gamma-Glutamyl-gamma-aminobutyrate	0.91	-0.01	1.74	0.015858
C ₅ H ₁₂ N ₂ O ₂			L-Ornithine	0.52	0.12	2.27	6.52E-06
C ₄ H ₉ NO ₂			4-Aminobutanoate	1.52	-0.41	-0.90	1.05E-05
C ₃ H ₈ O ₅		glutamate degradation V	(R)-2-Hydroxyglutarate	-0.36	0.04	1.96	9.42E-06
C ₅ H ₁₁ NO ₂		Glycine, serine and threonine	Betaine	-0.18	-0.02	1.87	0.000532
C ₃ H ₈ NO ₆ P			O-Phospho-L-serine	0.81	0.47	2.03	0.009689
C ₂ H ₈ NO ₄ P			Ethanolamine phosphate	0.52	0.26	-1.77	2.16E-05
C ₃ H ₇ NO ₃			L-Serine	-0.12	0.00	-2.01	0.000329
C ₆ H ₁₀ N ₂ O ₄		Histidine	N-Formimino-L-glutamate	-0.91	0.19	1.54	0.000103
C ₆ H ₆ N ₂ O ₂			Urocanate	-0.20	0.06	1.77	0.003070
C ₈ H ₁₆ N ₂ O ₃		Lysine biosynthesis	N2-Acetyl-L-lysine	-0.04	-0.03	2.07	8.41E-06
C ₆ H ₁₄ N ₂ O ₂			L-Lysine	0.60	0.12	2.24	2.27E-05
C ₇ H ₁₅ NO ₃			L-Carnitine	0.65	-0.57	1.56	0.003152
C ₅ H ₁₁ NO ₂			5-Aminopentanoate	-0.31	-0.14	1.90	2.70E-05
C ₆ H ₁₃ O ₇ PS		Methionine	S-Methyl-5-thio-D-ribose 1-phosphate	0.86	-0.30	1.95	0.000104
C ₆ H ₁₁ NO ₄			O-Acetyl-L-homoserine	-0.38	0.05	1.86	0.000147
C ₉ H ₈ O ₃		Phenylalanine	Phenylpyruvate	-0.29	-0.36	-1.96	0.006486
C ₉ H ₁₆ N ₂ O ₅ Se		Selenoamino acid	gamma-Glutamyl-Se-methylselenocysteine	-0.33	-0.41	1.92	3.63E-09
C ₂ H ₅ O ₅ P		Taurine and hypotaurine	Acetyl phosphate	-0.05	-0.04	2.19	3.49E-12
C ₁₁ H ₁₂ N ₂ O ₄		Tryptophan	L-Formylkynurenine	1.01	0.72	2.35	0.000375
C ₁₁ H ₁₂ N ₂ O ₂			L-Tryptophan	0.01	0.15	-1.77	0.003293
C ₉ H ₁₁ NO ₃		Tyrosine	L-Tyrosine	-0.06	0.23	2.01	0.000326
C ₆ H ₁₀ O ₄		Valine, leucine & isoleucine biosynthesis	(S)-2-Aceto-2-hydroxybutanoate	0.39	-0.30	-1.77	0.001388
C ₄ H ₈ O ₃		Valine, leucine & isoleucine degradation	(S)-3-Hydroxyisobutyrate	-0.32	-0.42	1.88	3.51E-07
C ₂₆ H ₄₄ N ₇ O ₁₈ P ₃ S			(2S,3S)-3-Hydroxy-2-methylbutanoyl-CoA	-0.04	-0.04	2.20	1.35E-13
C ₂₆ H ₄₄ N ₇ O ₁₇ P ₃ S			3-Methylbutanoyl-CoA	-0.04	-0.03	2.20	1.02E-13
C ₆ H ₁₀ O ₃			(S)-3-Methyl-2-oxopentanoic acid	-0.91	-0.82	-2.08	0.011798
C ₃ H ₈ O ₃			3-Methyl-2-oxobutanoic acid	-0.56	-0.55	-2.25	0.000530
C ₅ H ₁₁ NO ₂			L-Valine	0.46	-0.15	2.07	7.36E-05
C ₁₂ H ₁₈ O ₂	undefined	undefined	4-Hexyloxyphenol	-0.41	-0.01	-2.25	7.82E-07
C ₁₁ H ₁₆ O ₂			3-tert-Butyl-5-methylcatechol	-0.36	0.02	-2.23	6.28E-07
C ₁₃ H ₂₀ O ₂			4-Heptyloxyphenol	-0.41	0.06	-2.21	1.28E-06
C ₁₈ H ₁₁ NO ₈ S ₂			Quinoline yellow	0.21	-0.24	-2.20	9.40E-12
C ₇ H ₁₀			1-Methyl-1,3-cyclohexadiene	-0.50	0.05	-2.19	7.25E-06
C ₈ H ₁₉ N			Octylamine	-0.48	-0.39	-2.18	0.000582
C ₁₂ H ₁₆ O			Rhubafuran	-0.44	0.10	-2.17	5.15E-06
C ₆ H ₁₅ O ₈ P			Glycerophosphoglycerol	0.31	-0.34	-2.13	1.42E-08
C ₃ H ₉ O ₆ P			sn-glycerol-1-phosphate	0.33	-0.31	-2.11	3.53E-08
C ₈ H ₁₆ O ₃			Ethyl (R)-3-hydroxyhexanoate	-0.06	0.24	-2.03	6.81E-06
C ₆ H ₇ NO ₂			N-Ethylmaleimide	-0.92	-0.39	-1.88	0.024893
C ₉ H ₁₂			Cumene	-0.73	0.07	-1.86	0.004976
C ₂₁ H ₂₇ O ₅			19-oi-c-deoxycorticosterone	-0.11	-0.78	-1.83	0.015015
C ₃₁ H ₅₃ N ₁₁ O ₅			Argiotoxin 659	0.22	0.02	-1.79	0.001652
C ₁₂ H ₁₆ N ₂ O ₃			Carbetamide	0.23	-0.17	-1.78	0.003027
C ₁₆ H ₂₇ NO ₄			N-(3-Oxododecanoyl)homoserine lactone	-0.94	-0.03	-1.69	0.026048
C ₁₁ H ₁₂ N ₂ O ₄			N-Formyl-D-kynurenine	0.87	-0.53	-1.66	3.33E-06
C ₉ H ₁₉ O ₁₁ P			sn-glycero-3-Phospho-1-inositol	-0.01	-0.13	-1.66	0.02679
C ₃ H ₇ O ₅ P			Hydroxyacetone phosphate	-1.41	0.07	-1.59	0.005803
C ₁₂ H ₂₀ O			(Z,Z,Z)-3,6,9-Dodecatrien-1-ol	-1.58	0.05	-1.52	0.003495
C ₁₀ H ₁₃ NO ₃			Damascenine	-2.00	-0.11	-0.96	0.002310

C ₁₀ H ₂₈ C ₁₂ N ₂ OP ₂			Polixetonium chloride	-0.33	-0.34	1.50	0.008092
C ₁₀ H ₁₄ N ₄ O ₃			quinonoid dihydro-(6H)- biopterin	0.10	-0.73	1.63	0.000255
C ₁₁ H ₁₆ N ₄ O ₂			CPX	0.75	-0.18	1.68	0.014547
C ₇ H ₁₃ O ₉ P			α-(2,6-anhydro-3- deoxy-D-arabino- heptulopyranosid)onate 7- phosphate	-0.45	-0.28	1.90	5.65E-08
C ₅ H ₁₁ NO ₃			3-nitro-2-pentanol	0.30	-0.01	1.91	0.002885
C ₁₀ H ₁₅ N ₃ O ₅			5-Methylcytidine	-0.07	-0.04	1.91	0.000487
C ₈ H ₁₅ NO ₇			N-Acetyl-D-glucosamine	-0.06	-0.08	1.93	0.000289
C ₁₉ H ₃₀ N ₂ O ₁₂			glcNAc-1,6-anhMurNAc	0.20	0.33	1.95	0.004973
C ₁₁ H ₁₅ N ₅ O ₃			N6-Methyl-2'-deoxyadenosine	0.32	-0.20	2.07	2.19E-05
C ₆ H ₁₁ NO ₂			(R)-piperidine-3-carboxylate	-0.06	-0.12	2.13	5.80E-09
C ₁₄ H ₁₈ N ₂ O ₄			L-phenylalanyl-L- hydroxyproline	0.25	0.19	2.16	8.26E-05
C ₁₀ H ₁₅ N ₅ O ₄			formycin A	0.00	-0.04	2.17	1.37E-08
C ₇ H ₁₄ N ₂ O ₃			N5-Ethyl-L-glutamine	0.11	0.20	2.18	1.23E-05
C ₈ H ₁₂ O ₇			dihomocitrate	-0.04	-0.03	2.21	6.74E-14
C ₁₅ H ₂₄ N ₅ O ₁₇ P ₃			ADPribose 2'-phosphate	-0.03	-0.03	2.21	1.61E-14
C ₁₀ H ₁₃ N ₄ O ₈ P			Inosine2'-phosphate	0.00	0.30	2.22	1.30E-06
C ₅ H ₆ N ₂ O ₂			Imidazol-4-ylacetate	0.12	-0.08	2.23	8.71E-12
C ₁₆ H ₃₀ O ₄		cutin biosynthesis	hexadecanedioate	-0.53	-0.10	-2.27	4.40E-06
C ₁₄ H ₁₄ N ₂ O ₆		IAA degradation II	2-oxindole-3-acetyl-asp	-0.96	0.14	-1.75	0.006742
C ₁₈ H ₃₂ O ₃		vernolic acid biosynthesis	vernolate	-0.47	-0.16	-2.33	2.70E-07

Table 4.4 Significant metabolites ($p \leq 0.05$) of PAO1 after treatment with polymyxin B (PB) and rifampicin (RIF) alone and in combination (COMBO) at 4 hr. Significant fold-changes are highlighted in yellow.

Formula	Map	Pathway	Metabolite	PB	RIF	COMBO	p-value
C ₁₄ H ₁₈ N ₂ O ₄	Cofactors & Vitamins	Riboflavin	alpha-Ribazole	1.86	0.49	1.16	0.02681
C ₁₂ H ₁₀ N ₄ O ₂			Lumichrome	-0.08	-0.05	-2.07	9.29E-05
C ₂₇ H ₃₃ N ₉ O ₁₅ P ₂			FAD	-0.16	0.04	-2.02	0.000241
C ₈ H ₈ N ₂ O ₃		Nicotinate and nicotinamide	Nicotinurate	0.31	0.15	-1.72	0.001279
C ₆ H ₅ NO ₃			6-Hydroxynicotinate	-1.53	-0.47	-1.69	0.022608
C ₈ H ₁₄ O ₈	Glycan Biosynthesis & Metabolism	LPS biosynthesis	3-Deoxy-D-manno- octulosonate	-0.54	-0.07	1.85	5.25E-06
C ₂₁ H ₂₈ N ₇ O ₁₇ P ₃	Energy	Photosynthesis	NADP+	0.26	0.19	-2.01	1.44E-07
C ₁₀ H ₁₅ N ₅ O ₁₀ P ₂		Oxidative phosphorylation	ADP	-0.39	0.36	1.75	0.002137
C ₁₀ H ₁₆ N ₅ O ₁₃ P ₃			ATP	-0.41	0.59	1.82	0.000581
C ₆ H ₁₄ O ₁₂ P ₂		Carbon fixation	D-Fructose 1,6- bisphosphate	-0.40	0.03	2.02	6.79E-08
C ₁₂ H ₂₂ O ₁₁	Carbohydrate	Starch & sucrose	Maltose	0.32	0.07	1.80	0.013614
C ₆ H ₁₀ O ₅		Pyruvate	(R)-2-Ethylmalate	0.57	-0.28	-1.51	0.007338
C ₆ H ₁₀ O ₇		PPP	2-Dehydro-D-gluconate	-0.13	-0.02	-1.91	0.001998
C ₁₅ H ₂₄ N ₂ O ₁₇ P ₂		Pentose & glucuronate interconversions	UDP-glucose	-0.21	0.19	2.19	6.40E-11
C ₅ H ₁₀ O ₅			L-Arabinose	1.91	0.27	0.13	0.005576
C ₅ H ₁₀ O ₆			D-Xylate	-0.39	-0.19	-2.22	4.55E-05
C ₃ H ₇ O ₆ P		Glycolysis / Gluconeogenesis	Glycerone phosphate	-0.98	0.40	1.31	0.001131
C ₃ H ₇ O ₇ P			3-Phospho-D-glycerate	-0.81	0.06	1.57	0.000237
C ₂₁ H ₃₆ N ₇ O ₁₆ P ₃ S		TCA cycle	CoA	1.06	0.93	2.37	0.000450
C ₈ H ₁₅ NO ₆		Aminosugars	N-Acetyl-D-mannosamine	-1.31	-0.46	-2.32	5.03E-05
C ₁₅ H ₁₆ O ₁₀		0	Caffeic acid 4-O- glucuronide	0.29	0.27	-1.83	6.16E-05

C ₂₇ H ₃₈ O ₁₈			cis-Ferulic acid [arabiosyl-(1->3)-[glucosyl-(1->6)]-glucosyl] ester	-1.67	-0.03	0.70	0.000149
C ₄ H ₉ O ₇ P			Erythrulose 1-phosphate	-0.93	-0.11	1.55	2.22E-05
C ₁₆ H ₂₆ N ₂ O ₁₅ P ₂	Biosynthesis of Secondary Metabolites	Novobiocin biosynthesis	dTDP-6-deoxy-L-mannose	-0.48	0.34	1.97	1.56E-06
C ₈ H ₁₄ N ₂ O ₄		Clavulanic acid biosynthesis	Proclavaminic acid	1.97	0.32	1.42	0.002509
C ₅ H ₈ O ₃	Amino Acid	Valine, leucine and isoleucine degradation	3-Methyl-2-oxobutanoic acid	-0.66	-0.34	-2.22	0.000366
C ₂₆ H ₄₄ N ₇ O ₁₈ P ₃ S			(2S,3S)-3-Hydroxy-2-methylbutanoyl-CoA	0.10	0.05	2.28	1.08E-12
C ₅ H ₈ O ₄		Valine, leucine and isoleucine biosynthesis	(S)-2-Acetolactate	-1.32	-0.08	-2.08	0.000135
C ₆ H ₁₀ O ₄			(S)-2-Aceto-2-hydroxybutanoate	-0.59	0.94	-1.50	3.94E-05
C ₁₁ H ₁₂ N ₂ O ₂		Tryptophan	L-Tryptophan	-0.13	-0.11	-2.18	5.95E-06
C ₁₀ H ₉ NO ₄			4-(2-Aminophenyl)-2,4-dioxobutanoate	0.13	-0.43	-1.69	0.01778
C ₂ H ₅ O ₅ P		Taurine and hypotaurine	Acetyl phosphate	0.09	0.05	2.26	4.10E-11
C ₉ H ₁₆ N ₂ O ₅ Se		Selenoamino acid	gamma-Glutamyl-Se-methylselenocysteine	-0.73	-0.01	1.68	5.96E-05
C ₉ H ₈ O ₃		Phenylalanine	Phenylpyruvate	-0.84	-0.34	-2.38	6.00E-06
C ₆ H ₁₁ NO ₄		Methionine	O-Acetyl-L-homoserine	-0.52	0.48	1.75	0.000508
C ₅ H ₁₁ NO ₃ S			L-Methionine S-oxide	-0.84	-0.29	-2.18	0.000709
C ₁₄ H ₂₀ N ₆ O ₅ S			S-Adenosyl-L-homocysteine	-0.07	0.27	-1.67	0.007563
C ₅ H ₁₁ NO ₂		Lysine degradation	5-Aminopentanoate	0.16	0.13	2.17	1.43E-05
C ₆ H ₁₄ N ₂ O ₂			L-Lysine	-0.12	0.34	2.05	0.000118
C ₈ H ₁₃ NO ₅			N2-Acetyl-L-aminoadipate	-1.44	-0.30	-2.24	2.07E-05
C ₈ H ₁₆ N ₂ O ₃			N2-Acetyl-L-lysine	-0.37	0.15	1.64	0.006819
C ₆ H ₆ N ₂ O ₂		Histidine	Urocanate	-1.32	-0.50	-2.15	0.001406
C ₃ H ₇ NO ₃		Glycine, serine and threonine	L-Serine	0.77	-0.26	-1.48	0.002050
C ₂ H ₈ NO ₄ P			Ethanolamine phosphate	0.18	0.21	-2.03	1.55E-07
C ₃ H ₈ NO ₆ P			O-Phospho-L-serine	1.36	0.61	2.38	4.03E-05
C ₄ H ₆ O ₃		Glutamate	Succinate semialdehyde	0.65	-0.08	-1.58	0.001504
C ₅ H ₇ NO ₂			(S)-1-Pyrroline-5-carboxylate	-0.76	-0.20	-1.90	0.01267
C ₅ H ₈ O ₅		glutamate degradation V	(R)-2-Hydroxyglutarate	0.14	0.37	1.78	0.022091
C ₅ H ₁₂ N ₂ O ₂		Arginine and proline	L-Ornithine	0.72	0.45	2.34	5.25E-05
C ₆ H ₁₃ N ₃ O ₃			L-Citrulline	-1.21	-0.22	-2.07	0.001026
C ₄ H ₇ N ₃ O			Creatinine	-0.12	-0.30	-1.82	0.014178
C ₉ H ₁₃ NO ₇			N-Succinyl-L-glutamate	-2.12	0.03	-0.25	2.61E-05
C ₆ H ₁₁ NO ₂			N4-Acetylaminobutanal	-0.33	0.20	1.91	0.000163
C ₇ H ₁₄ N ₂ O ₃			N-Acetylornithine	-0.07	0.74	1.95	0.001648
C ₁₀ H ₁₈ N ₄ O ₅			N2-Succinyl-L-arginine	0.54	1.81	2.23	9.98E-06
C ₂ H ₅ O ₅ P		Aminophosphonate	Phosphonoacetate	-0.90	0.59	1.30	0.002012
C ₃ H ₁₁ NO ₂		Amino Fatty Acids	[FA amino(5:0)] 2S-amino-pentanoic acid	0.39	-0.04	-1.72	0.001519
C ₃ H ₇ NO ₂		Alanine and aspartate	L-Alanine	-0.51	0.46	-1.70	0.002230
C ₁₁ H ₁₂ N ₂ O ₂		Undefined	D-Tryptophan	0.41	0.02	-1.88	3.98E-05
C ₁₅ H ₂₉ N ₃ O ₅			Marimastat	0.63	0.14	-1.58	0.000932
C ₁₃ H ₁₄ N ₂ O ₂			(1xi,3xi)-1,2,3,4-Tetrahydro-1-methyl-beta-carboline-3-carboxylic acid	0.09	0.14	1.77	0.01317
C ₆ H ₆ N ₂ O	Undefined	Glycerophosphoinositols	Picolinamide	-0.03	0.21	-1.62	0.014068
C ₁₆ H ₂₅ N ₅ O ₁₄ P ₂		GDP-L-colitose biosynthesis	GDP-3,6-dideoxy-D-galactose	-0.17	0.02	-2.28	1.84E-15
C ₁₃ H ₂₄ O ₁₁		galactosylcyclitol biosynthesis	D-galactosylononitol	1.17	0.79	2.11	0.007762
C ₁₆ H ₃₀ O ₄		cutin biosynthesis	hexadecanedioate	-0.91	-0.38	-2.26	0.000291
C ₁₀ H ₉ NO		3-methylquinoline degradation	3-Methyl-quinolin-2-ol	0.08	-0.42	-2.06	0.000209
C ₈ H ₁₆ O ₃		Undefined	Ethyl (R)-3-hydroxyhexanoate	-0.81	-0.40	-2.30	0.000149
C ₁₁ H ₁₉ NO ₈			N-Acetylmuramate	-1.20	-0.34	-2.29	4.86E-05
C ₁₁ H ₁₇ NO ₇			1,6-anhydro-N-acetylmuramate	-1.37	-0.36	-2.28	3.29E-05
C ₁₆ H ₂₁ NO			Isobutylphenyldienamide	-0.10	-0.43	-2.26	3.36E-06
C ₁₇ H ₂₁ NO			Diphenhydramine	-0.08	-0.21	-2.25	2.01E-07
C ₂₂ H ₄₂ O ₅			1,2-dioctanoyl-1,2,6-hexanetriol	0.11	-0.22	-2.25	1.21E-14
C ₉ H ₁₉ NO ₇			Choline bitartrate	-0.36	-0.08	-2.23	5.96E-06
C ₁₆ H ₁₉ NO			Dehydroisochalciporone	-0.26	-0.98	-2.22	0.000203

C ₆ H ₁₄ NO ₈ P		glycerophosphoserine	-1.26	-0.21	-2.19	9.15E-05
C ₄ H ₄ O ₃		Succinic anhydride	-1.03	-0.11	-2.15	0.000171
C ₂₂ H ₄₀ O ₃		auricolate	0.06	0.16	-2.14	2.38E-11
C ₅ H ₇ NO ₂		3,4-Dihydro-2H-Pyrrole-2-carboxylate	-0.77	-0.22	-2.09	0.001571
C ₆ H ₇ NO ₂		N-Ethylmaleimide	-0.40	-0.41	-2.09	0.002174
C ₁₉ H ₂₅ NO		N-Dealkylated tolterodine	-0.15	-0.60	-2.08	0.001115
C ₁₂ H ₂₀ O		(Z,Z,Z)-3,6,9-Dodecatrien-1-ol	0.27	-0.37	-2.07	5.23E-06
C ₁₇ H ₂₁ NO ₃		Feruperine	-0.31	-0.35	-2.05	0.002073
C ₁₄ H ₁₁ N ₃ O ₂		aeruginosin A	0.54	-0.11	-2.00	3.14E-12
C ₁₅ H ₁₀ O ₅		phenoxy radical VII	0.54	-0.35	-1.93	2.25E-06
C ₇ H ₁₄ N ₂ O ₃		N5-Ethyl-L-glutamine	-1.27	0.00	-1.81	0.003110
C ₈ H ₆ N ₂ O ₂		Quindoxin	-0.02	0.26	-1.78	0.001754
C ₂₁ H ₂₉ NO ₂		17-Methylandrosta-2,4-dieno[2,3-d]isoxazol-17beta-ol	0.46	-0.22	-1.77	0.000675
C ₇ H ₁₀		1-Methyl-1,3-cyclohexadiene	-0.36	0.33	-1.77	0.002514
C ₁₅ H ₂₃ N ₅ O ₁₃ P ₂		NAD stem group	0.04	0.47	-1.76	0.000319
C ₁₆ H ₁₉ NO		N-Desmethyldiphenhydramine	-0.04	-0.23	-1.75	0.01671
C ₆ H ₉ NO ₃		Trimethadione	-0.97	0.05	-1.70	0.01602
C ₁₂ H ₁₆ O		Rhubafuran	0.16	0.67	-1.68	5.79E-05
C ₁₂ H ₁₈ O ₂		4-Hexyloxyphenol	-0.59	0.46	-1.66	0.003125
C ₁₈ H ₃₀ O ₅ S		2-Dodecylbenzenesulfonic acid	0.38	-0.06	-1.62	0.006936
C ₁₃ H ₂₀ O ₂		4-Heptyloxyphenol	-0.55	0.54	-1.55	0.005321
C ₁₁ H ₁₆ O ₂		3-tert-Butyl-5-methylcatechol	-0.40	0.78	-1.49	0.001468
C ₈ H ₁₉ N		Octylamine	0.74	0.29	-1.47	0.000917
C ₁₅ H ₂₁ N ₅ O ₁₃ P ₂		Cyclic ADP-ribose	0.79	0.63	-1.33	0.000815
C ₁₄ H ₁₈ NO ₁₀ S ₂		Sinalbin	1.75	0.53	-0.07	0.015673
C ₁₂ H ₁₆ N ₂ O ₃		Carbetamide	1.69	-0.11	0.64	0.020069
C ₁₉ H ₃₀ N ₂ O ₁₂		glcNAc-1,6-anhMurNAc	-1.42	-0.09	0.93	0.000609
C ₁₄ H ₁₈ N ₂ O ₄		L-phenylalanyl-L-hydroxyproline	-0.59	-0.38	1.56	0.000560
C ₇ H ₁₃ O ₉ P		α-(2,6-anhydro-3-deoxy-D-arabino-heptulopyranosid)onate 7-phosphate	-0.79	0.28	1.78	5.94E-07
C ₁₁ H ₁₅ N ₅ O ₃		N6-Methyl-2'-deoxyadenosine	0.25	-0.24	1.86	0.001222
C ₆ H ₁₁ NO ₂		(R)-piperidine-3-carboxylate	-0.48	-0.14	1.86	5.21E-06
C ₁₀ H ₁₆ N ₂ O ₄ S		d-biotin d-sulfoxide	0.95	0.47	1.93	0.019882
C ₈ H ₁₁ N ₃ O ₃		N-Acetyl-L-histidine	-0.20	0.11	1.96	0.000145
C ₃ H ₉ O ₆ P		sn-glycerol-1-phosphate	1.26	1.10	1.99	0.021653
C ₁₁ H ₁₉ N ₃ O ₆		Ophthalmicacid	-0.18	0.06	2.07	2.65E-06
C ₁₀ H ₁₃ N ₄ O ₈ P		Inosine2'-phosphate	-0.26	0.11	2.08	5.54E-07
C ₉ H ₁₄ N ₂ O ₅		(1R,2S,3R)-2-Acetyl-4(5)-(1,2,3,4-tetrahydroxybutyl)imidazole	0.98	0.55	2.13	0.004399
C ₆ H ₁₅ O ₈ P		Glycerophosphoglycerol	1.10	1.03	2.14	0.008293
C ₅ H ₆ N ₂ O ₂		Imidazol-4-ylacetate	-0.07	0.14	2.21	6.27E-09
C ₁₀ H ₁₅ N ₃ O ₅		5-Methylcytidine	0.69	0.67	2.22	0.001601
C ₈ H ₁₂ O ₇		dihomocitrate	0.10	0.05	2.25	1.37E-09
C ₈ H ₁₅ NO ₇		N-Acetyl-D-glucosamine	0.10	0.05	2.27	6.41E-11
C ₁₀ H ₁₄ N ₄ O ₃		quinonoid dihydro-(6H)-biopterin	0.78	0.67	2.33	0.000327
C ₁₀ H ₂₈ C ₁₂ N ₂ OP ₂		Polixetonium chloride	1.07	0.57	2.45	8.30E-06

Table 4.5 Significant metabolites ($p \leq 0.05$) of PAO1 after treatment with polymyxin B (PB) and rifampicin (RIF) alone and in combination (COMBO) at 24 hr. Significant fold-changes are highlighted in yellow.

FORMULA	MAP	PATHWAY	METABOLITE	PB	RIF	COMBO	p-value
C ₂₁ H ₃₆ N ₇ O ₁₆ P ₃ S	Carbohydrate	TCA cycle	CoA	0.10	1.92	1.72	0.000050
C ₅ H ₁₀ O ₆		D-arabinose degradation III	D-Arabinonate	-1.63	0.40	0.34	0.001078
C ₅ H ₁₁ NO ₃	undefined	undefined	3-nitro-2-pentanol	1.04	1.39	2.32	0.000944
C ₁₂ H ₂₀ O			(Z,Z,Z)-3,6,9-Dodecatrien-1-ol	-0.30	-1.85	-1.97	0.000046
C ₁₃ H ₂₀ O ₂			4-Heptyloxyphenol	0.38	1.80	2.16	4.46E-06
C ₁₃ H ₁₀ N ₂ O			2-Aminoacridone	1.46	-0.85	-0.62	0.000021
C ₁₄ H ₁₁ N ₃ O ₂			aeruginosin A	2.19	0.89	0.11	0.000124
C ₂₂ H ₄₂ O ₅			1,2-dioctanoyl-1,2,6-hexanetriol	-0.19	-1.86	-1.68	0.000513
C ₁₅ H ₂₄ N ₅ O ₁₇ P ₃			ADPribose 2'-phosphate	0.27	0.03	1.98	0.001260
C ₁₈ H ₃₂ O ₃		vernolic acid biosynthesis	vernolate	-0.65	0.41	1.73	0.000121

4.5 Discussion

Changes in bacterial genome and metabolome are predominantly influenced by the environmental conditions or external stimulus such as temperature, pH and also by the effects of drugs. The significant changes are generally manifestation of their cellular physiological and phenotypic responses and adaptations. Remarkably, bacteria can undergo various cellular biochemical modifications in response to antibiotic to develop resistance. A detailed understanding of the mechanism of drug action potentially can limit the emergence of antibiotic resistance bacterial population. In particular, metabolomics, a hypothesis-generating method has been successfully employed to systematically predict and determine the mechanism of action of new drugs based on global cellular metabolic changes (304-307, 421, 426). In this PhD project, untargeted metabolomics was performed to investigate the mechanism of synergistic killing of the combination of polymyxin B and rifampicin against *P. aeruginosa* PAO1 at four different time points, 15 min, 1 hr, 4 hr and 24 hr.

Close clustered and overlapped between groups of polymyxin B alone and the combination of polymyxin B and rifampicin were notified in the PCA plot at 15 min. Polymyxin B alone commonly induced 37 metabolites that were also significantly changed by the combination (Figure 4.3A). Together, these results suggesting that the early metabolic changes at 15 min of the combination of polymyxin B and rifampicin were predominantly driven by polymyxin B. However, polymyxin B alone indistinguishably clustered together with the control untreated group at 1 hr and 4 hr as shown in the PCA plots (Figures 4.3B and C). This was due to the sub-inhibitory concentration of polymyxin B (1 mg/L) against the high inoculum size of PAO1 culture ($\sim 10^8$ CFU/mL) which induced no bacterial killing and less number of significantly changed metabolites particularly at 1 and 4 hr (Figures 4.1, 4.3B and C). Similarly, rifampicin alone also induced no significant changes to the PAO1 metabolome as the concentration of

rifampicin (2 mg/L) used was remarkably lower than its MICs (32 mg/L) (Figures 4.1 and 4.3). On the contrary, the combination synergistically induced significant perturbations of major metabolic pathways of PAO1 including lipids, peptidoglycan and LPS biosynthesis, nucleotides, amino acids and central carbon metabolism (i.e. glycolysis, PPP, TCA cycle) across 4 hr.

Polymyxin-induced cell death is predominantly mediated by the interaction of polymyxins with the lipid A domain of LPS and outer membrane lipids to cause membrane disruption and osmotic imbalance (reviewed in Section 1.3.3) (98, 375). Significant perturbation of PAO1 membrane lipids mainly of FAs and GPs by polymyxin B alone and the combination at 15 min, 1 hr and 4 hr thus reflecting the general mode of action of polymyxin B in inducing membrane disturbance (Figure 4.6) (11, 87). Similar changes in the levels of FAs and GPs were previously notified in *A. baumannii* (i.e. polymyxin-susceptible ATCC 19606 and 03-149.1, and polymyxin-resistant 03-149.2) following treatment with colistin and doripenem, alone and in combination (Section 3.4.2). Unsurprisingly, the present metabolomics results further support that polymyxins (both colistin and polymyxin B) elicit their general action by the disruption of cell envelope structures of Gram-negative bacteria. Furthermore, the results demonstrated that the combined polymyxin B and rifampicin significantly induced up-regulation of amino sugar metabolites of peptidoglycan and LPS biosynthesis (i.e. UDP-GlcNAc, UDP-MurNAc, UDP-MurNAc-L-Ala-gamma-D-Glu-meso-2,6-diaminopimelate and UDP-MurNAc-L-Ala-gamma-D-Glu-meso-2,6-diaminopimeloyl-D-Ala-D-Ala, KDO) at 15 min, 1 hr and 4 hr (Figure 4.7). On the contrary, in the previous study, the effects of colistin and doripenem monotherapy and the combination has been shown predominantly down-regulated the levels of several metabolites of peptidoglycan and LPS biosynthesis in *A. baumannii* (Section 3.4.5). In addition to polymyxin primary effect to cause membrane disruption, the results also consistently suggest that polymyxins have

significantly secondary effects on peptidoglycan and LPS biosynthesis metabolism in Gram-negative bacteria.

The synergistic killing of the combination of polymyxin B and rifampicin predominantly increased the levels of a large number of purine and pyrimidine nucleotides and perturbed many of amino acid metabolites of PAO1 (Figure 4.8A and B). Notably, the levels of few nucleotides and amino acids were significantly decreased by polymyxin B alone but no significant changes were observed in response to rifampicin alone. Interestingly, the results showed that uracil, a pyrimidine nucleotide was steadily decreased by the combination of polymyxin B and rifampicin at 15 min, 1 hr and 4 hr. Uracil is an important nucleotide in cellular metabolism and it has been used as an anticancer drug (as an antimetabolite, 5-fluorouracil) which mechanistically acts during the nucleic acid replication process (427, 428). The consistent down-regulation of uracil suggesting that the metabolite likely has been utilised to protect the bacterial cells from the toxic effect conferred by the polymyxin B and rifampicin combination. Nucleotides are highly essential in many cellular biological processes, in particular for DNA and RNA biosynthesis, and also as intermediate products in lipid and protein biosynthesis (378). Several studies have shown that purine and pyrimidine nucleotides levels were significantly altered in bacteria induced in response to antibiotic stress (113, 421, 429). In addition, the result of the previous metabolomics study also demonstrated that treatment with colistin and doripenem alone and the combination significantly decreased the levels of many nucleotides in *A. baumannii* (Section 3.4.4). Ampicillin, kanamycin and norfloxacin treatments have been shown to significantly induce depletion of nucleotides levels in *Escherichia coli*, suggesting the acceleration of nucleotide turnover rate likely due to the elevated levels of DNA damage (113). On the contrary, treatment of ciprofloxacin (421) and rifampicin (429) have been shown to significantly increase the levels of nucleotides in *Staphylococcus aureus*. The increase of nucleotides levels by

rifampicin treatment suggested that the bacteria was under a secondary metabolic arrest in cell turnover and DNA replication (263, 429). The results of the combination of polymyxin B and rifampicin treatment that significantly accumulated a large number of nucleotides and many other metabolites (e.g. amino acid, carbohydrate metabolites) also suggesting an inactivation of PAO1 cellular metabolism (263, 429). Consistently, the results likely reflecting the mechanism of action of rifampicin elicited via strong and specific binding to the bacterial DNA-dependent RNA polymerase to inhibit the transcription elongation process of RNA synthesis (263, 429).

Previous studies have demonstrated that antibiotic-induced cell death predominantly was associated with a significant increase of cellular respiration and central metabolism via the carbon flux changes of TCA cycle (110, 429-436). Consistently, the synergistic killing of the combined polymyxin B and rifampicin treatment significantly perturbed PAO1 metabolic pathways of central carbon metabolism including glycolysis, TCA cycle and PPP (Figure 4.9). The significant changes in the metabolite levels of central metabolism highly suggest that PAO1 dynamically experienced cellular energy changes. The significant increases of two metabolites of PPP, D-sedoheptulose 7-phosphate and D-ribose 5-phosphate by the combination of polymyxin B and rifampicin predominantly induced the changes notified in peptidoglycan and LPS biosynthesis metabolites and nucleotides, respectively. D-sedoheptulose 7-phosphate is an important precursor for cell envelope biosynthesis while D-ribose 5-phosphate is a precursor metabolite for nucleotide biosynthesis. The previous results also demonstrated that TCA cycle and PPP were significantly perturbed following treatment with colistin and doripenem alone and the combination (Sections 3.4.3 and 3.4.4). Importantly, these results highlight that the central metabolic pathways particularly of glycolysis, TCA cycle and PPP are common cellular metabolic targets of antibiotic-induced killing in bacteria.

Polymyxin B and rifampicin display their bactericidal action against Gram-negative pathogens with distinguished modes of action owing to the different cellular targets (98, 263). The metabolic changes induced by the synergistic combination of polymyxin B and rifampicin suggesting that the effect was predominantly conferred by rifampicin that was initially facilitated by polymyxin B. Interestingly, the mechanism of synergy of the combination of colistin and rifampicin has been previously suggested by the “simple-uptake effect” model (234, 249). The studies proposed that the primary effect of colistin predominantly induced membrane disruption to facilitate the penetration of rifampicin to reach its intracellular target (234, 249). In addition, the relative hydrophobic property of rifampicin that is less permeable to the outer membrane layer of Gram-negative bacteria necessitates the action of polymyxin. This justified the insignificant effect of rifampicin alone to confer any metabolic changes in *P. aeruginosa* PAO1 as rifampicin itself was unable to reach its intracellular target (263).

4.6 Conclusions

Polymyxin combination therapy offers great potential of increasing polymyxins antimicrobial efficacy and limiting the emergence of bacterial resistance. In summary, the synergistic killing of the combination of polymyxin B and rifampicin against *P. aeruginosa* PAO1 significantly altered key metabolic pathways of lipid, peptidoglycan and LPS biosynthesis, nucleotide, amino acid and central carbon metabolism particularly at 15 min, 1 hr and 4 hr. The simple-uptake model sufficiently explains the mechanism of synergistic killing of the polymyxin B and rifampicin combination against *P. aeruginosa*; as polymyxin B significantly disrupts the integrity of the bacterial membrane structure to facilitate the penetration of rifampicin into its intracellular target. Importantly, this study further broadens our understanding on the underlying mechanism of polymyxin action which is invaluable in optimising its clinical use. Last but not

least, the results highlight the efficacy of metabolomics approach used for the analysis of drug modes of action that can suitably be applied in complementary with other omics methods.

Chapter Five

Chapter 5: The transcriptomic responses of the synergistic combination of polymyxin B and rifampicin against *Pseudomonas aeruginosa* PAO1

5.1 Abstract

The limited pharmacokinetics and pharmacodynamics profiles of polymyxin monotherapy necessitates a detailed understanding of its mechanism of action. Polymyxin combination treatment is often employed to enhance polymyxin therapeutic effect and minimise the emergence of resistance. In this study, the effect of polymyxin B (1 mg/L) and rifampicin (2 mg/L) mono- and combination therapy on *Pseudomonas aeruginosa* PAO1 transcriptome was investigated following treatment at 1 hr and 24 hr (n=3). Polymyxin B alone at 1 hr significantly up-regulated the genes essential for the modification of lipid A structure of the LPS, multidrug efflux protein and phenazine biosynthesis, indicating the development of polymyxin resistance and pathogenicity. The significant down-regulation of many quorum sensing (QS) regulated virulence factor genes by the synergistic killing of polymyxin B and rifampicin combination, signifying the suppression of PAO1 pathogenicity; the changes are predominantly driven by rifampicin as initially facilitated by polymyxin B. The combination also strongly up-regulated the nitrate uptake system as a result of the repressed terminal cytochrome oxidase, highlighting that *P. aeruginosa* essentially required nitrate as its alternative energy source and for the maintenance of redox homeostasis. Notable change in rifampicin resistance gene at 24 hr following treatment with rifampicin alone and the combination provides an indicative of the emergence of rifampicin resistance. Overall, this study highlights the polymyxin- and rifampicin-induced transcriptomics changes in the *P. aeruginosa* that may significantly contribute to the discovery of new drug targets, particularly of polymyxins.

5.2 Introduction

The global problem of antibiotic resistance of *P. aeruginosa* Gram-negative pathogen is an alarming concern. The pathogenicity of *P. aeruginosa* is predominantly influenced by cellular virulence factors, machineries that are essential to initiate bacterial colonisation and tissue invasion (50, 51). The superbug exhibits extraordinary ability to escape various classes of antibiotics via different resistance mechanisms relatively conferred by its large genome size which constituted of 6.26 Mbp encoding for 5,567 genes (56, 72, 77). Polymyxins have been re-established as the last-line arsenal for MDR *P. aeruginosa* infection. Polymyxins exert rapid bactericidal action via the electrostatic and hydrophobic interactions to its target binding sites, the lipid A component of LPS and also phospholipids in bacterial outer membranes. Worryingly, the emergence of polymyxin resistance has been reported due to the worldwide and uncontrolled use of polymyxins. Due to the limited pharmacokinetic/pharmacodynamic (PK/PD) profiles of polymyxins, polymyxin combination therapy has been strongly recommended (214). In particular, the combination of polymyxin plus rifampicin has been shown to be synergistic against MDR *P. aeruginosa*, *A. baumannii* and *K. pneumonia* in several *in vitro* and clinical studies (231-236). However, the detailed underlying mechanism of polymyxin action either as a single therapy or in combination remains unclear (212).

Systems pharmacology is increasingly applied to elucidate the mechanisms of drugs actions (275). Transcriptomics using RNA-seq method allows a comprehensive analysis of a genome which covers protein-coding genes, intergenic regions, non-coding RNA and small regulatory RNA population (437). In this study, we examined the global transcriptomic responses of *P. aeruginosa* PAO1 following treatment with polymyxin B and rifampicin alone and in combination at 1 hr and 24 hr. Our analyses revealed that, at 1 hr, polymyxin B alone significantly up-regulated genes associated with polymyxin resistance. Whereas the combination

significantly down-regulated many genes associated with bacterial virulence factors at 1 hr. In turn, at 24 hr, *P. aeruginosa* PAO1 appeared to develop resistance towards rifampicin following treatment with rifampicin alone and the combination. Overall, this transcriptomics study significantly highlights the changes elicited by polymyxin B and rifampicin alone and in combination that could be used to rationally optimise polymyxin PK/PD and discover novel drug target.

5.3 Materials and methods

5.3.1 Strain

P. aeruginosa was from the American Type Culture Collection (ATCC). The broth microdilution MICs of the PAO1 to polymyxin B and rifampicin were 0.5 mg/L (susceptible) and 32 mg/L (resistant), respectively. The strain was grown in cation-adjusted Mueller-Hinton broth (CaMHB; Oxoid, Australia; 20-25 mg/L Ca^{2+} and 10-12.5 mg/L Mg^{2+}).

5.3.2 Antibiotics and reagents

Polymyxin B was prepared using Milli-Q water (Millipore Australia, North Ryde, New South Wales, Australia). Prior to experiment, rifampicin was solubilised by DMSO and filtered with a 0.22- μm pore size Millex GP filter (Millipore, Bedford, MA).

5.3.3 Bacterial culture preparation

Preparation of PAO1 bacterial culture is described in Section 4.3.3 with slight modifications. *P. aeruginosa* PAO1 was prepared on a nutrient agar plate from the frozen stock (-80°C) and incubated for 16 - 18 hr at 37°C . A colony of PAO1 was inoculated into 10 mL CaMHB and incubated for 16 - 18 hr at 37°C with shaking at 150 rpm to prepare for the overnight culture. The overnight culture was diluted with 1:100 into four different reservoirs of 100 mL fresh

CaMHB. To obtain enough cells for the transcriptomics experiment, the culture was grown to an optical density at 600 nm (OD_{600}) of ~0.5 ($\sim 10^8$ CFU/mL). Bacterial culture of each reservoirs was treated with polymyxin B (1 mg/L), rifampicin (2 mg/L) and the combination of polymyxin B and rifampicin (1 mg/L + 2 mg/L); concentrations of polymyxin B and rifampicin were clinically relevant. Untreated bacterial culture served as a control sample. Samples (1.5 mL) were collected before treatment with polymyxin B, rifampicin and the combination (i.e. time = 0), and at 1 hr and 24 hr for RNA extraction. The study was conducted with three biological replicates independently from different colonies of PAO1 on different days.

5.3.4 RNA extraction

The preparation of RNA extract was according to the RNeasy Mini Kit manufacturer's protocol (Qiagen) (438). For each sample, one volume of bacterial culture was added to the two volumes of RNAprotect Bacteria Reagent (439). The mixture was vortexed immediately for 5 sec and incubated for 5 min at room temperature. The mixture was centrifuged for 10 min at $5,000 \times g$ and the supernatant was decanted. TE buffer containing lysozyme (added with Proteinase K) was added to the mixture pallet and resuspended by pipetting up and down several times. The mixture was further vortexed for 10 min and incubated for 10 min on a shaker-incubator. Buffer RLT was added and vortexed vigorously. Then, ethanol was added and shaken vigorously. The homogenised lysate was transferred to a gDNA Eliminator spin column (placed in a 2-mL collection tube) and centrifuged for 30 sec at $\geq 8,000 \times g$. The column was discarded and the flow-through was added with 70% ethanol and mixed by pipetting. About 700 μ L of the sample (including any precipitate) was transferred to an RNeasy spin column and centrifuged for 15 sec at $\geq 8,000 \times g$. The flow-through was discarded. 700 μ L of buffer RW1 was added to the RNeasy spin column and centrifuged for 15 sec at $\geq 8,000 \times g$. The flow-through was discarded. Then, 500 μ L buffer RPE was added to the RNeasy spin column and centrifuged for 15 sec at $\geq 8,000$

x g. The flow-through was discarded. Again, the step was repeated. 30 μ L of RNase-free water was added directly to the spin column membrane and centrifuged for 1 min at $\geq 8,000 \times g$ to get RNA elute (in a new 1.5 mL collection tube).

5.3.5 Analysis of RNA-seq data

RNA-seq of 27 samples in total was analysed using Illumina HiSeq 1500 at the Hudson Medical Research Institute (Clayton, Victoria, Australia). Preliminary RNA-seq analysis was conducted by Dr Yan Zhu. The reads were aligned to the PAO1 genome obtained from *Pseudomonas* Genome DB (440) using SubRead (441) with the standard settings. The counts of mapped reads were summarised by featureCounts (441). Differential gene expression was identified using Degust (www.vicbioinformatics.com/de gust), a graphic interface of Voom and Limma packages (442). Statistical significance of differential gene expression (DEG) was computed using the F-statistic with Benjamini Hochberg adjustment to control the false discovery rate (FDR) (443). DEG was defined with the cut-off as $\geq 1.0\text{-log}_2\text{-fold}$ and $\text{FDR} \leq 0.05$. Gene ontology enrichment analysis of DEGs particularly of the polymyxin B and rifampicin combination results was performed using Reduce and Visualise Gene ontology (REVIGO) software (444). iPath (<http://pathways.embl.de/index.html>) (445) was utilised to map the DEGs of polymyxin B and rifampicin alone and in combination results at 1 hr and 24 hr to demonstrate the general overview of the affected KEGG metabolic pathway.

5.4 Results

P. aeruginosa PAO1 was treated with polymyxin B (1 mg/L) and rifampicin (2 mg/L) alone and in combination at 1 hr and 24 hr to analyse its gene expression profiles. The number of DEGs (ANOVA; $\geq 1.0\text{-log}_2\text{-fold}$, $p \leq 0.05$, $\text{FDR} \leq 0.05$) of polymyxin B and rifampicin alone and the combination at each time point are summarised using Venn diagrams (Figure 5.1). Treatment of

polymyxin B and rifampicin alone differentially regulated approximately 0.6% and 0.5% of the total genes in PAO1 at 1 hr, respectively, as the majority of DEGs were up-regulated (Figure 5.1A). In turn, at 24 hr, about 0.3% and 3% of genes were significantly regulated by polymyxin B and rifampicin alone, respectively (Figure 5.1B). The synergistic killing of the polymyxin B and rifampicin combination significantly induced a larger number of genes approximately of 15% and 7.8% at 1 hr and 24 hr, respectively (Figure 5.1). Interestingly, no overlapping of DEGs were notified between all the antibiotic-treated groups at 1 hr whereas there were 15 DEGs that were commonly regulated at 24 hr (Figure 5.1A and B). At 1 hr, several DEGs of polymyxin B (17 DEGs) and rifampicin (8 DEGs) alone were commonly regulated by the combination of polymyxin B and rifampicin. The results showed that a large number of DEGs were commonly shared between rifampicin alone and the combination at 24 hr, as rifampicin presumably was the driven synergistic killing of the combination (Figures 5.1B).

REVIGO (444) was utilised for a Gene ontology (GO) enrichment analysis of the combination of polymyxin B and rifampicin at 1 hr and 24 hr to examine biological processes and cellular components that were enriched from the DEGs. At 1 hr, the total GO terms of the biological processes were reduced from 579 into 152, and the cellular components from 426 into 42. Whereas at 24 hr, the analysis reduced the biological processes from 445 into 190 and cellular components from 313 into 46 (Figures 5.2 and 5.3). Among the important GO terms for biological processes are quorum sensing (GO:0009372), denitrification pathway (GO:0019333), phenazine biosynthetic process (GO:0002047), phospholipid biosynthetic process (GO:0008654). Whereas, among the GO terms for cellular components are periplasmic space (GO:0042597), respiratory chain (GO:0070469), plasma membrane (GO:0005886) and integral component of cell outer membrane (GO:0045203). The overview of the metabolic pathways of

the significantly changed enzymatic reactions by the combination at 1 hr and 24 hr are presented (Figures 5.4 and 5.5).

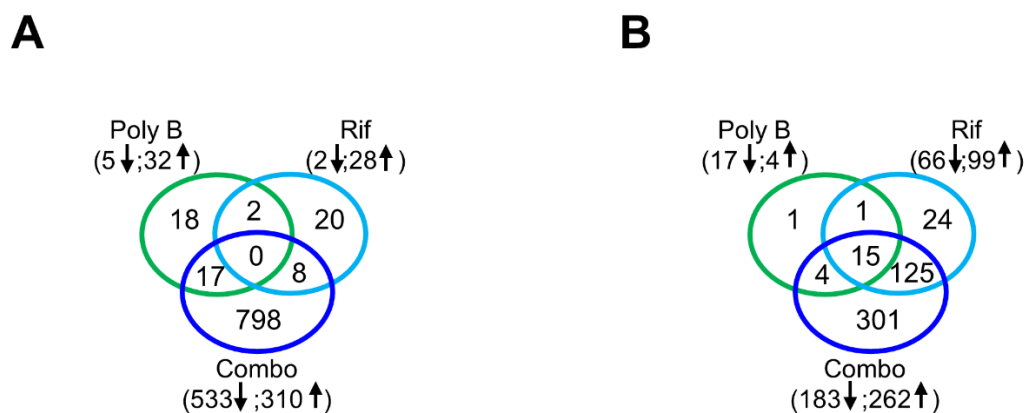


Figure 5.1. Transcriptomics response of *P. aeruginosa* PAO1. Venn diagrams represent the number of DEGs following treatment with polymyxin B and rifampicin alone and the combination at (A) 1 hr and (B) 24 hr. The numbers in brackets represent the number of DEGs that were significantly changed (up- and down-regulated). Polymyxin B alone = Poly B; Rifampicin alone = Rif; Polymyxin B and rifampicin combination = Combo. DEGs were selected with at least 1.0- \log_2 -fold, $p \leq 0.05$, FDR ≤ 0.05 .

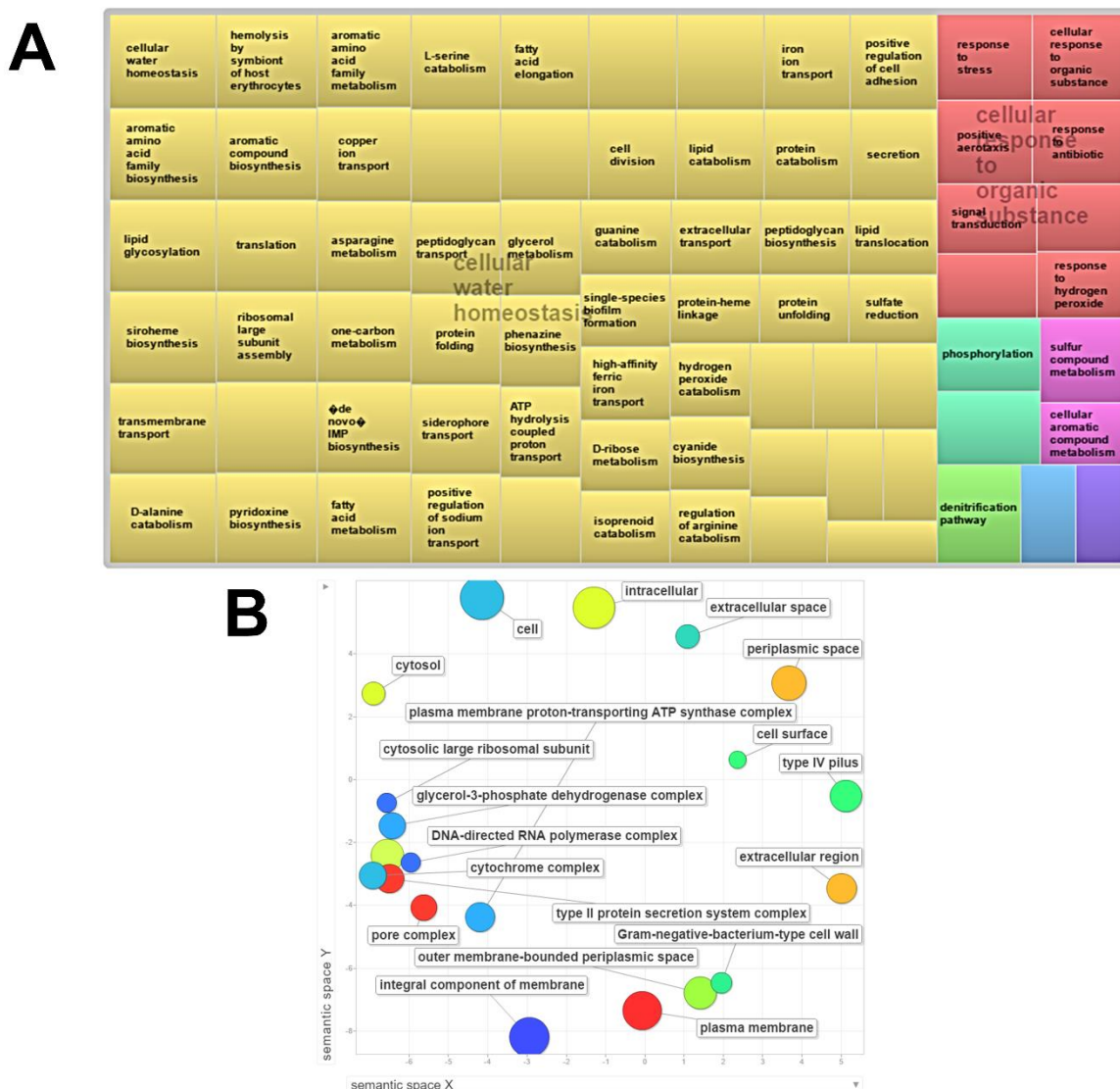


Figure 5.2. Gene ontology (GO) enrichment analysis of the combination of polymyxin B and rifampicin at 1 hr. (A) Summarised REVIGO TreeMap of the GO terms for biological processes. Similar colour represents semantic similarity related to similar functional category. The size of rectangle is proportional to the p -value for that category. **(B)** Summarised REVIGO scatter plot of the GO terms for cellular components. The circle represents the GO term and is plotted according to semantic similarity. The size of circle is proportional to the frequency of the GO term. The colour indicates the $\log_{10} p$ -value. DEGs including both the up- and down-regulated were selected with at least 1.0- \log_2 -fold, $p \leq 0.05$.

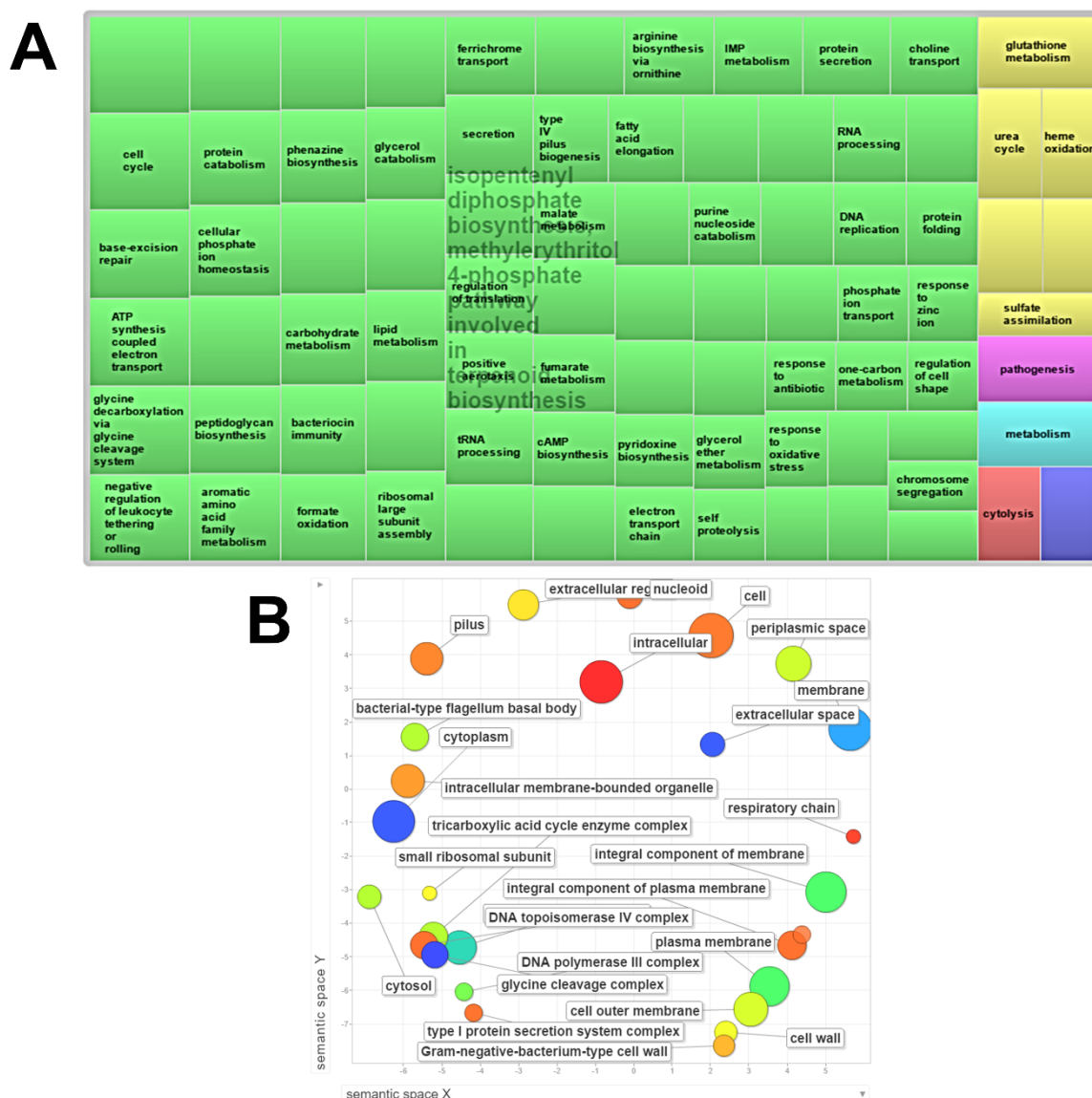


Figure 5.3. Gene ontology (GO) enrichment analysis of the combination of polymyxin B and rifampicin at 24 hr. (A) Summarised REVIGO TreeMap of the GO terms for biological processes. Similar colour represents semantic similarity related to similar functional category. The size of rectangle is proportional to the p -value for that category. **(B)** Summarised REVIGO scatter plot of the GO terms for cellular components. The circle represents the GO term and is plotted according to semantic similarity. The size of circle is proportional to the frequency of the GO term. The colour indicates the $\log_{10} p$ -value. DEGs including both the up- and down-regulated were selected with at least 1.0- \log_2 -fold, $p \leq 0.05$.

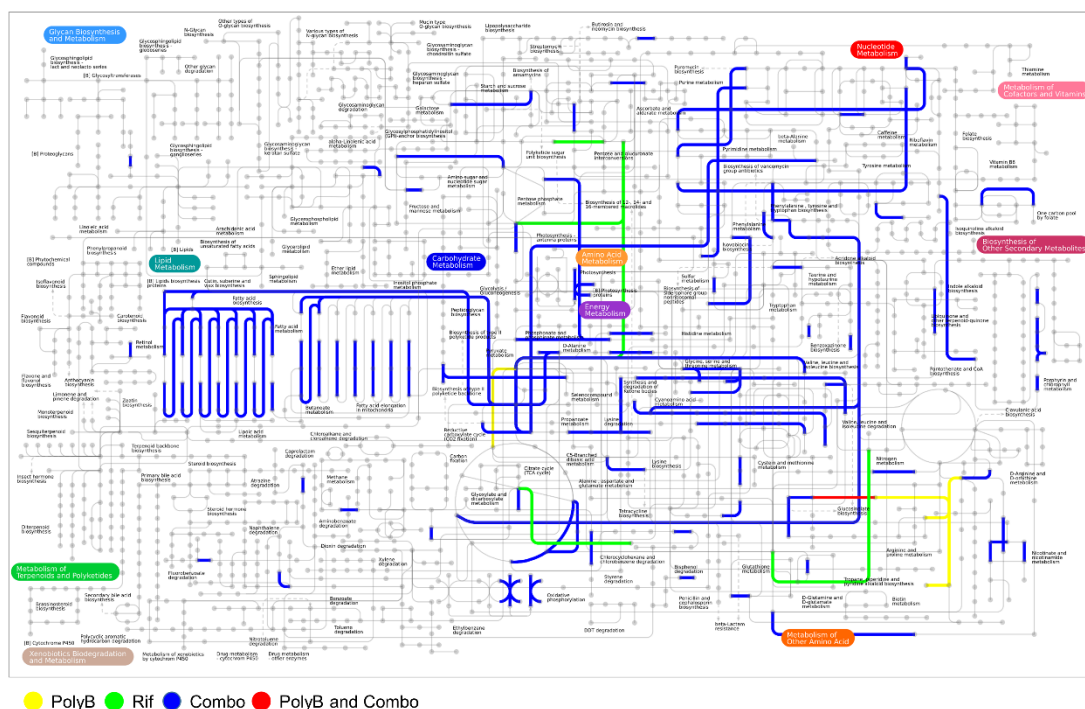
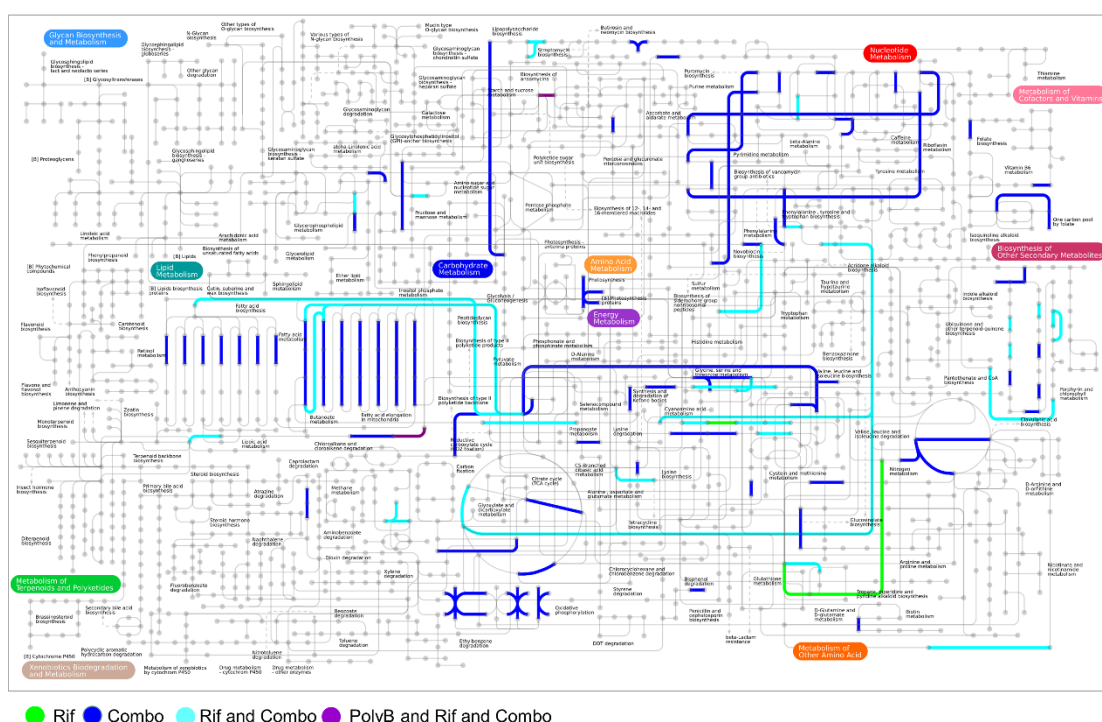
A**B**

Figure 5.4. The overview of metabolic pathways of the significantly changed enzymatic reactions (edges) of polymyxin B and rifampicin alone and the combination at (A) 1 hr and (B) 24 hr. Polymyxin B alone = Poly B; Rifampicin alone = Rif; Polymyxin B and rifampicin combination = Combo. DEGs including both the up- and down-regulated were selected with at least 1.0-log₂-fold, $p \leq 0.05$.

5.4.1 Polymyxin B differentially induced the expression of polymyxin resistance genes at 1 hr

Polymyxin B alone differentially induced over-expression of polymyxin resistance genes in PAO1 at 1 hr (Table 5.1). In particular, polymyxin B at sub-inhibitory concentration (1 mg/L) significantly up-regulated several genes on lipid A modification namely *arnA*, *arnB*, *arnC* and *arnE* ($\geq 2.5\text{-log}_2\text{-fold}$, $p \leq 0.05$) as well as *pagL* ($\geq 1.0\text{-log}_2\text{-fold}$, $p \leq 0.05$). At 1 hr, polymyxin B alone also significantly induced over-expression ($\geq 2.5\text{-log}_2\text{-fold}$, $p \leq 0.0001$) of genes of multidrug efflux protein, *mexX* and *mexY*; the changes that were also observed following the combination treatment. Notably, strong up-regulation of operon *msuE-msuD-PA2355-PA2354* was notified after treatment with polymyxin B alone and the combination ($\geq 2.5\text{-log}_2\text{-fold}$, $p \leq 0.01$). Interestingly, polymyxin B alone differentially up-regulated several genes on phenazine biosynthesis (*phzA1*, *phzM*; $>1.0\text{-log}_2\text{-fold}$, $p \leq 0.05$), a similar result as what has been previously reported in the literatures (68, 446). In addition, two genes of hypothetical proteins of the PA1559-PA1560 operon were strongly up-regulated by polymyxin B alone treatment ($\geq 2.5\text{-log}_2\text{-fold}$, $p \leq 0.01$). Three common DEGs (i.e. PA1797, PA0806 and PA2358) were steadily and strongly induced by both polymyxin B alone ($\geq 3.0\text{-log}_2\text{-fold}$, $p \leq 0.05$) and the combination ($\geq 1.5\text{-log}_2\text{-fold}$, $p \leq 0.05$) at 1 hr and 24 hr (Table 5.2).

Table 5.1 DEGs (at least 1.0-log₂-fold, $p \leq 0.05$) induced by polymyxin B alone at 1 hr.

Gene name/ locus tag	Product description	Expression ratio (log ₂)	Adjusted p -value
<i>arnB</i>	UDP-4-amino-4-deoxy-L-arabinose--oxoglutarate aminotransferase	2.68	0.00958
<i>arnC</i>	undecaprenyl-phosphate 4-deoxy-4-formamido-L-arabinose transferase	2.83	0.01278
<i>arnA</i>	bifunctional UDP-glucuronic acid decarboxylase/UDP-4-amino-4-deoxy-L-arabinose formyltransferase	2.83	0.00093
<i>arnE</i>	4-amino-4-deoxy-L-arabinose-phosphoundecaprenol flippase subunit ArnE	2.84	0.02206
<i>mexY</i>	RND multidrug efflux transporter	2.82	5.17E-08
<i>mexX</i>	RND multidrug efflux membrane fusion protein	2.89	5.27E-06
<i>pagL</i>	lipid A 3-O-deacylase	1.02	0.00283
PA2354	transcriptional regulator	2.96	0.00011
<i>msuC</i>	FMNH ₂ -dependent monooxygenase	3.83	0.00225
<i>msuD</i>	methanesulfonate sulfonase	4.24	0.00088
<i>msuE</i>	NADH-dependent FMN reductase	5.55	0.00062
<i>phzM</i>	Phenazine specific methyltransferase	1.34	0.00666
<i>phzA1</i>	Phenazine biosynthesis protein	1.13	0.04192
PA1559	Unknown	3.06	0.00015
PA1560	Unknown	2.55	0.00042
PA4774	Hypothetical protein	3.54	0.00066
PA4775	Hypothetical protein	1.44	0.00721
PA4773	Hypothetical protein	3.62	0.00014

Table 5.2 Common DEGs (at least 1.0-log₂-fold, $p \leq 0.05$) induced by polymyxin B alone and the combination of polymyxin B and rifampicin at 1 hr and 24 hr.

Locus tag	Product description	Expression ratio (log ₂)			
		Poly B (1hr)	Combo (1hr)	Poly B (24 hr)	Combo (24 hr)
PA1797	Hypothetical protein	5.20	3.40	3.05	1.82
PA0806	Hypothetical protein	5.11	2.89	5.50	3.03
PA2358	Hypothetical protein	5.72	3.81	5.00	3.47

5.4.2 Rifampicin-induced DEGs at 1 hr

At 1 hr, rifampicin alone predominantly up-regulated ($\geq 1.0\text{-log}_2\text{-fold}$, $p \leq 0.05$) the identified DEGs except the two genes of phenazine biosynthesis (*phzE2*, *phzF2*; $\leq 1.0\text{-log}_2\text{-fold}$, $p \leq 0.05$) (Table 5.3). Notably, DEGs that were significantly over-expressed by rifampicin alone were ABC transporter operon (PA3888-PA3891; $\geq 1.0\text{-log}_2\text{-fold}$, $p \leq 0.01$) and four hypothetical proteins (PA4738-PA4739, PA5481-PA5482; $\geq 1.5\text{-log}_2\text{-fold}$, $p \leq 0.01$).

Table 5.3 DEGs (at least $1.0\text{-log}_2\text{-fold}$, $p \leq 0.05$) induced by rifampicin alone at 1 hr.

Gene name/ locus tag	Product description	Expression ratio (\log_2)	Adjusted <i>p</i> -value
<i>phzE2</i>	Phenazine biosynthesis protein	-1.13	0.01090
<i>phzF2</i>	trans-2,3-dihydro-3-hydroxyanthranilate isomerase	-1.12	0.02225
PA1323	Hypothetical protein	1.19	0.00605
PA1324	Hypothetical protein	1.20	0.00416
PA3691	Hypothetical protein	1.35	0.00051
<i>lptF</i>	OM porin F	1.11	0.00147
<i>opuCD</i>	ABC transporter permease	1.15	0.00416
<i>opuCC</i>	ABC transporter	1.13	0.00605
<i>opuCB</i>	ABC transporter permease	1.25	0.00605
<i>opuCA</i>	ABC transporter ATP-binding protein	1.28	0.00096
PA4738	Hypothetical protein	2.01	0.00268
PA4739	Hypothetical protein	1.96	0.00661
PA5481	Hypothetical protein	2.04	0.00268
PA5482	Hypothetical protein	2.12	0.00514

5.4.3 Polymyxin B and rifampicin combination induced the repression of virulence factor genes at 1 hr

Exposure of the combination of polymyxin B and rifampicin treatment at 1 hr induced significant changes in many of PAO1 virulence factor genes (Table 5.4). Notably, the combination strongly suppressed the phenazine biosynthesis via the down-regulation ($\leq 2.0\text{-log}_2\text{-fold}$, $p \leq 0.05$) of *phzA1* and *phzA2* operons. A gene of the type IV pili (*flp*) and genes of the type VI secretion system (*vgrG6*, *hcpB*) were also strongly down-regulated ($\leq 4.0\text{-log}_2\text{-fold}$, $p \leq 0.05$) by the combination of polymyxin B and rifampicin at 1 hr. Other operons that were significantly down-

regulated ($\leq 1.0\text{-log}_2\text{-fold}$, $p \leq 0.05$) by the combination were the type II secretion system (PA3095-PA3105), biofilm formation protein (PA2231-PA2241) and the type IV fimbrial biogenesis protein (PA4551-PA4556). The combined polymyxin B and rifampicin also predominantly induced significant down-regulation ($\leq 1.0\text{-log}_2\text{-fold}$, $p \leq 0.05$) of genes of membrane porin protein (*oprB*, *oprD*); as both genes are associated with multidrug resistance mechanism. Importantly, the PA3327-PA3334 operon containing a gene of fatty acid biosynthesis (*fabH2*) was strongly down-regulated ($\leq 2.5\text{-log}_2\text{-fold}$, $p \leq 0.05$) in response to the polymyxin B and rifampicin combination.

5.4.4 *The combination of polymyxin B and rifampicin induced significant changes in central carbon metabolism*

The synergistic killing of the combination of polymyxin B and rifampicin significantly perturbed ($\geq 1.0\text{-log}_2\text{-fold}$, $p \leq 0.05$) the levels of genes involves in PAO1 central carbon metabolism (Table 5.4). In particular, several essential genes of glycolytic (*bkdB*, *lpdV*) and TCA cycle (*icd*, *mqaA*, *glcF*) pathways were significantly regulated following treatment with polymyxin B and rifampicin combination at 1 hr. The results also showed that genes associated with an aerobic electron transfer, particularly PA0521, *norB*, *cioB*, *cioA* and PA4133 were strongly down-regulated ($\leq 2.0\text{-log}_2\text{-fold}$, $p \leq 0.05$) by the combination at 1 hr. Interestingly, the combination significantly up-regulated ($\geq 2.0\text{-log}_2\text{-fold}$, $p \leq 0.05$) the *narK1K2GHJI* operon (PA3872-PA3877), which is important for the nitrate uptake system of denitrification process. Whereas cyanide-insensitive terminal oxidase operon (PA3928-PA3930) was significantly down-regulated by the combination. However, we found out that the combination significantly suppressed ($\leq 1.5\text{-log}_2\text{-fold}$, $p \leq 0.05$) the *nirSMCFDLGHJEN* operon (PA0509-PA0519) which is also functionally important for the denitrification process. Furthermore, an operon which

involved in chemotactic response (PA0173-PA0179) was significantly down-regulated (≤ 1.5 -log₂-fold, $p \leq 0.05$) by the polymyxin B and rifampicin combination at 1 hr.

Table 5.4 DEGs (at least 1.0-log₂-fold, $p \leq 0.05$) induced by the combination of polymyxin B and rifampicin at 1 hr.

Gene name/ locus tag	Product description	Expression ratio (log ₂)	Adjusted <i>p</i> -value
Virulence factors			
<i>phzA2</i>	Phenazine biosynthesis protein	-4.29	1.10E-06
<i>phzB2</i>	Phenazine biosynthesis protein	-5.01	1.46E-07
<i>phzC2</i>	Phenazine biosynthesis protein	-3.35	3.93E-08
<i>phzD2</i>	Phenazine biosynthesis protein	-4.47	5.08E-08
<i>phzE2</i>	Phenazine biosynthesis protein	-4.91	1.58E-08
<i>phzF2</i>	trans-2,3-dihydro-3-hydroxyanthranilate isomerase	-4.61	5.86E-08
<i>phzG2</i>	pyridoxamine 5'-phosphate oxidase	-3.68	1.45E-07
<i>phzA1</i>	phenazine biosynthesis protein	-4.56	5.10E-06
<i>phzB1</i>	phenazine biosynthesis protein	-4.71	9.09E-08
<i>phzC1</i>	phenazine biosynthesis protein	-4.43	0.00023
<i>phzG1</i>	pyridoxamine 5'-phosphate oxidase	-4.22	1.67E-06
<i>phzS</i>	hypothetical protein	-4.91	8.25E-08
<i>phzH</i>	phenazine-modifying protein	-2.43	3.87E-06
<i>phzM</i>	phenazine-specific methyltransferase	-3.94	9.90E-08
<i>flp</i>	type IVb pilin Flp	-4.33	3.14E-06
<i>lasA</i>	protease LasA	-1.47	5.01E-06
<i>lasB</i>	elastase LasB	-2.99	3.65E-07
<i>lasI</i>	Acyl-homoserine-lactone synthase	1.12	5.35E-06
<i>rhlI</i>	acyl-homoserine-lactone synthase	-1.33	1.08E-06
<i>rhlR</i>	transcriptional regulator RhlR	-1.98	7.03E-07
<i>rhlB</i>	rhamnosyltransferase subunit B	-3.15	3.98E-08
<i>rhlA</i>	rhamnosyltransferase subunit A	-3.53	3.93E-08
<i>xcpZ</i>	T2SS protein M	-2.03	9.83E-06
<i>xcpY</i>	T2SS protein L	-1.99	1.99E-06
<i>xcpX</i>	T2SS protein K	-1.76	4.14E-07
<i>xcpW</i>	T2SS protein J	-1.87	2.39E-08
<i>xcpV</i>	T2SS protein I	-1.84	1.45E-07
<i>xcpU</i>	T2SS protein H	-1.75	6.52E-07
<i>xcpT</i>	T2SS protein G	-1.75	1.96E-06
<i>xcpS</i>	T2SS protein F	-1.15	4.61E-05
<i>xcpR</i>	T2SS protein E	-1.34	9.81E-07
<i>xcpP</i>	T2SS protein N	-1.40	9.81E-06
<i>xcpQ</i>	T2SS protein D	-1.50	3.43E-07
<i>pslA</i>	biofilm formation protein PslA	-1.21	5.80E-07
<i>pslB</i>	biofilm formation protein PslB	-1.29	5.20E-07
<i>pslC</i>	biofilm formation protein PslC	-1.31	0.00010
<i>pslD</i>	biofilm formation protein PslD	-1.40	2.24E-07
<i>pslE</i>	biofilm formation protein PslE	-1.52	5.96E-07
<i>pslF</i>	biofilm formation protein PslF	-1.79	2.91E-05
<i>pslG</i>	biofilm formation protein PslG	-1.88	3.93E-08
<i>pslH</i>	biofilm formation protein PslH	-1.83	4.99E-07
<i>pslI</i>	biofilm formation protein PslI	-2.09	3.62E-07
<i>pslJ</i>	biofilm formation protein PslJ	-2.06	1.32E-07
<i>pslK</i>	biofilm formation protein PslL	-1.67	1.24E-05
<i>pilV</i>	type IV fimbrial biogenesis protein PilV	-1.28	7.18E-06
<i>pilW</i>	type IV fimbrial biogenesis protein PilW	-1.05	2.46E-05

<i>pilY1</i>	type IV fimbrial biogenesis protein PilY1	-1.04	8.79E-07
<i>pilY2</i>	type IV fimbrial biogenesis protein PilY2	-1.21	0.00014
<i>pilE</i>	type IV fimbrial biogenesis protein PilE	-1.20	2.88E-06
<i>oprD</i>	porin D	-1.07	0.00602
PA5265	hypothetical protein	-2.84	5.08E-06
<i>vgrG6</i>	Type VI secretion system, RhsGE-associated Vgr family subset	-4.36	5.46E-07
<i>hcpB</i>	Secreted protein Hcp	-4.55	5.20E-07
Central carbon metabolism/respiration			
PA3928	hypothetical protein	-2.86	2.67E-06
<i>cioB</i>	cyanide insensitive terminal oxidase	-3.20	5.23E-07
<i>cioA</i>	cyanide insensitive terminal oxidase	-3.43	7.44E-07
<i>narI</i>	respiratory nitrate reductase subunit gamma	2.64	0.01679
<i>narJ</i>	respiratory nitrate reductase subunit delta	2.31	0.02070
<i>narH</i>	respiratory nitrate reductase subunit beta	2.21	0.01753
<i>narG</i>	respiratory nitrate reductase subunit alpha	2.16	0.04273
<i>narK2</i>	nitrite extrusion protein 2	3.11	0.04253
<i>narK1</i>	nitrite extrusion protein 1	3.18	0.02028
<i>nirN</i>	cytochrome C	-2.51	2.24E-07
PA0510	uroporphyrin-III C-methyltransferase	-2.99	3.93E-08
<i>nirJ</i>	heme d1 biosynthesis protein NirJ	-3.15	3.93E-08
<i>nirH</i>	heme d1 biosynthesis protein NirH	-2.63	3.93E-08
<i>nirG</i>	heme d1 biosynthesis protein NirG	-2.31	4.23E-08
<i>nirL</i>	heme d1 biosynthesis protein NirL	-1.96	8.36E-08
<i>nirD</i>	heme d1 biosynthesis protein NirD	-1.95	2.67E-07
<i>nirF</i>	heme d1 biosynthesis protein NirF	-2.28	1.13E-07
<i>nirC</i>	cytochrome c55X	-2.26	5.33E-06
<i>nirM</i>	cytochrome C-551	-2.65	1.68E-06
<i>nirS</i>	nitrite reductase	-2.94	5.35E-06
<i>bkdB</i>	branched-chain alpha-keto acid dehydrogenase complex lipoamide acyltransferase	-2.76	2.68E-07
<i>lpdV</i>	branched-chain alpha-keto acid dehydrogenase complex dihydrolipoyl dehydrogenase	-3.36	7.61E-08
<i>Icd</i>	isocitrate dehydrogenase	-1.08	0.000615
<i>mqaA</i>	malate:quinone oxidoreductase	1.43	7.16E-07
<i>glcF</i>	glycolate oxidase iron-sulfur subunit	-2.27	0.013103
PA0521	cytochrome C oxidase subunit	-2.24	0.000649
PA4133	cbb3-type cytochrome C oxidase subunit I	-2.59	1.24E-05
Antibiotic Resistance			
<i>mexY</i>	RND multidrug efflux transporter	2.60	3.93E-08
<i>mexX</i>	RND multidrug efflux membrane fusion protein	2.85	9.60E-07
Others			
PA3328	FAD-dependent monooxygenase	-3.39	5.66E-07
PA3329	hypothetical protein	-3.33	4.37E-07
PA3330	short-chain dehydrogenase	-3.57	3.07E-07
PA3331	cytochrome P450	-2.85	3.62E-07
PA3332	hypothetical protein (Phenazine biosynthesis protein A/B)	-3.54	3.50E-07
<i>fabH2</i>	3-oxoacyl-ACP synthase III	-4.23	1.10E-07
PA3334	acyl carrier protein	-4.26	9.07E-08
<i>oprB</i>	porin B	-1.92	0.00056
PA3187	ABC transporter ATP-binding protein	-2.92	0.00012
PA3188	sugar ABC transporter permease	-2.13	0.00263

PA3189	sugar ABC transporter permease	-2.29	0.00375
<i>aprX</i>	hypothetical protein	-1.97	2.85E-07
<i>aprD</i>	alkaline protease secretion ATP-binding protein AprD	-2.29	1.04E-05
<i>aprE</i>	alkaline protease secretion protein AprE	-2.67	1.36E-06
<i>aprF</i>	alkaline protease secretion protein AprF	-2.95	4.96E-07
<i>opmD</i>	OM protein precursor	-3.75	2.66E-07
PA4607	hypothetical protein	-3.23	1.17E-06
<i>ampP</i>	Transmembrane transport	-3.45	6.39E-07
PA3335	hypothetical protein	-4.36	6.96E-08
PA3336	major facilitator superfamily transporter	-3.67	1.43E-07
PA0173	chemotaxis response regulator protein-glutamate methylesterase	-2.43	7.46E-06
PA0174	hypothetical protein	-2.98	5.75E-06
PA0175	chemotaxis protein methyltransferase	-3.48	7.65E-07
<i>aer2</i>	aerotaxis transducer Aer2	-2.52	8.15E-07
PA0177	purine-binding chemotaxis protein	-1.96	5.55E-05
PA0178	two-component sensor	-2.15	1.70E-07
PA0179	two-component response regulator	-2.63	5.20E-07
PA2354	transcriptional regulator	2.05	0.00035
PA2355	FMNH ₂ -dependent monooxygenase	2.59	0.00453
<i>msuD</i>	methanesulfonate monooxygenase	3.32	0.00069
<i>msuE</i>	NADH-dependent FMN reductase MsuE	4.36	0.00110

5.4.5 Rifampicin alone and the combination differentially regulated more genes at 24 hr

Rifampicin alone differentially regulated more genes at 24 hr than at 1 hr, as the similar changes were also notified by the combination of polymyxin B and rifampicin (Figure 5.1B and Table 5.5). However, only 21 DEGs were induced by polymyxin B alone at 24 hr which were less compared to its effect at 1 hr. Interestingly, a similar pattern of changes was observed in the 15 DEGs after exposure to polymyxin B and rifampicin alone and the combination (Table 5.6). At 24 hr, the combination differentially up-regulated several essential genes of bacterial virulence factors, as the effects were opposite from the changes observed at 1 hr. In particular, significant over-expressions ($1.0 \geq \log_2\text{-fold}$, $p \leq 0.05$) of regulatory genes of the quorum-sensing (QS) system, *rhlR*, *lasI* and *lasA* were notified following treatment with the combination. The combination also differentially up-regulated the genes of phenazine biosynthesis protein, *phzH*, *phzA1*, *phzA2*, and *phzB2* at 24 hr, as the changes were also induced by rifampicin alone. Several essential genes for transport and secretion of protease and lipase, *AprD*, *AprE* and *AprF* were significantly up-regulated ($2.0 \geq \log_2\text{-fold}$, $p \leq 0.05$) by the combination. Notably, the *AprE* was notified to be up-regulated ($3.0 \geq \log_2\text{-fold}$, $p \leq 0.05$) in response to rifampicin treatment. Furthermore, rifampicin alone and the combination significantly induced over-expression ($2.0 \geq \log_2\text{-fold}$, $p \leq 0.05$) of operon PA4468-PA6670 comprised of a gene encoding for antioxidant enzyme superoxide dismutase (SOD), *sodM*. The synergistic killing of the combination differentially induced suppression ($1.0 \leq \log_2\text{-fold}$, $p \leq 0.05$) of several genes involved in phosphate uptake protein, *phoU*, *pstB*, *pstS* and *pstA*. Importantly, at 24 hr *rpoB* encoding for the beta subunit of bacterial RNA polymerase was significantly down-regulated following treatment with rifampicin alone and the combination.

Table 5.5 Common DEGs (at least 1.0- \log_2 -fold, $p \leq 0.05$) induced by rifampicin alone and the combination of polymyxin B and rifampicin at 24 hr.

Gene name/ Locus tag	Product description	Expression ratio (\log_2)	
		Rif	Combo
<i>phzH</i>	phenazine-modifying protein	2.25	2.62
PA0133	HTH-type transcriptional activator BauR	1.42	1.23
<i>nuh</i>	nonspecific ribonucleoside hydrolase	1.44	1.47
<i>aer2</i>	aerotaxis transducer Aer2	2.52	2.91
PA0187	hypothetical protein	2.30	2.66
PA0188	hypothetical protein	1.88	1.98
<i>fiuA</i>	ferrichrome receptor FiuA	2.01	2.27
PA0493	acetyl-CoA carboxylase biotin carboxyl carrier protein subunit	1.64	1.40
PA0494	acetyl-CoA carboxylase biotin carboxylase subunit	1.70	1.36
PA0495	hypothetical protein	1.81	1.36
PA0572	hypothetical protein	1.44	1.85
PA0586	hypothetical protein	1.89	1.82
PA0587	hypothetical protein	1.07	1.44
<i>hemO</i>	heme oxygenase	2.06	2.43
<i>vreA</i>	hypothetical protein	2.05	2.38
PA0716	hypothetical protein	1.05	1.15
<i>recO</i>	DNA repair protein RecO	-2.10	-2.29
<i>hpd</i>	4-hydroxyphenylpyruvate dioxygenase	3.38	3.26
<i>phhB</i>	pterin-4- α -carbinolamine dehydratase	1.63	1.95
PA0894	hypothetical protein	-1.67	-1.91
PA0984	colicin immunity protein	2.00	2.16
<i>pyoS5</i>	pyocin S5	1.43	1.69
<i>braE</i>	branched-chain amino acid ABC transporter permease BraE	1.83	1.19
PA1131	major facilitator superfamily transporter	-1.12	-1.24
<i>aprE</i>	alkaline protease secretion protein AprE	3.00	3.76
PA1274	5,6-dimethylbenzimidazole synthase	-1.66	-2.69
<i>cobD</i>	cobalamin biosynthesis protein CobD	-2.04	-2.13
<i>cobC</i>	threonine-phosphate decarboxylase	-2.49	-2.49
PA1302	heme utilization protein	2.07	2.48
PA1351	ECF subfamily sigma-70 factor	1.30	1.15
<i>lasI</i>	acyl-homoserine-lactone synthase	1.38	1.11
<i>sucB</i>	2-oxoglutarate dehydrogenase complex dihydrolipoyllysine-residue succinyltransferase	-1.30	-1.24
<i>kdpB</i>	potassium-transporting ATPase subunit B	-2.98	-2.52
PA1833	Oxidoreductase	1.11	1.32
<i>phzA2</i>	phenazine biosynthesis protein PhzA	1.80	2.50
<i>maiA</i>	maleylacetoacetate isomerase	2.49	2.98
<i>fahA</i>	Fumarylacetoacetase	3.33	3.99
<i>liuC</i>	gamma-carboxygeranoyl-CoA hydratase	3.06	2.56
<i>liuB</i>	methylcrotonyl-CoA carboxylase subunit beta	2.12	1.76
<i>liuA</i>	isovaleryl-CoA dehydrogenase	2.28	1.76
PA2033	hypothetical protein	1.99	2.35
PA2034	hypothetical protein	1.68	1.93
PA2226	hypothetical protein	1.09	1.44
<i>vqsM</i>	HTH-type transcriptional regulator VqsM	1.27	1.38

<i>bkdB</i>	branched-chain alpha-keto acid dehydrogenase complex	1.01	1.35
	lipoamide acyltransferase		
<i>ansA</i>	L-asparaginase I	-1.49	-1.12
PA2381	hypothetical protein	1.28	1.26
PA2407	adhesion protein	2.54	2.81
<i>gcvP2</i>	glycine dehydrogenase	2.05	2.55
PA2465	hypothetical protein	2.51	2.13
PA2540	hypothetical protein	-1.18	-1.37
PA2552	acyl-CoA dehydrogenase	1.70	1.29
PA2553	acyl-CoA thiolase	1.93	1.74
PA2554	short-chain dehydrogenase	1.99	1.52
PA2561	methyl-accepting chemotaxis protein CtpH	1.04	1.72
PA2838	transcriptional regulator	-1.74	-1.49
PA2902	hypothetical protein	-1.06	-1.13
<i>cobJ</i>	precorrin-3 methylase CobJ	-1.31	-1.77
PA2914	ABC transporter permease	-1.77	-1.57
<i>nqrF</i>	Na(+)-translocating NADH-quinone reductase subunit F	-1.75	-2.19
<i>rmf</i>	ribosome modulation factor	1.36	1.86
<i>xcpT</i>	type II secretion system protein G	1.25	1.13
PA3122	transcriptional regulator	1.18	1.35
PA3174	transcriptional regulator	1.12	1.07
<i>glpD</i>	glycerol-3-phosphate dehydrogenase	-1.21	-2.05
<i>lpxB</i>	lipid-A-disaccharide synthase	-1.14	-1.31
<i>cdsA</i>	phosphatidate cytidylyltransferase	-1.71	-2.30
<i>wspE</i>	chemotaxis sensor/effector fusion protein	-1.04	-1.24
PA3711	transcriptional regulator	1.13	1.15
PA3723	FMN oxidoreductase	1.23	1.31
<i>exoS</i>	exoenzyme S	1.45	1.63
<i>rocR</i>	DNA-binding response regulator RocR	1.67	1.32
<i>sltB1</i>	soluble lytic transglycosylase B	-1.09	-1.12
<i>rodA</i>	rod shape-determining protein	-1.64	-1.79
PA4048	hypothetical protein	-1.49	-1.85
PA4090	hypothetical protein	1.81	1.51
<i>phzA1</i>	phenazine biosynthesis protein	2.60	2.06
<i>pchD</i>	2,3-dihydroxybenzoate-AMP ligase	2.59	3.20
<i>rpsN</i>	30S ribosomal protein S14	-2.83	-2.50
<i>rpsQ</i>	30S ribosomal protein S17	-2.56	-3.05
<i>rpmC</i>	50S ribosomal protein L29	-2.26	-3.02
<i>rpoB</i>	DNA-directed RNA polymerase subunit beta	-1.47	-1.88
<i>mvaT</i>	transcriptional regulator MvaT	1.05	1.13
<i>icmP</i>	insulin-cleaving metalloproteinase outer membrane protein	1.96	2.07
PA4467	hypothetical protein	2.90	3.48
<i>sodM</i>	superoxide dismutase	3.03	3.55
PA4469	hypothetical protein	3.06	3.74
<i>fumC1</i>	fumarate hydratase	2.44	3.05
PA4476	hypothetical protein	-1.23	-1.30
PA4497	ABC transporter	1.78	1.56
<i>opdP</i>	glycine-glutamate dipeptide porin OpdP	1.80	1.73
<i>lytB</i>	4-hydroxy-3-methylbut-2-enyl diphosphate reductase	-1.34	-1.63
PA4570	hypothetical protein	1.79	2.07
<i>mscL</i>	large-conductance mechanosensitive channel	1.06	1.23
<i>murI</i>	glutamate racemase	-1.27	-2.23
PA4680	hypothetical protein	2.40	2.31
PA4706	hemin importer ATP-binding subunit	1.53	1.35
<i>pnp</i>	polynucleotide phosphorylase	-1.15	-1.29

<i>rpsO</i>	30S ribosomal protein S15	-1.10	-1.24
<i>truB</i>	tRNA pseudouridine synthase B	-1.35	-1.48
PA4754	hypothetical protein	-1.16	-1.11
<i>greA</i>	transcription elongation factor GreA	-1.26	-1.48
<i>fdnI</i>	nitrate-inducible formate dehydrogenase subunit gamma	2.20	1.39
<i>fdnH</i>	nitrate-inducible formate dehydrogenase subunit beta	2.41	2.13
<i>retS</i>	sensor histidine kinase MifS	-1.92	-2.35
PA4889	Oxidoreductase	-1.16	-1.64
<i>parC</i>	DNA topoisomerase IV subunit A	-1.11	-1.47
PA5008	hypothetical protein	-1.76	-2.32
<i>pilQ</i>	type IV fimbrial biogenesis outer membrane protein PilQ	1.21	1.19
PA5061	hypothetical protein	1.22	1.19
<i>glnA</i>	glutamine synthetase	1.39	1.60
<i>dctP</i>	C4-dicarboxylate-binding protein	1.51	1.37
<i>dctQ</i>	dicarboxylate transporter	2.43	2.10
<i>dctM</i>	C4-dicarboxylate transporter	2.37	1.99
PA5230	ABC transporter permease	1.65	2.23
PA5312	aldehyde dehydrogenase	1.48	1.06
<i>pstB</i>	phosphate ABC transporter ATP-binding protein	-1.82	-2.04
<i>betA</i>	choline dehydrogenase	-1.20	-2.69
<i>betI</i>	BetI family transcriptional regulator	-1.17	-1.98
<i>wzm</i>	LPS efflux transporter membrane protein	1.75	1.25
<i>wbpW</i>	phosphomannose isomerase/mannose-1-phosphate guanylyl transferase	1.81	1.73
<i>atpC</i>	ATP synthase subunit epsilon	-2.82	-2.53
<i>atpD</i>	ATP synthase subunit beta	-2.97	-2.94

Table 5.6 Common DEGs (at least 1.0-log₂-fold, $p \leq 0.05$) induced by polymyxin B and rifampicin alone and the combination at 24 hr.

Gene name/ Locus tag	Product description	Expression ratio (log ₂)		
		Poly B	Rif	Combo
<i>cycH</i>	cytochrome c-type biogenesis protein CycH	-1.76	-1.87	-2.01
PA2006	major facilitator superfamily transporter	2.52	3.19	3.29
<i>nuoG</i>	NADH-quinone oxidoreductase subunit G	-1.33	-1.63	-1.88
PA2993	Hypothetical protein	-1.66	-1.94	-1.99
<i>nth</i>	endonuclease III	-1.63	-2.02	-1.66
PA3559	nucleotide sugar dehydrogenase	-2.46	-3.04	-3.42
<i>dxr</i>	1-deoxy-D-xylulose 5-phosphate reductoisomerase	-1.78	-2.78	-3.19
PA3800	OM protein assembly factor BamB	-1.67	-1.91	-1.81
PA3801	Hypothetical protein	-1.78	-2.27	-2.21
<i>rplE</i>	50S ribosomal protein L5	-2.53	-3.01	-2.88
<i>rplX</i>	50S ribosomal protein L24	-2.60	-3.08	-3.22
<i>rplN</i>	50S ribosomal protein L14	-2.25	-2.94	-3.16
PA5001	Hypothetical protein	-1.43	-1.96	-1.98
PA5007	Hypothetical protein	-2.09	-2.16	-2.14
<i>phoU</i>	phosphate uptake regulatory protein PhoU	-1.66	-2.25	-2.07

5.5 Discussion

The primary action of antibiotics is to cause either bacterial killing or inhibition. Importantly, at the cellular level, antibiotics essentially can induce gene regulations and expressions (446). Antibiotics at their sub-optimal concentrations can significantly modulate the expression of bacterial genes which likely can lead into resistance (447). In this thesis, transcriptomic changes of *P. aeruginosa* PAO1 in response to treatment with polymyxin B and rifampicin alone and in combination were profiled particularly at 1 hr and 24 hr.

The significant changes of the polymyxin-associated resistance genes at 1 hr indicated that PAO1 has become resistant to polymyxin B. The mechanism of polymyxin adaptive resistance in *P. aeruginosa* can be elucidated by two-component regulatory systems. The systems have been previously described which include five different classes, PmrA/PmrB (127-130), PhoP/PhoQ (131-134), ParR/ParS (135, 136), ColR/ColS and CprR/CprS (137). The PhoPQ and PmrAB two-component regulatory systems were first described in *P. aeruginosa* which functionally stimulate LPS modification independently of polymyxin induction (140). These two systems are predominantly regulated by the limited Mg^{2+} and phosphate conditions that induce lipid A modifications then finally cause polymyxin resistance (127, 131, 138). On the contrary, the ParRS system has been shown to be directly activated by the sub-inhibitory concentrations of cationic peptides (i.e. polymyxinB, colistin, indolicidin) to consequently induce LPS modification (135). Upon activation, response regulators (i.e. pmrA, phoP and parR) will induce the transcription of the *arnBCADTEF* operon to alter the lipid A structure of LPS by the addition of 4-aminoarabinose (127, 128, 448). The changes reduce the negative charge of LPS then inhibit polymyxins to bind and cross the outer membrane. In consistent with previous studies, the results demonstrated that the ParRS-regulated operons, PA1559-PA1560, PA4773-PA4775-pmrAB and *arnBCADTEF* (also regulated by the PmrAB and PhoPQ systems) were differentially over-

expressed by the sub-inhibitory concentration of polymyxin B at 1 hr (Table 5.1) (135, 140, 448). In addition, lipid A structure of LPS was also likely modified via the deacylation process as shown by the up-regulation of *pagL* gene (Table 5.1). An important hypothetical gene, PA1797 has been demonstrated to particularly involve in the cascade of ParRS system which directly or indirectly linked with the polymyxin resistance (135). The PA1797 is located downstream to but transcribed independently of the *parRS* operon and speculatively has a common function like β -lactamases (135). In addition, a gene, PA2358 encoding an unknown protein also was strongly up-regulated by polymyxin B alone and the combination at 1 and 24 hr. Interestingly, PA2358 also has been previously shown to be controlled by ParR (135, 140). In relation to these genes (PA1797 and PA2358), a gene PA0860 of hypothetical protein was also likely to be associated with polymyxin resistance as it was commonly over-expressed by polymyxin B alone and the combination.

Moreover, over-expression of the genes of multidrug efflux pump (*mexXY*) by polymyxin B alone also suggested the emergence of antibiotic resistance. Notably, the genes of multidrug efflux pump also were differentially induced by the combination. However, the synergistic killing of the combination importantly inhibited polymyxin resistance via the insignificant changes of the *arnBCADTEF* operon. No literature thus far has been reported on the direct association of polymyxin B-induced over-expression of *mexXY* system (449). Interestingly, a study showed that the activation of ParRS system significantly induced the up-regulation of *MexXY/OprM* system (140). Notably, *oprD* was significantly regulated by the combination but not by polymyxin B alone. Speculatively, *MexXY/OprM* and *OprD* may act together via active efflux and outer membrane impermeability to limit the intracellular accumulation of a toxic substrate directly or indirectly in response to polymyxin B (140). Furthermore, a previous study demonstrated that sub-inhibitory concentration of colistin significantly over-expressed

Pseudomonas quinolone signal biosynthesis genes and phenazine biosynthesis operon (68). Consistently, the present results showed that polymyxin B differentially up-regulated genes of phenazine biosynthesis, suggesting that the sub-inhibitory concentration of polymyxin B significantly influenced the *P. aeruginosa* pathogenicity.

Fatty acids are importantly used in many cellular processes including for structural component synthesis, as cofactors and energy storage reserves (450). A very strong suppression of a fatty acid biosynthesis gene, *fabH2* by the combination at 1 hr highly suggesting the inhibition of PAO1 membrane lipid production (Table 5.4). The synergistic model of the combination of polymyxin (specifically colistin) and rifampicin has been previously described by the “simple uptake effect”; as polymyxin predominantly induced membrane disorganisation to facilitate the entry of rifampicin into the cell (234, 249). Even though the result presented in this transcriptomics study cannot be used directly to explain the synergy mechanism of the combination but the significantly changed of the *fabH2* partly supports the proposed synergistic model.

The results demonstrated that the synergistic killing of the combination at 1 hr effectively suppressed the expression of many PAO1 virulence factors; the effects which have not been observed following treatment with polymyxin B and rifampicin alone (Table 5.4). The pathogenesis of *P. aeruginosa* infection is generally mediated by cellular virulence factors (50, 51). Importantly, this virulence machinery is highly regulated via the quorum sensing (QS) system (53, 451). *P. aeruginosa* displays two homologous QS systems, *las* and *rhl*, functionally regulate proteases and rhamnolipids production, respectively; as the *las* system systematically regulates the *rhl* system (451, 452). The *las* system comprised of an autoinducer synthase, *lasI*, functionally to produce AHL signal molecule *N*-(3-oxododecanoyl)-L-homoserine lactone (3O-

C₁₂-HSL) and a transcriptional activator protein, *lasR*, functionally to regulate *lasA* (protease) and *lasB* (elastase) expressions. In addition, the system also regulates *xcpP* and *xcpR*, genes encoding for secretory proteins. In turn, the *rhl* system comprised of an autoinducer synthase, *rhlI*, functionally to produce AHL *N*-butyryl-L-homoserine lactone (C₄-HSL) and a transcriptional activator protein which is important for the *rhlAB* operon expression. Also, the *rhl* system functionally regulate other extracellular virulence factors, *lasA* and *lasB* elastases, pyocyanin, cyanide, alkaline protease and *rpoS* (451). The importance of QS system to cause infection has been subjected it as a potential drug target (53, 58, 62, 63). The results revealed that the synergistic killing of the combination significantly down-regulated the QS regulatory genes (i.e. *lasA*, *lasB*, *rhlI*, *rhlR*, *rhlA*, *rhlB*); as the changes induced by the *rhl* system was stronger than the *las* system (Table 5.4). Furthermore, the synergistic action of the combination in reducing the potential of PAO1 to form biofilm is essential in avoiding the emergence of resistance. Consistently, the combination significantly suppressed rhamnolipids and associated biofilm formation proteins, particularly important for maintaining and establishing biofilm in *P. aeruginosa* (Table 5.4). Phenazine compounds (e.g. pyocyanin) are important bioactive secondary metabolites served as signals in *P. aeruginosa* QS system (446, 453). It has been shown to inhibit the ciliary function of respiratory epithelial cells and alter the host immune and inflammatory response (454, 455). The strong suppression of phenazine biosynthesis operons by the synergistic killing of the combination suggesting a significant reduction of PAO1 pathogenicity.

P. aeruginosa generally uses oxygen as terminal electron acceptor during aerobic respiration. Under anaerobic condition, nitrate and nitrite alternatively can be utilised in replacement for oxygen; the process known as denitrification (456-458). Denitrification is the process of nitrate reduction to dinitrogen that comprised of four steps (458). The first step is the reduction of nitrate

to nitrite that requires respiratory nitrate reductase. However, nitrate cannot simply diffuse through the cell membrane. Therefore, nitrate/nitrite transport protein(s) is required to facilitate its intracellular entry. Specifically, the *narK1K2GHJI* operon is encoding for both nitrate/nitrite transporters and nitrate reductase. In the second step, nitrite is reduced to nitric oxide which requires the periplasmic cytochrome *cd1* nitrite reductase, NirS (459). The enzyme generally comprised of a heme *c* and a heme *d₁* (encoded by the *nirSMCFDLGHJEN* operon) cofactor (459). Interestingly, the results suggested that the nitrate uptake system was activated in response to the combination as demonstrated by the significant over-expression of the *narK1K2GHJI* operon. The changes indicated that the treated PAO1 required nitrate likely to be used for respiration (Table 5.4) (458). In addition, the suppression of the terminal cytochrome oxidase (via PA3928-PA3930 operon) further supported the induction of denitrification process as an alternative mechanism of energy generation and maintenance of redox homeostasis (Table 5.4) (460). However, the significant down-regulation of the *nirSMCFDLGHJEN* operon suggesting that the process of denitrification was incomplete most likely left PAO1 at lower energy level (Table 5.4).

At 24 hr, a large number of DEGs were commonly identified between rifampicin alone and the combination signifying that the mechanism of synergy was driven predominantly by rifampicin (Figure 5.1B and Table 5.5). Interestingly, polymyxin B and rifampicin alone and the combination differentially regulated 15 common genes at 24 hr suggesting a general transcriptomics response of PAO1 to polymyxin B and rifampicin (Table 5.6). Notably, the significant over-expressions of genes associated with the QS regulatory proteins and virulence factors likely indicating the increase of bacterial pathogenicity. Rifampicin alone and the combination likely to induce the oxidative stress mechanism at 24 hr, an important defense system of a cell as notified by the up-regulation of SOD enzyme, *sodM* (Table 5.4) (461).

Moreover, rifampicin alone and the combination at 24 hr significantly repressed *rpoB*, a rifampicin resistance gene encoding for bacterial RNA polymerase β subunit, indicating the emergence of rifampicin resistance. The mechanism of rifampicin resistance is exclusively attributed to the missense mutation of *rpoB* which significantly induces structural changes in the bacterial RNA polymerase; and this has been demonstrated in *E. coli* and *Mycobacterium tuberculosis* (263, 462-464). We hypothesised that the significant down-regulation of *rpoB* expression likely resulted in reduced binding of rifampicin into its specific target, the β subunit of bacterial RNA polymerase conferring rifampicin resistance in *P. aeruginosa*.

5.6 Conclusions

Overall, this study demonstrates the dynamic transcriptomics changes of *P. aeruginosa* in response to polymyxin B and rifampicin alone and the combination treatments. Polymyxin B and rifampicin importantly induced the emergence of resistance in *P. aeruginosa* early at 1 hr and later at 24 hr, respectively. The results also highlight the importance of optimal dosage administration of both polymyxin B and rifampicin in monotherapy and the significance of polymyxin combination therapy to inhibit resistance. The synergistic killing of the combination to induce significant changes in QS-regulated virulence factors, fatty acid biosynthesis and denitrification process potentially provides novel drug targets, particularly for polymyxins.

Chapter Six

Chapter 6: Integrated metabolomic and transcriptomic analyses of the synergistic effect of polymyxin B and rifampicin combination against *Pseudomonas aeruginosa* PAO1

6.1 Abstract

Understanding the detailed mechanism of drug action is extremely important for improving current antimicrobial therapies. For the first time, integrated metabolomic and transcriptomic analyses of the synergistic combination of polymyxin B (1 mg/L) and rifampicin (2 mg/L) against *Pseudomonas aeruginosa* PAO1 at 1 hr and 24 hr was performed using a genome-scale metabolic network (GSMN) method. Polymyxin B alone and the combination induced significant lipid perturbations, predominantly of fatty acyls and glycerophospholipids, manifesting the known action of polymyxin to cause membrane disorganisation. Importantly, polymyxin B alone activated the two-component regulatory system, particularly the ParRS system to induce antibiotic resistance via lipid A modification, deacylation and multidrug efflux pump. Significant repression of a large number of PAO1 quorum sensing-regulated virulence determinants at 1 hr was evident by the synergistic combination. Notable changes in the peptidoglycan metabolism by the combination were presumably as a result of the secondary effect of polymyxin B. This study also highlights the dynamic respiratory changes of PAO1 to adopt the denitrification process in response to the combination. Accumulation of major metabolite classes (e.g. nucleotides, amino acids) by the combination indicates that PAO1 was in a state of metabolic arrest reflecting the action of rifampicin to inhibit bacterial DNA transcription. At 24 hr, the depletion of mRNA for a gene encoding for the RNA polymerase binding site for rifampicin suggests the emergence of rifampicin resistance. Overall, this study highlights the significant potential of integrative systems pharmacology in antimicrobial PK/PD optimisation.

6.2 Introduction

The rapid increase of antibiotic resistance across the globe is terrifying. *P. aeruginosa*, a versatile opportunistic Gram-negative pathogen has recently been ranked under the “Critical Priority” by the WHO (9). *P. aeruginosa* is metabolically flexible which produces a large number of cellular virulence factors and is able to develop different resistance mechanisms (reviewed in Section 1.2.2) (50, 51, 56). Polymyxins have been increasingly used as the last-line therapeutic arsenal, particularly for MDR *P. aeruginosa* infection. The well-established mode of bactericidal action of polymyxins is via the ‘self-promoted uptake’ pathway (Section 1.3.3) (11, 97), but the detailed mechanism of polymyxin-induced cell death remains unclear. As reviewed in Section 1.3.5, the PK/PD profiles of polymyxins showed that parenteral polymyxin monotherapy with current recommended dosages is unlikely to produce effective plasma exposure which tends to cause resistance (81, 189, 197, 213-216). Therefore, polymyxin combination therapy has been recommended to enhance its antibacterial activity and at the same time minimise the emergence of resistance (81, 214). *In vitro* and clinical evidence demonstrated that polymyxins in combination with rifampicin synergistically killed MDR *P. aeruginosa*, *A. baumannii* and *K. pneumoniae* (231-236).

At present, systems pharmacology of integrated omics is increasingly utilised to elucidate the detail mechanism of drug action (275, 281-285). The complement between metabolomics and transcriptomics information potentially can lead to the discovery of novel enzyme functions and metabolic pathways for comprehensive understanding of the basic cellular physiology (465). The general assumption that metabolites and genes are co-regulated in the same biochemical pathway allows the analysis of the unknown entities based on their pattern of changes with compounds of known functions of a defined metabolic pathways (465). In this study, integrated metabolomics and transcriptomics study of the synergistic killing of polymyxin B and rifampicin

combination against *P. aeruginosa* PAO1 was examined using a genome-scale metabolic network (GSMN). The results provide extensive mechanistic insights of the metabolic and regulatory bacterial networks affected by polymyxin B and rifampicin alone and in combination. The synergistic action of the combination significantly repressed the production of bacterial quorum sensing-regulated virulence factors and perturbed key metabolic pathways of cell envelope biosynthesis (i.e. lipids, peptidoglycan and LPS), central carbon metabolism (i.e. glycolysis, TCA and pentose phosphate pathway), nucleotides and amino acids. Whereas, polymyxin B and rifampicin monotherapy significantly induced the emergence of resistance at different time points highlighting the potential application of polymyxin combinations for effective treatment of MDR Gram-negative infections.

6.3 Materials and methods

P. aeruginosa PAO1 and antibiotics used in this study are detailed in Sections 4.3.1 and 4.3.2, respectively. Preparation for metabolomic and transcriptomic experiments are described in Sections 4.3 and 5.3, respectively

6.3.1 Genome-scale metabolic network (GSMN) reconstruction for *P. aeruginosa* PAO1

The GSMN of *P. aeruginosa* PAO1 was reconstructed by Dr Yan Zhu in our laboratory with reference to the iMO1056 (350) and Opt208964 (466) containing a total of 4,365 reactions, 3,022 metabolites and 1,458 genes. The reconstructed model was assigned as iPAO1. The reactions from iPAO1 were categorised into 110 pathways mainly based on classifications in MetaCyc and KEGG. The list of significantly changed metabolites and DEGs were uploaded in an Excel template of VANTED (367). Using the VANTED software, the experimental data from both metabolomics and transcriptomics studies were mapped into the GSMN iPAO1 construct to visualise the interaction between metabolites and genes (367). iPath (445) was utilised to map

the significantly changed metabolites and DEGs of the polymyxin B and rifampicin combination results at 1 hr and 24 hr into the KEGG map to demonstrate the general overview of the affected metabolic pathways.

6.4 Results

6.4.1 *Metabolomics*

Global metabolic profiling of PAO1 exposed to polymyxin B and rifampicin alone and in combination was conducted across four time points, 15 min, 1 hr, 4 hr and 24 hr (n=4). A total of 2,520 metabolite features (including their isomers) were putatively annotated and identified using the IDEOM software (341). Principal component analysis (PCA) plots and Venn diagrams are employed to show the global metabolic alterations and the number of significantly changed metabolites of PAO1 in response to polymyxin B and rifampicin alone or in combination (Figure 6.1). At 15 min, polymyxin B alone closely clustered with the combination as a large number of the significantly changed metabolites (1.5%) were commonly shared with the combination (Figure 6.1A). The effects of polymyxin B alone at 1 hr and 4 hr were very subtle as indicated by no bacterial killing (Figure 4.1) and a much less number of significantly changed metabolites (Figure 6.1B, C). At 1 and 4 hr, the PCA plots consistently demonstrated that polymyxin B alone indistinguishably grouped together with the control untreated (Figure 6.1B and C). Similarly, treatment with rifampicin alone showed no significant metabolic changes at 15 min, 1 hr and 4 hr as 2 mg/L used was also insufficient to induce significant metabolic changes (Figures 4.1 and 6.1A, B, C). On the contrary, the synergistic killing of the polymyxin B and rifampicin combination significantly perturbed key metabolic pathways of lipids, nucleotides, amino acids, carbohydrates, peptidoglycan and LPS biosynthesis over 4 hr (Figure 6.1A, B, C). At 24 hr, all antibiotic-treated groups noticeably clustered with the untreated control (Figure 6.1D).

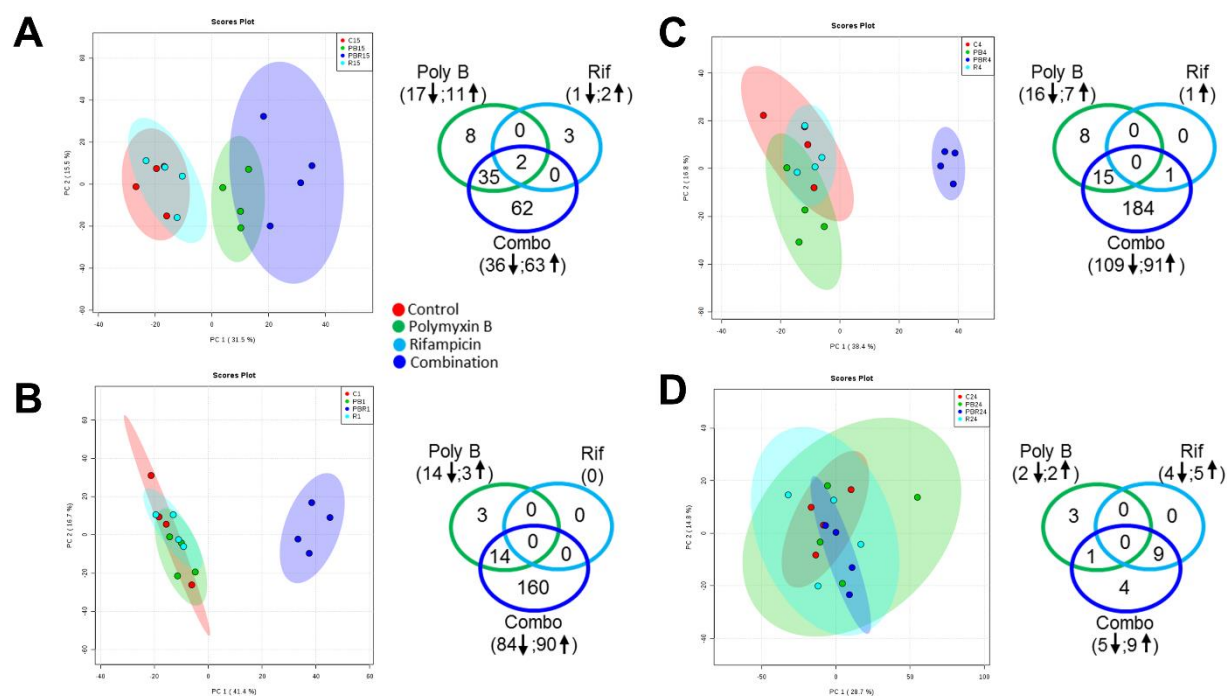


Figure 6.1. Global metabolic changes in *P. aeruginosa* PAO1 in response to polymyxin B (Poly B) and rifampicin (Rif) alone and in combination (Combo). PCA plots (left) of metabolic changes and Venn diagrams (right) of number of significantly changed metabolites at (A) 15 min, (B) 1 hr, (C) 4 hr and (D) 24 hr. The numbers in brackets represent the metabolites that were significantly changed (up- and down-regulated). Significantly changed metabolites were selected with at least 1.0- \log_2 -fold, $p \leq 0.05$.

6.4.2 Transcriptomics

The gene expression profile of PAO1 was analysed following treatment with polymyxin B, rifampicin and their combination at 1 hr and 24 hr (n=3). The RNA-seq data of 27 samples yielded overall 97,676,777 raw 100-bp single-end reads and 63.7-97.1% reads were successfully mapped to the coding regions of the PAO1 genome. Gene expression values indicated that a large number of DEGs were significantly regulated by the combination at 1 hr (Figure 6.2A (i)). Whereas, at 24, DEGs were predominantly regulated by rifampicin alone and the combination (Figure 6.2A (ii)). The numbers of DEGs following each antibiotic treatment at 1 and 24 hr were summarised by the Venn diagrams (Figure 6.2B). At 1 hr, polymyxin B and rifampicin alone significantly regulated approximately 0.6% and 0.5% of genes, respectively, as the majority of the DEGs were predominantly up-regulated (Figure 6.2B (i)). Whereas 0.3% and 3% of genes were significantly regulated by polymyxin B and rifampicin alone, respectively, at 24 hr (Figure 6.2B (ii)). The combination of polymyxin B and rifampicin induced a large number of DEGs approximately 15% and 7.8% at 1 hr and 24 hr, respectively, signified its persistent synergistic effect (Figure 6.2B). At 24 hr, approximately 2.5% of the DEGs induced by the combination were also commonly notified following treatment with rifampicin alone (Figure 6.2B (ii)). There were no overlapped DEGs between all the antibiotic treatment groups at 1 hr (Figure 6.2). Whereas at 24 hr 15 DEGs were commonly altered by the polymyxin and rifampicin mono- and combination therapy (Figure 6.2 and Table 5.6 [Section 5.4.5]).

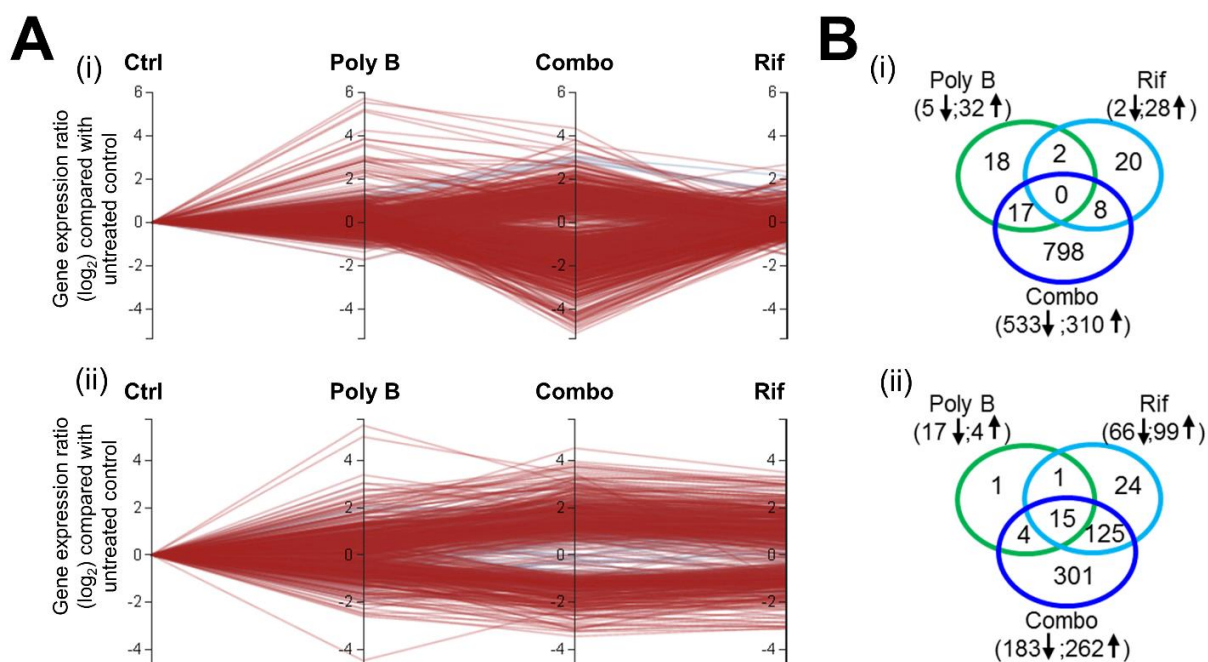


Figure 6.2. Gene expression changes in *P. aeruginosa* PAO1 following exposure to polymyxin B (Poly B) and rifampicin (Rif) alone and in combination (Combo). (A) Gene expression values for all the DEGs at (i) 1 hr and (ii) 24 hr. (B) Summary number of DEGs at (i) 1 hr and (ii) 24 hr. The numbers in brackets represent genes that were significantly changed (up- and down-regulated). DEGs were selected with at least 1.0- \log_2 -fold, $p \leq 0.05$.

6.4.3 Integration of metabolomic and transcriptomic data

The construct of PAO1 GSMN model, assigned as *i*PAO1 accounts for a total of 1,458 genes, 3,022 metabolites and 4,263 reactions. The significantly changed metabolites and DEGs which have KEGG ID numbers were mapped into the *i*PAO1 model. The overview of PAO1 metabolic pathways of the significantly changed enzymatic reactions and metabolites induced by the combination at 1 and 24 hr (Figure 6.3).

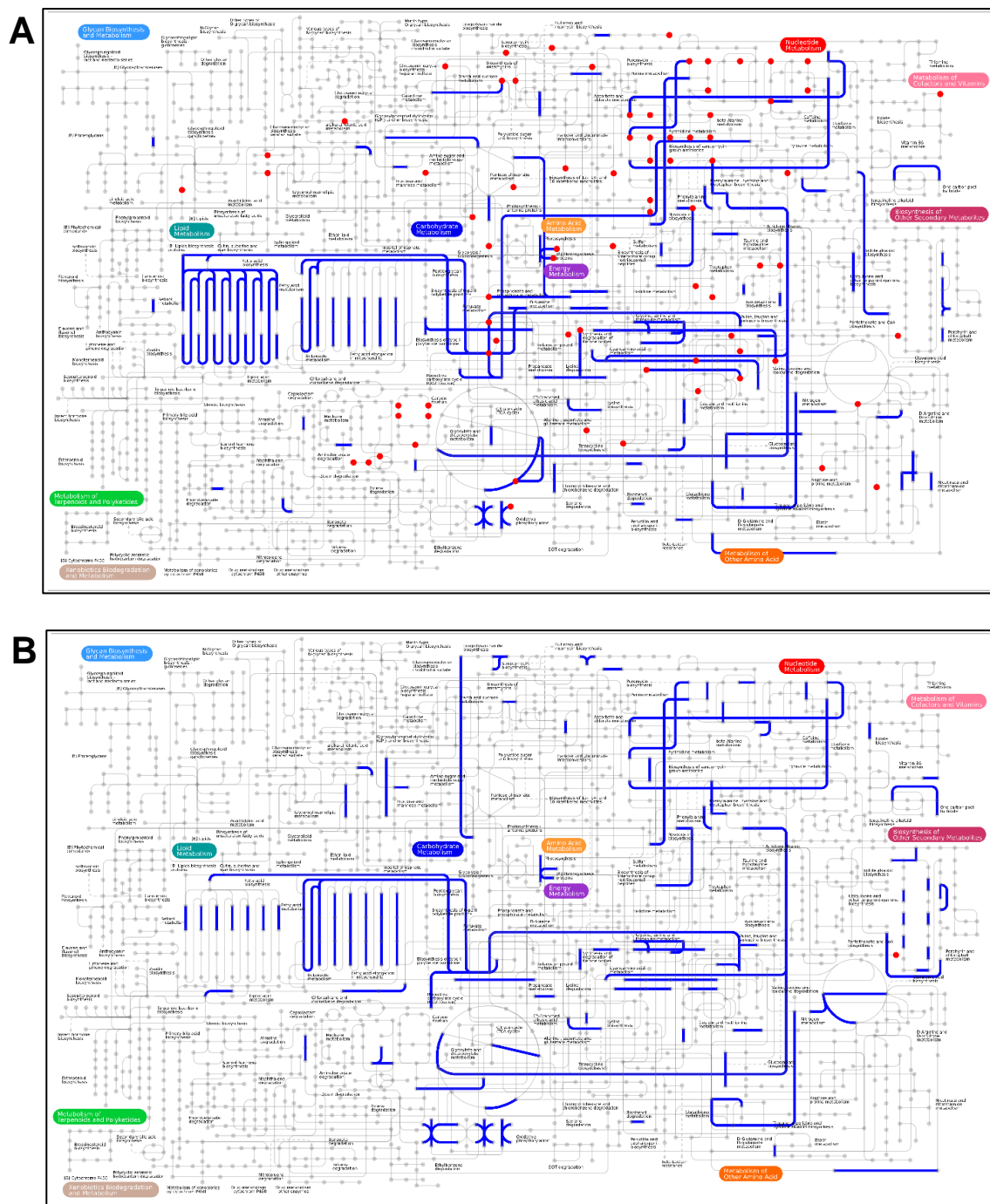


Figure 6.3. The overview of metabolic pathways of *P. aeruginosa* PAO1 affected by the combination of polymyxin B and rifampicin at (A) 1 hr and (B) 24 hr. Blue edges represent the significantly changed enzymatic reactions and red nodes represent the significantly changed metabolites. Significant metabolites and DEGs (including both the up- and down-regulated) were selected with at least 1.0-log₂-fold, $p \leq 0.05$.

6.4.4 Polymyxin-induced cell envelope changes

Polymyxin B alone and the combination significantly perturbed ($\geq 1.0\text{-log}_2\text{-fold}$, $p \leq 0.05$) the levels of PAO1 membrane lipids particularly of fatty acyls (FAs) and glycerophospholipids (GPs) at 15 min, 1 hr and 4 hr, whereas no appreciable changes following treatment with rifampicin alone at the same time points (Figure 6.4A). At 1 hr and 4 hr, the combination predominantly altered phosphatidylethanolamine (PE) and phosphatidylglycerol (PG) species of long fatty acyl chains (Figure 6.4A). Notable changes of the DEGs associated with fatty acid β -oxidation (*pldA*) and fatty acid biosynthesis (PA5524, PA0098, PA1806, PA3333) induced by the combination at 1 hr were consistent with the observed metabolomic changes in lipids (Figure 6.4B). In addition, a very strong suppression ($\leq 4.0\text{-log}_2\text{-fold}$, $p \leq 0.00001$) of genes involved in fatty acid biosynthesis, in particular *fabH2* and *atoB* by the polymyxin B and rifampicin combination at 1 hr supported the significant lipid perturbation observed in PAO1 (Figure 6.4B). Furthermore, rifampicin alone and the combination predominantly perturbed the levels of FAs at 24 hr which was consistent with the DEGs associated with phospholipid biosynthesis (*cdsA*) and fatty acid biosynthesis (PA049) (Figure 6.4B).

Significant metabolomics and transcriptomics changes of PAO1 cell wall synthesis, particularly peptidoglycan and LPS by the combination were notified. Metabolites of peptidoglycan biosynthesis, UDP-*N*-acetylglucosamine (UDP-GlcNAc), UDP-*N*-acetylmuramate (UDP-MurNAc), UDP-MurNAc-L-Ala- γ -D-Glu-meso-2,6-diaminopimelate and UDP-MurNAc-L-Ala- γ -D-Glu-meso-2,6-diaminopimeloyl-D-Ala-D-Ala were significantly up-regulated ($\geq 1.5\text{-log}_2\text{-fold}$, $p \leq 0.05$) following the combination treatment at 15 min, 1 hr and 4 hr (Figure 6.5). In addition, the combination also significantly increased ($\geq 1.5\text{-log}_2\text{-fold}$, $p \leq 0.05$) the levels of D-sedoheptulose 7-phosphate, a precursor metabolite for peptidoglycan and LPS synthesis, and 3-deoxy-D-manno-octulosonate (KDO), a metabolite in the LPS synthesis.

Consistently, following the combination treatment at 1 hr, several DEGs of peptidoglycan and lysine biosynthesis (i.e. *ampDh3*, *dapB*, PA0223, PA0530) were significantly over-expressed ($\geq 1.0\text{-log}_2\text{-fold}$, $p \leq 0.05$), in addition to the significant depletion ($\leq 1.0\text{-log}_2\text{-fold}$, $p \leq 0.05$) of a gene of lysine degradation (PA1252) (Figure 6.5). However, polymyxin B and rifampicin monotherapy induced no appreciable changes of PAO1 peptidoglycan and LPS biosynthesis metabolites across 24 hr. Several DEGs associated with the (KDO)₂-lipid A and peptidoglycan biosynthesis (i.e. *lpxA*, *lpxB* and *murl*) were significantly down-regulated by rifampicin alone and the combination at 24 hr but no significant metabolite changes detected.

6.4.5 Polymyxin B induced resistance and the expression of genes related to virulence factor

Polymyxin B alone exclusively up-regulated ($\geq 1.0\text{-log}_2\text{-fold}$, $p \leq 0.05$) the expression of lipid A modification genes, *arnA*, *arnB*, *arnC*, *arnE*, and *pagL* particularly at 1 hr and this was consistent with the significant increase ($\geq 1.4\text{-log}_2\text{-fold}$; $p \leq 0.05$) of a key LPS biosynthesis metabolite, UDP-glucuronate (Figure 6.6). Notably, no significant changes in the expression of the associated DEGs were identified by rifampicin alone and the combination. Three genes of hypothetical proteins linked with LPS modification, PA1797, PA0806 and PA2358 were significantly over-expressed ($\geq 1.5\text{-log}_2\text{-fold}$, $p \leq 0.05$) by polymyxin B alone and the combination at 1 hr and 24 hr. At 1 hr polymyxin B alone and the combination also significantly up-regulated ($\geq 1.0\text{-log}_2\text{-fold}$, $p \leq 0.05$) genes involved in multidrug efflux protein (*mexX*, *mexY*). Essentially, a number of genes of phenazine biosynthesis, *phzM* and *phzA1* of PAO1 virulence determinants were significantly increased ($\geq 1.0\text{-log}_2\text{-fold}$, $p \leq 0.05$) by polymyxin B alone at 1 hr.

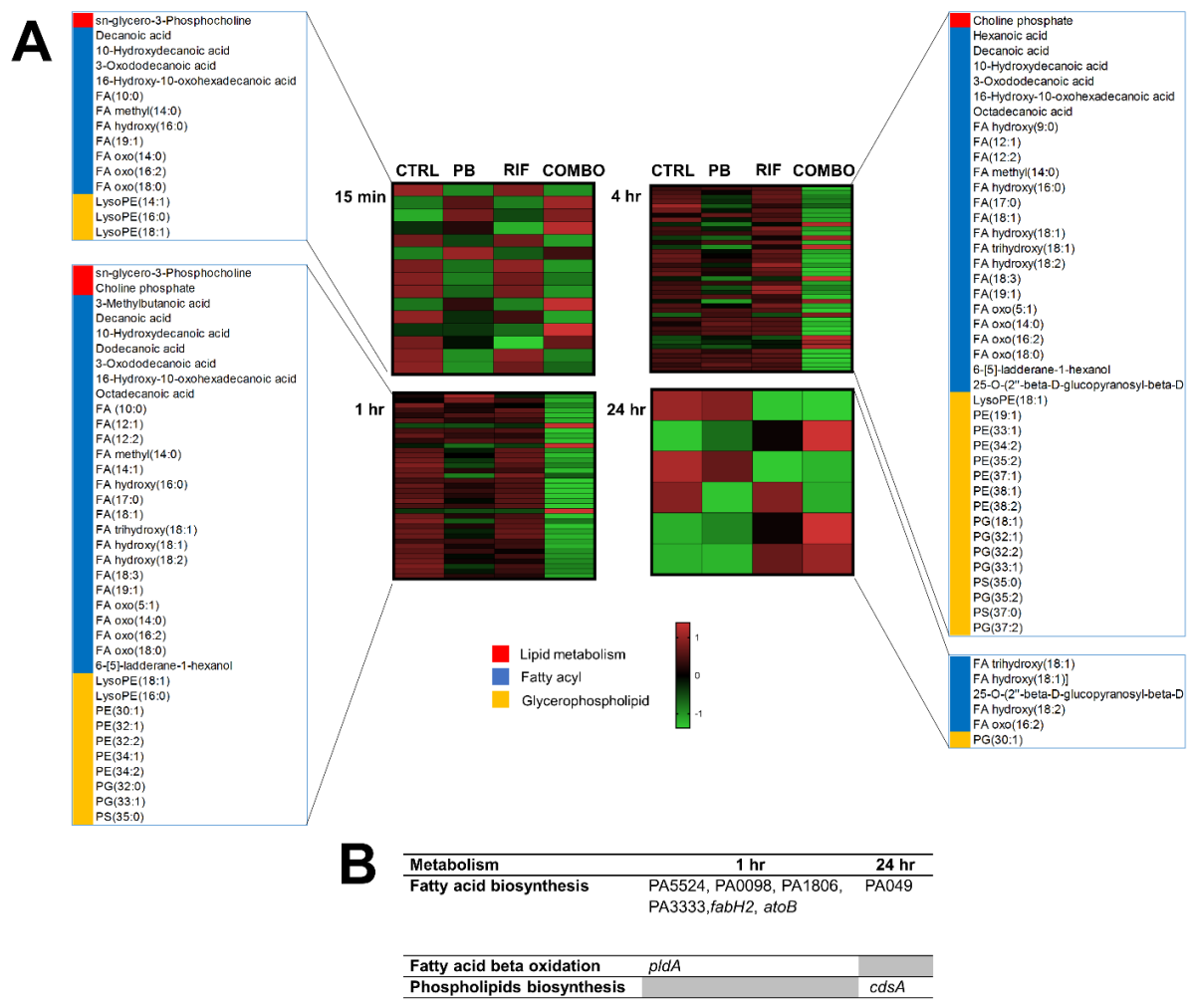


Figure 6.4. Perturbation of membrane lipids. (A) Heat map profiles of the significantly changed lipids at 15 min, 1 hr, 4 hr and 24 hr. Polymyxin B alone and the combination predominantly altered FAs and GPs of PAO1 at 15 min, 1 hr and 4 hr. Few FAs were perturbed by rifampicin alone and the combination at 24 hr. Lipids were putatively annotated with reference to accurate mass. (B) DEGs associated with lipid changes at 1 and 24 hr. Significantly changed metabolites and DEGs were selected with at least 1.0-log₂-fold, $p \leq 0.05$.

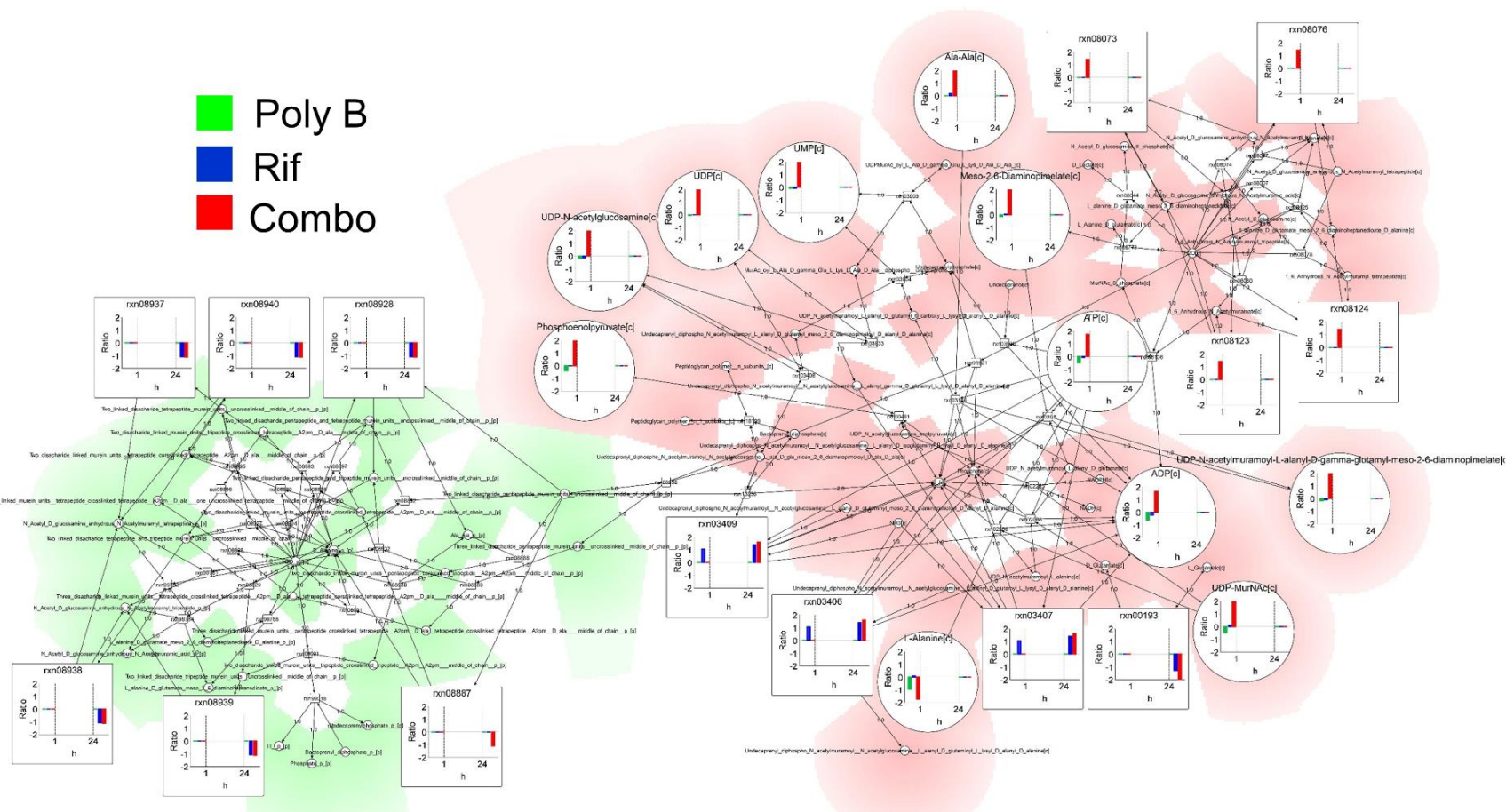


Figure 6.5 GSMN map of peptidoglycan biosynthesis pathway. Polymyxin B and rifampicin combination significantly up-regulated intracellular metabolites and DEGs associated with peptidoglycan biosynthesis at 1 hr. Cellular compartmentalisation represents green background as periplasmic space and red background as cytoplasmic space. Polymyxin B = Poly B; Rifampicin = Rif; Polymyxin B and rifampicin combination = Combo. Significantly changed metabolites and DEGs were selected with at least 1.0- \log_2 -fold, $p \leq 0.05$.

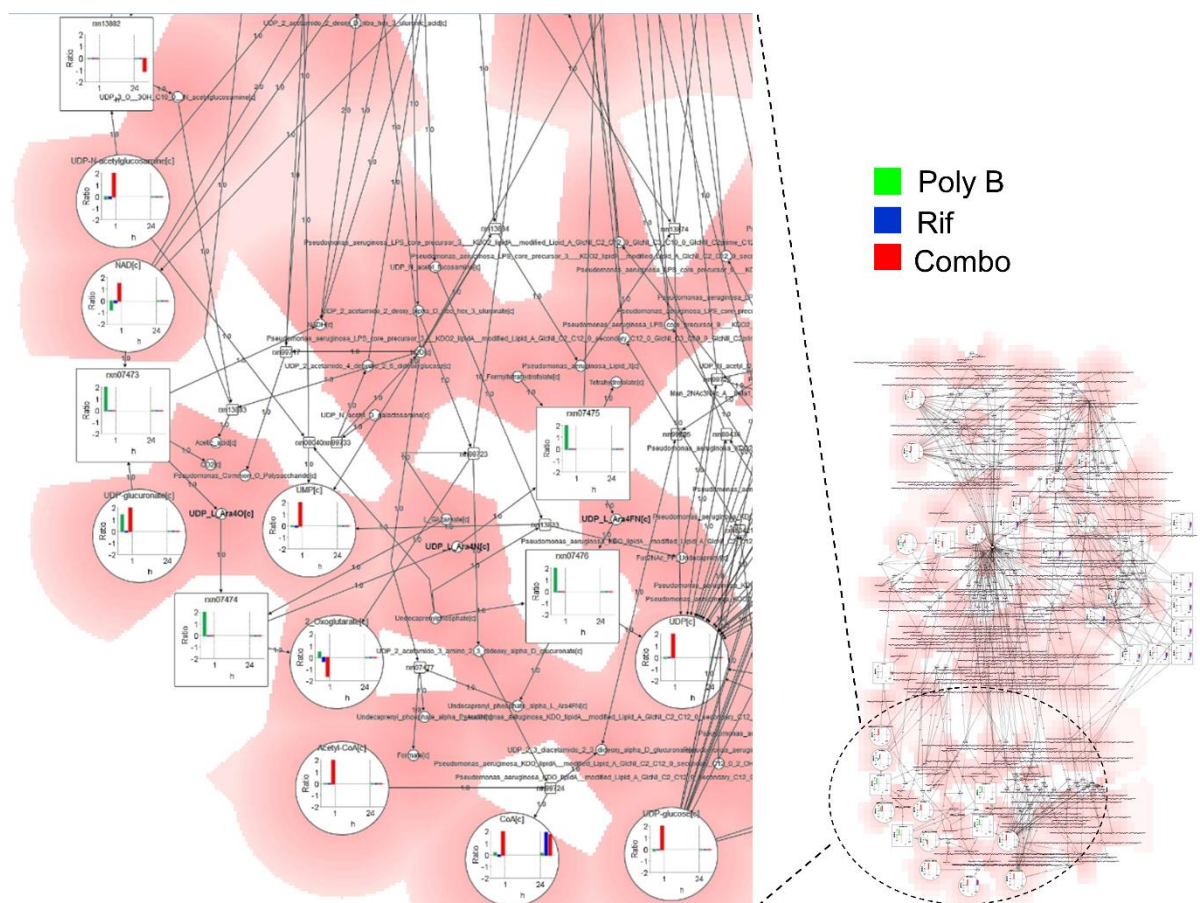


Figure 6.6 GSMN map of LPS modification pathway. Polymyxin B alone significantly up-regulated *arnA* (rxn 07473, rxn 07475), *arnB* (rxn 07474), *arnC* (rxn 07476) and UDP-glucuronate at 1 hr to induce the addition of 4-aminoarabinose to lipid A structure of LPS conferring to polymyxin resistance. Cellular compartmentalisation represents red background as cytoplasmic space. Polymyxin B = Poly B; Rifampicin = Rif; Polymyxin B and rifampicin combination = Combo. Significantly changed metabolites and DEGs were selected with at least 1.0-log₂-fold, $p \leq 0.05$.

6.4.6 *The combination of polymyxin B and rifampicin induced significant changes in nucleotide and amino acid metabolism*

The levels of purine and pyrimidine nucleotides mainly increased ($\geq 1.0\text{-log}_2\text{-fold}$, $p \leq 0.05$) by the combination of polymyxin B and rifampicin at 15 min, 1 hr and 4 hr (Figure 6.7A). Consistently, the combination significantly up-regulated DEGs associated with nucleotide biosynthesis (*atpC*, PA0531) and down-regulated a DEG involved in nucleotide degradation (PA1521) at 1 hr (Figure 6.7B). On the contrary, only very few nucleotides (mainly decreased) were significantly changed by polymyxin B alone at 15 min, 1 hr and 4 hr, whereas no significant changes were induced by rifampicin alone at any time point (Figure 6.7A). Notably, at 24 hr there were no significant changes in nucleotide levels following each antibiotic treatment.

Significant changes of PAO1 amino acid metabolism following exposure to the combination of polymyxin B and rifampicin at 1 hr were noticeable in both transcriptomics and metabolomics data (Table 6.1). In particular, the combination significantly altered the biosynthesis of phenylalanine, alanine, serine and glycine as well as degradation of valine, leucine, histidine and tyrosine at 1 hr. At 1 hr, the significant increase of 3-methylbutanoyl-CoA ($\geq 2.0\text{-log}_2\text{-fold}$, $p \leq 0.01$), a metabolite of leucine degradation was consistent with the notable decrease of associated genes (*liuA*, *liuB* and *liuE*) by the combination ($\leq 2.0\text{-log}_2\text{-fold}$, $p \leq 0.01$). The combination also significantly increased ($\geq 2.0\text{-log}_2\text{-fold}$, $p \leq 0.01$) a tyrosine metabolite while down-regulated the expression of tyrosine degradation genes, *phhC*, *hpd*, *hmgA*, *maiA* and *fahA* ($\leq 1.0\text{-log}_2\text{-fold}$, $p \leq 0.01$) at 1 hr. In contrast, the expression of leucine and tyrosine degradation genes was significantly up-regulated following treatment with rifampicin alone and the combination at 24 hr (Table 6.2).

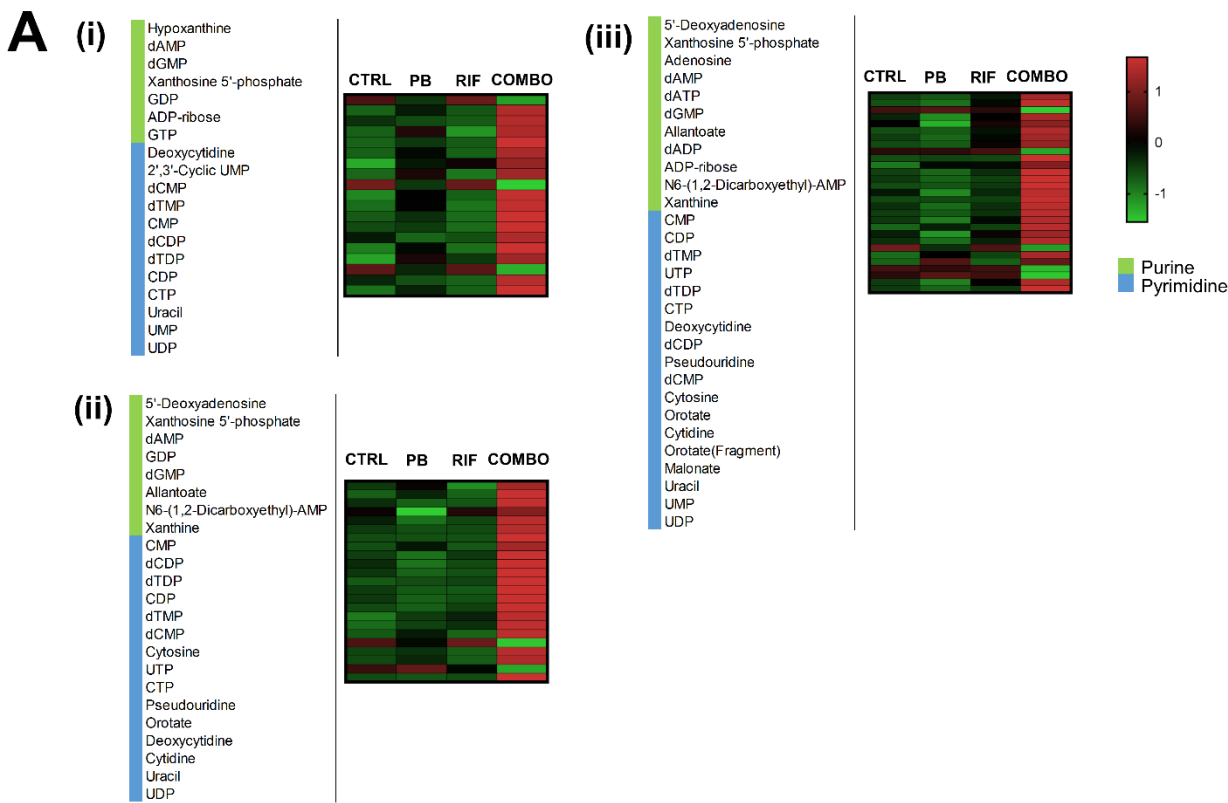


Figure 6.7. Perturbation of purine and pyrimidine nucleotides. (A) The combination of polymyxin B and rifampicin predominantly induced significant increases in the levels of nucleotides at (i) 15 min, (ii) 1 hr and (iii) 4 hr. (B) DEGs associated with purine and pyrimidine changes induced by the combination at 1 hr. There were no significant changes in nucleotide levels following each antibiotic treatment at 24 hr. Significantly changed metabolites and DEGs were selected with at least 1.0-log₂-fold, $p \leq 0.05$.

Table 6.1 Significantly changed metabolites and DEGs (at least 1.0-log₂-fold, $p \leq 0.05$) associated with amino acid metabolism induced by the polymyxin B and rifampicin combination at 1 hr.

Metabolism	Metabolite(s)	Log ₂ -fold	DEGs	Log ₂ -fold
Alanine biosynthesis	Pyruvate	-2.07	<i>iscS</i> ,	-1.17
	L-Alanine	-1.74	<i>dadX</i>	1.93
	Valine	2.07		
Serine and glycine biosynthesis	3-phospho-D-glycerate,	2.15	<i>glyA2</i>	1.34
	3-phospho-L-serine,	2.03		
	Serine	-2.01		
Phenylalanine biosynthesis	2-oxo-3-phenylpropanoate	-1.96	<i>phhC</i>	-1.02
Valine degradation	Valine,	2.07	<i>bkdA2</i> ,	-2.72
	(S)-3-hydroxy-isobutanoate	1.88	PA0744,	-2.47
			PA0743	-1.90
Leucine degradation	3-Methylbutanoyl-CoA	2.20	<i>liuA</i> ,	-2.68
			<i>liuB</i> ,	-2.64
			<i>liuE</i>	-3.51
Histidine degradation	Urocanate,	1.77	PA5106	1.12
	N-formimino L-glutamate	1.54		
Tyrosine degradation	Tyrosine	2.01	<i>phhC</i> ,	-1.02
			<i>hpd</i> ,	-3.37
			<i>hmgA</i> ,	-2.75
			<i>maiA</i> ,	-2.93
			<i>fahA</i>	-2.82

Table 6.2 DEGs (at least 1.0-log₂-fold, $p \leq 0.05$) associated with amino acid metabolism induced by the polymyxin B and rifampicin combination at 24 hr.

Metabolism	Rif	Log ₂ -fold	Combo	Log ₂ -fold
Leucine degradation	<i>liuA</i>	2.28	<i>liuA</i> ,	1.76
	<i>liuB</i>	2.12	<i>liuB</i>	1.76
Tyrosine degradation	<i>hpd</i> ,	3.38	<i>phhC</i> ,	1.79
	<i>maiA</i> ,	2.49	<i>hpd</i> ,	3.26
	<i>fahA</i>	3.33	<i>maiA</i> ,	2.98
			<i>fahA</i>	3.99

6.4.7 Synergistic polymyxin B and rifampicin combination induced suppression of virulence factors

The synergy of polymyxin B and rifampicin combination significantly induced the suppression of a large number of PAO1 cellular virulence factors at 1 hr; the effects that have not been reported by polymyxin B or rifampicin monotherapy (Table 6.3). Notably, the combination strongly repressed (≤ 2.0 -log₂-fold, $p \leq 0.05$) the expression of phenazine synthesis (via *phzA1* and *phzA2* operons), type IV pili (*flp*) and type VI secretion system (*vgrG6*, *hcpB*). Furthermore, the combination synergistically down-regulated (≤ 1.0 -log₂-fold, $p \leq 0.05$) the expression of genes associated with type II secretion system (PA3095-PA3105), type IV fimbrial biogenesis protein (PA4551-PA4556) and biofilm formation protein (PA2231-PA2241). Several virulence determinants are generally regulated by quorum sensing (QS) system where the results consistently revealed that the combination significantly suppressed (≤ 1.0 -log₂-fold, $p \leq 0.05$) the associated regulatory genes, *lasA*, *lasB*, *rhlI*, *rhlR*, *rhlA* and *rhlB* at 1 hr. The effect of combination treatment significantly down-regulated (≤ 1.0 -log₂-fold, $p \leq 0.01$) the expression of a sigma factor *RpoS*, the general stress response regulator in bacteria.

Table 6.3 DEGs (at least 1.0-log₂-fold, $p \leq 0.05$) induced by the polymyxin B and rifampicin combination at 1 hr.

Gene name/locus tag	Product description	Expression Ratio (log ₂)	Adjusted P-value
Virulence factor			
<i>lasA</i>	protease LasA	-1.47	5.01E-06
<i>lasB</i>	elastase LasB	-2.99	3.65E-07
<i>lasI</i>	acyl-homoserine-lactone synthase	1.12	5.35E-06
<i>rhlI</i>	acyl-homoserine-lactone synthase	-1.33	1.08E-06
<i>rhlR</i>	transcriptional regulator RhlR	-1.98	7.03E-07
<i>rhlB</i>	rhamnosyltransferase subunit B	-3.15	3.98E-08
<i>rhlA</i>	rhamnosyltransferase subunit A	-3.53	3.93E-08
<i>phzA2</i> , <i>phzB2</i> , <i>phzC2</i> , <i>phzD2</i> , <i>phzE2</i> , <i>phzF2</i> ,	phenazine biosynthesis protein	≤ -2.00	≤ 0.001

<i>phzG2, phzA1, phzB1, phzC1, phzG1, phzS, phzH, phzM</i>			
<i>flp</i>	type IVb pilin Flp	-4.33	3.14E-06
<i>xcpZ, xcpY, xcpX, xcpW, xcpV, xcpU, xcpT, xcpS, xcpR, xcpP, xcpQ</i>	type II secretion system protein	< -1.00	≤0.001
<i>pslA, pslB, pslC, pslD, pslE, pslF, pslG, pslH, pslI, pslJ, pslK</i>	biofilm formation protein	< -1.00	≤0.001
<i>pilV, pilW, pilY1, pilY2, pilE</i>	Type IV fimbrial biogenesis protein	< -1.00	≤0.001
PA5265	hypothetical protein	-2.84	5.08E-06
<i>vgrG6</i>	Type VI secretion system, RhsGE-associated Vgr family subset	-4.36	5.46E-07
<i>hcpB</i>	Secreted protein Hcp	-4.55	5.20E-07
Central carbon metabolism/respiration			
PA3928	hypothetical protein	-2.86	2.67E-06
<i>cioB</i>	cyanide insensitive terminal oxidase	-3.20	5.23E-07
<i>cioA</i>	cyanide insensitive terminal oxidase	-3.43	7.44E-07
<i>narI, narJ, narH, narG, narK2, narK1</i>	respiratory nitrate reductase subunit gamma	> 2.00	< 0.05
<i>nirN</i>	nitrite extrusion protein	> 3.00	< 0.05
PA0510	cytochrome C	-2.51	2.24E-07
<i>nirJ, nirH, nirG, nirL, nirD, nirF</i>	uroporphyrin-III C-methyltransferase	-2.99	3.93E-08
<i>nirC</i>	heme d1 biosynthesis protein	< 1.5	≤0.001
<i>nirM</i>	cytochrome c55X	-2.26	5.33E-06
<i>nirS</i>	cytochrome C-551	-2.65	1.68E-06
	nitrite reductase	-2.94	5.35E-06
Antibiotic resistance			
<i>oprB, oprD</i>	porin B, porin D	< -1.00	≤0.001
<i>mexY, mexX</i>	RND multidrug efflux	≥ 2.60	0.000001

6.4.8 Synergistic polymyxin B and rifampicin combination induced alterations in central carbon metabolism

Significant perturbation of PAO1 central carbon metabolism was evident following treatment with the polymyxin B and rifampicin combination. Both the transcriptomics and metabolomics results demonstrated that the synergistic killing of the combination predominantly altered (≥ 1.0 -log₂-fold, $p \leq 0.05$) the metabolic pathways of glycolysis, TCA cycle and PPP at 1 hr (Figure 6.8). Whereas, no significant changes were notified following treatment with polymyxin B and rifampicin monotherapy at each time point. The products of glycolytic reactions,

phosphoenolpyruvate and pyruvate, as well as metabolites of TCA cycle, 2-oxoglutarate and acetyl-CoA were significantly perturbed by the polymyxin B and rifampicin combination across 4 hr but with no common pattern of changes (Figure 6.8). Consistently, several essential genes of glycolysis and TCA cycle namely PA3416, PA3417, *lpdV*, *icd* and *mgoA* were significantly regulated following treatment with the combination at 1 hr. In addition, the combination also predominantly increased the abundance levels of PPP metabolites of D-sedoheptulose 7-phosphate, D-ribose 5-phosphate and fructose 6-phosphate across 4 hr (Figure 6.8). Moreover, the results showed that the combination caused strong down-regulation ($\leq 2.0\text{-log}_2\text{-fold}$, $p \leq 0.05$) of genes associated with aerobic electron transfer, namely PA0521, *norB*, *cioB*, *cioA* and PA4133 (Table 6.3). Interestingly, the synergistic action of the combination of polymyxin B and rifampicin significantly altered genes associated with denitrification process, via the up-regulation of the *narK1K2GHJI* operon and down-regulation of the *nirSMCFDLGHJEN* operon (Table 6.3).

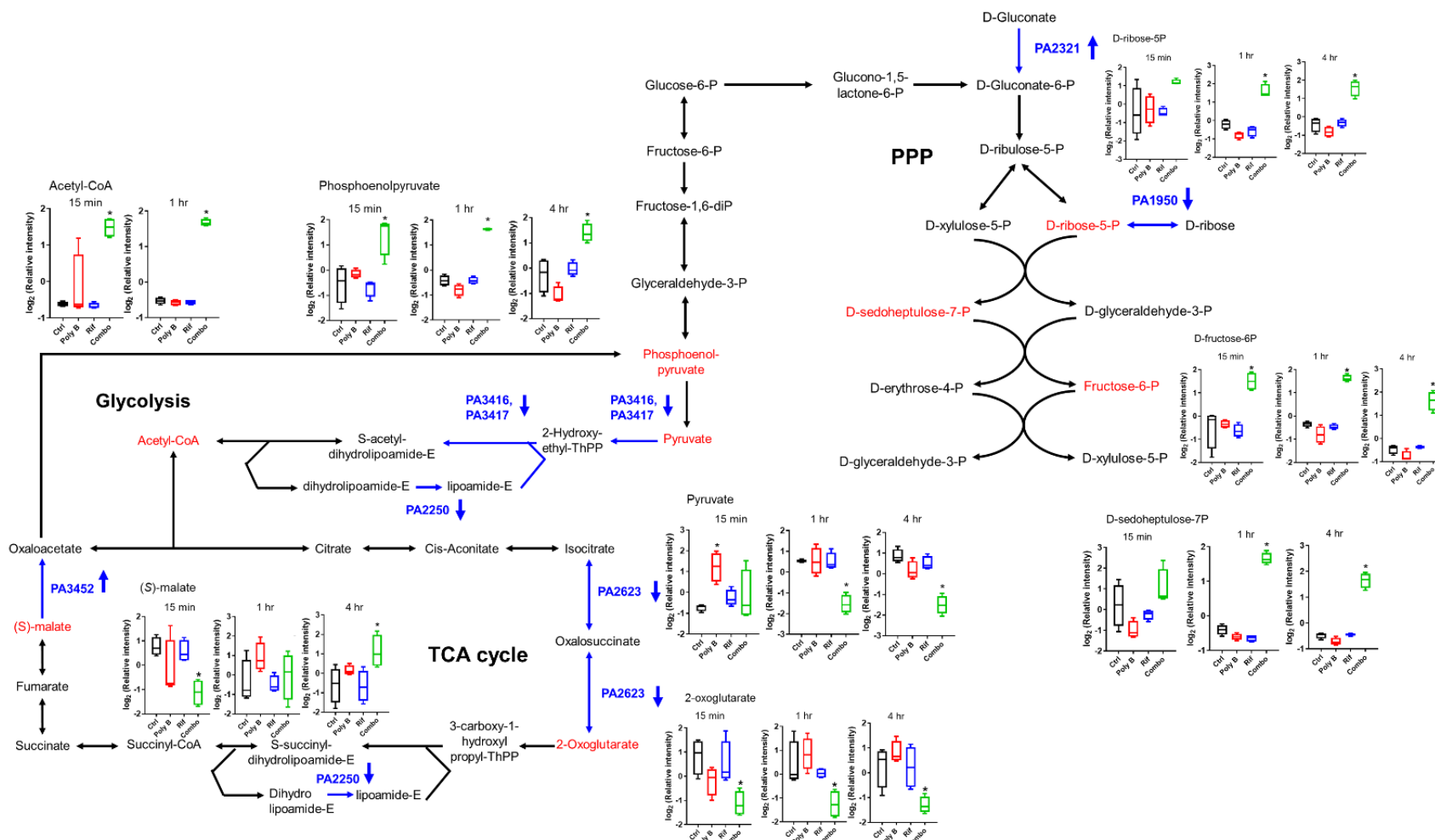


Figure 6.8. Perturbation of central carbon metabolism by the combination of polymyxin B and rifampicin. The combination significantly altered the metabolite and gene expression levels of metabolic pathways of TCA cycle, glycolysis and PPP. Metabolites of red colours represent the significantly changed metabolites (at 15 min, 1 hr and 4 hr); whereas genes of blue colours represent the DEGs (at 1 hr) either up-regulated or down-regulated (indicated with arrows). Box plots indicate upper and lower quartiles (top and bottom of box); median (line within box); and the spread of data that are not outliers (whiskers). Significantly changed metabolites (*) and DEGs were selected with at least 1.0- \log_2 -fold, $p \leq 0.05$. The figure is modified from the KEGG with reference to *P. aeruginosa* PAO1 strain.

6.4.9 Rifampicin predominantly induced transcriptomic changes in the polymyxin B and rifampicin combination at 24 hr

Analysis of the transcriptomic data showed that rifampicin alone induced more DEGs at 24 hr than at 1 hr, as the changes were predominantly in common with the combination of polymyxin B and rifampicin (Figure 6.2). A list of DEGs that were induced by both rifampicin alone and the combination at 24 hr is presented in Table 5.5 (Section 5.4.5). However, only few metabolites were significantly changed following treatment with rifampicin alone and the combination at 24 hr (Figure 6.1D and Table 4.5 [Section 4.4]). For polymyxin B alone, the changes in both metabolomics and transcriptomics at 24 hr were dramatically less than at 1 hr (Figures 6.1 and 6.2). At 24 hr, the combination predominantly up-regulated a large number of genes of PAO1 virulence determinants such as the QS regulatory genes (*rhlR*, *lasI*, *lasA*; $1.0 \geq \log_2$ -fold, $p \leq 0.05$), phenazine biosynthesis proteins (*phzH*, *phzA1*, *phzA2*, *phzB2*; $2.0 \geq \log_2$ -fold, $p \leq 0.05$) and protease secretion system (*AprD*, *AprE*, *AprF*; $2.0 \geq \log_2$ -fold, $p \leq 0.05$). Notably, rifampicin alone also differentially over-expressed ($2.0 \geq \log_2$ -fold, $p \leq 0.05$) those genes of phenazine biosynthesis at 24 hr. In addition, significant up-regulation of PA4468-PA6670 operon ($2.5 \geq$

\log_2 -fold, $p \leq 0.05$), which contains an important gene encoding for antioxidant enzyme superoxide dismutase, *sodM* was noted following treatment with rifampicin alone and the combination. Moreover, at 24 hr, rifampicin alone and the combination significantly down-regulated ($1.0 \leq \log_2$ -fold, $p \leq 0.05$) the expression of an essential gene, *rpoB*, particularly associated with rifampicin resistance.

6.5 Discussion

Polymyxin combination therapy has been increasingly applied clinically to enhance polymyxin antimicrobial efficacy and minimise the emergence of resistance to this last-line class antibiotic (81, 197, 213-216). The great prospect of polymyxins use in combination with other antibiotics requires extensive PK/PD optimisation, and this can be potentially achieved by systems pharmacology via detailed understanding of the mechanism of polymyxin action. At the present time, systems pharmacology is an important component in the drug development pipeline used to elucidate the mode of action of a new drug. In addition, evidence shows that the platform is increasingly used to provide information about potential novel drug targets. In particular, a genome-scale metabolic network (GSMN), a reconstruction of the metabolic pathways of a cell based on annotations of gene-protein-reaction (GPR) relationships with a mass- and energy balance, has been widely applied in systems medicine (348). In this PhD project, transcriptomics and metabolomics data were systematically integrated and analysed using a GSMN model to provide a comprehensive understanding of the mechanism of synergistic killing of the combination of polymyxin B and rifampicin against *P. aeruginosa* PAO1.

Significant metabolic perturbations induced by the combination treatment at 15 min suggesting polymyxin B was the driving force of the observed changes. Notable changes of PAO1 membrane lipids majorly of GPs and FAs at 15 min were exclusively as a result of the direct

action of polymyxin B to cause membrane disorganisation (Figure 6.4) (11, 87). In Section 3.4.2, the results showed that colistin alone and the combination with doripenem similarly induced significant perturbation in the levels of *A. baumannii* membrane lipids (GPs and FAs) particularly at 15 min and 1 hr. Moreover, the combination of polymyxin B and rifampicin significantly increased the levels of peptidoglycan and LPS biosynthesis metabolites in PAO1 (Figure 6.5). On the contrary, the changes that have been observed in *A. baumannii* demonstrated that colistin alone and the combination with doripenem significantly down-regulated the amino sugar metabolites of cell wall biosynthesis (e.g. UDP-GlcNAc, UDP-MurNAc) (Section 3.4.5). Even though the significant changes in the levels of peptidoglycan and LPS biosynthesis metabolites were only detected as a result of the polymyxin B and rifampicin combination, the previous results suggested that polymyxin itself presumably induced the secondary effect on the peptidoglycan and LPS biosynthesis (467). Thus, the present results further support the previous hypothesis on the potential of polymyxin to induce significant effect on peptidoglycan and LPS biosynthesis metabolism; the effect that resembles the primary mode of action of β -lactam antibiotic via inhibition of cell wall biosynthesis, specifically peptidoglycan (468, 469).

The significant transcriptomics and metabolomics changes induced by polymyxin B alone at 1 hr indicated that PAO1 became resistant to polymyxin B. Polymyxin resistance in *P. aeruginosa*, particularly via the adaptive resistance mechanism can lead to LPS modification; the mechanism that is tightly controlled by two-component regulatory systems (127-137). The most studied two-component systems, PmrAB and PhoPQ can be induced by a limited Mg^{2+} condition independently in the presence of polymyxins (127-134, 140). Interestingly, a novel ParRS system has been shown to be directly activated by the sub-inhibitory concentrations of polycationic peptides (e.g. polymyxin B, colistin, indolicidin) (135, 136). The two-component systems are generally comprised of sensor kinases (i.e. PmrB, PhoQ, ParS) which can either

phosphorylate or dephosphorylate the response regulators (i.e. PmrA, PhoP, ParR). The changes then activate the *arnBCADTEF* operon to modify the lipid A structure of LPS by the addition of 4-aminoarabinose (L-Ara4N). The reduced negative charge of LPS then inhibits the binding of polymyxins to permeabilise the outer membrane (127, 128, 448). The differentially over-expressed genes of the ParRS-regulated operons namely, PA1559-PA1560, PA4773-PA4775-*pmrAB* and *arnBCADTEF* only by the polymyxin B alone at 1 hr were consistent with previous studies (Figure 6.6) (135, 140, 448). In addition, the expression of these operons have also been reported to be up-regulated directly or indirectly by the PmrAB and PhoPQ systems (135, 140, 448). The occurrence of polymyxin resistance in PAO1 via lipid A modification was also highlighted by the up-regulation of UDP-glucuronate, a precursor metabolite for the L-Ara4N synthesis (Figure 6.6) (470). In addition, the mechanism of LPS alteration has been linked with a few ParRS-regulated putative genes. In particular, PA1797, a proposed lipoprotein with β -lactamases function has been speculated to play an essential role in the ParRS cascade of polymyxin resistance (135). Another gene encoding for unknown protein, PA2358, also has been previously suggested to be controlled by the ParR response regulator (135, 140). As the change pattern of PA0860 was similar to PA1797 and PA2358, the results likely suggested that the gene of PA0860 is also crucially involved in the ParRS-mediated polymyxin resistance. Interestingly, activation of the ParRS system by polymyxin B alone and the combination was likely to induce the MexXY/OprM system (140), and coincidentally, this was consistent with the significant up-regulation of MexXY genes. Furthermore, the over-expression of two DEGs of phenazine synthesis by polymyxin B alone indirectly suggests the increased PAO1 virulence, which potentially may lead to complications in patients under polymyxin monotherapy (68).

The results of metabolomics aligned well with the data of transcriptomics, as the combination synergistically increased the levels of a large number of purine and pyrimidine nucleotides of

PAO1 at 1 hr (Figure 6.7). On the contrary, the levels of a few nucleotides (e.g. 2',3'-cyclic UMP, GDP, dATP, orotate) were predominantly decreased by polymyxin B alone. The previous study showed that the effect of colistin alone and the combination with doripenem significantly depleted most of nucleotides levels in *A. baumannii* (Section 3.4.4); as the changes were similarly observed for polymyxin B alone in the present study. Nucleotides are basic components used for energy transfer in DNA and RNA biosynthesis and intermediates of lipid and protein synthesis (378, 471). Antibiotics can significantly induce nucleotide changes in bacteria and this has been shown in many studies (113, 421, 429, 467). Ciprofloxacin (421) and rifampicin (429) were reported to significantly enhance the levels of nucleotides in *Staphylococcus aureus*. The significant changes of nucleotides levels observed in the rifampicin study (429) suggested that *S. aureus* was in a state of metabolically inactive in cell turnover (i.e. turn off cell metabolism). Notably, changes in the nucleotide abundances both in the previous and our present studies were likely consistent with the effect of rifampicin to inhibit bacterial DNA transcription process, reflecting rifampicin's mode of action (262, 263, 429).

Several virulence factors in *P. aeruginosa* are regulated by the QS system (53, 451). Two homologous QS systems have been discovered in *P. aeruginosa*, *las* and *rhl* acyl-homoserine lactone (HSL) systems, generally vital for the regulation of bacterial secretory factors (451). The *las* system is composed of *lasI* (to produce *N*(3-oxo-dodecanoyl)-HSL; 3OC12-HSL) and *lasR* (as a transcriptional activator) which functionally regulate the expression of *lasA* (protease), *lasB* (elastase) and *xcpPR* (secretory pathway) (472, 473). The *rhl* system is composed of *rhlI* (to produce *N*-butyryl-HSL; C4-HSL) and *rhlR* (as a transcriptional activator) which functionally regulate the expression of *rhlAB* operon, *lasA* elastase, *lasB* elastase, pyocyanin, cyanide and alkaline protease (451). The two systems act upon each other as *lasR* activates the transcription of *rhl* system (both *rhlR* and *rhlI*) (474). Due to the significance pathogenic property of QS

system, it has been subjected as a potential antimicrobial target (53, 58, 62). Consistently, the synergistic action of the combination significantly down-regulated the expression of genes associated with QS-regulatory (i.e. *lasA*, *lasB*, *lasI*, *rhlI*, *rhlR*, *rhlB* and *rhlA*) and virulence factors (e.g. phenazine biosynthesis, *xcp* type II secretion system) at 1 hr (Table 6.3). Notably, our analysis indicated several metabolites that were significantly changed by the combination particularly can be linked to phenazine synthesis pathway. In particular, phenylpyruvate, indole, 2-oxo-3-phenylpropanoate and L-tryptophan, which are intermediate products of aromatic amino acid biosynthesis were significantly depleted by the polymyxin B and rifampicin combination. As an important precursor metabolite for aromatic amino acid biosynthesis, chorismate is also a precursor for phenazine biosynthesis particularly at the branch point of the shikimic acid pathway (475). As the aromatic amino acid pathway was significantly affected (i.e. observed by the depletion of the intermediated metabolites) by the synergistic effect of the combination, the results indirectly suggesting the metabolism of chorismate was significantly down-regulated which was consistent with repression of the phenazine biosynthesis operons (i.e. *phzA1* and *phzA2*) (Table 6.3). Furthermore, the general stress response regulator, a sigma factor *rpoS* was significantly down-regulated by the combination of polymyxin B and rifampicin (Table 6.3). In bacteria, *rpoS* is functionally regulated by the *rhl* system as a counter-measure to a variety of conditions including nutrient starvation during stationary phase, heat, osmotic and oxidative stress (476). Overall, the suppression of many genes of QS system and virulence factors in PAO1 by the synergistic killing of the combination highly supported the application of polymyxin combination therapy clinically.

Previous studies showed that antibiotic-induced cell death predominantly altered bacterial cellular respiration and central metabolism via carbon flux of TCA cycle (429, 430, 433, 434, 436). Notably, the effect of antibiotic killing also significantly increased the rate of cellular

metabolism as notified in several metabolomics and transcriptomics studies (110, 429, 431, 432). In spite of some contradictory findings, the mechanism of antibiotic killing, including polymyxins, appears to involve oxidative stress via the formation of reactive oxygen species (ROS) (108, 431, 436, 477). In particular, polymyxins have also been reported to inhibit respiratory chain enzymes (e.g. NADH-quinone oxidoreductase) (92, 109) and increase expression of superoxide dismutase (SOD) enzymes (e.g. HMPREF0010_02336, *sodB* encoding a predicted FeSOD) (412). In the present study, both metabolomics and transcriptomics data were consistent and complement each other which showed that the combination significantly induced perturbation of central carbon metabolic pathways of glycolysis, TCA cycle and PPP in PAO1 (Figure 6.8). In particular, the inhibition of phosphoenolpyruvate (via increased level) conversion to pyruvate (via decreased level) by the combination differentially down-regulated several associated genes (i.e. PA3416, PA3417), presumably suggesting the inhibition of central carbon metabolic pathway. Notably, the effect on TCA cycle and PPP perturbations has also been previously shown by colistin and doripenem alone and the combination treatment against *A. baumannii* (Section 3.4.4).

P. aeruginosa is capable of growing in both aerobic and anaerobic environments (458). Oxygen is required as the terminal electron acceptor in an aerobic respiration process, whereas, nitrate is alternatively used in anaerobic conditions, also known as the denitrification process (458). Denitrification is the process of nitrate reduction to dinitrogen, and is generally comprised of four sequential steps (458). The first step involves the reduction of nitrate to nitrite mediated by respiratory nitrate reductase. Nitrate needs to enter and bind to its binding site that is located on the cytoplasmic side of membrane and this requires a nitrate/nitrite transporter (encoded by the *narK1K2GHJI* operon). Nitrite is then reduced to nitric oxide catalysed by the periplasmic cytochrome cd1 nitrite reductase NirS. The enzyme contains heme *c* and heme *d₁* cofactors, as

the latter is the enzyme catalytic domain (encoded by the *nirSMCFDLGHJEN* operon) (459). In this study, the significant up-regulation of the *narK1K2GHJI* operon of the nitrate uptake system by the combination presumably suggests that PAO1 requires nitrate as their energy source to maintain redox homeostasis. The process of nitrate uptake was very likely initiated by the significant suppression of terminal cytochrome oxidase genes of aerobic electron transfer particularly PA0521, *norB*, *cioB*, *cioA* and PA4133 (Table 6.3). However, the significant down-regulation of the *nirSMCFDLGHJEN* operon (Table 6.3), functionally important for nitrite reduction likely suggests that the denitrification process was incomplete.

At 24 hr, a large number of DEGs were commonly induced by rifampicin alone and the combination, suggesting that rifampicin was primarily responsible for the transcriptomics response (Figure 6.1B and Table 5.5). However, only a few significantly changed metabolites could be identified in rifampicin alone and the combination at 24 hr likely indicating that PAO1 was metabolically stable. Interestingly, the identification of 15 common DEGs following treatment with polymyxin B and rifampicin mono- and the combination likely were the general antibiotic-induced changes of PAO1 at 24 hr (Table 5.6). The significant over-expression of several QS-regulatory and virulence factor genes by the combination at 24 hr highlighted the increase of virulence of the bacteria, in contrast to its effect at 1 hr. Moreover, at 24 hr rifampicin alone and the combination differentially up-regulated *sodM*, suggesting a mechanism of oxidative stress in PAO1, likely driven by the effect of rifampicin treatment (461). Rifampicin resistance is attributed by the missense mutation of *rpoB*, a gene encoding for the β subunit of bacterial RNA polymerase, rifampicin's specific binding target which leads into structural modification of the enzyme (263, 462-464). Significant suppression of *rpoB* by rifampicin alone and the combination likely indicating the reduced expression of RNA polymerase's β subunit

and binding capacity of rifampicin to the enzyme, importantly conferred the PAO1 resistance to rifampicin.

Polymyxin B and rifampicin distinctively display their primary modes of bacterial killing against different cellular targets (98, 263). Polymyxin-induced cell death is initiated by the ‘self-promoted uptake’ pathway via the electrostatic binding to a lipid A domain of LPS which leads to membrane disorganisation and osmotic imbalance (98, 375). Whereas, rifampicin exhibits strong and specific binding affinity towards bacterial RNA polymerase, which functionally inhibits the transcriptional elongation process during RNA synthesis (263). The overall metabolomic and transcriptomic changes of the combination suggested that the synergy was predominantly conferred by the intracellular effect of rifampicin, as its action was initially facilitated by polymyxin B. As the mode of action of rifampicin is functionally to block bacterial RNA synthesis, therefore this is consistent with the observed metabolomic and transcriptomic changes (263, 462-464). The abundance of metabolites (e.g. nucleotides, amino acids) induced by the combination suggesting that the PAO1 was in a state of metabolic inactivity. Interestingly, the synergistic killing of the combination has been previously elucidated which proposed that colistin predominantly caused outer membrane disturbance to facilitate the uptake of rifampicin into its intracellular target (234, 249). Notably, the relative hydrophobic property of rifampicin confers the antibiotic less permeable to cross the outer membrane of Gram-negative bacteria, likely supporting the lack of significant metabolomic changes when administered as a single treatment (263).

6.6 Conclusions

To the best of our knowledge, this PhD study is the first to investigate the synergistic mechanism of the combination of polymyxin B and rifampicin against *P. aeruginosa* applying an integrated

metabolomics and transcriptomics GSMN analysis. The association of cellular metabolite changes and gene expression changes is commonly influenced by several factors including post-transcriptional alterations and protein expression (478). Although complex interactions are expected, we identified that the metabolomic and transcriptomic data aligned well with each other. Overall, this study highlights the importance of understanding the complex bacterial metabolic and transcriptomic responses either to a single or to combination polymyxin treatments at different time points. Taking into consideration the early effect of polymyxin B alone to induce resistance, the synergistic killing of the combination and suppression of bacterial virulence highly supports the application of polymyxin combination therapy in patients. Lastly, the emergence of polymyxin B and rifampicin resistance at different time intervals, at 1 hr and 24 hr, respectively, signify the clinical importance of PK/PD optimisation of both antibiotics.

Chapter Seven

Chapter 7: Conclusions and Future Perspectives

The treatment of life-threatening infections using polymyxins has become indispensable due to two main factors; the rapid emergence of MDR clinical isolates and the failure of current drug discovery and development pipelines to supply novel antibiotic compounds (354). Polymyxins exhibit rapid bactericidal action against susceptible Gram-negative bacteria via an initial electrostatic interaction with the phosphate groups of the lipid A component of LPS, followed by non-polar interactions of the hydrophobic domains with the bacterial outer membrane (11, 400). Although much has been done to understand the complete action of polymyxin, the ultimate mechanism of polymyxin-induced cell death is still not completely understood.

The reported PK/PD profiles of polymyxins revealed that polymyxin monotherapy is unlikely to generate optimal plasma concentrations in patients (81, 189, 197, 213-216). Moreover, monotherapy likely to induce resistance in Gram-negative bacterial isolates (e.g. *A. baumannii* and *P. aeruginosa*) due to the existence of a small sub-population of polymyxin resistant cells (heteroresistant subpopulation) being present in largely polymyxin susceptible population (45, 227). Therefore, polymyxin combination therapy has been proposed as a solution to the problem of polymyxin monotherapy and is being increasingly utilised in the hospital setting (81, 214). As the use of polymyxins is an essential, last-line, treatment option that is currently available, full optimisation of its clinical potential is highly required. The key focus of this PhD research was to provide essential information on the mechanism of polymyxin action and bacterial resistance. This information is crucial to allow us to facilitate the optimisation of PK/PD of polymyxins and the discovery of potential novel drug targets.

In this project, for the first time, we performed a comparative, LCMS-based, untargeted metabolomics study of MDR *A. baumannii* to profile global metabolic differences between pairs

of polymyxin-susceptible and -resistant *A. baumannii* strains without antibiotic treatment (Chapter 2). Substantial metabolic state differences were identified between the polymyxin-susceptible parent strain, ATCC 19606 and its polymyxin-resistant strain, 19606R, which is resistant due to the complete loss of the LPS component lipid A, the initial target molecule for polymyxin (44, 122). Metabolic analysis of the LPS-deficient, polymyxin-resistant strain indicated there was significant perturbation in the production of specific amino acid and carbohydrate metabolites, particularly intermediates within the PPP and TCA cycle. The LPS-deficient 19606R also exhibited a lower abundance of nucleotides and had a unique lipid profile pattern that included a significant increase in short-chain glycerophospholipids. In contrast, there were few metabolic changes identified between the paired clinical isolates 03-149.1 (polymyxin-susceptible) and the derivative strain 03-149.2 (122). In contrast to the LPS-deficient 19606R, strain 03-149.2 is polymyxin-resistant due to a mutation in *pmrB* that is required for the modification of lipid A with phosphoethanolamine and galactosamine (122). Interestingly, both polymyxin-resistant strains, 19606R and 03-149.2 were significantly depleted in metabolites associated with peptidoglycan biosynthesis, compared to the parent strains.

A. baumannii can rapidly become resistant to many clinically available antibiotics, and the use of drug combinations can be effectively deployed to treat infections caused by this MDR superbug. *In vitro* studies using polymyxins and carbapenems in combination have shown that they have a synergistic action against a range of MDR Gram-negative bacteria including *A. baumannii*, *P. aeruginosa* and *K. pneumoniae* (222-226, 407). In Chapter 3, we undertook a study investigating the effect of combination treatment consisting of colistin (2 mg/L) plus doripenem (25 mg/L) against polymyxin-susceptible (ATCC 19606, 03-149.1) and polymyxin-resistant (03-149.2) MDR *A. baumannii* strains. To do this, time-kill experiments (with samples taken at 15 min, 1 hr and 4 hr) were conducted and the mechanism of synergy was elucidated

using untargeted metabolomics analysis. This study was the first to report that the colistin plus doripenem combination treatment synergistically killed *A. baumannii* via the time-dependent inhibition of a number of key metabolic pathways (467). In colistin-susceptible *A. baumannii*, colistin predominantly induced early (15 min and 1 hr) disruption of the bacterial outer membrane and the cell wall, as demonstrated by the perturbation of glycerophospholipid and fatty acid production. Doripenem acts via the inhibition of peptidoglycan cell wall synthesis and there was a notable decrease in the amount of peptidoglycan biosynthesis metabolites following treatment with doripenem alone (particularly at 4 hr) and in combination (across 4 hr). The synergistic action of the combination treatment significantly down-regulated the bacterial cell wall biosynthesis (via D-sedoheptulose 7-phosphate and D-ribulose 5-phosphate) and nucleotide metabolism (via D-ribose 5-phosphate and PRPP) predominantly via metabolic changes within the PPP. On the contrary, *A. baumannii* polymyxin-resistant strain, 03-149.2, displayed changes (e.g. increase levels of nucleotides and amino acid metabolites) that were presumably associated with the general antibiotic stress response that is induced by the colistin treatment, alone and in combination. Overall, this study highlights the significant potential of systems pharmacology to elucidate the mechanism of antibiotic synergy and to optimise antibiotic PK/PD.

The mode of action of polymyxins was further investigated using polymyxin B in combination with other antibiotics to treat MDR isolates from other bacterial species, particularly *P. aeruginosa*. The combination of polymyxin plus rifampicin has previously been demonstrated to be synergistic, both *in vitro* and in the clinical setting, against a number of MDR Gram-negative bacteria including *A. baumannii*, *P. aeruginosa* and *K. pneumoniae* (231-236). To investigate the synergistic action of a polymyxin B (1 mg/L) and rifampicin (2 mg/L) combination against *P. aeruginosa* PAO1, a series of a time interval experiments were performed followed by global metabolomics (Chapter 4) and transcriptomics (Chapter 5) analyses.

Polymyxin B, alone and in combination with rifampicin, significantly altered the PAO1 lipid metabolism at the 15 min, 1 hr and 4 hr time points, correlating well with its known effect to cause general membrane disruption and as has been observed in *A. baumannii* (Chapter 2). There was an increase in abundance of many metabolites in key metabolic pathways (i.e. nucleotides, amino acids, central carbon metabolism [TCA cycle, glycolysis, PPP], peptidoglycan and LPS biosynthesis) in response to polymyxin B and rifampicin combination treatment signifying synergistic action. The results also indicated that PAO1 was metabolically inactive (due to a halt in metabolism), correlating with the known action of rifampicin as an inhibitor of RNA synthesis. Furthermore, there was a significant over-expression of genes that is particularly involved in the ParRS two-component regulatory system in response to polymyxin B monotherapy at 1 hr. This up-regulated system controls lipid A modification (via an addition of 4-aminoarabinose [L-Ara4N]) and the expression of multidrug efflux proteins which resulted in the emergence of polymyxin resistance in PAO1. In addition, the up-regulation of phenazine biosynthesis suggesting the increase of PAO1 virulence by the polymyxin B monotherapy. The synergistic killing of polymyxin B and rifampicin combination treatment significantly down-regulated the production of many cellular virulence factors regulated by quorum sensing (QS) system perhaps signifying reduced bacterial pathogenicity which would be clinically important in treating PAO1 infection. In addition, the combination treatment led to an up-regulation in the nitrate uptake system and the down-regulation of terminal cytochrome oxidase suggesting that *P. aeruginosa* PAO1 required nitrate as an alternative energy source to maintain its redox homeostasis during treatment. Notably, there was a significant down-regulation of expression from the rifampicin resistance gene (*rpoB*) at the 24 hr time point during rifampicin alone and the combination therapy, indicating an emergence of rifampicin resistance.

In the final results chapter of this thesis (Chapter 6), the metabolomic and transcriptomic data were integrated and analysed using a genome-scale metabolic network (GSMN) constructed for the *P. aeruginosa* strain, PAO1. The results generated from the PAO1 metabolomic data proved to be complementary to the transcriptomic data as demonstrated by significant changes in key metabolic and regulatory pathways (i.e. perturbation of lipids, nucleotide, amino acid, central carbon metabolism [TCA cycle, glycolysis, PPP], peptidoglycan and LPS biosynthesis) particularly in response to the combination treatment of polymyxin B and rifampicin. The results of the integrated study showed that the synergistic action of the combination of polymyxin B and rifampicin fits well with the “simple uptake effect” model (250) as the observed response was driven predominantly by rifampicin and facilitated by the action of polymyxin B.

The vast information gained from this PhD project significantly provides invaluable insights into the mechanisms of polymyxin actions and resistance. Importantly, the many significant hypotheses generated from the global metabolomic and transcriptomic studies need to be further explored and confirmed by a targeted approach. In-depth understanding of structural and functional importance of the significantly changed metabolites and genes, including the known and unknown compounds is highly required as this can potentially lead to the discovery of new class of compounds. Structural annotation and elucidation of unknown entities can be reached by an extended analytical method for example by NMR and MS/MS spectrum analysis. Whereas it's functional significance can be potentially determined by the analysis of available mutant libraries. In addition, direct association between the significantly identified metabolites and genes of particular metabolic reactions potentially can be further detailed by subsequent recombinant protein study. To further investigate the mechanism of polymyxin action, other layers of omics approaches such as proteomics, peptidomics and lipidomics could be adopted. This integrative approach will provide information at different cellular levels that are

complementary to each other essential for developing and supporting new hypothesis. Furthermore, an advanced GSMN analysis of an integrated omics with a stoichiometric model of bacterial metabolism and flux simulation could be performed to analyse the metabolic potential and fates, particularly of *P. aeruginosa* (348, 479).

In conclusion, extensive data presented in this PhD project is a significant contribution towards advancing our knowledge on the mode of polymyxin action and the development of resistance. The complement of metabolomics and transcriptomics data set will provide comprehensive understanding of the complex cellular polymyxin interactions which will be invaluable for the PK/PD optimisation of polymyxins. In addition, our data provide key information that will aid in the discovery of novel drug targets particularly of polymyxins. Last but not least, this study will allow for improved use of polymyxins in the clinical setting and the development of a new generation of polymyxin drugs.

References

1. Jones KE, Patel NG, Levy MA, Storeygard A, Balk D, Gittleman JL, Daszak P. Global trends in emerging infectious diseases. *Nature*. 2008;451(7181):990-3.
2. Ventola CL. The antibiotic resistance crisis: part 1: causes and threats. *P T*. 2015;40(4):277-83.
3. Alekshun MN, Levy SB. Molecular mechanisms of antibacterial multidrug resistance. *Cell*. 2007;128(6):1037-50.
4. O'Neill J. Review on antimicrobial resistance. Antimicrobial resistance: tackling a crisis for the health and wealth of nations. 2014. Available at: https://www.his.org.uk/files/4514/1829/6668/AMR_Review_Paper_-_Tackling_a_crisis_for_the_health_and_wealth_of_nations_1.pdf (Accessed: 12 June 2017).
5. Schaberle TF, Hack IM. Overcoming the current deadlock in antibiotic research. *Trends Microbiol*. 2014;22(4):165-7.
6. Boucher HW, Talbot GH, Bradley JS, Edwards JE, Gilbert D, Rice LB, Scheld M, Bartlett J. Bad bugs, no drugs: no ESKAPE! An update from the Infectious Diseases Society of America. *Clin Infect Dis*. 2009;48(1):1-12.
7. Rice LB. Federal funding for the study of antimicrobial resistance in nosocomial pathogens: No ESKAPE. *J Infect Dis*. 2008;197(8):1079-81.
8. Eurosurveillance editorial team. CDC publishes report on antibiotic resistance threats in the United States for the first time. *Euro Surveill*. 2013;18(38):pii=20588. Available at: <http://www.eurosurveillance.org/ViewArticle.aspx?ArticleId=20588> (Accessed: 12 June 2017).
9. World Health Organization (WHO). Global priority list of antibiotic-resistant bacteria to guide research, discovery, and development of new antibiotics. 2017. Available at: <http://www.who.int/medicines/publications/global-priority-list-antibiotic-resistant-bacteria/en/> (Accessed: 12 June 2017).
10. Gilbert DN, Guidos RJ, Boucher HW, Talbot GH, Spellberg B, Edwards JE Jr, Scheld WM, Bradley JS, Bartlett JG. The 10 x '20 Initiative: pursuing a global commitment to develop 10 new antibacterial drugs by 2020. *Clin Infect Dis*. 2010;50(8):1081-3.
11. Velkov T, Roberts KD, Nation RL, Thompson PE, Li J. Pharmacology of polymyxins: new insights into an 'old' class of antibiotics. *Future Microbiol*. 2013;8(6):711-24.
12. Peleg AY, Seifert H, Paterson DL. *Acinetobacter baumannii*: emergence of a successful pathogen. *Clin Microbiol Rev*. 2008;21(3):538-82.
13. Maragakis LL, Perl TM. *Acinetobacter baumannii*: Epidemiology, antimicrobial resistance, and treatment options. *Clin Infect Dis*. 2008;46(8):1254-63.
14. Bassetti M, Righi E, Esposito S, Petrosillo N, Nicolini L. Drug treatment for multidrug-resistant *Acinetobacter baumannii* infections. *Future Microbiol*. 2008;3(6):649-60.
15. Shields RK, Kwak EJ, Potoski BA, Doi Y, Adams-Haduch JM, Silveira FP, Toyoda Y, Pilewski JM, Crespo M, Pasculle AW, Clancy CJ, Nguyen MH. High mortality rates among solid organ transplant recipients infected with extensively drug-resistant *Acinetobacter baumannii*: using in vitro antibiotic combination testing to identify the combination of a carbapenem and colistin as an effective treatment regimen. *Diagn Microbiol Infect Dis*. 2011;70(2):246-52.
16. Shields RK, Clancy CJ, Gillis LM, Kwak EJ, Silveira FP, Massih RCA, Eschenauer GA, Potoski BA, Nguyen MH. Epidemiology, clinical characteristics and outcomes of extensively drug-resistant *Acinetobacter baumannii* infections among solid organ transplant recipients. *PLoS One*. 2012;7(12).
17. Howard A, O'Donoghue M, Feeney A, Sleator RD. *Acinetobacter baumannii*: an emerging opportunistic pathogen. *Virulence*. 2012;3(3):243-50.

18. Choi CH, Lee EY, Lee YC, Park TI, Kim HJ, Hyun SH, Kim SA, Lee SK, Lee JC. Outer membrane protein 38 of *Acinetobacter baumannii* localizes to the mitochondria and induces apoptosis of epithelial cells. *Cell Microbiol.* 2005;7(8):1127-38.
19. McConnell MJ, Actis L, Pachon J. *Acinetobacter baumannii*: human infections, factors contributing to pathogenesis and animal models. *FEMS Microbiol Rev.* 2013;37(2):130-55.
20. Kim BN, Peleq AY, Lodise TP, Lipman J, Li J, Nation R, Peterson DL. Management of meningitis due to antibiotic-resistant *Acinetobacter* species. *Lancet Infect Dis.* 2009;9(4):245-55.
21. Akers KS, Chaney C, Barsoumian A, Beckius M, Zera W, Yu X, Guymon C, Keen EF, Robinson BJ, Mende K, Murray CK. Aminoglycoside resistance and susceptibility testing errors in *Acinetobacter baumannii-calcoaceticus* complex. *J Clin Microbiol.* 2010;48(4):1132-38.
22. Gao L, Lyu Y, Li Y. Trends in drug resistance of *Acinetobacter baumannii* over a 10-year period: nationwide data from the China surveillance of antimicrobial resistance program. *Chin Med J (Engl).* 2017;130(6):659-64.
23. Durante-Mangoni E, Zarrilli R. Global spread of drug-resistant *Acinetobacter baumannii*: molecular epidemiology and management of antimicrobial resistance. *Future Microbiol.* 2011;6(4):407-22.
24. Vallenet D, Nordmann P, Barbe V, Poirel L, Mangenot S, Bataille E, Dossat C, Gas S, Kreimeyer A, Lenoble P, Oztas S, Poulain J, Segurens B, Robert C, Abergel C, Claverie JM, Raoult D, Medigue C, Weissenbach J, Cruveiller S. Comparative analysis of *Acinetobacter*: three genomes for three lifestyles. *PLoS One.* 2008;3(3):e1805.
25. Iacono M, Villa L, Fortini D, Bordoni R, Imperi F, Bonnal RJ, Sicheritz-Ponten T, De Bellis G, Visca, Cassone A, Carattoli A. Whole-genome pyrosequencing of an epidemic multidrug-resistant *Acinetobacter baumannii* strain belonging to the European clone II group. *Antimicrob Agents Chemother.* 2008;52(7):2616-25.
26. Adams MD, Goglin K, Molyneaux N, Hujer KM, Lavender H, Jamison JJ, MacDonald IJ, Martin KM, Russo T, Campagnari AA, Hujer AM, Bonomo RA, Grill SR. Comparative genome sequence analysis of multidrug-resistant *Acinetobacter baumannii*. *J Bacteriol.* 2008;190(24):8053-64.
27. Poirel L, Nordmann P. Genetic structures at the origin of acquisition and expression of the carbapenem-hydrolyzing oxacillinase gene bla(OXA-58) in *Acinetobacter baumannii*. *Antimicrob Agents Chemother.* 2006;50(4):1442-8.
28. Zarrilli R, Vitale D, Di Popolo A, Bagattini M, Daoud Z, Khan AU, Afif C, Triassi M. A Plasmid-borne bla(OXA-58) gene confers imipenem resistance to *Acinetobacter baumannii* isolates from a Lebanese hospital. *Antimicrob Agents Chemother.* 2008;52(11):4115-20.
29. D'Andrea MM, Giani T, D'Arezzo S, Capone A, Petrosillo N, Visca P, Luzzaro F, Rosolini GM. Characterization of pABVA01, a plasmid encoding the OXA-24 carbapenemase from Italian isolates of *Acinetobacter baumannii*. *Antimicrob Agents Chemother.* 2009;53(8):3528-33.
30. Merino M, Acosta J, Poza M, Sanz F, Beceiro A, Chaves F, Bou G. OXA-24 carbapenemase gene flanked by XerC/XerD-like recombination sites in different plasmids from different *Acinetobacter* species isolated during a nosocomial outbreak. *Antimicrob Agents Chemother.* 2010;54(6):2724-7.
31. Chen TL, Wu RCC, Shaio MF, Fung CP, Cho WL. Acquisition of a plasmid-borne bla(OXA-58) gene with an upstream IS1008 insertion conferring a high level of carbapenem resistance to *Acinetobacter baumannii*. *Antimicrob Agents Chemother.* 2008;52(7):2573-80.
32. Adam MD, Chan ER, Molyneaux ND, Bonomo RA. Genome wide analysis of divergence of antibiotic resistance determinants in closely related isolates of *Acinetobacter baumannii*. *Antimicrob Agents Chemother.* 2010;54(9):3569-77.

33. Higgins PG, Wisplinghoff H, Stefanik D, Seifert H. Selection of topoisomerase mutations and overexpression of adeB mRNA transcripts during an outbreak of *Acinetobacter baumannii*. J Antimicrob Chemother. 2004;54(4):821-3.
34. Vila J, Ruiz J, Goni P, Marcos A, Jimenez de Anta T. Mutation in the *gyrA* gene of quinolone-resistant clinical isolates of *Acinetobacter baumannii*. Antimicrob Agents Chemother. 1995;39(5):1201-3.
35. Hu WS, Yao SM, Fung CP, Hsieh YP, Liu CP, Lin JF. An OXA-66/OXA-51-like carbapenemase and possibly an efflux pump are associated with resistance to imipenem in *Acinetobacter baumannii*. Antimicrob Agents Chemother. 2007;51(11):3844-52.
36. Coyne S, Courvalin P, Perichon B. Efflux-mediated antibiotic resistance in *Acinetobacter* spp. Antimicrob Agents Chemother. 2011;55(3):947-53.
37. Ruzin A, Keeney D, Bradford PA. AdeABC multidrug efflux pump is associated with decreased susceptibility to tigecycline in *Acinetobacter calcoaceticus*-*Acinetobacter baumannii* complex. J Antimicrob Chemother. 2007;59(5):1001-4.
38. Peleg AY, Adams J, D.L. P. Tigecycline efflux as a mechanism for nonsusceptibility in *Acinetobacter baumannii*. Antimicrob Agents Chemother. 2007;51(6):2065-9.
39. Gehrlein M, Leying H, Cullmann W, Wendt S, Opferkuch W. Imipenem resistance in *Acinetobacter baumannii* is due to altered penicillin-binding proteins. Chemotherapy. 1991;37(6):405-12.
40. Mussi MA, Limansky AS, Viale AM. Acquisition of resistance to carbapenems in multidrug-resistant clinical strains of *Acinetobacter baumannii*: natural insertional inactivation of a gene encoding a member of a novel family of beta-barrel outer membrane proteins. Antimicrob Agents Chemother. 2005;49(4):1432-40.
41. Beceiro A, Llobet E, Aranda J, Bengoechea JA, Doumith M, Hornsey M, Dhanji H, Chart H, Bou G, Livermore DM, Woodford N. Phosphoethanolamine modification of lipid A in colistin-resistant variants of *Acinetobacter baumannii* mediated by the *pmrAB* two-component regulatory system. Antimicrob Agents Chemother. 2011;55(7):3370-9.
42. Arroyo LA, Herrera CM, Fernandez L, Hankins JV, Trent MS, Hancock RE. The *pmrCAB* operon mediates polymyxin resistance in *Acinetobacter baumannii* ATCC 17978 and clinical isolates through phosphoethanolamine modification of lipid A. Antimicrob Agents Chemother. 2011;55(8):3743-51.
43. Pelletier MR, Casella LG, Jones JW, Adams MD, Zurawski DV, Hazlett KR, Doi Y, Ernst RK. Unique structural modifications are present in the lipopolysaccharide from colistin-resistant strains of *Acinetobacter baumannii*. Antimicrob Agents Chemother. 2013;57(10):4831-40.
44. Moffatt JH, Harper M, Harrison P, Hale JDF, Vinogradov E, Seemann T, Henry R, Crane B, St Michael F, Cox AD, Adler B, Nation RL, Li J, Boyce JD. Colistin resistance in *Acinetobacter baumannii* is mediated by complete loss of lipopolysaccharide production. Antimicrob Agents Chemother. 2010;54(12):4971-7.
45. Li J, Rayner CR, Nation RL, Owen RJ, Spelman D, Tan KE, Liolios L. Heteroresistance to colistin in multidrug-resistant *Acinetobacter baumannii*. Antimicrob Agents Chemother. 2006;50(9):2946-50.
46. Hawley JS, Murray CK, Jorgensen JH. Colistin heteroresistance in *Acinetobacter* and its association with previous colistin therapy. Antimicrob Agents Chemother. 2008;52(1):351-2.
47. Tan CH, Li J, Nation RL. Activity of colistin against heteroresistant *Acinetobacter baumannii* and emergence of resistance in an in vitro pharmacokinetic/pharmacodynamic model. Antimicrob Agents Chemother. 2007;51(9):3413-5.
48. Kassamali Z, Jain R, Danziger LH. An update on the arsenal for multidrug-resistant *Acinetobacter* infections: polymyxin antibiotics. Int J Infect Dis. 2015;30:125-32.

49. Lister PD, Wolter DJ, Hanson ND. Antibacterial-resistant *Pseudomonas aeruginosa*: clinical impact and complex regulation of chromosomally encoded resistance mechanisms. Clin Microbiol Rev. 2009;22(4):582-610.
50. Lyczak JB, Cannon CL, Pier GB. Establishment of *Pseudomonas aeruginosa* infection: lessons from a versatile opportunist. Microbes Infect. 2000;2(9):1051-60.
51. Sadikot RT, Blackwell TS, Christman JW, Prince AS. Pathogen-host interactions in *Pseudomonas aeruginosa* pneumonia. Am J Respir Crit Care Med. 2005;171(11):1209-23.
52. Overhage J, Schemionek M, Webb JS, Rehm BH. Expression of the *psl* operon in *Pseudomonas aeruginosa* PAO1 biofilms: *PslA* performs an essential function in biofilm formation. Appl Environ Microbiol. 2005;71(8):4407-13.
53. Wagner S, Sommer R, Hinsberger S, Lu C, Hartmann RW, Empting M, Titz A. Novel strategies for the treatment of *Pseudomonas aeruginosa* infections. J Med Chem. 2016;59(13):5929-69.
54. Winstanley C, O'Brien S, Brockhurst MA. *Pseudomonas aeruginosa* evolutionary adaptation and diversification in cystic fibrosis chronic lung infections. Trends Microbiol. 2016;24(5):327-37.
55. Hirsch EB, Tam VH. Impact of multidrug-resistant *Pseudomonas aeruginosa* infection on patient outcomes. Expert Rev Pharmacoecon Outcomes Res. 2010;10(4):441-51.
56. Gellatly SL, Hancock RE. *Pseudomonas aeruginosa*: new insights into pathogenesis and host defenses. Pathog Dis. 2013;67(3):159-73.
57. Whiteley M, Lee KM, Greenberg EP. Identification of genes controlled by quorum sensing in *Pseudomonas aeruginosa*. Proc Natl Acad Sci USA. 1999;96(24):13904-9.
58. Smith RS, Iglewski BH. *Pseudomonas aeruginosa* quorum sensing as a potential antimicrobial target. J Clin Invest. 2003;112(10):1460-5.
59. Chugani SA, Whiteley M, Lee KM, D'Argenio D, Manoil C, Greenberg EP. QscR, a modulator of quorum-sensing signal synthesis and virulence in *Pseudomonas aeruginosa*. Proc Natl Acad Sci USA. 2001;98(5):2752-7.
60. Rumbaugh KP, Griswold JA, Iglewski BH, Hamood AN. Contribution of quorum sensing to the virulence of *Pseudomonas aeruginosa* in burn wound infections. Infect Immun. 1999;67(11):5854-62.
61. Pearson JP, Feldman M, Iglewski BH, Prince A. *Pseudomonas aeruginosa* cell-to-cell signaling is required for virulence in a model of acute pulmonary infection. Infect Immun. 2000;68(7):4331-4.
62. Rasamiravaka T, Labtani Q, Duez P, El Jaziri M. The formation of biofilms by *Pseudomonas aeruginosa*: a review of the natural and synthetic compounds interfering with control mechanisms. Biomed Res Int. 2015;2015:759348.
63. Hentzer M, Wu H, Andersen JB, Riedel K, Rasmussen TB, Bagge N, Kumar N, Schembri MA, Song Z, Kristofferson P, Manefield M, Costerton JW, Molin S, Eberl L, Steinberg P, Kjelleberg S, Hoiby N, Giskov M. Attenuation of *Pseudomonas aeruginosa* virulence by quorum sensing inhibitors. EMBO J. 2003;22(15):3803-15.
64. Hentzer M, Givskov M. Pharmacological inhibition of quorum sensing for the treatment of chronic bacterial infections. J Clin Invest. 2003;112(9):1300-7.
65. Molinari G, Guzman CA, Pesce A, Schito GC. Inhibition of *Pseudomonas aeruginosa* virulence factors by subinhibitory concentrations of azithromycin and other macrolide antibiotics. J Antimicrob Chemother. 1993;31(5):681-8.
66. Morita Y, Tomida J, Kawamura Y. Responses of *Pseudomonas aeruginosa* to antimicrobials. Front Microbiol. 2014;4:422.
67. Skindersoe ME, Alhede M, Phipps R, Yang L, Jensen PO, Rasmussen TB, Bjarnsholt T, Tolker-Nielsen T, Hoiby N, Giskov M. Effects of antibiotics on quorum sensing in *Pseudomonas aeruginosa*. Antimicrob Agents Chemother. 2008;52(10):3648-63.

68. Cummins J, Reen FJ, Baysse C, Mooij MJ, O'Gara F. Subinhibitory concentrations of the cationic antimicrobial peptide colistin induce the pseudomonas quinolone signal in *Pseudomonas aeruginosa*. *Microbiology*. 2009;155(Pt 9):2826-37.
69. Hoffmann N, Lee B, Hentzer M, Rasmussen TB, Song Z, Johansen HK, Giskov M, Hoiby N. Azithromycin blocks quorum sensing and alginate polymer formation and increases the sensitivity to serum and stationary-growth-phase killing of *Pseudomonas aeruginosa* and attenuates chronic *P. aeruginosa* lung infection in Cftr(-/-) mice. *Antimicrob Agents Chemother*. 2007;51(10):3677-87.
70. Nalca Y, Jansch L, Bredenbruch F, Geffers R, Buer J, Haussler S. Quorum-sensing antagonistic activities of azithromycin in *Pseudomonas aeruginosa* PAO1: a global approach. *Antimicrob Agents Chemother*. 2006;50(5):1680-8.
71. Tateda K, Comte R, Pechere JC, Kohler T, Yamaguchi K, Van Delden C. Azithromycin inhibits quorum sensing in *Pseudomonas aeruginosa*. *Antimicrob Agents Chemother*. 2001;45(6):1930-3.
72. Lambert PA. Mechanisms of antibiotic resistance in *Pseudomonas aeruginosa*. *J R Soc Med*. 2002;95 Suppl 41:22-6.
73. Hoiby N, Ciofu O, Bjarnsholt T. *Pseudomonas aeruginosa* biofilms in cystic fibrosis. *Future Microbiol*. 2010;5(11):1663-74.
74. Costerton JW, Stewart PS, Greenberg EP. Bacterial biofilms: a common cause of persistent infections. *Science*. 1999;284(5418):1318-22.
75. Yoshimura F, Nikaido H. Permeability of *Pseudomonas aeruginosa* outer membrane to hydrophilic solutes. *J Bacteriol*. 1982;152(2):636-42.
76. Strateva T, Yordanov D. *Pseudomonas aeruginosa* - a phenomenon of bacterial resistance. *J Med Microbiol*. 2009;58(Pt 9):1133-48.
77. Stover CK, Pham XQ, Erwin AL, Mizoguchi SD, Warren P, Hickey MJ, Brinkman FS, Hufnagle WO, Kowalik DJ, Lagrou M, Garber RL, Goltry L, Tolentino E, Westbrook-Wadman S, Yuan Y, Brody LL, Coulter SN, Folger KR, Kas A, Larbig K, Lim R, Smith K, Spencer D, Wong GK, Wu Z, Paulsen IT, Reizer J, Saier MH, Hancock RE, Lory S, Olson MV. Complete genome sequence of *Pseudomonas aeruginosa* PAO1, an opportunistic pathogen. *Nature*. 2000;406(6799):959-64.
78. Livermore DM. Multiple mechanisms of antimicrobial resistance in *Pseudomonas aeruginosa*: our worst nightmare? *Clin Infect Dis*. 2002;34(5):634-40.
79. Storm DR, Rosenthal KS, Swanson PE. Polymyxin and related peptide antibiotics. *Annu Rev Biochem*. 1977;46:723-63.
80. Arnold TM, Forrest GN, Messmer KJ. Polymyxin antibiotics for Gram-negative infections. *Am J Health Syst Pharm*. 2007;64(8):819-26.
81. Bergen PJ, Landersdorfer CB, Zhang J, Zhao M, Lee HJ, Nation RL, Li J. Pharmacokinetics and pharmacodynamics of 'old' polymyxins: what is new? *Diagn Microbial Infect Dis*. 2012;74(3):213-23.
82. Falagas ME, Kasiakou SK. Toxicity of polymyxins: a systematic review of the evidence from old and recent studies. *Crit Care*. 2006;10(1):R27.
83. Orwa JA, Govaerts C, Busson R, Roets E, Van Schepdael A, Hoogmartens J. Isolation and structural characterization of colistin components. *J Antibiot (Tokyo)*. 2001;54(7):595-9.
84. Finking R, Marahiel MA. Biosynthesis of nonribosomal peptides. *Ann Rev Microbiol*. 2004;58:453-88.
85. Gallardo-Godoy A, Muldoon C, Becker B, Elliott AG, Lash LH, Huang JX, Butler MS, Pelingon R, Kavanagh AM, Ramu S, Phetsang W, Blacskovich MA, Cooper MA. Activity and predicted nephrotoxicity of synthetic antibiotics based on polymyxin B. *J Med Chem*. 2016;59(3):1068-77.

86. Yahav D, Farbman L, Leibovici L, Paul M. Colistin: new lessons on an old antibiotic. *Clin Microbiol Infect.* 2012;18(1):18-29.
87. Nikaido H. Molecular basis of bacterial outer membrane permeability revisited. *Microbiol Mol Biol Rev.* 2003;67(4):593-656.
88. Beveridge TJ. Structures of Gram-negative cell walls and their derived membrane vesicles. *J Bacteriol.* 1999;181(16):4725-33.
89. Needham BD, Trent MS. Fortifying the barrier: the impact of lipid A remodelling on bacterial pathogenesis. *Nat Rev Microbiol.* 2013;11(7):467-81.
90. Ruiz N, Kahne D, Silhavy TJ. Transport of lipopolysaccharide across the cell envelope: the long road of discovery. *Nat Rev Microbiol.* 2009;7(9):677-83.
91. Yu Z, Qin W, Lin J, Fang S, Qiu J. Antibacterial mechanisms of polymyxin and bacterial resistance. *Biomed Res Int.* 2015;2015:679109.
92. Deris ZZ, Akter J, Sivanesan S, Roberts KD, Thompson PE, Nation RL, Li J, Velkov T. A secondary mode of action of polymyxins against Gram-negative bacteria involves the inhibition of NADH-quinone oxidoreductase activity. *J Antibiot (Tokyo).* 2014;67(2):147-51.
93. Galizzi A, Cacco G, Siccardi AG, Mazza G. Mode of action of polymyxin B: physiological studies with *Bacillus subtilis*-resistant mutant. *Antimicrob Agents Chemother.* 1975;8(3):366-9.
94. HsuChen CC, Feingold DS. The mechanism of polymyxin B action and selectivity toward biologic membranes. *Biochemistry.* 1973;12(11):2105-11.
95. Mares J, Kumaran S, Gobbo M, Zerbe O. Interactions of lipopolysaccharide and polymyxin studied by NMR spectroscopy. *J Biol Chem.* 2009;284(17):11498-506.
96. Trimble MJ, Mlynarcik P, Kolar M, Hancock RE. Polymyxin: alternative mechanisms of action and resistance. *Cold Spring Harb Perspect Med.* 2016;6(10).pii:a025288.
97. Newton BA. The properties and mode of action of the polymyxins. *Bacteriol Rev.* 1956;20(1):14-27.
98. Zavascki AP, Goldani LZ, Li J, Nation RL. Polymyxin B for the treatment of multidrug-resistant pathogens: a critical review. *J Antimicrob Chemother.* 2007;60(6):1206-15.
99. Domingues MM, Inacio RG, Raimundo JM, Martins M, Castanho MA, Santos NC. Biophysical characterization of polymyxin B interaction with LPS aggregates and membrane model systems. *Biopolymers.* 2012;98(4):338-44.
100. Velkov T, Deris ZZ, Huang JX, Azad MA, Butler M, Sivanesan S, Kaminskas LM, Dong YD, Boyd B, Baker MA, Cooper MA, Nation RL, Li J. Surface changes and polymyxin interactions with a resistant strain of *Klebsiella pneumoniae*. *Innate Immun.* 2014;20(4):350-63.
101. Teuber M, Bader J. Action of polymyxin B on bacterial membranes. Binding capacities for polymyxin B of inner and outer membranes isolated from *Salmonella typhimurium* G30. *Arch Microbiol.* 1976;109(1-2):51-8.
102. Miller IR, Bach D, Teuber M. Effect of polymyxin B on the structure and the stability of lipid layers. *J Membr Biol.* 1978;39(1):49-56.
103. Zhang L, Dhillon P, Yan H, Farmer S, Hancock RE. Interactions of bacterial cationic peptide antibiotics with outer and cytoplasmic membranes of *Pseudomonas aeruginosa*. *Antimicrob Agents Chemother.* 2000;44(12):3317-21.
104. Schindler PR, Teuber M. Action of polymyxin B on bacterial membranes: morphological changes in the cytoplasm and in the outer membrane of *Salmonella typhimurium* and *Escherichia coli* B. *Antimicrob Agents Chemother.* 1975;8(1):95-104.
105. McCoy LS, Roberts KD, Nation RL, Thompson PE, Velkov T, Li J, Tor Y. Polymyxins and analogues bind to ribosomal RNA and interfere with eukaryotic translation in vitro. *Chembiochem.* 2013;14(16):2083-6.

106. Mortensen NP, Fowlkes JD, Sullivan CJ, Allison DP, Larsen NB, Molin S, Doktycz MJ. Effects of colistin on surface ultrastructure and nanomechanics of *Pseudomonas aeruginosa* cells. *Langmuir*. 2009;25(6):3728-33.
107. Lu S, Walters G, Parg R, Dutcher JR. Nanomechanical response of bacterial cells to cationic antimicrobial peptides. *Soft Matter*. 2014;10(11):1806-15.
108. Cabisco E, Tamarit J, Ros J. Oxidative stress in bacteria and protein damage by reactive oxygen species. *Int Microbiology*. 2000;3(1):3-8.
109. Sampson TR, Liu X, Schroeder MR, Kraft CS, Burd EM, Weiss DS. Rapid killing of *Acinetobacter baumannii* by polymyxins is mediated by a hydroxyl radical death pathway. *Antimicrob Agents Chemother*. 2012;56(11):5642-9.
110. Dwyer DJ, Kohanski MA, Hayete B, Collins JJ. Gyrase inhibitors induce an oxidative damage cellular death pathway in *Escherichia coli*. *Mol Syst Biol*. 2007;3:91.
111. Dwyer DJ, Kohanski MA, Collins JJ. Role of reactive oxygen species in antibiotic action and resistance. *Curr Opin Microbiol*. 2009;12(5):482-9.
112. Dong TG, Dong S, Catalano C, Moore R, Liang X, Mekalanos JJ. Generation of reactive oxygen species by lethal attacks from competing microbes. *Proc Natl Acad Sci USA*. 2015;112(7):2181-6.
113. Belenky P, Ye JD, Porter CBM, Cohen NR, Lobritz MA, Ferrante T, Jain S, Korry BJ, Schwarz EG, Walker GC, Collins JJ. Bactericidal antibiotics induce toxic metabolic perturbations that lead to cellular damage. *Cell Rep*. 2015;13(5):968-80.
114. Saugar JM, Alarcon T, Lopez-Hernandez S, Lopez-Brea M, Andreu D, Rivas L. Activities of polymyxin B and cecropin A-,melittin peptide CA(1-8)M(1-18) against a multiresistant strain of *Acinetobacter baumannii*. *Antimicrob Agents Chemother*. 2002;46(3):875-8.
115. Mogi T, Murase Y, Mori M, Shiomi K, Omura S, Paranagama MP, Kita K. Polymyxin B identified as an inhibitor of alternative NADH dehydrogenase and malate: quinone oxidoreductase from the Gram-positive bacterium *Mycobacterium smegmatis*. *J Biochem*. 2009;146(4):491-9.
116. Tochikubo K, Yasuda Y, Kozuka S. Decreased particulate NADH oxidase activity in *Bacillus subtilis* spores after polymyxin B treatment. *J Gen Microbiol*. 1986;132(2):277-87.
117. Brochmann RP, Toft A, Ciofu O, Briaies A, Kolpen M, Hempel C, Bjarnsholt T, Hoiby N, Jensen PO. Bactericidal effect of colistin on planktonic *Pseudomonas aeruginosa* is independent of hydroxyl radical formation. *Int J Antimicrob Agents*. 2014;43(2):140-7.
118. Keren I, Inocencia J, Mulcahy LR, Lewis K. Killing by bactericidal antibiotics does not depend on reactive oxygen species. *Science* 2013;339(6124):1213-6.
119. Kindrachuk KN, Fernandez L, Bains M, Hancock RE. Involvement of an ATP-dependent protease, PA0779/AsrA, in inducing heat shock in response to tobramycin in *Pseudomonas aeruginosa*. *Antimicrob Agents Chemother*. 2011;55(5):1874-82.
120. Paulander W, Wang Y, Folkesson A, Charbon G, Lobner-Olesen A, Ingmer H. Bactericidal antibiotics increase hydroxyphenyl fluorescein signal by altering cell morphology. *PLoS One*. 2014;9(3):e92231.
121. Raetz CR, Reynolds CM, Trent MS, Bishop RE. Lipid A modification systems in Gram-negative bacteria. *Annu Rev Biochem*. 2007;76:295-329.
122. Mahamad Maifiah MH, Cheah SE, Johnson MD, Han ML, Boyce JD, Thamlikitkul V, Forest A, Kaye KS, Hertzog P, Purcell AW, Song J, Velkov T, Creek DJ, Li J. Global metabolic analyses identify key differences in metabolite levels between polymyxin-susceptible and polymyxin-resistant *Acinetobacter baumannii*. *Sci Rep*. 2016;6:22287.
123. Boll JM, Tucker AT, Klein DR, Beltran AM, Brodbelt JS, Davies BW, Trent MS. Reinforcing lipid A acylation on the cell surface of *Acinetobacter baumannii* promotes cationic antimicrobial peptide resistance and desiccation survival. *MBio*. 2015;6(3):e00478-15.

124. Steeghs L, de Cock H, Evers E, Zomer B, Tommassen J, van der Ley P. Outer membrane composition of a lipopolysaccharide-deficient *Neisseria meningitidis* mutant. *The EMBO J*. 2001;20(24):6937-45.
125. Boll JM, Crofts AA, Peters K, Cattoir V, Vollmer W, Davies BW, Trent MS. A penicillin-binding protein inhibits selection of colistin-resistant, lipooligosaccharide-deficient *Acinetobacter baumannii*. *Proc Natl Acad Sci USA*. 2016;113(41):E6228-E37.
126. Owusu-Anim D, Kwon DH. Differential role of two-component regulatory systems (phoPQ and pmrAB) in polymyxin B susceptibility of *Pseudomonas aeruginosa*. *Adv Microbiol*. 2012;2(1).
127. McPhee JB, Lewenza S, Hancock REW. Cationic antimicrobial peptides activate a two-component regulatory system, PmrA-PmrB, that regulates resistance to polymyxin B and cationic antimicrobial peptides in *Pseudomonas aeruginosa*. *Mol Microbiol*. 2003;50(1):205-17.
128. Moskowitz SM, Ernst RK, Miller SI. PmrAB, a two-component regulatory system of *Pseudomonas aeruginosa* that modulates resistance to cationic antimicrobial peptides and addition of aminoarabinose to lipid A. *J Bacteriol*. 2004;186(2):575-9.
129. Moskowitz SM, Brannon MK, Dasgupta N, Pier M, Sgambati N, Miller AK, Selgrade SE, Miller SI, Denton M, Conway SP, Johansen HK, Hoiby N. PmrB mutations promote polymyxin resistance of *Pseudomonas aeruginosa* isolated from colistin-treated cystic fibrosis patients. *Antimicrob Agents Chemother*. 2012;56(2):1019-30.
130. Abraham N, Kwon DH. A single amino acid substitution in PmrB is associated with polymyxin B resistance in clinical isolate of *Pseudomonas aeruginosa*. *FEMS Microbiol Lett*. 2009;298(2):249-54.
131. Macfarlane EL, Kwasnicka A, Ochs MM, Hancock RE. PhoP-PhoQ homologues in *Pseudomonas aeruginosa* regulate expression of the outer-membrane protein OprH and polymyxin B resistance. *Mol Microbiol*. 1999;34(2):305-16.
132. Barrow K, Kwon DH. Alterations in two-component regulatory systems of phoPQ and pmrAB are associated with polymyxin B resistance in clinical isolates of *Pseudomonas aeruginosa*. *Antimicrob Agents Chemother*. 2009;53(12):5150-4.
133. Schurek KN, Sampaio JL, Kiffer CR, Sinto S, Mendes CM, Hancock RE. Involvement of pmrAB and phoPQ in polymyxin B adaptation and inducible resistance in non-cystic fibrosis clinical isolates of *Pseudomonas aeruginosa*. *Antimicrob Agents Chemother*. 2009;53(10):4345-51.
134. Miller AK, Brannon MK, Stevens L, Johansen HK, Selgrade SE, Miller SI, Hoiby N, Moskowitz SM. PhoQ mutations promote lipid A modification and polymyxin resistance of *Pseudomonas aeruginosa* found in colistin-treated cystic fibrosis patients. *Antimicrob Agents Chemother*. 2011;55(12):5761-9.
135. Fernandez L, Gooderham WJ, Bains M, McPhee JB, Wiegand I, Hancock RE. Adaptive resistance to the "last hope" antibiotics polymyxin B and colistin in *Pseudomonas aeruginosa* is mediated by the novel two-component regulatory system ParR-ParS. *Antimicrob Agents Chemother*. 2010;54(8):3372-82.
136. Fernandez L, Jenssen H, Bains M, Wiegand I, Gooderham WJ, Hancock RE. The two-component system CprRS senses cationic peptides and triggers adaptive resistance in *Pseudomonas aeruginosa* independently of ParRS. *Antimicrob Agents Chemother*. 2012;56(12):6212-22.
137. Gutu AD, Sgambati N, Strasbourger P, Brannon MK, Jacobs MA, Haugen E, Kaul RK, Johansen HK, Hoiby N, Moskowitz SM. Polymyxin resistance of *Pseudomonas aeruginosa* phoQ mutants is dependent on additional two-component regulatory systems. *Antimicrob Agents Chemother*. 2013;57(5):2204-15.

138. Lewenza S, Falsafi R, Bains M, Rohs P, Stupak J, Sprott GD, Hancock RE. The *olsA* gene mediates the synthesis of an ornithine lipid in *Pseudomonas aeruginosa* during growth under phosphate-limiting conditions, but is not involved in antimicrobial peptide susceptibility. *FEMS Microbiol Lett*. 2011;320(2):95-102.
139. Macfarlane EL, Kwasnicka A, Hancock REW. Role of *Pseudomonas aeruginosa* PhoP-PhoQ in resistance to antimicrobial cationic peptides and aminoglycosides. *Microbiology*. 2000;146(Pt 10):2543-54.
140. Muller C, Plesiat P, Jeannot K. A two-component regulatory system interconnects resistance to polymyxins, aminoglycosides, fluoroquinolones, and β -lactams in *Pseudomonas aeruginosa*. *Antimicrob Agents Chemother*. 2011;55(3):1211-21.
141. Wang DP, Seeve C, Pierson LS, Pierson EA. Transcriptome profiling reveals links between ParS/ParR, MexEF-OprN, and quorum sensing in the regulation of adaptation and virulence in *Pseudomonas aeruginosa*. *BMC Genomics*. 2013;14:618.
142. Llobet E, Tomas JM, Bengoechea JA. Capsule polysaccharide is a bacterial decoy for antimicrobial peptides. *Microbiology*. 2008;154(Pt 12):3877-86.
143. Padilla E, Llobet E, Domenech-Sanchez A, Martinez-Martinez L, Bengoechea JA, Alberti S. *Klebsiella pneumoniae* AcrAB efflux pump contributes to antimicrobial resistance and virulence. *Antimicrob Agents Chemother*. 2010;54(1):177-83.
144. Srinivasan VB, Rajamohan G. KpnEF, a new member of the *Klebsiella pneumoniae* cell envelope stress response regulon, is an SMR-type efflux pump involved in broad-spectrum antimicrobial resistance. *Antimicrob Agents Chemother*. 2013;57(9):4449-62.
145. Pamp SJ, Gjermansen M, Johansen HK, Tolker-Nielsen T. Tolerance to the antimicrobial peptide colistin in *Pseudomonas aeruginosa* biofilms is linked to metabolically active cells, and depends on the *pmr* and *mexAB-oprM* genes. *Mol Microbiol*. 2008;68(1):223-40.
146. Warner DM, Levy SB. Different effects of transcriptional regulators MarA, SoxS and Rob on susceptibility of *Escherichia coli* to cationic antimicrobial peptides (CAMPs): Rob-dependent CAMP induction of the *marRAB* operon. *Microbiology*. 2010;156(Pt 2):570-8.
147. Liu YY, Wang Y, Walsh TR, Yi LX, Zhang R, Spencer J, Doi Y, Tian G, Dong B, Huang X, Yu LF, Gu D, Ren H, Chen X, Lv L, He D, Zhou H, Liang Z, Liu JH, Shen J. Emergence of plasmid-mediated colistin resistance mechanism MCR-1 in animals and human beings in China: a microbiological and molecular biological study. *Lancet Infect Dis*. 2016;16(2):161-8.
148. Ye H, Li Y, Li Z, Gao R, Zhang H, Wen R, Gao GF, Hu Q, Feng Y. Diversified mcr-1-harboring plasmid reservoirs confer resistance to colistin in human gut microbiota. *MBio*. 2016;7(2):e00177.
149. Mediavilla JR, Patrawalla A, Chen L, Chavda KD, Mathema B, Vinnard C, Dever LL, Kreiswirth BN. Colistin- and carbapenem-resistant *Escherichia coli* harboring mcr-1 and blaNDM-5, causing a complicated urinary tract infection in a patient from the United States. *MBio*. 2016;7(4):e01191.
150. Irrgang A, Roschanski N, Tenhagen BA, Grobbel M, Skladnikiewicz-Ziemer T, Thomas K, Roesler U, Kasbohrer A. Prevalence of mcr-1 in *E. coli* from livestock and food in Germany, 2010-2015. *PLoS One*. 2016;11(7):e0159863.
151. Gao R, Hu Y, Li Z, Sun J, Wang Q, Lin J, Ye H, Liu F, Srinivas S, Li D, Zhu B, Liu YH, Tian GB, Feng Y. Dissemination and mechanism for the MCR-1 colistin resistance. *PLoS pathogens*. 2016;12(11):e1005957.
152. Poirel L, Kieffer N, Liassine N, Thanh D, Nordmann P. Plasmid-mediated carbapenem and colistin resistance in a clinical isolate of *Escherichia coli*. *Lancet Infect Dis*. 2016;16(3):281.
153. Zhang H, Seward CH, Wu Z, Ye H, Feng Y. Genomic insights into the ESBL and MCR-1-producing ST648 *Escherichia coli* with multi-drug resistance. *Sci Bull (Beijing)*. 2016;61:875-8.

154. Falgenhauer L, Waezsada SE, Yao Y, Imirzalioglu C, Kasbohrer A, Roesler U, Michael GB, Scharz S, Werner G, Kreinbrock L, Chakraborty T. Colistin resistance gene *mcr-1* in extended-spectrum β -lactamase-producing and carbapenemase-producing Gram-negative bacteria in Germany. *Lancet Infect Dis.* 2016;16(3):282-3.
155. Haenni M, Poirel L, Kieffer N, Chatre P, Saras E, Metayer V, Dumoulin R, Nordmann P, Madec JY. Co-occurrence of extended spectrum β -lactamase and MCR-1 encoding genes on plasmids. *Lancet Infect Dis.* 2016;16(3):281-2.
156. Du H, Chen L, Tang YW, Kreiswirth BN. Emergence of the *mcr-1* colistin resistance gene in carbapenem-resistant Enterobacteriaceae. *Lancet Infect Dis.* 2016;16(3):287-8.
157. Yao X, Doi Y, Zeng L, Lv L, Liu JH. Carbapenem-resistant and colistin-resistant *Escherichia coli* co-producing NDM-9 and MCR-1. *Lancet Infect Dis.* 2016;16(3):288-9.
158. Haenni M, Metayer V, Gay E, Madec JY. Increasing trends in *mcr-1* prevalence among extended-spectrum- β -lactamase-producing *Escherichia coli* isolates from French calves despite decreasing exposure to colistin. *Antimicrob Agents Chemother.* 2016;60(10):6433-4.
159. Olaitan AO, Morand S, Rolain JM. Mechanisms of polymyxin resistance: acquired and intrinsic resistance in bacteria. *Front Microbiol.* 2014;5:643.
160. Abdelraouf K, Braggs KH, Yin T, Truong LD, Hu M, Tam VH. Characterization of polymyxin B-induced nephrotoxicity: implications for dosing regimen design. *Antimicrob Agents Chemother.* 2012;56(9):4625-9.
161. Justo JA, Bosso JA. Adverse reactions associated with systemic polymyxin therapy. *Pharmacotherapy.* 2015;35(1):28-33.
162. Falagas ME, Rafailidis PI. Nephrotoxicity of colistin: new insight into an old antibiotic. *Clin Infect Dis.* 2009;48(12):1729-31.
163. Bergen PJ, Li J, Rayner CR, Nation RL. Colistin methanesulfonate is an inactive prodrug of colistin against *Pseudomonas aeruginosa*. *Antimicrob Agents Chemother.* 2006;50(6):1953-8.
164. Li J, Nation RL, Milne RW, Turnidge JD, Coulthard K. Evaluation of colistin as an agent against multi-resistant in Gram-negative bacteria. *Int J Antimicrob Agent.* 2005;25(1):11-25.
165. Nation RL, Li J, Cars O, Couet W, Dudley MN, Kaye KS, Mouton JW Paterson DL, Tam VH, Theuretzbacher U, Tsuji BT, Turnidge JD. Framework for optimisation of the clinical use of colistin and polymyxin B: the Prato polymyxin consensus. *Lancet Infect Dis.* 2015;15(2):225-34.
166. Tallgren LG, Liewendahl K, Kuhlbaeck B. The therapeutic success and nephrotoxicity of colistin in acute and chronic nephropathies with impaired renal function. *Acta Med Scand.* 1965;177:717-28.
167. Koch-Weser J, Sidel VW, Federman EB, Kanarek P, Finer DC, Eaton AE. Adverse effects of sodium colistimethate. Manifestations and specific reaction rates during 317 courses of therapy. *Ann Intern Med.* 1970;72(6):857-68.
168. Fekety FR, Jr., Norman PS, Cluff LE. The treatment of Gram-negative bacillary infections with colistin. The toxicity and efficacy of large doses in forty-eight patients. *Ann Intern Med.* 1962;57:214-29.
169. Olesen S, Madsen PO. Intravenous administration of sodium colistimethate in urinary tract infections. *Curr Ther Res Clin Exp.* 1967;9(6):283-7.
170. Baines RD, Jr., Rifkind D. Intravenous Administration of Sodium Colistimethate. *JAMA.* 1964;190:278-81.
171. Garnacho-Montero J, Ortiz-Leyba C, Jimenez-Jimenez FJ, Barrero-Almodovar AE, Garcia-Garmendia JL, Bernabeu-Wittel IM, Gallego-Lara SL, Madrazo-Osuna J. Treatment of multidrug-resistant *Acinetobacter baumannii* ventilator-associated pneumonia (VAP) with intravenous colistin: a comparison with imipenem-susceptible VAP. *Clin Infect Dis.* 2003;36(9):1111-8.

172. Hartzell JD, Neff R, Ake J, Howard R, Olson S, Paolino K, Vishnepolsky M, Weintrob A, Wortmann G. Nephrotoxicity associated with intravenous colistin (colistimethate sodium) treatment at a tertiary care medical center. *Clin Infect Dis*. 2009;48(12):1724-8.
173. Berg JR, Spilker CM, Lewis SA. Modulation of polymyxin B effects on mammalian urinary bladder. *Am J Physiol*. 1998;275(2 Pt 2):F204-15.
174. Berg JR, Spilker CM, Lewis SA. Effects of polymyxin B on mammalian urinary bladder. *J Membr Biol*. 1996;154(2):119-30.
175. Lewis JR, Lewis SA. Colistin interactions with the mammalian urothelium. *Am J Physiol Cell physiol*. 2004;286(4):C913-22.
176. Markou N, Apostolakis H, Koumoudiou C, Athanasiou M, Koutsoukou A, Alamanos I, Gregorakos L. Intravenous colistin in the treatment of sepsis from multiresistant Gram-negative bacilli in critically ill patients. *Crit Care*. 2003;7(5):R78-83.
177. Michalopoulos AS, Tsiodras S, Rellos K, Mentzelopoulos S, Falagas ME. Colistin treatment in patients with ICU-acquired infections caused by multiresistant Gram-negative bacteria: the renaissance of an old antibiotic. *Clin Microbiol Infect*. 2005;11(2):115-21.
178. Falagas ME, Rizos M, Bliziotis IA, Rellos K, Kasiakou SK, Michalopoulos A. Toxicity after prolonged (more than four weeks) administration of intravenous colistin. *BMC Infect Dis*. 2005;5:1.
179. Duncan DA. Colistin toxicity. Neuromuscular and renal manifestations. Two cases treated by hemodialysis. *Minn Med*. 1973;56(1):31-5.
180. Kubikowski P, Szreniawski Z. The mechanism of the neuromuscular blockade by antibiotics. *Arch Int Pharmacodyn Ther*. 1963;146:549-60.
181. Nation RL, Velkov T, Li J. Colistin and polymyxin B: peas in a pod, or chalk and cheese? *Clin Infect Dis*. 2014;59(1):88-94.
182. Cheah SE, Wang J, Nguyen VT, Turnidge JD, Li J, Nation RL. New pharmacokinetic/pharmacodynamic studies of systemically administered colistin against *Pseudomonas aeruginosa* and *Acinetobacter baumannii* in mouse thigh and lung infection models: smaller response in lung infection. *J Antimicrob Chemother*. 2015;70(12):3291-7.
183. Owen RJ, Li J, Nation RL, Spelman D. In vitro pharmacodynamics of colistin against *Acinetobacter baumannii* clinical isolates. *J Antimicrob Chemother*. 2007;59(3):473-7.
184. Poudyal A, Howden BP, Bell JM, Gao W, Owen RJ, Turnidge JD, Nation RL, Li J. In vitro pharmacodynamics of colistin against multidrug-resistant *Klebsiella pneumoniae*. *J Antimicrob Chemother*. 2008;62(6):1311-8.
185. Bergen PJ, Bulitta JB, Forrest A, Tsuji BT, Li J, Nation RL. Pharmacokinetic/pharmacodynamic investigation of colistin against *Pseudomonas aeruginosa* using an in vitro model. *Antimicrob Agents Chemother*. 2010;54(9):3783-9.
186. Li J, Nation RL, Turnidge JD, Milne RW, Coulthard K, Rayner CR, Paterson DL. Colistin: the re-emerging antibiotic for multidrug-resistant Gram-negative bacterial infections. *Lancet Infect Dis*. 2006;6(9):589-601.
187. Li J, Milne RW, Nation RL, Turnidge JD, Smeaton TC, Coulthard K. Use of high-performance liquid chromatography to study the pharmacokinetics of colistin sulfate in rats following intravenous administration. *Antimicrob Agents Chemother*. 2003;47(5):1766-70.
188. Plachouras D, Karvanen M, Friberg LE, Papadomichelakis E, Antoniadou A, Tsangaris I, Karaikos I, Poulakou G, Kontopidou F, Armaganidis A, Cars O, Giamarellou H. Population pharmacokinetic analysis of colistin methanesulfonate and colistin after intravenous administration in critically ill patients with infections caused by Gram-negative bacteria. *Antimicrob Agents Chemother*. 2009;53(8):3430-6.
189. Garonzik SM, Li J, Thamlikitkul V, Paterson DL, Shoham S, Jacob J, Silveira FP, Forrest A, Nation RL. Population pharmacokinetics of colistin methanesulfonate and formed colistin in

- critically ill patients from a multicenter study provide dosing suggestions for various categories of patients. *Antimicrob Agents Chemother.* 2011;55(7):3284-94.
190. Marchand S, Frat JP, Petitpas F, Lemaitre F, Gobin P, Robert R, Mimos O, Couet W. Removal of colistin during intermittent haemodialysis in two critically ill patients. *J Antimicrob Chemother.* 2010;65(8):1836-7.
 191. Markou N, Fousteri M, Markantonis SL, Zidianakis B, Hroni D, Boutzouka E, Baltopoulos G. Colistin pharmacokinetics in intensive care unit patients on continuous venovenous haemodiafiltration: an observational study. *J Antimicrob Chemother.* 2012;67(10):2459-62.
 192. Karvanen M, Plachouras D, Friberg LE, Paramythiotou E, Papadomichelakis E, Karaikos I, Tsangaris I, Armaganidis A, Cars O, Giamarellou H. Colistin methanesulfonate and colistin pharmacokinetics in critically ill patients receiving continuous venovenous hemodiafiltration. *Antimicrob Agents Chemother.* 2013;57(1):668-71.
 193. Sandri AM, Landersdorfer CB, Jacob J, Boniatti MM, Dalarosa MG, Falci DR, Behle TF, Saitovitch D, Wang J, Forrest A, Nation RL, Zavascki AP, Li J. Pharmacokinetics of polymyxin B in patients on continuous venovenous haemodialysis. *J Antimicrob Chemother.* 2013;68(3):674-7.
 194. Zavascki AP, Goldani LZ, Cao G, Superti SV, Lutz L, Barth AL, Ramos F, Boniatti MM, Nation RL, Li J. Pharmacokinetics of intravenous polymyxin B in critically ill patients. *Clin Infect Dis.* 2008;47(10):1298-304.
 195. Kwa AL, Lim TP, Low JG, Hou J, Kurup A, Prince RA, Tam VH. Pharmacokinetics of polymyxin B1 in patients with multidrug-resistant Gram-negative bacterial infections. *Diagn Microbiol Infect Dis.* 2008;60(2):163-7.
 196. Abdelraouf K, He J, Ledesma KR, Hu M, Tam VH. Pharmacokinetics and renal disposition of polymyxin B in an animal model. *Antimicrob Agents Chemother.* 2012;56(11):5724-7.
 197. Sandri AM, Landersdorfer CB, Jacob J, Boniatti MM, Dalarosa MG, Falci DR, Behli TF, Bordinhao RC, Wang J, Forrest A, Nation RL, Li J, Zavascki AP. Population pharmacokinetics of intravenous polymyxin B in critically ill patients: implications for selection of dosage regimens. *Clin Infect Dis.* 2013;57(4):524-31.
 198. Tam VH, Schilling AN, Vo G, Kabbara S, Kwa AL, Wiederhold NP, Lewis RE. Pharmacodynamics of polymyxin B against *Pseudomonas aeruginosa*. *Antimicrob Agents Chemother.* 2005;49(9):3624-30.
 199. Bergen PJ, Forrest A, Bulitta JB, Tsuji BT, Sidjabat HE, Paterson DL, Li J, Nation RL. Clinically relevant plasma concentrations of colistin in combination with imipenem enhance pharmacodynamic activity against multidrug-resistant *Pseudomonas aeruginosa* at multiple inocula. *Antimicrob Agents Chemother.* 2011;55(11):5134-42.
 200. Yau W, Owen RJ, Poudyal A, Bell JM, Turnidge JD, Yu HH, Nation RL, Li J. Colistin hetero-resistance in multidrug-resistant *Acinetobacter baumannii* clinical isolates from the Western Pacific region in the SENTRY antimicrobial surveillance programme. *J Infect.* 2009;58(2):138-44.
 201. Dudhani RV, Turnidge JD, Coulthard K, Milne RW, Rayner CR, Li J, Nation RL. Elucidation of the pharmacokinetic/pharmacodynamic determinant of colistin activity against *Pseudomonas aeruginosa* in murine thigh and lung infection models. *Antimicrob Agents Chemother.* 2010;54(3):1117-24.
 202. Dudhani RV, Turnidge JD, Nation RL, Li J. fAUC/MIC is the most predictive pharmacokinetic/pharmacodynamic index of colistin against *Acinetobacter baumannii* in murine thigh and lung infection models. *J Antimicrob Chemother.* 2010;65(9):1984-90.

203. Tran TB, Velkov T, Nation RL, Forrest A, Tsuji BT, Bergen PJ, Li J. Pharmacokinetics/pharmacodynamics of colistin and polymyxin B: are we there yet? *Int J Antimicrob Agents*. 2016;48(6):592-7.
204. Cheah S-E, Li J, Bergen PJ, Nation RL. Polymyxin pharmacokinetics and pharmacodynamics. In: Rotschafer JC, Andes DR, Rodvold KA. *Antibiotic pharmacodynamics*. Springer New York; 2016;10:221-60.
205. Tamma PD, Cosgrove SE, Maragakis LL. Combination therapy for treatment of infections with Gram-negative bacteria. *Clin Microbiol Rev*. 2012;25(3):450-70.
206. Zarkotou O, Pournaras S, Tselioti P, Dragoumanos V, Pitiriga V, Ranellou K, Prekates A, Themeli-Digalaki K, Tsakris A. Predictors of mortality in patients with bloodstream infections caused by KPC-producing *Klebsiella pneumoniae* and impact of appropriate antimicrobial treatment. *Clin Microbiol Infect*. 2011;17(12):1798-803.
207. Batirel A, Balkan, II, Karabay O, Agalar C, Akalin S, Alici O, Alp E, Altay FA, Altin N, Arslan T, Bekiroglu N, Cesur AD, Dogan M, Durdu B, Duygu F, Engin A, Engin DO, Gonen I, Guclu E, Guven T, Hatipoglu CA, Hosoglu S, Karahocagil MK, Kilic AU, Ormen B, Ozdemir D, Ozer S, Oztoprak N, Sezak N, Turhan V, Toker N, Yilmaz H. Comparison of colistin-carbapenem, colistin-sulbactam, and colistin plus other antibacterial agents for the treatment of extremely drug-resistant *Acinetobacter baumannii* bloodstream infections. *Eur J Clin Microbiol Infect Dis*. 2014;33(8):1311-22.
208. Daikos GL, Petrikos P, Psychogiou M, Kosmidis C, Vryonis E, Skoutelis A, Georgousi K, Tzouvelekis LS, Tassios PT, Bamia C, Petrikos G. Prospective observational study of the impact of VIM-1 metallo- β -lactamase on the outcome of patients with *Klebsiella pneumoniae* bloodstream infections. *Antimicrob Agents Chemother*. 2009;53(5):1868-73.
209. Tzouvelekis LS, Markogiannakis A, Piperaki E, Souli M, Daikos GL. Treating infections caused by carbapenemase-producing Enterobacteriaceae. *Clin Microbiol Infect*. 2014;20(9):862-72.
210. Kumar A, Zarychanski R, Light B, Parrillo J, Maki D, Simon D, Laporta D, Lapinsky S, Ellis P, Mirzanejad Y, Martinka G, Keenan S, Wood G, Arabi Y, Feinstein D, Kumar A, Dodek P, Kravetsky L, Doucette S. Early combination antibiotic therapy yields improved survival compared with monotherapy in septic shock: a propensity-matched analysis. *Crit Care Med*. 2010;38(9):1773-85.
211. Lehar J, Krueger AS, Avery W, Heilbut AM, Johansen LM, Price ER, Rickles RJ, Short GF 3rd, Staunton JE, Jin X, Lee MS, Zimmermann GR, Borisy AA. Synergistic drug combinations tend to improve therapeutically relevant selectivity. *Nat Biotechnol*. 2009;27(7):659-66.
212. Bollenbach T. Antimicrobial interactions: mechanisms and implications for drug discovery and resistance evolution. *Curr Opin Microbiol*. 2015;27:1-9.
213. Li J, Coulthard K, Milne R, Nation RL, Conway S, Peckham D, Etherington C, Turnidge J. Steady-state pharmacokinetics of intravenous colistin methanesulphonate in patients with cystic fibrosis. *J Antimicrob Chemother*. 2003;52(6):987-92.
214. Bergen PJ, Bulman ZP, Landersdorfer CB, Smith N, Lenhard JR, Bulitta JB, Nation RL, Li J, Tsuji BT. Optimizing polymyxin combinations against resistant Gram-negative bacteria. *Infect Dis Ther*. 2015;4(4):391-415.
215. Cheah SE, Johnson MD, Zhu Y, Tsuji BT, Forrest A, Bulitta JB, Boyce JD, Nation RL, Li J. Polymyxin resistance in *Acinetobacter baumannii*: genetic mutations and transcriptomic changes in response to clinically relevant dosage regimens. *Sci Rep*. 2016;6:26233.
216. Cheah SE, Li J, Tsuji BT, Forrest A, Bulitta JB, Nation RL. Colistin and polymyxin B dosage regimens against *Acinetobacter baumannii*: differences in activity and the emergence of resistance. *Antimicrob Agents Chemother*. 2016;60(7):3921-33.

217. Rigatto MH, Falci DR. Polymyxins combined with other antibiotics for the treatment of multi-resistant Gram negative bacteria: review of the literature. *PPCR*. 2016;1(4):91-6.
218. Elias LS, Konzen D, Krebs JM, Zavascki AP. The impact of polymyxin B dosage on in-hospital mortality of patients treated with this antibiotic. *J Antimicrob Chemother*. 2010;65(10):2231-7.
219. Kvitko CH, Rigatto MH, Moro AL, Zavascki AP. Polymyxin B versus other antimicrobials for the treatment of *Pseudomonas aeruginosa* bacteraemia. *J Antimicrob Chemother*. 2011;66(1):175-9.
220. Tuon FF, Rigatto MH, Lopes CK, Kamei LK, Rocha JL, Zavascki AP. Risk factors for acute kidney injury in patients treated with polymyxin B or colistin methanesulfonate sodium. *Int J Antimicrob Agents*. 2014;43(4):349-52.
221. Rigatto MH, Vieira FJ, Antochévis LC, Behle TF, Lopes NT, Zavascki AP. Polymyxin B in combination with antimicrobials lacking in vitro activity versus polymyxin B in monotherapy in critically ill patients with *Acinetobacter baumannii* or *Pseudomonas aeruginosa* infections. *Antimicrob Agents Chemother*. 2015;59(10):6575-80.
222. Bergen PJ, Tsuji BT, Bulitta JB, Forrest A, Jacob J, Sidjabat HE, Paterson DL, Nation RL, Li J. Synergistic killing of multidrug-resistant *Pseudomonas aeruginosa* at multiple inocula by colistin combined with doripenem in an in vitro pharmacokinetic/pharmacodynamic model. *Antimicrob Agents Chemother*. 2011;55(12):5685-95.
223. Deris ZZ, Yu HH, Davis K, Soon RL, Jacob J, Ku CK, Poudyal A, Bergen PJ, Tsuji BT, Bulitta JB, Forrest A, Paterson DL, Velkov T, Li J, Nation RL. The combination of colistin and doripenem is synergistic against *Klebsiella pneumoniae* at multiple inocula and suppresses colistin resistance in an in vitro pharmacokinetic/pharmacodynamic model. *Antimicrob Agents Chemother*. 2012;56(10):5103-12.
224. Jernigan MG, Press EG, Nguyen MH, Clancy CJ, Shields RK. The combination of doripenem and colistin is bactericidal and synergistic against colistin-resistant, carbapenemase-producing *Klebsiella pneumoniae*. *Antimicrob Agents Chemother*. 2012;56(6):3395-8.
225. Principe L, Capone A, Mazzarelli A, D'Arezzo S, Bordini E, Di Caro A, Petrosillo N. In vitro activity of doripenem in combination with various antimicrobials against multidrug-resistant *Acinetobacter baumannii*: possible options for the treatment of complicated infection. *Microb Drug Resist*. 2013;19(5):407-14.
226. Oleksiuk LM, Nguyen MH, Press EG, Updike CL, O'Hara JA, Doi Y, Clancy CJ, Shields RK. In vitro responses of *Acinetobacter baumannii* to two- and three-drug combinations following exposure to colistin and doripenem. *Antimicrob Agents Chemother*. 2014;58(2):1195-9.
227. Abdul Rahim N, Cheah SE, Johnson MD, Yu H, Sidjabat HE, Boyce J, Butler MS, Cooper MA, Fu J, Paterson DL, Nation RL, Bergen PJ, Velkov T, Li J. Synergistic killing of NDM-producing MDR *Klebsiella pneumoniae* by two 'old' antibiotics-polymyxin B and chloramphenicol. *J Antimicrob Chemother*. 2015;70(9):2589-97.
228. Tumbarello M, Viale P, Viscoli C, Trecarichi EM, Tumietto F, Marchese A, Spanu T, Ambretti S, Ginocchio F, Cristini F, Losito AR, Tadeschi S, Cauda R, Bassetti M. Predictors of mortality in bloodstream infections caused by *Klebsiella pneumoniae* carbapenemase-producing *K. pneumoniae*: importance of combination therapy. *Clin Infect Dis*. 2012;55(7):943-50.
229. Qureshi ZA, Paterson DL, Peleg AY, Adams-Haduch JM, Shutt KA, Pakstis DL, Sordillo E, Polsky B, Sandovsky G, Bhussar MK, Doi Y. Clinical characteristics of bacteraemia caused by extended-spectrum β -lactamase-producing Enterobacteriaceae in the era of CTX-M-type and KPC-type β -lactamases. *Clin Microbiol Infect*. 2012;18(9):887-93.
230. Zusman O, Avni T, Leibovici L, Adler A, Friberg L, Stergiopoulou T, Carmeli Y, Paul M. Systematic review and meta-analysis of in vitro synergy of polymyxins and carbapenems. *Antimicrob Agents Chemother*. 2013;57(10):5104-11.

231. Parchem NL, Bauer KA, Cook CH, Mangino JE, Jones CD, Porter K, Murphy CV. Colistin combination therapy improves microbiologic cure in critically ill patients with multi-drug resistant Gram-negative pneumonia. *Eur J Clin Microbiol Infect Dis*. 2016;35(9):1433-9.
232. Urena MT, Barasoain I, Espinosa M, Garcia E, Portoles A. Evaluation of different antibiotic actions combined with rifampicin. In vitro synergism against *Pseudomonas* and *Proteus*. *Chemotherapy*. 1975;21(2):82-9.
233. Lim TP, Tan TY, Lee W, Sasikala S, Tan TT, Hsu LY, Kwa AL. In-vitro activity of polymyxin B, rifampicin, tigecycline alone and in combination against carbapenem-resistant *Acinetobacter baumannii* in Singapore. *PLoS One*. 2011;6(4):e18485.
234. Lee HJ, Bergen PJ, Bulitta JB, Tsuji B, Forrest A, Nation RL, Li J. Synergistic activity of colistin and rifampin combination against multidrug-resistant *Acinetobacter baumannii* in an in vitro pharmacokinetic/pharmacodynamic model. *Antimicrob Agents Chemother*. 2013;57(8):3738-45.
235. Tascini C, Tagliaferri E, Giani T, Leonildi A, Flammini S, Casini B, Lewis R, Ferranti S, Rossolini GM, Menichetti F. Synergistic activity of colistin plus rifampin against colistin-resistant KPC-producing *Klebsiella pneumoniae*. *Antimicrob Agents Chemother*. 2013;57(8):3990-3.
236. Elemam A, Rahimian J, Doymaz M. In vitro evaluation of antibiotic synergy for polymyxin B-resistant carbapenemase-producing *Klebsiella pneumoniae*. *J Clin Microbiol*. 2010;48(10):3558-62.
237. Qureshi ZA, Paterson DL, Potoski BA, Kilayko MC, Sandovsky G, Sordillo E, Polsky B, Adam-Haduch JM, Doi Y. Treatment outcome of bacteremia due to KPC-producing *Klebsiella pneumoniae*: superiority of combination antimicrobial regimens. *Antimicrob Agents Chemother*. 2012;56(4):2108-13.
238. Linden PK, Kusne S, Coley K, Fontes P, Kramer DJ, Paterson D. Use of parenteral colistin for the treatment of serious infection due to antimicrobial-resistant *Pseudomonas aeruginosa*. *Clin Infect Dis*. 2003;37(11):E154-E60.
239. Furtado GH, d'Azevedo PA, Santos AF, Gales AC, Pignatari AC, Medeiros EA. Intravenous polymyxin B for the treatment of nosocomial pneumonia caused by multidrug-resistant *Pseudomonas aeruginosa*. *Int J Antimicrob Agents*. 2007;30(4):315-9.
240. Garnacho-Montero J, Amaya-Villar R, Gutierrez-Pizarra A, Espejo-Gutierrez de Tena E, Artero-Gonzalez ML, Corcia-Palomo Y, Bautista-Paloma J. Clinical efficacy and safety of the combination of colistin plus vancomycin for the treatment of severe infections caused by carbapenem-resistant *Acinetobacter baumannii*. *Chemotherapy*. 2013;59(3):225-31.
241. Petrosillo N, Giannella M, Antonelli M, Antonini M, Barsic B, Belancic L, Inkaya AC, De Pascale G, Grilli E, Tumbarello M, Akova M. Clinical experience of colistin-glycopeptide combination in critically ill patients infected with Gram-negative bacteria. *Antimicrob Agents Chemother*. 2014;58(2):851-8.
242. Sobieszczyk ME, Furuya EY, Hay CM, Pancholi P, Della-Latta P, Hammer SM, Kubin CJ. Combination therapy with polymyxin B for the treatment of multidrug-resistant Gram-negative respiratory tract infections. *J Antimicrob Chemother*. 2004;54(2):566-9.
243. Loewe S. The problem of synergism and antagonism of combined drugs. *Arzneimittel-Forschung*. 1953;3(6):285-90.
244. Tallarida RJ. Quantitative methods for assessing drug synergism. *Genes Cancer*. 2011;2(11):1003-8.
245. Chou TC. Drug combination studies and their synergy quantification using the Chou-Talalay method. *Cancer Res*. 2010;70(2):440-6.
246. Chen D, Zhang H, Lu P, Liu X, Cao H. Synergy evaluation by a pathway-pathway interaction network: a new way to predict drug combination. *Mol BioSyst*. 2016;12(2):614-23.

247. Li S, Zhang B, Zhang N. Network target for screening synergistic drug combinations with application to traditional Chinese medicine. *BMC Syst Biol.* 2011;5 Suppl 1:S10.
248. Jia J, Zhu F, Ma X, Cao Z, Li Y, Chen YZ. Mechanisms of drug combinations: interaction and network perspectives. *Nat Rev Drug Discov.* 2009;8(2):111-28.
249. Bolla JM, Alibert-Franco S, Handzlik J, Chevalier J, Mahamoud A, Boyer G, Kiec-Kononowicz K, Pages JM. Strategies for bypassing the membrane barrier in multidrug resistant Gram-negative bacteria. *FEBS Lett.* 2011;585(11):1682-90.
250. Zimmermann GR, Lehar J, Keith CT. Multi-target therapeutics: when the whole is greater than the sum of the parts. *Drug Discov Today.* 2007;12(1-2):34-42.
251. Yeh PJ, Hegreness MJ, Aiden AP, Kishony R. Drug interactions and the evolution of antibiotic resistance. *Nat Rev Microbiol.* 2009;7(6):460-6.
252. Pal C, Papp B, Lazar V. Collateral sensitivity of antibiotic-resistant microbes. *Trends in Microbiol.* 2015;23(7):401-7.
253. Chahine EB, Ferrill MJ, Poulakos MN. Doripenem: a new carbapenem antibiotic. *Am J Health Syst Pharm.* 2010;67(23):2015-24.
254. Hagerman JK, Knechtel SA, Klepser. Doripenem: A new extended-spectrum carbapenem antibiotic. *Formulary.* 2007;42(6):676-88.
255. Fritsche TR, Stilwell MG, Jones RN. Antimicrobial activity of doripenem (S-4661): a global surveillance report (2003). *Clin Microbiol Infect.* 2005;11(12):974-84.
256. Tsuji M, Ishii Y, Ohno A, Miyazaki S, Yamaguchi K. In vitro and in vivo antibacterial activities of S-4661, a new carbapenem. *Antimicrob Agents Chemother.* 1998;42(1):94-9.
257. Keam SJ. Doripenem: a review of its use in the treatment of bacterial infections. *Drugs.* 2008;68(14):2021-57.
258. Paterson DL, Depestel DD. Doripenem. *Clin Infect Dis.* 2009;49(2):291-8.
259. Papp-Wallace KM, Endimiani A, Taracila MA, Bonomo RA. Carbapenems: past, present, and future. *Antimicrob Agents Chemother.* 2011;55(11):4943-60.
260. Davies TA, Shang W, Bush K, Flamm RK. Affinity of doripenem and comparators to penicillin-binding proteins in *Escherichia coli* and *Pseudomonas aeruginosa*. *Antimicrob Agents Chemother.* 2008;52(4):1510-2.
261. Drug bank. Rifampicin. Available at: <https://www.drugbank.ca/drugs/DB01045> (Accessed: 12 June 2017).
262. Wehrli W. Rifampin: mechanisms of action and resistance. *Rev Infect Dis.* 1983;5 Suppl 3:S407-11.
263. Campbell EA, Korzheva N, Mustaev A, Murakami K, Nair S, Goldfarb A, Darst SA. Structural mechanism for rifampicin inhibition of bacterial RNA polymerase. *Cell.* 2001;104(6):901-12.
264. Hartmann G, Honikel KO, Knusel F, Nuesch J. The specific inhibition of the DNA-directed RNA synthesis by rifamycin. *Biochim Biophys Acta.* 1967;145(3):843-4.
265. Rifampin. Tuberculosis (Edinb). Available at: [https://doi.org/10.1016/S1472-9792\(08\)70024-6](https://doi.org/10.1016/S1472-9792(08)70024-6). 2008;88(2):151-4.
266. Crick F. Central dogma of molecular biology. *Nature.* 1970;227(5258):561-3.
267. Tang J. Microbial metabolomics. *Curr Genomics.* 2011;12(6):391-403.
268. Patti GJ, Yanes O, Siuzdak G. Innovation: Metabolomics: the apogee of the omics trilogy. *Nat Rev Mol Cell Biol.* 2012;13(4):263-9.
269. Roberts LD, Souza AL, Gerszten RE, Clish CB. Targeted metabolomics. In: Ausubel FM, Brent R, Kingston RE, Moore DD, Seidman JG, Struhl K. Current protocols in molecular biology. John Wiley & Son, Inc. 2012;98:30.2:30.2.1-30.2.24.
270. Oliver SG, Winson MK, Kell DB, Baganz F. Systematic functional analysis of the yeast genome. *Trends Biotechnol.* 1998;16(9):373-8.

271. Wang QZ, Wu CY, Chen T, Chen X, Zhao XM. Integrating metabolomics into a systems biology framework to exploit metabolic complexity: strategies and applications in microorganisms. *Appl Microbiol Biotechnol*. 2006;70(2):151-61.
272. Clish CB. Metabolomics: an emerging but powerful tool for precision medicine. *Cold Spring Harb Mol Case Stud*. 2015;1(1):a000588.
273. Bain JR, Stevens RD, Wenner BR, Ilkayeva O, Muoio DM, Newgard CB. Metabolomics applied to diabetes research: moving from information to knowledge. *Diabetes*. 2009;58(11):2429-43.
274. Kaddurah-Daouk R, Kristal BS, Weinshilboum RM. Metabolomics: a global biochemical approach to drug response and disease. *Ann Rev Pharmacol Toxicol*. 2008;48:653-83.
275. Johnson CH, Ivanisevic J, Siuzdak G. Metabolomics: beyond biomarkers and towards mechanisms. *Nat Rev Mol Cell Biol*. 2016;17(7):451-9.
276. Monteiro MS, Carvalho M, Bastos ML, Guedes de Pinho P. Metabolomics analysis for biomarker discovery: advances and challenges. *Curr Med Chem*. 2013;20(2):257-71.
277. Armitage EG, Barbas C. Metabolomics in cancer biomarker discovery: current trends and future perspectives. *J Pharm Biomed Analysis*. 2014;87:1-11.
278. Rhee EP, Gerszten RE. Metabolomics and cardiovascular biomarker discovery. *Clin Chem*. 2012;58(1):139-47.
279. Palama TL, Canard I, Rautureau GJ, Mirande C, Chatellier S, Elena-Herrmann B. Identification of bacterial species by untargeted NMR spectroscopy of the exo-metabolome. *Analyst*. 2016;141(15):4558-61.
280. Putri SP, Nakayama Y, Matsuda F, Uchikata T, Kobayashi S, Matsubara A, Fukusaki E. Current metabolomics: practical applications. *J Biosci Bioengin*. 2013;115(6):579-89.
281. Beyoglu D, Idle JR. Metabolomics and its potential in drug development. *Biochem Pharmacol*. 2013;85(1):12-20.
282. Robertson DG, Frevert U. Metabolomics in drug discovery and development. *Clin Pharmacol Ther*. 2013;94(5):559-61.
283. Wishart DS. Applications of metabolomics in drug discovery and development. *Drugs R D*. 2008;9(5):307-22.
284. Wishart DS. Emerging applications of metabolomics in drug discovery and precision medicine. *Nat Rev Drug Discov*. 2016;15(7):473-84.
285. Kumar B, Prakash A, Ruhela RK, Medhi B. Potential of metabolomics in preclinical and clinical drug development. *Pharmacol Rep*. 2014;66(6):956-63.
286. Gamache PH, Meyer DF, Granger MC, Acworth IN. Metabolomic applications of electrochemistry/mass spectrometry. *J Am Soc Mass Spectrom*. 2004;15(12):1717-26.
287. Vuckovic D. Current trends and challenges in sample preparation for global metabolomics using liquid chromatography-mass spectrometry. *Anal Bioanal Chem*. 2012;403(6):1523-48.
288. Bartel J, Krumsiek J, Theis FJ. Statistical methods for the analysis of high-throughput metabolomics data. *Comput Struct Biotechnol J*. 2013;4:e201301009.
289. Chubukov V, Gerosa L, Kochanowski K, Sauer U. Coordination of microbial metabolism. *Nat Rev Microbiol*. 2014;12(5):327-40.
290. Johnson CH, Gonzalez FJ. Challenges and opportunities of metabolomics. *J Cell Physiol*. 2012;227(8):2975-81.
291. Nielsen J, Oliver S. The next wave in metabolome analysis. *Trends Biotechnol*. 2005;23(11):544-6.
292. Goodacre R, Vaidyanathan S, Dunn WB, Harrigan GG, Kell DB. Metabolomics by numbers: acquiring and understanding global metabolite data. *Trends Biotechnol*. 2004;22(5):245-52.

293. Vinayavekhin N, Saghatelian A. Untargeted metabolomics. In: Asubel FM, Brent R, Kingston RE, David DM, Seidman JG, Struhl K. Current protocols in molecular biology. John Wiley & Son, Inc. 2010;30.1:30.1.1-24.
294. Theodoridis G, Gika HG, Wilson ID. LC-MS-based methodology for global metabolite profiling in metabonomics/metabolomics. *TrAC-Trends Anal Chem.* 2008;27(3):251-60.
295. Tautenhahn R, Cho K, Uritboonthai W, Zhu Z, Patti GJ, Siuzdak G. An accelerated workflow for untargeted metabolomics using the METLIN database. *Nat Biotechnol.* 2012;30(9):826-8.
296. Link H, Buescher JM, Sauer U. Targeted and quantitative metabolomics in bacteria. *Method Microbiol.* 2012;39:127-50.
297. Coates AR, Halls G, Hu Y. Novel classes of antibiotics or more of the same? *Br J Pharmacol.* 2011;163(1):184-94.
298. Bunnage ME. Getting pharmaceutical R&D back on target. *Nat Chem Biol.* 2011;7(6):335-9.
299. Brown D. Unfinished business: target-based drug discovery. *Drug Discov Today.* 2007;12(23-24):1007-12.
300. Halouska S, Fenton RJ, Barletta RG, Powers R. Predicting the in vivo mechanism of action for drug leads using NMR metabolomics. *ACS Chem Biol.* 2012;7(1):166-71.
301. Cox DG, Oh J, Keasling A, Colson KL, Hamann MT. The utility of metabolomics in natural product and biomarker characterization. *Biochim Biophys Acta.* 2014;1840(12):3460-74.
302. Vincent IM, Weidt S, Rivas L, Burgess K, Smith TK, Ouellette M. Untargeted metabolomic analysis of miltefosine action in *Leishmania infantum* reveals changes to the internal lipid metabolism. *Int J Parasitol Drugs Drug Resist.* 2013;4(1):20-7.
303. Trochine A, Creek DJ, Faral-Tello P, Barrett MP, Robello C. Benznidazole biotransformation and multiple targets in *Trypanosoma cruzi* revealed by metabolomics. *PLoS Negl Trop Dis.* 2014;8(5):e2844.
304. Vincent IM, Ehmann DE, Mills SD, Perros M, Barrett MP. Untargeted metabolomics to ascertain antibiotic modes of action. *Antimicrob Agents Chemother.* 2016;60(4):2281-91.
305. Chatzimitakos TG, Stalikas CD. Qualitative alterations of bacterial metabolome after exposure to metal nanoparticles with bactericidal properties: a comprehensive workflow based on (1)H NMR, UHPLC-HRMS, and metabolic databases. *J Proteome Res.* 2016;15(9):3322-30.
306. Creek DJ, Barrett MP. Determination of antiprotozoal drug mechanisms by metabolomics approaches. *Parasitology.* 2014;141(1):83-92.
307. Vincent IM, Creek DJ, Burgess K, Woods DJ, Burchmore RJS, Barrett MP. Untargeted metabolomics reveals a lack of synergy between nifurtimox and eflornithine against *Trypanosoma brucei*. *PloS Neglect Trop Dis.* 2012;6(5):e1618.
308. Gika HG, Theodoridis GA, Plumb RS, Wilson ID. Current practice of liquid chromatography-mass spectrometry in metabolomics and metabonomics. *J Pharm Biomed Anal.* 2014;87:12-25.
309. Marcinowska R, Trygg J, Wolf-Watz H, Mortiz T, Surowiec I. Optimization of a sample preparation method for the metabolomic analysis of clinically relevant bacteria. *J Microbiol Methods.* 2011;87(1):24-31.
310. Meyer H, Weidmann H, Lalk M. Methodological approaches to help unravel the intracellular metabolome of *Bacillus subtilis*. *Microb Cell Fact.* 2013;12:69.
311. Reaves ML, Rabinowitz JD. Metabolomics in systems microbiology. *Curr Opin Biotechnol.* 2011;22(1):17-25.
312. Rabinowitz JD. Cellular metabolomics of *Escherchia coli*. *Exp Rev Proteomics.* 2007;4(2):187-98.

313. Stipetic LH, Dalby MJ, Davies RL, Morton FR, Ramage G, Burgess KEV. A novel metabolomic approach used for the comparison of *Staphylococcus aureus* planktonic cells and biofilm samples. *Metabolomics*. 2016;12:75.
314. Patejko M, Jacyna J, Markuszewski MJ. Sample preparation procedures utilized in microbial metabolomics: an overview. *J Chromatogr B Analyt Technol Biomed Life Sci*. 2017;1;1043:150-157.
315. Faijes M, Mars AE, Smid EJ. Comparison of quenching and extraction methodologies for metabolome analysis of *Lactobacillus plantarum*. *Microb Cell Fact*. 2007;6:27.
316. Winder CL, Dunn WB, Schuler S, Broadhurst D, Jarvis R, Stephens GM, Goodacre R. Global metabolic profiling of *Escherichia coli* cultures: an evaluation of methods for quenching and extraction of intracellular metabolites. *Anal Chem*. 2008;80(8):2939-48.
317. Bordag N, Janakiraman V, Nachtigall J, Gonzalez Maldonado S, Bethan B, Laine JP, Elie Fux. Fast filtration of bacterial or mammalian suspension cell cultures for optimal metabolomics results. *PLoS One*. 2016;11(7):e0159389.
318. Alvarez-Sanchez B, Priego-Capote F, de Castro MDL. Metabolomics analysis II. Preparation of biological samples prior to detection. *TrAC-Trends Anal Chem*. 2010;29(2):120-7.
319. Li X, Long D, Ji J, Yang W, Zeng Z, Guo S, Ji Z, Qi G, Chen S. Sample preparation for the metabolomics investigation of poly- γ -glutamate-producing *Bacillus licheniformis* by GC-MS. *J Microbiol Methods*. 2013;94(1):61-7.
320. Lau SK, Lam CW, Curreem SO, Lee KC, Lau CC, Chow WN, Ngan AH, To KK, Chan JF, Hung IF, Yam WC, Yuen KY, Woo PC. Identification of specific metabolites in culture supernatant of *Mycobacterium tuberculosis* using metabolomics: exploration of potential biomarkers. *Emerg Microbes Infect*. 2015;4(1):e6.
321. Lee SH, Kim S, Kwon MA, Jung YH, Shin YA, Kim KH. Atmospheric vs. anaerobic processing of metabolome samples for the metabolite profiling of a strict anaerobic bacterium, *Clostridium acetobutylicum*. *Biotechnol Bioeng*. 2014;111(12):2528-36.
322. Villas-Boas SG, Bruheim P. Cold glycerol-saline: the promising quenching solution for accurate intracellular metabolite analysis of microbial cells. *Anal Biochem*. 2007;370(1):87-97.
323. Jaki BU, Franzblau SG, Cho SH, Pauli GF. Development of an extraction method for mycobacterial metabolome analysis. *J Pharm Biomed Anal*. 2006;41(1):196-200.
324. Park C, Yun S, Lee SY, Park K, Lee J. Metabolic profiling of *Klebsiella oxytoca*: evaluation of methods for extraction of intracellular metabolites using UPLC/Q-TOF-MS. *Appl Biochem Biotechnol*. 2012;167(3):425-38.
325. Villas-Boas SG, Hojer-Pedersen J, Akesson M, Smedsgaard J, Nielsen J. Global metabolite analysis of yeast: evaluation of sample preparation methods. *Yeast*. 2005;22(14):1155-69.
326. Lindon JC, Nicholson JK. Analytical technologies for metabonomics and metabolomics, and multi-omic information recovery. *TrAC-Trends Anal Chem*. 2008;27(3):194-204.
327. Moco S, Bino RJ, De Vos RCH, Vervoort J. Metabolomics technologies and metabolite identification. *TrAC-Trends Anal Chem*. 2007;26(9):855-66.
328. Zhang A, Sun H, Wang P, Han Y, Wang X. Modern analytical techniques in metabolomics analysis. *Analyst*. 2012;137(2):293-300.
329. Xiao JF, Zhou B, Ressom HW. Metabolite identification and quantitation in LC-MS/MS-based metabolomics. *Trends Analyt Chem*. 2012;32:1-14.
330. Martin JC, Maillot M, Mazerolles G, Verdu A, Lyan B, Migne C, Defoort C, Canlet C, Junot C, Guillou C, Manach C, Jacob D, Bouveresse DJ, Paris E, Pujos-Guillot E, Jourdan F, Giacomoni F, Courant F, Fave G, Le Gall G, Chassaigne H, Tabet JC, Martin JF, Antignac JP, Shintu L, Defernez M, Philo M, Alexandre-Gouaubau MC, Amiot-Carlin MJ, Bossis M, Triba MN, Stojilkovic N, Banzet N, Molinie R, Bott R, Goulitquer S, Caldarelli, Rutledge DN. Can

- we trust untargeted metabolomics? Results of the metabo-ring initiative, a large-scale, multi-instrument inter-laboratory study. *Metabolomics*. 2015;11(4):807-21.
331. Ward JL, Baker JM, Miller SJ, Deborde C, Maucourt M, Biais B, Rolin D, Moing A, Moco S, Vervoort J, Lommen A, Schafer H, Humpfer E, Beale MH. An inter-laboratory comparison demonstrates that ¹H-NMR metabolite fingerprinting is a robust technique for collaborative plant metabolomic data collection. *Metabolomics*. 2010;6(2):263-73.
332. Viant MR, Bearden DW, Bundy JG, Burton IW, Collette TW, Ekman DR, Ezernieks V, Karakach TK, Lin CY, Rochfort S, de Ropp JS, Teng Q, Tjeerdema RS, Walter JA, Wu H. International NMR-based environmental metabolomics intercomparison exercise. *Environ Sci Technol*. 2009;43(1):219-25.
333. Allwood JW, Erban A, de Koning S, Dunn WB, Luedemann A, Lommen A, Kay L, Loscher R, Kopka J, Goodacre R. Inter-laboratory reproducibility of fast gas chromatography-electron impact-time of flight mass spectrometry (GC-EI-TOF/MS) based plant metabolomics. *Metabolomics*. 2009;5(4):479-96.
334. Benton HP, Want E, Keun HC, Amberg A, Plumb RS, Goldfain-Blanc F, Walther B, Reily MD, Lindon JC, Holmes E, Nicholson JK, Ebbels TM. Intra- and interlaboratory reproducibility of ultra performance liquid chromatography-time-of-flight mass spectrometry for urinary metabolic profiling. *Anal Chem*. 2012;84(5):2424-32.
335. Ogata H, Goto S, Sato K, Fujibuchi W, Bono H, Kanehisa M. KEGG: Kyoto Encyclopedia of Genes and Genomes. *Nucleic Acids Res*. 1999;27(1):29-34.
336. Smith CA, O'Maille G, Want EJ, Qin C, Trauger SA, Brandon TR, Custodio DE, Abagyan R, Siuzdak G. METLIN: a metabolite mass spectral database. *Ther Drug Monit*. 2005;27(6):747-51.
337. Wishart DS, Knox C, Guo AC, Eisner R, Young N, Gautam B, Hau DD, Psychgiros N, Dong E, Bouatra S, Mandal R, Sinelnikov I, Xia J, Jia L, Cruz JA, Lim E, Sobsey CA, Shrivastava S, Huang P, Liu P, Fang L, Peng J, Fraddette R, Cheng D, Tzur D, Clements M, Lewis A, De Souza A, Zuniga A, Dawe M, Xiong Y, Clive D, Greiner R, Nazzyrova A, Shaykhutdinov R, Li L, Vogel HJ, Forsythe I. HMDB: a knowledgebase for the human metabolome. *Nucleic Acids Res*. 2009;37(Database issue):D603-10.
338. Fahy E, Subramaniam S, Murphy RC, Nishijima M, Raetz CR, Shimizu T, Spener F, Van Meer G, Wakelam MJ, Dennis EA. Update of the LIPID MAPS comprehensive classification system for lipids. *J Lipid Res*. 2009;50 Suppl:S9-14.
339. Ren S, Hinzman AA, Kang EL, Szczesniak RD, Lu LJ. Computational and statistical analysis of metabolomics data. *Metabolomics*. 2015;11(6):1492-513.
340. Steuer R, Morgenthal K, Weckwerth W, Selbig J. A gentle guide to the analysis of metabolomic data. *Methods Mol Biol*. 2007;358:105-26.
341. Creek DJ, Jankevics A, Burgess KE, Breitling R, Barrett MP. IDEOM: an Excel interface for analysis of LC-MS-based metabolomics data. *Bioinformatics*. 2012;28(7):1048-9.
342. Scheltema RA, Jankevics A, Jansen RC, Swertz MA, Breitling R. PeakML/mzMatch: a file format, Java library, R library, and tool-chain for mass spectrometry data analysis. *Anal Chem*. 2011;83(7):2786-93.
343. Smith CA, Want EJ, O'Maille G, Abagyan R, Siuzdak G. XCMS: Processing mass spectrometry data for metabolite profiling using nonlinear peak alignment, matching, and identification. *Anal Chem*. 2006;78(3):779-87.
344. Xia J, Sinelnikov IV, Han B, Wishart DS. MetaboAnalyst 3.0-making metabolomics more meaningful. *Nucleic Acids Res*. 2015;43(W1):W251-7.
345. Nicholson JK, Lindon JC. Systems biology: Metabonomics. *Nature*. 2008;455(7216):1054-6.
346. Nicholson JK, Wilson ID. Understanding 'global' systems biology: metabonomics and the continuum of metabolism. *Nat Rev Drug Discov*. 2003;2(8):668-76.

347. Schilling CH, Schuster S, Palsson BO, Heinrich R. Metabolic pathway analysis: basic concepts and scientific applications in the post-genomic era. *Biotechnol Prog.* 1999;15(3):296-303.
348. Zhang C, Hua Q. Applications of genome-scale metabolic models in biotechnology and systems medicine. *Front Physiol.* 2016;6:413.
349. Durot M, Bourguignon PY, Schachter V. Genome-scale models of bacterial metabolism: reconstruction and applications. *FEMS Microbiol Rev.* 2009;33(1):164-90.
350. Oberhardt MA, Puchalka J, Fryer KE, Martins dos Santos VA, Papin JA. Genome-scale metabolic network analysis of the opportunistic pathogen *Pseudomonas aeruginosa* PAO1. *J Bacteriol.* 2008;190(8):2790-803.
351. Dijkshoorn L, Nemec A, Seifert H. An increasing threat in hospitals: multidrug-resistant *Acinetobacter baumannii*. *Nat Rev Microbiol.* 2007;5(12):939-51.
352. Perez F, Hujer AM, Hujer KM, Decker BK, Rather PN, Bonomo RA. Global challenge of multidrug-resistant *Acinetobacter baumannii*. *Antimicrob Agents Chemother.* 2007;51(10):3471-84.
353. Gordon NC, Wareham DW. Multidrug-resistant *Acinetobacter baumannii*: mechanisms of virulence and resistance. *Int J Antimicrob Agents.* 2010;35(3):219-26.
354. Karageorgopoulos DE, Falagas ME. Current control and treatment of multidrug-resistant *Acinetobacter baumannii* infections. *Lancet Infect Dis.* 2008;8(12):751-62.
355. Hancock RE. Peptide antibiotics. *Lancet.* 1997;349(9049):418-22.
356. Henry R, Vithanage N, Harrison P, Seemann T, Coutts S, Moffatt JH, Nation RL, Li J, Harper M, Adler B, Boyce JD. Colistin-resistant, lipopolysaccharide-deficient *Acinetobacter baumannii* responds to lipopolysaccharide loss through increased expression of genes involved in the synthesis and transport of lipoproteins, phospholipids, and poly- β -1,6-N-acetylglucosamine. *Antimicrob Agents Chemother.* 2012;56(1):59-69.
357. van der Werf MJ, Overkamp KM, Muilwijk B, Coulter L, Hankemeier T. Microbial metabolomics: toward a platform with full metabolome coverage. *Anal Biochem.* 2007;370(1):17-25.
358. Snyder M, Li XY. Metabolomics as a robust tool in systems biology and personalized medicine: an open letter to the metabolomics community. *Metabolomics.* 2013;9(3):532-4.
359. Kim OS, Cho YJ, Lee K, Yoon SH, Kim M, Na H, Park SC, Jeon YS, Lee JH, Yi H, Won S, Chun J. Introducing EzTaxon-e: a prokaryotic 16S rRNA gene sequence database with phylotypes that represent uncultured species. *Int J Syst Evol Microbiol.* 2012;62(Pt 3):716-21.
360. Altschul SF, Madden TL, Schaffer AA, Zhang J, Zhang Z, Miller W, Lipman DJ. Gapped BLAST and PSI-BLAST: a new generation of protein database search programs. *Nucleic Acids Res.* 1997;25(17):3389-402.
361. Que NL, Lin S, Cotter RJ, Raetz CR. Purification and mass spectrometry of six lipid A species from the bacterial endosymbiont rhizobium etli. Demonstration of a conserved distal unit and a variable proximal portion. *J Biol Chem.* 2000;275(36):28006-16.
362. Bligh EG, Dyer WJ. A rapid method of total lipid extraction and purification. *Can J Biochem Physiol.* 1959;37(8):911-7.
363. Gika HG, Theodoridis GA, Wingate JE, Wilson ID. Within-day reproducibility of an HPLC-MS-based method for metabolomic analysis: application to human urine. *J Proteome Res.* 2007;6(8):3291-303.
364. Zhang T, Creek DJ, Barrett MP, Blackburn G, Watson DG. Evaluation of coupling reversed phase, aqueous normal phase, and hydrophilic interaction liquid chromatography with Orbitrap mass spectrometry for metabolomic studies of human urine. *Anal Chem.* 2012;84(4):1994-2001.

365. Leader DP, Burgess K, Creek D, Barrett MP. Pathos: a web facility that uses metabolic maps to display experimental changes in metabolites identified by mass spectrometry. *Rapid Commun Mass Spectrom*. 2011;25(22):3422-6.
366. Caspi R, Altman T, Billington R, Dreher K, Foerster H, Fulcher CA, Holland TA, Keseler IM, Kothari A, Kubo A, Krummenacker M, Latendresse M, Mueller LA, Ong Q, Paley S, Subhraveti P, Weaver DS, Weerasinghe D, Zhang P, Karp PD. The MetaCyc database of metabolic pathways and enzymes and the BioCyc collection of Pathway/Genome Databases. *Nucleic Acids Res*. 2014;42(Database issue):D459-71.
367. Junker BH, Klukas C, Schreiber F. VANTED: a system for advanced data analysis and visualization in the context of biological networks. *BMC bioinformatics*. 2006;7:109.
368. Kell DB, Goodacre R. Metabolomics and systems pharmacology: why and how to model the human metabolic network for drug discovery. *Drug Discov Today*. 2014;19(2):171-82.
369. Yeom J, Shin JH, Yang JY, Kim J, Hwang GS. (1)H NMR-based metabolite profiling of planktonic and biofilm cells in *Acinetobacter baumannii* 1656-2. *PloS One*. 2013;8(3):e57730.
370. Gjersing EL, Herberg JL, Horn J, Schaldach CM, Maxwell RS. NMR metabolomics of planktonic and biofilm modes of growth in *Pseudomonas aeruginosa*. *Anal Chem*. 2007;79(21):8037-45.
371. t'Kindt R, Scheltema RA, Jankevics A, Bruncker K, Rijal S, Dujardin JC, Breitling R, Watson DG, Coombs GH, Decuypere S. Metabolomics to unveil and understand phenotypic diversity between pathogen populations. *PloS Negl Trop Dis*. 2010;4(11):e904.
372. Vincent IM, Creek D, Watson DG, Kamleh MA, Woods DJ, Wong PE, Burchmore RJ, Barrett MP. A molecular mechanism for eflornithine resistance in African trypanosomes. *PLoS Pathog*. 2010;6(11):e1001204.
373. Derewacz DK, Goodwin CR, McNees CR, McLean JA, Bachmann BO. Antimicrobial drug resistance affects broad changes in metabolomic phenotype in addition to secondary metabolism. *Proc Natl Acad Sci USA*. 2013;110(6):2336-41.
374. Nowicki EM, O'Brien JP, Brodbelt JS, Trent MS. Characterization of *Pseudomonas aeruginosa* LpxT reveals dual positional lipid A kinase activity and co-ordinated control of outer membrane modification. *Mol Microbiol*. 2014;94(3):728-41.
375. Velkov T, Thompson PE, Nation RL, Li J. Structure-activity relationships of polymyxin antibiotics. *J Med Chem*. 2010;53(5):1898-916.
376. Wittmann C, Kromer JO, Kiefer P, Binz T, Heinzle E. Impact of the cold shock phenomenon on quantification of intracellular metabolites in bacteria. *Anal Biochem*. 2004;327(1):135-9.
377. Shin MH, Lee DY, Liu KH, Fiehn O, Kim KH. Evaluation of sampling and extraction methodologies for the global metabolic profiling of *Saccharophagus degradans*. *Anal Chem*. 2010;82(15):6660-6.
378. Armenta-Medina D, Segovia L, Perez-Rueda E. Comparative genomics of nucleotide metabolism: a tour to the past of the three cellular domains of life. *BMC Genomics*. 2014;15:800.
379. Maeda H, Dudareva N. The Shikimate pathway and aromatic amino acid biosynthesis in plants. *Annu Rev Plant Biol*. 2012;63:73-105.
380. Stincone A, Prigione A, Cramer T, Wamelink MM, Campbell K, Cheung E, Olin-Sandoval V, Gruning NM, Kruger A, Tauqeer Alam M, Keller MA, Breitenbach M, Brindle KM, Rabinowitz JD, Ralser M. The return of metabolism: biochemistry and physiology of the pentose phosphate pathway. *Biol Rev Camb Philos Soc*. 2015;90(3):927-63.
381. Taylor PL, Blakely KM, de Leon GP, Walker JR, McArthur F, Evdokimova E, Zhang K, Valvano MA, Wright GD, Junop MS. Structure and function of sedoheptulose-7-phosphate isomerase, a critical enzyme for lipopolysaccharide biosynthesis and a target for antibiotic adjuvants. *J Biol Chem*. 2008;283(5):2835-45.

382. Sarkar M, Maganti L, Ghoshal N, Dutta C. In silico quest for putative drug targets in *Helicobacter pylori* HPAG1: molecular modeling of candidate enzymes from lipopolysaccharide biosynthesis pathway. *J Mol Model*. 2012;18(5):1855-66.
383. Kneidinger B, Graninger M, Puchberger M, Kosma P, Messner P. Biosynthesis of nucleotide-activated D-glycero-D-manno-heptose. *J Biol Chem*. 2001;276(24):20935-44.
384. Valvano MA, Messner P, Kosma P. Novel pathways for biosynthesis of nucleotide-activated glycerol-manno-heptose precursors of bacterial glycoproteins and cell surface polysaccharides. *Microbiology*. 2002;148(Pt 7):1979-89.
385. Tian J, Bryk R, Itoh M, Suematsu M, Nathan C. Variant tricarboxylic acid cycle in *Mycobacterium tuberculosis*: Identification of α -ketoglutarate decarboxylase. *Proc Natl Acad Sci USA*. 2005;102(30):10670-5.
386. Lovering AL, Safadi SS, Strynadka NC. Structural perspective of peptidoglycan biosynthesis and assembly. *Annu Rev Biochem*. 2012;81:451-78.
387. Gordon E, Flouret B, Chantalat L, van Heijenoort J, Mengin-Lecreulx D, Dideberg O. Crystal structure of UDP-N-acetylmuramoyl-L-alanyl-D-glutamate: meso-diaminopimelate ligase from *Escherichia coli*. *J Biol Chem*. 2001;276(14):10999-1006.
388. Breidenstein EB, de la Fuente-Nunez C, Hancock RE. *Pseudomonas aeruginosa*: all roads lead to resistance. *Trends Microbiol*. 2011;19(8):419-26.
389. Dalebroux ZD, Matamouros S, Whittington D, Bishop RE, Miller SI. PhoPQ regulates acidic glycerophospholipid content of the *Salmonella Typhimurium* outer membrane. *Proc Natl Acad Sci USA*. 2014;111(5):1963-8.
390. Geiger O, Lopez-Lara IM, Sohlenkamp C. Phosphatidylcholine biosynthesis and function in bacteria. *Biochim Biophys Acta*. 2013;1831(3):503-13.
391. Garsin DA. Ethanolamine utilization in bacterial pathogens: roles and regulation. *Nat Rev Microbiol*. 2010;8(4):290-5.
392. Kendall MM, Gruber CC, Parker CT, Sperandio V. Ethanolamine controls expression of genes encoding components involved in interkingdom signaling and virulence in enterohemorrhagic *Escherichia coli* O157:H7. *MBio*. 2012;3(3):e00050.
393. Bowen BP, Northen TR. Dealing with the Unknown: metabolomics and metabolite atlases. *J Am Soc Mass Spectrom*. 2010;21(9):1471-6.
394. Nakabayashi R, Saito K. Metabolomics for unknown plant metabolites. *Anal Bioanal Chem*. 2013;405(15):5005-11.
395. Nagana Gowda GA, Raftery D. Can NMR solve some significant challenges in metabolomics? *J Magn Reson*. 2015;260:144-60.
396. Fishbain J, Peleg AY. Treatment of *Acinetobacter* infections. *Clin Infect Dis*. 2010;51(1):79-84.
397. Lim LM, Ly N, Anderson D, Yang JC, Macander L, Jarkowski A 3rd, Forrest A, Bulitta JB, Tsuji BT. Resurgence of colistin: a review of resistance, toxicity, pharmacodynamics, and dosing. *Pharmacotherapy*. 2010;30(12):1279-91.
398. Falagas ME, Rafailidis PI, Matthaiou DK. Resistance to polymyxins: mechanisms, frequency and treatment options. *Drug Resist Updat*. 2010;13(4-5):132-8.
399. Pogue JM, Cohen DA, Marchaim D. Editorial commentary: polymyxin-resistant *Acinetobacter baumannii*: urgent action needed. *Clin Infect Dis*. 2015;60(9):1304-7.
400. Clausell A, Garcia-Subirats M, Pujol M, Busquets MA, Rabanal F, Cajal Y. Gram-negative outer and inner membrane models: insertion of cyclic cationic lipopeptides. *J Phys Chem B*. 2007;111(3):551-63.
401. Cai Y, Chai D, Wang R, Liang B, Bai N. Colistin resistance of *Acinetobacter baumannii*: clinical reports, mechanisms and antimicrobial strategies. *J Antimicrob Chemother*. 2012;67(7):1607-15.

402. Bergen PJ, Bulman ZP, Saju S, Bulitta JB, Landersdorfer C, Forrest A, Li J, Nation RL, Tsuji BT. Polymyxin combinations: pharmacokinetics and pharmacodynamics for rationale use. *Pharmacotherapy*. 2015;35(1):34-42.
403. Nation RL, Garonzik SM, Li J, Thamlikitkul V, Giamarellos-Bourboulis EJ, Paterson DL, Turnidge JD, Forrest A, Silveira FP. Updated US and European dose recommendations for intravenous colistin: how do they perform? *Clin Infect Dis*. 2016;62(5):552-8.
404. Lesho E, Yoon EJ, McGann P, Snesrud E, Kwak Y, Milillo M, Onmus-Leone F, Preston L, St Clair K, Nikolich M, Viscount H, Wortmann G, Zapor M, Grillot-Courvalin C, Courvalin P, Clifford R, Waterman PE. Emergence of colistin-resistance in extremely drug-resistant *Acinetobacter baumannii* containing a novel pmrCAB operon during colistin therapy of wound infections. *J Infect Dis*. 2013;208(7):1142-51.
405. Rolain JM, Diene SM, Kempf M, Gimenez G, Robert C, Raoult D. Real-time sequencing to decipher the molecular mechanism of resistance of a clinical pan-drug-resistant *Acinetobacter baumannii* isolate from Marseille, France. *Antimicrob Agents Chemother*. 2013;57(1):592-6.
406. Snitkin ES, Zelazny AM, Gupta J, Palmore TN, Murray PR, Segre JA. Genomic insights into the fate of colistin resistance and *Acinetobacter baumannii* during patient treatment. *Genome Res*. 2013;23(7):1155-62.
407. Ly NS, Bulitta JB, Rao GG, Landersdorfer CB, Holden PN, Forrest A, Bergen PJ, Nation RL, Li J, Tsuji BT. Colistin and doripenem combinations against *Pseudomonas aeruginosa*: profiling the time course of synergistic killing and prevention of resistance. *J Antimicrob Chemother*. 2015;70(5):1434-42.
408. Chen C, Gonzalez FJ, Idle JR. LC-MS-based metabolomics in drug metabolism. *Drug Metab Rev*. 2007;39(2-3):581-97.
409. Mastrangelo A, Armitage EG, Garcia A, Barbas C. Metabolomics as a tool for drug discovery and personalised medicine. A Review. *Curr Top Med Chem*. 2014;14(23):2627-36.
410. Kaddurah-Daouk R, Weinshilboum RM, Network PR. Pharmacometabolomics: implications for clinical pharmacology and systems pharmacology. *Clin Pharmacol Ther*. 2014;95(2):154-67.
411. Kirwan JA, Weber RJ, Broadhurst DI, Viant MR. Direct infusion mass spectrometry metabolomics dataset: a benchmark for data processing and quality control. *Sci Data*. 2014;1:140012.
412. Henry R, Crane B, Powell D, Lucas DD, Li ZF, Aranda J, Harrison P, Nation RL, Adler B, Harper M, Boyce JD, Li J. The transcriptomic response of *Acinetobacter baumannii* to colistin and doripenem alone and in combination in an in vitro pharmacokinetics/pharmacodynamics model. *J Antimicrob Chemother*. 2015;70(5):1303-13.
413. Matthaiou DK, Michalopoulos A, Rafailidis PI, Karageorgopoulos DE, Papaioannou V, Ntani G, Samonis G, Falagas ME. Risk factors associated with the isolation of colistin-resistant Gram-negative bacteria: a matched case-control study. *Crit Care Med*. 2008;36(3):807-11.
414. Pritchard JR, Bruno PM, Gilbert LA, Capron KL, Lauffenburger DA, Hemann MT. Defining principles of combination drug mechanisms of action. *Proc Natl Acad Sci USA*. 2013;110(2):E170-9.
415. Malinverni JC, Silhavy TJ. An ABC transport system that maintains lipid asymmetry in the gram-negative outer membrane. *Proc Natl Acad Sci USA*. 2009;106(19):8009-14.
416. Martorana AM, Motta S, Di Silvestre D, Falchi F, Deho G, Mauri P, Sperandeo P, Polissi A. Dissecting *Escherichia coli* outer membrane biogenesis using differential proteomics. *PLoS One*. 2014;9(6):e100941.
417. Kneidinger B, Marolda C, Graninger M, Zamyatina A, McArthur F, Kosma P, Valvano MA, Messner P. Biosynthesis pathway of ADP-L-glycero-beta-D-manno-heptose in *Escherichia coli*. *J Bacteriol*. 2002;184(2):363-9.

418. Taylor PL, Sugiman-Marangos S, Zhang K, Valvano MA, Wright GD, Junop MS. Structural and kinetic characterization of the LPS biosynthetic enzyme D- α , β -D-heptose-1,7-bisphosphate phosphatase (GmhB) from *Escherichia coli*. *Biochemistry*. 2010;49(5):1033-41.
419. Brooke JS, Valvano MA. Molecular cloning of the *Haemophilus influenzae* *gmhA* (*lpcA*) gene encoding a phosphoheptose isomerase required for lipooligosaccharide biosynthesis. *J Bacteriol*. 1996;178(11):3339-41.
420. Kilstrup M, Hammer K, Ruhdal Jensen P, Martinussen J. Nucleotide metabolism and its control in lactic acid bacteria. *FEMS Microbiol Rev*. 2005;29(3):555-90.
421. Dorries K, Schlueter R, Lalk M. Impact of antibiotics with various target sites on the metabolome of *Staphylococcus aureus*. *Antimicrob Agents Chemother*. 2014;58(12):7151-63.
422. Hilaris O, Ezzo DC, Jodlowski TZ. Doripenem (doribax), a new carbapenem antibacterial agent. *P T*. 2008;33(3):134-80.
423. Macheboeuf P, Contreras-Martel C, Job V, Dideberg O, Dessen A. Penicillin binding proteins: key players in bacterial cell cycle and drug resistance processes. *FEMS Microbiol Rev*. 2006;30(5):673-91.
424. Scheffers DJ, Pinho MG. Bacterial cell wall synthesis: new insights from localization studies. *Microbiol Mol Biol Rev*. 2005;69(4):585-607.
425. t'Kindt R, Jankevics A, Scheltema RA, Zheng L, Watson DG, Dujardin JC, Breitling R, Coombs GH, Decuypere S. Towards an unbiased metabolic profiling of protozoan parasites: optimisation of a Leishmania sampling protocol for HILIC-orbitrap analysis. *Anal Bioanal Chem*. 2010;398(5):2059-69.
426. Hoerr V, Duggan GE, Zbytnuik L, Poon KKH, Grosse C, Neugebauer U, Methling K, Löffler B, Vogel HJ. Characterization and prediction of the mechanism of action of antibiotics through NMR metabolomics. *BMC Microbiol*. 2016;16:82.
427. Focaccetti C, Bruno A, Magnani E, Bartolini D, Principi E, Dallaglio K, Bucci EO, Finzi G, Sessa F, Noonan DM, Albin A. Effects of 5-fluorouracil on morphology, cell cycle, proliferation, apoptosis, autophagy and ROS production in endothelial cells and cardiomyocytes. *PLoS One*. 2015;10(2):e0115686.
428. Malet-Martino M, Martino R. Clinical studies of three oral prodrugs of 5-fluorouracil (capecitabine, UFT, S-1): a review. *Oncologist*. 2002;7(4):288-323.
429. Lobritz MA, Belenky P, Porter CBM, Gutierrez A, Yang JH, Schwarz EG, Dwyer DJ, Khalil AS, Collins JJ. Antibiotic efficacy is linked to bacterial cellular respiration. *Proc Natl Acad Sci USA*. 2015;112(27):8173-80.
430. Nandakumar M, Nathan C, Rhee KY. Isocitrate lyase mediates broad antibiotic tolerance in *Mycobacterium tuberculosis*. *Nat Commun*. 2014;5:4306.
431. Kohanski MA, Dwyer DJ, Hayete B, Lawrence CA, Collins JJ. A common mechanism of cellular death induced by bactericidal antibiotics. *Cell*. 2007;130(5):797-810.
432. Kohanski MA, Dwyer DJ, Wierzbowski J, Cottarel G, Collins JJ. Mistranslation of membrane proteins and two-component system activation trigger antibiotic-mediated cell death. *Cell*. 2008;135(4):679-90.
433. Baek SH, Li AH, Sassetti CM. Metabolic regulation of mycobacterial growth and antibiotic sensitivity. *PLoS Biol*. 2011;9(5):e1001065.
434. Thomas VC, Kinkead LC, Janssen A, Schaeffer CR, Woods KM, Lindgren JK, Peaster JM, Chaudhari SS, Sadykov M, Jones J, AbdelGhani SM, Zimmerman MC, Bayles KW, Somerville GA, Fey PD. A dysfunctional tricarboxylic acid cycle enhances fitness of *Staphylococcus epidermidis* during β -lactam stress. *MBio*. 2013;4(4):e00437-13.
435. Grant SS, Kaufmann BB, Chand NS, Haseley N, Hung DT. Eradication of bacterial persisters with antibiotic-generated hydroxyl radicals. *Proc Natl Acad Sci USA*. 2012;109(30):12147-52.

436. Dwyer DJ, Belenky PA, Yang JH, MacDonald IC, Martell JD, Takahashi N, Chan CT, Lobritz MA, Braff D, Schwarz EG, Ye JD, Pati M, Vercruysse M, Ralifo PS, Allison KR, Khalil AS, Ting AY, Wakler GC, Collins JJ. Antibiotics induce redox-related physiological alterations as part of their lethality. *Proc Natl Acad Sci USA*. 2014;111(20):E2100-9.
437. Wang Z, Gerstein M, Snyder M. RNA-Seq: a revolutionary tool for transcriptomics. *Nat Rev Genet*. 2009;10(1):57-63.
438. RNeasy Plus Mini Kit. Qiagen. 2011. Available at <https://www.qiagen.com/us/resources/resourcedetail?id=1d882bbe-c71d-4fec-bdd2-bc855d3a4b55&lang=en> (Accessed: 12 June 2017).
439. RNAprotect bacteria reagent and RNeasy protect bacteria kits. Qiagen. 2011. Available at: <https://www.qiagen.com/us/resources/resourcedetail?id=cda8a33c-d9ae-456e-8597-f002758e58b6&lang=en> (Accessed: 12 June 2017).
440. Winsor GL, Griffiths EJ, Lo R, Dhillon BK, Shay JA, Brinkman FS. Enhanced annotations and features for comparing thousands of *Pseudomonas* genomes in the *Pseudomonas* genome database. *Nucleic Acids Res*. 2016;44(D1):D646-53.
441. Liao Y, Smyth GK, Shi W. The Subread aligner: fast, accurate and scalable read mapping by seed-and-vote. *Nucleic Acids Res*. 2013;41(10):e108.
442. Ritchie ME, Phipson B, Wu D, Hu Y, Law CW, Shi W, Smyth GK. limma powers differential expression analyses for RNA-sequencing and microarray studies. *Nucleic Acids Res*. 2015;43(7):e47.
443. Benjamini Y, Hochberg Y. Controlling the false discovery rate - a practical and powerful approach to multiple testing. *J Roy Stat Soc B Met*. 1995;57(1):289-300.
444. Supek F, Bosnjak M, Skunca N, Smuc T. REVIGO summarizes and visualizes long lists of gene ontology terms. *PLoS One*. 2011;6(7):e21800.
445. Yamada T, Letunic I, Okuda S, Kanehisa M, Bork P. iPath2.0: interactive pathway explorer. *Nucleic Acids Res*. 2011;39(Web Server issue):W412-5.
446. Liang H, Li L, Dong Z, Surette MG, Duan K. The YebC family protein PA0964 negatively regulates the *Pseudomonas aeruginosa* quinolone signal system and pyocyanin production. *J Bacteriol*. 2008;190(18):6217-27.
447. Hancock RE. The complexities of antibiotic action. *Mol Syst Biol*. 2007;3:142.
448. McPhee JB, Bains M, Winsor G, Lewenza S, Kwasnicka A, Brazas MD, Brinkman FS, Hancock RE. Contribution of the PhoP-PhoQ and PmrA-PmrB two-component regulatory systems to Mg²⁺-induced gene regulation in *Pseudomonas aeruginosa*. *J Bacteriol*. 2006;188(11):3995-4006.
449. Masuda N, Sakagawa E, Ohya S, Gotoh N, Tsujimoto H, Nishino T. Substrate specificities of MexAB-OprM, MexCD-OprJ, and MexXY-oprM efflux pumps in *Pseudomonas aeruginosa*. *Antimicrob Agents Chemother*. 2000;44(12):3322-7.
450. Yuan YQ, Sachdeva M, Leeds JA, Meredith TC. Fatty acid biosynthesis in *Pseudomonas aeruginosa* is initiated by the FabY Class of beta-ketoacyl acyl carrier protein synthases. *J Bacteriol*. 2012;194(19):5171-84.
451. Van Delden C, Iglewski BH. Cell-to-cell signaling and *Pseudomonas aeruginosa* infections. *Emerg Infect Dis*. 1998;4(4):551-60.
452. Sharma G, Rao S, Bansal A, Dang S, Gupta S, Gabrani R. *Pseudomonas aeruginosa* biofilm: potential therapeutic targets. *Biologicals*. 2014;42(1):1-7.
453. Lau GW, Hassett DJ, Ran H, Kong F. The role of pyocyanin in *Pseudomonas aeruginosa* infection. *Trends Mol Med*. 2004;10(12):599-606.
454. Rada B, Leto TL. Pyocyanin effects on respiratory epithelium: relevance in *Pseudomonas aeruginosa* airway infections. *Trends Microbiol*. 2013;21(2):73-81.

455. Hall S, McDermott C, Anoopkumar-Dukie S, McFarland AJ, Forbes A, Perkins AV, Davey AK, Chess-Williams R, Kiefel MJ, Arora D, Grant GD. Cellular effects of pyocyanin, a secreted virulence factor of *Pseudomonas aeruginosa*. *Toxins* (Basel). 2016;8(8):E236.
456. Haas D, Holloway BW, Schambeck A, Leisinger T. The genetic organization of arginine biosynthesis in *Pseudomonas aeruginosa*. *Mol Gen Genet*. 1977;154(1):7-22.
457. Hassett DJ, Schweizer HP, Ohman DE. *Pseudomonas aeruginosa* sodA and sodB mutants defective in manganese- and iron-cofactored superoxide dismutase activity demonstrate the importance of the iron-cofactored form in aerobic metabolism. *J Bacteriol*. 1995;177(22):6330-7.
458. Sharma V, Noriega CE, Rowe JJ. Involvement of NarK1 and NarK2 proteins in transport of nitrate and nitrite in the denitrifying bacterium *Pseudomonas aeruginosa* PAO1. *Appl Environ Microbiol*. 2006;72(1):695-701.
459. Adamczack J, Hoffmann M, Papke U, Haufschildt K, Nicke T, Broring M, Sezer M, Weimar R, Kuhlmann U, Hildebrandt P, Layer G. NirN protein from *Pseudomonas aeruginosa* is a novel electron-bifurcating dehydrogenase catalyzing the last step of heme d(1) biosynthesis. *J Biol Chem*. 2014;289(44):30753-62.
460. Zaborin A, Gerdes S, Holbrook C, Liu DC, Zaborina OY, Alverdy JC. *Pseudomonas aeruginosa* overrides the virulence inducing effect of opioids when it senses an abundance of phosphate. *PLoS One*. 2012;7(4):e34883.
461. McCord JM, Fridovich I. Superoxide dismutase. An enzymic function for erythrocuprein (hemocuprein). *J Biol Chem*. 1969;244(22):6049-55.
462. Jin DJ, Gross CA. Mapping and sequencing of mutations in the *Escherichia coli* rpoB gene that lead to rifampicin resistance. *J Mol Biol*. 1988;202(1):45-58.
463. Comas I, Borrell S, Roetzer A, Rose G, Malla B, Kato-Maeda M, Galagan J, Niemann S, Gagneux S. Whole-genome sequencing of rifampicin-resistant *Mycobacterium tuberculosis* strains identifies compensatory mutations in RNA polymerase genes. *Nat Genet*. 2011;44(1):106-10.
464. Taniguchi H, Aramaki H, Nikaido Y, Mizuguchi Y, Nakamura M, Koga T, Yoshida S. Rifampicin resistance and mutation of the *rpoB* gene in *Mycobacterium tuberculosis*. *FEMS Microbiol Lett*. 1996;144(1):103-8.
465. Prosser GA, Larrouy-Maumus G, de Carvalho LP. Metabolomic strategies for the identification of new enzyme functions and metabolic pathways. *EMBO Rep*. 2014;15(6):657-69.
466. Henry CS, DeJongh M, Best AA, Frybarger PM, Linsay B, Stevens RL. High-throughput generation, optimization and analysis of genome-scale metabolic models. *Nat Biotechnol*. 2010;28(9):977-82.
467. Maifiah MH, Creek DJ, Nation RL, Forrest A, Tsuji BT, Velkov T, Li J. Untargeted metabolomics analysis reveals key pathways responsible for the synergistic killing of colistin and doripenem combination against *Acinetobacter baumannii*. *Sci Rep*. 2017;7:45527.
468. Konaklieva MI. Molecular targets of β -lactam-based antimicrobials: beyond the usual suspects. *Antibiotics* (Basel). 2014;3(2):128-42.
469. Zeng X, Lin J. B-lactamase induction and cell wall metabolism in Gram-negative bacteria. *Front Microbiol*. 2013;4:128.
470. Wang X, Quinn PJ. Lipopolysaccharide: biosynthetic pathway and structure modification. *Prog Lipid Res*. 2010;49(2):97-107.
471. Moffatt BA, Ashihara H. Purine and pyrimidine nucleotide synthesis and metabolism. *Arabidopsis Book*. 2002;1:e0018.
472. Chapon-Herve V, Akrim M, Latifi A, Williams P, Lazdunski A, Bally M. Regulation of the xcp secretion pathway by multiple quorum-sensing modulons in *Pseudomonas aeruginosa*. *Mol Microbiol*. 1997;24(6):1169-78.

- 473. Senf F, Tommassen J, Koster M. Polar secretion of proteins via the Xcp type II secretion system in *Pseudomonas aeruginosa*. Microbiology. 2008;154(Pt 10):3025-32.
- 474. Latifi A, Foglino M, Tanaka K, Williams P, Lazdunski A. A hierarchical quorum-sensing cascade in *Pseudomonas aeruginosa* links the transcriptional activators LasR and RhIR (VsmR) to expression of the stationary-phase sigma factor RpoS. Mol Microbiol. 1996;21(6):1137-46.
- 475. Mavrodi DV, Blankenfheldt W, Thomashow LS. Phenazine compounds in fluorescent *Pseudomonas* spp. biosynthesis and regulation. Annu Rev Phytopathol. 2006;44:417-45.
- 476. Schuster M, Hawkins AC, Harwood CS, Greenberg EP. The *Pseudomonas aeruginosa* RpoS regulon and its relationship to quorum sensing. Mol Microbiol. 2004;51(4):973-85.
- 477. Foti JJ, Devadoss B, Winkler JA, Collins JJ, Walker GC. Oxidation of the guanine nucleotide pool underlies cell death by bactericidal antibiotics. Science. 2012;336(6079):315-9.
- 478. Zelezniak A, Sheridan S, Patil KR. Contribution of network connectivity in determining the relationship between gene expression and metabolite concentration changes. PLoS Comput Biol. 2014;10(4):e1003572.
- 479. Baart GJ, Martens DE. Genome-scale metabolic models: reconstruction and analysis. Methods Mol Biol. 2012;799:107-26.

Appendix-I

Publications in support of this thesis

SCIENTIFIC REPORTS

OPEN

Global metabolic analyses identify key differences in metabolite levels between polymyxin-susceptible and polymyxin-resistant *Acinetobacter baumannii*

Received: 03 July 2015
Accepted: 11 February 2016
Published: 29 February 2016

Mohd Hafidz Mahamad Maifiah¹, Soon-Ee Cheah¹, Matthew D. Johnson¹, Mei-Ling Han¹, John D. Boyce², Visanu Thamlikitkul³, Alan Forrest⁴, Keith S. Kaye⁵, Paul Hertzog^{6,7}, Anthony W. Purcell⁸, Jiangning Song⁸, Tony Velkov^{1,*}, Darren J. Creek^{1,*} & Jian Li^{1,*}

Multidrug-resistant *Acinetobacter baumannii* presents a global medical crisis and polymyxins are used as the last-line therapy. This study aimed to identify metabolic differences between polymyxin-susceptible and polymyxin-resistant *A. baumannii* using untargeted metabolomics. The metabolome of each *A. baumannii* strain was measured using liquid chromatography-mass spectrometry. Multivariate and univariate statistics and pathway analyses were employed to elucidate metabolic differences between the polymyxin-susceptible and -resistant *A. baumannii* strains. Significant differences were identified between the metabolic profiles of the polymyxin-susceptible and -resistant *A. baumannii* strains. The lipopolysaccharide (LPS) deficient, polymyxin-resistant 19606R showed perturbation in specific amino acid and carbohydrate metabolites, particularly pentose phosphate pathway (PPP) and tricarboxylic acid (TCA) cycle intermediates. Levels of nucleotides were lower in the LPS-deficient 19606R. Furthermore, 19606R exhibited a shift in its glycerophospholipid profile towards increased abundance of short-chain lipids compared to the parent polymyxin-susceptible ATCC 19606. In contrast, in a pair of clinical isolates 03–149.1 (polymyxin-susceptible) and 03–149.2 (polymyxin-resistant, due to modification of lipid A), minor metabolic differences were identified. Notably, peptidoglycan biosynthesis metabolites were significantly depleted in both of the aforementioned polymyxin-resistant strains. This is the first comparative untargeted metabolomics study to show substantial differences in the metabolic profiles of the polymyxin-susceptible and -resistant *A. baumannii*.

Acinetobacter baumannii is a Gram-negative, aerobic bacterium and a major cause of nosocomial infections worldwide, particularly in critically-ill patients¹. *A. baumannii* infections include hospital-acquired pneumonia, bloodstream infection, urinary tract infection, skin and soft tissue infections^{2,3}. *A. baumannii* has become a significant global threat and is one of the six 'superbugs' identified by the Infectious Diseases Society of America (IDSA) which required urgent attention for discovery of novel antibiotics⁴. Recently, the United States Centers for Disease Control and Prevention (CDC) classified multi-drug resistant (MDR) *A. baumannii* as a microorganism

¹Drug Delivery, Disposition and Dynamics, Monash Institute of Pharmaceutical Sciences, Monash University, Parkville, VIC, 3052, Australia. ²Department of Microbiology, Faculty of Medicine, Nursing & Health Sciences, Monash University, Clayton, VIC, 3800, Australia. ³Faculty of Medicine Siriraj Hospital, Mahidol University, Bangkok, 10700, Thailand. ⁴UNC Eshelman School of Pharmacy, The University of North Carolina at Chapel Hill, Chapel Hill, NC, 27599-7569, USA. ⁵Detroit Medical Centre and Wayne State University, University Health Centre, Detroit, MI, 48201, USA. ⁶Hudson Institute of Medical Research, Clayton, VIC, 3168, Australia. ⁷Faculty of Medicine, Nursing & Health Sciences, Monash University, Clayton, VIC, 3800, Australia. ⁸Department of Biochemistry and Molecular Biology, Faculty of Medicine, Nursing & Health Sciences, Monash University, Clayton, VIC, 3800, Australia. *These authors jointly supervised this work. Correspondence and requests for materials should be addressed to J.L. [REDACTED]

with a threat level of “Serious”⁵. *A. baumannii* has been characterised as ‘naturally transformable’, since it can rapidly acquire diverse resistance mechanisms and undergo genetic modifications that confer resistance to all current clinically used antibiotics^{1,2,6}.

The clinical use of polymyxins waned in the 1970s due to potential nephrotoxicity and neurotoxicity^{7,8}. However, over the last decade colistin (polymyxin E) and polymyxin B have been widely used as the only effective therapeutic option for patients infected with MDR *A. baumannii*^{9–11}. Polymyxins are amphipathic, cationic lipopeptides that contain five L- α , γ -diaminobutyric acid (Dab) residues^{7,8}. The bactericidal activity of polymyxins is exerted via the ‘self-promoted uptake’ pathway, initiated by electrostatic interaction with the lipid A of lipopolysaccharide (LPS) on the outer leaflet of the bacterial outer membrane^{7,12}. In addition, a recent study suggested that polymyxins exert bacterial killing through a specific mechanism via the formation of hydroxyl radicals¹³. Polymyxin resistance in *A. baumannii* can be acquired via the addition of phosphoethanolamine^{14,15} or galactosamine¹⁶ to lipid A structure. Our group firstly reported that *A. baumannii* ATCC 19606 spontaneously acquired colistin resistance following exposure to high levels of colistin, via the loss of its initial target, LPS¹⁷. Further analyses revealed LPS loss was due to single random mutations in the lipid A biosynthesis genes, *lpxA*, *lpxC* and *lpxD*¹⁷. Moreover, transcriptomic analyses of the *A. baumannii* LPS-deficient strain 19606R revealed significant up-regulation of genes involved in the cell envelope and membrane biogenesis, in particular of the Lol lipoprotein transport system and the Mla-retrograde phospholipid transport system¹⁸. We therefore hypothesised that the LPS-deficient strain 19606R exhibits significant changes in its metabolic profile in response to LPS loss. For bacteria, metabolomics is a powerful systems biology tool for understanding cell physiology and can complement and validate data from genomics, transcriptomics and proteomics^{19–21}. In this study, we report the first comparative untargeted metabolomics analyses of paired polymyxin-susceptible and polymyxin-resistant (via LPS loss or lipid A modifications) *A. baumannii* strains.

Results

Comparative untargeted metabolomics was employed to identify differences in the metabolic profile between polymyxin-susceptible and polymyxin-resistant *A. baumannii* strains. Two pairs of *A. baumannii* strains were examined: a laboratory-derived polymyxin-resistant, LPS-deficient *lpxA*-mutant strain, 19606R and its polymyxin-susceptible parent strain, ATCC 19606; and two clinical isolates, polymyxin-susceptible 03–149.1 and polymyxin-resistant 03–149.2 obtained from a patient before and after colistin treatment, respectively. The polymyxin-resistant strain 19606R displayed a slower growth rate compared to the parent strain ATCC 19606, as previously reported¹⁷. Whereas, there was no significant difference in the growth rate between the paired polymyxin-susceptible 03–149.1 and polymyxin-resistant 03–149.2 clinical isolates.

Genomics and lipid A structural analysis of *A. baumannii* clinical isolates 03–149.1 and 03–149.2. The paired *A. baumannii* clinical isolates of polymyxin-susceptible 03–149.1 and polymyxin-resistant 03–149.2 strains were initially identified using 16S rDNA gene sequencing; and showed 96.17% and 97.15% sequence similarity to the *A. baumannii* ATCC 19606, respectively (Supplementary Table S1). Furthermore, a comparison of the polymyxin-susceptible 03–149.1 and the polymyxin-resistant 03–149.2 by high-throughput sequencing and variant calling revealed 3 variations unique to the 03–149.2 isolate (Supplementary Table S2). One variation found in 03–149.2 was a deletion of 3 bases in the *pmrB* gene, which conferred an in-frame deletion of alanine 28. We also investigated the mechanism(s) of polymyxin resistance in the clinical isolate 03–149.2 with lipid A structural analysis. Lipid A samples isolated from both polymyxin-susceptible 03–149.1 and polymyxin-resistant 03–149.2 were characterised with electrospray ionization (ESI) high-resolution mass spectrometry in the negative-ion mode (Fig. 1). The mass spectrum of lipid A from the polymyxin-susceptible 03–149.1 shows a predominant peak at m/z 1911.28, which represents a hepta-acylated lipid A with four primary fatty acyls (i.e. two 3-hydroxylaurate [C_{12} (3-OH)] acyl chains and two 3-hydroxymyristate [C_{14} (3-OH)] acyl chains), and three secondary fatty acyls (i.e. one C_{12} (3-OH) acyl chain and two laurate (C_{12}) acyl chains); while the peak at m/z 1933.26 represents the sodium adduct of the hepta-acylated lipid A mentioned above (Fig. 1A). The peak at m/z 1883.25 is for a hepta-acylated lipid A with four primary C_{14} (3-OH) acyl chains and three secondary fatty acyls (i.e. one C_{12} acyl chain, one C_{12} (3-OH) acyl chain, and one myristate (C_{14}) acyl chain). The peak at m/z 1729.12 corresponds to a hexa-acylated lipid A, indicating the loss of a laurate acyl chain from the hepta-acylated lipid A at m/z 1911.28 ($\Delta m/z = -182$). Additional peaks at m/z 1649.15, 1803.29, 1831.32 differ from the peaks listed above by dephosphorylation at the 1 or 4' position of lipid A ($\Delta m/z = -80$), while the peaks at m/z 1712.12, 1867.26, and 1895.29 were only different from the corresponding peaks at m/z 1729.12, 1883.25, and 1911.28 by the mass of one oxygen atom ($\Delta m/z = -16$), indicating the absence of 3-hydroxylation at the secondary laurate acyl chain.

Mass spectrometry analyses of lipid A from the polymyxin-resistant 03–149.2 isolate revealed several different types of modifications in the lipid A structure (Fig. 1B). The predominant peak at m/z 2034.29 represents the hepta-acylated lipid A at m/z 1911.28 modified with a phosphoethanolamine (pEtN) residue ($\Delta m/z = +123$), while the peak at m/z 1954.32 indicates its dephosphorylated form ($\Delta m/z = -80$). Minor peaks at m/z 1990.26, 2006.26, and 2018.29 correspond to lipid A at m/z 1867.26, 1883.25, and 1895.29 which were modified with a pEtN group, respectively. The peak at m/z 2157.30 represents a modified lipid A with the addition of two pEtN moieties to the parent structure at m/z 1911.28. Interestingly, lipid A modified with galactosamine (GalN) was also detected in polymyxin-resistant 03–149.2. In detail, the peaks at m/z 2078.25 and 2094.33 represent lipid A at m/z 1895.29 and 1911.28 modified with a GalN residue ($\Delta m/z = +161$) along with a sodium adduct, respectively, and the peak at m/z 2195.36 corresponds to a lipid A (m/z 1911.28) with both pEtN and GalN additions ($\Delta m/z = +284$) (Fig. 1B).

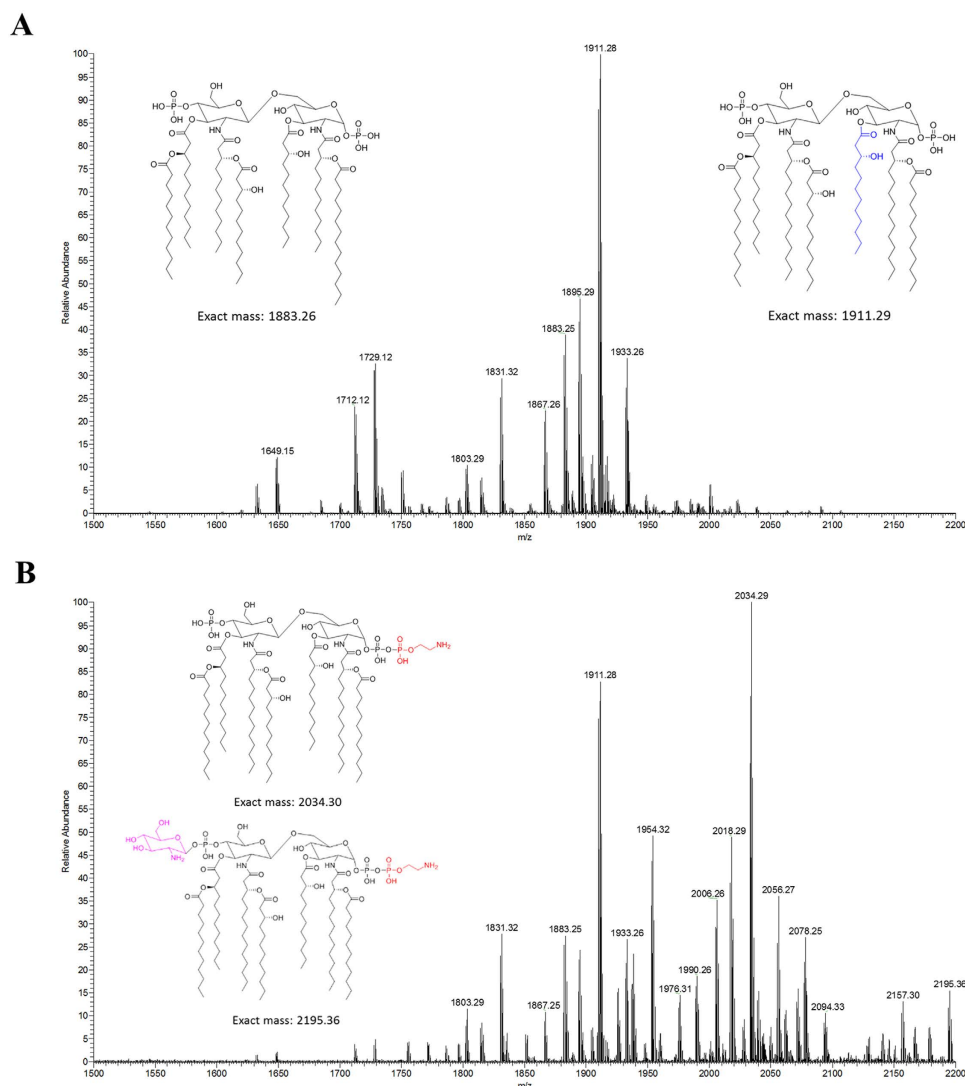


Figure 1. The mass spectra of lipid A isolated from the *A. baumannii* clinical isolates. (A) Polymyxin-susceptible 03-149.1 without lipid A modification. (B) Polymyxin-resistant 03-149.2 with lipid A modifications with phosphoethanolamine (pEtN) and galactosamine (GalN).

Optimal metabolite recovery of MDR *A. baumannii* by washing with 0.9% NaCl and extraction using chloroform:methanol:water (1:3:1). Optimisation of the metabolite sampling method was performed prior to the metabolomics analysis of paired polymyxin-susceptible and polymyxin-resistant strains. The potential for metabolite leakage during the washing step was examined by comparing washed and unwashed cell extracts, and analysing the washing waste supernatant. The hierarchical clustered heat map demonstrated that the washing step with 0.9% NaCl successfully removed the majority of culture media components (Fig. 2A). Recovery of intracellular metabolites (those not present in the broth) was not substantially impacted by washing. Analysis of the supernatant from the washing waste detected leakage of certain cell-derived metabolites, but at very low levels relative to the levels within the cell pellets. Furthermore, evaluation of four extraction solvents showed a total of 1099, 1104, 1070 and 1089 metabolites detected from the LC-MS analyses of metabolite samples extracted by the chloroform:methanol (CM; 1:2, v/v), chloroform:methanol:water (CMW; 1:3:1, v/v), 60% ethanol (60EtOH) and absolute methanol (MeOH) solvents, respectively. CMW was the most promising solvent, demonstrating efficient extraction of a wide range of metabolite classes (Fig. 2B). In addition, the median relative standard deviation (RSD) for all metabolites in the CMW samples was 22%, which is within an acceptable range and is comparable to the standard MeOH extraction solvent (Table 1). In comparison, CM and 60EtOH extraction solvents showed median RSD values of 25% and 24%, respectively. Peak intensities and RSD values for a number of common metabolites are provided in Table 1, showing that CMW was the most reproducible compared to the other three extraction solvents.

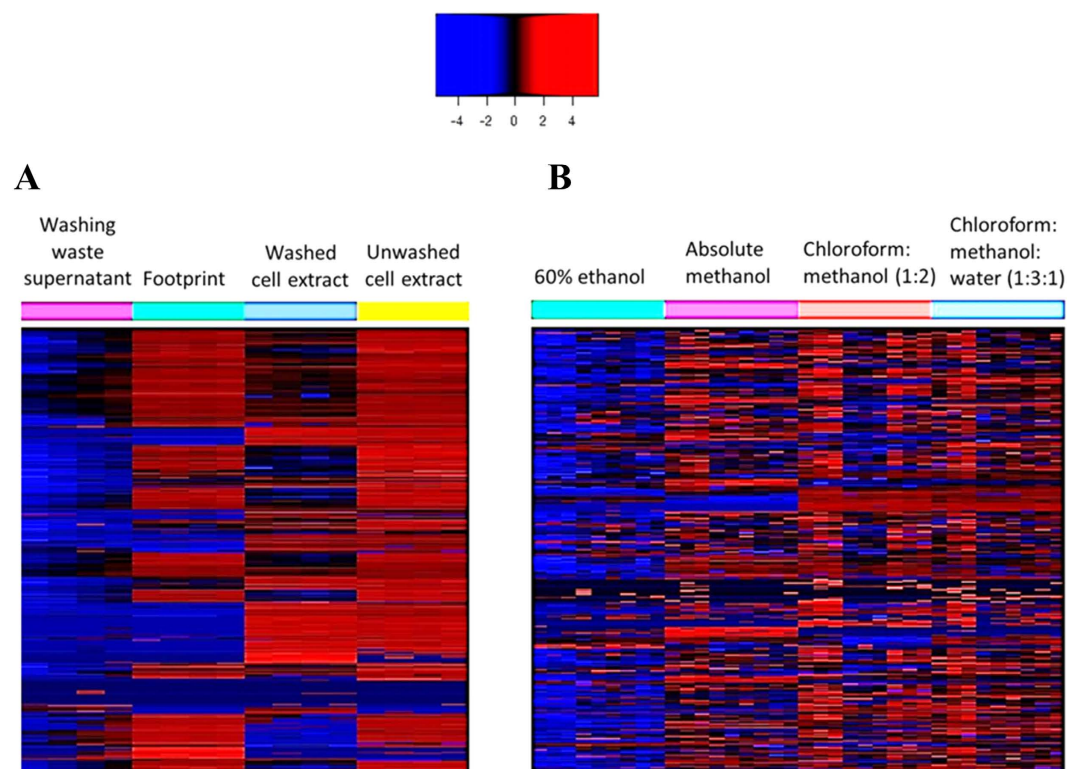


Figure 2. Evaluation of washing step and extraction solvents in the sample pre-treatment method. (A) Clustered heat map distinguished the total metabolite recovery between cells subjected to washing with 0.9% NaCl and without washing. (B) Comparison of four different extraction solvents on the global metabolite recovery in *A. baumannii*: 60% ethanol, absolute methanol, chloroform:methanol (1:2, v/v), and chloroform:methanol:water (1:3:1, v/v).

Multivariate and univariate metabolomics analyses were able to identify key differences between the polymyxin-susceptible and polymyxin-resistant *A. baumannii* strains. The metabolomics data from the present LCMS-based comparative untargeted metabolomics study were highly reproducible. The pooled quality control samples clustered tightly in the PCA plot, indicating small analytical variations among the samples (Supplementary Figure S1). Furthermore, the median RSD value for all metabolites in this study was less than 10%. Global metabolome differences between four *A. baumannii* strains were visualised using PCA score plots (Fig. 3A) and heat map profiles (Fig. 4), and demonstrate that the polymyxin-resistant and polymyxin-susceptible strains differed significantly in their levels of a number of key cellular metabolites. PCA score plots also clearly show that there were global metabolic differences between the paired *A. baumannii* strains (Fig. 3B,C). Interestingly, nearly 25% of metabolites in the LPS-deficient polymyxin-resistant strain 19606R, were significantly more abundant than the corresponding polymyxin-susceptible parent strain ATCC 19606 (Fig. 3D). Peptides were highly enriched in 19606R, and it appears that many of the more abundant metabolites in this polymyxin-resistant strain 19606R were derived from the growth medium (Fig. 4). The accumulation of medium components within cells was unique to the LPS-deficient 19606R, and was not apparent in the polymyxin-resistant clinical isolate 03–149.2.

For univariate analyses, all the putatively identified cellular metabolites (i.e. those more abundant in cell pellets than in footprint samples) were further analysed to reveal those that showed at least 2-fold differences ($*p < 0.05$ and $**p < 0.01$) in relative abundance between the polymyxin-resistant and polymyxin-susceptible *A. baumannii* strains. Several cellular metabolites were differentially abundant in the polymyxin-susceptible ATCC 19606 and polymyxin-resistant 19606R strains including carbohydrate, amino acid, nucleotide and lipid metabolites. In comparison, there were very few metabolic differences observed in the polymyxin-resistant clinical isolate 03–149.2 and polymyxin-susceptible clinical isolate 03–149.1 (Fig. 3D).

Perturbations in sugar and nucleotide metabolism. The polymyxin-resistant strain 19606R showed significant perturbations of several putative sugar phosphate metabolites, including metabolites associated with the pentose phosphate pathway (PPP). In particular, over 2-fold ($p < 0.01$) higher levels were observed for two PPP metabolites, D-erythrose 4-phosphate and D-sedoheptulose 7-phosphate, whereas the PPP-derived nucleotide precursor, 5-phospho- α -D-ribose 1-diphosphate (PRPP) was more than 3-fold ($p < 0.01$) lower than the polymyxin-susceptible parent strain ATCC 19606 (Fig. 5). On the contrary, the polymyxin-resistant clinical isolate 03–149.2 showed significantly lower abundance of the detected PPP metabolites, D-erythrose 4-phosphate, D-sedoheptulose 7-phosphate, D-glyceraldehyde 3-phosphate, and D-ribose 5-phosphate

	CM	CMW	60EtOH	MeOH
Median RSD value (%)	25	22	24	20
Identified compound				
Amino acids				
L-Lysine	4.1×10^7 (20.7)	5.7×10^7 (16.1)	4.1×10^7 (20.4)	4.2×10^7 (27.6)
L-Serine	1.7×10^7 (22.2)	1.7×10^7 (13.7)	1.3×10^7 (15.7)	1.8×10^7 (7.3)
L-Tyrosine	9.7×10^7 (14.0)	9.5×10^7 (12.8)	5.6×10^7 (17.6)	1.1×10^8 (11.2)
L-Methionine	1.8×10^8 (11.9)	1.7×10^8 (13.9)	1.2×10^8 (14.5)	1.9×10^8 (10.4)
L-Phenylalanine	3.0×10^8 (13.4)	2.7×10^8 (13.0)	1.8×10^8 (10.8)	2.7×10^8 (9.5)
L-Valine	1.0×10^7 (14.1)	9.6×10^6 (10.2)	7.4×10^6 (13.7)	1.0×10^7 (5.6)
L-Aspartate	2.8×10^7 (11.8)	2.5×10^7 (9.4)	2.2×10^7 (10.5)	2.6×10^7 (6.3)
Energy				
NADPH	5.4×10^5 (45.0)	1.6×10^6 (11.5)	3.8×10^5 (48.3)	6.9×10^5 (35.1)
NAD ⁺	4.6×10^7 (33.0)	7.6×10^7 (9.8)	3.4×10^7 (16.1)	5.5×10^7 (23.4)
FMN	4.7×10^5 (31.3)	6.2×10^5 (7.6)	NA*	4.0×10^5 (61.7)
Nucleotides				
Adenine	6.7×10^6 (46.7)	5.1×10^6 (15.6)	2.3×10^6 (41.8)	8.8×10^6 (26.6)
Cytidine	9.1×10^6 (24.1)	8.7×10^6 (11.9)	4.0×10^6 (10.9)	8.1×10^6 (10.1)
Guanine	2.1×10^5 (38.6)	2.1×10^5 (12.6)	1.5×10^5 (28.2)	2.5×10^5 (12.9)
Uridine	8.7×10^6 (19.2)	8.2×10^6 (14.0)	5.0×10^6 (15.2)	1.0×10^7 (17.3)
Carbohydrate				
Pyruvate	3.0×10^5 (19.8)	3.0×10^5 (17.0)	2.4×10^5 (25.2)	2.8×10^5 (10.7)
Sucrose	2.0×10^6 (39.2)	1.9×10^6 (13.5)	1.1×10^6 (13.7)	1.8×10^6 (14.7)
Citrate	1.7×10^7 (38.7)	2.8×10^7 (14.9)	2.7×10^7 (20.4)	2.2×10^7 (18.6)
cis-Aconitate	2.3×10^5 (29.3)	4.5×10^5 (14.9)	2.6×10^5 (17.8)	3.3×10^5 (19.5)
Oxalate	2.5×10^5 (22.7)	2.7×10^5 (19.3)	2.8×10^5 (29.2)	2.3×10^5 (22.9)
(R,R)-Tartaric acid	3.2×10^4 (19.4)	4.0×10^4 (17.3)	3.4×10^4 (23.3)	3.3×10^4 (22.3)

Table 1. Validation and reproducibility of metabolite extraction procedure for four different extraction solvents. CM, chloroform:methanol (1:2, v/v); CMW, chloroform:methanol:water (1:3:1, v/v); 60EtOH, 60% ethanol; MeOH, absolute methanol (3 biological samples with 3 technical replicates per condition). *NA, not available as the metabolite was not detected. Data are expressed as mean relative intensity (relative standard deviation, RSD, %).

($p < 0.05$) than the paired susceptible isolate 03–149.1. Besides, the levels of most nucleotides were significantly lower in the polymyxin-resistant 19606R than the parent polymyxin-susceptible ATCC 19606 strain (Fig. 6). However, there were no clear differences in nucleotide levels between the paired clinical isolates. Furthermore, two essential tricarboxylic acid (TCA) cycle intermediates, 2-oxoglutarate and *cis*-aconitate were identified at least 2-fold ($p < 0.05$) lower in relative abundance in the polymyxin-resistant 19606R cells (Fig. 7). Other TCA cycle metabolites, acetyl-CoA, citrate, and succinate, showed a consistent pattern of lower relative abundance in the polymyxin-resistant strain 19606R, albeit with less than two-fold difference. Interestingly, a similar pattern of metabolic changes were observed in the polymyxin-resistant clinical isolate 03–149.2; which showed lower abundance of citrate, *cis*-aconitate, 2-oxoglutarate and succinate than the polymyxin-susceptible clinical isolate 03–149.1.

Variations of amino acid related metabolites in the polymyxin-resistant 19606R. The abundance of several metabolites involved in phenylalanine, tyrosine, tryptophan and histidine metabolic pathways were significantly ($p < 0.01$) perturbed in the polymyxin-resistant 19606R strain (Table 2). Most notably, two putative metabolites associated with the shikimate pathway, shikimate-3-phosphate and 5-O-(1-Carboxyvinyl)-3-phosphoshikimate were significantly higher in abundance (between 11- to 14-fold) in the polymyxin-resistant 19606R compared to the polymyxin-susceptible parent strain ATCC 19606. Significant depletion was observed in three important peptidoglycan biosynthesis intermediates, *N*-succinyl-L,L-2,6-diaminopimelate, *meso*-diaminopimelate and UDP-*N*-acetylmuramoyl-L-alanyl- γ -D-glutamyl-*meso*-2,6-diaminopimelate which were 2- to 5-fold lower in the polymyxin-resistant 19606R (Fig. 8A). In addition, levels of these metabolites also decreased in the clinical polymyxin-resistant strain, 03–149.2. Interestingly, choline was undetectable in the polymyxin-resistant 19606R strain (Fig. 8B), suggesting differential uptake or utilisation of this metabolite from the growth medium. Footprint analysis revealed complete depletion of choline from the growth medium for the polymyxin-resistant 19606R, but not for the polymyxin-susceptible ATCC 19606 or both of the clinical isolates.

Perturbation of lipids levels in the LPS-deficient polymyxin-resistant 19606R. Analyses of cellular lipid metabolites in the polymyxin-resistant 19606R and polymyxin-susceptible ATCC 19606 revealed profound alteration ($p < 0.05$) of several putatively identified lipid metabolites. The observed accurate masses

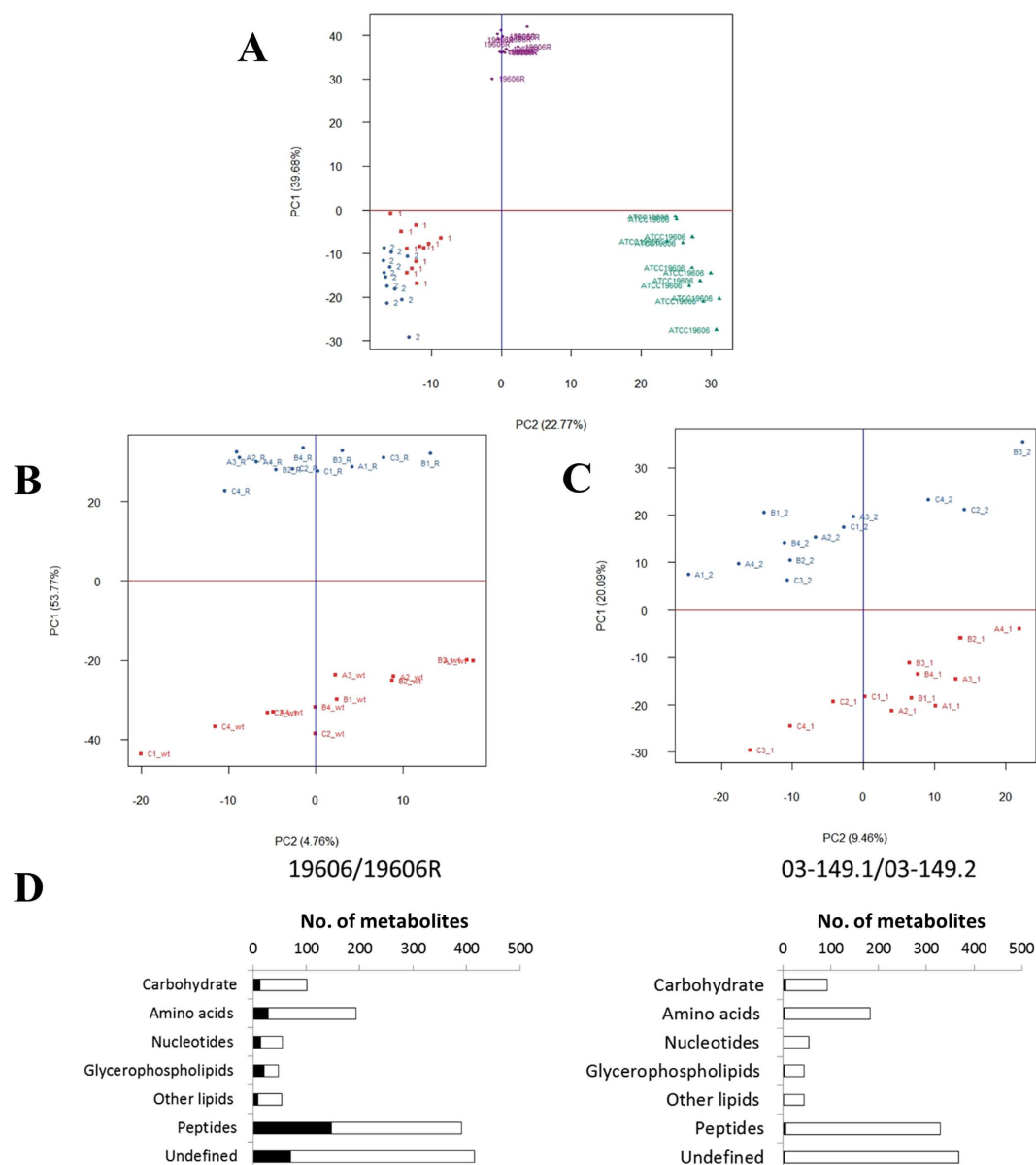


Figure 3. (A) PCA score plot of four *A. baumannii* strains. (B) PCA score plot of paired polymyxin-resistant 19606R and the wild-type ATCC 19606. (C) PCA score plot of paired polymyxin-resistant 03-149.2 and polymyxin-susceptible 03-149.1 clinical isolates. Each data set for individual strains represents a total of 12 sample replicates (3 biological replicates and each with 4 technical replicates). (D) Pathway-focused representation of the significant metabolites (black bars) and total number of putatively identified metabolites (open bars) for the polymyxin-resistant 19606R relative to the wild-type ATCC 19606 (left) and the polymyxin-resistant clinical isolate 03-149.2 relative to the polymyxin-susceptible isolate 03-149.1 (right). Significant metabolites were selected by at least 2-fold difference ($p < 0.05$) in the metabolites levels of polymyxin-resistant strain relative to the polymyxin-susceptible strain.

and retention times indicated that many of these lipids were unsaturated and oxidised fatty acids; precise identification of these fatty acids is beyond the scope of this study. High level identification of glycerophospholipids (GPs) based on molecular formula revealed significant perturbations in the major phospholipid species, glycerophosphoethanolamine (PE), glycerophosphoserine (PS), and glycerophosphoglycerol (PG). In general, GPs with shorter-chain fatty acids (total ≤ 32 carbons) were enriched in the polymyxin-resistant LPS-deficient 19606R, in addition to the shorter-chain lysophospholipids (≤ 18 carbons) (Fig. 9A). Notably, lipids with longer-chain fatty acids (> 32 carbons) were generally depleted in the LPS-deficient 19606R. However, these trends were not observed in *A. baumannii* of both clinical isolates, polymyxin-susceptible 03-149.1 and polymyxin-resistant 03-149.2 (Fig. 9B). Furthermore, two key metabolites linked with glycerophospholipid metabolism, ethanolamine phosphate and glycerophosphoethanolamine phosphate were significantly ($p < 0.05$) lower in abundance in the

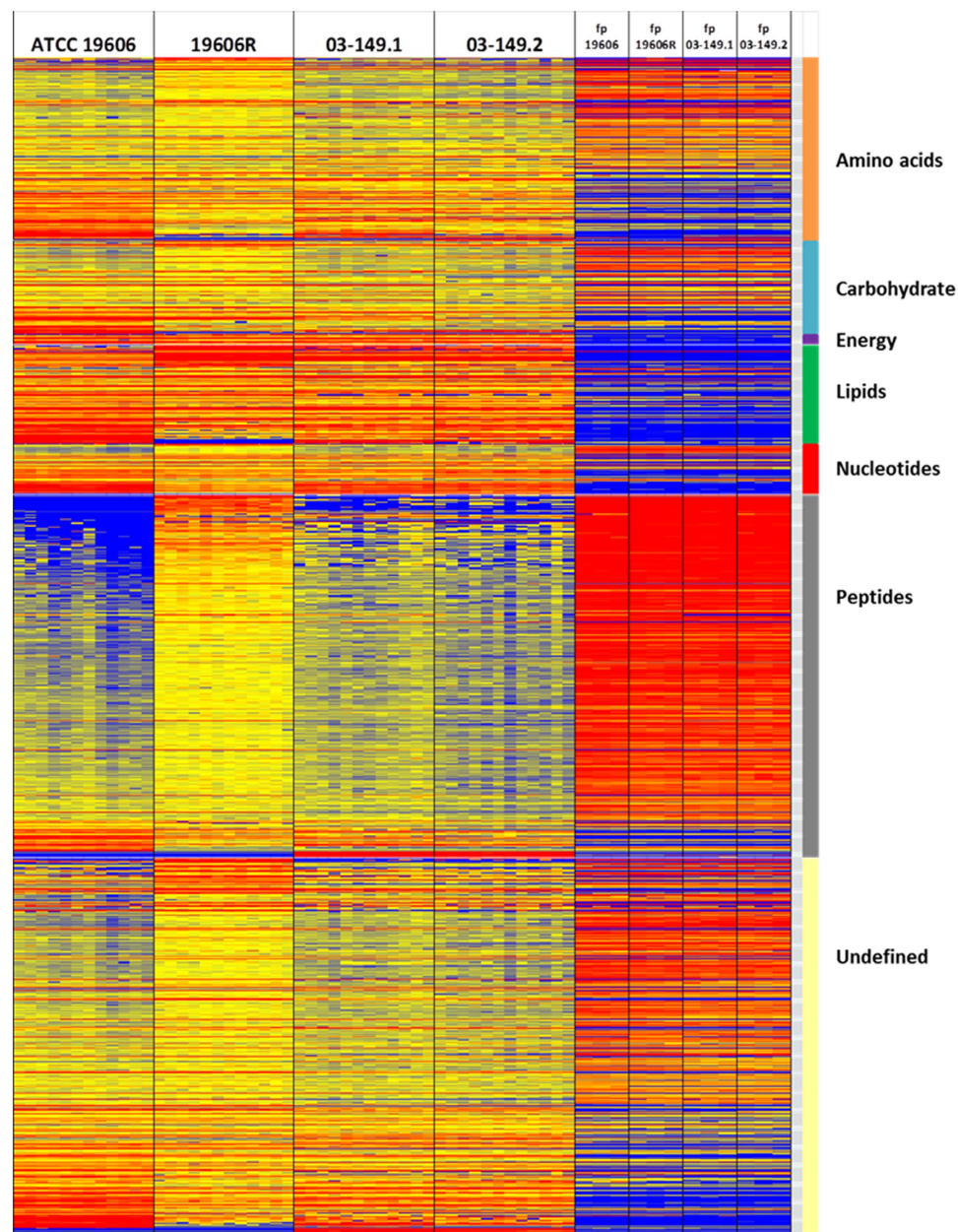


Figure 4. Heat map profiles of metabolite peak intensities in *A. baumannii*. Left: paired strains of ATCC 19606 and polymyxin-resistant 19606R, Right: paired clinical isolates polymyxin-susceptible 03–149.1 and polymyxin-resistant 03–149.2. Metabolites are grouped into different classes: amino acids, carbohydrates, energy, lipids, nucleotides, peptides and undefined. Metabolites derived from the footprint (fp) also represented in the heat map. The colors indicate the relative abundance of metabolites based on the relative peak intensity (red = high, yellow = no change, blue = undetectable).

polymyxin-resistant 19606R than the polymyxin-susceptible parent strain ATCC 19606, but not significantly changed in both *A. baumannii* clinical isolates (Fig. 9C).

Untargeted analysis reveals unknown metabolites that are common to both polymyxin-resistant strains. Four unidentified features were uniquely detected in both polymyxin-resistant strains and not in either of the polymyxin-susceptible strains. Whilst these features could not be identified based on existing bacterial metabolite databases, formula determination based on accurate mass, isotope abundance and retention time suggests that these unique metabolites may be complex amino-sugars: $C_{12}H_{24}N_2O_8$ (mass 324.153; t_R 14.7 min), $C_{30}H_{57}N_2O_{12}P_3$ (mass 730.312; t_R 17.2 min), $C_{13}H_{26}N_2O_6$ (mass 306.179; t_R 19.8 min), and $C_{16}H_{28}N_2O_{11}[Cl^-]$ (mass 460.146; t_R 13.7 min). Notably, three unidentified metabolites were detected in both polymyxin-susceptible strains, but were absent in both of the polymyxin-resistant strains. Accurate mass indicates that these features likely represent metabolites with the formulas $C_9H_{14}N_2O_5S$ (mass 262.063; t_R 13.4 min),

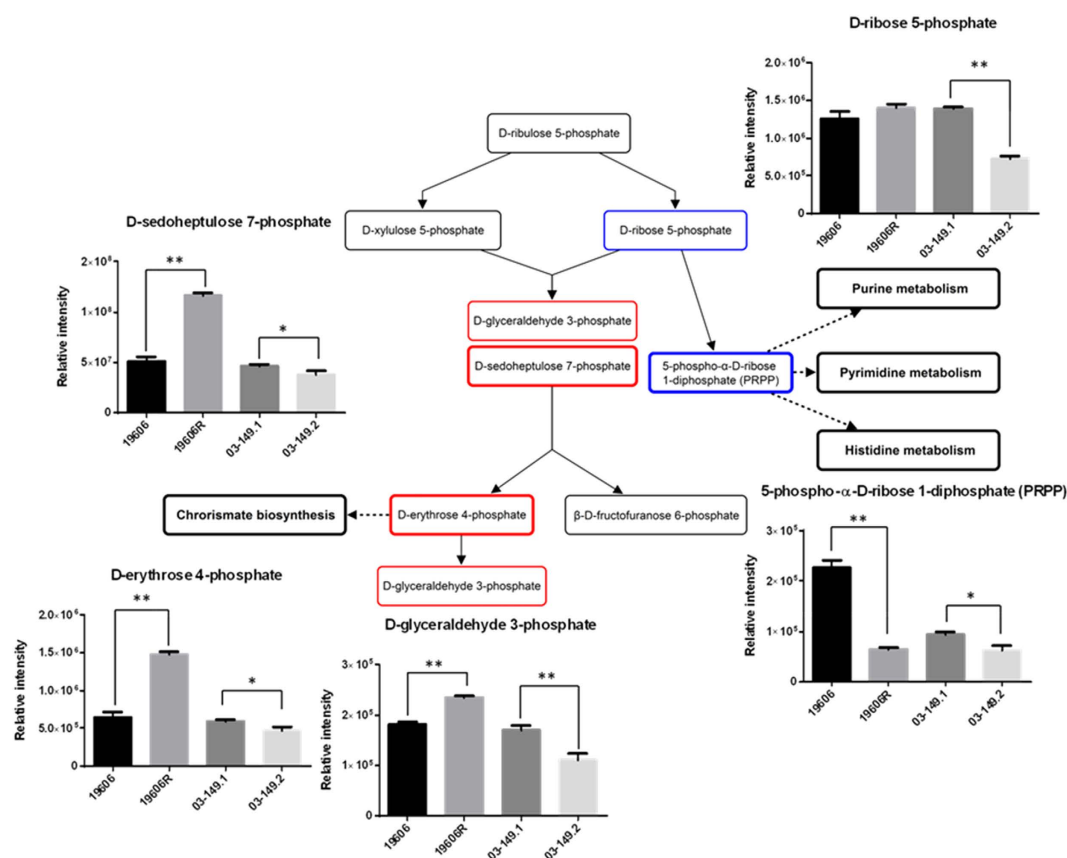


Figure 5. Perturbations of identified sugar phosphates in *A. baumannii*. Pentose phosphate pathway (PPP) of *A. baumannii*. PPP intermediates showed significant differences between polymyxin-resistant and polymyxin-susceptible *A. baumannii* strains. Metabolites in the red bold box indicate metabolites that were at least 2-fold more abundant in polymyxin-resistant 19606R strain than polymyxin-susceptible ATCC 19606 strain. Metabolites in the red box indicate metabolites that were less than 2-fold more abundant in the 19606R strain. The blue bold box indicates the metabolite that was at least 2-fold less abundant in 19606R than ATCC 19606. The blue box indicates the metabolite that was less than 2-fold less abundant in the 03–149.2 polymyxin-resistant strain than polymyxin-susceptible 03–149.1 strain. The black boxes indicate metabolites that were not detected. * $p < 0.05$; ** $p < 0.01$.

$C_7H_{11}NO_3S$ (mass 189.046; t_R 7.5 min) and $C_{11}H_{19}N_3O_7S_2$ (mass 369.066, t_R 16.8 min). The latter formula corresponds to γ -glutamyl cystine, and the presence of sulfur in the other formulas suggest that they may also be cysteine conjugates.

Discussion

In recent times, untargeted metabolomics has been successfully applied towards the investigation of global metabolic profiles, particularly in microbiology and pharmacology^{22–24}. Advantageously, the untargeted metabolomics platform enables the detection of both known and unknown metabolites and has allowed the elucidation of complex interactions between cellular metabolites²¹. Significantly, this global metabolomics approach has been beneficial in enhancing our understanding of the biological nature of antimicrobial resistance mechanisms. Global metabolic profiling distinguished differential metabolic patterns between antibiotic-susceptible and antibiotic-resistant strains of *A. baumannii*, *Pseudomonas aeruginosa*, *Nocardia* spp., as well as the protozoan parasites *Trypanosoma brucei* and *Leishmania donovani*^{25–29}. In a previous study, both planktonic and biofilm forms of *A. baumannii* were compared to identify metabolic profiles associated with biofilm synthesis²⁵. In the present study, we employed a global metabolic profiling strategy to identify key metabolic differences between two pairs of polymyxin-susceptible and polymyxin-resistant *A. baumannii* strains, specifically conferred by two different mechanisms of polymyxin resistance, LPS loss and lipid A modifications.

Gram-negative bacteria can develop resistance to most current antimicrobial agents because of their extraordinary metabolic versatility and adaptability to a wide range of environmental conditions². The main mechanisms used for conferring polymyxin resistance in Gram-negative bacteria involved modifications of lipid A, the membrane embedded component of lipopolysaccharides (LPS)⁷. In a previous study, we discovered that *A. baumannii* can develop resistance to very high colistin concentrations through a complete loss of LPS, due to spontaneous mutations in any one of the three key lipid A biosynthetic genes¹⁷. Polymyxin resistance in 19606R was shown to be conferred by a spontaneous single mutation in *lpxA* gene, resulting in LPS loss¹⁷. RNA expression profiling of polymyxin-resistant 19606R by our group indicated that significant outer-membrane remodelling

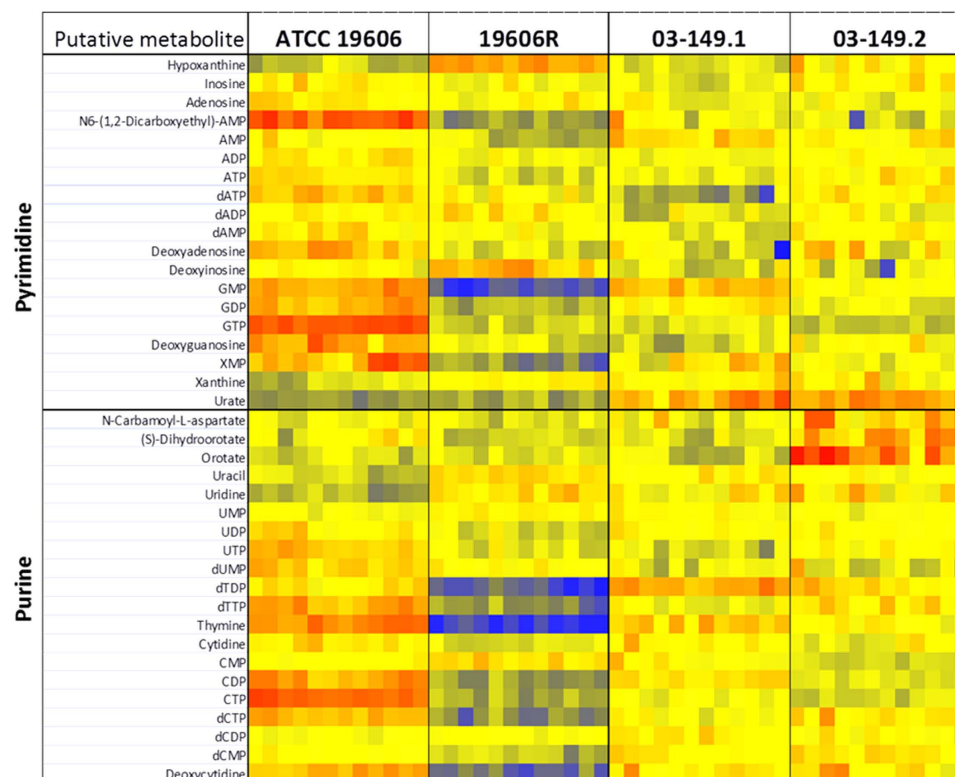


Figure 6. Heat map profiles of relative abundance of nucleotides. The polymyxin-resistant 19606R and its parent ATCC 19606 (left) and the clinical isolates polymyxin-resistant 03–149.2 and polymyxin-susceptible 03–149.1 (right). The colors indicate the relative abundance of metabolites based on the relative peak intensity (red = high, yellow = no change, blue = undetectable).

occurs due to LPS loss¹⁸. This included increased expression of genes involved in cell envelope and membrane biogenesis, in particular the Lol lipoprotein transport system, the Mla-retrograde phospholipid transport system and poly- β -1,6-*N*-acetylglucosamine (PNAG) biosynthesis¹⁸. In addition, polymyxin-resistant 19606R displays a decreased expression of genes predicted to encode the fimbrial subunit FimA and components involved in the type VI secretion system (T6SS)¹⁸.

Our genome sequencing data for the polymyxin-resistant isolate 03–149.2 show that the deletion of 3 bases in the *pmrB* gene conferred an in-frame deletion of alanine 28. This particular mutation has not been characterized previously. However, mutations in *pmrB* have repeatedly been shown to cause polymyxin resistance in *A. baumannii* by the upregulation of the phosphoethanolamine transferase, *pmrC*, and subsequent lipid A modification³⁰. Furthermore, structural analyses of lipid A from both polymyxin-susceptible 03–149.1 and polymyxin-resistant 03–149.2 clinical isolates revealed lipid A modifications with phosphoethanolamine (pEtN) and galactosamine (GalN) in the polymyxin-resistant 03–149.2 strain (Supplementary Figure S2). These lipid A modifications play a role in polymyxin resistance similar to that of aminoarabinose modification in other Gram-negative bacteria^{31,32} which reduce the initial electrostatic interaction with polymyxins by reducing the negative charge on the bacterial outer membrane^{7,33,34}. The results clearly indicate that the mechanism of polymyxin resistance in the polymyxin-resistant 03–149.2 isolate differs from the *A. baumannii* 19606R resistant strain, which was due to the complete loss of LPS¹⁷.

Careful assessment of sample preparation methods is an important pre-requisite step to generate physiological metabolome data based on the differences in cell composition and culture condition³⁵. In our study, the effect of the washing step and the efficiency of four different extraction solvents were firstly examined. Since a very rich culture medium, cation-adjusted Mueller-Hinton broth (MHB) was used in this study, a washing process was essential to avoid medium effects and to ensure that detected metabolites solely derive from cells³⁶. Desirably, the leakage of intracellular metabolites into its extracellular environment should be avoided during the washing step³⁷. As washing with organic solvents at sub-zero temperature leads to the leakage of cellular metabolites³⁸, we implemented a quenching step at 0°C and washing in aqueous buffer 0.9% NaCl (4°C). The washing process was effective in eliminating most of the extracellular contaminants from the rich growth media whilst avoiding significant leakage of intracellular metabolites. Furthermore, the ideal extraction solvent should be able to extract a broad range of metabolites with different physicochemical properties in high and reproducible yield³⁹. Several extraction solvents have been reported in the literature for bacterial metabolomics, and four promising solvent compositions were selected to determine the optimal extraction method specifically for *A. baumannii* in the present study. Unsurprisingly, our analyses showed that different extraction solvents preferentially extract certain metabolites depending on the polarity of the solvent. Overall, CMW (1:3:1, v/v) provided the greatest

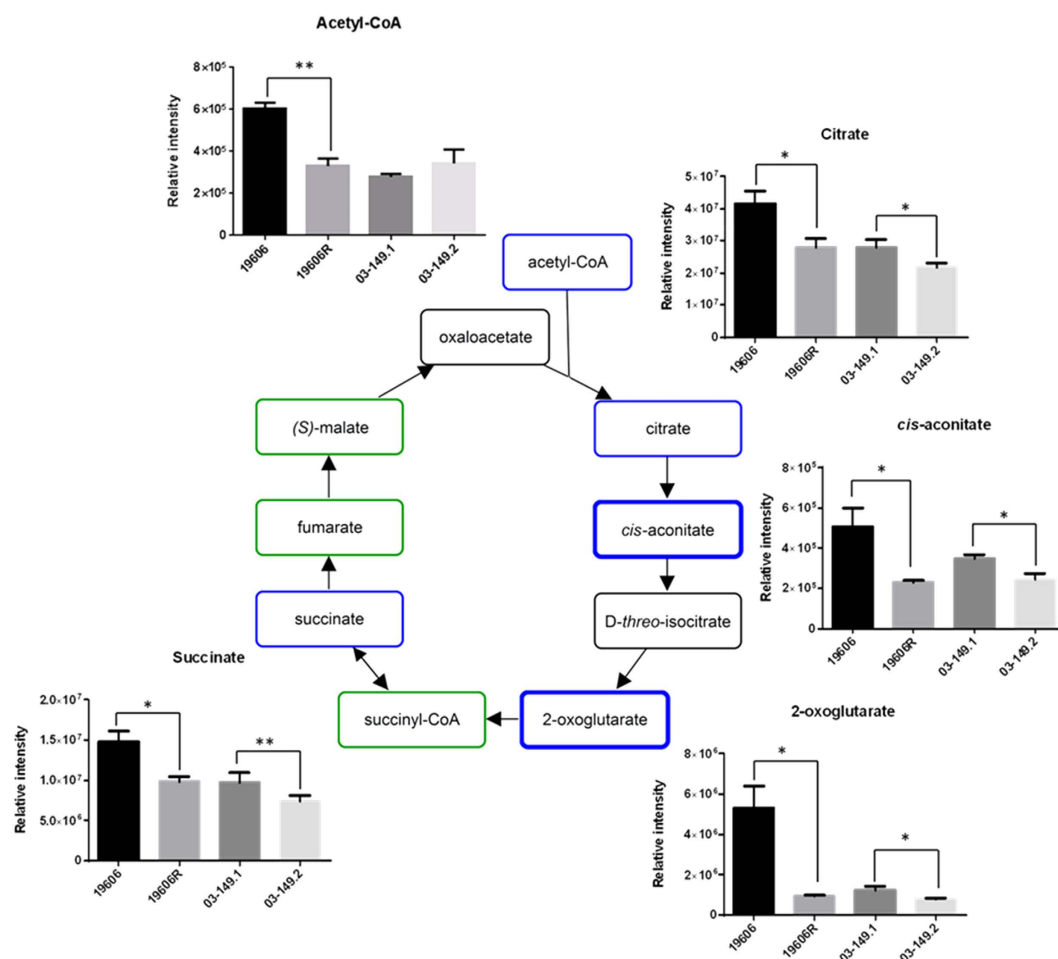


Figure 7. Perturbations of TCA cycle intermediates in *A. baumannii*. TCA cycle of *A. baumannii*. The blue bold box indicates metabolites that were at least 2-fold less abundant in the polymyxin-resistant 19606R strain than polymyxin-susceptible ATCC 19606. Metabolites in the blue box indicate metabolites that were less than 2-fold less abundant in 19606R than ATCC 19606. The green boxes indicate metabolites that were detected but not significant. The black boxes indicate metabolites that were not detected. * $p < 0.05$; ** $p < 0.01$.

recovery and reproducibility for the largest number of different classes of metabolites, and is suitable to be used as a one-step method for untargeted metabolomics studies of *A. baumannii*.

Metabolic fingerprinting of two pairs of polymyxin-susceptible and polymyxin-resistant *A. baumannii* strains demonstrated accumulation or depletion of specific metabolite pools, indicating differential regulation of particular metabolic pathways. Interestingly, PCA plots clearly distinguished the metabolic profile differences between the polymyxin-resistant strain 19606R and the three other *A. baumannii* strains, signifying that the metabolic differences were substantially driven by the complete loss of outer membrane LPS. Notably, there were clear metabolic differences between the polymyxin-susceptible ATCC 19606 and polymyxin-resistant 19606R. In contrast, relatively very few metabolite differences were identified between the *A. baumannii* clinical isolates, polymyxin-susceptible 03-149.1 and polymyxin-resistant 03-149.2, demonstrating that lipid A modifications had minimal impact on the global metabolic profile. In general, the results show that different mechanisms of polymyxin resistance lead to unique changes in global metabolic profiles.

Our results demonstrate that peptides derived from the medium component were substantially accumulated in the polymyxin-resistant strain 19606R compared to other *A. baumannii* strains, and suggested that the uptake was facilitated significantly as a result of loss membrane integrity from the total LPS loss. The analyses of carbohydrate associated metabolites displayed higher levels of pentose phosphate pathway (PPP) intermediates in the polymyxin-resistant 19606R than in its susceptible parent strain ATCC 19606. In contrast, the polymyxin-resistant 03-149.2 showed significantly lower levels of detected PPP-associated metabolites than the polymyxin-susceptible 03-149.1. However, a major end-product of the PPP, 5-phospho- α -D-ribose 1-diphosphate (PRPP), was 3.5-fold lower in abundance in the polymyxin-resistant 19606R, suggesting diversion of flux through the non-oxidative branch of the PPP. PRPP is an essential precursor for both purine and pyrimidine nucleotide biosynthesis as well as for the biosynthesis of amino acids histidine and tryptophan⁴⁰. Coincidentally, decreased levels of nucleotides was observed in 19606R, as well as depletion of two histidine metabolites, *N*-formimino-L-glutamate (24-fold) and urocanate (3-fold), which may be secondary to the

Formula	Putative metabolite ^a	Pathway/metabolism	Fold change	P-value
Carbohydrate				
C ₅ H ₁₂ O ₅	Xylitol	Pentose and glucuronate interconversions	3.47	0.00017
C ₁₂ H ₂₃ O ₁₄ P	Lactose 6-phosphate	Galactose metabolism	2.14	0.0018
C ₃ H ₆ O ₉ P ₂	Cyclic 2,3-bisphospho-D-glycerate	Carbohydrate metabolism	-3.01	0.0035
Amino acids				
C ₇ H ₁₁ O ₈ P	Shikimate 3-phosphate	Phenylalanine, tyrosine, tryptophan biosynthesis	14.41	0.0012
C ₁₀ H ₁₃ O ₁₀ P	5-O-(1-Carboxyvinyl)-3-phosphoshikimate	Phenylalanine, tyrosine, tryptophan biosynthesis	11.30	0.0079
C ₈ H ₈ O ₅	3,4-Dihydroxymandelate	Tyrosine	3.03	0.00074
C ₄ H ₆ O ₃	2-Methyl-3-oxopropanoate	Valine, leucine and isoleucine degradation	2.19	0.00060
C ₂ H ₅ O ₃ P	Acetyl phosphate	Taurine and hypotaurine	2.15	9.2E-05
C ₉ H ₈ O ₃	Phenylpyruvate	Phenylalanine	-2.00	5.9E-05
C ₉ H ₁₀ O ₄	3-(2,3-Dihydroxyphenyl)propanoate	Phenylalanine	-2.03	0.0011
C ₁₃ H ₁₅ NO ₆	4-Hydroxyphenylacetylglutamic acid	Tyrosine	-2.08	0.0077
C ₇ H ₁₃ NO ₃	L-Carnitine	Lysine degradation	-2.57	0.00049
C ₆ H ₆ N ₂ O ₂	Urocanate	Histidine	-3.75	0.0031
C ₆ H ₁₀ N ₂ O ₄	N-Formimino-L-glutamate	Histidine	-24.86	0.00095

Table 2. Fold changes (relative intensity) in the abundance of metabolites detected in the LPS-deficient polymyxin-resistant 19606R, relative to the parent strain ATCC 19606. ^aPutative metabolites, identified by exact mass, with at least 2-fold differences at p value < 0.01 between the polymyxin-resistant 19606R and the polymyxin-susceptible ATCC 19606.

decreased concentration of PRPP. However, the significant depletion of nucleotide levels was not observed in the polymyxin-resistant 03–149.2 clinical isolate. The increased level of D-erythrose 4-phosphate (2-fold) generated in the PPP of the polymyxin-resistant 19606R strain appears to facilitate biosynthesis of the aromatic amino acids: phenylalanine, tyrosine, and tryptophan through the shikimate pathway, as shown by the significant accumulation of two intermediates, shikimate-3-phosphate (14-fold) and 5-O-(1-Carboxyvinyl)-3-phosphoshikimate (11-fold)⁴¹. Apart from the importance of PPP to conserve stable carbon equilibrium, to generate nucleotide and amino acid biosynthesis precursors and to supply reducing molecules for anabolism, PPP also has been found to be essential in the biosynthesis of LPS in Gram-negative bacteria⁴². SHI, an enzyme that has been characterised in *Escherichia coli*, *P. aeruginosa*⁴³ and *Helicobacter pylori*⁴⁴ converts sedoheptulose 7-phosphate into the LPS precursor, glycerol-manno-heptose 7-phosphate^{43,45,46}. Interestingly, we identified that the level of this particular metabolite, D-sedoheptulose 7-phosphate was about 2-fold higher ($**p < 0.01$) than the other three *A. baumannii* strains. We hypothesised that, as the polymyxin-resistant 19606R is characterised by the total LPS loss¹⁷, the metabolite, sedoheptulose 7-phosphate was significantly accumulated in the cells since it was not converted into the LPS precursor. The TCA cycle is another essential central metabolic pathway in bacterial cells, providing substrates for energy and biosynthetic reactions, including precursors for lipids and amino acids⁴⁷. Notably, both polymyxin-resistant strains, 19606R and clinical isolate 03–149.2 showed lower abundance of TCA cycle metabolites than their respective polymyxin-susceptible strains. This suggested that, in general, the polymyxin-resistant strains produced less energy through TCA cycle indicating lower cellular metabolism than the polymyxin-susceptible strains and this was significantly observed particularly in the polymyxin-resistant strains, 19606R.

Three intracellular metabolites engaged in the peptidoglycan biosynthesis pathway, *meso*-diaminopimelate, UDP-*N*-acetylmuramoyl-L-alanyl- γ -D-glutamyl-*meso*-2-6-diaminopimelate, and *N*-succinyl-L-L-2,6-diaminopimelate were detected 2- to 5-fold less abundant in the polymyxin-resistant 19606R strain, compared to the parent strain ATCC 19606. Interestingly, these metabolites were also significantly decreased (2- to 3-fold) in the polymyxin-resistant clinical isolate 03–149.2. *Meso*-diaminopimelate is derived from lysine degradation and is conjugated with UDP-*N*-acetylmuramoyl-L-alanyl-D-glutamate (catalysed by MurE ligase) in the cytoplasm to form UDP-*N*-acetylmuramoyl-L-alanyl- γ -D-glutamyl-*meso*-2-6-diaminopimelate⁴⁸. This is followed by the addition of dipeptide D-alanyl-D-alanine to form UDP-*N*-acetylmuramoyl-L-alanyl-D-glutamyl-6-carboxy-L-lysyl-D-alanyl-D-alanine (catalysed by MurF ligase). In *E. coli*, the MurE and MurF ligases are encoded by the *murE* and *murF* genes, respectively, co-localised in the genome; these ligases are essential for bacterial viability and are targets for antibacterial chemotherapy⁴⁹. The lower levels of the peptidoglycan biosynthesis metabolites indicate that the polymyxin-resistant 19606R and clinical isolate 03–149.2 synthesised less peptidoglycan compared to their polymyxin-susceptible parent strains. Interestingly, choline levels were significantly depleted in the 19606R strain and its culture medium. In our recent transcriptomics study, the expression of choline dehydrogenase, choline-glycine betaine transporter and choline transport protein BetT was significantly increased (3.0, 3.0 and 4.6 folds, respectively) in the polymyxin-resistant *A. baumannii* 19606R¹⁸. As choline uptake and metabolism have been associated with maintenance of osmotic balance in Gram-negative bacteria^{45,50}, our transcriptomics and metabolomics data collectively indicate that choline was required by 19606R in response

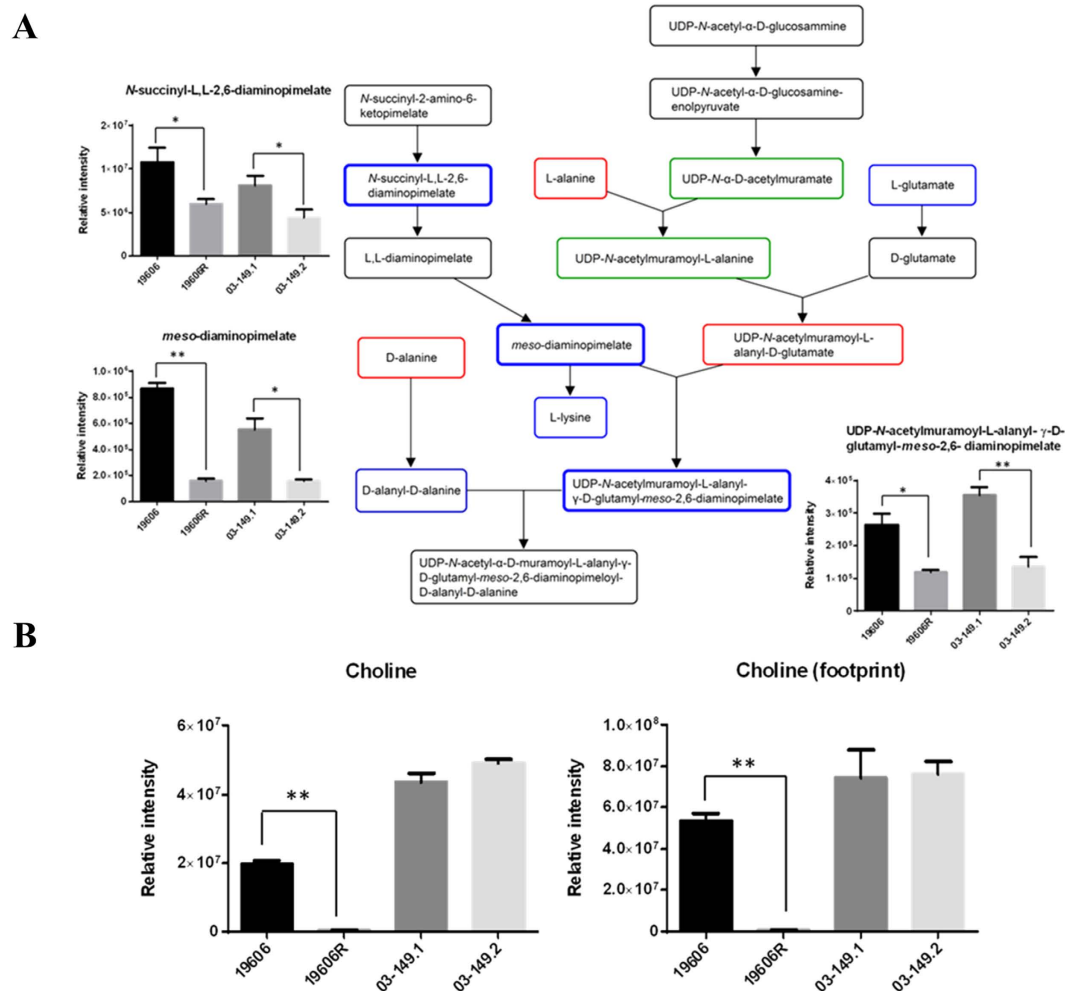


Figure 8. Levels of peptidoglycan biosynthesis metabolites and choline in *A. baumannii*. (A) Peptidoglycan synthesis pathway of *A. baumannii*. Metabolites in the red box indicate metabolites that were less than 2-fold higher in polymyxin-resistant strains than polymyxin-susceptible strains. The blue and bold boxes indicate metabolites that were at least 2-fold lower in polymyxin-resistant strains than polymyxin-susceptible strains. Metabolites in the blue box indicate less than 2-fold lower abundance in polymyxin-resistant strains than polymyxin-susceptible strains. The green box indicates metabolites that were detected but not significant. Metabolites in the black box were not detected. (B) Intracellular and footprint (extracellular) choline shows significantly lower abundance in the polymyxin-resistant 19606R than the parent wild-type ATCC 19606. * $p < 0.05$; ** $p < 0.01$.

to the osmolarity pressure due to the less peptidoglycan caused by polymyxin resistance. However, there was no profound change in choline level in the polymyxin-resistant clinical isolate 03-149.2 proposing that choline was not utilised and the level was in equilibrium state between intracellular and extracellular.

The outer membrane (OM) of Gram-negative bacterial cells is composed of an asymmetrical bilayer consisting of an outer leaflet with LPS as a major component, and the inner leaflet mainly containing glycerophospholipids (GPs)⁵¹. The OM serves as an efficient permeability barrier and a first-line defence mechanism, and GPs are the most prevalent component of lipids in the bacteria OM⁵². Compared to GPs species in the samples obtained from ATCC 19606, the LPS-deficient, polymyxin-resistant 19606R produced relatively high levels of GP species PE, PS and PG with shorter fatty acyl chains (less than 32 carbons in both chains) and concomitantly less GP species with more than 34 carbons in their fatty acyl chains. This finding agrees with a previous report that showed a LPS-deficient *Neisseria meningitidis* mutant preferentially incorporated saturated PE and PG species with shorter fatty acyl chains into its OM⁵³. Furthermore, the higher abundance of lyso-GPs (those with a single fatty acid chain less than 18 carbons) in the polymyxin-resistant 19606R, compared to the parent strain ATCC 19606, indicate significant GPs turnover; hence, our result supports the hypothesis that the OM structure of polymyxin-resistant bacterial cells is dramatically altered due to LPS loss. The observed increase in the production of GPs, which we hypothesise are mainly exported to the outer leaflet of the OM of the LPS-deficient strain 19606R, further supports the previously described compensatory mechanism for the LPS loss which associated with increase in cell envelope and membrane biosynthesis¹⁸. Transcriptomics analyses of the LPS-deficient strain 19606R revealed that there was a significant increase in the expression of genes involved in phospholipid

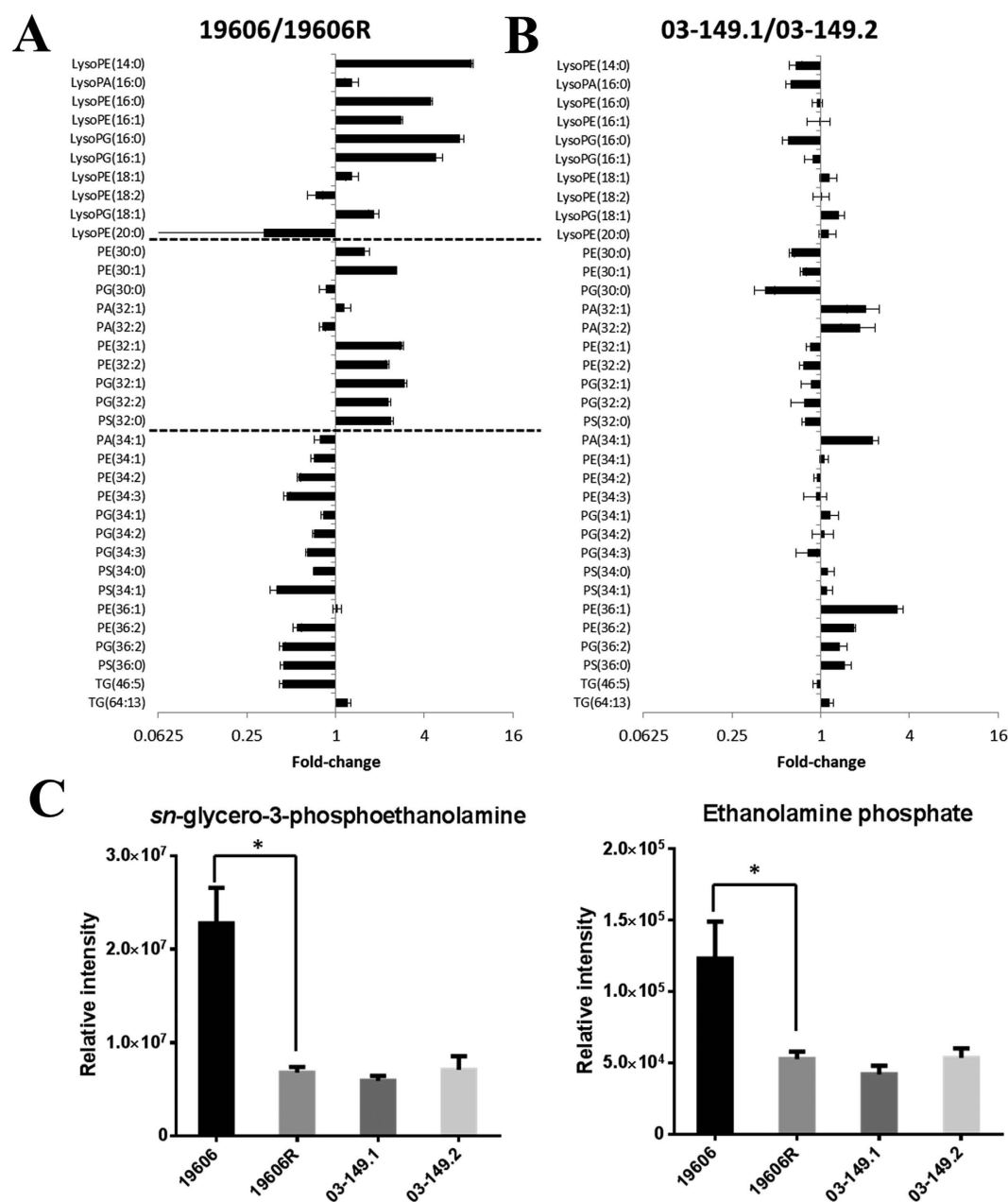


Figure 9. Relative intensity of glycerophospholipids levels. (A) LPS-deficient polymyxin-resistant 19606R and its parent strain ATCC 19606; and (B) polymyxin-resistant 03-149.2 and polymyxin-susceptible 03-149. (C) Glyceroethanolamine phosphate and ethanolamine phosphate showed significantly lower levels in the polymyxin-resistant 19606R than its parent ATCC 19606. PE, glycerophosphoethanolamine; PS, glycerophosphoserine; PG, glycerophosphoglycerols; PA, glycerophosphates. Fatty acyl carbon atom number and double bond number are shown in brackets. * $p < 0.05$.

transport (*mlaBCD*) in response to the LPS loss¹⁸. Remarkably, glycerethanolamine phosphate and ethanolamine phosphate showed significantly lower levels in the polymyxin-resistant 19606R than its parent ATCC 19606. Ethanolamine utilisation was suggested to associate with bacterial pathogenesis and virulence^{54,55}. Our results support the claim and suggest that ethanolamine is crucial for bacterial metabolism, in particular in the polymyxin-resistant 19606R. The present study utilising HILIC chromatography does not represent the total phospholipid composition and does not reveal the relative distribution of each GP species in the inner and outer membranes of *A. baumannii*. Future membrane lipidomics analysis of LPS-deficient, polymyxin-resistant *A. baumannii* is underway and will further define the total lipid abundance and distribution.

In addition to the perturbations to known metabolic pathways, our untargeted metabolomics analysis revealed four unidentified metabolite features which are consistent with amino-sugars that were unique to the polymyxin-resistant strains, and not in either of the polymyxin-susceptible strains. Metabolite identification is a

major bottleneck in untargeted metabolomics, and accurate identification of metabolites that are not present in existing databases requires large-scale fractionation and extensive structural analysis^{56–58}. Precise structural identification of the unknown metabolites that are unique to polymyxin-resistant strains is beyond the scope of the present study. Nevertheless, with the high-resolution MS applied here, features can be annotated with the most likely molecular formulas. Whilst not conclusive, these unique unidentified metabolites suggest the involvement of glycan metabolism in the molecular mechanisms of polymyxin resistance in *A. baumannii*. Further studies are warranted to characterise these unknown metabolites and their biological functions. Together with our metabolomics and transcriptomics results¹⁸, it will provide additional information about the metabolic differences between polymyxin-susceptible and polymyxin-resistant *A. baumannii* (Figs 3 and 4).

To the best of our knowledge, this comparative untargeted metabolomics study is the first to demonstrate significant global metabolic changes in polymyxin-resistant *A. baumannii* strains. In particular, global metabolic differences are associated with different mechanisms of polymyxin resistance due to LPS loss and lipid A modifications. Our study provides a valuable insight into the global metabolism of polymyxin-resistant *A. baumannii* and potentially offers new therapeutic targets.

Materials and Methods

Strains. The *A. baumannii* wild-type strain ATCC 19606 was obtained from the American Type Culture Collection. The *lpxA* mutant strain 19606R (MIC > 128 mg/L) is an LPS-deficient, polymyxin-resistant derivative of ATCC 19606¹⁷. The two clinical isolates used in this study were polymyxin-susceptible 03–149.1 (MIC 1 mg/L) and polymyxin-resistant 03–149.2 (MIC > 32 mg/L); both were isolated from the same patient⁵⁹. Bacterial strains were grown in cation-adjusted Mueller-Hinton broth (MHB; Oxoid, England; 20–25 mg/L Ca^{2+} and 10–12.5 mg/L Mg^{2+}).

Identification of 16S rDNA, genome sequencing and lipid A structural analysis of *A. baumannii* clinical isolates 03–149.1 and 03–149.2.

The *A. baumannii* clinical isolates 03–149.1 and 03–149.2 16S were identified using rDNA gene sequencing (Supplementary Method). Their genome sequences were determined using 36-bp paired-end sequencing chemistry on an Illumina Genome Analyzer II apparatus (Illumina) at the Micromon Sequencing Facility (Monash University) as previously described¹⁷. Furthermore, lipid A of the clinical isolates 03–149.1 and 03–149.2 was prepared by mild acid hydrolysis as previously described⁶⁰. In detail, 100 mL of broth cultures were harvested at $\text{OD}_{600\text{nm}} = 0.8$ via centrifugation at $3,220 \times g$ for 20 min and washed twice with phosphate-buffered saline (PBS). Initially, the cells were re-suspended in 4 mL PBS, methanol (10 mL) and chloroform (5 mL) were then added to the suspension, making a single-phase Bligh-Dyer (chloroform/methanol/water, 1:2:0.8, v/v)⁶¹. The mixture was centrifuged at $3,220 \times g$ for 15 min and supernatant was removed. The pellet was washed once with chloroform/methanol/water (1:2:0.8, v/v), re-suspended in the hydrolysis buffer (50 mM sodium acetate pH 4.5, 1% sodium dodecyl sulphate (SDS)), and incubated in a boiling water bath for 45 min. To extract lipid A, the SDS solution was converted into a double-phase Bligh-Dyer mixture by adding 6 mL of chloroform and 6 mL of methanol for a final mixture of chloroform/methanol/water (1:1:0.9, v/v)⁶¹. The lower phase containing lipid A was finally extracted and samples were dried and stored at -20°C . Structural analysis of lipid A was performed in negative mode on a Q-Exactive Hybrid Quadrupole-Orbitrap Mass Spectrometer (Thermo Fisher).

Bacterial culture preparation for metabolomics experiments. Bacterial strains, subcultured from -80°C frozen stocks, were inoculated onto nutrient agars and incubated for 16–18 h at 37°C . For the polymyxin-resistant strains, *lpxA* mutant 19606R and clinical isolate 03–149.2, the Mueller-Hinton plates were supplemented with polymyxin B (10 mg/L) to maintain the selection pressure. For each culture, a single colony was used to inoculate 10 mL MHB for incubation overnight (16–18 h) at 37°C with constant shaking (180 rpm). Three biological replicate reservoirs for different *A. baumannii* colonies, each consisting of 50 mL MHB, were prepared for each *A. baumannii* strain. Each reservoir was inoculated with 500 μL of overnight culture and grown at 37°C with shaking (180 rpm) to an $\text{OD}_{600\text{nm}} \sim 0.5$ (mid-exponential growth phase). The polymyxin-resistant strains 19606R and 03–149.2 were grown in MHB without colistin. For the blank controls, two MHB reservoirs without bacterial inoculation were included in the experiment.

Sample preparation for metabolomic study. Metabolomic sample was prepared as previously described with slight modifications³⁶. The sample pre-treatment method, washing step and extraction solvents were optimised for improved recovery of cellular metabolites. The final method for cell pellet analyses employed four technical replicates, each consisting of 10 mL mid-exponential culture ($\text{OD}_{600\text{nm}} \sim 0.5$) collected in 50 mL Falcon tubes (Thermo Fisher). The tubes were centrifuged at $3,220 \times g$ at 4°C for 5 min and the supernatant discarded. For each sample, extracellular metabolites and medium components were removed by washing cell pellets twice with 0.5 mL of 0.9% NaCl (4°C). Following each wash, cells were pelleted by centrifugation at $3,220 \times g$ at 4°C for 3 min. To evaluate the washing effect on the metabolite leakage, washing waste supernatant samples were collected and analysed (below). Furthermore, the efficiency of four different extraction solvents were evaluated: (i) absolute methanol (MeOH), (ii) 60% ethanol (60EtOH), (iii) chloroform:methanol:water (CMW; 1:3:1, v/v), and (iv) chloroform:methanol (CM; 1:2, v/v). In our comparison study of different *A. baumannii* strains, washed cell pellets were resuspended in 0.5 mL metabolite extraction solvent consisting of CMW (1:3:1, v/v; -80°C); the solvent mixture contained the internal standards (CHAPS, CAPS, PIPES and TRIS; 1 μM of each). These compounds were selected as the internal standards as they are physicochemically diverse small molecules that are not naturally occurring in any microorganism and can be spiked at known concentrations to determine the analytical performance of the method used. Samples were frozen in liquid nitrogen and thawed on ice, and freeze-thaw was repeated three times in order to permeabilise the cells and release intracellular metabolites. The mixtures were

centrifuged for 10 min at $3,220 \times g$ at 4°C and 300 μL of the supernatants containing the extracted metabolites were collected in 1.5-mL centrifuge tubes and stored at -80°C immediately. For analysis, the samples were thawed and further centrifuged at $14,000 \times g$ for 10 min at 4°C and 200 μL of particle-free supernatant was transferred into the injection vial for LC-MS analysis. For footprint samples, an aliquot of approximately 1.5 mL of the culture was rapidly filtered through a 0.22- μm filter and stored at -80°C . Prior to analysis, these samples were thawed and 10 μL combined with 250 μL extraction solvent (chloroform:methanol:water, 1:3:1, v/v) and then centrifuged at $14,000 \times g$ for 10 min at 4°C to collect 200 μL supernatant for LC-MS analysis (below). Equal volumes from each of the *A. baumannii* strains samples were mixed for a quality control sample (QC). This pooled quality control sample was used to estimate a composite sample profile representing all the analytes that will be encountered during the LC-MS analysis⁶².

LC-MS analysis. Hydrophilic interaction liquid chromatography (HILIC)—high-resolution mass spectrometry (HRMS) was employed in this study. Samples were analysed on a Dionex high-performance liquid chromatography (HPLC) system (RSLCU3000, Thermo Fisher) using a ZIC-PHILIC column (5 μm , polymeric, $150 \times 4.6\text{ mm}$; SeQuant, Merck) coupled to a Q-Exactive Orbitrap mass spectrometer (Thermo Fisher) operated at 35000 resolution in both positive and negative electro-spray ionization (ESI) mode and a detection range of 85 to 1,275 m/z . The LC solvent consisted of 20 mM ammonium carbonate (A) and acetonitrile (B) with a multi-step gradient system from 80% B to 50% B over 15 min, then to 5% B at 18 min, followed by wash with 5% B for 3 min, and 8 min re-equilibration with 80% B at a flow rate of 0.3 mL/min⁶³. The run time was 32 min and the injection sample volume was 10 μL . All samples (3 biological replicates, each with 4 technical replicates) were randomized and analysed in a single LC-MS batch to reduce batch-to-batch variation. The chromatographic peaks, signal reproducibility and analyte stability were monitored by assessment of pooled quality control sample analysed periodically throughout the run, internal standards and total ion chromatograms for each sample. Mixtures of pure standards containing over 250 metabolites of different classes were analysed within the batch to aid in the identification of metabolites.

Data processing, bioinformatics and statistical analyses. Global metabolomics analyses were performed using mzMatch⁶⁴ and IDEOM (<http://mzmatch.sourceforge.net/ideom.php>) free software⁶⁵. Raw LC-MS data were converted to mzXML format and chromatogram peaks were detected using XCMS⁶⁶ and saved in the peakML format. The program Mzmatch.R was used to align samples and filter peaks based on minimum detectable intensity (100000), reproducibility (relative standard deviation (RSD) for all replicates < 0.5) and peak shape (codaw > 0.8). Mzmatch.R was also used to retrieve LC-MS peak intensities for missing peaks and for the annotation of related peaks. Unwanted noise and artefact peaks were eliminated using IDEOM with default parameters. Metabolites were putatively identified by the exact mass within 2 ppm, after correction for loss or gain of a proton in negative and positive ESI mode, respectively. Retention time was employed to confirm the identification of each metabolite based on the available authentic standards. Putative identification of other metabolites was determined using exact mass and predicted retention time based on the Kyoto Encyclopedia of Genes and Genomes (KEGG), MetaCyc and LIPIDMAPS databases, with preference given to bacterial metabolites annotated in EcoCyc. Quantification of each metabolite was calculated using the raw peak height and is expressed relative to the average peak height for their paired susceptible strain. Univariate statistical analyses utilised a Welch's T-test ($\alpha = 0.01$) and multivariate analyses utilised the metabolomics R package. Metabolic pathway analyses were performed using the free web-based metabolomics tool Pathos (<http://motif.gla.ac.uk/Pathos/>)⁶⁷, BioCyc (<http://biocyc.org/>)⁶⁸, and Visualization and Analysis of Networks containing Experimental Data (Vanted) software⁶⁹.

References

- Peleg, A. Y., Seifert, H. & Paterson, D. L. *Acinetobacter baumannii*: emergence of a successful pathogen. *Clin. Microbiol. Rev.* **21**, 538–582 (2008).
- Dijkshoorn, L., Nemec, A. & Seifert, H. An increasing threat in hospitals: multidrug-resistant *Acinetobacter baumannii*. *Nat. Rev. Microbiol.* **5**, 939–951 (2007).
- Maragakis, L. L. & Perl, T. M. *Acinetobacter baumannii*: Epidemiology, antimicrobial resistance, and treatment options. *Clin. Infect. Dis.* **46**, 1254–1263 (2008).
- Boucher, H. W. *et al.* Bad bugs, no drugs: No ESCAPE! An update from the Infectious Diseases Society of America. *Clin. Infect. Dis.* **48**, 1–12 (2009).
- Centers for Disease Control and Prevention (CDC). Antibiotic resistance threats in the United States, 2013. (2013). Available at: <http://www.cdc.gov/drugresistance/threat-report-2013/pdf/ar-threats-2013-508.pdf>. (Accessed: 17th February 2016).
- Perez, F. *et al.* Global challenge of multidrug-resistant *Acinetobacter baumannii*. *Antimicrob. Agents Chemother.* **51**, 3471–3484 (2007).
- Velkov, T., Roberts, K. D., Nation, R. L., Thompson, P. E. & Li, J. Pharmacology of polymyxins: new insights into an 'old' class of antibiotics. *Future Microbiol.* **8**, 711–724 (2013).
- Li, J. *et al.* Colistin: the re-emerging antibiotic for multidrug-resistant Gram-negative bacterial infections. *Lancet Infect. Dis.* **6**, 589–601 (2006).
- Gordon, N. C. & Wareham, D. W. Multidrug-resistant *Acinetobacter baumannii*: mechanisms of virulence and resistance. *Int. J. Antimicrob. Agents.* **35**, 219–226 (2010).
- Arnold, T. M., Forrest, G. N. & Messmer, K. J. Polymyxin antibiotics for Gram-negative infections. *Am. J. Health Syst. Pharm.* **64**, 819–826 (2007).
- Karageorgopoulos, D. E. & Falagas, M. E. Current control and treatment of multidrug-resistant *Acinetobacter baumannii* infections. *Lancet Infect. Dis.* **8**, 751–762 (2008).
- Hancock, R. E. W. Peptide antibiotics. *Lancet* **349**, 418–422 (1997).
- Sampson, T. R. *et al.* Rapid killing of *Acinetobacter baumannii* by polymyxins is mediated by a hydroxyl radical death pathway. *Antimicrob. Agents Chemother.* **56**, 5642–5649 (2012).
- Beceiro, A. *et al.* Phosphoethanolamine modification of lipid A in colistin-resistant variants of *Acinetobacter baumannii* mediated by the pmrAB two-component regulatory system. *Antimicrob. Agents Chemother.* **55**, 3370–3379 (2011).

15. Arroyo, L. A. *et al.* The pmrCAB operon mediates polymyxin resistance in *Acinetobacter baumannii* ATCC 17978 and clinical isolates through phosphoethanolamine modification of lipid A. *Antimicrob. Agents Chemother.* **55**, 3743–3751 (2011).
16. Pelletier, M. R. *et al.* Unique structural modifications are present in the lipopolysaccharide from colistin-resistant strains of *Acinetobacter baumannii*. *Antimicrob. Agents Chemother.* **57**, 4831–4840 (2013).
17. Moffatt, J. H. *et al.* Colistin resistance in *Acinetobacter baumannii* is mediated by complete loss of lipopolysaccharide production. *Antimicrob. Agents Chemother.* **54**, 4971–4977 (2010).
18. Henry, R. *et al.* Colistin-resistant, lipopolysaccharide-deficient *Acinetobacter baumannii* responds to lipopolysaccharide loss through increased expression of genes involved in the synthesis and transport of lipoproteins, phospholipids, and poly- β -1,6-N-acetylglucosamine. *Antimicrob. Agents Chemother.* **56**, 59–69 (2012).
19. Van der Werf, M. J., Overkamp, K. M., Muijlwijk, B., Coulter, L. & Hankemeier, T. Microbial metabolomics: toward a platform with full metabolome coverage. *Anal. Biochem.* **370**, 17–25 (2007).
20. Snyder, M. & Li, X. Y. Metabolomics as a robust tool in systems biology and personalized medicine: an open letter to the metabolomics community. *Metabolomics* **9**, 532–534 (2013).
21. Putri, S. P. *et al.* Current metabolomics: practical applications. *J. Biosci. Bioeng.* **115**, 579–589 (2013).
22. Beyoglu, D. & Idle, J. R. Metabolomics and its potential in drug development. *Biochem. Pharmacol.* **85**, 12–20 (2013).
23. Kell, D. B. & Goodacre, R. Metabolomics and systems pharmacology: why and how to model the human metabolic network for drug discovery. *Drug Discov. Today* **19**, 1828–1828 (2014).
24. Tang, J. Microbial metabolomics. *Curr. Genomics* **12**, 391–403 (2011).
25. Yeom, J., Shin, J. H., Yang, J. Y., Kim, J. & Hwang, G. S. H-1 NMR-based metabolite profiling of planktonic and biofilm cells in *Acinetobacter baumannii* 1656-2. *Plos One* **8**, e57730 (2013).
26. Gjersing, E. L., Herberg, J. L., Horn, J., Schaldach, C. M. & Maxwell, R. S. NMR metabolomics of planktonic and biofilm modes of growth in *Pseudomonas aeruginosa*. *Anal. Chem.* **79**, 8037–8045 (2007).
27. t'Kindt, R. *et al.* Metabolomics to unveil and understand phenotypic diversity between pathogen populations. *Plos Negl. Trop. Dis.* **4**, e904 (2010).
28. Vincent, I. M. *et al.* A molecular mechanism for efloornithine resistance in African trypanosomes. *PLoS Pathog.* **6**, e1001204 (2010).
29. Derewacz, D. K., Goodwin, C. R., McNeese, C. R., McLean, J. A. & Bachmann, B. O. Antimicrobial drug resistance affects broad changes in metabolomic phenotype in addition to secondary metabolism. *Proc. Natl. Acad. Sci. USA* **110**, 2336–2341 (2013).
30. Iacono, M. *et al.* Whole-genome pyrosequencing of an epidemic multidrug-resistant *Acinetobacter baumannii* strain belonging to the European clone II group. *Antimicrob. Agents Chemother.* **52**, 2616–2625 (2008).
31. Raetz, C. R., Reynolds, C. M., Trent, M. S. & Bishop, R. E. Lipid A modification systems in Gram-negative bacteria. *Annu. Rev. Biochem.* **76**, 295–329 (2007).
32. Nowicki, E. M., O'Brien, J. P., Brodbelt, J. S. & Trent, M. S. Characterization of *Pseudomonas aeruginosa* LpxT reveals dual positional lipid A kinase activity and co-ordinated control of outer membrane modification. *Mol. Microbiol.* **94**, 728–741 (2014).
33. Velkov, T., Thompson, P. E., Nation, R. L. & Li, J. Structure-activity relationships of polymyxin antibiotics. *J. Med. Chem.* **53**, 1898–1916 (2009).
34. Yu, Z., Qin, W., Lin, J., Fang, S. & Qiu, J. Antibacterial mechanisms of polymyxin and bacterial resistance. *BioMed Res. Int.* **2015**, 1–11 (2015).
35. Meyer, H., Weidmann, H. & Lalk, M. Methodological approaches to help unravel the intracellular metabolome of *Bacillus subtilis*. *Microb. Cell Fact.* **12**, 69 (2013).
36. Marcinowska, R., Trygg, J., Wolf-Watz, H., Mortiz, T. & Surowiec, I. Optimization of a sample preparation method for the metabolomic analysis of clinically relevant bacteria. *J. Microbiol. Methods* **87**, 24–31 (2011).
37. Rabinowitz, J. D. Cellular metabolomics of *Escherichia coli*. *Expert Rev. Proteomic* **4**, 187–198 (2007).
38. Wittmann, C., Kromer, J. O., Kiefer, P., Binz, T. & Heinzel, E. Impact of the cold shock phenomenon on quantification of intracellular metabolites in bacteria. *Anal. Biochem.* **327**, 135–139 (2004).
39. Shin, M. H., Lee, D. Y., Liu, K. H., Fiehn, O. & Kim, K. H. Evaluation of sampling and extraction methodologies for the global metabolic profiling of *Saccharophagus degradans*. *Anal. Chem.* **82**, 6660–6666 (2010).
40. Armenta-Medina, D., Segovia, L. & Perez-Rueda, E. Comparative genomics of nucleotide metabolism: a tour to the past of the three cellular domains of life. *BMC Genomics* **15** (2014).
41. Maeda, H. & Dudareva, N. The shikimate pathway and aromatic amino acid biosynthesis in plants. *Annu. Rev. Plant Biol.* **63**, 73–105 (2012).
42. Stincone, A. *et al.* The return of metabolism: biochemistry and physiology of the pentose phosphate pathway. *Biol. Rev.* **90**, 927–963 (2015).
43. Taylor, P. L. *et al.* Structure and function of sedoheptulose-7-phosphate isomerase, a critical enzyme for lipopolysaccharide biosynthesis and a target for antibiotic adjuvants. *J. Biol. Chem.* **283**, 2835–2845 (2008).
44. Sarkar, M., Maganti, L., Ghoshal, N. & Dutta, C. In silico quest for putative drug targets in *Helicobacter pylori* HPAG1: molecular modeling of candidate enzymes from lipopolysaccharide biosynthesis pathway. *J. Mol. Model.* **18**, 1855–1866 (2012).
45. Kneidinger, B., Graninger, M., Puchberger, M., Kosma, P. & Messner, P. Biosynthesis of nucleotide-activated D-glycero-D-manno-Heptose. *J. Biol. Chem.* **276**, 20935–20944 (2001).
46. Valvano, M. A., Messner, P. & Kosma, P. Novel pathways for biosynthesis of nucleotide-activated glycerol-manno-heptose precursors of bacterial glycoproteins and cell surface polysaccharides. *Microbiol. SGM.* **148**, 1979–1989 (2002).
47. Tian, J., Bryk, R., Itoh, M., Suematsu, M. & Nathan, C. Variant tricarboxylic acid cycle in *Mycobacterium tuberculosis*: Identification of α -ketoglutarate decarboxylase. *Proc. Natl. Acad. Sci. USA* **102**, 10670–10675 (2005).
48. Lovering, A. L., Safadi, S. S. & Strynadka, N. C. Structural perspective of peptidoglycan biosynthesis and assembly. *Annu. Rev. Biochem.* **81**, 451–478 (2012).
49. Gordon, E. *et al.* Crystal structure of UDP-N-acetylmuramoyl-L-alanyl-D-glutamate: meso-diaminopimelate ligase from *Escherichia coli*. *J. Biol. Chem.* **276**, 10999–11006 (2001).
50. Rudulier, D. L. Elucidation of the role of osmoprotective compounds and osmoregulatory genes: The key role of bacteria. (eds. Lieth, H. & Al Masoom, A.) *Towards the rational use of high salinity tolerant plants*. I, 313–322 (Kluwer Academic Publishers, 1993).
51. Dalebroux, Z. D., Matamouros, S., Whittington, D., Bishop, R. E. & Miller, S. I. PhoPQ regulates acidic glycerophospholipid content of the *Salmonella Typhimurium* outer membrane. *Proc. Natl. Acad. Sci. USA* **111**, 1963–1968 (2014).
52. Geiger, O., Lopez-Lara, I. M. & Sohlenkamp, C. Phosphatidylcholine biosynthesis and function in bacteria. *BBA-Mol. Cell Biol. L.* **1831**, 503–513 (2013).
53. Steeghs, L. *et al.* Outer membrane composition of a lipopolysaccharide-deficient *Neisseria meningitidis* mutant. *EMBO J.* **20**, 6937–6945 (2001).
54. Garsin, D. A. Ethanolamine utilization in bacterial pathogens: roles and regulation. *Nature Rev. Microbiol.* **8**, 290–295 (2010).
55. Kendall, M. M., Gruber, C. C., Parker, C. T. & Sperandio, V. Ethanolamine controls expression of genes encoding components involved in interkingdom signaling and virulence in enterohemorrhagic *Escherichia coli* O157:H7. *mBio*. **3**, e00050–12 (2012).
56. Bowen, B. P. & Northen, T. R. Dealing with the unknown: metabolomics and metabolite atlases. *J. Am. Soc. Mass Spectr.* **21**, 1471–1476 (2010).
57. Nakabayashi, R. & Saito, K. Metabolomics for unknown plant metabolites. *Anal. Bioanal. Chem.* **405**, 5005–5011 (2013).
58. Gowda, G. A. N. & Rafferty, D. Can NMR solve some significant challenges in metabolomics? *J. Magn. Reson.* **260**, 144–160 (2015).

59. Garonzik, S. M. *et al.* Population pharmacokinetics of colistin methanesulfonate and formed colistin in critically ill patients from a multicenter study provide dosing suggestions for various categories of patients. *Antimicrob. Agents Chemother.* **55**, 3284–3294 (2011).
60. Que, N. L., Lin, S., Cotter, R. J. & Raetz, C. R. Purification and mass spectrometry of six lipid A species from the bacterial endosymbiont *Rhizobium etli*. Demonstration of a conserved distal unit and a variable proximal portion. *J. Biol. Chem.* **275**, 28006–28016 (2000).
61. Bligh, E. G. & Dyer, W. J. A rapid method of total lipid extraction and purification. *Can. J. Biochem. Physiol.* **37**, 911–917 (1959).
62. Gika, H. G., Theodoridis, G. A., Wingate, J. E. & Wilson, I. D. Within-day reproducibility of an HPLC-MS-based method for metabolomic analysis: application to human urine. *J. Proteome Res.* **6**, 3291–3303 (2007).
63. Zhang, T., Creek, D. J., Barrett, M. P., Blackburn, G. & Watson, D. G. Evaluation of coupling reversed phase, aqueous normal phase, and hydrophilic interaction liquid chromatography with orbitrap mass spectrometry for metabolomic studies of human urine. *Anal. Chem.* **84**, 1994–2001 (2012).
64. Scheltema, R. A., Jankevics, A., Jansen, R. C., Swertz, M. A. & Breitling, R. PeakML/mzMatch: a file format, Java library, R library, and tool-chain for mass spectrometry data analysis. *Anal. Chem.* **83**, 2786–2793 (2011).
65. Creek, D. J., Jankevics, A., Burgess, K. E., Breitling, R. & Barrett, M. P. IDEOM: an Excel interface for analysis of LC-MS-based metabolomics data. *Bioinformatics* **28**, 1048–1049 (2012).
66. Smith, C. A., Want, E. J., O'Maille, G., Abagyan, R. & Siuzdak, G. XCMS: Processing mass spectrometry data for metabolite profiling using nonlinear peak alignment, matching, and identification. *Anal. Chem.* **78**, 779–787 (2006).
67. Leader, D. P., Burgess, K., Creek, D. & Barrett, M. P. Pathos: A web facility that uses metabolic maps to display experimental changes in metabolites identified by mass spectrometry. *Rapid Commun. Mass Spectrom.* **25**, 3422–3426 (2011).
68. Caspi, R. *et al.* The MetaCyc database of metabolic pathways and enzymes and the BioCyc collection of Pathway/Genome Databases. *Nucleic Acids Res.* **42**, 459–471 (2014).
69. Junker, B. H., Klukas, C. & Schreiber, F. VANTED: a system for advanced data analysis and visualization in the context of biological networks. *BMC bioinform.* **7**, 109 (2006).

Acknowledgements

J.L., D.J.C., T.V., J.S., A.W.P., P.H., A.F. and K.S.K. are supported by the National Institute of Allergy and Infectious Diseases of the National Institutes of Health (R01 AI111965). The content is solely the responsibility of the authors and does not necessarily represent the official views of the National Institute of Allergy and Infectious Diseases or the National Institutes of Health. J.L. and A.W.P. are Australian NHMRC Senior Research Fellows. D.J.C. and T.V. are Australian NHMRC Career Development Research Fellows. P.H. is an Australian NHMRC Senior Principal Research Fellow.

Author Contributions

J.L. conceived the project. J.L., M.H.M.M., S.-E.C., M.D.J., M.H., J.D.B., V.T., A.F., K.S.K., P.H., A.W.P., J.S., T.V. and D.J.C. involved in the design of the experiments. M.H.M.M., M.H., J.D.B. and M.D.J. performed the experiments, and M.H.M.M., D.J.C., S.-E.C., M.H., M.D.J., J.D.B. and J.L. analysed the results. All authors, J.L., M.H.M.M., S.-E.C., M.D.J., M.H., J.D.B., V.T., A.F., K.S.K., P.H., A.W.P., J.S., T.V. and D.J.C. reviewed the manuscript.

Additional Information

Supplementary information accompanies this paper at <http://www.nature.com/srep>

Competing financial interests: The authors declare no competing financial interests.

How to cite this article: Maifiah, M. H. M. *et al.* Global metabolic analyses identify key differences in metabolite levels between polymyxin-susceptible and polymyxin-resistant *Acinetobacter baumannii*. *Sci. Rep.* **6**, 22287; doi: 10.1038/srep22287 (2016).



This work is licensed under a Creative Commons Attribution 4.0 International License. The images or other third party material in this article are included in the article's Creative Commons license, unless indicated otherwise in the credit line; if the material is not included under the Creative Commons license, users will need to obtain permission from the license holder to reproduce the material. To view a copy of this license, visit <http://creativecommons.org/licenses/by/4.0/>

SCIENTIFIC REPORTS

OPEN

Untargeted metabolomics analysis reveals key pathways responsible for the synergistic killing of colistin and doripenem combination against *Acinetobacter baumannii*

Mohd Hafidz Mahamad Maifiah¹, Darren J. Creek^{1,*}, Roger L. Nation¹, Alan Forrest², Brian T. Tsuji³, Tony Velkov¹ & Jian Li^{4,*}

Received: 07 November 2016

Accepted: 28 February 2017

Published: 30 March 2017

Combination therapy is deployed for the treatment of multidrug-resistant *Acinetobacter baumannii*, as it can rapidly develop resistance to current antibiotics. This is the first study to investigate the synergistic effect of colistin/doripenem combination on the metabolome of *A. baumannii*. The metabolite levels were measured using LC-MS following treatment with colistin (2 mg/L) or doripenem (25 mg/L) alone, and their combination at 15 min, 1 hr and 4 hr ($n = 4$). Colistin caused early (15 min and 1 hr) disruption of the bacterial outer membrane and cell wall, as demonstrated by perturbation of glycerophospholipids and fatty acids. Concentrations of peptidoglycan biosynthesis metabolites decreased at 4 hr by doripenem alone, reflecting its mechanism of action. The combination induced significant changes to more key metabolic pathways relative to either monotherapy. Down-regulation of cell wall biosynthesis (via D-sedoheptulose 7-phosphate) and nucleotide metabolism (via D-ribose 5-phosphate) was associated with perturbations in the pentose phosphate pathway induced initially by colistin (15 min and 1 hr) and later by doripenem (4 hr). We discovered that the combination synergistically killed *A. baumannii* via time-dependent inhibition of different key metabolic pathways. Our study highlights the significant potential of systems pharmacology in elucidating the mechanism of synergy and optimizing antibiotic pharmacokinetics/pharmacodynamics.

Multidrug-resistant (MDR) *Acinetobacter baumannii* has been classified by the Centers for Disease Control and Prevention (CDC) as a “Serious Threat” which is responsible for a plethora of nosocomial infections including pneumonia, bacteraemia, wound infections, urinary tract infections and meningitis^{1–3}. As one of the six significant ESKAPE ‘superbugs’ identified by the Infectious Diseases Society of America (IDSA), *A. baumannii* represents a challenge as it can rapidly develop resistance to all clinically available antibiotics^{4–7}. *A. baumannii* exhibits a wide array of antibiotic resistance strategies, including degradation and modification of enzymes, alteration of target binding sites, and activation of efflux pumps⁸.

Due to the dry antibiotic discovery pipeline, the re-utilization of the ‘old’ polymyxin class of antibiotics has become essential for the treatment of life-threatening infections caused by MDR *A. baumannii*⁹. Polymyxin B and colistin (i.e. polymyxin E) are non-ribosomal cyclic lipopeptides that contain six basic L- α - γ -diaminobutyric acid (Dab) residues, two hydrophobic amino acids, and an N-terminal fatty acyl group¹⁰. Polymyxins interact electrostatically with the phosphate groups of the lipid A component of lipopolysaccharide (LPS) followed by non-polar interactions of hydrophobic domains on both molecules to initiate the rapid bactericidal effect^{10,11}. Destabilization of the LPS leaflet of the outer membrane has generally been thought to cause local disturbance, osmotic

¹Drug Delivery, Disposition and Dynamics, Monash Institute of Pharmaceutical Sciences, Monash University, Parkville, VIC, 3052, Australia. ²UNC Eshelman School of Pharmacy, The University of North Carolina at Chapel Hill, Chapel Hill, NC, 27599-7569, USA. ³Department of Pharmacy Practice, University at Buffalo, Buffalo, NY, USA.

⁴Monash Biomedicine Discovery Institute, Department of Microbiology, Monash University, VIC 3800, Australia.

*These authors jointly supervised this work. Correspondence and requests for materials should be addressed to J.L.

imbalance and finally cell death, although the ultimate mechanism of cell death is not completely understood¹². Polymyxin monotherapy may lead to treatment failure as it is not always possible to generate reliably efficacious plasma exposure and bacterial resistance may emerge^{13–18}. *A. baumannii* can become resistant to polymyxins by the addition of phosphoethanolamine (pEtN), galactosamine (GalN) or both^{19–24} to its lipid A structure, or by the loss of LPS²⁵. These modifications significantly reduce the negative charge on the bacterial outer membrane, thus diminishing the binding of polymyxins¹⁰. A number of *in vitro* studies have shown that colistin and doripenem combination therapy is synergistic against MDR *Pseudomonas aeruginosa*, *Klebsiella pneumoniae* and *A. baumannii*^{26–31}. In addition, the colistin-carbapenem combination has been shown to significantly limit the emergence of colistin resistance in *A. baumannii*³². Therefore, polymyxin-carbapenem combinations are often employed to enhance therapeutic response and minimize potential polymyxin resistance.

The mechanisms that underlie the synergistic action of polymyxins and carbapenems have not been fully elucidated. Metabolomics provides the opportunity to gain a system-wide snapshot of cellular biochemical networks under defined conditions^{33–35}, and has been increasingly employed in bacterial physiology³⁴ and drug discovery to elucidate the mechanism of drug action³⁶. Furthermore, a detailed understanding of cellular metabolic perturbations in response to antibiotic treatment can potentially facilitate the discovery of novel alternative drug targets³⁷. To elucidate the mechanism of synergistic killing of the colistin and doripenem combination against *A. baumannii*, we conducted an untargeted metabolomics study. Our study is the first to reveal that the metabolic perturbations induced by the combination were predominantly associated with the effect of colistin in the early time points, followed by doripenem at 4 hr. Notably, significant metabolic changes via disorganization of membrane lipids and depletion of nucleotides, energy, and amino sugar metabolites were evident following treatment with colistin alone, and were enhanced by its combination with doripenem. Our data provide a novel insight into the mechanism of synergistic killing against *A. baumannii* by the colistin-doripenem combination.

Results

Untargeted metabolomics was applied to profile the metabolic changes in *A. baumannii* ATCC 19606 treated with monotherapy of colistin and doripenem and the combination at 15 min, 1 hr and 4 hr. Four biological replicates were independently prepared from different cultures on separate days, and all the samples were analyzed in a single LC-MS batch. The within-experiment technical (analytical) variations were monitored based on periodic analysis of pooled biological quality control (PBQC) samples in the batch. We showed that the median relative standard deviation (RSD) of the PBQC, an indicator for analytical reproducibility, was 14% (Supplementary Figure S1A) which is well within the acceptable limits for metabolomics³⁸. In addition, the PCA plot showed the PBQC samples tightly clustered together, indicating minimal technical variation (Supplementary Figure S1B). The median RSD value for each sample group was between 19–30%, showing the dynamics of bacterial metabolism due to antibiotic treatments (Supplementary Figure S1A). Principal component analysis (PCA) (Fig. 1A) and heatmaps (Supplementary Figure S2) revealed global metabolic changes in *A. baumannii* after antibiotic treatment at each time point. A total of 1,577, 1,583 and 1,637 unique metabolites (carbohydrates, energy, amino acids, nucleotides, lipids, peptides, and others) were putatively identified at 15 min, 1 hr and 4 hr, respectively. Univariate analysis of these features revealed that 5–11% of metabolites were significantly altered ($\geq 1.5\text{-log}_2\text{-fold}$; ANOVA, $p \leq 0.05$, FDR ≤ 0.1) following treatment with monotherapy and the combination at each time point (Fig. 1B, and Supplementary Tables 1 and 2).

Colistin induced significant global metabolic changes as early as at 15 min. In contrast, the most substantial metabolic changes associated with doripenem monotherapy were observed at 4 hr, signifying the time-dependent effect of doripenem. Treatment with the colistin and doripenem combination affected 31 additional metabolites that were not altered by either colistin or doripenem treatment alone at 15 min and 1 hr, indicating a synergistic effect of this combination. Interestingly, the PCA plot (Fig. 1A) and heatmaps (Supplementary Figure S2) show relatively similar metabolic profiles between the treatment with colistin monotherapy and the combination of colistin and doripenem at 15 min. There was also considerable overlap at 1 hr as almost half of the perturbed metabolites from the combination treatment were also perturbed by colistin alone. However, at 4 hr the impact of colistin alone was minimal and the combination treatment shared many metabolic features with the doripenem monotherapy (Fig. 1B).

Colistin alone and in combination with doripenem predominantly induced disruption of bacterial lipids.

Unique patterns of changes in the levels of lipids were observed in samples treated with either colistin monotherapy or combination with doripenem at 15 min, 1 hr and 4 hr. Treatment with colistin alone induced significant perturbation in the levels of membrane lipids at 15 min and 1 hr, predominantly the glycerophospholipids (GPLs) and fatty acids (FAs) ($\geq 1.5\text{-log}_2\text{-fold}$; ANOVA, $p \leq 0.05$, FDR ≤ 0.1) (Fig. 2A). Significant changes in levels of GPLs were observed after treatment with colistin and doripenem combination at all three time points, including the depletion of several lysophosphatidylethanolamines (lysoPE) while only very few FAs were affected. Interestingly, the metabolite arising from PE metabolism, *sn*-glycero-3-phosphoethanolamine, significantly decreased ($\geq 1.5\text{-log}_2\text{-fold}$; ANOVA, $p \leq 0.0001$, FDR ≤ 0.1) after treatment with colistin monotherapy and combination across all the time points (Fig. 2B). In addition, the combination therapy significantly decreased the level of *sn*-glycero-3-phosphate ($\geq 1.5\text{-log}_2\text{-fold}$; ANOVA, $p \leq 0.001$, FDR ≤ 0.1), another metabolite associated with GPL metabolism (Fig. 2B). Doripenem alone showed no significant changes to lipid levels at 15 min and 1 hr. However, doripenem alone caused substantial perturbation in the levels of cellular lipids, predominantly accumulation of FAs at 4 hr.

Combination of colistin and doripenem induced global metabolic changes via Pentose Phosphate Pathway (PPP) metabolism.

The combination of colistin and doripenem caused significant decreases in the levels of metabolites of central carbon metabolism, primarily associated with bacterial anabolic

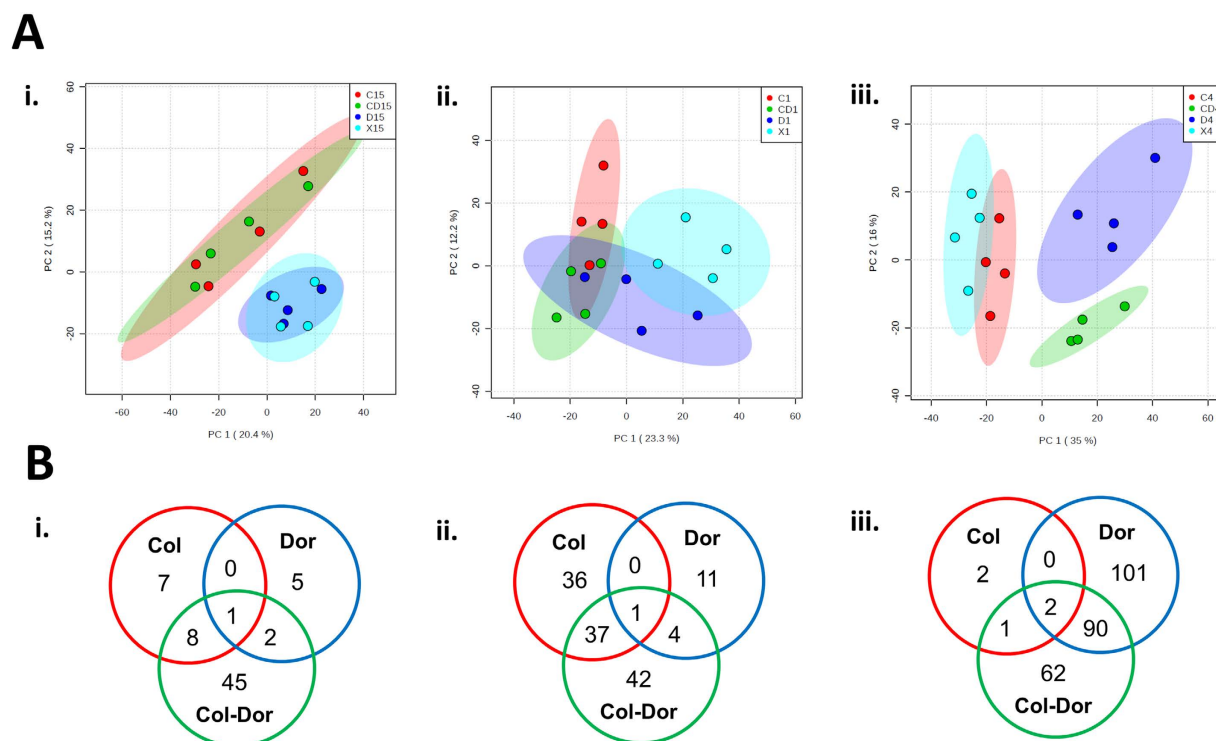


Figure 1. Multivariate and univariate analyses of global metabolic changes. (A) PCA score plots of the first two principal components for metabolite levels from samples treated with colistin, doripenem and the combination at (i) 15 min, (ii) 1 hr, and (iii) 4 hr. Each data set represents a total of 16 samples of 4 biological replicates of each condition. Red = colistin alone (C); Dark blue = doripenem alone (D); Green = colistin and doripenem combination (CD); Light blue = untreated control (X). (B) Venn diagrams represent the number of metabolites significantly affected by each treatment at (i) 15 min, (ii) 1 hr, and (iii) 4 hr. Significant metabolites were selected with ≥ 1.5 -log₂-fold, $p \leq 0.05$, FDR ≤ 0.1 (one-way ANOVA for multiple comparison).

metabolism of the PPP at 15 min, 1 hr and 4 hr (≥ 1.5 -log₂-fold; ANOVA, $p \leq 0.001$, FDR ≤ 0.1) (Fig. 3). In particular, the combination of colistin and doripenem induced significant decreases in the levels of three essential metabolites of PPP at all time-points, D-ribose 5-phosphate, D-sedoheptulose 7-phosphate, and D-erythrose 4-phosphate, key precursors for biosynthesis of nucleotides, lipopolysaccharides (LPS) and aromatic amino acids, respectively. These metabolites were depleted by colistin monotherapy at early time-points, but not by doripenem (significant at 1 hr); whereas significant depletion at 4 hr was observed for doripenem monotherapy, but not colistin. In addition to these PPP metabolites, a related metabolite, 2-deoxy-D-ribose-5-phosphate was consistently decreased as a result of the combination of colistin and doripenem at 1 hr and 4 hr.

Colistin and doripenem caused depletion of metabolite levels of energy and nucleotide metabolism. Significant depletion in the levels of intracellular metabolites of energy metabolism, namely ATP, NAD⁺ and NADP⁺, was observed following treatment with colistin and doripenem combination across all three time points (≥ 1.5 -log₂-fold; ANOVA, $p \leq 0.01$, FDR ≤ 0.1) (Fig. 4A). Treatment with colistin alone decreased the levels of these energy metabolites at 15 min and 1 hr, while doripenem-associated depletion was only significant at 4 hr. Notably, significant perturbations of tricarboxylic acid (TCA) cycle intermediates, fumarate and cis-aconitate were identified in samples treated with colistin and doripenem alone and in combination in particular at 15 min and 4 hr (Supplementary Table 1). In addition, significant depletion in the levels of nucleotides, both purines and pyrimidines, were observed after colistin alone at 1 hr, doripenem alone at 4 hr and combination treatment at each time point (≥ 1.5 -log₂-fold; ANOVA, $p \leq 0.01$, FDR ≤ 0.1) (Fig. 4B).

Colistin and doripenem induced depletion of amino sugar metabolites for cell wall biosynthesis. Colistin alone significantly decreased the intracellular levels of several important metabolites associated with amino sugar and nucleotide sugar metabolism, in particular at 1 hr (≥ 1.5 -log₂-fold; ANOVA $p \leq 0.05$, FDR ≤ 0.1) (Fig. 5A). The levels of two major precursor metabolites of cell wall biosynthesis significantly decreased after treatment with colistin alone at 1 hr, namely UDP-N-acetylmuramate (UDP-MurNAc) and UDP-N-acetylglucosamine (UDP-GlcNAc) (≥ 1.5 -log₂-fold; ANOVA $p \leq 0.01$, FDR ≤ 0.1). Significant decreases in the levels of both metabolites were also observed following treatment with the combination of colistin and doripenem at 1 hr and 4 hr. Doripenem alone significantly decreased the amino sugar associated metabolites only at 4 hr. In addition to these metabolites, another two metabolites of peptidoglycan biosynthesis were identified to significantly decrease at 4 hr after doripenem treatment, meso-2,6-Diaminoheptanedioate and UDP-N-acetylmuramoyl-L-alanyl-D-glutamyl-6-carboxy-L-lysyl-D-alanyl-D-alanine (≥ 1.5 -log₂-fold; ANOVA

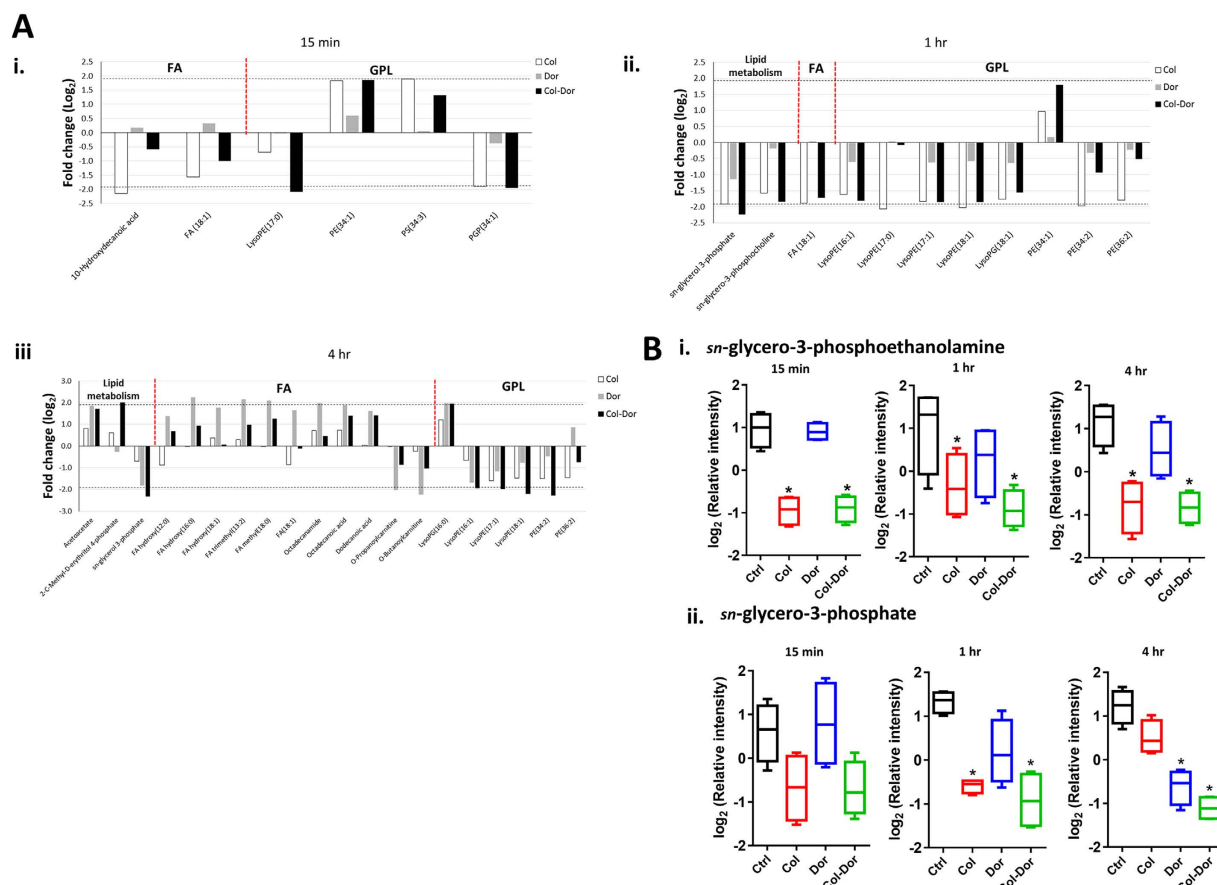


Figure 2. Perturbations of bacterial lipids. (A) Significantly perturbed lipids in *A. baumannii* ATCC 19606 following treatment with colistin (Col, white), doripenem (Dor, grey) and the combination (Col-Dor, black) for (i) 15 min, (ii) 1 hr, and (iii) 4 hr. Lipid names are putatively assigned based on accurate mass. (B) Depletion of (i) *sn*-glycero-3-phosphoethanolamine, and (ii) *sn*-glycero-3-phosphate after treatment with colistin, doripenem, and the combination across all three time points. Box plots indicate upper and lower quartiles (top and bottom of box); median (line within box); and the spread of data that are not outliers (whiskers). * ≥ 1.5 -log₂-fold, $p \leq 0.05$, FDR ≤ 0.1 (one-way ANOVA).

$p \leq 0.01$, FDR ≤ 0.1). Only UDP-*N*-acetylmuramoyl-L-alanyl-D-glutamyl-6-carboxy-L-lysyl-D-alanyl-D-alanine was found to significantly decrease after treatment with combined colistin/doripenem at 4 hr.

Colistin and doripenem induced alterations in peptide metabolism. Treatment with doripenem alone and the combination of colistin and doripenem showed unique changes in the levels of short peptides (Supplementary Figure S3 and Tables 1–3). The number of significantly perturbed peptides increased across the time points after treatment with doripenem alone and the combination of colistin and doripenem (≥ 1.5 -log₂-fold; ANOVA $p \leq 0.05$, FDR ≤ 0.1). However, colistin alone showed significant changes in the levels of only a few cellular peptides. Interestingly, a unique putative metabolite, tyramine ($m/z = 137.08$, $t_R = 9.03$ min; MSI level 2), which is associated with tyrosine metabolism was found to significantly increase only after treatment with doripenem alone and the combination of colistin and doripenem across all the time points (≥ 1.5 -log₂-fold; ANOVA $p \leq 0.0001$, FDR ≤ 0.1).

Discussion

The global spread of MDR Gram-negative bacteria is alarming and it is crucial to understand the detailed mechanisms of antibiotic action and resistance. Bacterial metabolic responses to antibiotics have not been well examined with cutting-edge metabolomics, and deciphering the metabolome of bacterial cells can potentially lead to innovative strategies for effective antibacterial therapy. Polymyxins and carbapenems display their primary antibacterial activity via initial interactions with LPS and binding to penicillin-binding proteins (PBPs), respectively^{10,39}. Notwithstanding, increasing evidence indicates that the rarely explored effects on bacterial metabolism are crucial for the antibacterial activity of antibiotics⁴⁰. The combination of polymyxins with carbapenems has been shown to be synergistic against MDR Gram-negative bacteria; albeit, the detailed mechanism of their synergistic action(s) has not been examined^{26–30}. Previously, our transcriptomics data revealed that the combination of colistin and doripenem altered the gene expression profiles in *A. baumannii* at 1 hr in a similar manner to that of colistin treatment alone. These genes were primarily associated with outer membrane biogenesis, fatty acid metabolism and phospholipid trafficking⁴¹. Interestingly, similar transcriptional changes were also

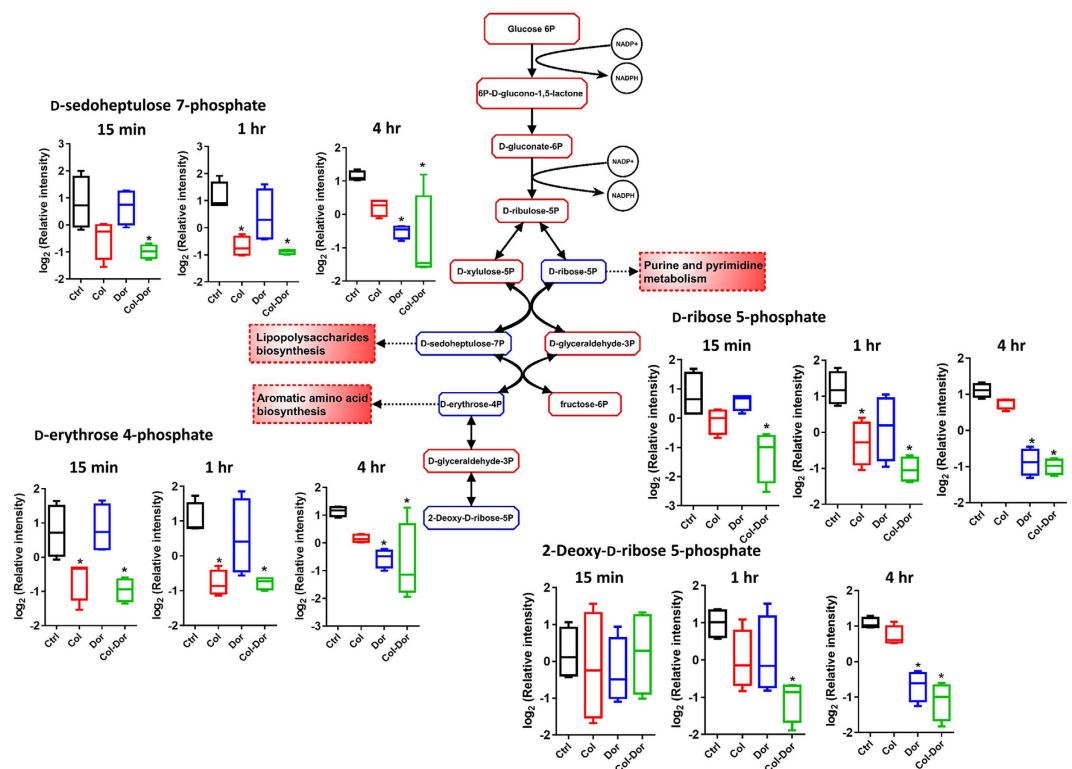


Figure 3. Central metabolic changes in the pentose phosphate pathway (PPP). Antibiotic treatment of *A. baumannii* ATCC 19606 significantly decreased the levels of three PPP metabolites (D-sedoheptulose 7-phosphate, D-erythrose 4-phosphate, and D-ribose 5-phosphate) that are essential anabolic precursors of related pathways. The combined colistin/doripenem significantly decreased the levels of the three precursor metabolites at all the time points. Additionally, 2-deoxy-D-ribose 5-phosphate significantly decreased followed by the combination at 1 hr and 4 hr. In the pathway flow chart (adapted from biocyc.org with reference to *E. coli* K-12), blue boxes indicate the metabolites that were significantly decreased and red boxes indicate the metabolites that were not significantly changed. Box plots indicate upper and lower quartiles (top and bottom of box); median (line within box); and the spread of data that are not outliers (whiskers). ≥ 1.5 -log₂-fold, $p \leq 0.05$, FDR ≤ 0.1 (one-way ANOVA).

observed in the *A. baumannii* LPS-deficient strain without colistin treatment⁴². Our present study is the first to elucidate the synergistic killing mechanism of the combination of colistin and doripenem against *A. baumannii*. The most significant findings on the synergistic combination in this metabolomics study include: (1) differential time-dependent inhibition of key metabolic pathways; (2) perturbation of the PPP and the downstream metabolism of LPS and nucleotides; and (3) inhibition of cell wall synthesis via different targets.

In the present study, global metabolic changes of MDR *A. baumannii* were investigated following exposure to colistin and doripenem individually and in combination over 4 hr. Our results show, for the first time, that colistin, doripenem and the combination induced common global metabolic perturbations in *A. baumannii*, and metabolisms of cellular lipids, nucleotides, amino sugars and energy are common pathways involved in the synergistic action of colistin and doripenem (Figs 2–5). The initial cellular metabolic perturbations following treatment with colistin monotherapy at 15 min and 1 hr impacted several essential metabolic pathways, namely lipid metabolism, nucleotide metabolism, amino sugar metabolism and energy metabolism (Figs 2, 4, and 5). Similar metabolic alterations were observed following treatment with doripenem alone at 4 hr (Figs 2, 4, and 5), indicating the effects of each antibiotic occur in a differential time-dependent manner. With the combination treatment, the perturbations were observed across all of the time points. This mechanistic finding has important implications for the pharmacokinetics/pharmacodynamics (PK/PD) of the colistin and doripenem combination, supporting its use in the clinic for maintaining persistent antibacterial effect and minimizing the potential bacterial regrowth due to colistin monotherapy^{43,44}.

Two key models have been proposed to explain mechanisms of drug synergism, the parallel pathway inhibition model and the bioavailability model^{45–48}. The parallel pathway inhibition model suggests that two drugs are synergistic if they inhibit two different targets in parallel pathways that are essential for an observed phenotype⁴⁷. The bioavailability model suggests that two drugs are synergistic if one drug's action enhances another drug's availability in the target cell, either by increasing the second drug's entry into the cell or by decreasing the second drug's degradation or efflux⁴⁸. As doripenem itself can access its target in the periplasmic space in *A. baumannii*, the bioavailability model is unlikely to explain the synergistic activity of colistin and doripenem, and is not supported by our metabolomics data. Our metabolomics analysis indicates that the parallel pathway inhibition model explains well the synergistic killing by colistin and doripenem against *A. baumannii*. Notably, treatment

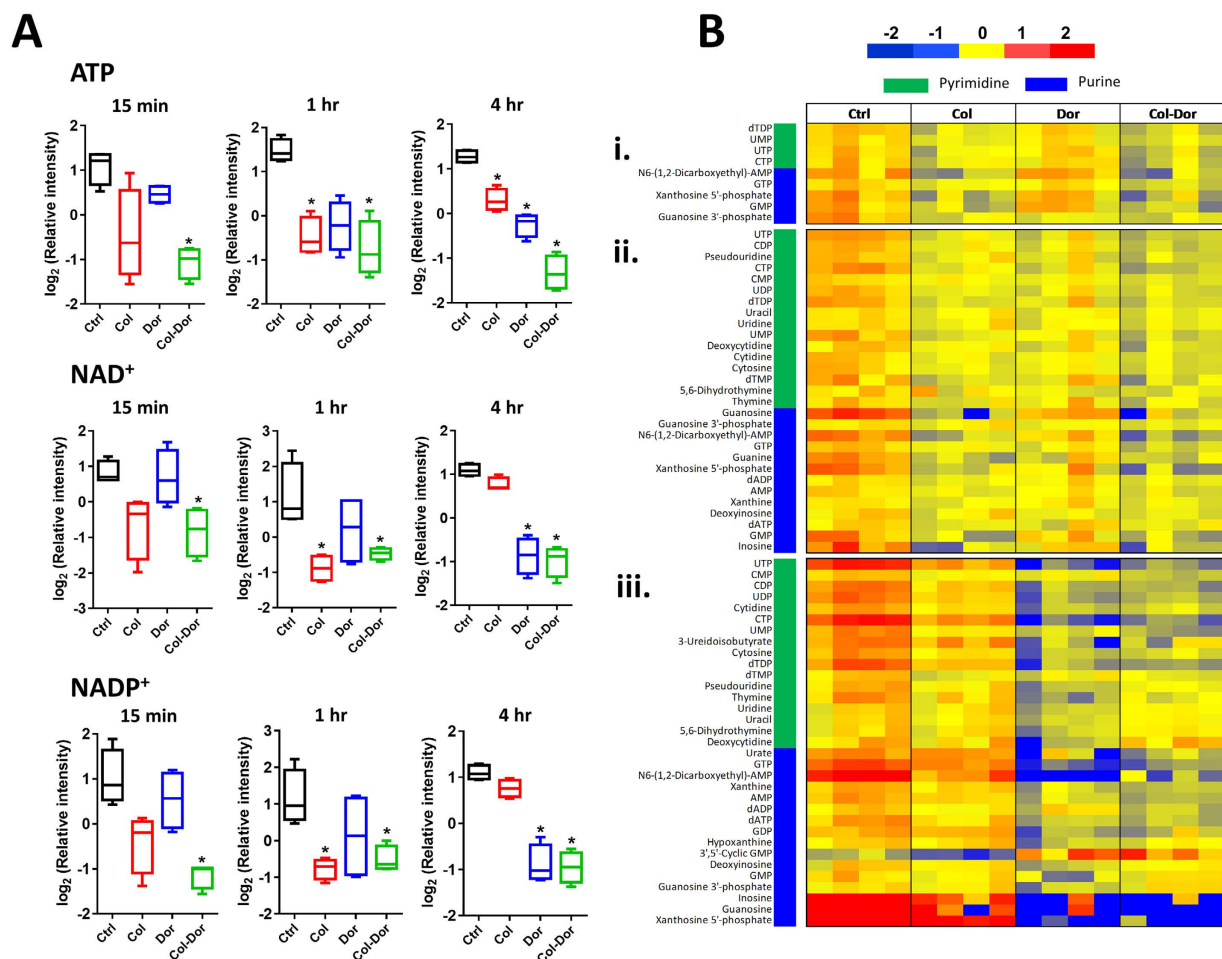


Figure 4. Depletion of energy and nucleotide metabolite levels. (A) Decreased levels of key energy-associated metabolites, ATP, NAD⁺ and NADP⁺ induced by colistin, doripenem, and the combination in *A. baumannii* ATCC 19606. Box plots indicate upper and lower quartiles (top and bottom of box); median (line within box); and the spread of data that are not outliers (whiskers). * ≥ 1.5 -log₂-fold, $p \leq 0.05$, FDR ≤ 0.1 (one-way ANOVA). (B) Heatmap profile of relative abundance of significantly perturbed nucleotides at (i) 15 min, (ii) 1 hr, and (iii) 4 hr after treatment with colistin (Col), doripenem (Dor) and the combination (Col-Dor) (n = 4). Antibiotics decreased the levels of nucleotides, both purines and pyrimidines, in *A. baumannii* ATCC 19606.

with colistin or doripenem alone or in combination at different time points significantly decreased the cellular levels of PPP intermediates (e.g. D-sedoheptulose 7-phosphate), UDP-GlcNAc and UDP-MurNAc, which are key precursor metabolites for the biosynthesis of peptidoglycan and LPS (Figs 3 and 5). Our metabolomics data also demonstrate that colistin and doripenem perturb various key pathways related to cell envelope biosynthesis, namely GPLs, FAs, LPS and peptidoglycan biosynthesis (Figs 2 and 5). Importantly, our study is the first to reveal that colistin itself also caused inhibition of cell wall synthesis by decreasing the essential precursor metabolites (i.e. UDP-GlcNAc and UDP-MurNAc), a different mechanism from doripenem which acts via binding to PBPs.

The Gram-negative bacterial cell envelope is composed of an asymmetrical outer membrane (OM), a thin cell wall, and a symmetrical inner membrane⁴⁹. The outer leaflet of the OM is predominantly constituted of LPS and the inner leaflet is mainly comprised of phospholipids^{49,50}. In line with the primary mode of action of colistin, our metabolomics data revealed that colistin treatment at 15 min and 1 hr caused significant perturbations in the levels of OM lipids, specifically GPLs and FAs (Fig. 2A). In keeping with this finding, our previous transcriptomics results showed that colistin treatment up-regulated the expression of the Mla system (Maintenance of OM lipid asymmetry) in *A. baumannii* ATCC 19606, which is responsible for transporting excess phospholipids in the outer leaflet back to the inner membrane to maintain the OM asymmetry^{41,51,52}. Significant changes to the OM lipids, as observed at both the transcriptomics and metabolomics levels, are highly consistent with the proposed bactericidal mechanism of colistin via lipid exchange between the inner and outer membrane¹¹. Furthermore, our previous transcriptomics data showed that colistin treatment induced the up-regulation of genes involved in fatty acid β -oxidation/degradation and down-regulation of genes involved in fatty acid biosynthesis⁴¹, which well explains the colistin-induced fatty acid perturbations observed here (Fig. 2A). Notably, doripenem treatment at 15 min and 1 hr did not produce any appreciable changes in the levels of GPLs and FAs relative to the untreated control (Fig. 2A), and the expression of lipid metabolism genes was not affected at 15 min, although

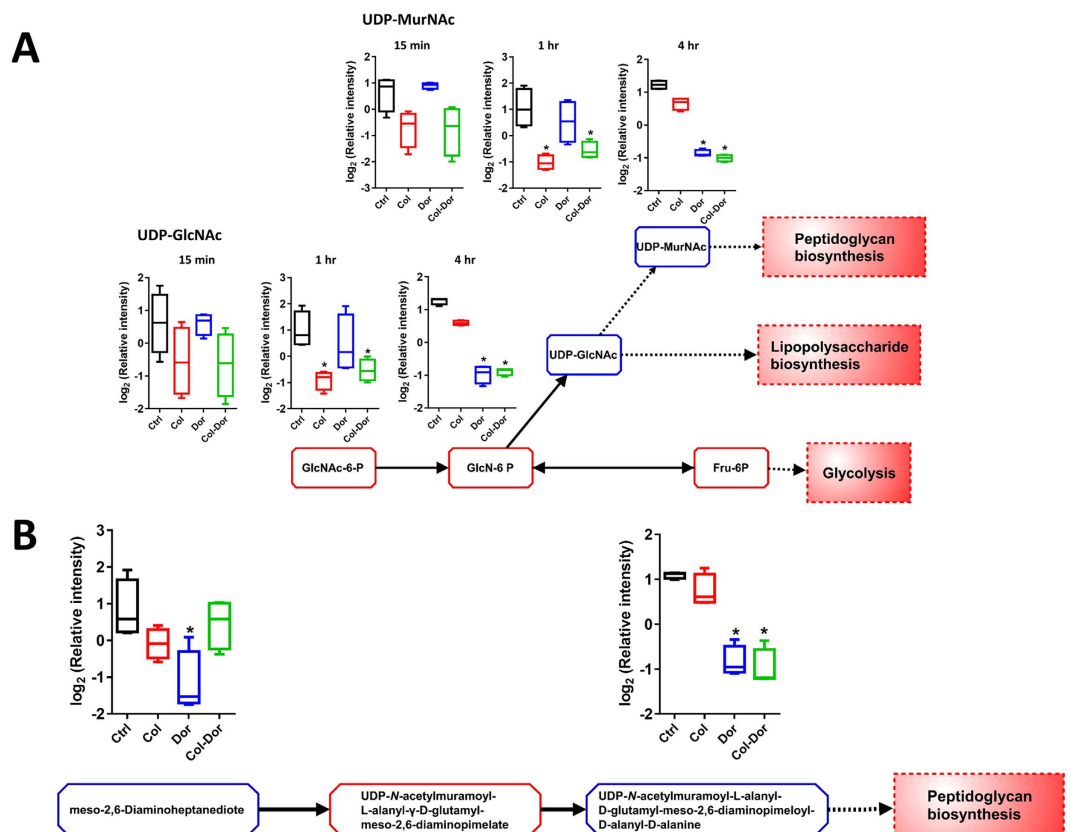


Figure 5. Depletion of amino sugar metabolites for peptidoglycan and lipopolysaccharide biosynthesis.

(A) Significant decrease in the levels of two amino sugar metabolites at 1 hr and 4 hr by colistin, doripenem and the combination, and perturbation of the cell envelope biosynthesis (peptidoglycan and lipopolysaccharide biosynthesis) in *A. baumannii* ATCC 19606. UDP-N-acetyl-D-glucosamine (UDP-GlcNAc) is a key precursor metabolite for LPS and peptidoglycan biosynthesis. (B) Levels of two key metabolites of peptidoglycan biosynthesis significantly decreased after treatment with doripenem alone at 4 hr. The combination of colistin and doripenem also significantly decreased UDP-N-acetylmuramoyl-L-alanyl-D-glutamyl-meso-2,6-diaminopimeloyl-D-alanyl-D-alanine (>2.0 -log₂-fold) at 4 hr. The blue boxes in the flow charts indicate the metabolites that were significantly decreased. The red boxes indicate the metabolites that were not significantly changed. Box plots indicate upper and lower quartiles (top and bottom of box); median (line within box); and the spread of data that are not outliers (whiskers). ≥ 1.5 -log₂-fold, $p \leq 0.05$, FDR ≤ 0.1 (one-way ANOVA).

significant transcriptomic changes were reported for doripenem treatment at 1 hr (i.e. retrograde phospholipid transport and lipoprotein transport)⁴¹. However, doripenem treatment at 4 hr produced a similar pattern of lipid changes (both GPLs and FAs) as per the aforementioned colistin treatment at 15 min and 1 hr. Interestingly, the entire time-course of the combination treatment displayed a distinct pattern of lipid changes, wherein only the GPLs were significantly perturbed while the FA levels remained largely unaffected. One metabolite involved in glycerophospholipid metabolism, *sn*-glycero-3-phosphoethanolamine, was specifically associated with colistin treatment, both alone and in combination, but *sn*-glycero-3-phosphoethanolamine was also significantly depleted in the LPS-deficient polymyxin-resistant strain *A. baumannii* 19606 R relative to the wild-type ATCC 19606 strain in the absence of polymyxin treatment⁵³.

In terms of the impact on energy metabolism, treatment with the colistin/doripenem combination significantly decreased intracellular ATP, NADP⁺ and NAD⁺ levels and the levels of three major metabolites of PPP, namely D-sedoheptulose-7-phosphate, D-ribose 5-phosphate and D-erythrose 4-phosphate. ADP-heptose, a key downstream metabolite of the heptose biosynthesis pathway, is an important component of the LPS inner core^{54,55}. Mutations in the gene (*GmhA*) associated with ADP-glyceromannoheptose synthesis in *Haemophilus influenza*, which cause deficiencies in heptose biosynthesis, result in an avirulent phenotype, increased membrane permeability and increased susceptibility to antibiotics^{55–57}. Excitingly, our data revealed significant depletion in the levels of D-sedoheptulose-7-phosphate under all treatment conditions (Fig. 3). As D-sedoheptulose-7-phosphate is also a key early precursor metabolite in the heptose biosynthesis pathway, our data suggest that colistin, doripenem, and their combination perturb the biosynthesis of ADP-heptose in *A. baumannii* via inhibition of the PPP. Another metabolite in the PPP, D-ribose 5-phosphate, was depleted after treatment with colistin, doripenem and the combination (Fig. 3). D-Ribose 5-phosphate is a key initial precursor metabolite in purine and pyrimidine metabolism, and hence all treatment conditions caused significant decreases in the levels of nucleotides, both purine and pyrimidine (Fig. 4B). Previous metabolomics studies have shown total depletion of

the nucleotide pool following antibiotic treatment (ampicillin, kanamycin, norfloxacin, and vancomycin) in both Gram-negative (*Escherichia coli*) and Gram-positive (*Staphylococcus aureus*) bacteria^{40,58}. The significant changes in nucleotide levels in antibiotic-treated samples were suggestive of nucleotide degradation⁴⁰. Interestingly, significant depletion in the levels of nucleotides in the polymyxin-resistant LPS-deficient strain *A. baumannii* 19606 R was observed even without polymyxin treatment⁵³. Significant depletion in the levels of ATP, NADP⁺ and NAD⁺ is likely secondary to the nucleotide pool depletion, but may also be indicative of altered oxidative phosphorylation. It has been reported that polymyxins induce inhibition of respiration which reduces the level of the intracellular ATP pool⁵⁹, and altered levels of TCA metabolites (fumarate and *cis*-aconitate) were observed in the present study. It is likely that the depletion of energy related metabolites by colistin, doripenem and the combination is a secondary effect of their antibacterial activity against *A. baumannii*.

The broad-spectrum antibacterial effect of doripenem against Gram-positive and Gram-negative bacteria is by virtue of its ability to inhibit biosynthesis of the key building block of the bacterial cell wall, peptidoglycan^{39,60,61}. Fundamentally, doripenem is a substrate analogue that binds to the C-terminal transpeptidase active site of PBPs in a non-reversible manner, thus inhibiting the peptidoglycan polymerization process⁶². Notably, following treatment with doripenem alone or in combination at 4 hr, we observed a significant decrease in the levels of the peptidoglycan biosynthesis metabolites, meso-2,6-diaminoheptanedioate and UDP-N-acetylmuramoyl-L-alanyl-D-glutamyl-6-carboxy-L-lysyl-D-alanyl-D-alanine (Fig. 5B). As mentioned above, colistin monotherapy also significantly decreased the levels of the essential peptidoglycan precursor metabolites UDP-GlcNAc and UDP-MurNAc (Fig. 5A). Interestingly, our previous transcriptomics results showed that peptidoglycan-associated lipoproteins were significantly up-regulated in *A. baumannii* in response to treatment with colistin and doripenem alone or in combination⁴¹. The up-regulation of peptidoglycan-associated lipoproteins may be a protective action by *A. baumannii* to cope with the inhibition of peptidoglycan synthesis by doripenem and/or colistin. Taken together, our current metabolomic study reveals that, in addition to disorganizing the OM, colistin also interferes cell wall synthesis via inhibition of peptidoglycan metabolism; this mechanism also explains the synergistic killing effect of its combination with a carbapenem.

Studies have shown that the mechanism of polymyxin activity was partly associated with oxidative stress via the formation of hydroxyl radicals, with reactive oxygen species mainly targeting DNA, RNA, proteins and lipids⁶³, or by inhibition of respiratory chain enzymes (e.g. NADH-quinone oxidoreductase)^{64,65}. However, the association of free radicals in the mechanism of antibiotic bacterial killing is disputable^{66–70}. In our analysis the reduced form of glutathione (GSH), an important indicator of oxidative stress, was not detected, as it was likely oxidized to glutathione disulfide (GSSG) during sample preparation and/or storage⁷¹. Nevertheless, the total glutathione content, measured as GSSG, was significantly depleted following exposure to colistin and doripenem alone and in combination (Supplementary Table 1); this result is in line with the utilization of glutathione pools to compensate for antibiotic-induced oxidative damage, albeit not consistent with the increased levels of reduced glutathione previously reported⁴⁰. Even though we were unable to detect specific markers of oxidative stress from the TCA cycle intermediate (i.e. α -ketoglutarate) and product (i.e. NADH), the changes to other TCA metabolites (i.e. fumarate and *cis*-aconitate) clearly indicate the perturbation of the TCA cycle in response to single and combination treatments of colistin and doripenem. Our group previously demonstrated that *A. baumannii* ATCC 19606 treated with colistin significantly increased the expression of superoxide dismutase (SOD) enzyme, HMPREF0010_02336 (*sodB* encoding a predicted FeSOD) and HMPREF0010_02564 (encoding a predicted Cu-ZnSOD), suggesting the association of hydroxyl radicals in colistin antibacterial activity⁴¹.

To the best of our knowledge, this is the first metabolomics study to investigate the mechanism of action of colistin either as monotherapy, or in combination with doripenem, against *A. baumannii*. Our study discovered significant perturbations to cell envelope biosynthesis, nucleotide metabolism, and energy metabolism by colistin and its synergistic combination with doripenem. The convergence of antibiotic-induced metabolic profiles on the depletion of PPP and amino-sugar metabolites indicates that these pathways play key roles in the antibacterial activity of colistin alone and its combination with doripenem. Importantly, we are the first to demonstrate that the combination of colistin with doripenem synergistically kills *A. baumannii* via inhibiting different key metabolic pathways in a time-dependent manner, which highlights the essentiality of mechanism-based optimization of this combination using pharmacokinetics/pharmacodynamics. Overall, this study highlights the importance of elucidating the complex and dynamic interaction of multiple cellular metabolic pathways due to antibiotic treatment, and the significant potential of systems pharmacology in paradigm-shifting optimization of antibiotic use in patients.

Materials and Methods

Strain, antibiotics and reagents. *A. baumannii* ATCC 19606 (American Type Culture Collection [ATCC], Manassas, USA) was susceptible to both colistin and doripenem with MICs of 1 mg/L for both antibiotics. The strain was grown in cation-adjusted Mueller-Hinton broth (MHB; Oxoid, Australia; 20–25 mg/L Ca²⁺ and 10–12.5 mg/L Mg²⁺). Colistin (Sigma-Aldrich, Saint Louis, USA) and doripenem (Doribax, Shinogi Inc, Osaka, Japan) were prepared using Milli-Q water (Millipore Australia, North Ryde, New South Wales, Australia) prior to each experiment and sterilized by filtration with a 0.22- μ m pore size Millex GP filter (Millipore, Bedford, MA).

Bacterial culture preparation. Culture of *A. baumannii* ATCC 19606 was prepared on a nutrient agar plate from the frozen stock (−80 °C) and incubated for 16–18 hr at 37 °C. For the overnight culture, a colony of ATCC 19606 was inoculated into 15 mL MHB and incubated for 16–18 hr at 37 °C with shaking at 150 rpm. For the main culture, 1:100 dilution of the overnight culture was sub-cultured into four different reservoirs containing 200 mL fresh MHB and grown to an optical density at 600 nm (OD₆₀₀) of ~0.5 to achieve the starting inoculum ~10⁸ cfu/mL (in order to obtain enough cells) of an early exponential growth phase. Bacterial culture was treated with colistin

(2 mg/L), doripenem (25 mg/L), and combination of colistin and doripenem (2 mg/L + 25 mg/L, respectively); concentrations of colistin and doripenem were chosen based on their pharmacokinetics in patients²⁶. Bacterial culture without any antibiotic treatment served as a control. Four biological replicates were prepared independently from different colonies of ATCC 19606 on different days.

Preparation of cellular metabolite extracts. The untargeted metabolomics study was performed to investigate global metabolic alterations in *A. baumannii* ATCC 19606 due to colistin, doripenem and the combination treatments in an *in vitro* static time-kill study. Cellular metabolites of *A. baumannii* were extracted by the previously optimized method with slight modifications⁵³. Samples were collected before treatment with colistin, doripenem and the combination (i.e. time = 0), and at 15 min, 1 hr, and 4 hr for metabolite extraction and viable counting. For the fingerprint samples (i.e. intracellular metabolites), 15 mL of the bacterial culture was collected and immediately transferred on ice. All the samples were rapidly quenched in a dry ice/ethanol bath and preserved on ice for all following steps. Samples were normalized by optical density ($OD_{600\text{ nm}}$) and centrifuged for 10 min at 3,220 g at 4 °C. The supernatant was collected for extracellular metabolites (i.e. footprint). The cell pellets were washed three times with sterile saline (4 °C) and centrifuged for 3 min at 3,220 g at 4 °C. Cellular metabolites were extracted with chloroform:methanol:water (1:3:1, v/v; -80 °C) (total volume of 300 µL) containing generic internal standards (CHAPS, CAPS, PIPES and TRIS) at 1 µM. Samples were immediately frozen in liquid nitrogen and allowed to thaw on ice, and the freeze-thaw process was repeated three times to lyse the cells and release cellular metabolites. The extracted samples were centrifuged for 10 min at 3,220 g at 4 °C and the supernatant was collected and further centrifuged at 14,000 g for 10 min at 4 °C. The final supernatant samples (200 µL) were collected into injector vials for LC-MS analysis. For footprint samples, aliquots of the culture supernatant were rapidly filtered through a 0.22-µm membrane filter, and 10 µL of the supernatant was mixed with 250 µL of chloroform:methanol:water (1:3:1, v/v) and centrifuged at 14,000 g for 10 min at 4 °C to collect particle-free supernatant for LC-MS analysis.

LC-MS analysis of metabolites. Samples were analyzed on a Q-Exactive Orbitrap mass spectrometer (Thermo Fisher), coupled to a Dionex high-performance liquid chromatograph (U3000 RSLC HPLC, Thermo Fisher) with a ZIC-pHILIC column (5 µm, polymeric, 150 × 4.6 mm; SeQuant, Merck). The MS system was operated at 35,000 resolution in both positive and negative electro-spray ionization (ESI) mode (rapid switching) and a detection range of 85 to 1,275 *m/z*. The LC solvent consisted of 20 mM ammonium carbonate (A) and acetonitrile (B) with a multi-step gradient system from 80% B to 50% B over 15 min, then to 5% B at 18 min, followed by a wash with 5% B for 3 min, and re-equilibration for 8 min with 80% B at a flow rate of 0.3 mL/min⁵³. The injection sample volume was 10 µL and the run time was 32 min. All samples were analyzed in the same run and the chromatographic peaks, signal reproducibility and analyte stability were monitored by assessment of pooled biological quality control (PBQC) samples (aliquot of 10 µL of each sample, including both footprints and fingerprints) analyzed periodically throughout the batch, internal standards and total ion chromatograms for each sample. Mixtures of pure standards containing over 200 metabolites were analyzed within the batch to aid in the identification of metabolites.

Data processing, bioinformatics and statistical analyses. Metabolomics data analyses were performed as previously described⁵³ using *mzMatch*⁷² and *IDEOM* (<http://mzmatch.sourceforge.net/ideom.php>)⁷³. Quantification of each metabolite was conducted using the raw peak height. Univariate and multivariate analyses utilized *MetaboAnalyst 3.0*⁷⁴. Prior to analysis, relative peak intensity data were normalized by the median, log transformed and scaled (by auto scale function) to reduce variance between the samples. The global metabolic profiles of samples with antibiotic treatments at each time point were analyzed using multivariate statistical analysis by unsupervised principal component analysis (PCA). One-way Analysis of Variance (ANOVA) ($p < 0.05$, $FDR \leq 0.1$) for multiple comparison and post hoc analysis using Tukey's Honestly Significant Difference (Tukey's HSD) were applied to identify significant metabolite changes between treated and untreated control samples at each time point. Metabolites that were detected as isomeric peaks with opposite abundance changes (increased and decreased levels) were excluded. To further increase the reliability of the data, significant metabolites were filtered by selection of only those that showed a ≥ 1.5 -log₂-fold change relative to the untreated control samples and an identification confidence score of 6 or more in *IDEOM* (i.e. removing likely LC-MS artefacts). Metabolic pathway analysis was performed based on the statistically significant identified metabolites (≥ 1.5 -log₂-fold; $p \leq 0.05$, $FDR \leq 0.1$, one-way ANOVA for multiple comparison). Visualization and Analysis of Networks containing Experimental Data (Vanted) software was utilized to visualize the associated metabolic pathways⁷⁵.

References

1. Dijkshoorn, L., Nemec, A. & Seifert, H. An increasing threat in hospitals: multidrug resistant *Acinetobacter baumannii*. *Nat. Rev. Microbiol.* **5**(12), 939–951 (2007).
2. Fishbain, J. & Peleg, A. Y. Treatment of *Acinetobacter* infections. *Clin. Infect. Dis.* **51**(1), 79–84 (2010).
3. Eurosurveillance editorial team. CDC publishes report on antibiotic resistance threats in the United States for the first time. *Eurosurveillance* **18**(38), 28–28 (2013).
4. Boucher, H. W. *et al.* Bad Bugs, No Drugs: No ESCAPE! An update from the Infectious Diseases Society of America. *Clin. Infect. Dis.* **48**(1), 1–12 (2009).
5. Lim, L. M. *et al.* Resurgence of colistin: a review of resistance, toxicity, pharmacodynamics, and dosing. *Pharmacotherapy* **30**(12), 1279–1291 (2010).
6. Falagas, M. E., Rafailidis, P. I. & Matthaïou, D. K. Resistance to polymyxins: mechanisms, frequency and treatment options. *Drug Resist. Updates* **13**(4–5), 132–138 (2010).
7. Cai, Y., Chai, D., Wang, R., Liang, B. B. & Bai, N. Colistin resistance of *Acinetobacter baumannii*: clinical reports, mechanisms and antimicrobial strategies. *J. Antimicrob. Chemother.* **67**(7), 1607–1615 (2012).

8. Pogue, J. M., Cohen, D. A. & Marchaim, D. Editorial commentary: polymyxin-resistant *Acinetobacter baumannii*: urgent action needed. *Clin. Infect. Dis.* **60**(9), 1304–1307, (2015).
9. Karageorgopoulos, D. E. & Falagas, M. E. Current control and treatment of multidrug-resistant *Acinetobacter baumannii* infections. *Lancet Infect. Dis.* **8**(12), 751–762 (2008).
10. Velkov, T., Roberts, K. D., Nation, R. L., Thompson, P. E. & Li, J. Pharmacology of polymyxins: new insights into an 'old' class of antibiotics. *Future Microbiol.* **8**(6), 711–724 (2013).
11. Clausell, A. *et al.* Gram-negative outer and inner membrane models: insertion of cyclic cationic lipopeptides. *J. Phys. Chem. B.* **111**(3), 551–563 (2007).
12. Trimble, M. J., Mlynarcik, P., Kolar, M. & Hancock, R. E. Polymyxin: alternative mechanisms of action and resistance. *Cold Spring Harb. Perspect. Med.* **6**(10), (2016).
13. Li, J. *et al.* Heteroresistance to colistin in multidrug-resistant *Acinetobacter baumannii*. *Antimicrob. Agents Chemother.* **50**(9), 2946–2950 (2006).
14. Cai, Y., Chai, D., Wang, R., Liang, B. & Bai, N. Colistin resistance of *Acinetobacter baumannii*: clinical reports, mechanisms and antimicrobial strategies. *J. Antimicrob. Chemother.* **67**(7), 1607–1615 (2012).
15. Bergen, P. J. *et al.* Polymyxin combinations: pharmacokinetics and pharmacodynamics for rationale use. *Pharmacotherapy* **35**(1), 34–42 (2015).
16. Bollenbach, T. Antimicrobial interactions: mechanisms and implications for drug discovery and resistance evolution. *Curr. Opin. Microbiol.* **27**, 1–9 (2015).
17. Kassamali, Z., Jain, R. & Danziger, L. H. An update on the arsenal for multidrug-resistant *Acinetobacter* infections: polymyxin antibiotics. *Int. J. Infect. Dis.* **30**, 125–132 (2015).
18. Nation, R. L. *et al.* Updated US and European dose recommendations for intravenous colistin: how do they perform? *Clin. Infect. Dis.* **62**(5), 552–558 (2016).
19. Beceiro, A. *et al.* Phosphoethanolamine modification of lipid A in colistin-resistant variants of *Acinetobacter baumannii* mediated by the pmrAB two-component regulatory system. *Antimicrob. Agents Chemother.* **55**(7), 3370–3379 (2011).
20. Arroyo, L. A. *et al.* The pmrCAB operon mediates polymyxin resistance in *Acinetobacter baumannii* ATCC 17978 and clinical isolates through phosphoethanolamine modification of lipid A. *Antimicrob. Agents Chemother.* **55**(8), 3743–3751 (2011).
21. Pelletier, M. R. *et al.* Unique structural modifications are present in the lipopolysaccharide from colistin-resistant strains of *Acinetobacter baumannii*. *Antimicrob. Agents Chemother.* **57**(10), 4831–4840 (2013).
22. Lesho, E. *et al.* Emergence of colistin-resistance in extremely drug-resistant *Acinetobacter baumannii* containing a novel pmrCAB operon during colistin therapy of wound infections. *J. Infect. Dis.* **208**(7), 1142–1151 (2013).
23. Rolain, J. M. *et al.* Real-time sequencing to decipher the molecular mechanism of resistance of a clinical pan-drug-resistant *Acinetobacter baumannii* isolate from Marseille, France. *Antimicrob. Agents Chemother.* **57**(1), 592–596 (2013).
24. Snitkin, E. S. *et al.* Genomic insights into the fate of colistin resistance and *Acinetobacter baumannii* during patient treatment. *Genome Res.* **23**(7), 1155–1162, (2013).
25. Moffatt, J. H. *et al.* Colistin resistance in *Acinetobacter baumannii* is mediated by complete loss of lipopolysaccharide production. *Antimicrob. Agents Chemother.* **54**(12), 4971–4977 (2010).
26. Bergen, P. J. *et al.* Synergistic killing of multidrug-resistant *Pseudomonas aeruginosa* at multiple inocula by colistin combined with doripenem in an *in vitro* pharmacokinetic/pharmacodynamic model. *Antimicrob. Agents Chemother.* **55**(12), 5685–5695 (2011).
27. Deris, Z. Z. *et al.* The combination of colistin and doripenem is synergistic against *Klebsiella pneumoniae* at multiple inocula and suppresses colistin resistance in an *in vitro* pharmacokinetic/pharmacodynamic model. *Antimicrob. Agents Chemother.* **56**(10), 5103–5112 (2012).
28. Jernigan, M. G., Press, E. G., Nguyen, M. H., Clancy, C. J. & Shields, R. K. The combination of doripenem and colistin is bactericidal and synergistic against colistin-resistant, carbapenemase-producing *Klebsiella pneumoniae*. *Antimicrob. Agents Chemother.* **56**(6), 3395–3398 (2012).
29. Principe, L. *et al.* *In vitro* activity of doripenem in combination with various antimicrobials against multidrug-resistant *Acinetobacter baumannii*: possible options for the treatment of complicated infection. *Microb. Drug Resist.* **19**(5), 407–414 (2013).
30. Oleksiuk, L. M. *et al.* *In vitro* responses of *Acinetobacter baumannii* to two- and three-drug combinations following exposure to colistin and doripenem. *Antimicrob. Agents Chemother.* **58**(2), 1195–1199 (2014).
31. Ly, N. S. *et al.* Colistin and doripenem combinations against *Pseudomonas aeruginosa*: profiling the time course of synergistic killing and prevention of resistance. *J. Antimicrob. Chemother.* **70**(5), 1434–1442 (2015).
32. Shields, R. K. *et al.* Epidemiology, clinical characteristics and outcomes of extensively drug-resistant *Acinetobacter baumannii* infections among solid organ transplant recipients. *Plos One* **7**(12), (2012).
33. Chen, C., Gonzalez, F. J. & Idle, J. R. LC-MS-based metabolomics in drug metabolism. *Drug Metab. Rev.* **39**(2–3), 581–597 (2007).
34. Mastrangelo, A., Armitage, E. G., Garcia, A. & Barbas, C. Metabolomics as a tool for drug discovery and personalised medicine. A review. *Curr. Top. Med. Chem.* **14**(23), 2627–2636 (2014).
35. Kaddurah-Daouk, R., Weinshilboum, R. M. & Network, P. R. Pharmacometabolomics: implications for clinical pharmacology and systems pharmacology. *Clin. Pharmacol. Ther.* **95**(2), 154–167 (2014).
36. Vincent, I. M., Ehmann, D. E., Mills, S. D., Perros, M. & Barrett, M. P. Untargeted metabolomics to ascertain antibiotic modes of action. *Antimicrob. Agents Chemother.* **60**(4), 2281–2291 (2016).
37. Jia, J. *et al.* Mechanisms of drug combinations: interaction and network perspectives. *Nat. Rev. Drug Discov.* **8**(2), 111–128 (2009).
38. Kirwan, J. A., Weber, R. J., Broadhurst, D. I. & Viant, M. R. Direct infusion mass spectrometry metabolomics dataset: a benchmark for data processing and quality control. *Sci. Data* **1**, 140012 (2014).
39. Paterson, D. L. & Depestel, D. D. Doripenem. *Clin. Infect. Dis.* **49**(2), 291–298 (2009).
40. Belenky, P. *et al.* Bactericidal antibiotics induce toxic metabolic perturbations that lead to cellular damage. *Cell Rep.* **13**(5), 968–980 (2015).
41. Henry, R. *et al.* The transcriptomic response of *Acinetobacter baumannii* to colistin and doripenem alone and in combination in an *in vitro* pharmacokinetics/pharmacodynamics model. *J. Antimicrob. Chemother.* **70**(5), 1303–1313 (2015).
42. Henry, R. *et al.* Colistin-resistant, lipopolysaccharide-deficient *Acinetobacter baumannii* responds to lipopolysaccharide loss through increased expression of genes involved in the synthesis and transport of lipoproteins, phospholipids, and poly-beta-1,6-N-acetylglucosamine. *Antimicrob. Agents Chemother.* **56**(1), 59–69 (2012).
43. Bergen, P. J. *et al.* Pharmacokinetic/pharmacodynamic investigation of colistin against *Pseudomonas aeruginosa* using an *in vitro* model. *Antimicrob. Agents Chemother.* **54**(9), 3783–3789 (2010).
44. Matthaiou, D. K. *et al.* Risk factors associated with the isolation of colistin-resistant Gram-negative bacteria: a matched case-control study. *Crit. Care Med.* **36**(3), 807–811, (2008).
45. Pritchard, J. R. *et al.* Defining principles of combination drug mechanisms of action. *Proc. Natl. Acad. Sci. USA.* **110**(2), 170–179 (2013).
46. Bolla, J. M. *et al.* Strategies for bypassing the membrane barrier in multidrug resistant Gram-negative bacteria. *FEBS Lett.* **585**(11), 1682–1690 (2011).
47. Yeh, P. J., Hegreness, M. J., Aiden, A. P. & Kishony, R. Drug interactions and the evolution of antibiotic resistance. *Nat. Rev. Microbiol.* **7**(6), 460–466 (2009).

48. Zimmermann, G. R., Lehar, J. & Keith, C. T. Multi-target therapeutics: when the whole is greater than the sum of the parts. *Drug Discov. Today* **12**(1–2), 34–42 (2007).
49. Nikaido, H. Molecular basis of bacterial outer membrane permeability revisited. *Microbiol. Mol. Biol. Rev.* **67**(4), 593–656 (2003).
50. Beveridge, T. J. Structures of Gram-negative cell walls and their derived membrane vesicles. *J. Bacteriol.* **181**(16), 4725–4733 (1999).
51. Malinverni, J. C. & Silhavy, T. J. An ABC transport system that maintains lipid asymmetry in the Gram-negative outer membrane. *Proc. Natl. Acad. Sci. USA* **106**(19), 8009–8014 (2009).
52. Martorana, A. M. *et al.* Dissecting *Escherichia coli* outer membrane biogenesis using differential proteomics. *PLoS One* **9**(6), (2014).
53. Mahamad Maifiah, M. H. *et al.* Global metabolic analyses identify key differences in metabolite levels between polymyxin-susceptible and polymyxin-resistant *Acinetobacter baumannii*. *Sci. Rep.* **6**, 22287 (2016).
54. Kneidinger, B. *et al.* Biosynthesis pathway of ADP-L-glycero-beta-D-manno-heptose in *Escherichia coli*. *J. Bacteriol.* **184**(2), 363–369 (2002).
55. Taylor, P. L. *et al.* Structure and function of sedoheptulose-7-phosphate isomerase, a critical enzyme for lipopolysaccharide biosynthesis and a target for antibiotic adjuvants. *J. Biol. Chem.* **283**(5), 2835–2845 (2008).
56. Taylor, P. L. *et al.* Structural and kinetic characterization of the LPS biosynthetic enzyme D-alpha, beta-D-heptose-1,7-bisphosphate phosphatase (GmhB) from *Escherichia coli*. *Biochemistry* **49**(5), 1033–1041 (2010).
57. Brooke, J. S. & Valvano, M. A. Molecular cloning of the *Haemophilus influenzae* *gmhA* (*lpcA*) gene encoding a phosphoheptose isomerase required for lipooligosaccharide biosynthesis. *J. Bacteriol.* **178**(11), 3339–3341 (1996).
58. Dorries, K., Schlueter, R. & Lalk, M. Impact of antibiotics with various target sites on the metabolome of *Staphylococcus aureus*. *Antimicrob. Agents Chemother.* **58**(12), 7151–7163 (2014).
59. Storm, D. R., Rosenthal, K. S. & Swanson, P. E. Polymyxin and related peptide antibiotics. *Annu. Rev. Biochem.* **46**, 723–763 (1977).
60. Lister, P. D. Carbapenems in the USA: focus on doripenem. *Expert Rev. Anti. Infect. Ther.* **5**(5), 793–809 (2007).
61. Macheboeuf, P., Contreras-Martel, C., Job, V., Dideberg, O. & Dessen, A. Penicillin binding proteins: key players in bacterial cell cycle and drug resistance processes. *FEMS Microbiol. Rev.* **30**(5), 673–691 (2006).
62. Scheffers, D. J. & Pinho, M. G. Bacterial cell wall synthesis: new insights from localization studies. *Microbiol. Mol. Biol. Rev.* **69**(4), 585–607 (2005).
63. Cabiscot, E., Tamarit, J. & Ros, J. Oxidative stress in bacteria and protein damage by reactive oxygen species. *Int. Microbiol.* **3**(1), 3–8 (2000).
64. Sampson, T. R. *et al.* Rapid killing of *Acinetobacter baumannii* by polymyxins is mediated by a hydroxyl radical death pathway. *Antimicrob. Agents Chemother.* **56**(11), 5642–5649 (2012).
65. Deris, Z. Z. *et al.* A secondary mode of action of polymyxins against Gram-negative bacteria involves the inhibition of NADH-quinone oxidoreductase activity. *J. Antibiot.* **67**(2), 147–151 (2014).
66. Dwyer, D. J., Kohanski, M. A., Hayete, B. & Collins, J. J. Gyrase inhibitors induce an oxidative damage cellular death pathway in *Escherichia coli*. *Mol. Syst. Biol.* **3**, 91 (2007).
67. Dwyer, D. J., Kohanski, M. A. & Collins, J. J. Role of reactive oxygen species in antibiotic action and resistance. *Curr. Opin. Microbiol.* **12**(5), 482–489 (2009).
68. Dong, T. G. *et al.* Generation of reactive oxygen species by lethal attacks from competing microbes. *Proc. Natl. Acad. Sci. USA* **112**(7), 2181–2186 (2015).
69. Brochmann, R. P. *et al.* Bactericidal effect of colistin on planktonic *Pseudomonas aeruginosa* is independent of hydroxyl radical formation. *J. Antimicrob. Agents* **43**(2), 140–147 (2014).
70. Iris Keren, Y. W., Juli Inocencia, Lawrence R. Mulcahy & Kim Lewis. Killing by bactericidal antibiotics does not depend on reactive oxygen species. *Science* **339**(6124), 1213–1216 (2013).
71. t'Kindt, R. *et al.* Towards an unbiased metabolic profiling of protozoan parasites: optimization of a *Leishmania* sampling protocol for HILIC-orbitrap analysis. *Anal. Bioanal. Chem.* **398**(5), 2059–2069 (2010).
72. Scheltema, R. A., Jankevics, A., Jansen, R. C., Swertz, M. A. & Breitling, R. PeakML/mzMatch: a file format, Java library, R library, and tool-chain for mass spectrometry data analysis. *Anal. Chem.* **83**(7), 2786–2793 (2011).
73. Creek, D. J., Jankevics, A., Burgess, K. E., Breitling, R. & Barrett, M. P. IDEOM: an Excel interface for analysis of LC-MS-based metabolomics data. *Bioinformatics* **28**(7), 1048–1049 (2012).
74. Xia, J., Sinelnikov, I. V., Han, B. & Wishart, D. S. MetaboAnalyst 3.0-making metabolomics more meaningful. *Nucleic Acids Res.* **43**(W1), W251–257 (2015).
75. Junker, B. H., Klukas, C. & Schreiber, F. VANTED: a system for advanced data analysis and visualization in the context of biological networks. *BMC Bioinformatics* **7**, 109 (2006).

Acknowledgements

J.L., D.J.C., T.V., R.L.N., B.T.T., and A.F. are supported by the National Institute of Allergy and Infectious Diseases of the National Institutes of Health (R01 AI111965 [J.L., D.J.C., T.V., and A.F.] and AI111990 [B.T.T., J.L., R.L.N. and A.F.]). The content is solely the responsibility of the authors and does not necessarily represent the official views of the National Institutes of Health. J.L. is an Australian National Health and Medical Research Council (NHMRC) Senior Research Fellow. D.J.C. and T.V. are Australian NHMRC Career Development Research Fellows.

Author Contributions

J.L. conceived the project and all authors involved in the design of the experiments. M.H.M.M. performed the experiments, and M.H.M.M., D.J.C., T.V., and J.L. analyzed the results. All authors reviewed the manuscript.

Additional Information

Supplementary information accompanies this paper at <http://www.nature.com/srep>

Competing Interests: The authors declare no competing financial interests.

How to cite this article: Maifiah, M. H. M. *et al.* Untargeted metabolomics analysis reveals key pathways responsible for the synergistic killing of colistin and doripenem combination against *Acinetobacter baumannii*. *Sci. Rep.* **7**, 45527; doi: 10.1038/srep45527 (2017).

Publisher's note: Springer Nature remains neutral with regard to jurisdictional claims in published maps and institutional affiliations.



This work is licensed under a Creative Commons Attribution 4.0 International License. The images or other third party material in this article are included in the article's Creative Commons license, unless indicated otherwise in the credit line; if the material is not included under the Creative Commons license, users will need to obtain permission from the license holder to reproduce the material. To view a copy of this license, visit <http://creativecommons.org/licenses/by/4.0/>

© The Author(s) 2017

Acinetobacter baumannii phenylacetic acid metabolism influences infection outcome through a direct effect on neutrophil chemotaxis

Md Saruar Bhuiyan^{a,b}, Felix Ellett^c, Gerald L. Murray^{a,b}, Xenia Kostoulas^{a,b}, Gustavo M. Cerqueira^{a,b}, Keith E. Schulze^d, Mohd Hafidz Mahamad Maifiah^e, Jian Li^e, Darren J. Creek^e, Graham J. Lieschke^c, and Anton Y. Peleg^{a,b,f,1}

^aInfection and Immunity Program, Monash Biomedicine Discovery Institute, Melbourne, VIC 3800, Australia; ^bDepartment of Microbiology, Monash University, Melbourne, VIC 3800, Australia; ^cAustralian Regenerative Medicine Institute, Monash University, Clayton, VIC 3800, Australia; ^dMonash Micro Imaging, Monash University, Clayton, VIC 3800, Australia; ^eMonash Institute of Pharmaceutical Sciences, Monash University, Parkville, VIC 3052, Australia; and ^fDepartment of Infectious Diseases, The Alfred Hospital and Central Clinical School, Monash University, Melbourne, VIC 3004, Australia

Edited by Ralph R. Isberg, Howard Hughes Medical Institute, Tufts University School of Medicine, Boston, MA, and approved June 27, 2016 (received for review November 23, 2015)

Innate cellular immune responses are a critical first-line defense against invading bacterial pathogens. Leukocyte migration from the bloodstream to a site of infection is mediated by chemotactic factors that are often host-derived. More recently, there has been a greater appreciation of the importance of bacterial factors driving neutrophil movement during infection. Here, we describe the development of a zebrafish infection model to study *Acinetobacter baumannii* pathogenesis. By using isogenic *A. baumannii* mutants lacking expression of virulence effector proteins, we demonstrated that bacterial drivers of disease severity are conserved between zebrafish and mammals. By using transgenic zebrafish with fluorescent phagocytes, we showed that a mutation of an established *A. baumannii* global virulence regulator led to marked changes in neutrophil behavior involving rapid neutrophil influx to a localized site of infection, followed by prolonged neutrophil dwelling. This neutrophilic response augmented bacterial clearance and was secondary to an impaired *A. baumannii* phenylacetic acid catabolism pathway, which led to accumulation of phenylacetate. Purified phenylacetate was confirmed to be a neutrophil chemoattractant. These data identify a previously unknown mechanism of bacterial-guided neutrophil chemotaxis in vivo, providing insight into the role of bacterial metabolism in host innate immune evasion. Furthermore, the work provides a potentially new therapeutic paradigm of targeting a bacterial metabolic pathway to augment host innate immune responses and attenuate disease.

Acinetobacter baumannii | zebrafish | neutrophils | chemotaxis | phenylacetate

The opportunistic Gram-negative bacterium, *Acinetobacter baumannii*, is now threatening our current antimicrobial armamentarium. This bacterium has a particular predilection for infecting patients with compromised innate immune defenses such as those in intensive care units, where it is responsible for a diverse range of infections including ventilator-associated pneumonia, bacteremia, and urinary tract, skin, and wound infection (1). Despite an increase in *A. baumannii* infections and outbreaks in health care facilities (1), relatively little is known about its pathogenesis. As with other Gram-negative bacteria, *A. baumannii* lipopolysaccharide plays a critical role in immune stimulation, particularly through Toll-like receptor 4 (TLR4) and CD14, leading to the production of the neutrophil chemotactic factor IL-8 (2) and the proinflammatory cytokine TNF- α (3). Mice lacking TLR4 and CD14 are more susceptible to *A. baumannii* pulmonary infection (3). Neutrophil recruitment is also critical, with neutrophil depletion being associated with more severe disease and greater bacterial burdens and dissemination (4, 5). The specific drivers of neutrophil trafficking during *A. baumannii* infection have not yet been defined.

Fundamental advances in the understanding of host–pathogen interactions have recently emerged through the use of the vertebrate model system *Danio rerio* (zebrafish) (6). The zebrafish is a tropical freshwater fish that has a remarkably similar immune system to humans, with elaborate innate and adaptive immune response pathways (7). As embryos, zebrafish rely solely on innate immune defenses, including soluble components such as opsonins, cytokines, chemokines, and complement, as well as the innate cellular repertoire of antigen presenting and phagocytic cells (7, 8). The establishment of a functional adaptive immune system is delayed to approximately 3 wk postfertilization (7). This distinction in immune development makes zebrafish embryos ideally suited to study host innate immune responses to bacterial pathogens (9, 10). High-resolution, real-time imaging enables the mechanistic dissection of how host innate immune cells migrate and respond to a bacterial pathogen in vivo (6). For example, work in zebrafish has led to a paradigm change in the understanding of the importance of macrophages harboring and disseminating mycobacterial infection (11, 12), and the conserved role for nerve growth factor β and its receptor tyrosine kinase TrkA signaling in pathogen-specific host immunity against *Staphylococcus aureus* (13).

In the present study, we exploited the advantages of zebrafish to better understand *A. baumannii* pathogenesis and interrogated

Significance

Acinetobacter baumannii is one of the most significant hospital-acquired bacterial pathogens, able to cause life-threatening infections and develop resistance to all currently available antibiotic agents. Here, we established zebrafish as a model to study real-time interactions between innate immune cells and *A. baumannii* during infection. We identified a bacterial metabolic pathway that, when inhibited, leads to enhanced immune responses toward the bacteria, improving bacterial clearance and reducing severity of disease. The enhanced immune response was secondary to accumulation of a metabolic by-product, which acted as a direct, bacterial-mediated attractant of neutrophils, the key immune cell important in response to bacterial infections. These results pave the way for novel therapeutic targeting of bacterial metabolism to stimulate immune responses to fight off infection.

Author contributions: M.S.B., G.J.L., and A.Y.P. designed research; M.S.B., F.E., X.K., G.M.C., and M.H.M.M. performed research; F.E., G.L.M., G.M.C., K.E.S., M.H.M.M., J.L., D.J.C., G.J.L., and A.Y.P. contributed new reagents/analytic tools; M.S.B., F.E., G.L.M., X.K., D.J.C., G.J.L., and A.Y.P. analyzed data; and M.S.B., G.L.M., and A.Y.P. wrote the paper.

The authors declare no conflict of interest.

This article is a PNAS Direct Submission.

¹To whom correspondence should be addressed.

This article contains supporting information online at www.pnas.org/lookup/suppl/doi:10.1073/pnas.1523116113/-DCSupplemental.

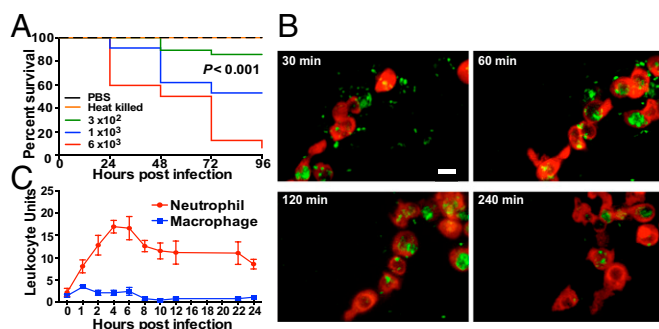


Fig. 1. *A. baumannii* infection in zebrafish. (A) Survival after bloodstream infection with live *A. baumannii* ($n = 30$ embryos, three biological replicates; P value is a comparison of 3×10^2 and 1×10^3 cfu per embryo by log-rank test). (B) Time-lapse confocal scanning laser microscopy showing red neutrophils [Tg(*lyz:DsRed*)^{nz50}] phagocytosing and clearing *A. baumannii*-GFP. (Scale bar: 20 μ m.) (C) LUs after infection into the somatic muscle of zebrafish after adjustment for trauma (PBS solution injection; mean \pm SEM, $n = 5$ per experiment, three biological replicates).

bacterial factors that determine neutrophil behavior in vivo. We showed that *A. baumannii* causes a lethal systemic infection in zebrafish, and that bacterial drivers of disease are conserved between zebrafish and mammals. Neutrophils were the dominant phagocyte responders to *A. baumannii* infection, and we identified that the *A. baumannii* phenylacetic acid catabolism pathway is an important mechanism used by the bacteria to assist in immune evasion. Loss of function of this metabolic pathway led to by-product accumulation dominated by phenylacetate (PA), which acted as a potent bacterial chemoattractant. These data identify a previously unknown mechanism of bacterial-guided neutrophil behavior in vivo and provide an example of the interaction between bacterial metabolism and host immunology.

Results

Systemic Infection with Live *A. baumannii* Causes Lethal Disease in Zebrafish. One of the most life-threatening forms of *A. baumannii* disease is bloodstream infection (1). As *A. baumannii* is not known to be a natural zebrafish pathogen, we assessed its capacity to cause disease in zebrafish embryos. A reference hospital-acquired *A. baumannii* strain [American Type Culture Collection (ATCC) 17978] was inoculated into the circulation of embryos 48 h postfertilization (hpf). As few as 300 cfu of bacteria caused lethal disease, with mortality dependent on the infecting inoculum (Fig. 1A). Similar findings were observed for other clinical *A. baumannii* strains (AB307, A9844, AB0059, ATCC 19606) (Fig. S1A–D). Neither injection of washed, heat-killed bacteria (Fig. 1A) nor culture filtrates from exponential or stationary-phase growth caused disease. These data show that live bacterial cells are required for *A. baumannii* pathogenesis in zebrafish.

To determine the ability of zebrafish to mount an effective response to *A. baumannii* bloodstream infection, we performed in vivo bacterial growth kinetic studies after infection with 1×10^3 cfu of *A. baumannii* per embryo (Fig. S1E). The bacterial burden increased to 20 h postinfection (hpi) but then subsided by 44 h to undetectable levels (Fig. S1E), suggesting that zebrafish can mount an innate immune response that clears an initially expanding bacterial population. Conversely, after inoculation of *A. baumannii* into the zebrafish yolk sac, a site devoid of innate immune cells (14), zebrafish were hypersusceptible to lethal disease (Fig. S1F), further supporting a role of innate immune responses in the defense against *A. baumannii*.

Protective Phagocyte Responses to *A. baumannii* Infection in Zebrafish. In mammals, neutrophils play an important role in response and clearance of *A. baumannii* infection (4, 5). To examine phagocyte–*A. baumannii* interactions in zebrafish, we used transgenic embryos

with fluorescently labeled leukocytes. Localized infection with GFP-expressing bacteria (*A. baumannii*) was established within somatic muscle. Within minutes of inoculation, neutrophils migrated to the site of *A. baumannii* infection, where they accumulated, phagocytosed bacteria, and then migrated away, clearing the bulk of infection by 4 h (Fig. 1B and Movie S1). Histopathology of the infection site confirmed neutrophilic phagocytosis of bacteria (Fig. S1G). Macrophages, which have also been shown to be important first responders to *A. baumannii* infection in mammals (15), were also recruited to the infection site but appeared to have less phagocytic activity (Movie S2), and similar numbers were seen with a tissue trauma control (PBS solution injection) (Fig. 1C). These data highlight the specificity of neutrophils in responding to pathogen-associated factors and macrophages in responding to tissue damage.

Within neutrophils, pathogen degradation typically occurs by hydrolytic enzymes within acidic phagolysosomes, whereas the remainder of the cytoplasm remains at neutral pH (16). To characterize the intracellular handling of *A. baumannii* following phagocytosis by neutrophils in vivo, we labeled *A. baumannii* with pHrodo-dextran, which emits red fluorescence only under low pH conditions. In Tg(*mpx:GFP*) zebrafish with green fluorescent neutrophils, red pHrodo-dependent fluorescence emerged within cytoplasmic vacuoles at 50 min postinfection (Fig. 2A, Fig. S2A, and Movie S3), confirming that intracellular handling and degradation of *A. baumannii* following neutrophil phagocytosis is within acidic phagolysosomes.

To further characterize the functional role of leukocytes in *A. baumannii* infection, we depleted zebrafish of neutrophils by knocking down the gene encoding the zebrafish ortholog of the granulocyte colony stimulating factor receptor [colony stimulating factor 3 receptor (*csf3r*)] (17). This led to greater susceptibility of zebrafish embryos to lethal *A. baumannii* infection (Fig. 2B). In contrast, *irf8* knockdown, which depletes macrophages but expands the neutrophil population (18), did not impact on *A. baumannii* infection survival (Fig. 2C and Fig. S2B and C). These data suggest a greater functional requirement for neutrophils than macrophages in controlling *A. baumannii* infection.

Bacterial Determinants of Virulence in Mammals Are Conserved in Zebrafish. Although a number of bacterial virulence mechanisms are host-specific (19), some are likely conserved across a range of higher-order species, including insects, fish, and mammals (20). To assess the predictive potential of zebrafish for *A. baumannii* virulence, we first assessed *A. baumannii* mutants with deletions in genes that encode a sensor histidine kinase (Δ *gacS*) and a response regulator (Δ *gacA*), both of which have displayed marked attenuation for virulence in a murine septicemia model (21). *A. baumannii* Δ *gacS* and Δ *gacA* were significantly attenuated for virulence compared with wild-type *A. baumannii* in a zebrafish bloodstream infection model (Fig. 3A).

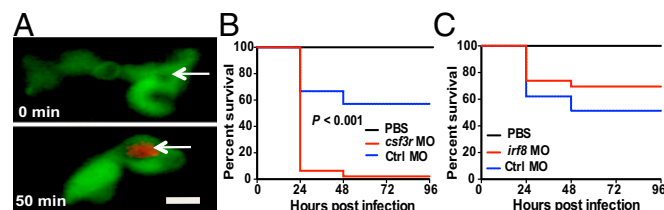


Fig. 2. Neutrophils are indispensable for zebrafish survival from *A. baumannii* infection. (A) Phagocytosed *A. baumannii* (pHrodo-dextran stain, white arrow) is handled within acidic phagolysosomes within a neutrophilic vacuole at 50-min postinfection [Tg(*mpx:GFP*)^{ll14} embryos with green fluorescent neutrophils were used]. (Scale bar: 20 μ m.) (B) Survival of neutrophil-depleted embryos (*csf3r* MO) (B) or macrophage-depleted embryos (*irf8* MO) (C) after bloodstream infection with *A. baumannii*. Comparison is made vs. *A. baumannii*-infected embryos injected with control morpholino (Ctrl MO); $P < 0.001$; $n = 30$ embryos, three biological replicates).

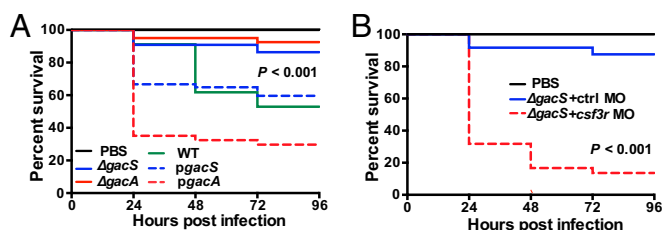


Fig. 3. *A. baumannii* virulence is conserved between zebrafish and mammals. (A) Zebrafish survival after bloodstream infection with *A. baumannii* mutants defective in virulence regulation ($\Delta gacS$ and $\Delta gacA$) and corresponding complemented strains (*pgacS* and *pgacA*); P value is comparison between $\Delta gacS$ and *pgacS*; $n = 30$ embryos, three biological replicates). (B) Neutrophil depletion using a *csf3r* morpholino (MO) restored the virulence of *A. baumannii* $\Delta gacS$ compared with zebrafish injected with a control morpholino (Ctrl MO; $P < 0.001$).

Complementation by expressing the full-length copies of the deleted genes restored virulence to wild-type *A. baumannii* levels (Fig. 3A). Moreover, neutrophil depletion using the *csf3r* morpholino restored the virulence capabilities of *A. baumannii* $\Delta gacS$ (Fig. 3B), suggesting that the virulence attenuation of this mutant was neutrophil-dependent.

Quorum-sensing is an evolutionary conserved signaling mechanism between cells within a population that facilitates the control of growth, nutrient acquisition, virulence, and other biological processes in bacteria (22, 23). Quorum sensing is yet to be established as a virulence factor in *Acinetobacter*. We tested an *Acinetobacter* M2 mutant with a deletion of the autoinducer synthase gene (*abaI*), which is necessary for 3-hydroxy- C_{12} -homoserine lactone production (24). Compared with wild-type *Acinetobacter* M2 infection, zebrafish infected with *Acinetobacter* $\Delta abaI$ had significantly greater survival (Fig. S2D). Virulence was partly restored with complementation. These findings were then corroborated in a mammalian septicemia model (Fig. S2E). Together, these data show that diverse intrinsic *Acinetobacter* virulence determinants are shared for infections in zebrafish and mammals, and support the use of zebrafish to study established, as well as new, mechanisms of *Acinetobacter* disease.

An *A. baumannii* Global Virulence Regulator Drives Extravascular Neutrophil Migration Patterns During Infection. We have shown that neutrophils orchestrate a coordinated response to a localized *A. baumannii* infection including rapid migration to the site of infection, phagocytosis, and bacterial processing within phagolysosomes, followed by migration away. Thus far, infection model studies have concentrated on host-derived factors that determine neutrophil chemotaxis such as IL-8, leukotriene B₄, C₅a, and hydrogen peroxide (2, 10, 25, 26). Less is known about bacterial factors that directly drive neutrophil migratory patterns and trafficking. During localized tissue infections into the zebrafish somatic muscle, we observed a difference in neutrophil behavior with the *A. baumannii* $\Delta gacS$ mutant. Although the neutrophils migrated to the infection site and phagocytosed bacteria, they failed to migrate away as occurred in wild-type *A. baumannii* infection (Fig. 4A and Movie S4). This resulted in persisting clusters of neutrophils at the infection site until 48 hpi (Fig. 4B and Fig. S3A). Importantly, complementation of $\Delta gacS$ restored neutrophil migratory patterns to those of wild-type (Fig. 4B). As a control, other virulence-attenuating *A. baumannii* deletion mutants ($\Delta abaI$ and $\Delta argH$) were tested but showed wild-type neutrophil migratory patterns (Fig. 4B), highlighting the specificity of this response to *A. baumannii* $\Delta gacS$. To control for site of infection, we also infected zebrafish in the otic vesicle, which, under normal conditions, is devoid of neutrophils, but is another established site for studying a localized infection. Similar findings were observed (Fig. 4C and Fig. S3B).

To characterize neutrophil dynamics in more detail, we used time-lapse confocal microscopy and 3D cell tracking software to

quantify neutrophil migratory parameters (Fig. 4D and Fig. S3C). Following infection with wild-type *A. baumannii*, neutrophils migrated to and from the site of infection consistently during the 5-h observation period (Fig. 4D). However, following infection with *A. baumannii* $\Delta gacS$, there was intense neutrophil migration to the site of infection during the first 75 min, followed by minimal further neutrophil ingress or egress for the remainder of the observation period (Fig. 4D). To determine if this neutrophil response coincided with increased host-derived chemotactic stimuli, we quantified at 1 h and 12 h after tail muscle infection the expression of mRNA encoding the chemokine IL-8, which is an established host-derived chemotaxin in tissue infection (2), and leukotriene A₄ (LTA₄) hydrolase that converts LTA₄ to LTB₄ (27). The expression of both mRNAs increased with infection, but no difference was seen between wild-type and *A. baumannii* $\Delta gacS$ (Fig. S4A). Collectively, these data indicate the presence of a strong and persistent chemoattractant in *A. baumannii* $\Delta gacS$ infection driving vigorous neutrophil influx followed by migratory arrest, and opens the possibility that this is bacterially derived.

Neutrophil Dwelling in *A. baumannii* Infected Tissue Is Mediated by an Impaired Phenylacetic Acid Catabolic Pathway. *A. baumannii* GacS is a global virulence regulator, controlling 674 genes across diverse functions (21). Interestingly, after deletion of *A. baumannii* *gacS*, the genes with greatest repression (as much as 200-fold) belonged to a single operon made up of 15 coding sequences known as the *paa* operon (21). The function of this operon is to degrade aromatic compounds such as PA, which is derived from phenylalanine, to form acetyl- and succinyl-CoA used in the TCA cycle (28). We therefore hypothesized that *A. baumannii* $\Delta gacS$ is altering neutrophil responses through repression of the *paa* operon, leading to accumulation of aromatic compounds and subsequent bacterial-driven chemoattraction.

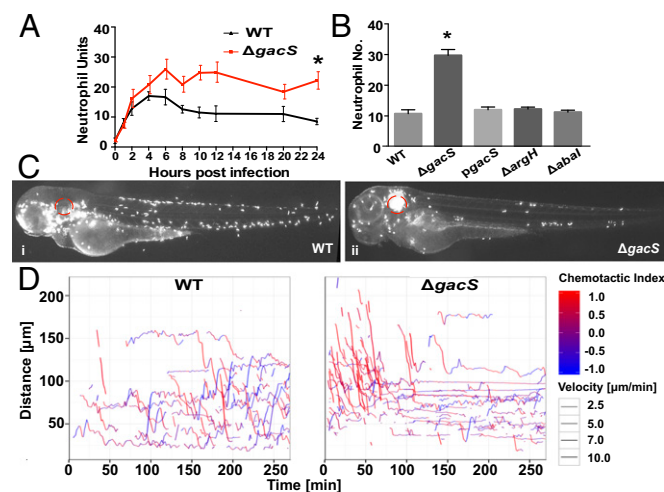


Fig. 4. Altered in vivo neutrophil migratory patterns during *A. baumannii* infection. (A) Localized somatic muscle infection with *A. baumannii* $\Delta gacS$ led to greater neutrophil units at the site of infection and a loss of migration away compared with wild-type *A. baumannii* infection (mean \pm SEM from three biological replicates). (B) Neutrophil units at the site of a localized somatic muscle infection 48 hpi showed restoration of neutrophil numbers with *gacS* complementation (*pgacS*) and no abnormalities with other *A. baumannii* virulence-associated mutants ($\Delta argH$, $\Delta abaI$; mean \pm SEM, three biological replicates). (C) Infection of the otic vesicle (red circle) with wild-type *A. baumannii* (i) and $\Delta gacS$ (ii) imaged at 48 hpi. (Magnification: 10 \times .) (D) Cell tracking analysis of neutrophil movement after infection with WT and $\Delta gacS$ strains. A chemotactic index (red, movement toward infection; blue, movement away) and velocity (thickness of the line) are indicated (representative experiment from five biological replicates). Asterisks in A and B denote comparison between wild-type *A. baumannii* and $\Delta gacS$ (* $P \leq 0.05$).

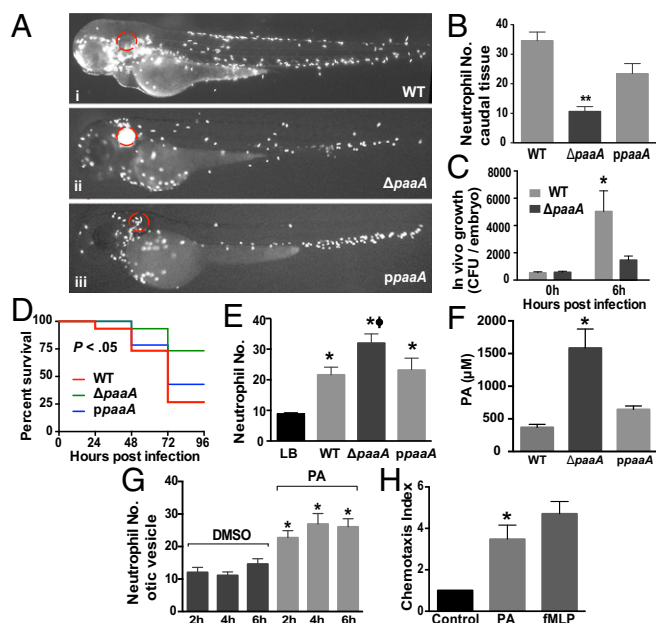


Fig. 5. PA is a bacterial-driven chemoattractant. (A) Neutrophil accumulation imaged 48 hpi of the otic vesicle (red circle). (B) The observed neutrophil clustering was associated with a reduction in neutrophils normally resident in the caudal hematopoietic tissue assessed at 48 h. The functional effect of this neutrophilic response to *A. baumannii* $\Delta paaA$ infection was a reduced bacterial burden (C) and increased zebrafish survival (D) compared with wild-type *A. baumannii* and the complemented strain (*ppaaA*; *P* value is a comparison of $\Delta paaA$ and *ppaaA* by log-rank test). (E) Attraction of neutrophils to the otic vesicle 6 hpi of culture filtrate. (F) Concentration of PA in culture filtrates. (G) Injection of purified PA into the otic vesicle was sufficient to attract a greater number of neutrophils within 2 h of injection compared with PBS solution. (H) Neutrophil chemotaxis toward PA (0.05 M) in an ex vivo neutrophil transwell migration assay using mouse-derived neutrophils. fMLP was used as a positive control. For all experiments, column bars represent the mean \pm SEM, performed at least in triplicate, and the asterisks denote comparison between wild-type *A. baumannii* and $\Delta paaA$ for B, C, and F, between LB and wild-type, $\Delta paaA$, and *ppaaA* for E, and between PA and PBS control for G and H; letter ϕ denotes comparison between wild-type and $\Delta paaA$ for E by one-way ANOVA (Kruskal–Wallis test, $*P \leq 0.05$, $**P < 0.01$, and $^{\phi}P \leq 0.05$). (Magnification: 10 \times .)

To test whether the $\Delta gacS$ -mediated neutrophil response is caused by loss of the PA catabolic pathway, we induced a localized infection in the zebrafish otic vesicle with an early PA pathway *A. baumannii* mutant ($\Delta paaA$). As shown in Fig. 5A, neutrophil responses were the same as that seen for *A. baumannii* $\Delta gacS$ (Fig. 4C), with prolonged neutrophil dwelling at the site of infection compared with wild-type *A. baumannii*. The phenotype was restored to wild-type levels with complementation (*ppaaA*) (Fig. 5A). Consistent with there being neutrophil relocation and clustering in the otic vesicle and not local neutrophil proliferation, we documented that neutrophil aggregation in the otic vesicle during *A. baumannii* $\Delta paaA$ infection was concurrent with reduction of neutrophils normally resident in the caudal hematopoietic tissue (Fig. 5B). Highlighting the specificity of this neutrophilic response to *A. baumannii* $\Delta paaA$, we infected zebrafish with another isogenic *A. baumannii* mutant with a deletion in a *GacS*-regulated gene *csuD* (21). No difference in neutrophil trafficking compared with wild-type was seen (Fig. S4B).

To determine the functional impact of this neutrophil dwelling response on bacterial survival, we assessed bacterial densities at 6 hpi for wild-type *A. baumannii*, $\Delta paaA$, and complement strains (all grow similarly in vitro). Significantly fewer bacteria were found for $\Delta paaA$ (Fig. 5C), and this was associated with attenuated virulence for the $\Delta paaA$ mutant compared with wild-

type and complement strains (Fig. 5D). Together, these data indicate that the *A. baumannii* PA catabolic pathway is important in mediating neutrophil chemotaxis and tissue responses to acute infection, and may be a mechanism by which *A. baumannii* uses for immune evasion and disease progression.

PA Mediates Neutrophil Chemotaxis. To confirm whether a metabolic by-product was accumulating in the tissues after infection with *A. baumannii* $\Delta paaA$, we first injected the otic vesicle of zebrafish with *A. baumannii* culture filtrate taken from stationary-phase in vitro growth (Fig. 5E). Neutrophil chemotaxis and dwelling occurred with supernatant taken from *A. baumannii* $\Delta paaA$, whereas neutrophil chemotaxis was less with supernatant from wild-type and complemented *A. baumannii* strains (Fig. 5E). Interestingly, injection of washed, heat-killed *A. baumannii* $\Delta paaA$ caused neutrophil chemotaxis, but neutrophil dwelling was not observed (Fig. S4C), indicating that metabolism from live bacteria is required for the production of the causative factor.

To identify the molecule responsible for the observed neutrophil responses, we performed untargeted global metabolomics by MS on culture filtrate taken from wild-type *A. baumannii*, $\Delta paaA$ and the complemented strain. In total, more than 1,600 metabolite features were detected, and the only metabolite that showed a significant accumulation (more than twofold; $P < 0.05$) in *A. baumannii* $\Delta paaA$ compared with the wild-type and complemented strains was putatively identified as PA (Fig. S5 and Dataset S1). Subsequent identification and accurate quantification of PA by using targeted liquid chromatography (LC)/MS confirmed fourfold accumulation of PA in $\Delta paaA$ supernatant compared with wild-type (Fig. 5F). PA is an intermediate product of the bacterial phenylalanine metabolic pathway, and a direct substrate of *paaA*. To confirm that PA was the causative driver of the observed neutrophil tissue responses, we injected purified PA (Sigma) into the otic vesicle of zebrafish at varying concentrations. This showed a bell-curve dose–response relationship characteristic of chemoattractants (29), with a concentration as low as 3.4 ng per embryo having an effect, and peaking at 37 ng per embryo (Fig. S6A). Neutrophil migration was seen within 2 hpi (Fig. 5G). When purified PA was added to wild-type culture filtrate and injected into the otic vesicle of zebrafish, we observed the same neutrophil trafficking characteristics as observed for infection with *A. baumannii* $\Delta paaA$ (Fig. S6B). Furthermore, the addition of purified PA to wild-type *A. baumannii* cells before infection led to greater embryo survival compared with infection with wild-type *A. baumannii* alone (Fig. S6C). Finally, to determine if PA was acting directly on neutrophils rather than through stimulation of endogenous cytokines, and to assess whether this effect was observed with mammalian neutrophils, we performed ex vivo neutrophil migration assays by using murine bone marrow-derived neutrophils. Purified PA caused significantly greater neutrophil transmigration compared with the control (Fig. 5H). Together, these data confirm that, in the absence of a functional PA catabolic pathway, PA accumulates with live bacterial cells and then acts as a bacterial-driven neutrophil chemoattractant.

Discussion

A. baumannii continues to be a problematic Gram-negative bacterial pathogen within health care institutions, with reports of pandrug resistance threatening our modern-day antibiotic armamentarium. As a consequence, we urgently require an improved understanding of the interactions between *A. baumannii* and the host during acute infection to provide the foundations for future therapeutic strategies. We developed a zebrafish model to study the molecular mechanisms of *A. baumannii*–host interactions. Through use of real-time fluorescent microscopy and cell tracking, we demonstrated an interaction between bacterial metabolism and host innate immune response. Inhibition of the *A. baumannii* phenylacetic acid catabolism pathway led to the accumulation of PA as a metabolic by-product, which was shown to be a direct bacterial-driven chemoattractant, causing

neutrophils to avidly migrate to the site of infection and dwell. The functional impact of this pronounced neutrophilic response was a reduction in bacterial burden and attenuated disease. Targeting a metabolic pathway with the intention of augmenting host innate immune response provides a potentially new paradigm for the treatment of challenging superbugs such as *A. baumannii*.

Zebrafish have now been used as a model to study the pathogenesis of diverse infectious diseases (9, 30–33). Bacteria such as *Mycobacterium marinum*, *Salmonella enterica* serovar Typhimurium, *S. aureus*, and *Shigella flexneri* have all displayed inoculum-dependent acute lethality in zebrafish, with survival correlating with bacterial growth in the host. By testing defined *A. baumannii* mutants, we were able to show that, for some virulence factors, virulence in zebrafish correlated with that observed in a mammalian model. *A. baumannii* GacS is a two-component signal transduction system that is essential for disease in a mouse septicemia model (21); likewise, mutants in this system were highly attenuated for disease in zebrafish. We also showed that quorum sensing is required for *A. baumannii* virulence in zebrafish and a mammalian host. These data support the utility of zebrafish as a facile, in vivo model for the study of new, as well as established, bacterial virulence mechanisms, and strengthen the idea that conservation of bacterial virulence may exist across a range of multicellular eukaryotic species.

Zebrafish and humans share very similar immune systems in terms of cellular anatomy and genetic regulation (6). Young zebrafish embryos (< 3 wk post fertilization) rely solely on innate immunity, which makes them ideal for the study of initial host responses to bacterial pathogens. By using several lines of evidence, we showed that innate immune cells, particularly neutrophils, were indispensable for zebrafish survival from *A. baumannii* infection. A lower inoculum of *A. baumannii* administered i.v. was cleared by zebrafish after ~44 h, whereas administration of the same dose into the yolk sac (devoid of phagocytic cells) was lethal. In a localized somatic muscle infection, neutrophils predominated as infection-specific first responders and showed greater phagocytic function than macrophages. Finally, selective depletion of zebrafish neutrophils increased susceptibility to acute lethal infection, whereas depletion of macrophages had no significant effect. Neutrophil depletion also restored the virulence of bacterial mutants that were attenuated for disease. These data support findings observed in mammalian hosts whereby depletion of neutrophils exacerbated *A. baumannii* infection (5, 34), whereas macrophage depletion had a limited impact on disease (15).

An impressive feature of zebrafish is the ability to visualize real-time infection dynamics at the cellular level, made possible by their optical transparency and the availability of well-characterized transgenic reporter fish lines that selectively fluoresce host innate immune cells. By using fluorophore-marked bacteria, we used high-resolution, time-course imaging experiments to delineate individual leukocyte responses to *A. baumannii* invasion in vivo, and, more specifically, study the drivers of neutrophil migration during an acute infection. For one of our bacterial mutants (Δ gacS), we observed that neutrophils avidly migrated to the site of infection and then failed to migrate away as seen with wild-type bacterial infection. By using a series of isogenic *A. baumannii* mutants, we showed that a mutant in the phenylacetic acid catabolism pathway mirrored the phenotype observed with Δ gacS. Δ paaA culture filtrate alone was sufficient to replicate the phenotype, but this was abolished with infection of washed, heat-killed Δ paaA cells, both suggesting that a bacterial-driven metabolic by-product was responsible for the altered neutrophil behavior.

Bacterial-guided leukocyte chemotaxis has thus far been well described for molecules such as LPS, lipopeptides, peptidoglycan, flagellin, and nucleic acids (35). However, these microorganism-associated molecular patterns lead to leukocyte recruitment indirectly via Toll-like receptors and activation of chemokines (e.g., IL-8). Very little is known about directly acting bacterial factors that drive neutrophil recruitment and behavior. By using global

metabolomic analyses of culture supernatants, we showed that PA was significantly and specifically increased for the Δ paaA mutant compared with supernatants taken from wild-type and complemented bacteria. To confirm the independent effect of this metabolite on neutrophil migration, purified PA was injected into the otic vesicle of zebrafish. Neutrophil chemotaxis and dwelling was observed. Purified PA was also sufficient to recreate the phenotype when added to culture supernatant from wild-type bacteria. These observations were then extended using ex vivo mammalian neutrophils, which showed that purified PA was independently capable of inducing neutrophil recruitment. Together, these data confirmed the role of PA as a direct bacterial-driven chemoattractant for zebrafish and mammalian neutrophils.

The role of PA in bacterial metabolism has not been fully elucidated. In *Burkholderia cenocepacia*, a Gram-negative pathogen related to *A. baumannii*, deletion of genes in the phenylalanine degradation pathway (*paaABCDE*) led to accumulation of phenylacetic acid and inhibited bacterial quorum sensing (36). Virulence attenuation has also been shown with disruption of the *paa* catabolic pathway; however, the mechanism of this remains unclear (37). Here we propose a mechanism that is driven by augmentation of host innate immune response. By deleting the *A. baumannii* phenylacetic acid catabolism pathway, an accumulation of PA ensues that enhances neutrophil migration and clustering at the site of infection, leading to greater bacterial killing and improved host survival. The significance of these data are that inhibition of this bacterial metabolic pathway could form a novel adjunctive therapy. The global emergence of antimicrobial resistance has led to a desperate need in identifying antimicrobials with new mechanisms of action. Augmentation of host immune responses to a bacterial pathogen could provide an alternative treatment strategy in the face of extreme drug-resistant and pandrug-resistant Gram-negative bacteria such as *A. baumannii*.

Methods and Materials

Bacterial Strains and Growth Conditions. *A. baumannii* strains (Table S1) were grown in LB liquid or solid media at 37 °C supplemented with carbenicillin (150 μ g/mL) or kanamycin (50 μ g/mL) as appropriate. GFP expression and complementation of *Acinetobacter* M2 Δ abai and ATCC 17978 Δ paaA were performed by using pWH1266 as described elsewhere (38). Primers used for this study are shown in Table S2.

Zebrafish Strains and Maintenance. Wild-type Tübingen, Tg(*lyz*:DsRed)ⁿ²⁵⁰ (39), Tg(*mpeg1*:mCherry)^{g123} (40), Tg(*mpx*:GFP)^{l14} (41), and Tg(*mpeg1*:Gal4FF)^{g125} \times Tg(*UAS-E1b*:Eco.NsfB-mCherry)^{c264} zebrafish embryos were maintained in the Monash University FishCore facility according to standard protocols (SI Materials and Methods).

Microinjection of *A. baumannii* into Zebrafish Embryos. Overnight bacterial cultures were adjusted to OD₆₀₀ of 1, washed, and resuspended in 2% (wt/vol) polyvinylpyrrolidone in PBS solution. Microinjections were performed at 48 hpf, and all inocula were confirmed by colony counts (42, 43). Embryos were monitored daily for survival to 96 hpi, and survival analyses were performed by using the Kaplan–Meier method. The Mantel–Cox test was used for statistical significance ($P < 0.05$). A range of 500–800 cfu of bacteria were injected into the muscle or otic vesicle for neutrophil and macrophage migration assays. Methods for in vivo *A. baumannii* growth kinetics and quantitative real-time PCR are shown in SI Materials and Methods.

Morpholino Depletion of *cfs3r* and *irf8*. Antisense morpholino oligomers (MOs) directed at *cfs3r* (30) and *irf8* (18) were purchased from Gene Tools. Volumes of 1 nL were microinjected into the yolk of one-cell embryos, delivering MOs at the following final concentration in distilled water: 25 μ M of *cfs3r*^{ATG} MO and 25 μ M of *irf8*^{ATG} MO. A standard control MO was used as a negative control.

Leukocyte Enumeration. Leukocyte units (LUs), a surrogate parameter proportional to leukocyte numbers determined by analysis of digital images, were computed as previously described and validated (43). When appropriate, LUs are referred to as “neutrophil units” or “macrophage units.” Leukocyte numbers were referred to when the total number of neutrophils was counted. A Mann–Whitney test was used for statistical significance ($P < 0.05$).

Microscopy and Image Processing. For microscopy, zebrafish were immobilized in 1% low melting temperature agar. Routine bright-field and fluorescence imaging was performed by using a Zeiss Lumar V12 stereo dissecting microscope with an AxioCam MRm camera running AxioVision 4.8 software. Confocal microscopy was performed with a Zeiss LSM 710 device with a Plan-Apochromat 20x, 0.8 N.A. objective, and Zen software (v4.0) (*SI Materials and Methods*). Images were processed in Imapris (Bitplane) for cell-tracking mode, and data were analyzed in the R program using ggplot2 (26). Vibratome sectioning, histopathology, and pHrodo staining are described in *SI Materials and Methods*.

Murine Disseminated Infection Model. The model was performed as described previously (21) using female BALB/c mice aged 6–8 wk ($n = 15$ per group) infected via intraperitoneal injection (*SI Materials and Methods*). Animal protocols were approved by the Monash University Animal Ethics Committee.

Metabolomics. Metabolite samples were prepared from cell culture supernatants by solvent extraction and analyzed by LC/MS with hydrophilic interaction liquid chromatography (HILIC) and high-resolution accurate MS (44) (*SI Materials and Methods*). Metabolomics data were analyzed with the

IDEOM software (45), and PA abundance confirmed with Tracefinder (Thermo). Quantification of PA was confirmed by using a complementary analytical method, reversed-phase chromatography coupled to high-resolution MS (Q-Exactive; Thermo; *SI Materials and Methods*).

Ex Vivo Neutrophil Chemotaxis Assay. Neutrophils were isolated from the bone marrow of C57BL/6 mice by Histopaque density gradient centrifugation, and chemotaxis was performed as described previously (46) (*SI Materials and Methods*).

ACKNOWLEDGMENTS. We thank Dr. Connie Wong and Alyce Nicholls for supporting the chemotaxis assay; Monash Micro Imaging for use of the imaging facilities; Monash FishCore facilities for the care and maintenance of zebrafish; and Max Cryle and Matthew Belousoff for assistance with the metabolomics assays. This work was supported by an Australian National Health and Medical Research Council (NHMRC) Career Development fellowship (to A.Y.P. and D.J.C.), and an Australian Leadership Award by the Australian government (to M.S.B.). G.J.L. is an NHMRC Senior Research Fellow. The Australian Regenerative Medicine Institute is supported by funds from the State Government of Victoria and the Australian Federal Government.

- Peleg AY, Seifert H, Paterson DL (2008) *Acinetobacter baumannii*: Emergence of a successful pathogen. *Clin Microbiol Rev* 21(3):538–582.
- Deng Q, et al. (2013) Localized bacterial infection induces systemic activation of neutrophils through Cxcr2 signaling in zebrafish. *J Leukoc Biol* 93(5):761–769.
- Knapp S, et al. (2006) Differential roles of CD14 and toll-like receptors 4 and 2 in murine *Acinetobacter pneumoniae*. *Am J Respir Crit Care Med* 173(1):122–129.
- Breslow JM, et al. (2011) Innate immune responses to systemic *Acinetobacter baumannii* infection in mice: Neutrophils, but not interleukin-17, mediate host resistance. *Infect Immun* 79(8):3317–3327.
- van Faassen H, et al. (2007) Neutrophils play an important role in host resistance to respiratory infection with *Acinetobacter baumannii* in mice. *Infect Immun* 75(12):5597–5608.
- Tobin DM, May RC, Wheeler RT (2012) Zebrafish: A see-through host and a fluorescent toolbox to probe host-pathogen interaction. *PLoS Pathog* 8(1):e1002349.
- Lieschke GJ, Trede NS (2009) Fish immunology. *Curr Biol* 19(16):R678–R682.
- Henry KM, Loynes CA, Whyte MK, Renshaw SA (2013) Zebrafish as a model for the study of neutrophil biology. *J Leukoc Biol* 94(4):633–642.
- Mostowy S, et al. (2013) The zebrafish as a new model for the in vivo study of *Shigella flexneri* interaction with phagocytes and bacterial autophagy. *PLoS Pathog* 9(9):e1003588.
- Tobin DM, et al. (2010) The *Ita4h* locus modulates susceptibility to mycobacterial infection in zebrafish and humans. *Cell* 140(5):717–730.
- Adams KN, et al. (2011) Drug tolerance in replicating mycobacteria mediated by a macrophage-induced efflux mechanism. *Cell* 145(1):39–53.
- Davis JM, Ramakrishnan L (2009) The role of the granuloma in expansion and dissemination of early tuberculous infection. *Cell* 136(1):37–49.
- Hepburn L, et al. (2014) Innate immunity. A Spaetzle-like role for nerve growth factor β in vertebrate immunity to *Staphylococcus aureus*. *Science* 346(6209):641–646.
- Crowhurst MO, Layton JE, Lieschke GJ (2002) Developmental biology of zebrafish myeloid cells. *Int J Dev Biol* 46(4):483–492.
- Qiu H, et al. (2012) Role of macrophages in early host resistance to respiratory *Acinetobacter baumannii* infection. *PLoS One* 7(6):e40019.
- Cech P, Lehrer RI (1984) Phagolysosomal pH of human neutrophils. *Blood* 63(1):88–95.
- Liongue C, Hall CJ, O'Connell BA, Crosier P, Ward AC (2009) Zebrafish granulocyte colony-stimulating factor receptor signaling promotes myelopoiesis and myeloid cell migration. *Blood* 113(11):2535–2546.
- Li L, Jin H, Xu J, Shi Y, Wen Z (2011) Irf8 regulates macrophage versus neutrophil fate during zebrafish primitive myelopoiesis. *Blood* 117(4):1359–1369.
- Morgan E, et al. (2004) Identification of host-specific colonization factors of *Salmonella enterica* serovar Typhimurium. *Mol Microbiol* 54(4):994–1010.
- Rahme LG, et al. (1995) Common virulence factors for bacterial pathogenicity in plants and animals. *Science* 268(5219):1899–1902.
- Cerqueira GM, et al. (2014) A global virulence regulator in *Acinetobacter baumannii* and its control of the phenylacetic acid catabolic pathway. *J Infect Dis* 210(1):46–55.
- Slamti L, Lereclus D (2002) A cell-cell signaling peptide activates the PlcR virulence regulon in bacteria of the *Bacillus cereus* group. *EMBO J* 21(17):4550–4559.
- Zhu J, et al. (2002) Quorum-sensing regulators control virulence gene expression in *Vibrio cholerae*. *Proc Natl Acad Sci USA* 99(5):3129–3134.
- Niu C, Clemmer KM, Bonomo RA, Rather PN (2008) Isolation and characterization of an autoinducer synthase from *Acinetobacter baumannii*. *J Bacteriol* 190(9):3386–3392.
- de Oliveira S, et al. (2013) Cxcl8 (IL-8) mediates neutrophil recruitment and behavior in the zebrafish inflammatory response. *J Immunol* 190(8):4349–4359.
- Lämmermann T, et al. (2013) Neutrophil swarms require LTB4 and integrins at sites of cell death in vivo. *Nature* 498(7454):371–375.
- Haeggström JZ, Funk CD (2011) Lipoxigenase and leukotriene pathways: Biochemistry, biology, and roles in disease. *Chem Rev* 111(10):5866–5898.
- Teufel R, et al. (2010) Bacterial phenylalanine and phenylacetate catabolic pathway revealed. *Proc Natl Acad Sci USA* 107(32):14390–14395.
- Schiffmann E, Corcoran BA, Wahl SM (1975) N-formylmethionyl peptides as chemoattractants for leucocytes. *Proc Natl Acad Sci USA* 72(3):1059–1062.
- Palha N, et al. (2013) Real-time whole-body visualization of *Chikungunya* virus infection and host interferon response in zebrafish. *PLoS Pathog* 9(9):e1003619.
- Prajsnar TK, Cunliffe VT, Foster SJ, Renshaw SA (2008) A novel vertebrate model of *Staphylococcus aureus* infection reveals phagocyte-dependent resistance of zebrafish to non-host specialized pathogens. *Cell Microbiol* 10(11):2312–2325.
- Runft DL, et al. (2014) Zebrafish as a natural host model for *Vibrio cholerae* colonization and transmission. *Appl Environ Microbiol* 80(5):1710–1717.
- van der Sar AM, et al. (2003) Zebrafish embryos as a model host for the real time analysis of *Salmonella typhimurium* infections. *Cell Microbiol* 5(9):601–611.
- Gandhi JA, et al. (2014) Alcohol enhances *Acinetobacter baumannii*-associated pneumonia and systemic dissemination by impairing neutrophil antimicrobial activity in a murine model of infection. *PLoS One* 9(4):e95707.
- Bloes DA, Kretschmer D, Peschel A (2015) Enemy attraction: Bacterial agonists for leukocyte chemotaxis receptors. *Nat Rev Microbiol* 13(2):95–104.
- Pribytkova T, et al. (2014) The attenuated virulence of a *Burkholderia cenocepacia* paaABCDE mutant is due to inhibition of quorum sensing by release of phenylacetic acid. *Mol Microbiol* 94(3):522–536.
- Law RJ, et al. (2008) A functional phenylacetic acid catabolic pathway is required for full pathogenicity of *Burkholderia cenocepacia* in the *Caenorhabditis elegans* host model. *J Bacteriol* 190(21):7209–7218.
- Tomaras AP, Flagler MJ, Dorsey CW, Gaddy JA, Actis LA (2008) Characterization of a two-component regulatory system from *Acinetobacter baumannii* that controls biofilm formation and cellular morphology. *Microbiology* 154(pt 11):3398–3409.
- Hall C, Flores MV, Storm T, Crosier K, Crosier P (2007) The zebrafish lysozyme C promoter drives myeloid-specific expression in transgenic fish. *BMC Dev Biol* 7:42.
- Ellett F, Pase L, Hayman JW, Andrianopoulos A, Lieschke GJ (2011) *mpeg1* promoter transgenes direct macrophage-lineage expression in zebrafish. *Blood* 117(4):e49–e56.
- Renshaw SA, et al. (2006) A transgenic zebrafish model of neutrophilic inflammation. *Blood* 108(13):3976–3978.
- Benard EL, et al. (2012) Infection of zebrafish embryos with intracellular bacterial pathogens. *J Vis Exp* Mar 15(61):61.
- Ellett F, Lieschke GJ (2012) Computational quantification of fluorescent leukocyte numbers in zebrafish embryos. *Methods Enzymol* 506:425–435.
- Zhang T, Creek DJ, Barrett MP, Blackburn G, Watson DG (2012) Evaluation of coupling reversed phase, aqueous normal phase, and hydrophilic interaction liquid chromatography with Orbitrap mass spectrometry for metabolomic studies of human urine. *Anal Chem* 84(4):1994–2001.
- Creek DJ, Jankevics A, Burgess KE, Breitling R, Barrett MP (2012) IDEOM: An Excel interface for analysis of LC-MS-based metabolomics data. *Bioinformatics* 28(7):1048–1049.
- Green TD, et al. (2012) Directed migration of mouse macrophages in vitro involves myristoylated alanine-rich C-kinase substrate (MARCKS) protein. *J Leukoc Biol* 92(3):633–639.